Enhanced Iridium Complexes for Amino Acid and Peptide Isotope Labelling Processes

Adele E. Queen

PhD Thesis

2020

Author Declaration

This thesis is the result of the author's original research. It has been composed by the author and has not been previously submitted for examination which has led to the award of a degree.

Signature:

Adele E. Queen

2/6/2020

Abstract

Over the last decade, the number of new chemical entities approved as drugs within the pharmaceutical industry has greatly increased. Although this may seem promising, the attrition rate remains obtusely high, posing a major issue for pharmaceutical drug development. In an attempt to combat these problems, metabolism studies are utilised much earlier in the drug discovery process, to enable the identification of potential issues before a candidate is entered into expensive pre-clinical or clinical trials. The use of heavy isotopes to label drug candidates play a central role in metabolism studies and as such methods of synthesising these are incredibly useful. Hydrogen isotopes are often utilised for this purpose, and are often introduced *via* hydrogen isotope exchange (HIE).

Iridium has adopted a central role in HIE processes, and a large library of iridium(I) catalysts have been developed within the Kerr group for the efficient *ortho*-labelling of a large array of aromatic compounds. Iridium catalysed HIE utilises a directing group within a molecule, meaning a large range of functionality can be employed. The Kerr group have presented an impressive advancement within the area of HIE, with efficient catalysts under mild conditions and high levels of labelling, however, labelling of sp^3-rich, and more biologically relevant, molecules remains in its infancy.

More and more peptides are emerging on the market as therapeutics, providing a 'sweet' spot between small molecules and large biologics. Therefore, it is imperative that such molecules can also be istopically labelled to allow metabolism studies much like their small molecule counterparts. In a similar vein, amino acids, the building blocks of peptide molecules, also represent an important class of molecules to be labelled.

This report describes development of a method to label amino acid and small peptide substrates under iridium(I) catalysis, with high incorporations observed under mild conditions. Isotopic labelling of peptides on solid resin support has been investigated in an

attempt to combat the solubility issues associated with these HIE substrates. In addition, Density Functional Theory (DFT) studies have been utilised to design new Ir(I) catalysts, targeted for the labelling of more complex amino acid and peptide motifs, which are, to date, significantly more challenging.

Acknowledgements

First and foremost I would like to thank Professor Billy Kerr, not only for allowing me the opportunity to be part of his research group, but for providing a motivated atmosphere which has allowed me to develop. I am endlessly grateful for all of the opportunities you have given me throughout my studies.

Particular thanks go to Dr David Lindsay and Dr Laura Paterson, your support has been invaluable throughout the duration of my PhD. Laura, I am grateful for your help day-to-day, both with my research project and emotional wellbeing, especially in stressful times. Dave, I cannot thank you enough for the advice and input you have given me with both my project and career aspects. Thanks also for your help in the preparation of this thesis. I thank you both for always having an open door policy, even though I'm sure in my times of stress you very much wanted to lock it closed.

I would also like to thank the various technical staff at the University of Strathclyde, especially to Craig Irving, who always helped out when there was an NMR issue.

My thanks also go to Dr Sumei Ren and her colleagues at Merck. Your help, inputs and encouragement on our regular telecoms have been invaluable and have led to fruitful outputs within this project.

During my PhD I was fortunate to undergo a placement at Research Triangle Institute (RTI) in North Carolina. I would like to extend my thanks to all of the staff there for welcoming me with open arms, and for the opportunity you gave me, making this a very fulfilling experience. A special thanks must go to Dr David Hesk. Not only were you a fantastic support to me during your time at Merck (travelling up to Scotland for an update, even when you were on holiday), but the invitation to work with you at RTI was extremely kind and accommodating. I feel extremely privileged to have worked with such an experienced isotope chemist and you made the whole experience very enjoyable. I would like to also extend my thanks to your wife Claudia, whom together your hospitality was second to none. Thank you again for making this such an enjoyable and rewarding experience.

I would like to thank all of the Kerr group members, past and present, that I have had the opportunity to work with throughout my time. A special thanks go to past team iridium members: Dr Marc Reid, Dr Richard Mudd, Dr Philippa Owens, Dr Renan Zorzatto and Dr Gary Knox for your endless support. Thanks must also go to Dr Peter Katai for his continuous practical jokes! Dr Liam McLean, I am extremely grateful for the help and support you have provided throughout my PhD and it was great to share the lab corner with you, even if you tried to murder Mega-Buchi. I am sorry you had to endure the thesis writing process in lock-down, you have the patience of a Saint (and the ability to know when I need tea and a cake!). I would also like to extend my thanks to my fellow year group: Raymond, Giorgia and Paul. Special thanks go to Raymond for our morning rants, good DJ'ing skills and endless support. I will never forget being stranded homeless with you in the middle of San Francisco. Nathan and Conor, it has been great to work with you both. Conor, I hope one day you will learn not to insult people immediately before asking for help! To Megan, Paul and Andrew- it has been a pleasure to work with you for a short time I wish you all the best for your PhD and Megan I hope you enjoy the peptides. A special mention must also got to Dr Jack Washington (honorary group member), for always making me laugh, listening to my rants and getting excited about baked goods with me!

I would also like to thank Laura Bain and Jemma MacLachlan. Laura, we have gone through both our undergraduate and PhD together, and in all honesty I couldn't think of a better person to have by my side. Thanks for always being there for a laugh, rant, drink or an emergency lunchtime walk! Jemma, you were a pleasure to have in the lab in the time you were there, and I don't think I have laughed as much as I did then. I am grateful to have you as a friend and continued support.

Finally I would like to extend my thanks to my family. To my mum, dad and brother, I will never be able to thank you enough for the love and support you have given me throughout my life, and mum and dad the sacrifices you, as parents, have given for your children. Thank you for always being a phone call away, and encouraging me throughout. Finally, I would like to dedicate this thesis to my gramps, who has always been my most proud supporter.

Abbreviations

AA – Amino Acid

Ac – Acetyl

ADMET – Adsorption, Distribution, Metabolism, Excretion and Toxicology

Ar – Aryl

Ala – L-Alanine

Avg – Average

BAr^F - Tetrakis[3,5-bis(trifluoromethyl)phenyl]borate

Bn – Benzyl

Boc – *tert*-butoxycarbonyl

BSSE – Basis Set Superposition Error

Cat – Catalyst

Cbz – Benzyloxy Carbonate

Ci – Curie

CM – ChemMatrix

CNS – Central Nervous System

COD – Cyclooctadiene

Cp – Cyclopentadienyl

Cp* – Pentamethylcyclopentadienyl

CPME – Cyclopentyl methyl ether

CuAAC – Copper catalysed Azide Alkyne Cycloaddition

Cy – Cyclohexyl

DABCO – 1,4-diazabicyclo[2.2.2]octane

DCC – Dicyclohexycarbodiimide

DCE – Dichloroethane

DIBALH – Di*iso*butylaluminium Hydride

DIC – *N,N*-Di*iso*propylcarbodimide

DCM – Dichloromethane

DFT – Density Functional Theory

DG – Directing Group

DIPEA – *N,N*-di-*iso*-propylethylamine

DiPP – Di-*iso*-propylphenyl

DMAP – *N,N*-dimethylaminopyridine

DMF – *N,N*-dimethyl Formamide

DMSO – Dimethyl Sulfoxide

DoE – Design of Experiment

ESI – Electrospray Ionisation

Et – Ethyl

eq – Equivalents

FDA – Food and Drug Administration

FG – Functional Group

Fmoc – Fluorenylmethoxy carbonyl

g – Gram(s)

Gly – Glycine

h – Hour(s)

HAT – Hydrogen Atom Transfer

HATU – (1-[Bis(dimethylamino)methylene]-1H-1,2,3-triazolo[4,5-b]pyridinium3-oxido hexafluorophosphate)

HBA – Hydrogen Bond Acceptor

HBD – Hydrogen Bond Donor

HIE – Hydrogen Isotope Exchange

HPLC – High Performance Liquid Chromatography

HRMS – High Resolution Mass Spectrometry

HTS – High Throughput Screen

Hz – Hertz

IAd – 1,3-Di(adamantyl)imidazolylidene

ICy – 1,3-Di(cyclohexyl)imidazolylidene

Ile – L-Isoleucine

IMes – 1,3-Dimesitylimidazolylidene

IMes^{Me} – 1,3-Di(mesity)-dimethyllimidazolylidene

IPA – *iso*-propanol

IPr - 1,3-Bis(2,6-di-*iso*-propylphenyl)imidazolylidene

^{i}Pr – *Iso*-propyl

IR – Infrared

kcal – Kilocalorie

KIE – Kinetic Isotope Effect

KHMDS – Potassium bis(trimethylsilyl)amide

L– Ligand

LCMS– Liquid Chromatography-Mass Spectrometry

Leu– L-Leucine

Log P – Lipophilicity

LOS– Lead Orientated Synthesis

M – Molar

Me – Methyl

Mes – Mesityl

Met –Methionine

MHz – Megahertz

MIC – Mesoionic Carbene

min – Minute

mmi – Membered Metallocyclic Intermediate

mmol – Millimoles

mol – Moles

mol% – Mole Percent

MS – Mass Spectrometry

MTBE – Methyl *tert*-Butyl Ether

MW – Molecular Weight

m/z – Mass to Charge Ratio

NAsc – Sodium Ascorbate

***n*Bu** – *n*-Butyl

NCE – New Chemical Entity

NCL – Native Chemical Ligation

NHC – *N*-Heterocyclic Carbene

NHCP – *N*-Heterocyclic Carbene-Phosphine

NMP – *N*-Methyl-2-pyrrolidinone

NMR – Nuclear Magnetic Resonance

appt – Apparent Triplet

bs – Broad Singlet

d – Doublet

dd – Doublet of Doublets

ddd – Doublet of Doublet of Doublets

J – Coupling Constant

m - Multiplet

ppm – Parts Per Million

q – Quartet

sep – Septet

t – Triplet

td – Triplet of Doublets

NSI – Nanospray Ionisation

OTf – Acetate

OTf – Triflate

Ph – Phenyl

Phe – L-Phenylalanine

Phen – 1,10-phenanthroline

Pro – L-Proline

Psi– Pounds Per Square Inch

Py – Pyridyl

R – Substituent

r - Radius

R&D – Research and Development

RDS – Rate Determining Step

RuNP – Ruthenium Nanoparticles

rt – Room Temperature

RTI – Research Triangle Institute

S – Solvent Molecule

SA – Specific Activity

Ser – L-Serine

SIMes – 1,3-Dimesityl-4,5-dihydro Imidazolylidene

SIPr – 1,3-Bis(2,6-di-*iso*-propylphenyl) dihydro imidazolylidene

SPPS – Solid Phase Peptide Synthesis

^{t}Bu – *tert*-Butyl

temp – Temperature

TEP – Tolman Electronic Parameter

tert – Tertiary

TFA – Trifluoro Acetic Acid

THF – Tetrahydrofuran

TLC – Thin Layer Chromatography

TMEDA – Tetramethylethylenediamine

TMes – 1,3-Dimesityltriazolylidene

TMDS – Tetramethyldis

Tol – Toluene

Trp – L-Tryptophan

trz – triazolylidene

Ts – tosyl

UPLC – Ultra-high Performance Liquid Chromatography

UV – Ultraviolet

Val – L-valine

%V$_{Bur}$ – Percent Buried Volume

WDI – World Drug Index

Chapter One

1.1 Introduction

1.1.1 Pharmaceutical Industry: The Drug Discovery Process

Over the last decade, the number of new chemical entities (NCEs) approved within the pharmaceutical industry has increased significantly, with an impressive 309 new drugs approved between 2011-2018. In 2018 alone, there were a total of 59 NCEs accepted to market, many of these targeting rare diseases (34 of 59).[1] Although this may convey an improvement in the drug development process, the discovery of new drugs to treat disease remains a challenging process. This is often attributed to the difficulty of finding molecules that are both active and display good pharmacokinetic profiles. For a number of years, medicinal chemists have utilised the 'Rule of five' approach to the design of new drug candidates, as described by Lipinski *et al.* in 1997.[2] The aforementioned rules were the result of a study conducted by Lipinski, in which marketed drugs from the World Drug Index (WDI) were studied, and their common physicochemical properties evaluated. This subsequently formed the 'Rule of five' which the authors suggested, if adhered to, would allow development of a compound with drug-like properties and little to no physicochemical issues. Lipinski's rules suggested that a molecule should have a molecular weight of <500, a Log P (lipophilicity) <5, less than 5 hydrogen bond donors (HBD) and, finally, less than 10 hydrogen bond acceptors (HBA) within the molecule.[2] Although Lipinski's work allowed medicinal chemists to focus on the relationship between a compound's physicochemical properties and its likelihood of progressing to a marketed drug, there are several shortfalls with this approach. The rules are optimised for the binding of a generally more hydrophobic protein target comparative to the bulk solution which the drug must travel through. This can mean that following the rules alone could lead to a drug compound with good binding affinity at the target, but low bioavailability. A molecule with high lipophilicity may also reside in apolar cell membranes and allow for off-site binding, leading to toxic properties and subsequently failure of the drug candidate. As a result, the rules have since been modified, with decreased lipophilicities and molecular weight suggested as lower risk.[3,4]

As it currently stands, more than 60% of NCEs fail in pre-clinical trials. The cost of the research and development effort to develop a candidate suitable for pre-clinical trials is thought to be in the region of $674 million dollars.[5] The high attrition rate is thought to be caused by NCEs displaying low bioavailability, high rates of metabolism, poor cell permeation or unattractive pharmacokinetic properties. Therefore, medicinal chemists have focused their efforts on finding more effective drug development methods. Traditional methods used at the start of drug discovery programs, such as High Throughput Screening (HTS), often fail to provide successful lead molecules due to the limited chemical libraries utilised, enhancing the rate of attrition.[6,7] These chemical libraries also tend to provide compounds that are rich in sp^2 character and have little diversity, accounted for by the ubiquitous use of sp^2-sp^2 cross couplings throughout their generation. High levels of unsaturation within a drug candidate can lead to problems with solubility and bioavailability, detrimental to a drug candidates progression. To this end, the concept of Lead Orientated Synthesis (LOS) was introduced by Churcher *et al.*[8] Lead orientated synthesis aims to create, from the outset, large libraries of compounds which contain drug-like properties from the outset. Simple reagents are used and prevention of a lipophilicity drift throughout the discovery process is managed by introduction of polar functional groups, using aqueous or highly polar reaction media. Additionally, LOS allows molecules with a higher degree of three-dimensional (3D) shape to be introduced. Saturation is considered favourable to avoid bioavailability issues through an increase in solubility, whilst maintaining low molecular weight. NCEs with enhanced 3D shape can also result in increased selectivity at the desired target, compared to more unsaturated molecules. Marsden and Nelson have pioneered LOS in recent years, conducting various studies to highlight the move to the construction of more diverse libraries.[9–11] One such study is depicted in Figure 1.1. Compounds generated through LOS (shown in orange) were compared to 90,000 commercial compounds (shown in blue) in order to assess differences in three-dimensional shape and saturation. It was concluded from the study that the fraction of molecules containing sp^3 character (wider spread of orange compounds across chemical space comparative to blue, where a build up is observed in the linear space) in the LOS library was significantly higher than that observed in commercially available compounds, highlighting a move towards a more diverse library. This being said, although the studies portray a favourable shift, LOS remains a relatively young technique and its utility remains to be seen, as lead molecules from these studies are carried through the drug discovery process and into pre-clinical trials.

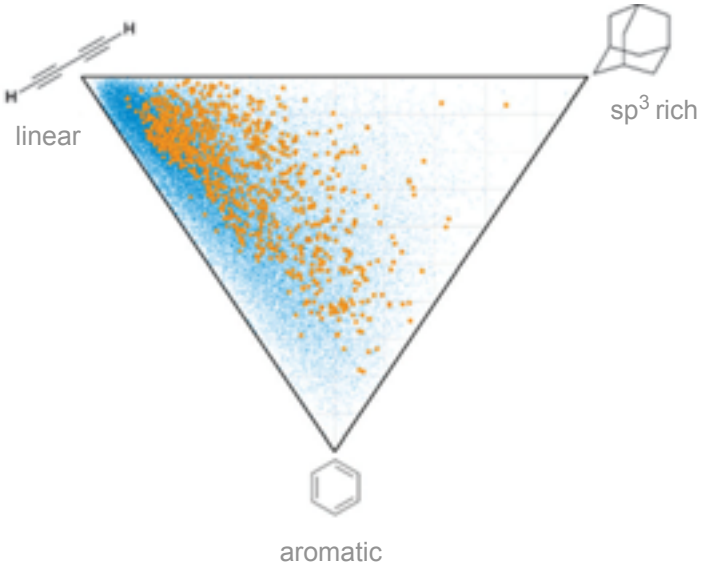

Figure 1.1

Another useful approach in increasing a drug candidate's bioavailability is through the design of prodrugs. Prodrugs are biologically inactive molecules that are metabolised within the body to produce the active pharmaceutical. Within this arena, incorporation of amino acid residues is commonplace.[12] Many amino acids are pharmacologically active compounds, exhibiting low toxicity as a result, meaning they are very attractive delivery vehicles in the pro-drug approach. Incorporation of such a residue, with the availability to be zwitterionic, affords enhanced water solubility and subsequent bioavailability. Anti-viral drug acyclovir, Figure 1.2, displays poor oral bioavailability owing to the lack of a capable transport system which can bind this substrate. Incorporation of a valine residue, affording Valacyclovir, affords a prodrug which is rapidly metabolised to the parent compound after administration. The successful transport of this prodrug by a peptide transport highly expressed in the intestine, allowed a 5-fold increase in bioavailability of Valacyclovir compared to Acyclovir, highlighting the applicability of prodrugs.[13]

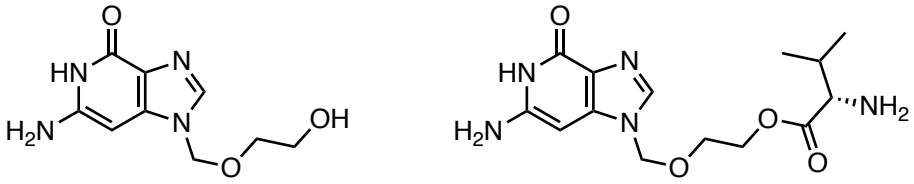

Acyclovir **Valacyclovir**

Figure 1.2

As well as being incorporated into prodrugs, amino acid residues are often found within parent drug structures (Figure 1.3).[14,15] Amino acids are an excellent source of saturation as well as providing vital hydrogen bonding sites. Incorporation of such moieties into drug candidates highlights further their importance and validity within the pharmaceutical industry.

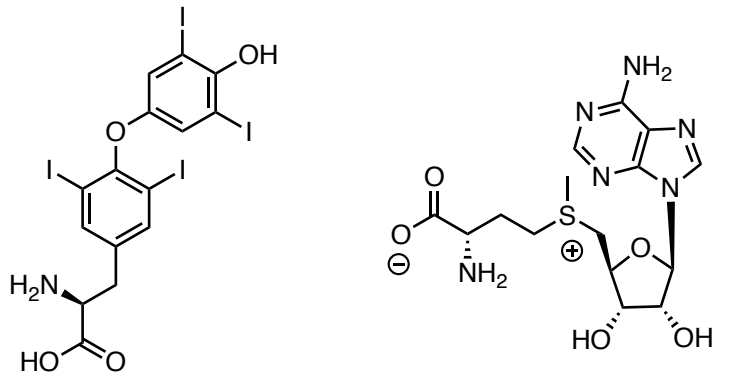

levothyroxine
(hypothyroidism)

Ademetionine
(chronic liver disease)

Figure 1.3

Alongside incorporation of single amino acid residues into small molecule drugs, medicinal chemistry has also observed the emergence of peptides as pharmaceuticals. More than 7000 naturally occurring peptides with central roles in physiology have been identified. One such example of a peptide pharmaceutical is the development and approval of carfilzomib, developed by Onyx Pharmaceuticals for the treatment of multiple myeloma in 2012 (Figure 1.4).[16] Peptides are generally very target selective and so form a good basis for the design and exploration of new peptidic drug molecules. Protein targets within the same family often

have active sites that are very similar in structure, meaning the medicinal chemists' job to obtain a drug with selectivity for one particular target can be very challenging, especially when considering small molecule drugs. Peptides, however, have the advantage of being larger, with more substrate-site interactions, and can therefore increase selectivity even if there are only a few amino acid residues different in the active site comparative to another member of the protein family. In addition, peptidic drugs offer potency and a more predictable metabolism comparative to small molecule drugs. Peptides are easier to synthesise than biologics and so offer a 'sweet spot' between biopharmaceuticals and small molecules.[17] Due to these advantages, the past two decades have seen 60 approved peptide drugs across the US, Europe and Japan. A compound annual growth rate of 9.1% is predicted from 2016 to 2024 and it is expected that the sales of peptide drugs will exceed $70 billion for 2019.

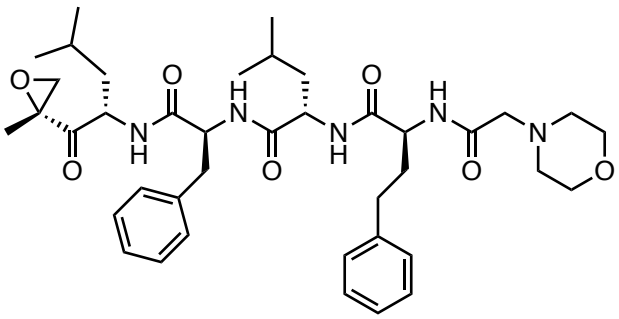

Carfilzomib

Figure 1.4

Owing to this advancement in the number of marketed peptide drug molecules, there are an estimated 400 peptidic molecules in clinical trials globally. Although a large increase from previous decades, there are still significant problems associated with peptide molecules as drugs. Namely, peptides can be unstable both chemically and physically, and can be prone to oxidation or hydrolysis. Additionally, they often have aggregation issues and a short half-life compared to small molecules. Oral availability and low membrane permeability of peptides also remain significant challenges for the medicinal chemist in the coming years. It is therefore key to understand the pharmacokinetic behaviour of potential peptide therapeutics from an early stage of their development.

Despite ongoing efforts within the pharmaceutical industry to explore alternative areas of drug development, the attrition rate remains a major issue and the use of LOS or peptide drugs to combat this could take many years for a significant effect to be observed. Therefore, it is important to tackle this problem in other ways. As previously discussed, many NCEs fail in pre-clinical trials due to high rates of metabolism or a poor pharmacokinetic profile. Assessment of these properties earlier in the drug discovery process has become key in aiding reduction of attrition within pre-clinical trials. Key to this are adsorption, distribution, metabolism, excretion and toxicology studies (ADMET). Use of isotopically labelled drugs within these studies is of great importance, wherein an atom of the drug molecule is replaced by a less common isotope, for example $^{2}H/^{3}H$ or $^{13}C/^{14}C$. Isotopic labelling is the most common approach, with no other technique able to provide detection and quantification of drug substances in convoluted systems with similar efficacy. Therefore, the ability to synthesise isotopically labelled drug molecules is of paramount importance within the pharmaceutical industry, whether this be small molecules or peptide therapeutics.

1.1.2 Isotopic Labelling

Isotopically labelled compounds are extremely important in studying the metabolic behaviour of drug molecules, however, this is not their sole use. Typically, isotopic labelling is utilised in the understanding of organic and organometallic reaction mechanisms within many research laboratories.[18] The understanding of reaction mechanism allows further control and optimisation of a process and labelled compounds are typically utilised in kinetic isotope effect (KIE) experiments. This provides the chemist with information of where and when certain bonds within a molecule are made or broken. It can also aid elucidation of potential transition states through an understanding of which bonds are cleaved.[19]

ADMET and reaction mechanism studies traditionally utilise heavy isotopes of either carbon or hydrogen. The former can be installed from isotopically enriched starting materials; however, these are often expensive and the label may have to be carried through a lengthy synthesis. If the labelled starting material for the designed route from medicinal chemists is

unavailable, a new route may have to be designed from alternative labelled starting materials. Additionally, for those isotopes which are radioactive, a lengthy synthesis is extremely undesirable as these compounds are difficult to handle, with large amounts of undesirable radioactive waste generated at each step. Another factor hindering the use of carbon labelled molecules is the relatively low abundance of the heavy isotopes compared to hydrogen. Consequently, the radioactive level may be too low to be detected in ADMET studies, rendering the technique invalid. Due to the relative scarcity of methods of installing and observing carbon labelled molecules for ADMET and mechanism elucidations, labelling using hydrogen isotopes is much more common and of great interest. This method allows incorporation of a heavy hydrogen isotope in a single step late in the synthesis, often on the active pharmaceutical or target molecule itself. The development of mild processes to achieve this transformation has been a large focus within the research community and improved methods ultimately lead to a more time- and cost efficient strategy for drug development within the pharmaceutical industry.

1.1.3 Hydrogen Isotope Exchange

Several methods can be employed to install hydrogen labels within a molecule. The simplest of these is exchange of one atom of hydrogen for a heavier analogue through acid or base catalysis. Such methods have been widely employed, however, poor functional group tolerance and harsh conditions often render these techniques inappropriate. Qiao-Xia *et al.* reported the acid catalysed deuteration of several simple aromatics with minimal substitution, one example being diphenylmethane **1** (Scheme 1.1).[20] Deuteration at all aromatic C-H positions was observed, with 96% incorporation of deuterium and a yield of 79%. This method allows high levels of deuterium incorporation under mild reaction conditions, albeit in an unselective manner and on simple, un-functionalised molecules.

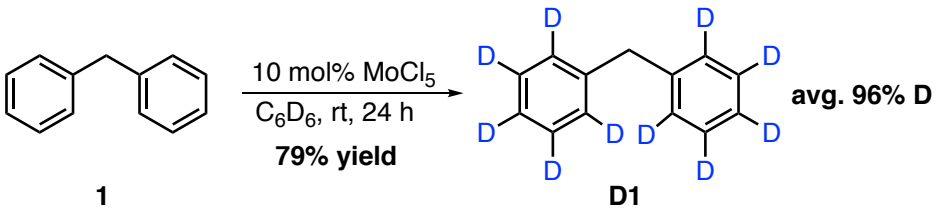

Scheme 1.1

To a similar end, the cough suppressant drug Dextromethorphan **2** has also been labelled *via* an acid catalysed H/D exchange, as reported by Murdter and Heinkele (Scheme 1.2).[21] Through this methodology, the authors were able to synthesise key metabolite **D2**, with high deuterium incorporations observed at all aryl positions. This method utilised a melt of pyridinium deuterochloride at 220 °C for a reaction time of six hours. De-methylation of the methoxy group also occurs under the reaction conditions.

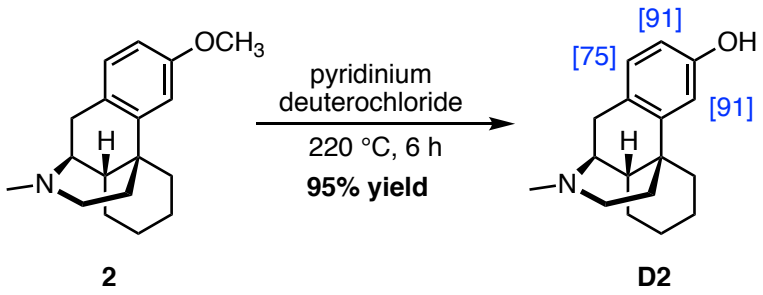

2 **D2**

Scheme 1.2

Base-catalysed methods are also employed to mediate HIE reactions. This strategy makes use of acidic hydrogen atoms, mainly *via* keto-enol equilibria. Such a strategy is shown in Scheme 1.3.[22] Steroid d_2-androstenedione **3** was further labelled through H/D exchange, employing sodium deuteroxide in deuterated water. This allowed the formation of d_8-androstenedione **D3** with incorporations of more than 90% attained.

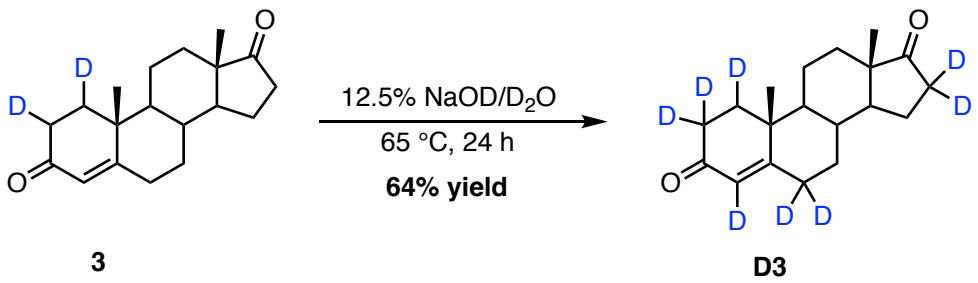

3 **D3**

Scheme 1.3

The installation of ^1H atoms in a molecule through hydrogenation reactions has been widely studied throughout the literature and so it was perhaps a natural progression for the chemist to employ similar methodology for the introduction of chemically similar deuterium atoms (^2H). Sajiki and co-workers reported the impressive HIE reaction of a range of aromatic

compounds bearing alkyl chains using Pd/C in D_2O (Scheme 1.4).[23] This methodology allows access to a range of compounds with high deuterium incorporation on alkyl positions. Ketone functionality can be tolerated within the substrate scope, as shown with compound **D5**. Unfortunately, aromatic positions displayed low incorporations of deuterium (36% compound **D5**), if any. Positions within close proximity to the phenyl moieties were labelled to near quantitative levels, showing the utility of this method for HIE.

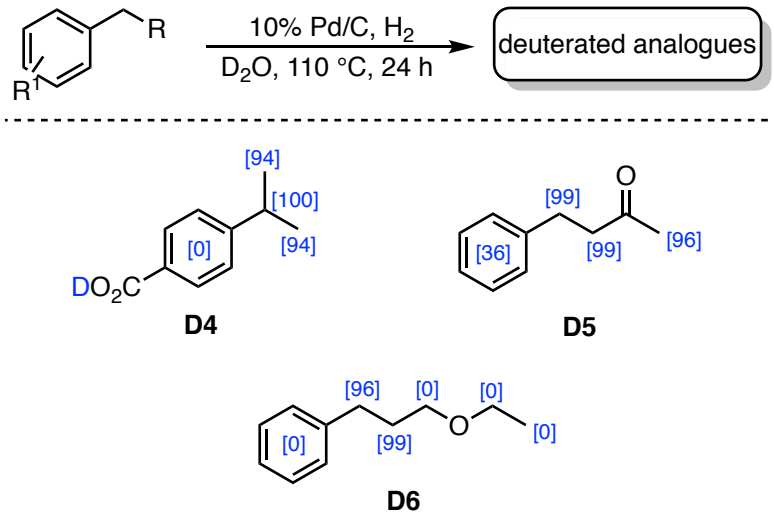

Scheme 1.4

The main advantage of such heterogeneous methods is the ease of catalyst removal. In the work discussed from Sajiki *et al.*, the Pd/C used in the reactions can be easily filtered from the reaction media and no further work up or purification is required. In contrast to this, the reaction conditions remain harsh for these types of processes, with high temperatures and/or long reaction times. Additionally, selectivity is low and often several or all positions within the molecule are labelled with deuterium. The limitations described above also apply to the acid or base catalysed methods, where selectivity can be restricted and substrate scope constrained. As a result, alternative methods are required to introduce an enhanced level of selectivity and wider substrate scope compatibility for the HIE process as a whole. This is often achieved through homogenous catalysis.

1.1.4 Undirected Homogeneous HIE Catalysis

The limitations displayed by the earlier methods discussed has led to the emergence of homogeneous catalysis as a front runner in HIE, alongside many other synthetic processes. Such methods allow for milder reaction conditions and greatly increased functional group tolerance. Compatibility with a range of chemical moieties is a key aspect for HIE, as late stage functionalisation of molecules is vital within both a pharmaceutical setting and indeed the investigation of reaction mechanisms. This offers homogeneous catalysis an advantage over the more traditional acid- or base- catalysed processes which exhibit low compatibility in this area. Homogeneous catalysis generally employs a transition metal catalyst, which inserts into an inert C-H bond *via* a process called C-H activation (Scheme 1.5).[24,25] Subsequently, the now activated species can react with 'X', which in the case of HIE is a source of deuterium or tritium, to form a new desired C-X bond.

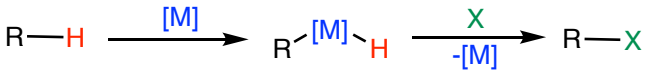

Scheme 1.5

This process has no requirement of prior activation of the C-H bond, for example by the conversion to a more reactive C-X bond (where X is a halogen or pseudo halogen). This can be extremely useful, not only for HIE processes, but also in the field of natural product synthesis. C-X bonds installed at the start of a synthesis could cause significant chemoselectivity issues throughout the synthetic sequence. Therefore, utilising unfunctionalised C-H bonds can be a very attractive approach.

The application of undirected deuterium incorporation through homogenous catalysis has been well studied over recent years. In 2018, Prakash and co-workers reported a regioselective deuteration of alcohols catalysed by iron and manganese pincer complexes *via* a hydrogen borrowing mechanism (Scheme 1.6).[26] The selectivity for the α or β position was highly dependent on the base metal used. In general, manganese-based pincer complexes

afforded deuterium incorporation at both positions, whereas the iron complex mostly gave exclusively α incorporation. The difference in selectivity is suggested to be a result of the difference in the hydrogenation rate of the *in situ* generated aldehyde. There are, however, some exceptions to this, such as with substrate **D11** where deuterium enrichment is observed at both positions, independent of the nature of the catalyst. To better understand this, the authors looked to the mechanism. It is thought that H/D exchange at the metal centre and subsequent hydrogenation of the aldehyde is generally faster for iron compared to manganese where keto-enol tautomerisation competes and allows additional incorporation at the β position. This is supported when considering substrate **D11,** where the rate of keto-enol tautomerisation is higher and therefore competes with the rate of hydrogenation, resulting in both positions being isotopically labelled regardless of the metal employed.

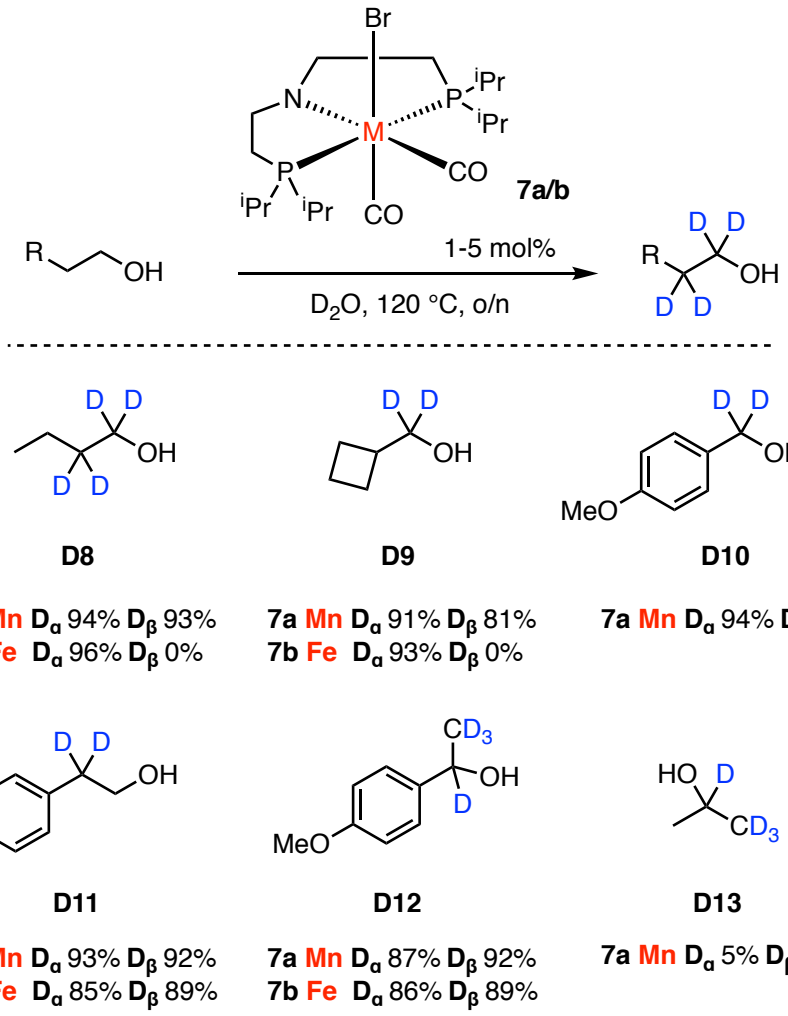

Scheme 1.6

Secondary alcohols could also be labelled efficiently under this methodology, such as with substrate **D12**. Compared to primary alcohol substrates, a slower reactivity was observed and increased reaction times were required. Unfortunately, alcohols such as *iso*-propanol **D13** could not be labelled efficiently and the reason for this is likely to be a difficult initial dehydrogenation step.

Another prominent example of undirected HIE comes from the Chirik group.[27] Similar to the work *above*, an iron pincer complex was utilised in the isotopic labelling of pharmaceutically relevant molecules (Scheme 1.7). Advantageously, the deuterium/tritium source used within this publication was D_2/T_2 respectively. This is an advancement on the work of Prakash where D_2O was utilised. While this is an adequate source for installation of deuterium, T_2O required for tritiation under a similar methodology would have several drawbacks: T_2O is prepared from tritium gas; undergoes decomposition through autoradiolysis, and presents handling challenges due to a high radioactivity to volume ratio, meaning it often has to be diluted with natural abundance water. Initially, Chirik *et al.* targeted small aromatic molecules to investigate the activity of their iron pincer complex (substrates **D15** to **D18**). The authors suggest that the selectivity is governed by the most sterically accessible position. Whilst the level of incorporation varies across the substrates, appreciable levels of deuterium are incorporated and this becomes particularly noteworthy when considering the isotopic labelling of complex drug molecules. Interestingly, as well as sterically accessible positions, C-H bonds *ortho* to a fluorine group were also activated, as can be seen in **MK-6096** and **Paroxetine**. Drug molecule **Papaverine** displayed excellent selectivity for the most sterically accessible position.

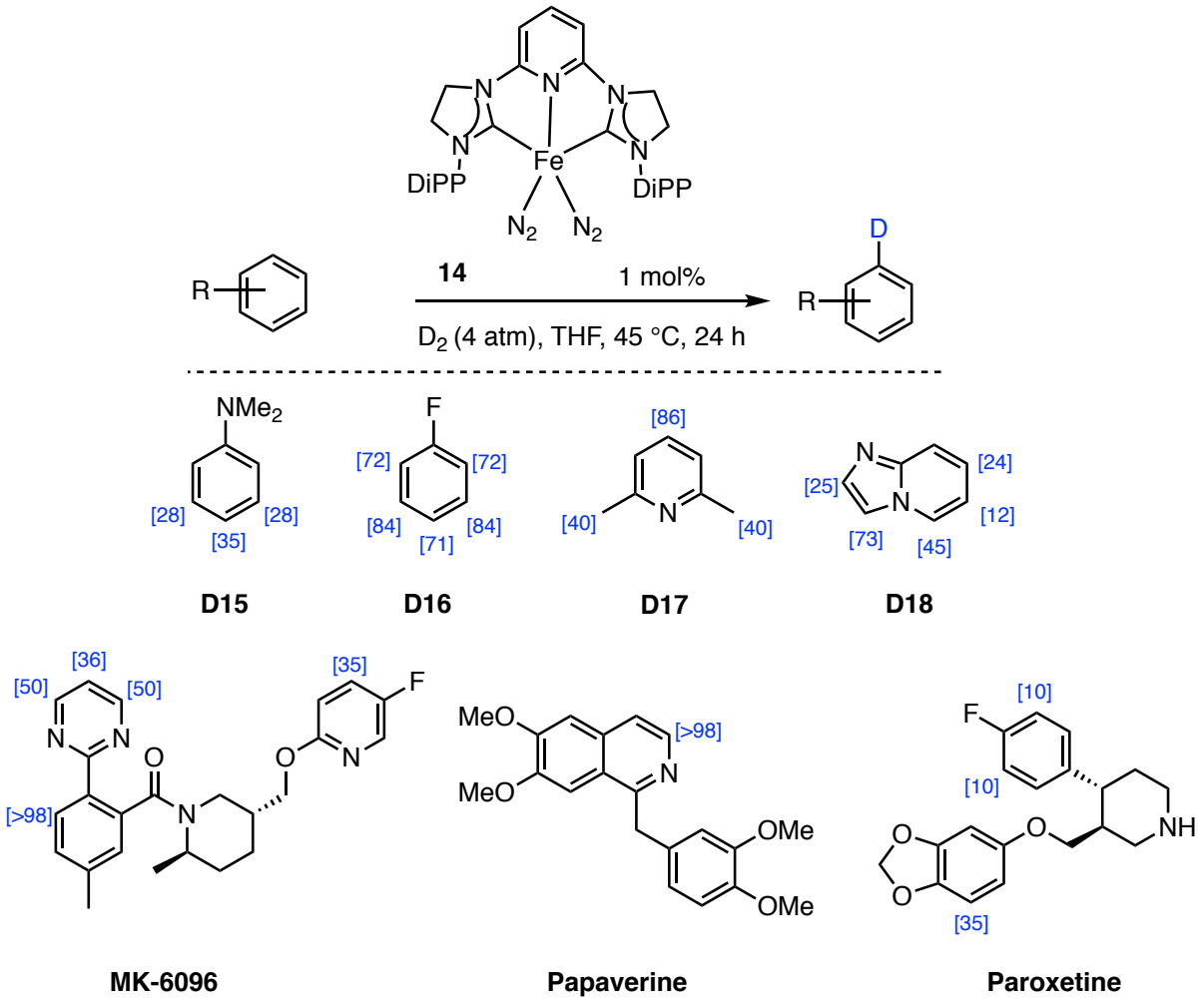

Scheme 1.7

With a competent deuterium labelling strategy in hand, Chirik and co-workers proceeded to investigate tritiation using their iron pincer complexes. Two notable examples are shown in Scheme 1.8. **MK-6096** gave an impressive specific activity of 57 Ci mmol^{-1} with tritium incorporated at a variety of unhindered sites. **Flumazenil** could also be competently tritiated under these conditions with a very useable specific activity of 16.1 Ci mmol^{-1}.

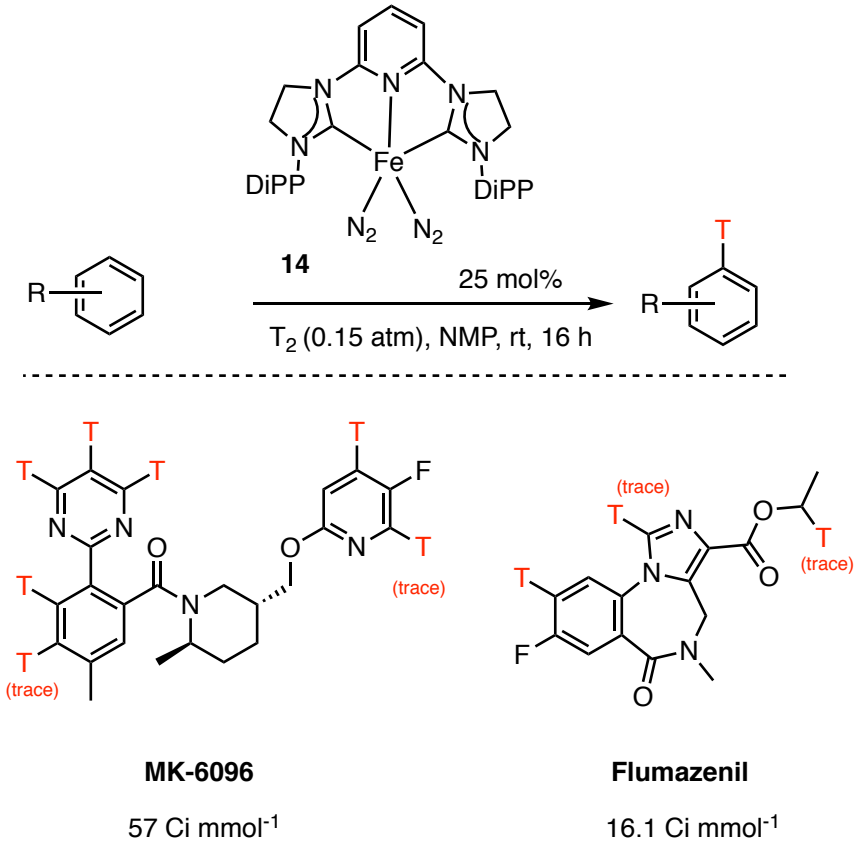

Scheme 1.8

The Chirik group, amongst others, have also investigated the use of non-precious transition metals, such as nickel and cobalt, for undirected HIE processes.[28,29] Whilst these are very attractive methods with mild reaction conditions, often the catalysts are not air stable and the chemistry must be performed within a glovebox. This limits their use and commercial availability for the industrial chemist. In addition, although undirected methods for HIE allow incorporation of several labelled atoms, often for metabolism or reaction mechanism studies a specific site within a molecule is required to be labelled and so the method must deliver excellent site selectivity. This is often achieved through directed, homogenous HIE.

1.1.5 Directed Homogenous HIE Catalysis

C-H activation strategies have wide utility and it is no surprise that this method has been of large interest to both academia and industry alike. Although there has been a significant

increase in the development of such processes, the ubiquitous nature of C-H bonds within most organic molecules poses a great problem. Selective installation of a deuterium or tritium at the end of a synthetic sequence is of paramount importance and therefore the number of C-H bonds within a molecule can become a key issue. In order to avoid such problems, the chemist employs a directing group (DG), such as a nitrogen or oxygen atom, which can bind to the metal catalyst and arrange the metal centre close to the C-H bond of interest (Scheme 1.9). This allows the formation of an agostic interaction between the metal centre and the C-H bond, which lengthens and therefore 'activates' the C-H bond to enable cyclometallation. Aryl systems bearing directing groups are often activated at the C-H bond *ortho* to the DG. In this instance, generally a five or six membered metallocyclic intermediate (5- or 6-mmi) is formed, which is lower in energy and more stable than, say, activation through a larger 7-mmi. As a result, many researchers have employed the use of directing groups for the *ortho* activation of aromatic compounds.

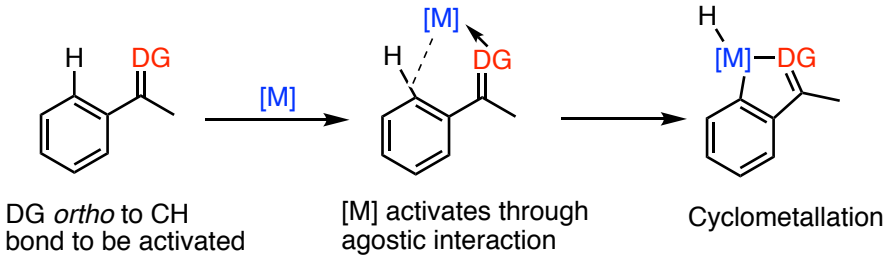

Scheme 1.9

One of the earliest applications of C-H activation for HIE was reported in seminal work using rhodium by Garnett *et al*. in 1975, where they demonstrated the use of $[RhCl_3(H_2O)_3]$ for the isotopic labelling of aromatic molecules.[30] Although this introduced the use of homogeneous rhodium catalysts for HIE, this process was once again unselective in the positions it labelled as no directing groups were present. In 1982, Lockley *et al.* paved the way for the use of homogeneous rhodium catalysed directed HIE when he reported the *ortho*-selective deuteration of a range of aromatic molecules (Scheme 1.10).[31] In contrast to Garnett, excellent selectivity was observed through employment of this methodology. Lockley suggested that the selective nature of the process was governed by the carbonyl directing group, which enabled activation of the *ortho* C-H bond through a 5-mmi, as discussed above.

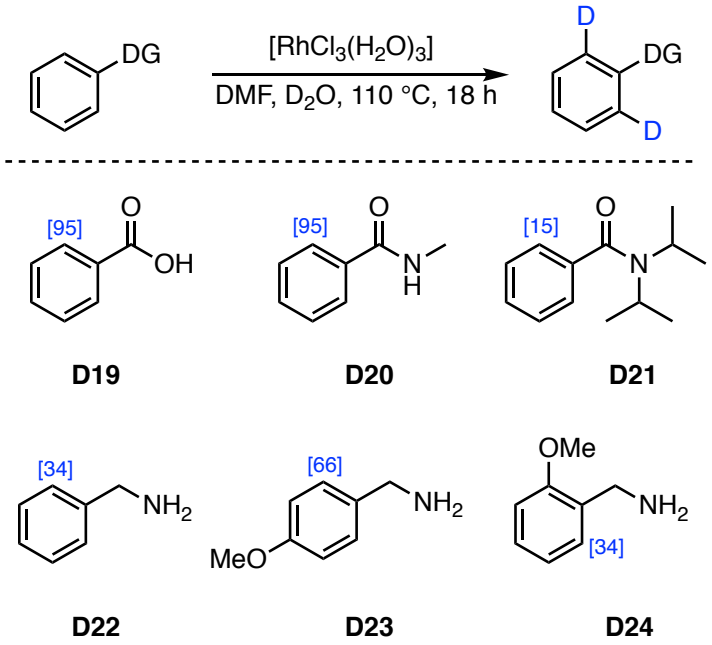

Scheme 1.10

When amides were employed as directing groups, such as secondary amide **20**, an impressive deuterium incorporation of 95% was achieved. However, when moving to a tertiary substituted amide **21**, incorporation falls dramatically to a mere 15% incorporation, suggesting the steric bulk of the DG is affecting the proximity of the metal centre to the *ortho* C-H bond. When moving to benzylamines, disappointingly the incorporations were much lower, with only 34% labelling at the *ortho* position of benzylamine **D22**. Despite some obvious limitations, Lockley's advances in the field of homogenous catalysis not only allowed the selective labelling of aromatic substrates but also led to the aforementioned rhodium catalyst dominating the area for many years. As such, this catalyst was utilised in the labelling of many drug molecules at the time.

1.1.6 Iridium Catalysed HIE

Hydrogen isotope exchange in the 1980-90s became dominated by homogenous cationic iridium complexes. One of the earliest examples utilised for HIE was complex **25**, shown in Scheme 1.11**.** This complex was originally synthesised and isolated by Osborn *et al.* as early as 1969.[32] Complex **25** was prepared by reaction of cycloctadiene iridium chloride dimer

$[Ir(COD)Cl]_2$ with triphenylphosphine. This cationic intermediate was then activated under an atmosphere of hydrogen in acetone, and the desired complex **25** isolated. More than twenty years after the reported isolation of complex **25**, Heys reported a more general use of the complex in HIE.[33] Heys' 1992 publication exploited various directing groups to achieve *ortho* selective hydrogen isotope exchange under mild conditions. Directing groups utilised by Heys included esters, amides and *N*-heterocycles. The sterically demanding *tert*-butyl ester in compound **D26** was a compatible directing group, with 90% incorporation observed at the *ortho* positions of the aryl ring. Substitution at the 3- position of aromatic esters was also tolerated under these reaction conditions, with both electron-donating and electron-withdrawing substituents allowing for HIE (compounds **D27** and **D28**). Substrate **D28** contains two potential directing groups with both an ester and nitro substituent on the aryl ring, and incorporation was observed *ortho* to both functionalities. Limitations of this method for HIE become apparent when considering substrate **D32**. Moving the directing group one carbon further away from the aryl ring results in a directing group which would have to form a 6-mmi- with the iridium centre in order to achieve a C-H activation process, and in this case, no incorporation is observed.

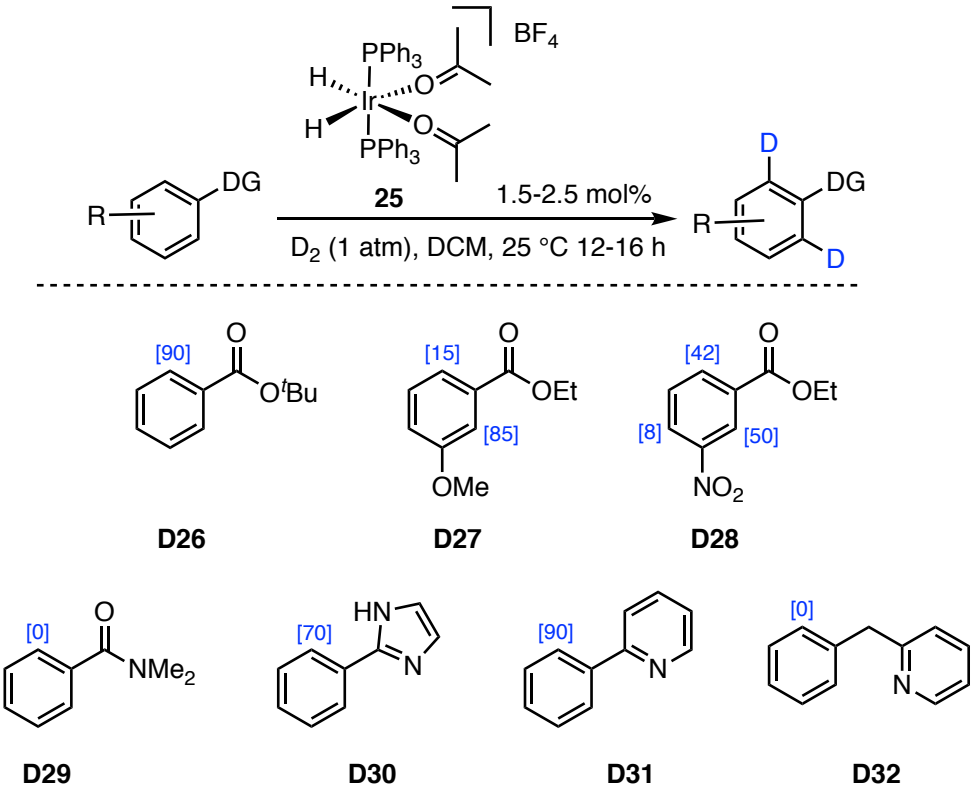

Scheme 1.11

In an advance of original work above, in 1993 Heys reported *ortho* selective labelling of *para* substituted aryl esters and amides.[34] Investigation of the nature of this process and substrate expansion was of high priority to the authors. Interestingly, the results highlight that the *para* substituted analogues were labelled to a greater extent, and indeed, more rapidly than the parent unsubstituted rings. In an attempt to elucidate further details as to why the *para* substituted substrates led to higher levels of deuterium incorporation, Heys observed the rate of exchange on each ring of mono-*p*-substituted benzophenone. The *ortho* positions of the substituted ring showed a much faster rate of deuteration compared to the unsubstituted ring, and Heys therefore hypothesised that perhaps it was not the coordination of the directing group which controls the rate of reaction but instead the C-H insertion process which was rate determining.

In addition to the emergence of complex **25,** as early as 1977, Crabtree was investigating the use of cationic iridium complex **33** for olefin hydrogenation reactions (Figure 1.5).[35] This catalyst was extremely competent for such transformations and quickly became the industry standard for hydrogenation reactions.

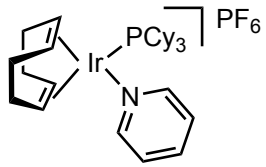

33

Figure 1.5

Recognizing the applicability of complex **33** in hydrogenation reactions, and from the propensity for hydrogenation catalysts to also be competent in the HIE arena, Hesk and co-workers first applied Crabtree's catalyst **33** as a tool for HIE in 1995.[36] Reported was the efficient *ortho* labelling of a range of acetanilides under mild conditions (Scheme 1.12). Largely, the reaction conditions are insensitive to substituent effects, with both electron-donating and electron-withdrawing substituents tolerated in the *para* position (**D36** and **D37**). Substrate **D38**, bearing a nitro group in the *para* position, undergoes labelling through direction from both functional handles, with the amide being a more competent directing group, achieving high levels of incorporation (73%) compare to direction through the nitro group (8%). Compounds bearing a nitrile group display no deuterium incorporation,

suggesting that the nitrile group may irreversibly bind to the iridium centre. *Meta* substituted acetanilides were mainly mono-deuterated, with most examples displaying inhibition of labelling at the 2- position by the *meta* substituent, for example with substrate **D41**. An exception to this was *meta*-fluoroacetanilide **D42**, which displayed incorporation in both *ortho* positions of the aromatic ring. The authors suggested that this may be attributed to the small van der Waals radius of the fluorine atom. It is interesting to note that monodentate Crabtree's catalyst can activate these acetanilides through a 6-mmi, where previous monodentate system **25** was unable to. This could be attributed to the small pyridine ligand, affording more space around the iridium centre for substrate binding and less opportunity for ligand/substrate clash.

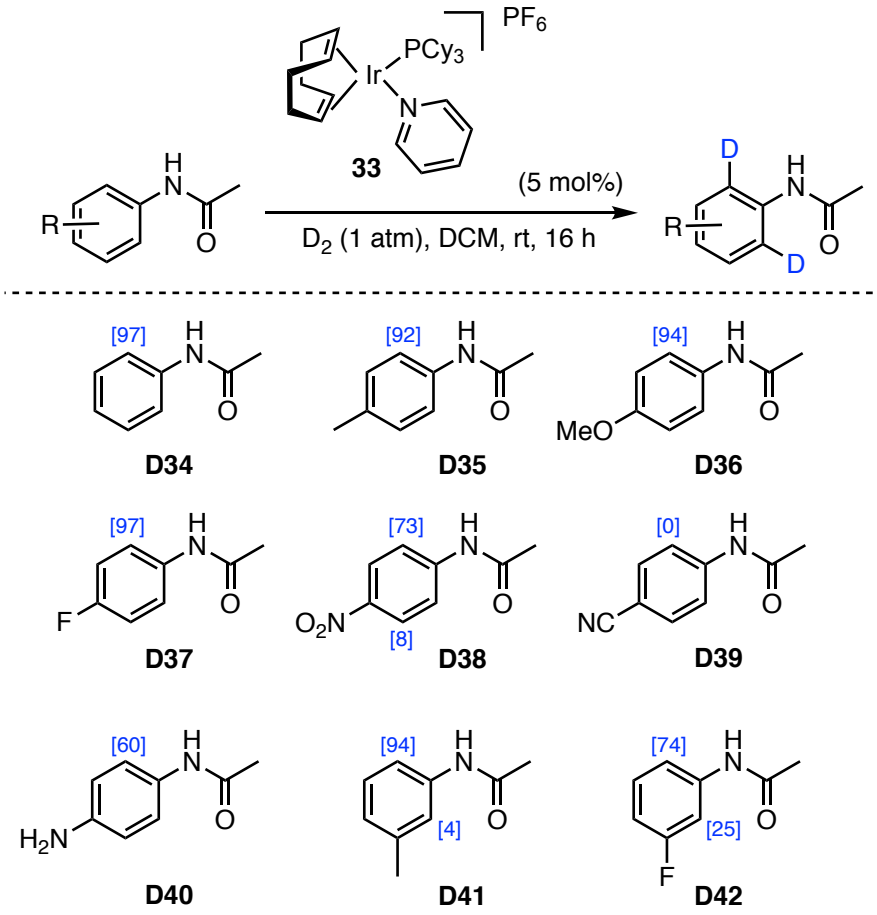

Scheme 1.12

Hesk's report using Crabtree's catalyst prompted widespread application in HIE processes within industry. Although the catalyst became used frequently in the labelling of pharmaceuticals, the low catalyst loading reported by Hesk could not be applied in a more general sense for compounds bearing alternative directing groups. Often, extremely high loadings were required, even stoichiometric amounts, in order to observe labelling. It was not until 2001 that a wider range of substrates were investigated and reported by Herbert *et al*.[37] In this study, high levels of catalyst loading were required (1.15 eq). A range of substrates were tested, including esters, ketones and amides, as shown in Scheme 1.13. Amides proved to be excellent directing groups, which is unsurprising considering the previous work in this field. No substituent effects were observed in the *para* position, with both electron-donating and electron-withdrawing groups well tolerated (**c**ompounds **D44** and **D45**). The authors hypothesised that the amide groups direct *via* the carbonyl oxygen bound to the metal centre. This was confirmed by bulkier amine groups (such as *iso*-propyl, compound **D21**) showing no reduction in labelling. Additionally, with this substrate, it was interesting to observe incorporation into the methine position of the *iso*-propyl group, which is also proceeding through a 5-mmi. Upon moving to ester directing groups, incorporation was generally lower (e.g. substrate **D45** *vs* substrate **D48**). This is thought to be a result of the relative electron-donating ability of the acid *vs* ester carbonyl groups when bound to iridium. Unlike amides, *para* substituents on the ester substrates had a significant effect on the level of incorporation observed. Whilst the electron-donating, *para* methoxy substituted **D47** was deuterated to an impressive 85%, the electron-poor, nitro-containing **D48** displayed diminished levels of incorporation at 20%. It is proposed that the electron-donating group can increase the Lewis basicity of the ester directing group and hence allow for more efficient binding, and in turn, higher levels of incorporation. In opposition to this, the electron-poor nitro group will withdraw electron density from the aryl ring and the directing group, and subsequently make it a much poorer directing group for the HIE process. Further to this, ketone directing groups also delivered excellent levels of labelling; however, they did not follow the same trend of substituent effects as esters, suggesting that there could be more than one pathway at play.

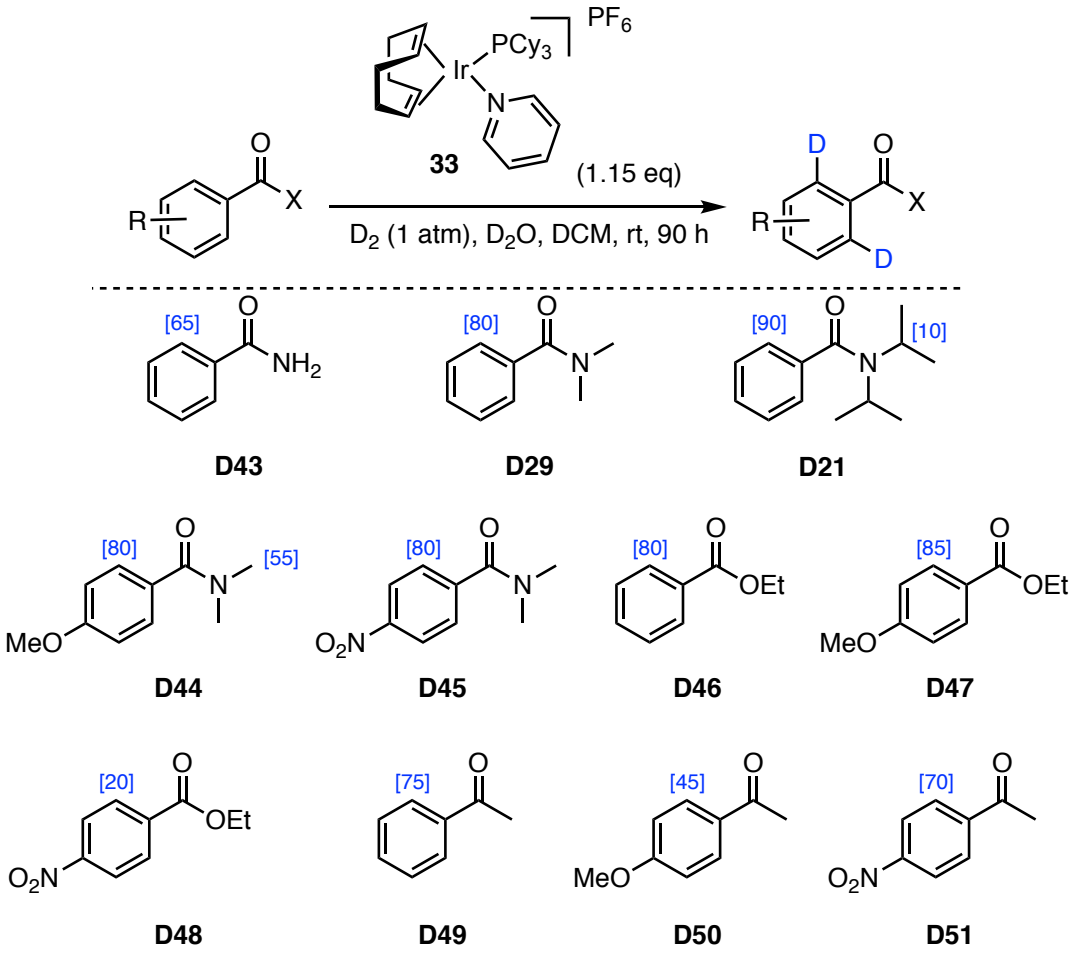

Scheme 1.13

Although Crabtree's catalyst **33** displays promising results with carbonyl-based directing groups such as amides and esters, extremely high (super-stoichiometric) catalysts loadings are required. This is a limiting factor for this methodology and is thought to be as a result of its tendency to form inactive hydride clusters in solution under the reaction conditions (Figure 1.6).[37,38]

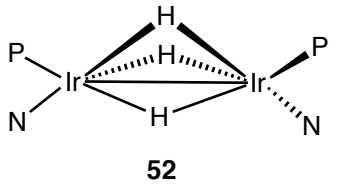

Figure 1.6

In an attempt to avoid complexes plagued with thermal stability issues, Heys and co-workers continued to investigate complexes akin to complex **53**, bearing two phosphine ligands. However, in order to combat the incapability of complex **53** to accommodate substrates which require formation of a 6-mmi to allow C-H activation, a bidentate phosphine ligand was investigated **54** (Figure 1.7).[39]

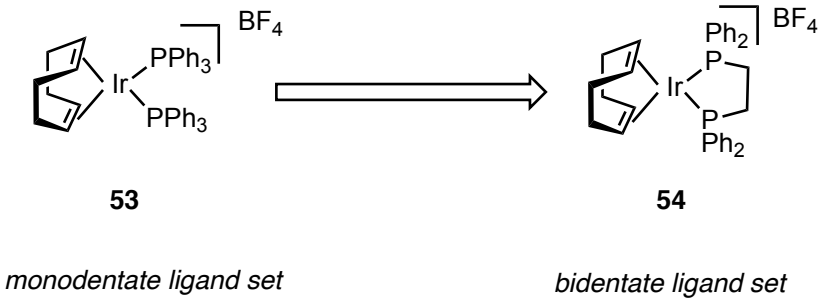

53 **54**

monodentate ligand set *bidentate ligand set*

Figure 1.7

Results from the deuteration of ethyl 1-naphthoate with complexes **53** and **54** are presented in Table 1.1. Incorporation *ortho* (D^a) *via* a 5-mmi is catalysed by both complexes. Monodentate catalyst **53** selectively affords deuterium incorporation at this position, and at high levels. Interestingly, the bidentate phosphine complex allows incorporation at both D^a and D^b, with the latter requiring activation *via* a 6-mmi. The level of labelling at D^a is significantly lower with the chelate complex **54**.

Table 1.1

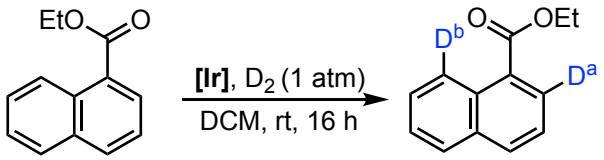

55 **D55**

Entry	Complex	Catalyst Loading (mol%)	D^a (%)	D^b (%)
1	**53**	2.2	90	0
2	**54**	2.5	54	35

It was postulated that the enhanced activity for chelating complex **54** through a 6-mmi is a result of the smaller ligand sphere, which can better accommodate the less planar metallocycle, where the monodentate catalyst cannot. This is explained in Figure 1.8. When monodentate complex **53** is activated *via* reduction of the COD ligand, the two phosphine ligands adopt a *trans* relationship to minimise steric repulsion between the ligands. With the phosphine ligands in this geometry, significant steric repulsion is observed between one of the phosphine ligands and the substrate bound through a 6-mmi (**56**). In comparison, the tethered phosphine ligands in complex **54** are forced to adopt a *cis* relationship, meaning there is significantly more space around the metal centre for the C-H activation to occur (**57**).

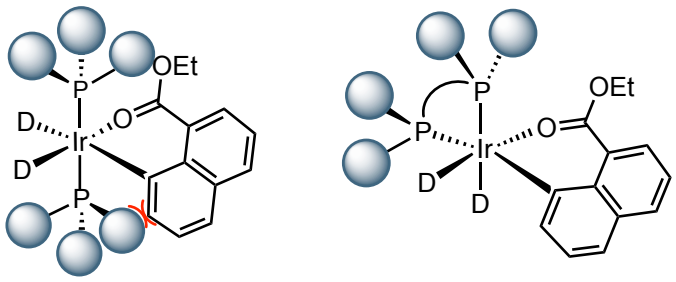

56 **57**

Figure 1.8

The investigation by Heys highlighted the importance of the ligand set around the iridium centre and highlighted the effects of such ligands on HIE through metallocycles of differing sizes. This prompted investigation of alternative ligand combinations by other researchers within the field.

In an attempt to overcome the thermal instability issues associated with Crabtree's catalyst, Nolan *et al.* hypothesised that replacement of the phosphine ligand with a bulky *N*-heterocyclic carbene (NHC) could allow access to a more active complex.[40] NHCs had been previously branded as 'phosphine mimics' as they are sterically demanding σ-donating ligands and can allow improved thermal stability. Nolan and co-workers investigated the replacement of PCy_3 in complex **33** with SIMes, in complex **60** (Mes = mesityl). The desired complex was synthesised *via in situ* generation of the free carbene **59** from reaction of

SIMes•HCl with ^{t}BuOK, and subsequent ligand displacement with **58** in toluene. This procedure afforded complex **60** in an 80% yield (Scheme 1.14).

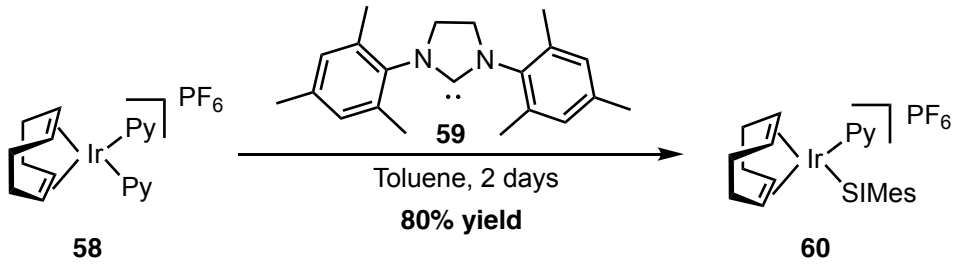

Scheme 1.14

The catalytic activity of complex **60** was compared to Crabtree's catalyst in the hydrogenation of 1-methly-1-clyclohexene. At low pressure of hydrogen, Crabtree's catalyst **33** out-performed **60**; however, when moving to more forcing conditions (60 psi, 50 °C), **60** allowed quantitative conversion to the saturated analogue where Crabtree's catalyst **33** displayed very poor activity. The authors proposed that this difference in activity could be attributed to the increased thermal stability of NHC-containing complex **60**, which hinders formation of inactive iridium clusters.

In 2002, Buriak *et al.* further investigated the use of iridium NHC complexes in hydrogenation processes.[41] Previously, Nolan and co-workers had described the enhanced stability of Crabtree's catalyst **33** by replacement of the phosphine ligand with an NHC; however, Buriak was instead interested in replacement of the pyridine ligand with an NHC. The hypothesis was that the combination of both a bulky phosphine and sterically demanding NHC could concomitantly enhance both stability and activity. The authors reported the synthesis of a variety of complexes bearing different phosphine and NHC combinations. Sterically unencumbered IMe (which is unstable as the free carbene) and the more stable and sterically hindered IMes were investigated in combination with alkyl phosphines (Figure 1.9). Unfortunately, bulky phosphines such as PCy_3 could not be complexed to an iridium centre containing the sterically encumbered IMes NHC and this was a limitation of the investigation. Pleasingly, all three complexes **61-63** were competent hydrogenation catalysts.

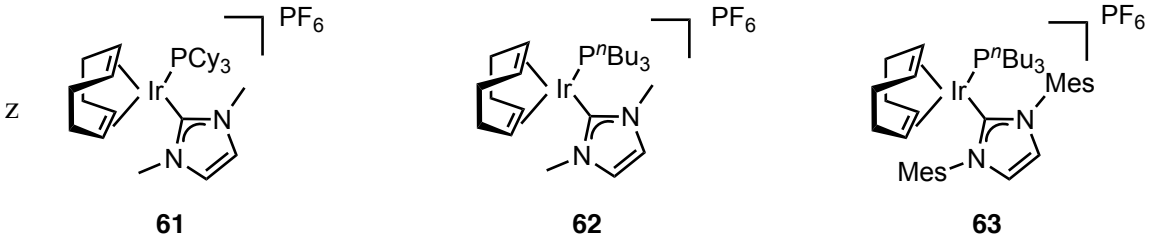

Figure 1.9

Buriak *zt al*.reported that the use of NHC/phosphine ligands around the iridium centre led to extremely high catalytic activity in the hydrogenation of several substituted olefins. In addition, both Buriak and Nolan have again demonstrated the importance of the ligand set complexed to iridium in terms of both activity and stability. Due to the compatibility of these complexes in both hydrogenation and HIEzalize, Kerr and co-workers became interested in the use of NHC/phosphine ligand combinations for HIE studies. Additionally, through investigations in this field (*vide infra*), it was noted by Kerr that if iridium catalysts could be prepared bearing both bulky phosphines and sterically hindered NHCs, activity towards HIE processes could be further enhanced. This became a focus of the Kerr group, not only to be able to access such complexes, but also to develop an understanding of the properties of NHC and phosphine ligands was considered essential to this effort.

1.1.7 Phosphines as Ligands

Ligand choice plays a central role in organometallic chemistry and catalysis. Judicious choice of a ligand set aids in fine tuning the electronic properties of a metal and how it performs. Additionally, ligands have a steric presence around the metal centre, also impacting the activity of the complex significantly. Tri-substituted phosphines are ubiquitous within organometallic chemistry, and the importance of this class of ligand arises from their wide range of steric and electronic properties which can be accessed through alteration of the substituents on the central phosphorus atom. In addition, phosphine ligands have been shown to stabilise and influence a wide range of metals, in a range of oxidation states, and so their use has grown exponentially within the field of catalysis. Phosphines are typically spectator ligands, which is ideal for several organometallic processes, where ligand influence on the

metal centre is essential, but participation of the ligand in the reaction mechanism is not required. The range of phosphines available has vastly increased due to the emergence of metal-catalysed cross coupling reactions, in which phosphine ligands are widely utilised. Phosphines display similar characteristics to the NR_3 class of ligands as they are also strong σ- donors (from a lone pair on their central atom to the metal centre) as shown below (Figure 1.10). Unlike their nitrogen counterparts, phosphines are also competent π-acids, with the orientation of the σ* orbital enabling donation of an electron pair into this empty orbital on the phosphine ligand.

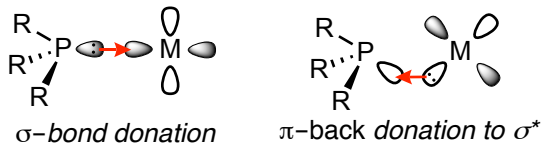

Figure 1.10

Variation of the R substituents on the phosphine can have a large influence on the ligand's ability as both a σ-donator and its π-acidity. This in turn significantly effects the nature of the metal complex and subsequently how it behaves. It is therefore important that the ability of a phosphine ligand to donate or accept electron density can be quantified, to allow the chemist to exploit phosphines with the properties that they desire. As the R group becomes more electron-donating, the σ-donation increases, while the π-acidity is attenuated (Figure 1.11).

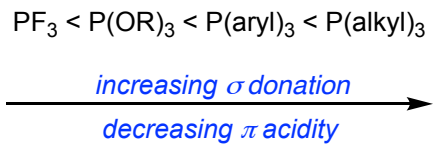

Figure 1.11

As early as 1970, Tolman introduced a method to quantify the electron donor-acceptor properties of various phosphine ligands.[42] Tolman utilised A_1 carbonyl stretching frequencies in nickel carbonyl complexes to parameterise the electronic influence of various R groups in phosphine ligands. Substitution of one of the CO ligands in $[Ni(CO)_4]$ with the phosphine of choice produces complexes of the form $[Ni(CO)_3PR_3]$. This results in a change in electron

density at the metal centre, which in turn affects the π back donation to the carbonyl ligands, resulting in differences in the A_1 carbonyl frequency (Figure 1.12).

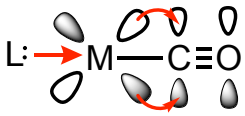

Figure 1.12

As phosphines become more electron-rich, and therefore more competent electron donors, the σ-donation increases. The resulting electron density residing on the metal centre is dispersed through the M-L π-system *via* back-bonding to the π* orbital of a CO ligand. A stronger M-C bond is formed, leading to a weaker C-O bond, which lowers the C-O frequency, ν(CO), measured by infrared (IR) spectroscopy. This stretching frequency became known as the Tolman Electronic Parameter (TEP) and is one of the most widely used techniques for quantification of ligand electronics. This has become a robust method of quantifying the electronics of novel phosphine ligands, with the values for some common phosphines depicted in Table 1.2.

Table 1.2

Entry	Phosphine	ν_{CO} (cm^{-1})
1	P^nBu_3	2051.6
2	P^iPr_3	2059.2
3	PMe_3	2064.1
4	PMe_2Ph	2065.3
5	PBn_3	2066.2
6	PPh_3	2068.9
7	$POMe_3$	2079.5

With a robust method to quantify the electronics of phosphine ligands, Tolman turned his attention to quantifying the steric properties, as these were also deemed influential to the activity of a metallic complex. In 1979, Tolman introduced the cone angle, θ (Figure 1.13). In accordance with the TEP, Tolman employed nickel carbonyl complexes substituted with a phosphine ligand in order to quantify their steric impact.[43] In such complexes, the phosphine substituents adopt a conformation whereby they are 'folded back' from the metal centre. A cone is then drawn from the metal centre at the apex in a vector which reaches the edges of the R substituent set on the phosphine being investigated. The angle can then be measured between the metal centre and the cone, denoted by θ.

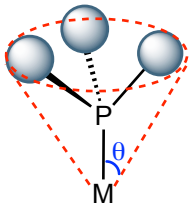

Figure 1.13

This technique has been shown experimentally to be an accurate depiction of steric properties for phosphine ligands, and is therefore widely used during catalyst design. Although this approach has been validated as a good predictor of phosphine steric properties, it considers the ligands in a static environment. This can fall short when considering ligands such as PBn_3, where although it may display an identical cone angle to another phosphine, its flexibility can result in a significantly different steric environment when complexed to the metal centre.

The ability to asses both the electronic and steric properties of ligands is extremely important in the design of metal complexes and their associated processes. The exploitation of ligands with similar steric properties but vastly different electronics could have a positive impact on a key step of a reaction mechanism without alteration of the ligand sphere, a key influencer on the reaction profile.

1.1.8 N-Heterocyclic Carbenes as Ligands

Free *N*-heterocyclic carbenes (NHCs) have historically been regarded as much too reactive and poorly stable to allow isolation and further characterisation. Therefore, it was not until 1991 that the first free NHC was reported. Arduengo *et al.* described the synthesis and isolation of 1,3-di(adamantyl)imidazol-2-ylidene (IAd) **64**.[44] The carbene was synthesised *via* deprotonation of its parent imidazolium salt (Figure 1.14). Since this pioneering work, a plethora of publications employing NHCs as ligands in metal complexes has emerged.

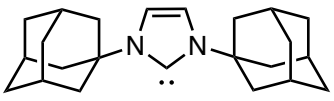

64

Figure 1.14

NHCs bear a pair of electrons on the carbenic carbon, which can occupy either a singlet or triplet state, with the former being inherently more stable (Figure 1.15). The electrons in the

triplet state are unpaired in adjacent p-orbitals residing on the carbonic carbon. In the singlet state, the unpaired electrons form a lone pair, leaving an empty p-orbital which may be stabilised *via* π-donation from the adjacent heteroatoms. NHCs are stabilised both electronically, as discussed, and sterically, through the R groups on the nitrogen atoms. They are electron-rich, neutral σ-donor ligands and the electron donating ability of NHCs span a tighter range when compared to phosphine analogues. Electronics are typically modified *via* alteration of the azole ring.

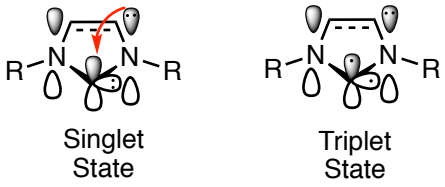

Figure 1.15

NHCs can be 'fine-tuned' with relative ease, as the N1, N3, C4 and C5 positions and the ring size are all available for further modification and optimisation. This allows a wider variation in steric properties comparative to phosphine ligands. Additionally, NHCs form much stronger M-L bonds, meaning they are often utilised within organometallic complexes. As a result of these favourable properties, investigation of NHC parameters and properties was widely sought in a manner akin to phosphines.

Similarly to their phosphine counterparts, electronic properties of NHCs can be quantified through the TEP. Once again, nickel carbonyl species can be prepared with an NHC complexed and the CO frequency measured. One issue with this method is the toxicity of the NHC bound nickel complexes. Nolan *et al.* overcame this issue by reporting the use of [Ir(Cl(CO)$_2$NHC] complexes to investigate the electronic properties.[45] A variety of NHC and phosphine ligands were parameterised as shown in Table 1.3. As can be seen from the results, the NHCs are significantly more electron donating than the phosphine ligands. This is a result of the strong σ donation of the NHC compared to the phosphines, alongside the lower levels of back-bonding, which means that NHCs can donate more electron density to the metal centre.

Table 1.3

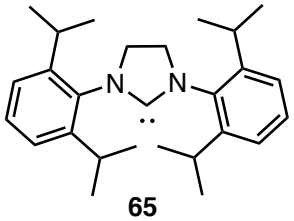

65

SIPr

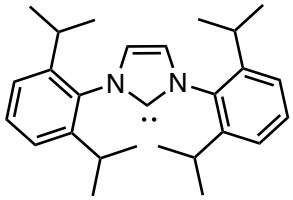

66

IPr

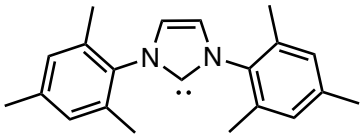

67

IMes

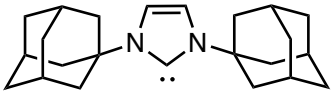

68

IAd

Entry	Ligand	TEP (cm^{-1})
1	**PPh_3**	2068.9
2	**PCy_3**	2056.4
3	**SIPr**	2052.2
4	**IPr**	2051.5
5	**IMes**	2050.7
6	**IAd**	2049.5

NHCs were traditionally regarded as solely σ-donating ligands, however, it was recognized that they also displayed significant π-acidity. The TEP was a competent method for parameterising the σ-donating strength of a variety of NHCs as discussed above; however, this parameter was not as effective in parameterising the π-acceptor strength of NHCs. In 2013, Ganter introduced the use of NHC selenium adducts for the quantification of this

property.[46] It is known that ^{77}Se NMR chemical shifts can appear over a range of ~800 ppm. Upon complexation with an NHC, it was hypothesised that the selenium shift would be significantly altered depending upon the π-accepting ability of the carbene. Figure 1.16 shows both an NHC with poor π-acidity and one with high π-acidity. When the NHC is acting only as a σ-donator, a highly shielded selenium atom results. This produces a ^{77}Se signal with high field chemical shift. On the other hand, NHCs with good π-acidity allow for a less shielded selenium atom, with the chemical shift now residing at lower field.

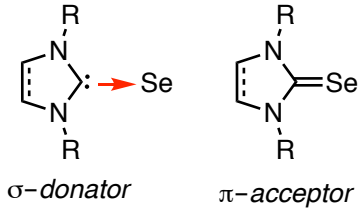

Figure 1.16

A small selection of NHC selenium adducts were investigated by Ganter to quantify their π-accepting ability (Figure 1.17). Adduct **69** is a strong σ-donating NHC with poor π-accepting properties and so exhibits a high field resonance. The low π-acceptance is due to the rigid ring structure, allowing for sufficient donation from the heteroatom lone pairs. Moving to the saturated version, **70**, the ring becomes more flexible, and donation from nitrogen lone pairs decreases, increasing the π-acidity and shifting the signal to lower field. When investigating the six- membered analogue **71**, it was observed that this NHC was extremely π-acidic. This is thought to be a result of a wider NCN angle, allowing the vacant p-orbital to be at lower energy and therefore better equipped for π back-donation from the selenium. Additionally, this is an NHC which contains increased flexibility, decreasing the lone pair/p-orbital overlap.

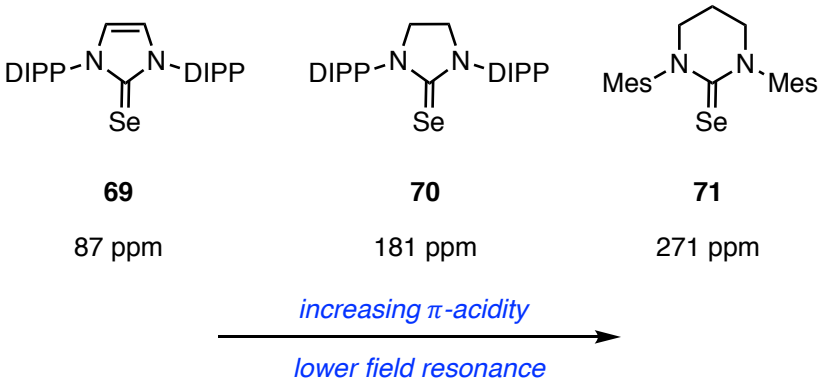

Figure 1.17

The π-acidity of NHCs has also been determined through the NMR spectroscopic analysis of NHC phosphinidene complexes by Bertrand *et al.*[47] The structures investigated are represented in Figure 1.18 as two canonical forms; either **A**, where there is a P-C dative bond with two lone pairs centred at phosphorus, or **B**, where a formal P=C bond is shown.

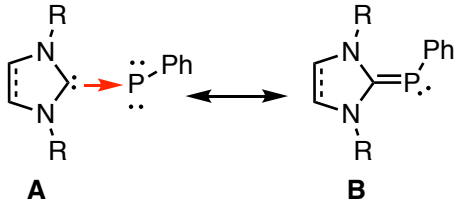

Figure 1.18

Such molecules display an extremely high field shift in ^{31}P NMR spectrum (in the region of -10 to -60 ppm) compared to the chemical shift usually expected for a non-polarised phospha-alkene (230-420 ppm). This highlights that the phosphorus atom is electron rich, and agrees more with the resonance structure shown in **A**. An increase in the π-acidity of the carbene will favour back- donation from phosphorus and increase the resonance form **B**. As a result, the more π-acidic the carbene ligand is, the more downfield the phosphorus chemical shift will be. A comparison of ^{31}P shifts for some selected NHCs are shown in Figure 1.19, as well as their corresponding TEP and ^{77}Se shift (the latter calculated from selenium adducts as described *vide infra*). Comparing IPr **66** and SIPr **65**, it can be seen that the ^{31}P shift becomes more downfield in **65**, suggesting that the donation from the nitrogen lone pairs is reduced and the π-acidity increased. When moving to **72**, a significantly lower field shift is observed

in the ^{31}P NMR. This is a result of the wider NCN angle and the π-accepting ability of the carbonyl group. It can be seen that whilst the trends match nicely when comparing the selenium and phosphorus shifts, there is some discrepancy when considering the TEP. This is, as previously discussed, a result of the TEP not accounting for the π-acidity of the NHC competently. Also noteworthy, is the wider range of shifts observed in Ganter and Bertrand's work compared to the TEP. This allows a much more thorough investigation of the electronics and allows the chemist to tease out electronic differences between ligand structures which are relatively similar, but may have significant impact when employed in catalysis.

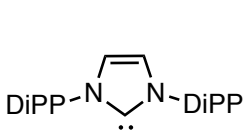

66

TEP: 2051.5

^{77}Se: 87 ppm

^{31}P: -18.9 ppm

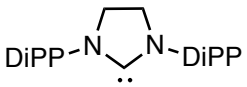

65

TEP: 2052.2

^{77}Se: 181 ppm

^{31}P: -10.2 ppm

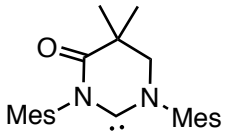

72

TEP: 2050.0

^{77}Se: 472 ppm

^{31}P: 39.7 ppm

Figure 1.19

Although TEP is the most widely utilised parameter for investigating the electronic properties of a ligand set, the emergence of new techniques allows a multicomponent analysis of the electronic properties and a larger data set to be investigated. It perhaps also gives a truer picture of the electronic component with both donor and acceptor properties being considered.

In accordance with their phosphorus analogues, the steric properties of an NHC ligand are vastly important to the design of an organometallic complex and its reactivity. Therefore, it is imperative that these properties can be measured and used to the chemist's advantage in catalyst design. Whilst for electronic considerations, the TEP can be utilised for both phosphines and NHCs alike, some discrepancies appear when utilising Tolman's cone angle for parameterisation of steric properties of NHCs. Phosphines display C_3 symmetry, whilst their NHC analogues are usually C_2 symmetric, or display no symmetry. Phosphine R groups

are ‘folded backwards’ from the metal centre, however NHC *N*-substituents are typically pointing towards the plane of the metal centre. As a result, both a height and length parameter would have to be considered for NHC ligands, and therefore a more accurate method for steric quantification is required.

Seminal work by Nolan *et al*. introduced the concept of ‘percentage buried volume’ ($\%V_{bur}$) as a descriptor of the steric contribution of an NHC ligand (Figure 1.20).[48] This method utilises a sphere of an assigned radius, with a metal fixed at the centre. The steric congestion of the ligand around the metal centre can be investigated through the percentage volume of the sphere that is occupied by the ligand. This method has been used to quantify a variety of NHC ligands and their steric properties. Buried volume can be calculated from either crystallographic data or through computational methods. Not only can the buried volume calculations be used for NHCs, but also other ligand sets including phosphine motifs. One drawback of this method is often when comparing buried volumes derived from computational methods or crystallographic data, some discrepancies are observed. This being said, buried volume remains the most widely used investigation tool for NHC ligand sets to quantify their steric influence.

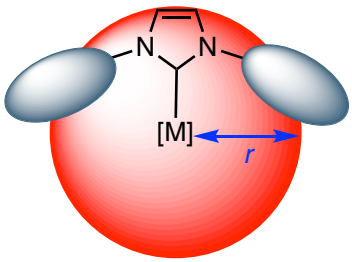

Figure 1.20

1.1.9 Kerr Group Investigations – HIE

Returning to hydrogen isotope exchange reactions, over the last decade, Kerr and co-workers. have turned their attention to phosphine/NHC complexes to overcome some of the fundamental issues displayed by Crabtree’s catalyst **33**. New catalysts were required for

utilisation in both HIE and hydrogenation processes, with the desire to design complexes which were highly active at mild temperatures and low catalyst loading. Following on from the work of Nolan and Buriak on phosphine/NHC complexes, work within the Kerr group focused on the generation of free carbenes *in situ,* in an effort to access complexes bearing both a bulky phosphine and a sterically demanding NHC.[49] A practically convenient method was developed which required no glovebox manipulations, and allowed access to a variety of novel iridium complexes in moderate to good yields (Scheme 1.15). Complexes bearing IMes and a variety of phosphines were synthesised, including PBn_3, PPh_3 and PMe_2Ph, all in moderate to good yields through a synthetically useful strategy.

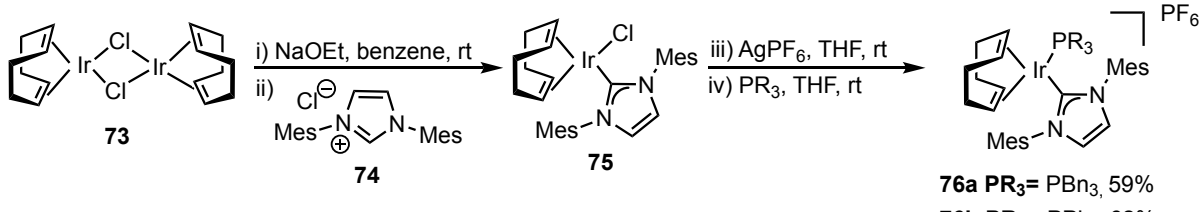

Scheme 1.15

With the novel complexes in hand, HIE reactions on a variety of different substrates were investigated to ascertain their relative activities. All three complexes afforded excellent levels of incorporation over a wide variety of substrates, as shown in Scheme 1.16. Although Crabtree's catalyst **33** has shown excellent levels of incorporation with a number of the substrates, such as **D49** and **D43**, stoichiometric amounts of catalyst were required. Work within the Kerr group has demonstrated the ability to obtain the same excellent levels of incorporation, if not higher in some cases, whilst only utilising 5 mol% of catalyst under mild conditions. The Kerr catalysts could access *ortho* sites *via* both 5- and 6-mmi with, for example, the latter being diminished in acetanilide **D34**. Nitro groups were previously regarded as poor directing groups in HIE reactions under iridium catalysis, however, as shown by **D79**, the nitro group was a very efficient directing group with excellent incorporations of ~98% observed with all three catalysts.

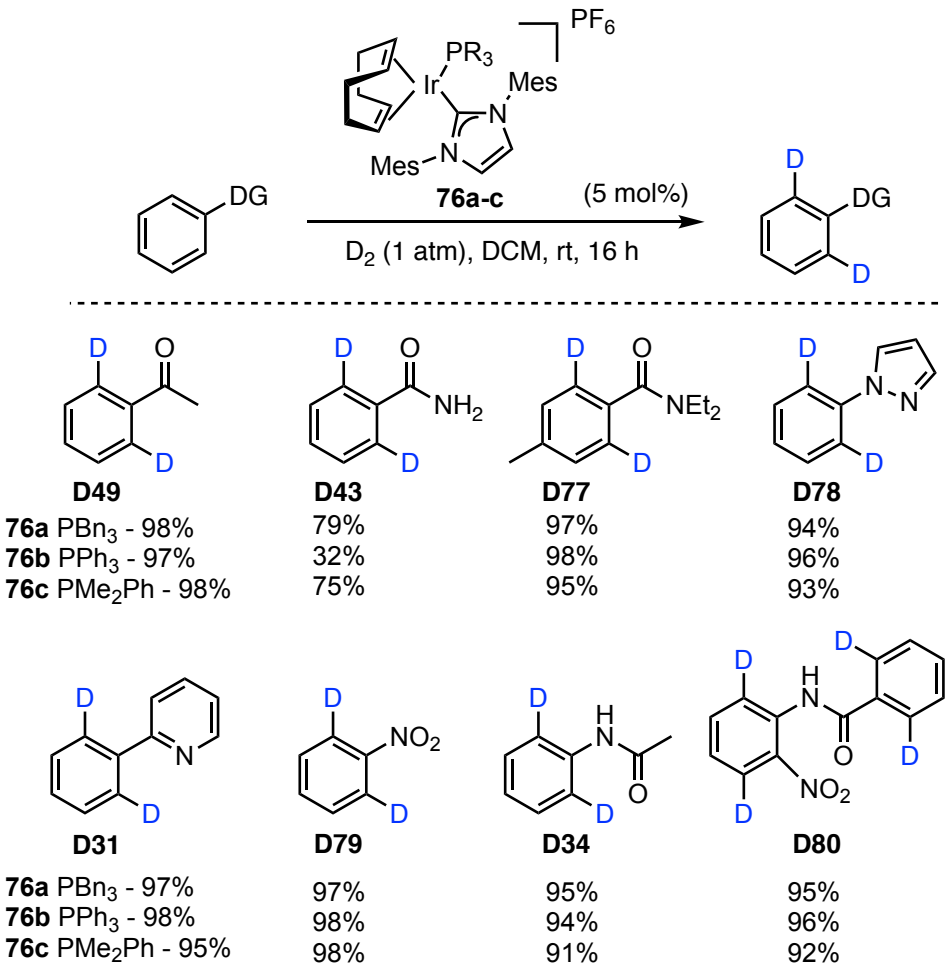

Scheme 1.16

It was hypothesised that the high catalytic activity observed was due to the combination of two bulky ligands on the catalyst complex. This could allow enhanced stability of the catalytic intermediates, blocking formation of inactive iridium clusters. Additionally, the electron rich and sterically bulky ligand sphere may assist in the insertion/elimination steps. With an impressive substrate scope in hand, investigations were then focused on developing selectivity over labelling through 5- or 6-mmi. In order to probe this, benzanilide **81**, which can be labelled *via* a 5-mmi at D^a or a 6-mmi at D^b was labelled under standard conditions using, initially, 5 mol% of complex **76c** (Table 1.4). At this level of catalyst loading, the incorporation at both *ortho* positions was extremely high, with over 90% labelling at both sites (**Entry 1)**. Interestingly, when lowering the catalyst loading to 0.5 mol%, significant levels of labelling were only observed at D^a through a 5-mmi. Under these low loadings, the energetically more demanding labelling through a 6-mmi appears to be inaccessible. This

provides a very attractive route to obtain site selectivity, which could easily be applied to pharmaceutical drug molecules.

Table 1.4

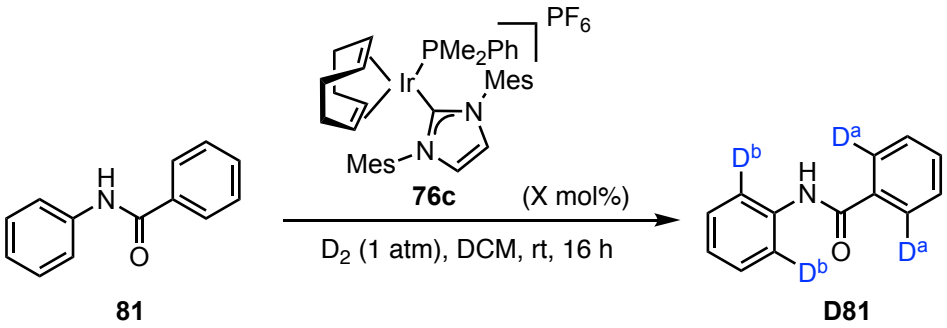

Entry	Catalyst Loading (mol%)	% D^a	% D^b
1	5	95	93
2	0.5	94	2

The Kerr group expanded their impact on HIE reactions by turning their attention to developing a more industrially applicable process.[50] Previous iridium catalysed HIE reactions relied upon the use of chlorinated solvents, which are generally avoided within the pharmaceutical industry due to their carcinogenic properties. In an attempt to combat this, acetophenone was chosen as a model substrate to investigate the solvent scope of the reaction with Kerr catalysts (Table 1.5). Labelling of this substrate with PPh_3 complex **76b** at 5 mol% loading, under one atmosphere of deuterium at room temperature for 16 h, was investigated with a range of ethereal solvents alongside acetone. Pleasingly, the move to ethereal solvents such as diethyl ether and *tert*-butylmethyl ether (MTBE), delivered the isotopically enriched **D49** in excellent levels of incorporation (entries 2 and 3) and remained comparable to the corresponding labelling reactions in dichloromethane (DCM) (entry 1). When moving to a more coordinating solvent such as acetone, a significant decrease in labelling was observed, with only 43% incorporation reported (entry 4). It was suggested by the authors that the more Lewis basic nature of acetone compared to the other solvents could cause a competition between substrate and solvent for efficient binding to the iridium centre. This was supported by examining the calculated enthalpy of displacement (ΔH_{exc}). It can be seen from the results that displacement of DCM or ethereal solvents by the substrate is an exothermic process and

is therefore energetically favourable. On the contrary, displacement of acetone is an endothermic process, with the equilibrium shifted towards the bis-solvated complex, lowering levels of the substrate bound complex, and, subsequently, the experimental levels of deuterium incorporation observed. 2-MeTHF could also be utilised as a solvent for labelling, and this solvent is generally regarded as a good replacement for DCM within industry. By switching to ethereal solvents, not only are carcinogenic substances avoided, but it also allows an opportunity for substrate expansion due to increased solubility of many substrates in these solvents.

Table 1.5

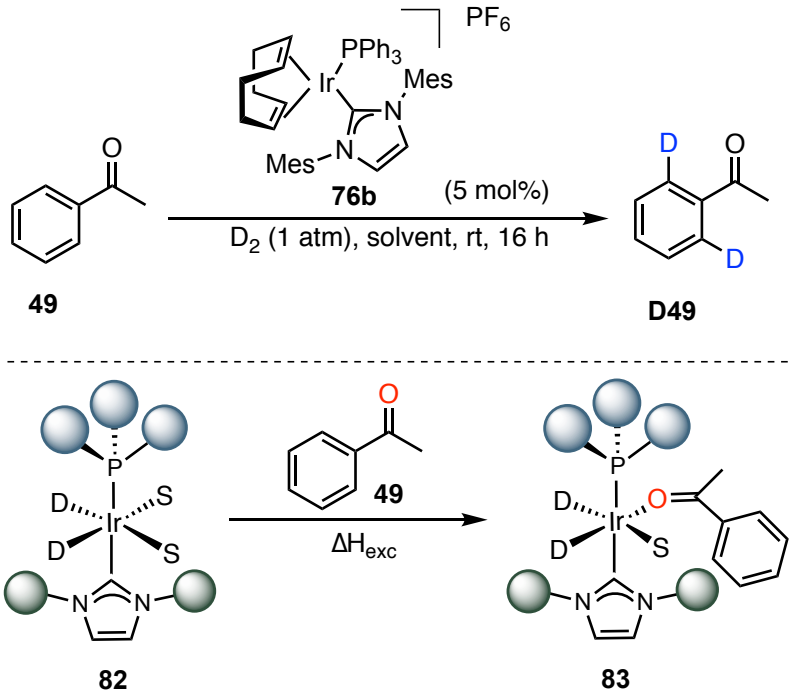

Entry	Solvent	ΔH_{exc} (kcal mol^{-1})	% D
1	**DCM**	-13.3	98
2	**Et_2O**	-7.3	94
3	**MTBE**	-12.8	91
4	**Acetone**	0.3	43
5	**2-MeTHF**	-3.7	95

Having developed a catalyst system bearing a ligand set which allowed unprecedented levels of substrate and solvent scope, the Kerr group in 2014 reported the use of complexes bearing alternative counterions, which allowed enhanced activity of their already robust catalyst systems.[51] Work from the Pfaltz group in hydrogenation reactions had shown that the move to a larger, non-coordinating anion such as terakis[3,5-bis(trifluoromethyl)phenyl]borate (BAr^F) could enhance the performance of catalysts.[52,53] Additionally, it was thought that the move to such counter ions, which are inherently more diffuse, could allow access to further solvents than those already employed successfully by the Kerr group. To investigate this hypothesis, variants of catalyst **76**, bearing both larger and smaller counterions, were synthesised (Figure 1.21). These catalyst were then employed in the deuteration of acetophenone and the rate of incorporation measured. Although all complexes delivered high levels of incorporation, the larger counterions reached maximum incorporation at a much faster rate.[51]

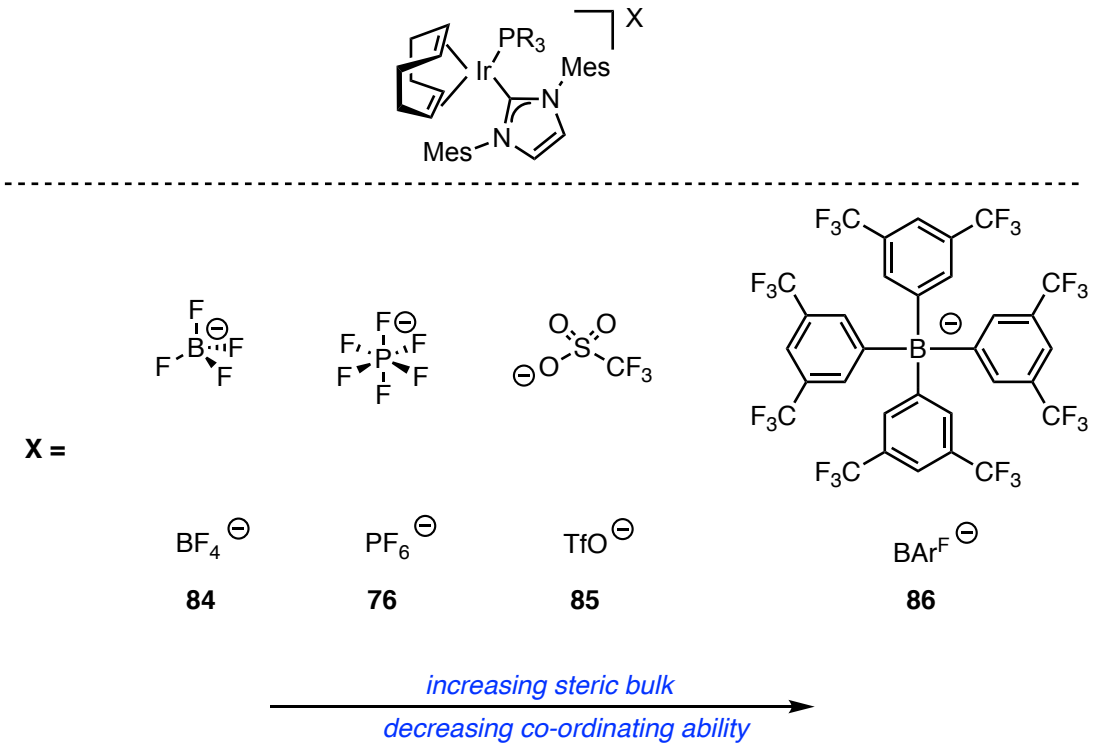

Figure 1.21

In an attempt to investigate the hypothesis that the move to a less coordinating counterion could enhance solvent applicability, the Kerr group investigated the labelling of

acetophenone with both complex **76b** and **86b**, with the former bearing the small, strongly coordinating PF_6 counterion and the latter bearing the larger, more diffuse BAr^F counterion.[51] It can be seen from Graph 1.1 that complex **86b** (red) allows for similar, if not significantly enhanced, incorporations over a variety of solvents, once again enhancing the number of solvents which can be applied with the Kerr catalysts.

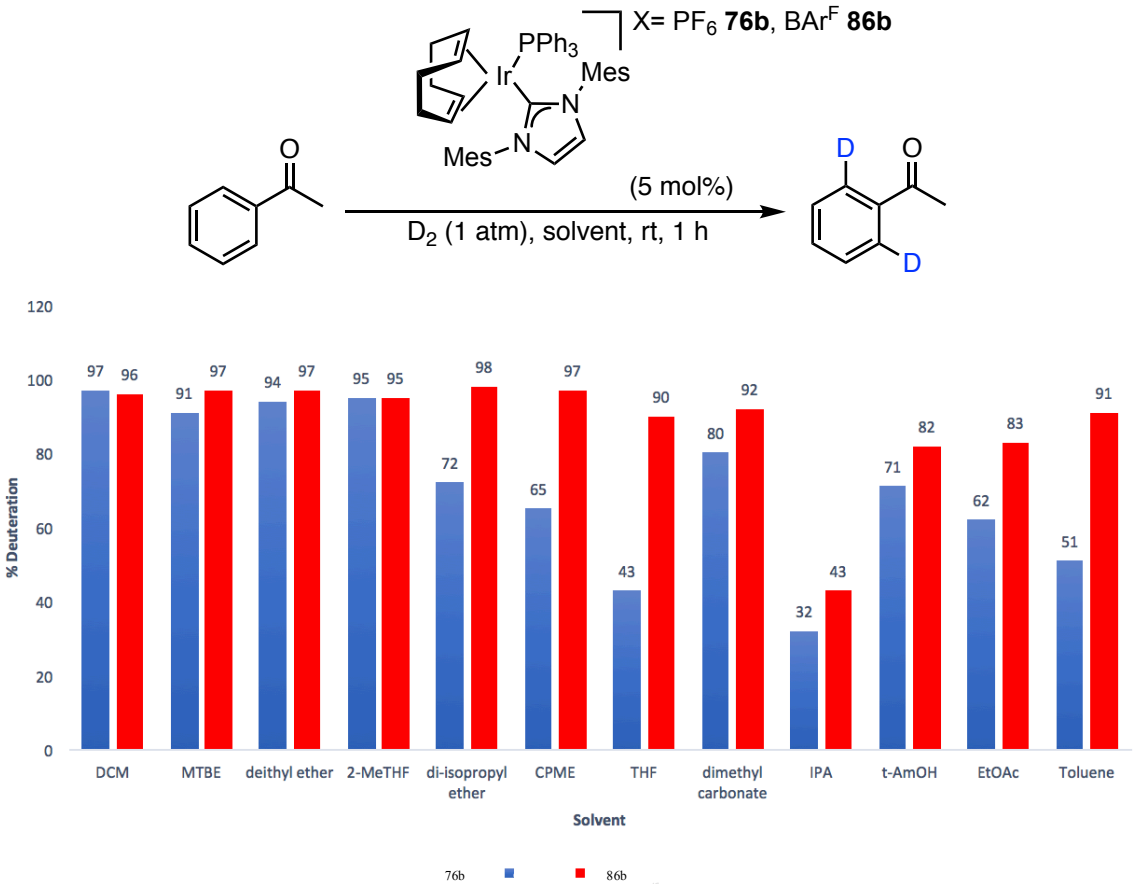

Graph 1.1

As a result of these studies, Kerr *et al.* successfully developed a catalyst system which was tolerant of a wider range of solvents, making the iridium catalysed HIE process significantly more viable for industry. The Kerr group then combined experimental and theoretical techniques to investigate the mechanism for this Ir(I) catalysed HIE, based on a cycle originally proposed by Heys in 1996.[39] Although several years had passed since its proposal, little evidence to support it had surfaced. It was speculated within the Kerr group that thorough understanding of the reaction mechanism would be key in the future design of catalyst systems which could further expand upon the HIE process. NMR analysis and DFT

calculations were used to further elucidate and support the mechanism already proposed in the field.[54] The mechanism elucidated was similar to Heys' original proposal, with the addition of a key intermediate (Scheme 1.17, note all complexes are cationic within the cycle). After initial activation of the catalyst and subsequent displacement of one molecule of solvent through substrate association, the second molecule of solvent is displaced by the formation of an agostically coordinated *ortho* C-H bond on the aryl ring to the iridium centre (step 2). Further findings included the elucidation of the rate determining step (RDS) of the reaction, which was found to be the C-H activation step, which was 3.5 kcal/mol higher in energy than the C-D bond forming event. In addition, the catalyst cycle was confirmed to be isohypsic: after initial activation of the Ir(I) pre-catalyst, the active Ir(III) catalyst species remains in this oxidation state throughout the cycle.

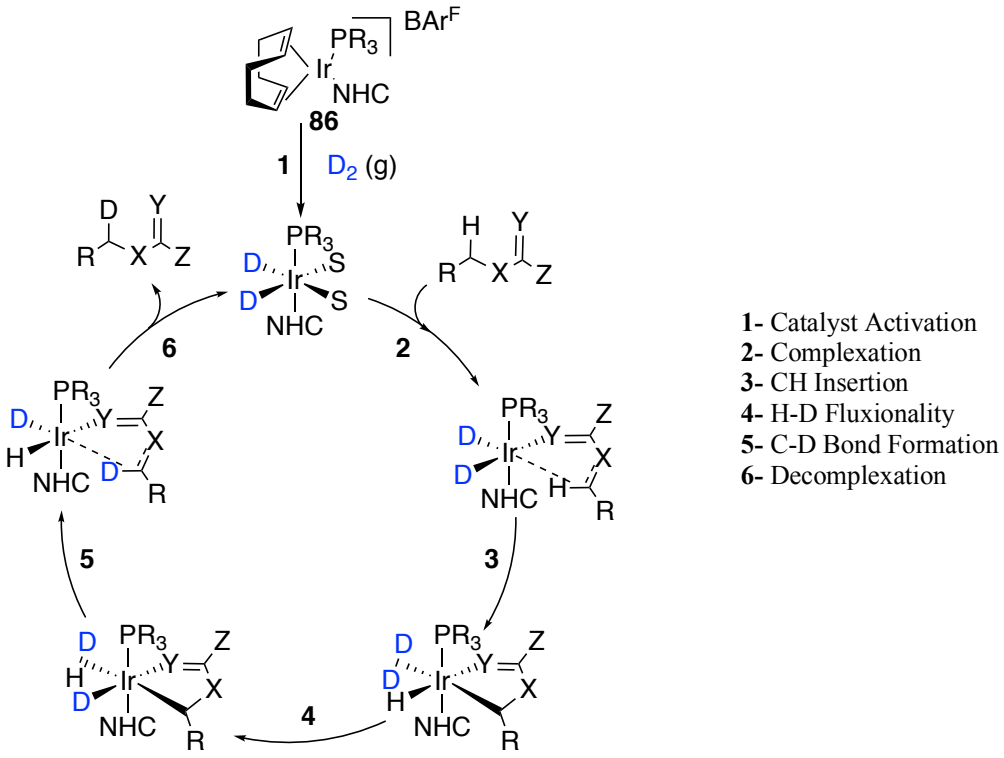

Scheme 1.17

Over recent years, the Kerr group have expanded the substrate scope of the phosphine/NHC complexes considerably, with the emergence of several newly applicable directing groups, and substrates labelled which have previously been inaccessible under iridium catalysed HIE

reactions. One such directing group was carboxylic acids (Scheme 1.18).[55] This methodology tolerated a range of substituents in the *para* position, regardless of their electronic nature. A dimethylamino substituent in the *meta* position **D91** hampered reactivity at the *ortho* sites, with only limited incorporation at the position also *ortho* to the amine group. The strongly electron-donating nature of this group could be strengthening the C-H bonds which are *ortho* and *para* to it. Secondly, this substrate could form a pincer type complex with the metal, generating an off-cycle species which limits the desired reactivity. *Ortho* substitution was also well tolerated, as shown by **D93**.

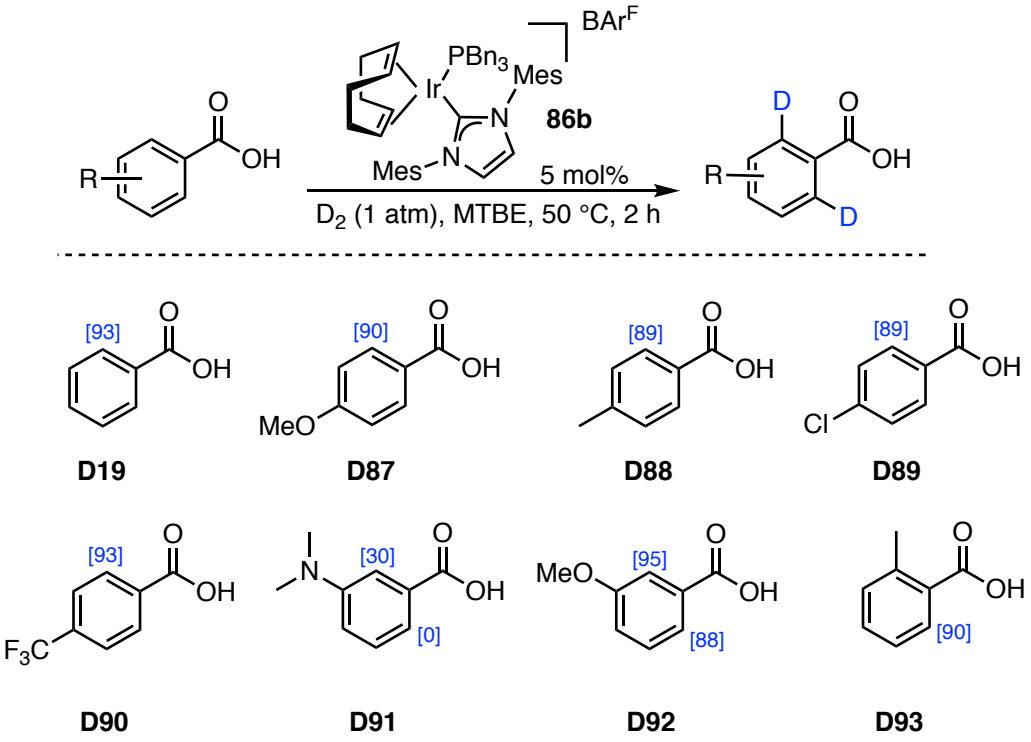

Scheme 1.18

Kerr next showed the application of the first generation catalysts (with PF_6 counterion) in the labelling of indole motifs (Scheme 1.19).[56] Employing an acetyl group on the nitrogen as a directing group allowed for activation of the C2 position and outstanding levels of deuterium were incorporated. The directing group could be modified to an ethyl carbamate **D95** with no detriment to the incorporations observed. Additional sp^2 nitrogen atoms within the ring system were well tolerated, as observed with substrate **D96**. Pleasingly, the indole nitrogen could be left unprotected if an alternative directing group was positioned at C3. The Weinreb

amide in **D97** provided near quantitative labelling at C2 with minimal incorporation observed on the directing group itself. In an industrially-relevant addition to this work, the authors efficiently labelled the ethyl carbamate of migraine drug sumatriptan **D98**, highlighting the applicability of the Kerr catalysts to active pharmaceutical ingredients.

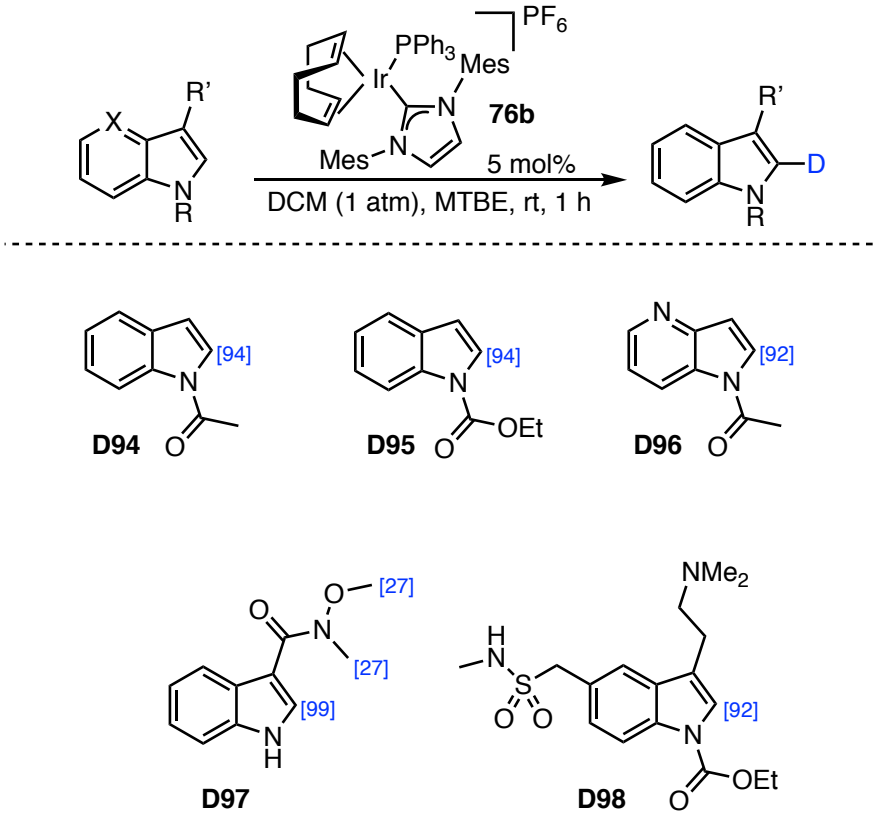

Scheme 1.19

Alongside the labelling of aromatic positions, the Kerr group also wanted to investigate whether the catalyst systems could introduce an isotopic label at a non-aromatic sp^2 centre within a molecule. In 2014, the group published the labelling of α,β-unsaturated carbonyl derivatives, Scheme 1.20.[57] A key challenge in this work was finding a ligand set which would avoid any hydrogenation reactivity due to the promiscuity of the olefin. To their delight, catalyst **76b**, combining PPh_3 and IMes ligands, was a competent HIE catalyst, but afforded only small amounts of hydrogenation. The numbers represented in parenthesis are the ratio of HIE product:hydrogenation product. Substitution on the aryl ring was well tolerated with both electron-donating and electron-withdrawing groups affording good to excellent levels of deuterium incorporation (**D99** and **D100**). The presence of a

pharmaceutically relevant heterocycle, thiophene, in **D102** also led to high isotopic enrichment with little hydrogenation. Investigation of the directing group revealed that good levels of incorporation were observed with various directing groups (compounds **D103-D104**) however, these substrates had a detrimental effect on the selectivity between HIE and hydrogenation. Having said this, the level of HIE product was significantly more for each substrate.

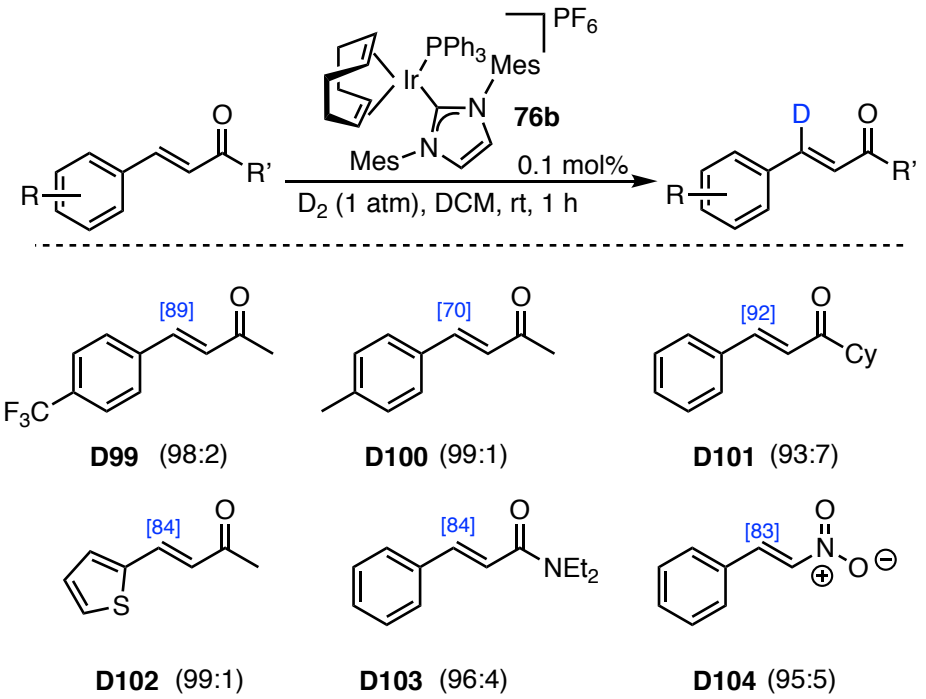

Scheme 1.20

Although the combination of a bulky phosphine and sterically encumbered NHC ligand set had allowed Kerr to access an unprecedented array of substrates for HIE, these catalysts were not competent in the labelling of substrates with a large tetrahedral directing group such as a primary sulfonamide. The Kerr group hypothesised that perhaps a smaller ligand set, with enhanced electron density, would allow more facile coordination of the directing group and allow C-H activation to occur more successfully. Sulfonamides were regarded as an important class of substrate owing to their prevalence in drug motifs. Interestingly, employment of chlorocarbene iridium complexes allowed deuterium incorporation in an aromatic sulfonamide (Table 1.6).[58] A range of NHCs with varying steric bulk and electronic properties were investigated in the labelling reaction. The use of buried volume calculations

and TEP analysis allowed some conclusive information to be drawn from the study. Firstly, NHCs with a percentage buried volume below 30% were inactive in the HIE process (**105**). This could be a result of the need for a larger ligand set to allow facile elimination of the sulfonamide substrate. Secondly, for NHCs of a similar size and structure, the more electron rich, the more active the catalyst becomes for HIE (entry 3 *vs* entry 4).

Table 1.6

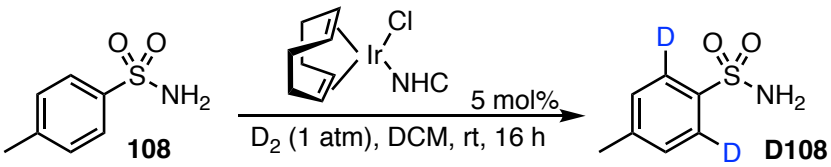

Entry	NHC	%V_{bur}	TEP/cm^{-1}	% D
1	**ICy 105**	26.4	2049.5	2
2	**IMes 75**	33.3	2049.6	90
3	**$IMes^{Me}$ 106**	34.9	2046.7	96
4	**IPr 107**	35.8	2050.2	93

An impressive array of aromatic primary sulfonamides were presented with high deuterium incorporation, and a range of substitution tolerated around the ring. Interestingly, employment of this distinct ligand set allowed excellent chemoselectivity within various competition studies where an aromatic amide was labelled to a poor extent with [Ir(COD)Cl$IMes^{Me}$] **106** but the aromatic sulfonamide maintained incorporations of over 90%. Additionally, drug molecule celecoxib **109** could be selectively deuterated at the positions *ortho* to the sulfonamide, whilst labelling through the pyrazole was minimal, Scheme 1.21. This gives complementary selectivity to what is achieved when one of the more traditional phosphine/NHC catalysts is employed with this pharmaceutical motif.

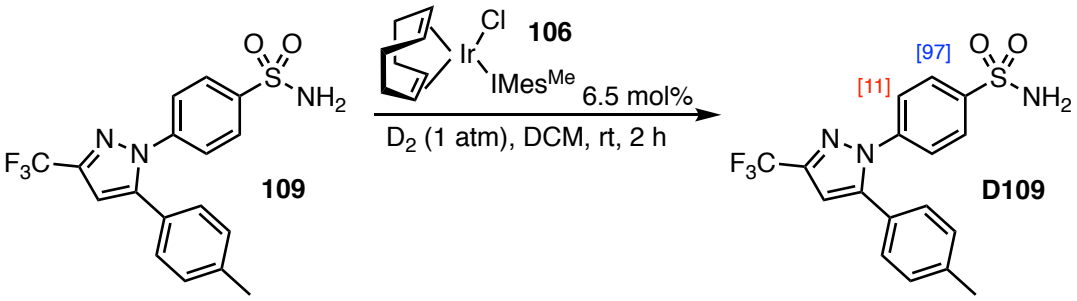

Scheme 1.21

Further application of the chlorocarbene complexes described above has been found by Kerr *et al* for the formyl labelling of aromatic aldehydes.[59] This allows complete selectivity over the *ortho* positions and is another example of the utility of these complexes as HIE catalysts in their own right.

Whilst opening up the ligand sphere using the chlorocarbene complexes was an effective strategy to achieve the labelling of challenging directing groups such as primary sulfonamides, this strategy was less fruitful for other challenging groups. Aryl carbamates are an important class of substrates owing to their widespread presence within pharmaceuticals and the utility of carbamates as protecting groups. For HIE processes, however, they are challenging motifs. The most ubiquitous carbamate protecting groups are often sterically encumbered. In combination with this, C-H activation must be achieved through a 6-mmi. Whilst the Kerr catalysts have been shown to achieve labelling through a 6-mmi, the combination of the more strained metallocycle and the steric constraints of the directing group on the system renders the monodentate phosphine/NHC complexes considerably less active in the labelling of carbamates. It was hypothesised that tethering the NHC and phosphine, to generate a bidentate ligand would reduce the steric hindrance around the iridium and allow better stability of the resulting 6-mmi, whilst maintaining similar electronics to the parent complexes. Therefore, new chelating iridium complexes were developed and the most active complex prepared is shown in Scheme 1.22.[60] Encouragingly, the bidentate complex **111** was inherently more active in HIE of carbamates than the corresponding monodentate Kerr catalyst, with outstanding levels of deuterium incorporation observed.

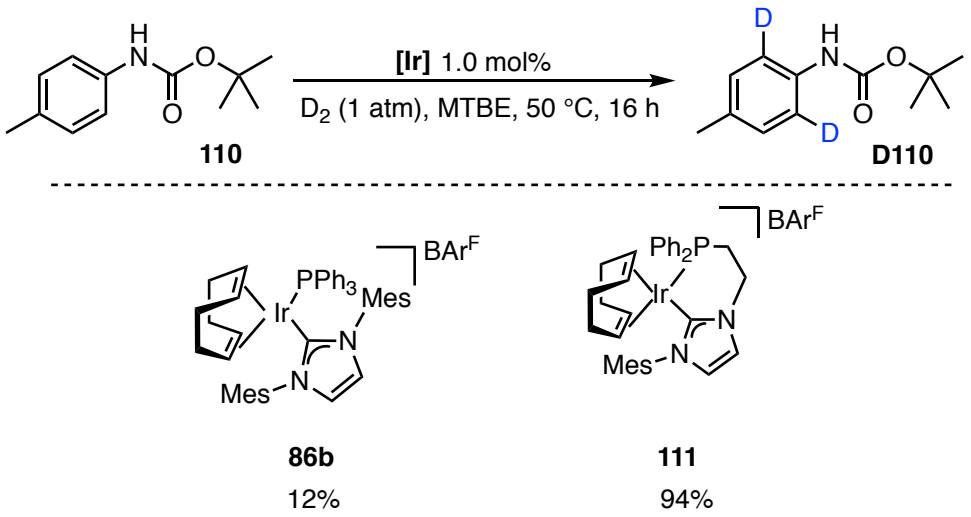

Scheme 1.22

An impressive substrate scope was also developed, once again with a variety of substitution of varying electronic effects tolerated around the aromatic ring system. The derivation of the traditional Kerr catalyst to a chelating ligand system widens the scope of HIE and highlights the invaluable impact that understanding the ligand properties of a catalyst system can have to allow advancement within a catalytic process.

1.1.10 HIE of sp³ C-H bonds in Amines and Amino Acids

Although the isotopic labelling of aryl C-H bonds has been widely studied and is now replete with excellent methods to achieve this transformation, the labelling of sp^3 C-H bonds is much less advanced. Alkyl C-H bonds are much stronger than aryl bonds and, as such, are much less activated towards C-H activation by a metal centre. If the C-H bond to be activated resides next to an electronegative heteroatom or electron-withdrawing group, it is generally accepted that the activation of that bond will be much more facile. Figure 1.22 shows the ease of C-H activation for a range of C-H bonds in different hybridisation and positions.

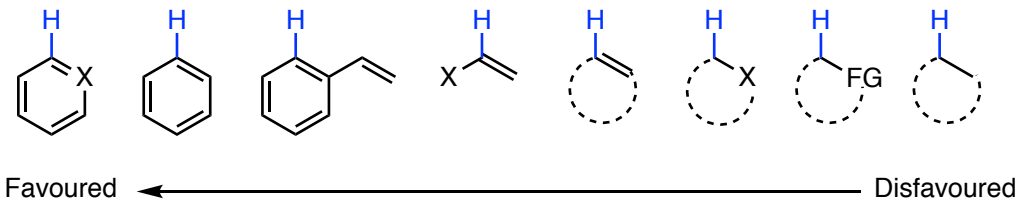

Figure 1.22

Within the HIE arena, over recent years the labelling of sp^3 centres has focused mainly on aliphatic amines and amino acid molecules. Additionally, many of these methods have been centred around the use of ruthenium catalysis. Early reports, in 2014/2015, came from the Pieters lab, where in two separate publications they reported the labelling of alkyl amines, and amino acids. and small peptides (Scheme 1.23).[61,62] The method employed heterogeneous ruthenium nanoparticle catalysts to install deuterium α to a nitrogen. At stereogenic centres, complete retention of configuration was observed. Both linear and cyclic amines were efficiently labelled under these conditions (**D112** and **D113**). Natural amino acid residues were also enriched with deuterium very efficiently. All positions adjacent to the nitrogen were labelled, as exemplified by proline **D116**. Substrate **D115**, Ac-Val-OH, was not labelled under these conditions, confirming the author's hypothesis that a free amine site is required for activation. If another coordinating atom was present within the molecule, such as in threonine, labelling was also observed α to it. With phenylalanine derivative **D118**, the ability of the phenyl rings to coordinate to the ruthenium centre may be the cause of the lower incorporation observed. Unfortunately, with an amino acid such as histidine, containing an imidazole ring, sp^2 C-H activation on the imidazole ring prevailed, with only low incorporation at the sp^3 centre. Interestingly, this method could also be employed to install deuterium in a chemoselective fashion on small di- and tri- peptide molecules. However, a limitation here is that only the residue with a free primary amine at the *N* terminus is labelled. Finally, this methodology was also utilised for the labelling of drug molecules, with Imipramine **122** shown as an example here. Although the reaction conditions for this transformation are relatively mild, high deuterium pressures will require a pressurised vessel and the ruthenium nanoparticles used require glovebox manipulation. This is a drawback compared with some other methods, described later.

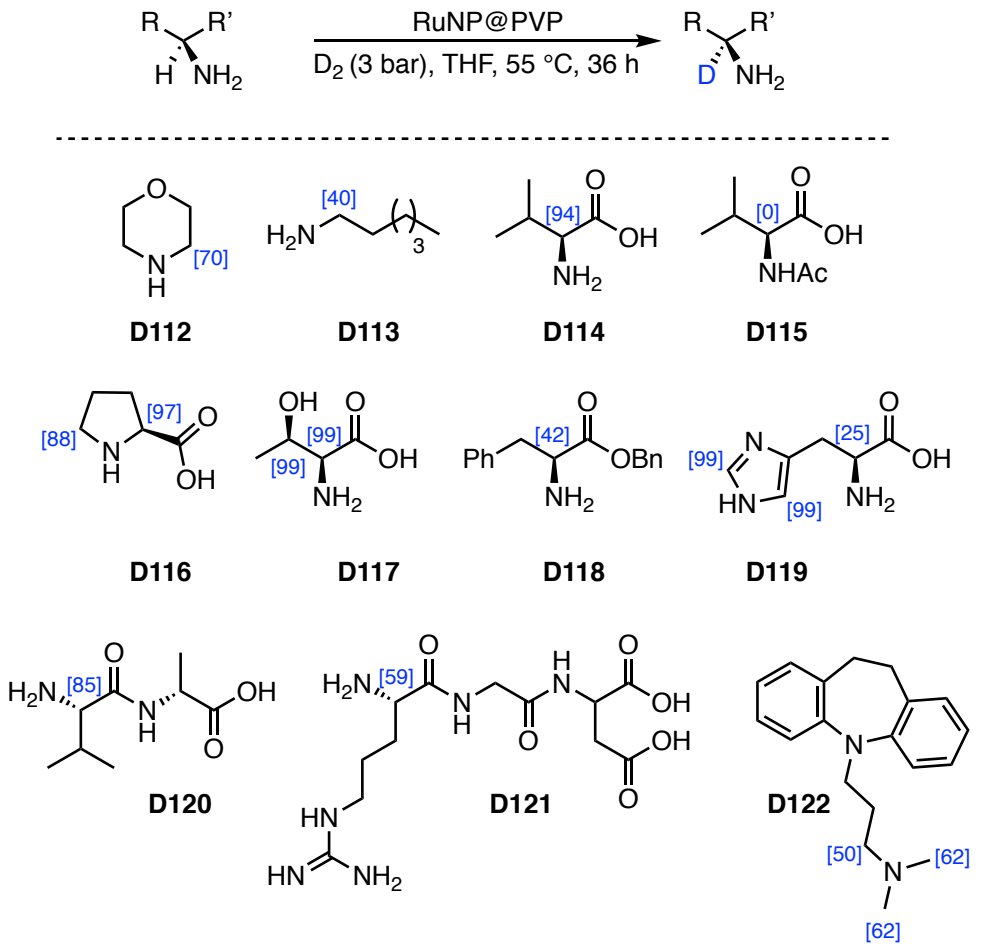

Scheme 1.23

Continuing the theme of heterogenous ruthenium catalysis, Roche and co-workers published the deuterium labelling of amino acid molecules in 2017.[63] This method employed ruthenium on charcoal under a hydrogen atmosphere, with deuterium oxide as the isotopic source. This methodology was stereoretentive and allowed efficient labelling of a variety of residues (Scheme 1.24). Similarly to Pieters' work, if another coordinating moiety was present in the molecule, such as the second carboxylic acid group in glutamic acid, labelling was also observed adjacent to this site. Another shared characteristic between these two methodologies was in dipeptide substrates. The labelling of Gly-Gly **D125** afforded isotopic enrichment only at the *N* terminus residue. The final comparison between the two methods was the use of a nitrogen protecting group. This has a detrimental effect on the HIE process, as depicted by substrate **D126**. Unfortunately, Roche's conditions did not extend to the labelling of sulfur

containing amino acids, e.g., **D127**. Overall, although this method has the benefit of a bench stable catalyst system, the use of D_2O as the deuterium source is a drawback.

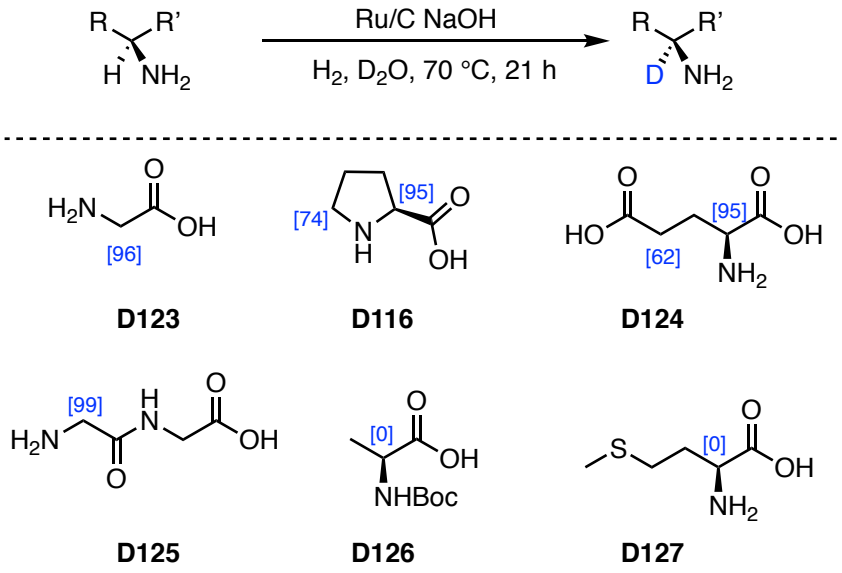

Scheme 1.24

Keeping within the realms of ruthenium catalysis, but moving to a homogeneous catalyst system, Gunanathan and co-workers reported the use of a monohydrido-bridged dinuclear complex which was able to deliver deuteration of alkyl amines and amino acids (Scheme 1.25).[64] Linear and cyclic alkyl amines were labelled to good levels under the reaction conditions. Parent amino acids were incompatible under these conditions, and this was attributed to the deactivation of the ruthenium catalyst in the presence of the carboxylic acid functionality. To circumvent this, the acids were first converted to their potassium salts. A range of amino acid residues could be labelled efficiently, with high incorporation seen for phenylalanine **D133**, in contrast to the methods described above. Additionally, methionine **D134** was also labelled to a good extent. Unlike the methods for amino acid labelling described previously, the harsh reaction conditions of this method meant that stereoretention was not observed, which is a considerable shortcoming of this strategy.

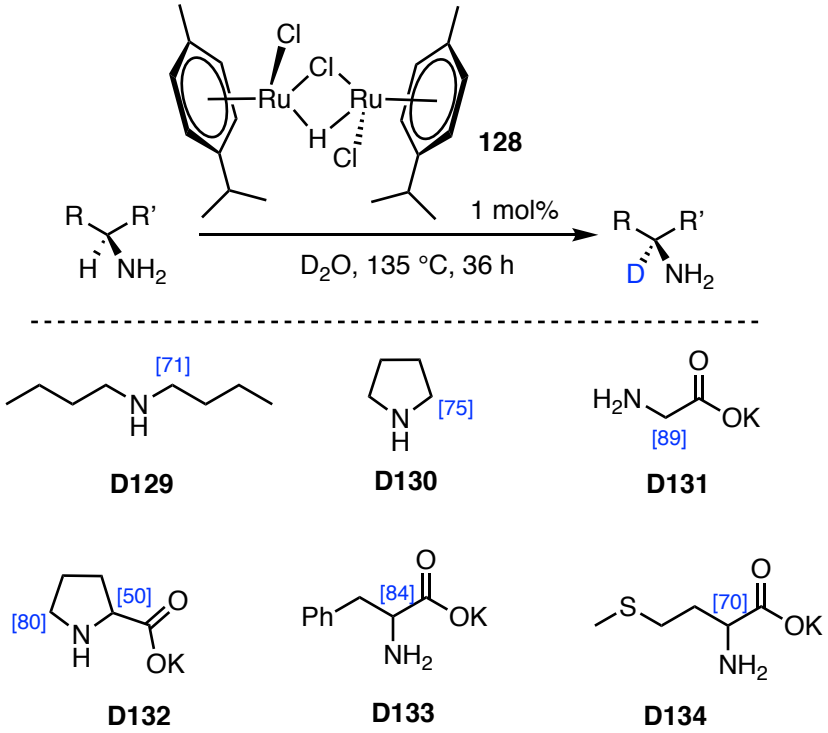

Scheme 1.25

Whilst there is an abundance of aromatic C-H HIE reactions catalysed by iridium, the use of this metal for sp^3 HIE is in its infancy. In a departure from the traditional Ir(I) catalysed HIE reactions traditionally used for HIE, a seminal piece of work from the MacMillan lab employed an Ir(III) photocatalyst to install deuterium and tritium through a hydrogen atom transfer (HAT) protocol (Scheme 1.26).[65] The excited photocatalyst can oxidise the amine substrate to generate an α-amino radial through deprotonation. Employment of a thiol HAT catalyst **135** allows exchange with T_2O to afford a tritiated thiol, which acts as the source of tritium through HAT. MacMillan and co-workers utilized this method to install deuterium or tritium in an impressive range of pharmaceuticals. The authors focussed their deuterium work for application in internal mass spectrometry standards, where four deuterium atoms are required per molecule. These reactions could be performed on a 1 g scale, providing sufficient material for Mass Spectrometry (MS) studies. Various saturated nitrogen containing rings could be deuterated to high levels. Positions α to an oxygen atom also deuterated, as shown in substrate **D137**. The deuteration protocol was extended to high molecular weight macrolide drugs, motifs which would be challenging through more traditional HIE techniques. Impressive levels of deuterium were incorporated into challenging substrate **D138**. In a further advancement, MacMillan successfully tritiated **138**

to give **T138**, with a good specific activity (SA) of 28.6 Ci mmol^{-1}. This is more than ample levels for use in ligand binding studies, where a specific activity of >15 Ci mmol^{-1} is generally accepted.

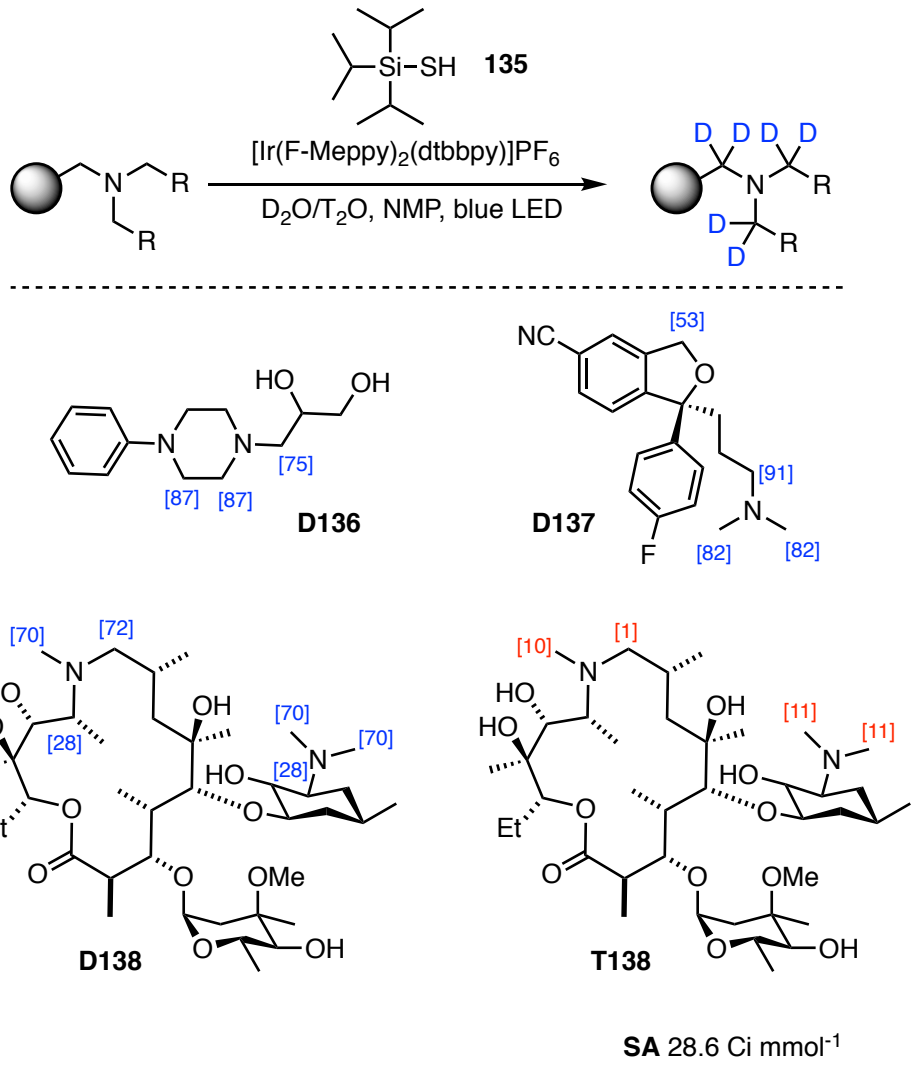

Scheme 1.26

Returning to the more traditional Ir(I) HIE catalysis, and owing to the success of their complexes in sp^2 HIE, Kerr and co-workers investigated these complexes to assess their activity in the labelling of saturated heterocycles. *N*-(pyridin-2-yl)morpholine **139** was used as a model substrate (Scheme 1.27).[66] The combination of both a bulky NHC and phosphine was found to be imperative for high levels of incorporation to be observed, whilst chlorocarbene **75** showed no activity towards the sp^3 activation. It was also noted that the incorporations for complexes bearing the more diffuse BAr^F counterion were much higher

than their PF_6 analogues (**76b** *vs* **86b**). Additionally, Crabtree's catalyst **33** only allowed poor incorporations of 24% on the morpholine ring, once again confirming the superior nature of the Kerr catalysts. It was noted, however, that varying the phosphine ligand did not significantly impart changes upon the levels of labelling observed, with incorporations of ~80% reported for complexes **86a-c**.

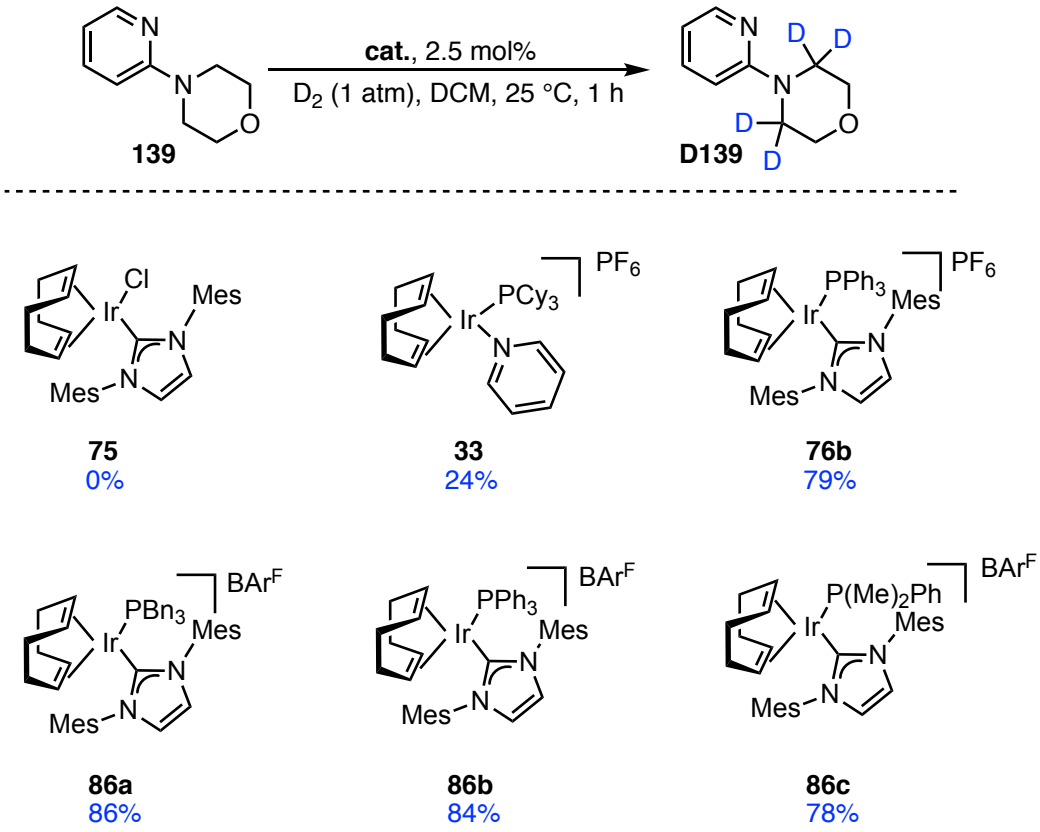

Scheme 1.27

Having achieved excellent levels of labelling with substrate **139**, attention was then focused on widening the substrate scope (Scheme 1.28).[55] The labelling reactions were performed under extremely mild conditions of 1 mol% catalyst at room temperature for 1 h. A variety of heterocyclic directing groups could be employed under the reaction conditions including pyridine, pyrimidine and thiazoles. The scope of the saturated heterocycles to be labelled was also expanded upon, moving to piperidine **D140** with high levels of incorporation observed (95%). Piperazine **D141** could also be labelled to high levels of 92%, however, longer reaction times of three hours and a higher catalyst loading were required for this substrate. Non-heterocyclic directing groups also performed well under the reaction conditions

(substrat**es 145** and **146**). Linear saturated systems, such as **D143** and **D144**, also allowed deuterium incorporation, albeit in low to moderate levels.

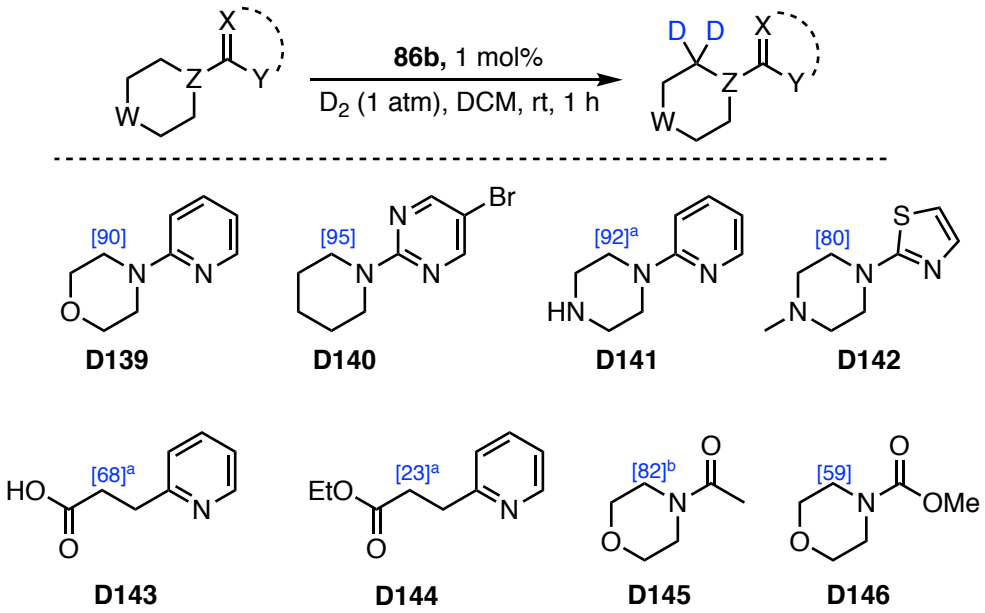

[a] 5 mol%, 3 h
*[b] **86a**, 5 mol%, 50°C, MTBE, 3 h*

Scheme 1.28

With a robust method of labelling saturated heterocycles in place, application of the methodology to drug molecules was investigated (Figure 1.23). Azaperone could be labelled on the piperazine ring, directed through the pyridine, to almost quantitative levels. Interestingly, only minimal amounts of aryl C-H activation was observed, which could also be directed through the carbonyl *via* a 5-mmi. This shows how the judicious choice of catalyst from the Kerr group suite and careful choice of conditions can allow access to labelling at sp^3-centres over aryl C-H bonds in an unprecedented manner for Ir(I) catalysed HIE.

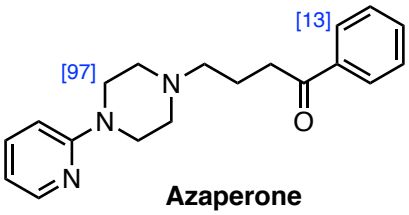

Figure 1.23

The applicability of bench stable Ir(I) Kerr catalysts which utilised D_2 as a deuterium source is very advantageous over some of the ruthenium chemistry discussed, where harsh reaction conditions destroy stereochemical integrity in some instances, some ruthenium catalysts cannot be utilised outside the glovebox, selectivity is often an issue, and many of the methods employ the unfavourable D_2O as a deuterium source. It is therefore unsurprising that scientists at Sanofi have investigated a range of Ir(I) catalysts for sp^3 labelling. At the onset of this project, there were no reports of Ir(I) HIE catalysis for the deuteration of amino acids and peptides. In 2018, Derdau *et al* from Sanofi reported the labelling of aliphatic amides.[67] A range of commercial Ir(I) catalysts were investigated, and, pleasingly Kerr catalyst **86b** was the most active compared to Crabtree's catalyst **33** and a variety of new Ir(I) catalysts from other groups. Derdau and co-workers employed the same catalyst motif to Kerr's sp^3 labelling methodology, however the more complex nature of the amino acid substrates required more forcing conditions. Increased catalyst loading and a higher boiling point solvent, *iso*-propyl acetate (^{i}PrOAc) at 80 °C were required to observe appreciable levels of deuterium incorporation (Scheme 1.29). With the secondary amino acid glycine, excellent levels of incorporation were observed for Ac-Gly-OMe **D147a**. Disappointingly, moving to synthetically more tractable protecting groups commonly used within amino acid chemistry such as Cbz-, Fmoc- and Boc-, the level of incorporation decreased significantly, with no incorporation observed at all for the Boc- protected substrate **D147d**. This is a severe limitation to this methodology and the authors reasoned that this could be a result of the bulky Boc- directing group resulting in a significant steric clash with the sterically encumbered ligand set. Nonetheless, good to excellent levels of incorporation were observed for glycine containing dipeptides **D151** and **D152**, regardless of which terminus the glycine was positioned at. Tertiary amino acid residues such as alanine derivative **D148** appeared to be much more challenging, with incorporation dropping to a still very respectable 65%.

When the substituent was made larger, such as in valine **D149**, or phenylalanine **D150**, isotopic labelling was completely hampered. Interestingly, high levels of labelling were observed at the methionine residue in **D153**, highlighting the tolerability of the sulfur functionality with Kerr's catalyst. It appears from the results presented, that secondary amino acid residues will be preferentially labelled over more substituted residues.

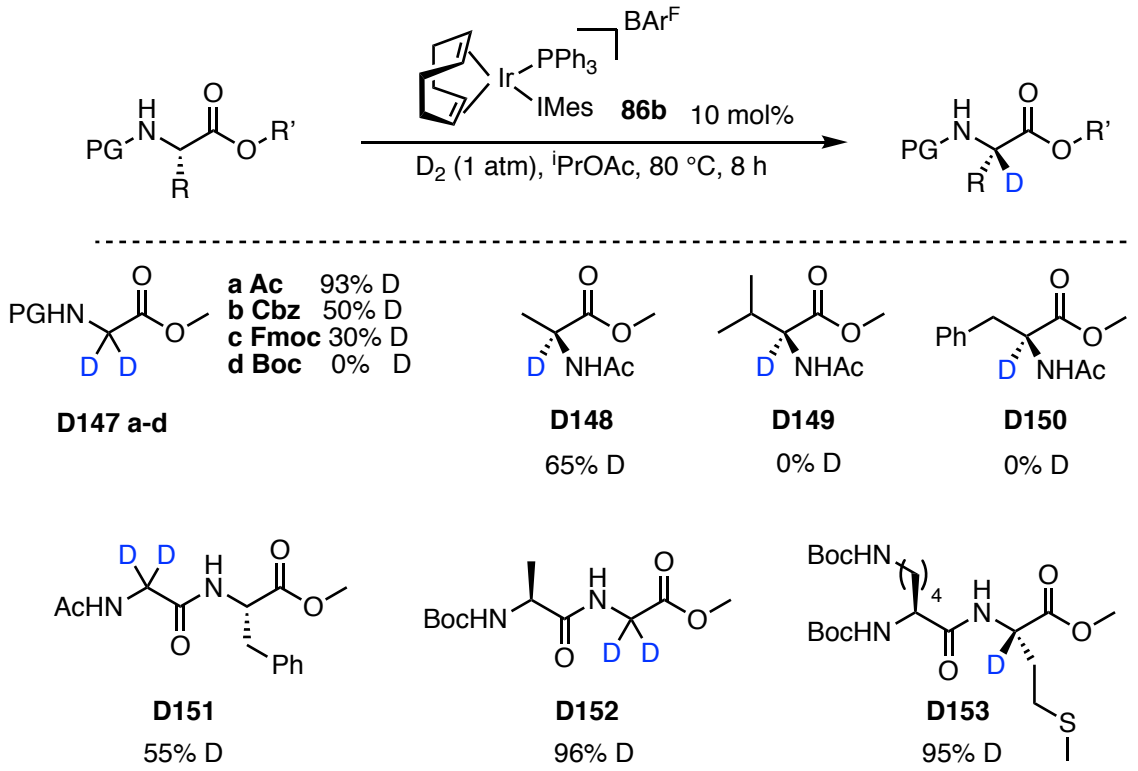

Scheme 1.29

The application and development of new catalyst structures to enable the HIE of various substrate classes is a well studied area. This being said, the extension of this methodology into the labelling of sp^3 C-H labelling remains in its infancy compared to the labelling of aromatic molecules. This affords an interesting arena for research and allows the opportunity to develop more robust catalyst systems for this application.

1.2 Proposed Work

1.2.1 Isotopic Labelling of Amino Acids

As discussed previously, within the Kerr group, a suite of complexes bearing NHC/phosphine or NHC/chloride ligands have been developed and successfully utilised within aryl HIE processes. Recent work has seen the extension of this methodology to activated sp^3 bonds and has laid the foundations for further expansion and development of this area. Lead drug candidates which are more sp^3 rich have become more prevalent over the recent years and, as such, a general method of labelling these systems is required. With seminal work within the Kerr group having targeted the labelling of saturated heterocycles, a move to investigate biologically relevant molecules is envisaged. Amino acids and peptides play a crucial role in drug discovery, with the number of peptide drugs on the market increasing every year. In order to enable the labelling of such molecules, amino acids will first be studied in order to find a robust and industrially-friendly isotopic labelling methodology (Scheme 1.30). In light of the work published by Derdau and co-workers during the course of this project, a specific effort was made to ensure catalyst development allowed common amino acid directing groups to be efficiently employed in the HIE process. Utilisation of the Kerr group catalysts may allow labelling of the α- position through a 5-mmi from the amine protecting group (Scheme 1.30, highlighted in green) or directed *via* the ester group through a 5-mmi to the ß—position (Scheme 1.30, shown in blue). As can be seen from Scheme 1.30, even simple amino acids provide a complex system which could be labelled through various groups to different positions within the molecule, and may depend greatly on the nature of the ligand set.

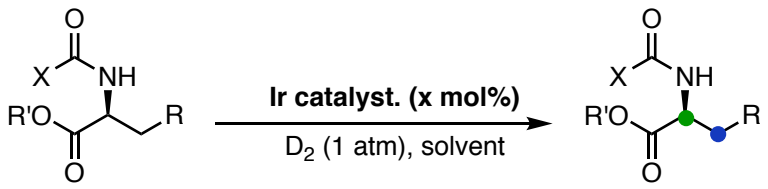

Scheme 1.30

Application of new and modified Kerr iridium catalysts could revolutionalise the area of amino acid labelling, which remains limited and plagued with issues. With this in mind, it is hoped that a method can be developed which will allow the stereochemical integrity of amino

acid substrate to remain intact. A range of catalysts are already available, including NHC/P and NHC/Cl complexes, and both monodentate and bidentate catalysts will be investigated to probe the reactivity of the Kerr catalysts with an amino acid system (Figure 1.24).

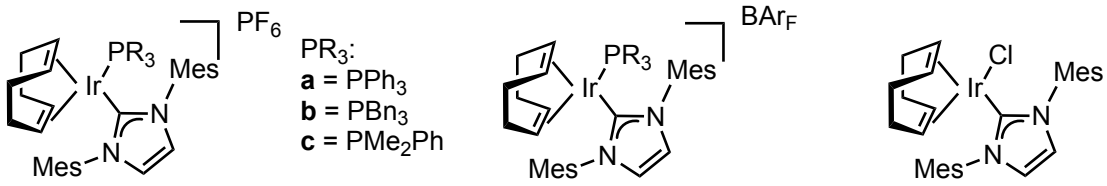

76a-c **86a-c** **75**

Figure 1.24

Initial investigations will be centred upon a model substrate, namely glycine (Gly) and its derivatives (Figure 1.25). A variety of amine protecting groups will be used as directing groups alongside differing combinations of ester groups at the R' position. A thorough solvent screen, catalyst loading and concentration study will be undertaken for amino acid substrates to optimise the labelling reactions further. Selectivity of the labelling reactions will be investigated thoroughly at each stage of the project.

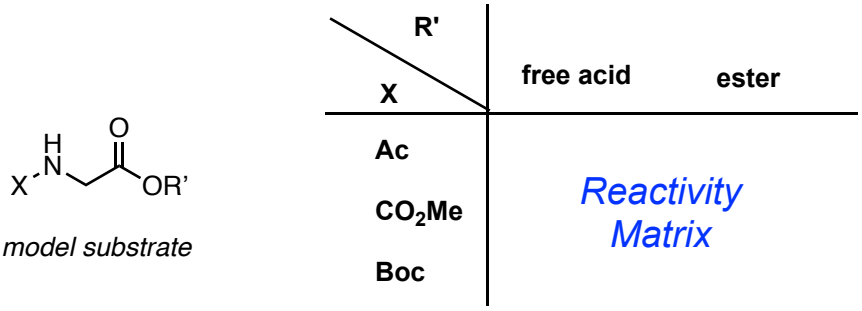

Figure 1.25

With an optimised labelling protocol for glycine derivatives in hand, the most efficient combination of protecting group X and R' will be chosen to investigate alternative amino acid residues to expand the scope of the methodology, and generality of the conditions. A range of amino acid substrates will be investigated, including; alanine, valine and proline, alongside sulfur containing residues, expanding the labelling protocol from secondary to tertiary amino acid residues (Figure 1.26).

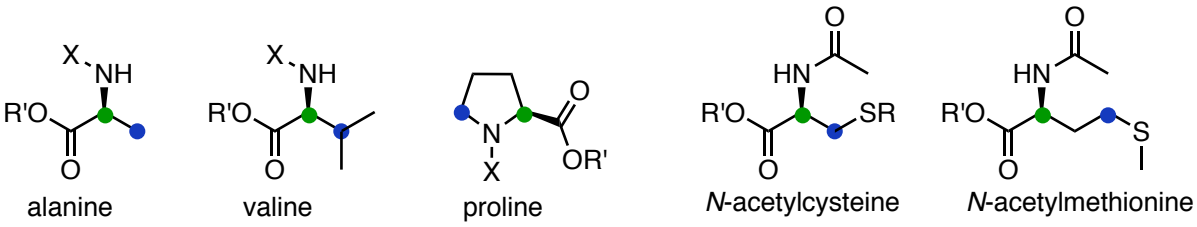
X
NH
R'O
O
alanine
X
NH
R'O
O
valine
O
N
X
OR'
proline
O
HN
R'O
SR
O
N-acetylcysteine
O
HN
R'O
S
O
N-acetylmethionine

Figure 1.26

1.3 Results and Discussion

1.3.1 Investigating the Labelling of Model Substrate Ac-Gly-OMe

To initiate our studies, we sought to investigate the isotopic labelling of Ac-Gly-OMe. To enable this, a suite of Kerr Ir(I) catalysts were synthesised. In line with previous investigations within the Kerr group, it was hypothesised that evaluating the activity of the Ir(I) chelated catalyst systems, as well as the monodentate systems, would be beneficial with challenging amino acid substrates. Not only do they often employ sterically encumbered directing groups (such as Boc- or Fmoc-), but the site to be activated is often a methine position, implying a sterically congested environment for the catalyst (Figure 1.27) whilst this is not an issue for secondary amino acid glycine, it was imperative to consider this as a factor moving forward.

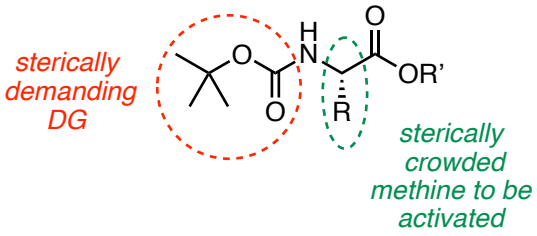

Figure 1.27

In order to explain the rationale as to why the chelated NHC/P ligands could potentially better accommodate the steric demand of our amino acid substrates, it is worth looking to the mechanism of HIE, Scheme 1.31. Catalytic cycles for both monodentate and bidentate catalyst systems are depicted. Both catalyst systems are activated by reduction of the COD ligand under an atmosphere on D_2 (step 1). This is where the first difference in the two systems arises. In **155**, the activated monodentate complex, the encumbered steric nature of the phosphine and NHC provide a *trans* relationship between the ligands. However, for the chelated catalyst system, the tether forces a *cis* P/NHC relationship, thereby decreasing the ligand sphere around the metal centre. The two cycles then follow the same elementary steps; 2- substrate association and formation of an agostic interaction; 3- C-H activation; 4- H-D fluxionality; 5- C-D bond formation; and 6- product dissociation. Whilst the catalytic steps

are identical, when we compare the intermediates **156** and **162**, where the substrate is agostically bound pre C-H activation, it is obvious that the substrate will experience a distinct steric environment in each case. For the bidentate cycle, there is significantly more 'free space' for the substrate to bind and undergo C-H activation. This could be particularly useful for substrates with a large R group. Exploring the reactivity of these catalyst systems therefore was a key consideration at the onset of this process.

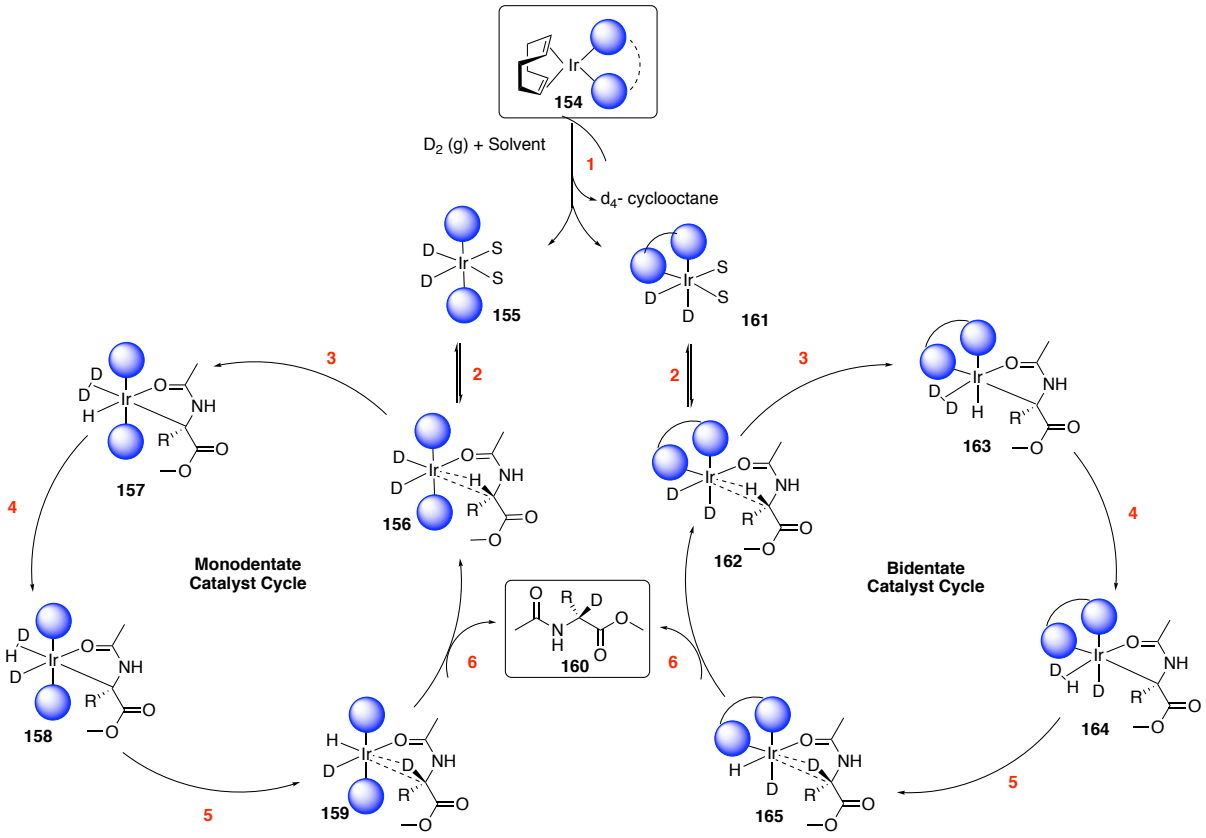

Scheme 1.31

As a result of their widespread utility in HIE reactions, many of the Kerr catalysts of the type [Ir(COD)PR_3NHC]X (where X= PF_6 or BAr^F) are available commercially from Strem Chemicals Inc. For the purpose of our HIE studies, the required monodentate complexes were prepared on scale and included some novel Ir(I) complexes. As previously discussed, the phosphine/NHC monodentate complexes were traditionally synthesised *via* formation and isolation of neutral chlorocarbene complexes such as **75**.[68] Over recent years, further

development of the protocol has resulted in more optimal conditions, enhancing the ease of synthesis.[69] Commercially available **73** was stirred with ^{t}BuOK, before addition of the IMes•HCl salt **74**, allowing *in situ* deprotonation and complexation (Scheme 1.32). It was pleasing that good to excellent yields of product **75** were achieved on both small and large scales.

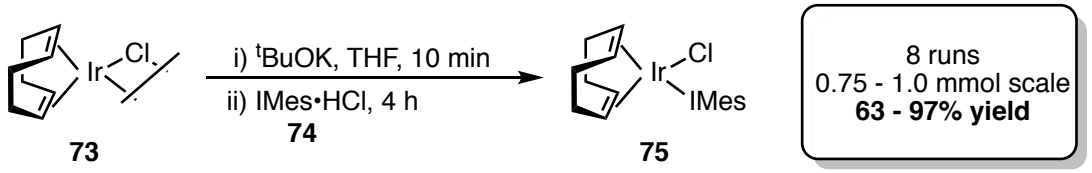

73 **75**

Scheme 1.32

Reaction of the generated chlorocarbene complex **75** with $NaBAr^F$ and the required phosphine subsequently afforded the desired complexes of the form $[Ir(COD)PR_3IMes]BAr^F$ (Scheme 1.33). Good to excellent yields were achieved for all complexes, highlighting the applicability of the adapted synthetic procedure.

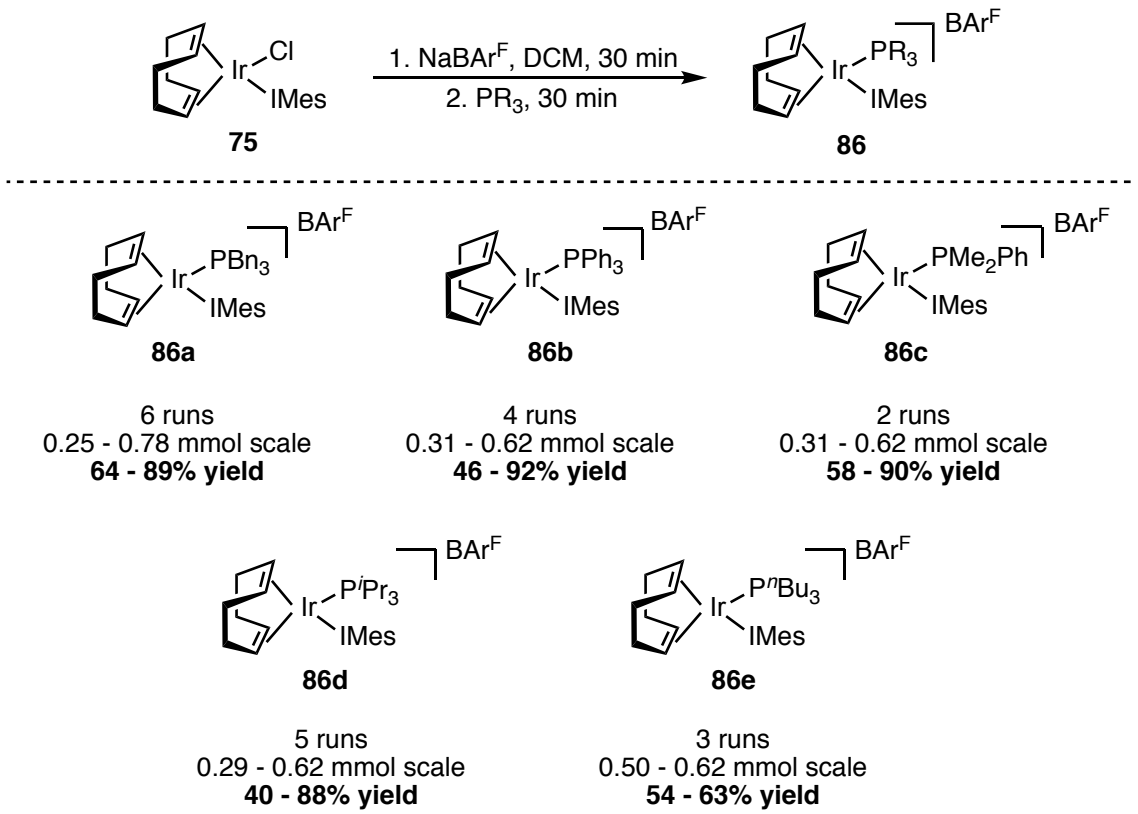

75 **86**

86a **86b** **86c** **86d** **86e**

Scheme 1.33

Whilst some of the chelated iridium catalysts to be investigated for HIE of amino acids were available in-house, complex **111** had to be synthesised. The NHC/P ligand was synthesised in five steps from 2,4,6-trimethylaniline **166** (Scheme 1.34).[70] A one pot multi-component synthesis of mesitylimidazole **169** in moderate yield, followed by alkylation with bromo-ethanol under reflux, afforded excellent yields of the alcohol salt **171**. This intermediate was then subjected to bromination conditions, generating moderate yields of the desired product **172**. Installation of the phosphine group required pre-formation of the diphenylphosphide anion using potassium *tert*-butoxide in dimethyl sulfoxide (DMSO), before careful addition of the resulting solution into a secondary flask containing **172** in DMSO. The phosphinated product was unstable and immediately subjected to anion exchange to afforded the desired ligand **173** in moderate yield. Although the yields for this step are poor, the ligand has been found to be sensitive to oxidation on silica. Complexation to iridium was achieved *via* deprotonation of imidazolium ligand **173** with potassium *tert*-butoxide to give complex **111**.

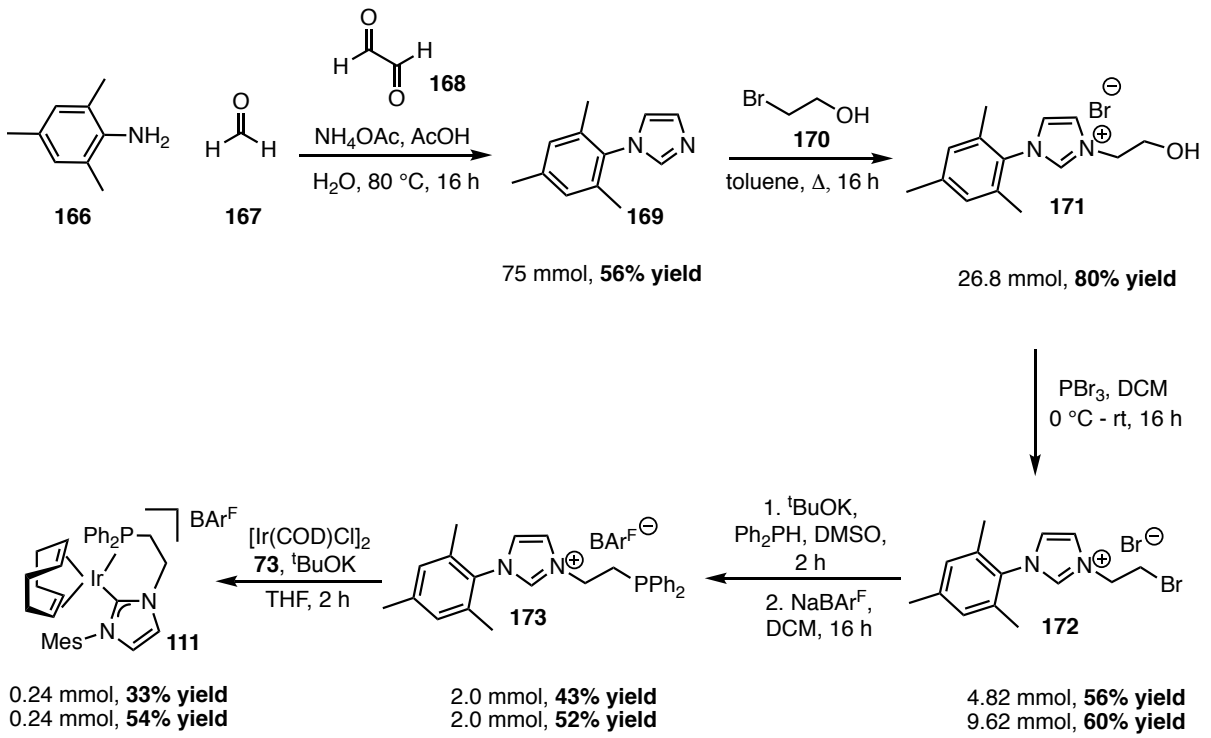

Data represented as: reaction scale, product yield

Scheme 1.34

With a suite of iridium (I) complexes synthesised (**86a-e** and **111**), and with **174** and **175** available,[71] these complexes were employed as catalysts in the labelling of Ac-Gly-OMe **147a**. Small protecting groups were initially sought at the *N* and *C* termini in the hope of finding an active catalyst. The use of an acetyl protecting group affords an amide directing group on the nitrogen, and such functionality has shown to be a competent directing group with the Ir(I) complexes previously. This would furnish an energetically favourable 5-mmi, allowing activation at the methylene position. Additionally, there is potential for the ester group to direct through a 5-mmi onto the methyl group, however, this was unexpected. To test our bank of catalysts, conditions from the Kerr groups sp^3 labelling studies of acetyl protected glycine were employed (Scheme 1.35). To note, the preparation of all amino acid substrates is given in the Experimental section before each first use, but for the sake of brevity, the details of synthesis are not discussed within this section

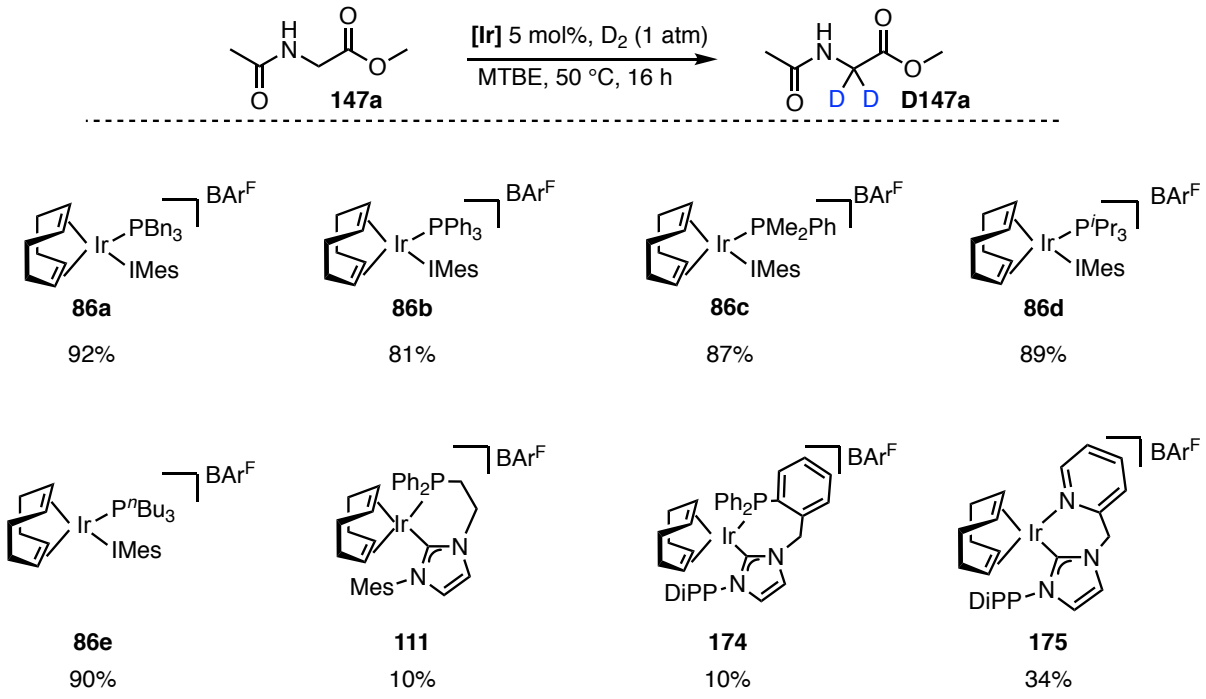

Scheme 1.35

To our delight, monodentate catalysts **86a** through to **86e** all displayed extremely high activity for the HIE process, with **86a** and **86e** showing remarkable incorporations of 92 and

90% respectively. It was extremely pleasing to confirm that the Kerr catalysts could indeed facilitate deuterium incorporation into these extremely interesting amino acid substrates, which are more complex than the sp^3 labelling substrates investigated to date. Variation in the size of the phosphine seemed to play no significant role in effecting the levels of incorporation with this substrate, suggesting the C-H activation and labelling of this process is very favourable. It was however, a very different outcome for the chelating NHC/P catalysts. Contrary to what we expected, these complexes showed only moderate incorporation at best, with complex **175** delivering 34% labelled product.

Although the lack of activity observed with the chelated catalysts was very intriguing and worthy of further investigation (which will be described below), the extremely high activity of a range of monodentate phosphine containing catalysts in the HIE of Ac-Gly-OMe prompted us to further expand the scope of the glycine derivatives. It was proposed to look further at which alternative amine and ester protecting groups could be tolerated. Whilst it looks like the nature of the phosphine is not important in the HIE process from the results with Ac-Gly-OMe **147a**, we were aware that when moving to larger, and arguably more synthetically useful, directing groups such as Boc-, the steric influence of the phosphine may have a significant impact. As a result, three classes of phosphine were investigated; benzyl phosphines, aryl phosphines and alkyl phosphines (complexes **86a**, **86b** and **86d**) and their steric parameters were evaluated.

To investigate the steric properties, percentage buried volume ($\%V_{bur}$) calculations were employed. DFT calculations were utilised to achieve an optimised geometry of the proposed *bis*-solvated intermediate on the catalytic cycle (Figure 1.28).

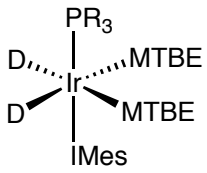

Figure 1.28

On completion of the required DFT optimisation, SambVca online software was used to

calculate $\%V_{bur}$ from the optimised coordinates.[72] The values obtained are depicted in Table 1.7.

Table 1.7

Complex	PR_3	$\%V_{bur}P$	$\%V_{bur}P+NHC$	Cone Angle θ[73]
86a	**PBn_3**	24.6	55.0	165
86b	**PPh_3**	26.7	58.5	145
86d	**P^iPr_3**	27.7	62.0	160

In addition to calculating the $\%V_{bur,}$ steric maps could also be obtained from the SambVca software, allowing us to visualise the steric environment (Figure 1.29). The iridium metal resides in the middle of the map, and a view down the Z axis is shown. Dark blue sections represent areas of the ligand furthest from the metal centre, where green areas highlight a steric build up. From the reported Tolman cone angles shown in Table 1.7, tribenzyl phosphine appears to be the largest ligand, whilst triphenyl phosphine is the smallest of the set. However, when examining the calculated $\%V_{bur}$ of the ligands within the three complexes, tribenzyl phosphine is in fact the smallest. Although it has the largest cone angle, in solution this phosphine will display a large degree of flexibility compared to the other phosphine ligands, this may account for the decrease in steric impact displayed. To gain further understanding, we can consider the steric maps generated (Figure 1.29). What we observe with tribenzyl phosphine is a build up of ligand volume concentrated in the south east quadrant of the steric map. This allows a lot of 'space' in all other quadrants around the metal centre which is not being occupied by the phosphine, highlighting the flexibility of this ligand motif. When we compare this to the other two phosphine ligands, it is obvious that there is steric build up in more than one quadrant. This could explain why their $\%V_{bur}$ is larger than the which might be expected from the cone angle calculations.

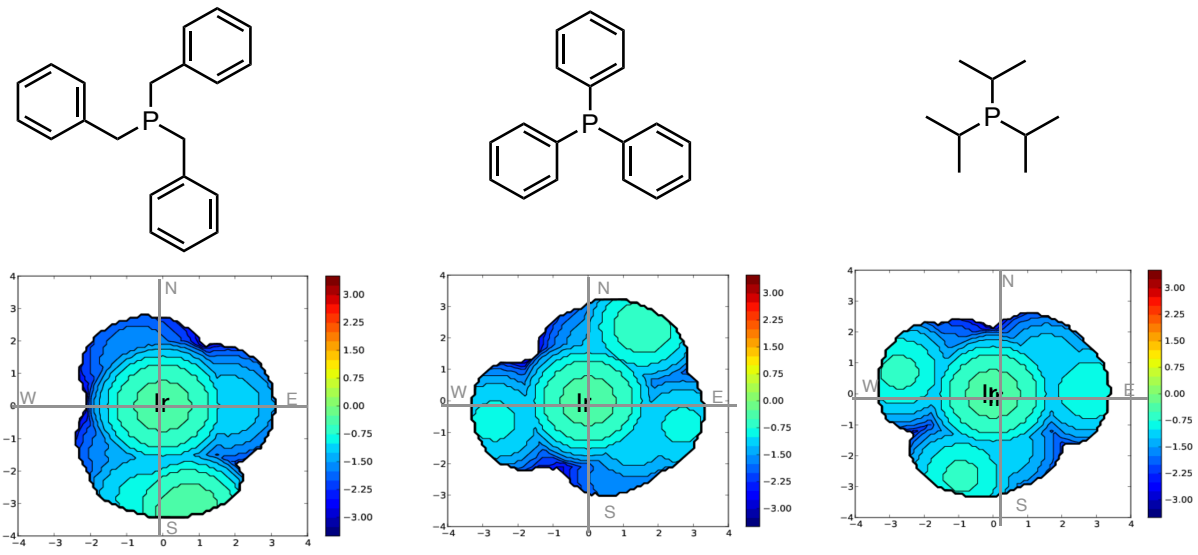

Figure 1.29

Owing to its high levels of incorporation and proposed flexibility, complex **86a** was deemed the most suitable catalyst choice moving forward. The flexible nature of the phosphine ligand could allow enhanced tolerability of bulky directing groups and activation of sterically congested methine positions within tertiary amino acids. In an attempt to confirm its superiority over the other monodentate catalyst systems, labelling of two Boc-Gly-OR' derivatives were investigated, Scheme 1.36. It was extremely pleasing to note that the Kerr catalysts, under our developed HIE conditions, could accommodate a Boc- directing group, something which previous reports with Kerr catalysts had been unable to achieve.[67] Incorporations were lower in general than those for Ac-Gly-OMe, but nonetheless, complex **86a** afforded very useful incorporations for both Boc-Gly-OMe **147d** and the even more sterically encumbered Boc-Gly-O^{t}Bu **176**, with the latter outperforming the smaller substrate.

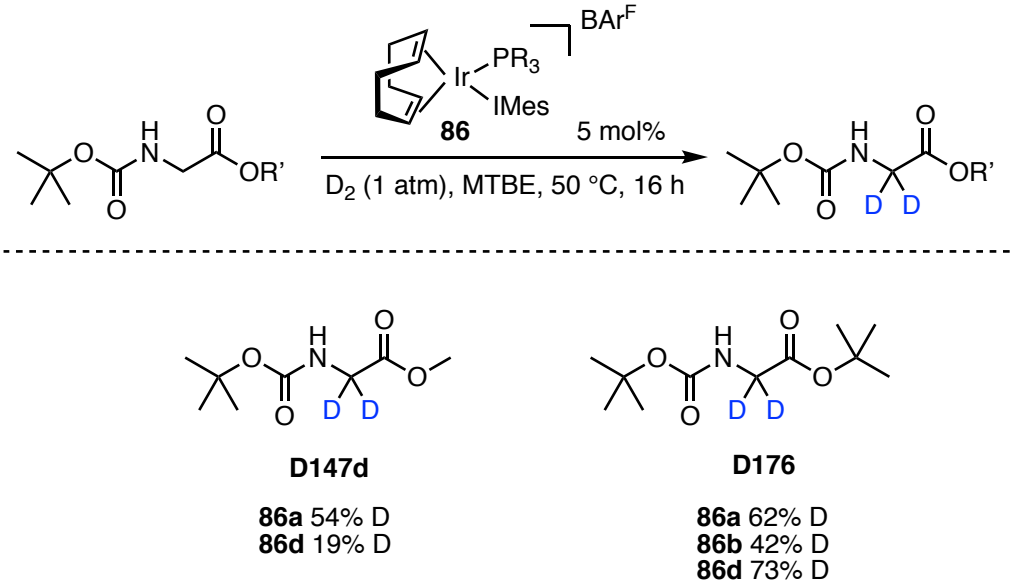

Scheme 1.36

In contrast to the report by Derdau and co-workers,[67] using our methodology, complex **86b** was in fact a competent catalyst to allow HIE directed through a Boc- group. Whilst those authors had put the lack of activity down to a steric clash between directing group and ligand, this discrepancy led us to believe this may in fact have been a solvent incompatibility. The nature of the solvent is extremely important for HIE processes and this has been demonstrated regularly throughout the literature. In order for the catalytic cycle to function, solvent molecules must be displaced by the substrate. If the solvent binds significantly better than the substrate, this displacement will not occur. This could indeed be the problem in Derdau's methodology where ^{i}PrOAc is used as the solvent. This solvent may bind more strongly to iridium than the carbamate directing group. In contrast, our method utilises a poorer binding solvent, MTBE. In this instance, the solvent is more easily displaced by the carbamate directing group. These results highlight the crucial importance of combining a suitable solvent with the desired directing group to allow C-H activation. Additionally, this study reiterates that moving from an amide directing group to a carbamate group can impart significant differences in reactivity.

Returning to our labelling results in Scheme 1.36, although complex **86b** was active, the drop in incorporation compared to **86a** was notable, and so this catalyst looked to be less optimal moving forward. Although complex **86d**, bearing an alkyl phosphine, performed outstandingly with Boc-Gly-O^{t}Bu **176**, it was not an efficient catalyst in the labelling of Boc-

Gly-OMe **147d**. This confirms our hypothesis that complex **86a**, with the flexible phosphine ligand PBn_3, appears to be the most suitable complex for the labelling of a range of glycine derivatives.

With a highly active catalyst motif in hand, we next investigated the tolerance of our catalyst system to a variety of synthetically useful directing groups (Scheme 1.37). As observed with the Boc- protected glycine derivatives, it was gratifying to note catalyst **86a** was remarkably tolerant of the larger ester group, with a high incorporation of 89% observed for Ac-Gly-O^{t}Bu **3**. Cbz- also afforded high levels of labelling at the glycine methylene, however, deuterium incorporation into the benzylic position of the protecting group was also observed in **D147b** and **D178**. Whilst this protecting group may not be preferred for α-selective labelling of amino acid residues, if the chemist requires high levels of isotopic incorporation, the advantage of this protecting group becomes apparent. Lastly, common amino acid protecting group Fmoc- was also well tolerated, with an impressive 80% incorporation when used in combination with the larger ester group **D179**.

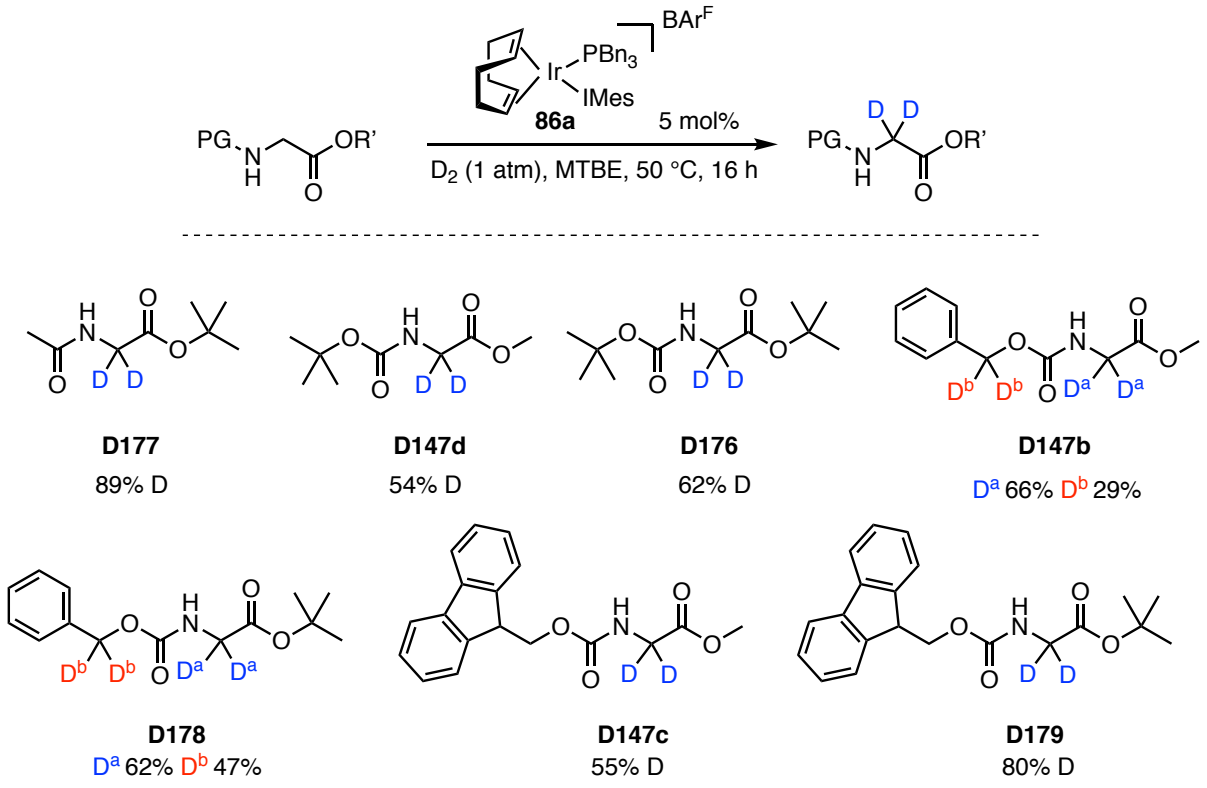

Scheme 1.37

The above results show an impressive versatility of catalyst **86a** and the chosen conditions to a wide variety of common amino acid protecting groups. This is an imperative characteristic when designing methodology aimed at use in an industrial setting, where a universal catalyst and conditions are highly preferred and sought after, and it was extremely pleasing that this could be achieved with the Kerr catalysts.

To investigate the transferability of our HIE process to tritium chemistry, collaborators at Merck performed the tritiation of Ac-Gly-OMe (Scheme 1.38).[74] The catalyst loading was increased to 12 mol%, a routine process when translating a deuteration protocol to tritium work. Owing to the hazardous nature of T_2 gas, the tritiation reactions are run at reduced pressure, resulting in a significantly more challenging process than a deuteration reaction. To our delight, a respectable specific activity of 10.7 Ci $mmol^{-1}$ was achieved under the conditions. This could perhaps be further improved by a move to a higher boiling solvent such as cyclopentyl methyl ether (CPME), as solvent evaporation was observed with MTBE at 50 °C under reduced pressure.

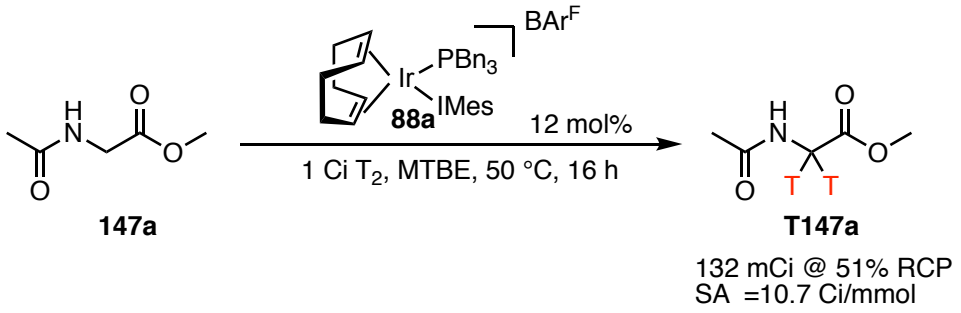

Scheme 1.38

1.3.2 Expansion of Deuterium Labelling to Tertiary Amino Acids

Following our success with glycine derivatives, we next turned our attention to the more challenging tertiary amino acid residues. Under the premise that the methine position would be significantly more challenging to activate compared to the methylene position in glycine,

it was deemed appropriate to conduct a full catalyst screen for chosen model substrate Ac-Ala-OMe **148**. Despite the surprising lack of activity of the chelated catalyst systems with Ac-Gly-OMe **147a**, their activity was also tested in the activation of a more sterically congested C-H bond (Scheme 1.39). Under our optimised conditions, it was discouraging to find Ac-Ala-OMe **148** afforded a mere 15% deuterium incorporation with the previously most active complex **86a**. Across the suite of catalysts, both monodentate and bidentate, the levelling of isotopic enrichment achieved was extremely poor, with the highest incorporation obtained only 23% (complex **86e**).

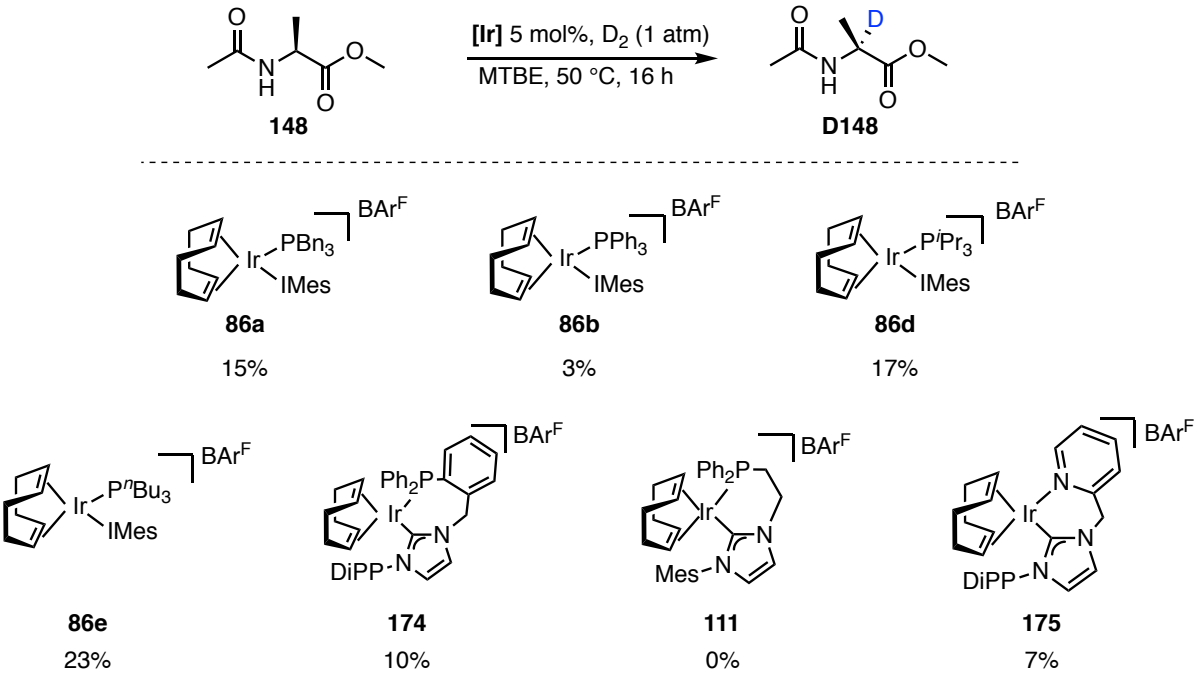

Scheme 1.39

The results generated to this point raised two main questions: firstly, why was there a severe lack of activity with chelating iridium(I) catalysts; and, secondly, why was there such a discrepancy in activity between Ac-Gly-OMe **147a** and Ac-Ala-OMe **148**. In an effort to understand these issues, we turned to DFT calculations. To address the difference in activity between monodentate and bidentate complexes, key intermediates in the catalytic cycle were investigated, employing Ac-Gly-OMe **147a** as the substrate. From the bis solvated active complex **180** (Scheme 1.40), it is known from previous work in Ir(I) catalysed HIE that substrate coordination should afford agostically-bound substrate complex **181**. This

intermediate leads to productive labelling reactivity through C-H activation. It was hypothesised, however, that for these amino acid substrates, coordination of a second carbonyl group from the ester functionality, forming a 7 membered chelate, could lead to an unfavourable "bis-carbonyl" bound species **182**. This is a catalytically inactive, off-cycle species, which would limit the amount of agostically-bound substrate in solution, thereby impeding desired reactivity. It was proposed that the relative binding energies for the substrate in each of these modes could be significantly different between catalyst classes.

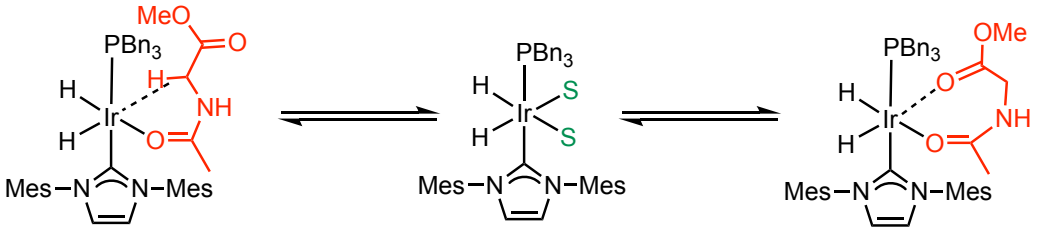

181 - agostically bound substrate
catalytically active

182 - bis-carbonyl bound substrate
catalytically inactive

Scheme 1.40

In order to support this hypothesis *in silico*, we calculated the binding energy of the substrate through both modes (agostically bound and bis-carbonyl bound) to a monodentate and bidentate catalyst, respectively. The energy associated with binding for each geometry was calculated using the basis set superposition error (BSSE) counterpoise method.[75] In addition, the Gibbs free energy (ΔG_{rel}) was also calculated for each structure. It can be seen from Scheme 1.41 that for the monodentate catalyst system, complex **181**, where the substrate is agostically bound, is energetically more favourable by 2.9 kcal mol^{-1}. In addition, this mode of binding is more favourable in terms of binding energy (E_{bind}) by around 1.2 kcal mol^{-1}. This suggests that the equilibrium will favour the agostically bound substrate, therefore allowing the productive C-H activation step to occur, leading to high levels of labelling. This is indeed confirmed by what we observe experimentally for this catalyst and substrate combination (incorporations of 92%). For the chelated catalyst systems, the situation is entirely different. The bis-carbonyl bound substrate complex **184** is inherently more stable in terms of ΔG_{rel}, with a large difference of 10.4 kcal mol^{-1}. Examination of the E_{bind} highlights

that the complex where the substrate is bound through both carbonyls (**184**) is a stronger binder to iridium than the agostically bound substrate **183** by an excess of 10 kcal mol^{-1}. An E_{bind} value of -46.6 kcal mol^{-1} is extremely strong, approaching the strength of binding for acetonitrile, which irreversibly binds to the iridium centre and is often practically used to inhibit the catalytic cycle at the end of a reaction. It is therefore no great surprise that the levels of incorporation are extremely low for this complex, as this will be by far the major species in solution, limiting the amount of agostically bound substrate and therefore inhibiting productive C-H activation. The chelated catalysts are significantly more 'open' around the metal centre and so appear to have ample space to accommodate the chelate of the bis-carbonyl bound substrate.

Monodentate catalyst system:

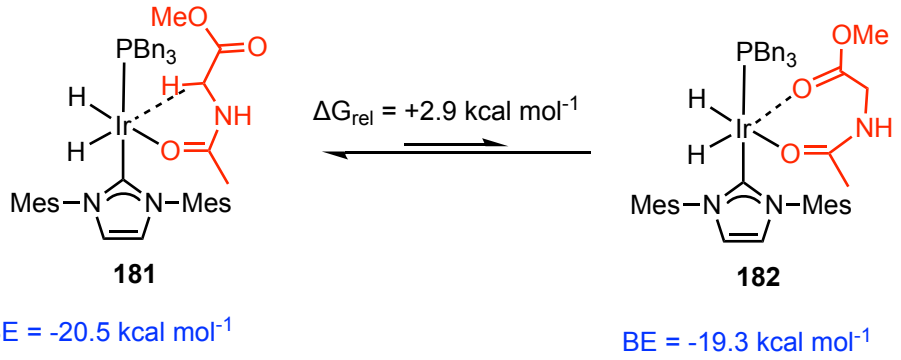

181 BE = -20.5 kcal mol^{-1}

182 BE = -19.3 kcal mol^{-1}

Bidentate catalyst system:

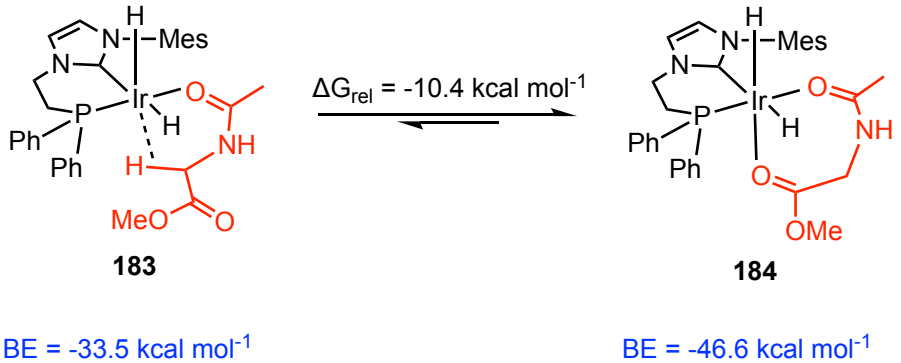

183 BE = -33.5 kcal mol^{-1}

184 BE = -46.6 kcal mol^{-1}

Scheme 1.41

Based on our observations, we proposed that if the groups on the *N* and *C* terminus were made large enough, a significant steric clash could be induced between ligand and substrate in the chelated catalyst system and therefore disfavour the formation of the chelate required to allow binding through both carbonyls. It was hoped that this would allow an increased concentration of the catalytically active, agostically bound substrate, which could undergo the C-H activation, allowing greater isotopic enrichment. To aid our proposal, experimental labelling reactions were carried out for Boc-Gly-O^{t}Bu **176** and compared to Ac-Gly-OMe **147a** which exhibited extremely poor levels of labelling with catalyst **111** (Scheme 1.42). To our delight, a significant increase was observed from 10% with Ac-Gly-OMe **147a** to 45% with Boc-Gly-O^{t}Bu **176**. Although this complex was still less active than the monodentate systems, it was pleasing to experimentally validate deeper understanding of this class of ligands gained from our DFT studies, and to determine the reason for lack of activity and offer a potential solution.

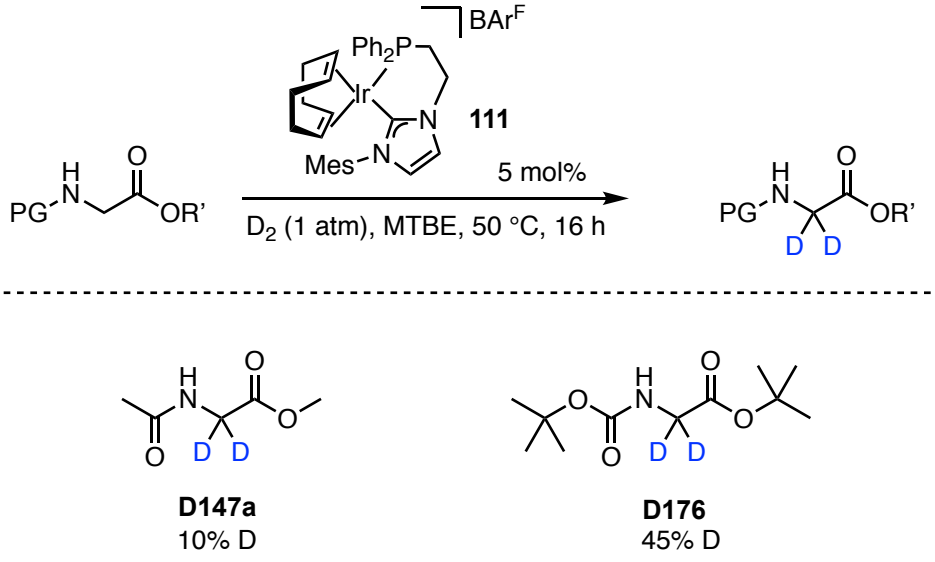

Scheme 1.42

To further deepen the relationship between our theoretical studies and experimental observations, the binding energies for Boc-Gly-O^{t}Bu **176** with catalyst **111** were then calculated. If our methods are to be in agreement, we would expect the bis-carbonyl bound intermediate **186** to be less strongly bound compared to Ac-Gly-OMe, Scheme 1.43.

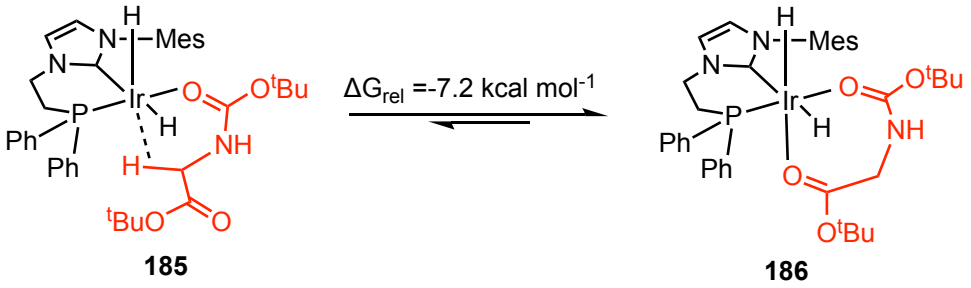

185 BE= -.28.1 kcal mol^{-1}

186 BE= -34.4 kcal mol^{-1}

Scheme 1.43

The DFT results clearly show that there is now much less of a difference in the strength of binding between the agostic complex **185** and the bis-carbonyl bound **186**, comparative to the Ac-Gly-OMe counterparts. Although the bis-carbonyl bound substrate remains a more efficient binding mode, this is now at a level where we would expect to see catalytic turnover by displacement of deuterated product by the reaction solvent. This agrees with the increase in labelling observed experimentally for this substrate.

We next sought to understand the difference in activity of our suite of catalysts between glycine and alanine. Our hypothesis was that, owing to the restricted rotation experienced with alanine compared to glycine, the unproductive bis-carbonyl bound chelate could be prevalent even with the bulky monodentate catalysts. This could offer some explanation as to why said complexes allow high incorporation with Ac-Gly-OMe **147a** but not with Ac-Ala-OMe **148**. Upon exposure to deuterium, complex **86a** loses the COD ligand *via* reduction, resulting in a coordinately unsaturated Ir species which can be stabilised by two molecules of solvent. Taking this as our lowest free energy (G_{rel}= 0 kcal mol^{-1}) species pre-activation, we evaluated the relative free energies and, indeed, binding energies, for both the agostically bound substrate **A** and the bis-carbonyl species **B**, as previously (Table 1.8). These parameters were investigated for Ac-Gly-OMe **147a**, Ac-Ala-OMe **148**, Boc-Gly-O^{t}Bu **176** and Boc-Ala-O^{t}Bu **187**. When considering the relative free energies for glycine analogues **147a** and **176**, the agostic complex **A** is approximately 3-5 kcal mol^{-1} more stable, suggesting this is a feasible intermediate in the reaction pathway, with the unproductive bis-carbonyl species **B** less favourable and therefore less likely to hinder the HIE process. On the other hand, with the alanine analogues, we observe more closely matched relative free energies of the agostic complex **A** and bis-carbonyl **B**, suggesting formation of these species may be

competitive, and the presence of bis-carbonyl **B** as a resting state could explain the drop in activity with the alanine substrates, in particular with Ac-Ala-OMe **148**. The energetic cost of the amino acid derivatives binding to the iridium centre (E_{bind}) was also calculated for each substrate through both plausible binding modes. For those substrates which display significant levels of deuterium incorporation (Ac-Gly-OMe **147a**, Boc-Gly-O^{t}Bu **176**) and in addition the sterically encumbered Boc-Ala-O^{t}Bu **187**, the binding energy of the agostic complex is more favourable compared with the unproductive bis-carbonyl species, allowing a productive HIE pathway to proceed. In sharp contrast, for Ac-Ala-OMe **148**, which shows low incorporation, the binding energy for the bis-carbonyl **B** is more favourable (-38.9 kcal mol^{-1}) compared to the agostic complex **A** (-27.3 kcal mol^{-1}). This suggests binding mode **B** could be the resting state in this case, therefore inhibiting the formation of the agostically bound substrate and subsequently hindering the HIE pathway.

Table 1.8

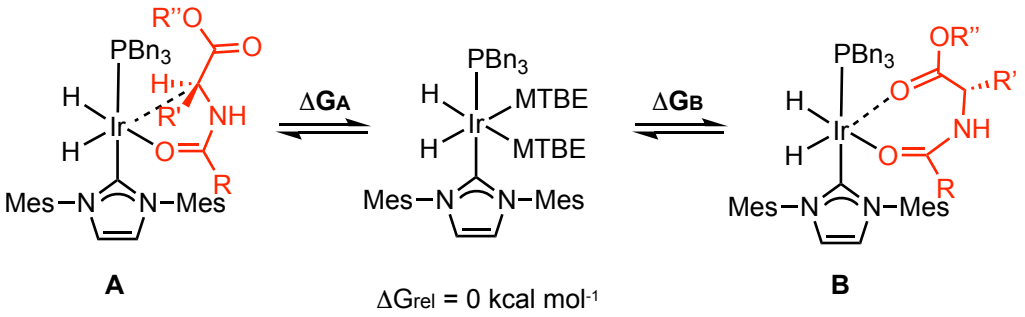

Entry	AA	ΔG_A (kcal mol^{-1})	ΔG_B (kcal mol^{-1})	ΔE_{bindA} (kcal mol^{-1})	ΔE_{bindB} (kcal mol^{-1})
1	Ac-Gly-OMe **147a**	-17.4	-14.5	-20.5	-19.2
2	Ac-Ala-OMe **148**	-14.6	-13.0	-27.3	-38.9
3	Boc-Gly-O^{t}Bu **176**	-22.7	-18.3	-23.2	-20.4
4	Boc-Ala-O^{t}Bu **187**	-13.3	-12.8	-16.8	-15.2

Following these findings, it was proposed to investigate the potential energy surfaces (PESs) for the C-H activation event for each of the four substrates discussed (Graph 1.2). Ac-Gly-OMe **147a**, which displays the highest deuterium incorporation (92% D), has an activation

energy of 25.7 kcal mol^{-1}, which suggests a feasible C-H activation event at 50 °C. The activation of Ac-Ala-OMe **148** is marginally higher in energy (+4.1 kcal mol^{-1}), and this suggests that although C-H activation seems a feasible process at 50 °C, the deuteration of this substrate is governed by the energy of binding. In comparison, although the energy for C-H activation of Boc-Ala-O^{t}Bu **187** is higher still at 32.6 kcal mol^{-1} (remaining a feasible reaction barrier at 50 °C), the favourable agostic binding of the substrate compared to the unproductive bis-chelate results in successful deuteration of this substrate.

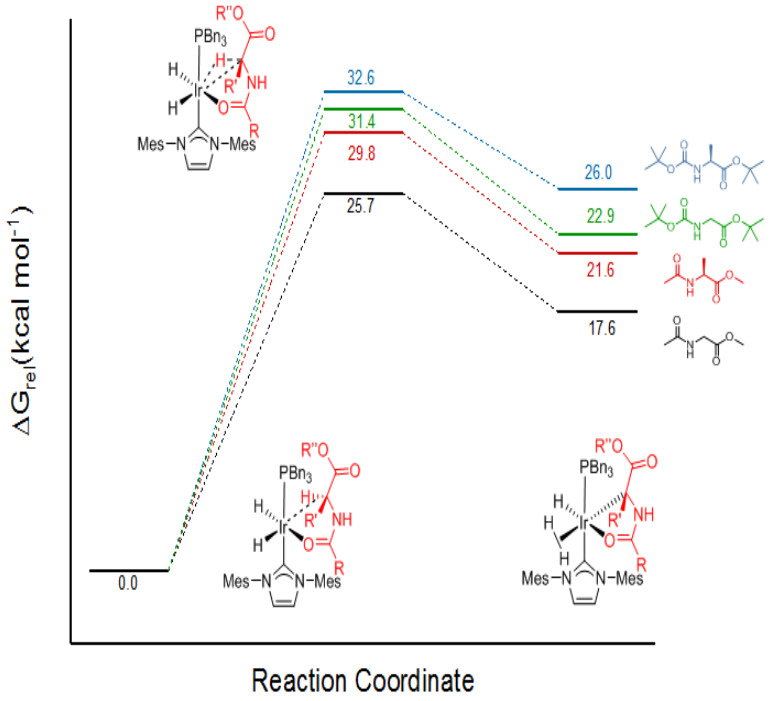

Graph 1.2

As previously, we wanted to affirm the synergy between our theoretical and experimental results, and validate our DFT findings. Based on the results of our calculations, Boc-Ala-O^{t}Bu **187** should label similarly to its glycine derivative. The labelling reaction was therefore carried out under the conditions reported previously. Gratifyingly, Boc-Ala-O^{t}Bu **187** was isotopically labelled to almost identical levels as its glycine analogue (62% D). This was a landmark result within the project, and validates the combined theoretical and experimental approach taken in our investigations.

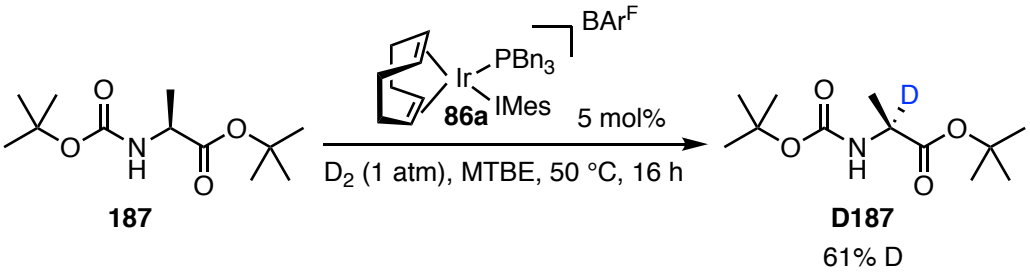

Scheme 1.44

Whilst the tertiary amino acid residues appear to be more challenging than the secondary amino acid glycine, through judicious choice of protecting group, labelling of such residues using our Ir(I) catalysts was enabled. Additionally, the use of Boc- protecting groups was advantageous as these groups are commonly utilised within amino acid chemistry and are set up for further synthetic manipulation. To this end, for substrate **D187**, universal deprotection under acidic conditions would allow access to the deuterated parent amino acid in one step, if so desired. Importantly for tertiary amino acid residues, complete stereo-retention was observed under the labelling conditions. This attribute it somewhat expected when considering the catalytic cycle, where stereospecific C-H insertion and C-D formation occur.

1.3.3 Optimisation of Tertiary Amino Acid Labelling

Based on the encouraging results with Boc-Ala-O^{t}Bu **187** and complex **86a**, we wanted to explore the opportunity to optimise the reaction conditions and enhance the level of isotopic labelling further. Whilst the choice of the protecting groups for this substrate allowed some steric control over the productive and unproductive binding modes, we considered more general improvement by altering the electronics of the catalyst system. Having screened a variety of different phosphine ligands previously, we wanted turned our attention towards the NHC ligand. Specifically, increasing the σ-donating ability of the NHC would afford enhanced electron density at the metal centre. This is turn could disfavour the binding of a second carbonyl, and instead encourage formation of the agostically bound substrate, where the now less Lewis acidic iridium is more likely to donate electron density into the C-H bond of interest. To explore this, an NHC which is more σ-donating (IMes^{Me}) and one which is

slightly less σ-donating (IPr) compared to IMes were synthesised (procedures can be found in the experimental section) and investigated in the labelling of Boc-Ala-O^{t}Bu **187** (Scheme 1.45). %V_{bur} were also calculated for the complexes to highlight the steric impact of the NHC on the metal centre. Pleasingly, a move to the more electron-rich IMes^{Me} NHC in complex **188** allowed a significant enhancement in the level of incorporation to 84%. In contrast, the less electron-rich IPr ligand in **189** resulted in poorer levels of incorporation. These results confirm the hypothesis that by manipulating the electronics of the catalyst, we could disfavour the formation of the unproductive bis-carbonyl species. This being said, it cannot be deduced that this is a purely electronic factor alone. Whilst IMes and IMes^{Me} show similar %V_{bur}, and so the difference in activity of **86a** and **188** appears to be purely an electronic bias, the larger %V_{bur} values of IPr in **189** could potentially hamper the reactivity of this complex.

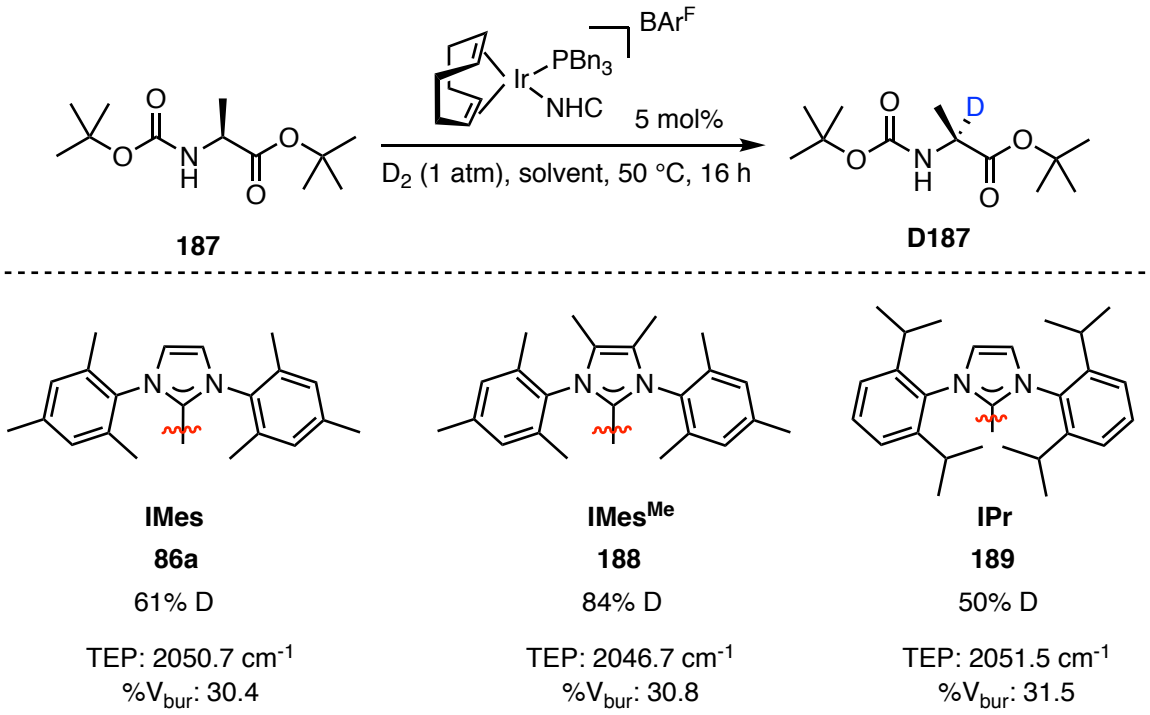

Scheme 1.45

With an improved NHC ligand in hand, further optimisation was undertaken using a Design of Experiments (DoE) approach. A two-level, 3-factor design was used to investigate the effects of catalyst loading (5-10 mol%), time (4-10 h) and concentration (0.05-0.2 M). This

technique minimises the number of experiments necessary while maximizing the chemical space screened within the optimisation. The optimised conditions are shown in Scheme 1.46. Increasing the catalyst loading modestly to 7.5 mol% allows for excellent levels of incorporation at 90%. If this loading is enhanced even further, incorporations are pushed to an outstanding 93%.

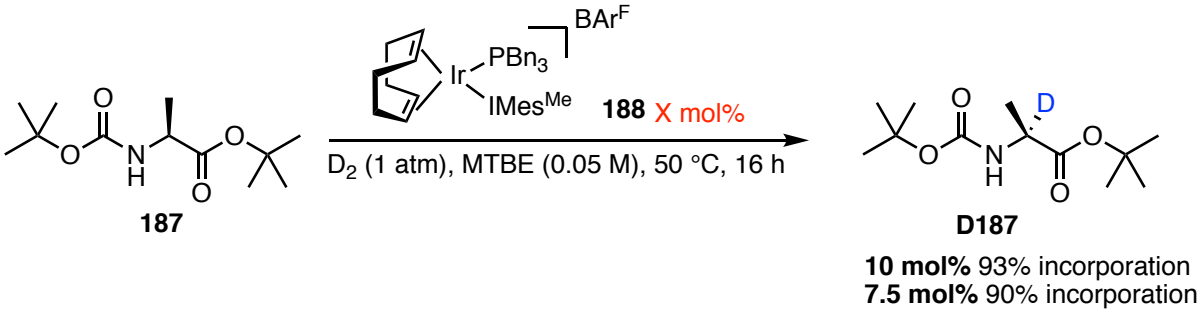

Scheme 1.46

The statistical software utilised allows generation of a visual representation depicting the significance of each factor in the form of a half-normal plot (Graph 1.3). The most significant factors are presented furthermost from the line, and the least significant factors reside closest. Not only does the half-normal show dependencies on singular factors, two-factor interactions are also considered. It can be seen from the graph that solvent volume (i.e. concentration) is the most important factor for the HIE of our amino acid substrate, with catalyst loading also being an important factor. Whilst singularly time does not seem important, the combination of time and concentration is crucial. In addition, there is an importance on the two factor interaction between catalyst loading and concentration.

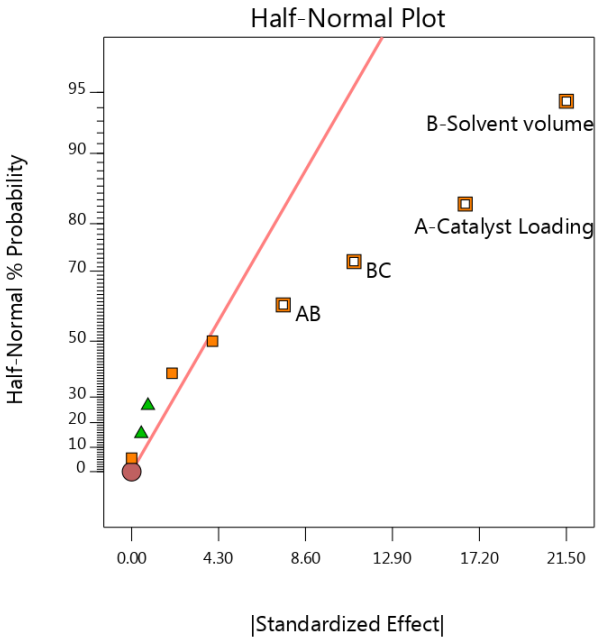

Graph 1.3

Since our DoE had demonstrated that concentration of solvent was extremely important, the reaction was then repeated with a variety of different solvents to investigate the compatibility of various solvent classes (Graph 1.4). Higher boiling point ethereal solvent CPME was compatible with this process, although a drop to 57% incorporation was observed. This solvent could be useful for tritiation procedures where a reduced pressure environment is used. Increase of catalyst loading or a subtle increase in temperature may allow an increase in incorporation observed in this case. Acetate solvents were somewhat compatible although incorporation was low. Chlorinated solvents such as DCE and PhCl also allowed incorporation but only to a small extent. It was therefore abundantly clear from our solvent screen that the most suitable solvent class for this process was ethereal solvents, with MTBE remaining the optimal solvent.

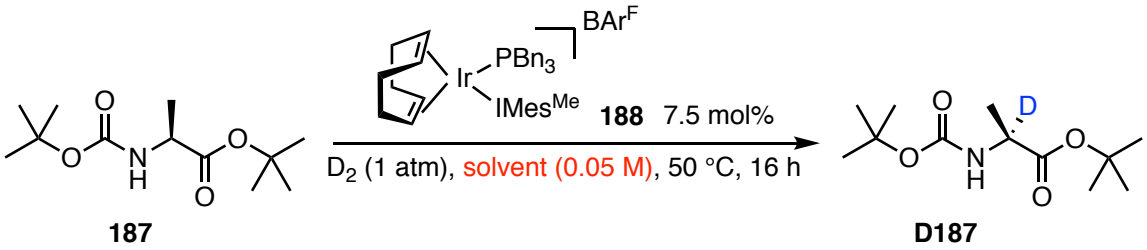

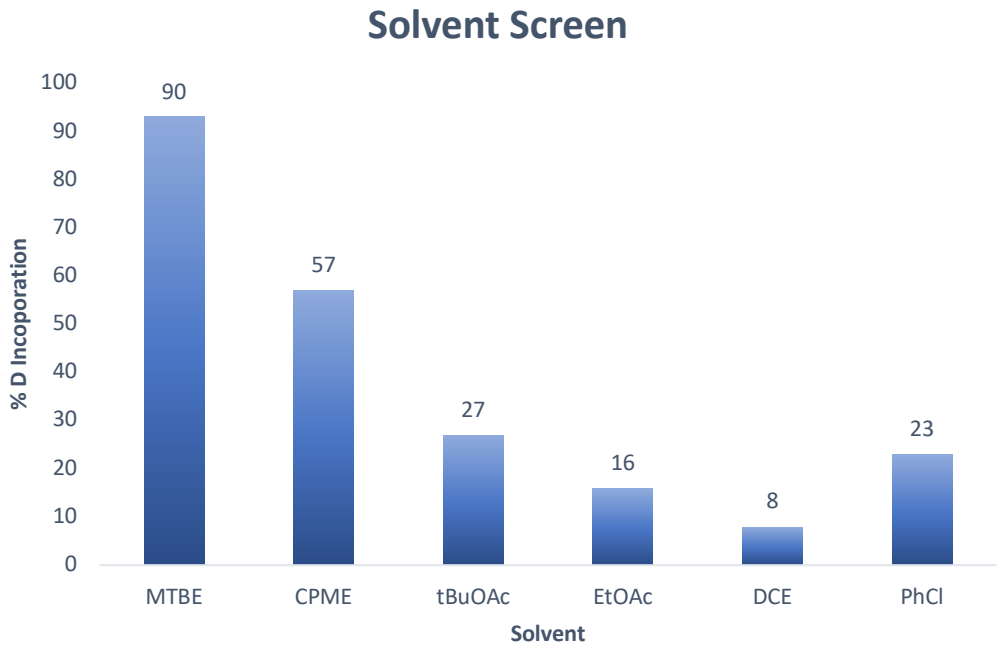

Graph 1.4

1.3.4 Tertiary Amino Acid Labelling Substrate Scope

At this stage, with optimal conditions derived for the labelling of tertiary amino acids we concentrated our efforts on expanding the scope of our HIE process, Scheme 1.47. Revisiting Ac-Ala-OMe **148** with the newly developed catalyst **188** and optimised conditions, it was encouraging to observe 85% deuterium incorporation at the methine position. Additionally, similarly to glycine derivatives **D147b** and **D179**, Fmoc- was also a competent directing group for the labelling of alanine **D190**, with an increase to 73% deuterium incorporation with the slightly higher catalyst loading of 10 mol %. Moving to amino acids with enhanced steric bulk at the labelling centre, such as Boc-Val-O^{t}Bu **D191** and Boc-Leu-O^{t}Bu **D192**, an

increase in catalyst loading to 10 mol% afforded high levels of labelling (91% in both cases). Interestingly, the isoleucine analogue, that is Boc-Ile-O^{t}Bu **D193**, afforded excellent deuterium incorporations of 94% at the lower catalyst loading of 7.5 mol%. Amino acids bearing heteroatoms, such as serine, could be protected as the *tert*-butyl ether, allowing 92% incorporation (10 mol% loading) of Boc-Ser(^{t}Bu)-O^{t}Bu **D194**. Proline based substrate **D195** labelled well under the reaction conditions, although disappointingly, highest levels of labelling were observed on the carbamate directing group. Essential amino acid phenylalanine could also be successfully labelled under our conditions. Unfortunately, however, use of a Boc- directing group in this case was unsuccessful, regardless of the ester size, suggesting sp^2 substitution at this position is not well tolerated. In an attempt to overcome this issue, the smaller, more electron-rich acyl group was utilised as the directing group in combination with a methyl ester, Ac-Phe-OMe **D150**. To our delight, 74% deuterium incorporation was observed for this substrate at 10 mol% catalyst loading. In contrast to other amino acid substrates investigated, incorporation at the acyl position was also observed. Ac-Trp-OMe **D196** was also well tolerated under the conditions developed with no indole labelling observed. Low incorporations of 36% were observed when the free NH on the indole was utilised. A tosyl protecting group of the indole NH in **D197** allowed an increased incorporation to 71%. Extremely pleasing, was the tolerance of our catalyst system to sulfur-containing amino acid Ac-Met-OMe **D198** (59% D).

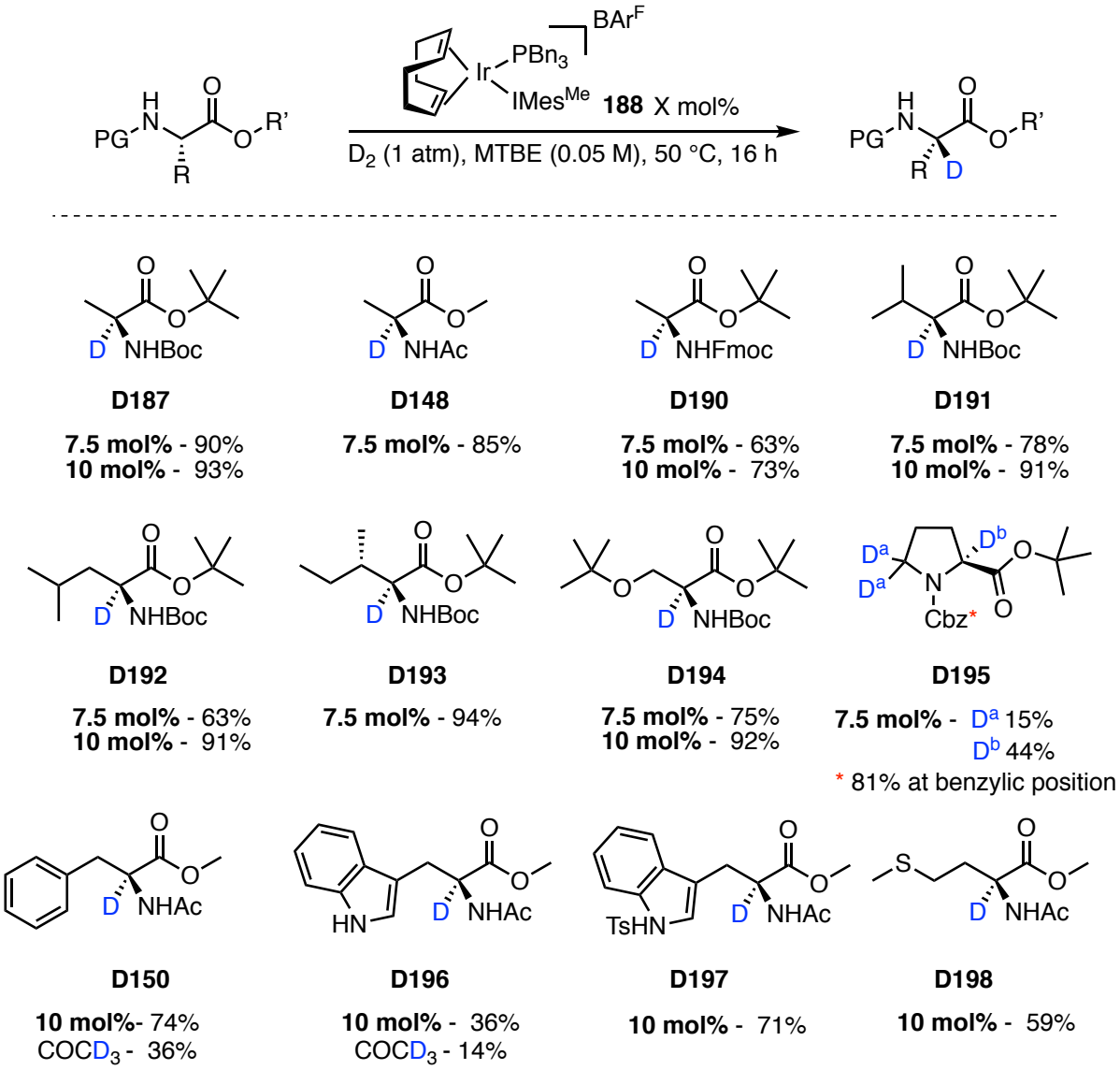

Scheme 1.47

1.3.5 Limitation of Current Catalyst System

Whilst our novel Ir(I) catalyst allows an unprecedented array of amino acid residues to be labelled, and tolerates a selection of commonly used protecting groups, there remains some limitations. Under our current conditions, the isotopic labelling of aromatic amino acid residues is highly dependent on the protecting groups chosen. Whilst small protecting groups like acetyl allow successful deuteration, a move to a synthetically more tractable directing

group such as Boc- completely diminishes reactivity in the case of phenylalanine and tryptophan (Scheme 1.48).

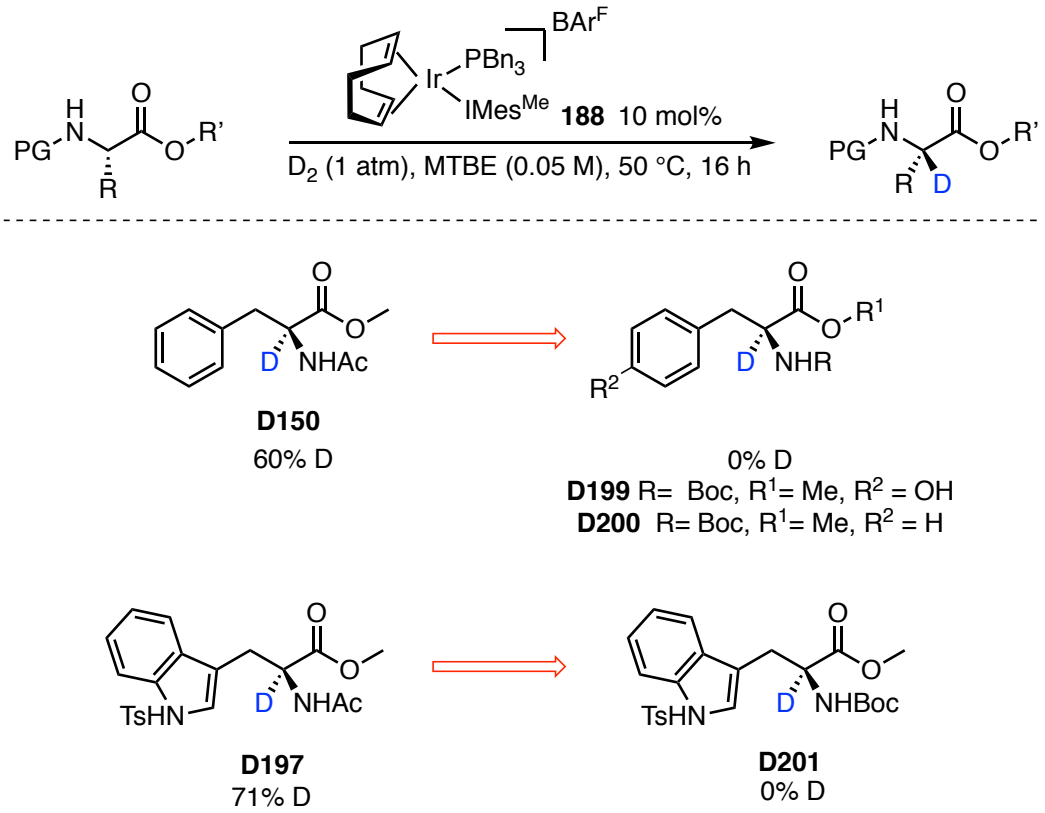

Scheme 1.48

In addition to the issues observed with these sp^2 substituted amino acids, and with the anticipation that Lewis basic sulfur could irreversibly bind to our metal complex, we designed substrates which would disfavour this. To this end, a range of protecting groups on sulfur (R^1) were sought (Figure 1.30).

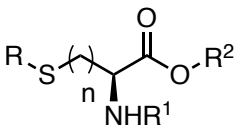

Figure 1.30

Akin to sp^2 substituted amino acids, methionine could not be labelled if protected with a Boc-group **D202** (Scheme 1.49). Whilst initially this was somewhat expected due to the Lewis basic nature of the sulfur atom, which we envisaged could cause problems for our HIE reactions, the successful labelling of Ac-Met-OMe **D198** led us to consider that the problem with our sulfur containing amino acids was not because of sulfur coordination, but instead another factor akin to that involved in the poor labelling of aromatic amino acids. There are few iridium catalysed methods which can tolerate sulfur functionality such as those shown, and so this was considered an important class of molecules to engage with.

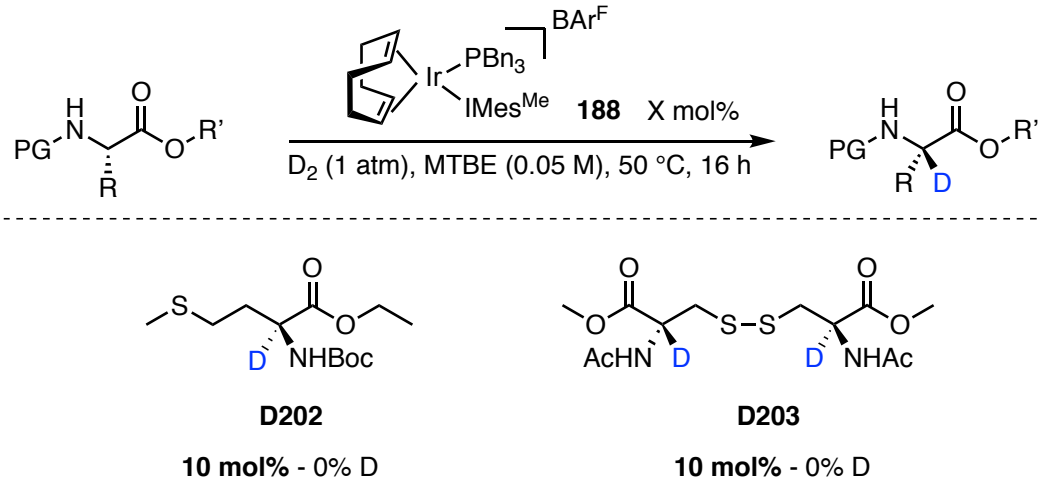

Scheme 1.49

Although our catalyst system allowed deuteration of these challenging amino acids with careful choice of directing group, we deemed it important to better understand the negligible activity observed. On the premise of being able to ascertain the reason for no activity, we were motivated to finding a catalyst motif that could afford universal labelling of these specific amino acid residues, and accommodate a variety of the more common protecting groups, to ensure an industrially applicable and useful methodology was achieved. Progress in this area will be discussed in Chapter 3.

1.3.6 Mixed Solvent Systems for Amino Acid Labelling

MTBE has been the standard solvent utilised within the amino acid labelling studies throughout the project thus far and has previously shown wide utility in the Kerr group in a variety of HIE processes. MTBE has a few key advantages: MTBE can be dissociated by many substrate classes (required within the catalytic cycle); it is a strong enough binder to iridium to stabilise the catalyst resting state; and MTBE is considered a green solvent, with industry employing it in several process scale reactions. Unfortunately, the solubility of amino acids and peptides is not optimal or indeed, for the latter, very good at all in non-polar ethereal solvents such as MTBE. At the outset of this project, we wanted to design a process which could label small peptide molecules as well as single amino acid residues. We felt at this stage of the project it was important to investigate solvents more suitable for peptidic substrates. Whilst solvents such as DMF and water are widely utilised within peptide chemistry, it was recognized that these would be far too Lewis basic to be compatible with our Ir(I) complexes. As a result, our attention turned to chloroform and alcoholic solvents. Previously within the Kerr group, alcohol solvents have been employed with substrates for sp^3 labelling reactions (Scheme 1.50).[55] Although bulky alcohols were required to observe good levels of labelling in this substrate, it was pleasing to see moderate incorporation even in methanol.

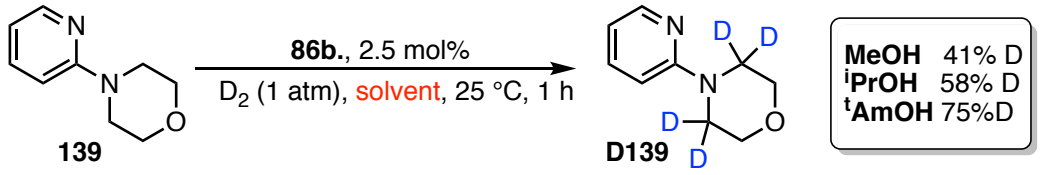

Scheme 1.50

To facilitate investigation of more suitable options for application in HIE of peptide molecules, we sought to conduct a solvent screen for, initially, the labelling of Ac-Gly-OMe **147a** under the standard developed conditions (Scheme 1.51). This would allow us to bench mark the alternative solvents against MTBE in a system we know labels very effectively. The results show that for this small amino acid substrate, MTBE remained the best solvent. However, it was encouraging to observe high levels of 76% incorporation were also achieved

in chloroform, a much more polar solvent and for more complex peptides, one that could allow better solubility and subsequently enhanced levels of incorporation. It was disappointing to note that all labelling was inhibited in each of the alcohol solvents investigated. The discrepancy in reactivity in alcoholic solvents between amino acid substrates and the labelling of previous sp^3 systems could be attributed to the decreased Lewis basicity of the acyl directing group comparative to that of the pyridine (Scheme 1.50). Key displacement of the alcoholic solvent molecules by amino acid substrates may not be a feasible process, thereby hampering the catalytic cycle for HIE.

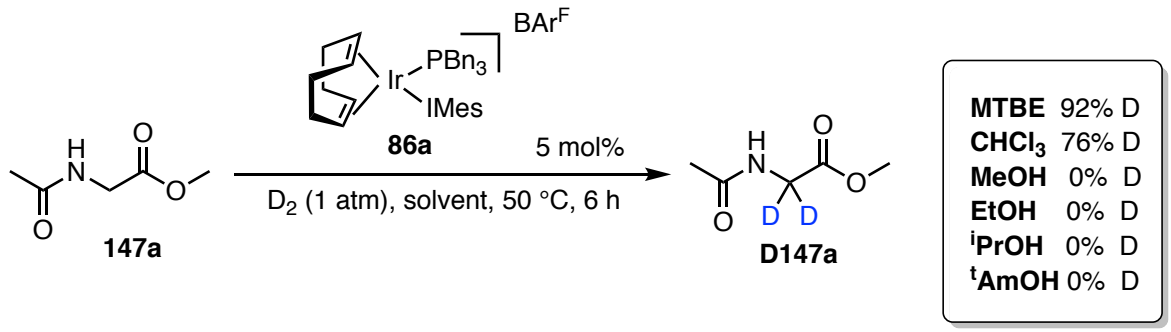

Scheme 1.51

Whilst purely alcoholic solvent systems were not tolerated in the HIE of Ac-Gly-OMe **147a**, it was hypothesised that a mixed solvent system may allow deuterium incorporation. Although not required for small amino acid substrates like **147a**, the investigation of mixed systems was deemed important for larger, more challenging peptide substrates. Due to the high activity observed with labelling of **147a** in MTBE, investigation of MTBE/alcohol mixtures were conducted. To initiate our studies, the sterically hindered, and therefore weakest binding alcohol, ^{t}AmOH was investigated as the co-solvent (Graph 1.5). Various percentages of ^{t}AmOH in MTBE were investigated, ranging from 0.4% to 50%. Very small amounts of alcohol in MTBE (~1%) hinder the labelling significantly, with a drop from 92% in pure MTBE to a mere 50% in the mixed solvent system. However, as we move to a higher percentage of alcoholic solvent (10-30%), we start to observe much less detriment to the labelling process, with incorporations of 70-80% observed. Although the effects of varying the alcohol levels within the mixed system is not fully understood, the trend observed could be attributed to a fine balance between the improvement of substrate solubility in alcoholic solvents, and indeed, the deleterious effect of having high percentages of alcohol which can bind strongly to the iridium metal centre, hindering the catalytic cycle. There appears to be a

'sweet spot' in alcohol concentration as a move to 40-50% alcohol in MTBE results in a gradual decline in the levels of labelling observed.

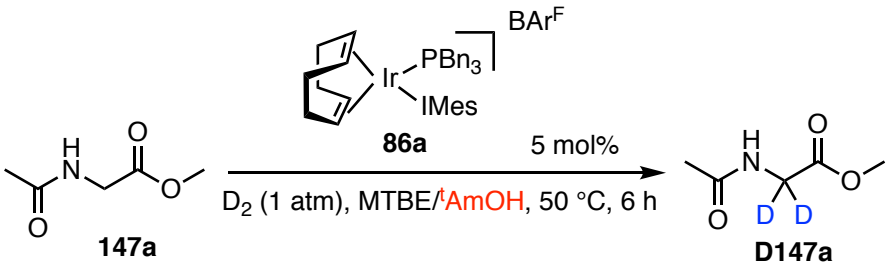

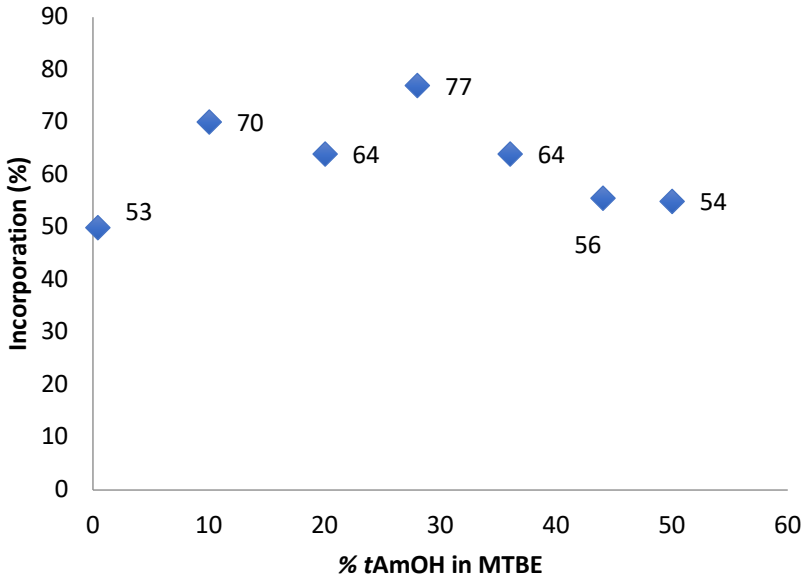

Graph 1.5

With 30% of ^{t}AmOH in MTBE appearing to be the optimal co-solvent system studied thus far, various alcohols were investigated at 30% in MTBE (Graph 1.6). As expected, sterically encumbered ^{t}AmOH /MTBE mixtures provided the best labelling results. When moving to alcohols with less steric bulk and enhanced Lewis basicity such as *iso*-propanol and ethanol, the labelling decreased from 77% to approximately 30%. Moving to the strongly coordinating solvent methanol led to even poorer levels of incorporation. Although the labelling results were low for some of the MTBE/alcohol mixtures, it was pleasing to see that the HIE process was not completely hindered upon addition of the alcohol. Although pure MTBE allows much better results for the Ac-Gly-OMe substrate, the addition of alcohol solvent could allow

enhanced incorporation in substrates which are scarcely soluble in ethereal solvents. A focus on mixed solvent systems in HIE processes has been extremely limited within the Kerr group to date and so it was very encouraging to note that these could be applicable in the future, not only within amino acid and peptide labelling but also other areas of the research.

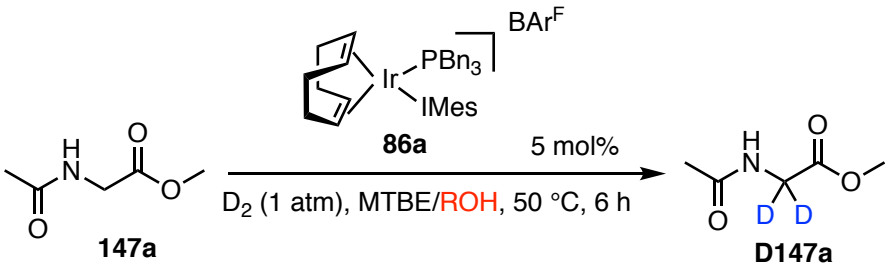

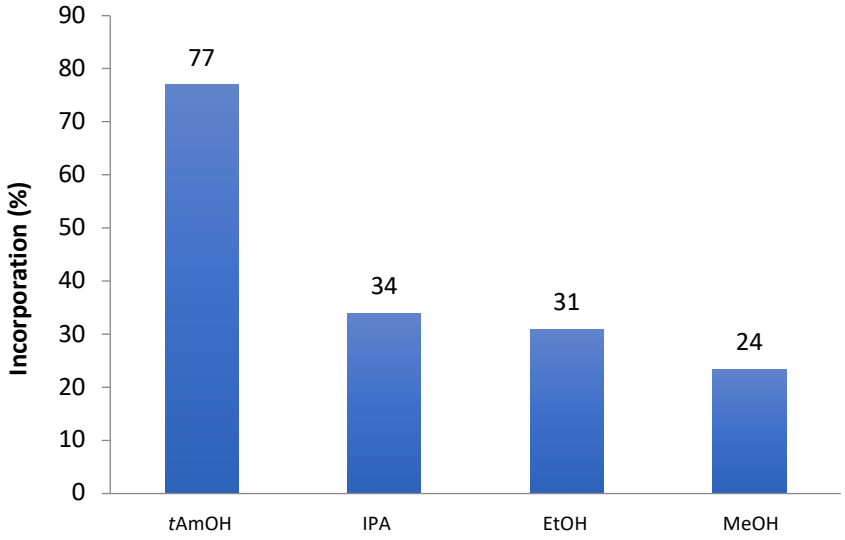

Graph 1.6

In a further extension of our mixed solvents systems, and to align our labelling solvent better with those co-solvent systems employed within peptide chemistry, chloroform/alcohol mixtures were investigated (Graph 1.7) Chloroform/*iso*-propanol solutions are routinely utilised to solubilise peptides and so it was considered an important co-solvent system to investigate. Small volumes of *iso*-propanol (20:1 $CHCl_3$/^{i}PrOH) were well tolerated in the reaction, however labelling levels started to decrease when moving to larger volumes (10:1, 4:1 of $CHCl_3$/^{i}PrOH). Mixtures of both 20:1 and 10:1 chloroform/^{t}AmOH afforded incorporations of ~65%.

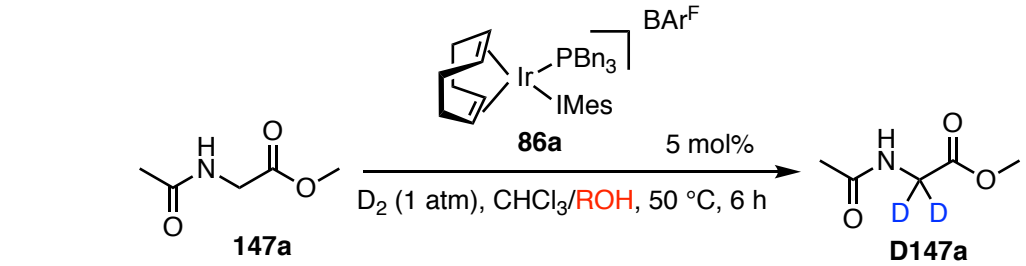

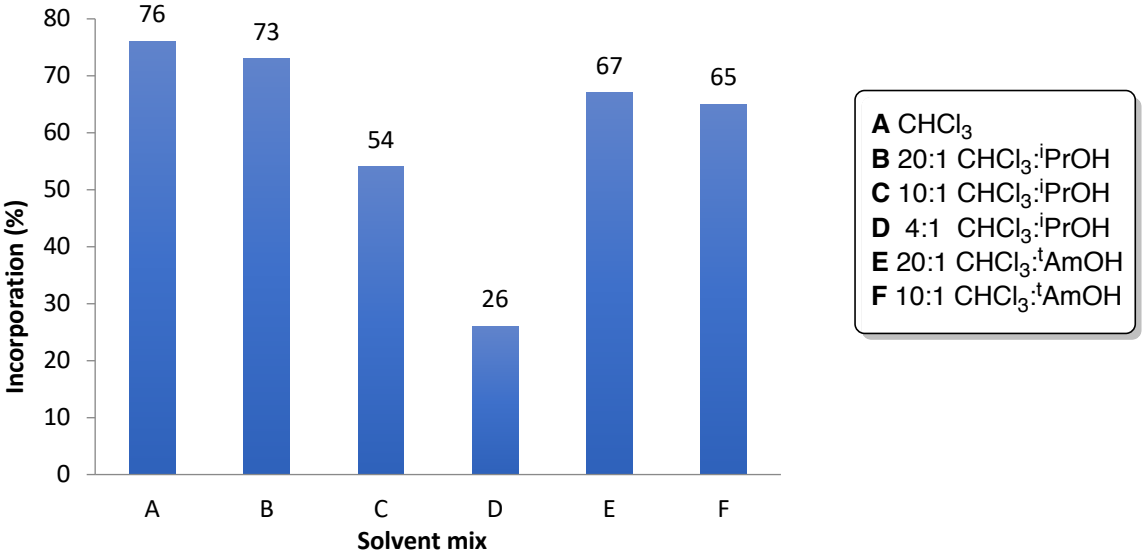

Graph 1.7

Whilst labelling in alcoholic solvents alone is unsuccessful with an acyl directing group, it is promising to see that large volumes of alcohol in a mixed solvent system with MTBE or chloroform are well tolerated, with good levels of labelling being observed. Although for the more simple amino acid substrates such as Ac-Gly-OMe **147a**, the incorporations are lowered with the introduction of alcohols, this is a very valuable proof of concept for future peptide work, where substrates may require addition of the more polar alcohol solvents to achieve solubility and therefore labelling.

1.4 Conclusions

To conclude this chapter, we have developed a mild and highly selective process for the labelling of α-amino acids. Utilising both previously established and novel Ir(I) catalysts we have developed a mild process which is extremely tolerant of a range of protecting groups, allowing high deuterium incorporations across the amino acid substrates. Pleasingly our HIE method allows complete stereo-retention at the α-centre.

Firstly, we screened a range of previously established and novel Ir(I) catalysts (both monodentate and bidentate complexes) and assessed their activity in the labelling of our model substrate Ac-Gly-OMe (Scheme 1.52). Pleasingly, a range of monodentate complexes were active and the use of DFT and $\%V_{bur}$ allowed careful analysis of the most suitable complex for substrate expansion. Several glycine derivatives were then labelled to high levels and a remarkable tolerance to a range of commonly used protecting groups was observed. To our delight, our deuteration protocol could be successfully transferred to tritiation procedures, with appreciable levels of tritiated Ac-Gly-OMe generated.

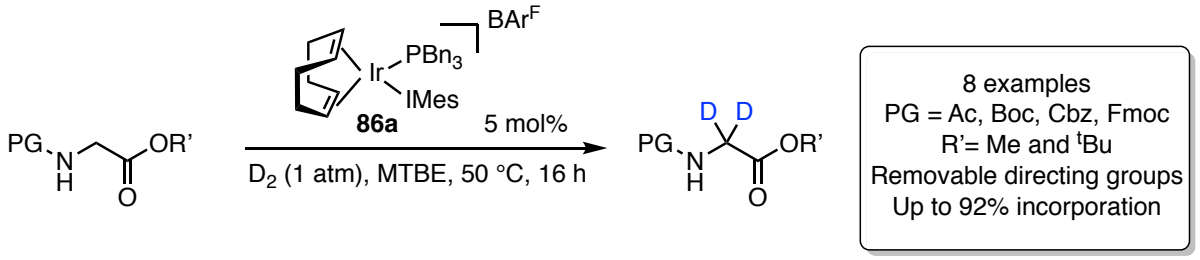

Scheme 1.52

Next, we wanted to expand our amino acid labelling methodology to include tertiary amino acid substrates. Using Ac-Ala-OMe as a probe for this, it was initially disappointing to observe a complete lack of reactivity for both monodentate and bidentate iridium(I) complexes. To compliment our experimental observations, and in hope to better understand both the lack of activity of Ir(I) bidentate complexes and the difference in activity observed with glycine and alanine, DFT calculations were utilised. This study uncovered a potential off

cycle unproductive binding mode of substrate to catalyst, and its likelihood of formation was significantly more pronounced within bidentate catalyst systems. Although for glycine derivatives this unproductive bis-carbonyl bound resting state did not appear to be an issue for monodentate complexes (both theoretically and experimentally), formation of this intermediate seemed plausible for Ac-Ala-OMe even within the sterically encumbered catalysts (Scheme 1.53). Excellent agreement between experimental and theoretical observations was found.

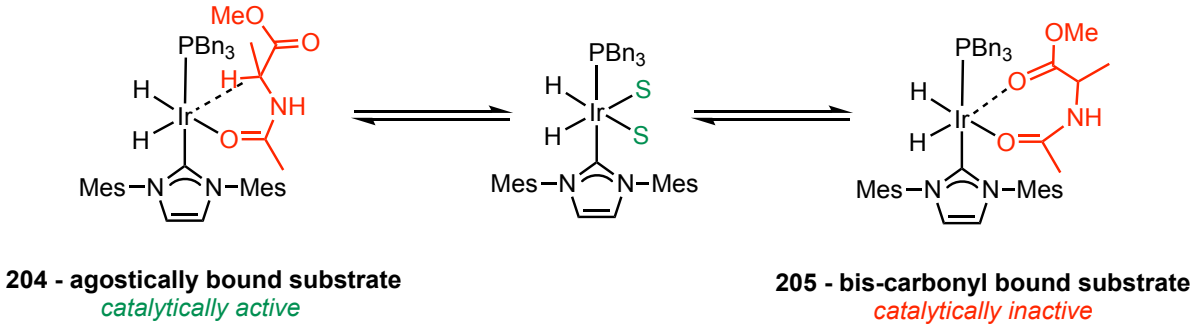

204 - agostically bound substrate
catalytically active

205 - bis-carbonyl bound substrate
catalytically inactive

Scheme 1.53

As a direct result of our DFT studies, uncovering the unproductive off cycle species, manipulation of the protecting groups utilised with alanine derivatives allowed successful deuteration of this residue (Scheme 1.54). To our delight, the optimal protecting groups were very synthetically tractable, allowing for a user friendly method to achieving deuterated amino acids.

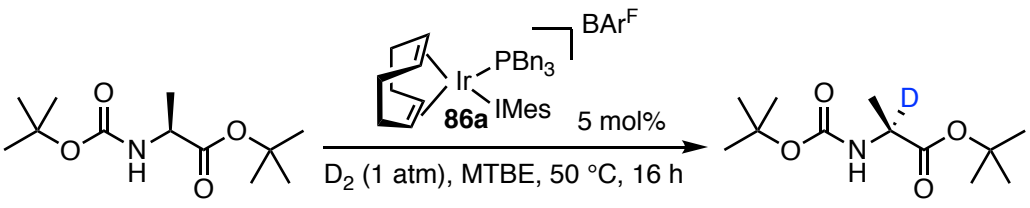

187

D187
61% D

Scheme 1.54

Further investigation of the ligand set, with a focus on the NHC, allowed development of novel catalyst **188** (Scheme 1.55). Optimisation through DoE and solvent screening afforded a mild and extremely efficient process for the labelling of tertiary amino acid residues.

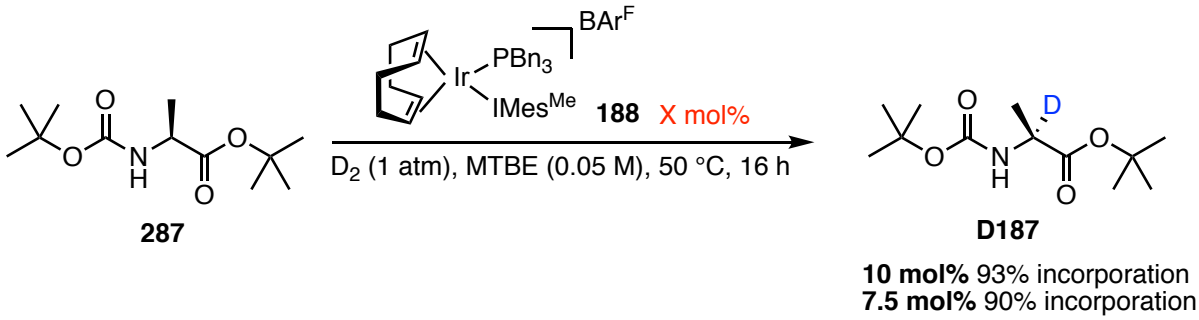

Scheme 1.55

Expansion of the substrate scope of the reaction highlighted the applicability and tolerance of the developed HIE process. Several natural α-amino acid residues were labelled to excellent levels of incorporation (up to 93%), Scheme 1.56. As with glycine analogues, a variety of common protecting groups were tolerated, showing an unprecedented substrate scope and applicability compared to previously reported methods in the area.

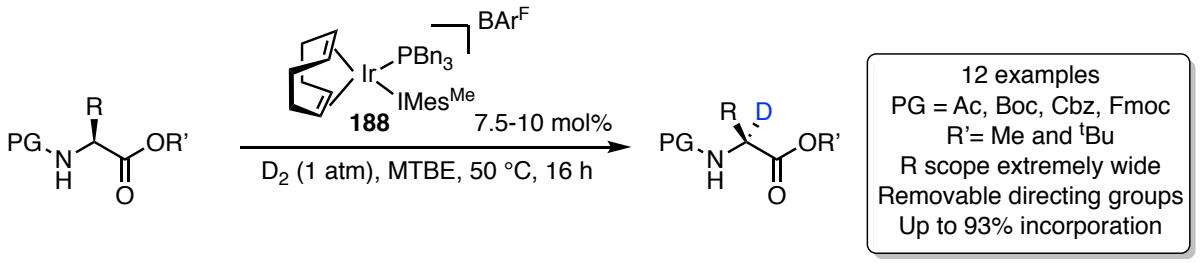

Scheme 1.56

Lastly, with the vision of expanding our HIE protocol to small peptide molecules, we wanted to investigate more suitable solvent systems for said substrates. As a benchmark we investigated the use of solvents more widely utilised within peptide chemistry in the deuterium labelling of our amino acid substrate Ac-Gly-OMe. Interestingly, although purely alcoholic systems were not well tolerated within the labelling reactions, co-solvent systems such as MTBE/ROH or $CHCl_3$ mixtures allowed high levels of incorporation in some cases.

Although MTBE remained optimal on its own for our amino acid substrates, this was an interesting proof of concept and a technique which when employed with less soluble peptidic substrates, could allow us access to a more efficient labelling protocol.

1.5 Experimental

1.5.1 General Information

All reagents were obtained from commercial suppliers (Alfa Aesar, Sigma Aldrich, Apollo Scientific, Fluorochem or Strem) and were used without further purification unless otherwise stated. If purification was required this was carried out using standard laboratory methods.[76] All glassware was flame-dried and cooled under a stream of nitrogen, unless otherwise stated.

Tetrahydrofuran was purified by heating to reflux over sodium wire, employing benzophenone ketyl as an indicator, before being distilled under a nitrogen atmosphere. All other solvents were distilled over calcium hydride under an argon atmosphere and stored over molecular sieves. Petroleum ether refers to ether with a boiling point range of 40-60°C.

Thin layer chromatography was carried out using Camlab silica plates coated with fluorescent indicator UV254. Plates were analysed using a Mineralight UVGL-25 lamp, or developed using vanillin or $KMnO_4$ solution.

Flash column chromatography was carried out using Prolab silica gel (230-400 μm mesh).

IR spectra were obtained on a Perking Elmer Spectrometer 1. All samples were analysed neat unless otherwise stated, and wavenumbers are reported in cm^{-1}.

^{1}H, ^{13}C, ^{11}B, ^{19}F, and ^{31}P NMR spectra were recorded on a Bruker DPX 400 spectrometer at 400 MHz, 101 MHz, 128 MHz, 376 MHz, and 162 MHz, respectively. Chemical shifts are reported in ppm. Coupling constants are reported in Hz and refer to $^{3}J_{HH}$ interactions unless stated otherwise.

High resolution mass spectra were recorded on a Finnigan MAT 90XLT instrument at either the EPSRC Mass Spectrometry facility at the University of Wales, Swansea or the Mass Spectrometry facility at the University of Edinburgh.

DFT theory was used to calculate gas-phase electronic structures and associated energies. All structures were optimized using the M06L functional. This was utilised in conjunction with the 6-31G9D basis set for the main group atoms. The Stuttgart RSC effective core potential with associated basis set was utilised for iridium. All calculations were performed using the Gaussian 09 quantum package.[77] Please see section 1.5.9 and the appendix for coordinates and further information.

1.5.2 General Procedures

General Procedure A - Preparation of complexes of the type [Ir(COD)Cl(NHC)] [68]

Bis(1,5-cyclooctadiene)diiridium(I) dichloride (1.0 eq) and potassium *tert*-butoxide (2.0 eq) were added to a flame-dried, argon cooled Schlenk tube and stirred under vacuum for 5 min. THF (20 mL / mmol Ir dimer) was added and the mixture stirred under argon for 10 min. The relevant imidazolium chloride (2.0 eq) was then added and the resulting reaction mixture stirred for 4 -16 h. The solvent was then removed *in vacuo*, and flash column chromatography (50% ethyl acetate in petrol) afforded the title compound.

General Procedure B - Preparation of complexes of the type [Ir(PR_3)(NHC)]BAr^F [78]

To a flame dried Schlenk tube under an atmosphere of argon was added [Ir(COD)Cl(NHC)] (1.0 eq) and $NaBAr^F$ (1.0 eq). The mixture was then dissolved in dry DCM (32 mL / mmol Ir complex) and the mixture stirred for 30 min. The respective phosphine ligand (1.0 eq) was then added slowly, initiating an orange to red colour change. After a further 30 min stirring, the reaction mixture was filtered through celite and concentrated *in vacuo*, resulting in a red oil. This residue was purified by flash chromatography (50% DCM in petrol) to afforded a

red crystalline solid. The isolated catalyst was dried in a vacuum oven (40 °C, 1 mbar) for 24 h before use.

General Procedure C - Acylation of Amino Ester Hydrochlorides with Acyl Chloride [79]

To a suspension of amino ester hydrochloride (1 eq) in dry $CHCl_3$ at 0 °C was added Et_3N (X eq) dropwise under argon. The resulting suspension was stirred for 10 min. Acetyl chloride (X eq) was then added dropwise at 0 °C and the reaction mixture left to stir for 1-16 h. The reaction was then carefully quenched by the addition saturated sodium bicarbonate, and then extracted with $CHCl_3$. The combined organic phases were dried with Na_2SO_4, filtered and concentrated *in vacuo*. The resulting oil was then purified by flash column chromatography (0-5% MeOH/DCM) to afford the title compounds.

General Procedure D - Boc Protection of Amino Ester Hydrochlorides [80]

To a suspension of amino ester hydrochloride in the solvent at 0 °C was added Et_3N (X eq) dropwise under argon. The resulting suspension was stirred for 10 min. Di-*tert*-butyl dicarbonate, Boc_2O, (X eq) was then added dropwise at 0 °C and the reaction mixture left to stir for 2-16 h. The reaction mixture was then washed with brine and the organic phase was separated, dried with Na_2SO_4, filtered and concentrated *in vacuo*. The resulting residue was then purified by flash column chromatography to afford the title compound.

General Procedure E - Formation of tert-butyl Esters [81]

To a round-bottom flask was added amino acid (1.0 eq) and *tert*-butyl acetate. The suspension was stirred at 0 °C and a solution 70% perchloric acid in water (X eq) was added *via* a syringe pump (5 mL/h). The resulting solution was stirred overnight at room temperature. After this time, the reaction mixture was diluted with water and carefully quenched at 0 °C with saturated potassium carbonate solution then basified to pH 9. The

resulting solution was then extracted with chloroform. The combined organic phases were dried with sodium sulfate, and concentrated *in vacuo.* The resulting residue was then purified by column chromatography (EtOAc/petrol) to afford the title compounds.

General Procedure F - Formation of Methyl Esters [79]

To a round-bottom flask was added the respective amino acid (1 eq) and methanol. Thionyl chloride (3-5 eq) was added dropwise at 0 °C, and the resulting solution heated to reflux for 6 h. The reaction mixture was then concentrated *in vacuo* to afford a white solid. This residue was then azeotroped with a DCM/hexane mixture to remove residual acid, affording the title compound.

General Procedure G - Acylation of Amino Ester Hydrochlorides with Acetic Anhydride [82]

To a suspension of amino ester hydrochloride (1 eq) in dry DCM at 0 °C was added Et_3N dropwise under argon. The resulting suspension was stirred for 10 min. Acetic anhydride (3 eq) was then added dropwise at 0 °C and the reaction mixture left to stir for 16 h. The reaction was then carefully quenched with saturated sodium bicarbonate and extracted with $CHCl_3$. The combined organic phases were dried with Na_2SO_4, filtered and concentrated *in vacuo*. The resulting oil was then purified by column chromatography (0-5% MeOH/DCM) to afford the title compounds.

General Procedure H – HIE protocol

Reactions were all performed using a Radley's 12-chamber carousel. Each of the carousel tubes was dried overnight in an oven at 180 °C. and allowed to cool under vacuum. Each tube was charged with the *N*-protected amino ester (0.011mmol or 0.215 mmol) and the relevant catalyst (X mol%). To each tube was added MTBE or DCM depending upon the study (X mL), and the solutions cooled to -78 °C. The atmosphere was exchanged with three vacuum/D_2 cycles and the tubes were sealed and immediately placed in a heating block pre-heated to the desired temperature (25 °C or 50 °C). The reactions were stirred for 16 h, after

which time the solvent was removed *in vacuo*. The resulting residue was triturated or purified by column chromatography to remove catalyst. The level of incorporation was determined by ^{1}H NMR spectroscopic analysis, with the integrals of the labelling positions measured against a peak corresponding to a position where labelling was not expected. The level of deuteration was then calculated using the formula:

$$Deuteration\,(\%) = \; 100 - [100 \times \left(\frac{Residual\ Integral}{Expected\ Integral}\right)$$

1.5.3 Investigating the Labelling of Glycine Derivatives

Chloro(η^4-Cycloocta-1,5-diene(1,3-bis(mesityl) imidazole-2-ylidene)iridium(I), **75** [68]

Scheme 1.32

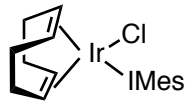

75

Chemical Formula: $C_{29}H_{36}ClIrN_2$
Molecular Weight: 640.29

Prepared according to *General Procedure A*

Table 1.9

Entry	Amount of dimer 73		Amount of IMes·HCl		Amount of ^{t}BuOK		Volume THF	Product Yield	
	mg	mmol	mg	mmol	mg	mmol	mL	mg	%
1	500	0.75	510	1.5	167	1.5	15	930	97
2	500	0.75	510	1.5	167	1.5	15	853	89
3	500	0.75	510	1.5	167	1.5	15	805	84
4	500	0.75	510	1.5	167	1.5	15	700	73
5	500	0.75	510	1.5	167	1.5	15	911	95
6	667	1.00	680	2.00	223	2.00	20	1128	88
7	750	1.12	760	2.24	251	2.24	22	1249	87
8	1000	1.50	1020	3.00	330	3.00	30	1211	63

Product appearance: yellow solid.

Melting point: >190 °C (decomposition) .

FTIR (neat): 3121, 2978, 2916, 1607, 1485 cm^{-1}.

^{1}H NMR (400 MHz, $CDCl_3$): δ 7.04 - 6.99 (m, 4H, Ar-H), 6.95 (s, 2H, NCH=CHN), 4.20 - 4.12 (m, 2H, COD CH), 2.99 - 2.94 (m, 2H, COD CH), 2.36 (s, 12H, *o*-CH_3Ar), 2.16 (s, 6H, *p*-CH_3), 1.79 -1.56 (m, 4H, COD CH_2), 1.39 - 1.19 (m, 4H, COD CH_2) ppm.

^{13}C NMR (101 MHz, $CDCl_3$): δ 180.9, 138.8, 137.5, 136.2, 134.6y, 129.7, 128.3, 123.4, 82.7, 51.6, 33.7, 29.1, 21.3, 19.8, 18.4 ppm.

[Ir(COD)(PBn$_3$)(IMes)] BAr^F **86a** [66]

Scheme 1.33

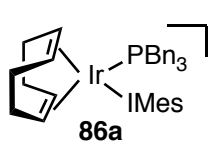

86a

Chemical Formula: $C_{82}H_{69}BF_{24}IrN_2P$

Molecular Weight: 1772.4304

Prepared according to *General Procedure B*.

Table 1.10

Entry	Amount of 75		Amount of $NaBAr^F$		Amount of PBn_3		Volume DCM	Product Yield		
	g	mmol	g	mmol	g	mmol	mL	g	mmol	%
1	0.17	0.25	0.23	0.25	0.08	0.25	8	0.25	0.14	56
2	0.17	0.25	0.23	0.25	0.08	0.25	8	0.28	0.16	64
3	0.40	0.62	0.55	0.62	0.19	0.62	20	0.77	0.43	70
4	0.40	0.62	0.55	0.62	0.19	0.62	20	0.78	0.44	71
5	0.46	0.71	0.63	0.71	0.22	0.71	23	1.12	0.63	89
6	0.50	0.78	0.69	0.78	0.24	0.78	25	1.23	0.69	88

Product appearance: orange solid.

Melting point: >170 °C (decomposition).

FTIR (neat): 2542, 2365, 1609, 1352 cm^{-1}.

^{1}H NMR (400 MHz, $CDCl_3$): δ 7.70 (bs, 8H, Ar-H BAr^F), 7.50 (bs, 4H, Ar-H BAr^F), 7.25 - 7.19 (m, 9H, Ar-H), 7.15 (s, 4H, Ar-H), 6.82 (d, J = 8.0, 6H, Ar-H), 6.59 – 6.48 (m, 2H, Ar-H), 4.58 – 4.55 (m, 2H, COD CH), 3.21 – 3.18 (m, 2H, COD CH), 2.82 (d, $^2J_{P\text{-}H}$ = 8.7 Hz, 6H, P-CH_2-Ar), 2.43 (s, 12H, ArCH_3), 2.25 (s, 6H, ArCH_3), 1.80 – 1.61 (m, 4H, COD CH_2), 1.50 – 1.21 (m, 4H, COD CH_2) ppm.

^{13}C NMR (101 MHz, $CDCl_3$) δ 176.5 (d, $^2J_{C\text{-}P}$ = 8.7 Hz), 161.2 (q, $^1J_{C\text{-}B}$ = 49.7 Hz), 140.4, 135.5, 135.2, 134.3, 132.2, 132.0, 130.0, 129.5, 129.3, 128.3 (q, $^2J_{C\text{-}F}$ = 31.5 Hz), 125.6, 125.2 (q, $^1J_{C\text{-}F}$ = 274 Hz), 116.2, 86.5, 85.9, 75.4, 31.3, 31.1, 29.9, 29.3, 20.5, 19.7, 19.0 ppm.

^{11}B NMR (128 MHz, $CDCl_3$): δ -6.64 ppm (BAr^F $B(Ar_4)$).

^{31}P NMR (162 MHz, $CDCl_3$): δ -8.0 ppm PBn_3.

^{19}F NMR (376 MHz, Methanol-d_4): δ -64.3 ppm (BAr^F $ArCF_3$).

[Ir(COD)(PPh_3)(IMes)] BAr^F **86b** [51]

Scheme 1.33

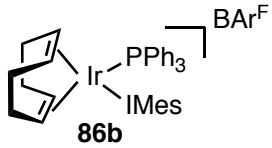

86b

Chemical Formula: $C_{79}H_{63}BF_{24}IrN_2P$
Molecular Weight: 1730.35

Prepared according to *General Procedure B*.

Table 1.11

Entry	Amount of 75		Amount of $NaBAr^F$		Amount of PPh_3		Volume DCM	Product Yield		
	g	mmol	g	mmol	g	mmol	mL	g	mmol	%
1	0.20	0.31	0.28	0.31	0.08	0.31	10	0.24	0.14	46
2	0.20	0.31	0.28	0.31	0.08	0.31	10	0.43	0.25	80
3	0.30	0.47	0.42	0.47	0.12	0.47	15	0.74	0.43	92
4	0.40	0.62	0.55	0.62	0.16	0.62	20	0.52	0.30	48

Product appearance: red solid.

Melting point: 148-150 °C.

FTIR (neat):2989, 2909, 1609, 1350 cm^{-1}.

^{1}H NMR (400 MHz, $CDCl_3$): δ 7.75 - 7.71 (m, 8H, Ar-H BAr^F), 7.51 (bs, 4H, Ar-H BAr^F), 7.46 – 7.38 (m, 3H, Ar-H), 7.32 – 7.23 (m, 8H, Ar-H and NCH=CHN), 7.18 – 7.10 (m, 6H, Ar-H), 7.00 (s, 2H, Ar-H), 6.66 (s, 2H, Ar-H), 4.41 – 4.30 (m, 2H, COD CH), 3.41 – 3.30 (m, 2H, COD CH), 2.33 (s, 6H, ArCH_3), 2.08 (s, 6H, ArCH_3), 1.75 (s, 6H, ArCH_3), 1.69 – 1.44 (m, 6H, COD CH_2), 1.35 - 1.27 (m, 2H, COD CH_2) ppm.

^{13}C NMR (101 MHz, $CDCl_3$) δ 178.1 (d, $^2J_{C\text{-}P}$ = 9.7 Hz), 161.9 (q, $^1J_{C\text{-}B}$ = 50.7 Hz), 140.3, 135.6, 135.3, 134.9, 134.8, 132.3, 132.2, 131.4, 130.6, 129.9, 129.2, 128.8, 128.7, 123.4 (q $^1J_{C\text{-}F}$ = 270 Hz), 117.6, 80.7, 80.6, 78.7, 32.0, 21.2, 21.0, 19.1 ppm.

^{11}B NMR (128 MHz, $CDCl_3$): δ -6.60 ppm (BAr^F $B(Ar_4)$).

^{31}P NMR (162 MHz, $CDCl_3$): δ 16.4 ppm (PPh_3).

^{19}F NMR (376 MHz, $CDCl_3$): δ -62.4 ppm. (BAr^F $ArCF_3$).

[Ir(COD)(PMe_2Ph)(IMes)] BAr^F **86c** [83]

Scheme 1.33

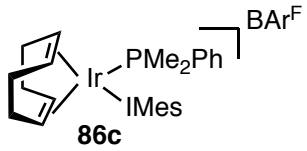

86c

Chemical Formula: $C_{69}H_{59}BF_{24}IrN_2P$
Molecular Weight: 1606.2074

Prepared according to *General Procedure B*.

Table 1.12

Entry	Amount of 75		Amount of $NaBAr^F$		Amount of PMe_2Ph		Volume DCM	Product Yield		
	g	mmol	g	mmol	mL	mmol	mL	g	mmol	%
1	0.20	0.31	0.28	0.31	0.08	0.31	10	0.29	0.18	58
2	0.40	0.62	0.55	0.62	0.09	0.62	20	0.90	0.56	90

Product appearance: red solid.

Melting point: 146-148 °C.

FTIR (neat): 3046, 2931, 1732, 1654, 1352 $cm^{-1.}$

^{1}H NMR (400 MHz, $CDCl_3$): δ 7.73 – 7.70 (m, 8H, Ar-H BAr^F), 7.51 (bs, 4H, Ar-H BAr^F), 7.44 – 7.40 (m, 1H, Ar-H), 7.35 – 7.27 (m, 4H, Ar-H), 7.15 (s, 2H, NCH=CHN), 7.06 (s, 2H, Ar-H), 6.91 (s, 2H, Ar-H), 4.32 – 4.25 (m, 2H, COD CH), 3.46- 3.44 (m, 2H, COD CH), 2.37 (s, 6H, Ar-CH_3), 2.19 (s, 6H, Ar-CH_3), 2.09 (s, 6H, Ar-CH_3), 1.78 – 1.58 (m, 8H, COD CH_2), 1.44 (s, 3H, P-CH_3), 1.42 (s, 3H, P-CH_3) ppm.

^{13}C NMR (101 MHz, $CDCl_3$) δ 178.0 (d, $^{2}J_{C\text{-}P}$ = 11.2 Hz), 161.9 (q, $^{1}J_{C\text{-}B}$ = 49.1 Hz), 140.5, 135.6, 135.4, 135.0, 134.3, 131.7, 131.6, 131.1, 129.2, 129.0, 128.9, 126.1, 125.6 (q $^{1}J_{C\text{-}F}$ = 274 Hz), 117.7, 84.0, 83.9, 76.5, 31.5, 30.6, 21.1, 20.2, 19.0, 16.7, 16.1 ppm.

^{11}B NMR (128 MHz, $CDCl_3$): δ -6.60 ppm (BAr^F $B(Ar_4)$).

^{31}P NMR (162 MHz, $CDCl_3$): δ -14.48 ppm (PMe_2Ph).

^{19}F NMR (376 MHz, $CDCl_3$): δ -62.4 ppm. (BAr^F $ArCF_3$).

[Ir(COD)(P^iPr_3)(IMes)] BAr^F **86d**

Scheme 1.33

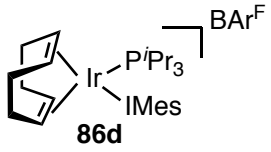

86d

Chemical Formula: $C_{70}H_{69}BF_{24}IrN_2P$

Molecular Weight: 1628.2984

Prepared according to *General Procedure B*.

Table 1.13

Entry	Amount of 75		Amount of $NaBAr^F$		Amount of P^iPr_3		Volume DCM	Product Yield		
	g	mmol	g	mmol	mL	mmol	mL	g	mmol	%
1	0.19	0.29	0.26	0.29	0.055	0.29	9	0.19	0.12	40
2	0.32	0.50	0.44	0.50	0.095	0.50	16	0.42	0.26	52
3	0.32	0.50	0.44	0.50	0.095	0.50	16	0.43	0.27	53
4	0.40	0.62	0.55	0.62	0.19	0.62	20	0.86	0.53	85
5	0.40	0.62	0.55	0.62	0.12	0.62	20	0.89	0.55	88

Product appearance: dark red solid.

Melting point: >120 °C (decomposition).

FTIR (neat): 2891, 2181, 1608, 1352, 1275 $cm^{-1.}$

^{1}H NMR (400 MHz, $CDCl_3$): δ 7.70 (bd, 8H, Ar-H BAr^F), 7.52 (bs, 4H, Ar-H BAr^F), 7.10 (s, 2H, NCH=CHN), 7.07 – 6.89 (m, 4H, Ar-H), 4.08-4.02 (s, 2H, COD CH), 3.97 – 3.87 (m, 2H, COD CH), 2.32 (s, 6H, Ar-CH_3), 2.28 (s, 6H, Ar-CH_3), 2.17 (s, 6H, Ar-CH_3), 1.67 – 1.64 (m, 2H), 1.63 – 1.53 (m, 6H), 1.41 – 1.17 (m, 10H), 1.08 – 1.00 (m, 11H) ppm.

^{13}C NMR (101 MHz, $CDCl_3$) δ 178.0 (d, $^2J_{C\text{-}P}$ = 9.4 Hz), 165.0 (q, $^1J_{C\text{-}B}$ = 49.1 Hz), 140.8, 139.7, 138.9, 136.3, 135.9, 135.0, 130.4, 130.1, 129.9, 129.7, 129.3, 129.0, 128.7, 126.4, 124.5 (q $^1J_{C\text{-}F}$ = 272 Hz), 117.7, 82.7, 72.3, 51.8, 33.7, 31.9, 31.3, 29.2, 26.5, 25.1, 24.5, 21.3, 20.2, 19.6, 19.2, 17.7, 16.6 ppm.

^{11}B NMR (128 MHz, $CDCl_3$): δ -6.60 ppm (BAr^F $B(Ar_4)$).

^{31}P NMR (162 MHz, $CDCl_3$): δ 21.92 ppm (P^iPr_3).

^{19}F NMR (376 MHz, $CDCl_3$): δ -62.4 ppm. (BAr^F $ArCF_3$).

HRMS (positive ESI): m/z calculated for $C_{38}H_{57}N_2$ $[M - BAr^F]^+$ 765.3885 found: 765.3889.

[Ir(COD)(P^nBu_3)(IMes)]BAr^F ***86e*** [55]

Scheme 1.33

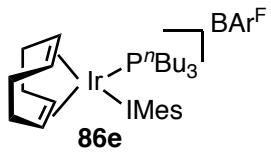

86e

Chemical Formula: $C_{73}H_{75}BF_{24}IrN_2P$

Molecular Weight: 1670.3794

Prepared according to *General Procedure B*.

Table 1.14

Entry	Amount of 75		Amount of $NaBAr^F$		Amount of P^nBu_3		Volume DCM	Product Yield		
	g	mmol	g	mmol	mL	mmol	mL	g	mmol	%
1	0.32	0.50	0.44	0.50	0.123	0.50	16	0.46	0.27	54
2	0.32	0.50	0.44	0.50	0.123	0.50	16	0.54	0.32	63
3	0.40	0.62	0.55	0.62	0.153	0.62	20	0.62	0.37	59

Product appearance: dark red solid.

Melting point:162-164 °C

FTIR (neat): 2962, 2876, 1609, 1458, 1352 cm^{-1}

^{1}H NMR (400 MHz, $CDCl_3$): δ 7.70 (bs, 8H, Ar-H BAr^F), 7.51 (bs, 4H, Ar-H BAr^F), 7.08 (s, 2H, NHC=CHN), 7.03 (s, 2H,ArH), 6.99 (s, 2H, ArH), 4.18 – 4.09 (m, 2H, COD CH), 3.68-

3.54 (m, 2 H, COD C<u>H</u>), 2.36 (s, 6H, Ar-<u>CH$_3$</u>), 2.29 (s, 6H, Ar-<u>CH$_3$</u>), 2.18 (s, 6H, Ar-<u>CH$_3$</u>), 2.00 – 1.79 (m, 2H, COD C<u>H$_2$</u>), 1.77 – 1.57 (m, 2H, COD C<u>H$_2$</u>), 1.51 – 1.31 (m, 10H, COD C<u>H$_2$</u> & CH$_2$-C<u>H$_2$</u>-CH$_2$), 1.28 (sextet, 6H, *J*= 8.0 Hz, CH$_2$-C<u>H$_2$</u>-CH$_3$), 1.03 – 0.90 (m, 6H, P-C<u>H$_2$</u>-CH$_2$), 0.87 (t, *J*=8.9 Hz, 9H, CH$_2$-C<u>H$_3$</u>) ppm.

^{13}C NMR (101 MHz, CDCl$_3$) δ 178.0 (d, $^2J_{C\text{-}P}$ = 8.7 Hz), 161.9 (q, $^1J_{C\text{-}B}$ = 52.4 Hz), 140.6, 135.9, 135.8, 135.0, 134.3, 130.2, 129.9, 128.4 (q $^2J_{C\text{-}F}$ = 35.7 Hz), 126.1, 125.6 (q $^1J_{C\text{-}F}$ = 268 Hz), 117.6, 82.3, 82.2, 74.5, 31.4, 31.0, 26.8, 24.6, 24.5, 24.2, 20.4, 19.5, 17.1, 13.8 ppm.

^{11}B NMR (128 MHz, CDCl$_3$): δ -6.62 ppm (BAr^F B(Ar$_4$)).

^{31}P NMR (162 MHz, CDCl$_3$): δ -2.46 ppm (P^{n}Bu$_3$).

^{19}F NMR (376 MHz, CDCl$_3$): δ -62.4 ppm. (BAr^F ArCF$_3$).

Toward the synthesis of η^4-Cycloocta-1,5-diene(3-(2-(diphenylphosphanyl)ethyl)-1-mesityl imidazole-2-ylidene)iridium BAr$_F$ **111** [69]

Scheme 1.34

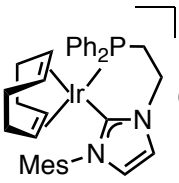

Chemical Formula: $C_{66}H_{51}BF_{24}IrN_2P$
Molecular Weight: 1562.1104

111

1-Mesitylimidazole **169** [84]

Scheme 1.34

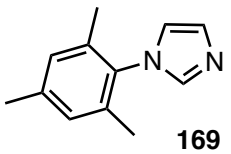

Chemical Formula: $C_{12}H_{14}N_2$
Molecular Weight: 186.2580

169

To a 500 mL three-necked round-bottom flask equipped with a condenser and addition funnel was added glyoxal **168** (40% wt. in water, 16.3 mL, 142 mmol, 1.10 eq), formaldehyde (37% wt. in water, 10.8 mL, 145 mmol, 1.10 eq) and acetic acid (35.0 mL). The reaction mixture

was heated to 80 °C. In a separate conical flask was added NH_4OAc (10.9 g, 140 mmol, 1.10 eq), 2,4,6-trimethylaniline (18.3 mL, 130 mmol, 1.00 eq), acetic acid (35.0 mL) and water (3.00 mL) and the mixture was stirred until a viscous solution formed. The resulting solution was transferred to the addition funnel and slowly added over a period of 10 minutes. The reaction was stirred for 16 h at 80 °C. After this time, the reaction mixture was cooled to room temperature and transferred to a dropping funnel. The solution was then added to an excess amount of aqueous saturate sodium bicarbonate solution, with very vigorous stirring. Once the quench was completed, the aqueous suspension was then filtered and the filter cake washed with water and allowed to dry in air. The filtrand was transferred to a beaker and petroleum ether added. The suspension was heated to boiling and the hot solution decanted. This process was repeated until the petroleum ether remained clear upon boiling, at which point the remaining solid residue was discarded. The decanted liquid was concentrated *in vacuo* to yield mesityl imidazole **169** (14.01 g, 75.3 mmol, 56%) as a brown solid.

Melting point: 111-115 °C (lit. 112-114 °C)[84]

FTIR (neat): 3093, 2918, 1637, 1593, 1497 $cm^{-1.}$

^{1}H NMR (400 MHz, $CDCl_3$): δ 7.42 (t, ^4J = 1.2 Hz, 1H, Ar-H), 7.22 (t, ^4J = 1.2 Hz, 1H, Ar-H), 6.96 (s, 2H, Ar-H), 6.88 (t, ^4J = 1.2 Hz, 1H, Ar-H), 2.33 (s, 3H, $ArCH_3$), 1.98 (s, 6H, $ArCH_3$) ppm.

^{13}C NMR (101 MHz, $CDCl_3$) δ 139.0, 137.6, 136.3, 133.6, 129.7, 129.1, 120.2, 21.2, 17.5 ppm.

3-(2-Hydroxyethyl)-1-mesitylimidazolium bromide **171** [85]

Scheme 1.34

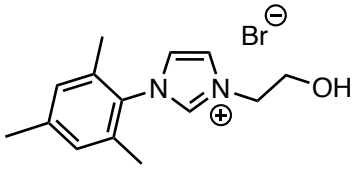

Chemical Formula: $C_{14}H_{19}BrN_2O$
Molecular Weight: 311.2230

171

To a 100 mL round-bottom flask was added mesityl imidazole **169** (5.00 g, 26.8 mmol). Toluene (80.0 mL) was added to dissolve the brown solid and 2-bromoethanol (2.40 mL,

33.5 mmol, 1.25 eq) was added. The resulting reaction mixture was heated to reflux for 16 h, after which the reaction was cooled to 0 °C and the resulting precipitate was allowed to settle. The solvent was then removed by pipette and the product washed with diethyl ether, yielding 3-(2-hydroxyethyl)-1-mesitylimidazolium bromide **171** (4.99 g, 21.6 mmol, 80% yield) as a brown solid.

Melting point: 162-164 °C (lit. 164-166 °C).[85]

FTIR (neat): 3290, 3055, 2020, 1560, 1535 cm^{-1}.

^{1}H NMR (400 MHz, DMSO-*d*$_6$) δ 9.41 (t, *J* = ^{4}*J* = 1.6 Hz, 1H, Ar-H), 8.06 (t, *J* = ^{4}*J* = 1.8 Hz, 1H, Ar-H), 7.93 (t, *J* = ^{4}*J* = 1.8 Hz, 1H, Ar-H), 7.15 (s, 2H, Ar-H), 5.24 (s, 1H, OH), 4.34 (t, *J* = 5.1 Hz, 2H, CH_2), 3.82 (t, *J* = 4.9 Hz, 2H, CH_2), 2.34 (s, 3H, $ArCH_3$), 2.03 (s, 6H, $ArCH_3$) ppm.

^{13}C NMR (101 MHz, DMSO-*d*$_6$) δ 140.1, 137.7, 134.2, 131.1 129.2, 123.6, 123.4, 59.0, 51.9, 20.6, 16.9 ppm.

3-(2-Bromoethyl)-1-mesitylimidazolium bromide **172** [85] [70]

Scheme 1.34

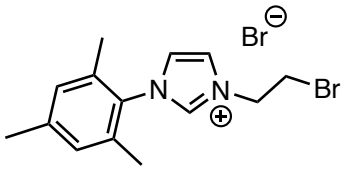

Chemical Formula: $C_{14}H_{18}Br_2N_2$
Molecular Weight: 374.1200

172

To a 100 mL round-bottom flask was added 3-(2-hydroxyethyl)-1-mesityl imidazolium bromide **171** (1.0 eq) and DCM. The solution was cooled to 0 °C and PBr_3 (0.87 eq) was added dropwise. The reaction mixture was stirred at room temperature for 16 h, and then cooled to 0 °C and quenched with saturated aqueous sodium bicarbonate. The mixture was then extracted with DCM and organic phases collected, dried with sodium sulfate and concentrated *in vacuo* to yield 3-(2-bromoethyl)-1-mesityl imidazolium bromide **172** as an off-white solid.

Prepared according to above procedure. Data presented as: (a) amount of 3-(2-hydroxyethyl)-1-mesityl imidazolium bromide **171**, (b) volume of DCM mL, (c) amount of PBr_3, and (d) yield.

Run 1

(a) 1.50 g, 4.82 mmol, 1.0 eq, (b) 25.0 mL, (c) 0.420 mL, 4.17 mmol, 0.87 eq, and (d) 1.01 g, 2.70 mmol, 56 % yield.

Run 2

(a) 3.00 g, 9.62 mmol, 1.0 eq, (b) 50.0 mL, (c) 0.840 mL, 8.34 mmol, 0.87 eq, and (d) 2.16 g, 5.78 mmol, 60 % yield.

Melting point: 152-154 °C

FTIR (neat): 3115, 3065, 2939, 1547, 1442 cm^{-1}.

^{1}H NMR (400 MHz, $CDCl_3$) δ 10.28 (t, ^4J = 1.6 Hz, 1H, NC<u>H</u>N), 7.93 (t, ^4J = 1.8 Hz, 1H, Ar-<u>H</u>), 7.15 (t, ^4J = 1.8 Hz, 1H, Ar-<u>H</u>), 7.03 (dd, J = 1.4, 0.7 Hz, 2H, Ar-<u>H</u>), 5.28 (t, J = 5.4 Hz, 2H, CH_2), 4.09 (t, J = 5.4 Hz, 2H, CH_2), 2.36 (s, 3H, ArC<u>H</u>$_3$), 2.10 (s, 6H, ArC<u>H</u>$_3$) ppm.

^{13}C NMR (101 MHz, $CDCl_3$) δ 141.4, 137.9, 134.4, 130.7, 129.9, 124.4, 123.1, 51.2, 31.8, 21.2, 17.7 ppm.

3-(2-(Diphenylphosphanyl)ethyl)-1-mesitylimidazolium BAr^F **173** [70]

Scheme 1.34

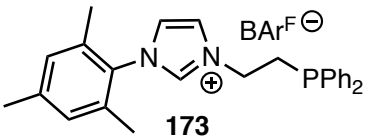

173

Chemical Formula: $C_{58}H_{39}BF_{24}N_2P$
Molecular Weight: 1261.7094

A flame-dried 10 mL round-bottom flask was placed under inert atmosphere *via* three vacuum/argon cycles. The flask was charged with potassium *tert*-butoxide (0.224 g, 2.0 mmol, 1.0 eq) and DMSO (3.0 mL). To this was added diphenylphosphine (0.340 mL, 2.10 mmol, 1.05 eq) and the reaction mixture stirred for 1 h. A separate flame-dried 10 mL round-

bottom flask was placed under an inert atmosphere *via* three vacuum/argon cylces and subsequently charged with 3-(2-bromoethyl)-1-mesitylimidazolium bromide **172** (0.750 g, 2.0 mmol, 1.00 eq) and DMSO (3.00 mL). The DMSO solution of potassium diphenylphosphide was then added dropwise, *via* syringe, and the reaction mixture stirred for 2 h. The reaction mixture was then transferred to a larger vessel and water (30.0 mL) added and the product subsequently extracted with DCM (3 × 30 mL). The combined organic phases were separated, and placed under an inert atmosphere. $NaBAr^F$ (1.95 g, 2.20 mmol, 1.10 eq) was added and the reaction stirred for 16 h at room temperature. After this time, the reaction mixture was concentrated *in vacuo*, and the product purified by flash column chromatography (50% DCM/petrol) to yield 3-(2-(diphenylphosphanyl)ethyl)-1-mesitylimidazolium BAr^F **173** as a tan solid.

Run 1: yield of **173** = 1.09 g, 0.86 mmol, 43% yield.

Run 2: yield of **173** = 1.32 g, 1.04 mmol, 52% yield.

Melting point: 115-117 °C.

FTIR (neat): 3064, 2939, 1547, 1443 cm^{-1}.

^{1}H NMR (400 MHz, $CDCl_3$) δ 8.30 (s, 1H, NCHN), 7.71 (bs, 8H, Ar-H BAr^F), 7.50 (s, 4H, Ar-H BAr^F), 7.42 – 7.33 (m, 11H, Ar-H), 7.22 (t, ^4J = 1.8 Hz, 1H, Ar-H), 7.01 (s, 2H, Ar-H), 4.33 (dt, $^2J_{P\text{-}H}$ = 10.7 Hz, J = 7.1 Hz, 2H, PCH_2), 2.64 (td, J = 7.1, 1.3 Hz, 2H, CH_2), 2.30 (s, 3H, ArMe), 1.92 (s, 6H, ArMe) ppm.

^{13}C NMR (101 MHz, $CDCl_3$) δ 161.9 (q, $^1J_{C\text{-}B}$ = 49.6 Hz), 143.0, 137.7, 135.0, 134.1, 133.9, 133.4, 132.8, 132.6, 130.6, 129.6 (q, $^2J_{C\text{-}F}$ = 35.7 Hz), 129.4, 124.0 (q, $^1J_{C\text{-}F}$ = 270.4 Hz), 123.1, 120.7, 117.7, 48.5 (d, $^1J_{C\text{-}P}$ = 21.1 Hz), 29.1 (d, $^2J_{C\text{-}P}$ = 12.7 Hz), 21.2, 17.2 ppm.

^{31}P NMR (162 MHz, $CDCl_3$): δ -25.4 ppm.

*η^4–Cycloocta-1,5-diene(3-(2-(diphenylphosphanyl)ethyl)-1-mesityl imidazole-2-ylidene)iridium terakis[3,5-bis(trifluoromethyl)phenyl]borate **111*** [70]

Scheme 1.34

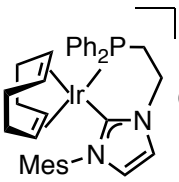

Chemical Formula: $C_{66}H_{51}BF_{24}IrN_2P$
Molecular Weight: 1562.1104

111

To a flame-dried Schlenk tube was added $[Ir(COD)Cl]_2$ **73** (0.161 g, 0.240 mmol, 0.5 eq) and **173** (0.606 g, 0.480 mmol, 1.0 eq). The mixture was then dissolved in THF (4.50 mL) and ^{t}BuOK (0.056 g, 0.50 mmol,1.0 eq) was added. The reaction was stirred at room temperature for 2 h, after which time the solvent was removed *in vacuo*. The resulting residue was purified by flash column chromatography (50% DCM/petrol). The resulting oil was then triturated with petrol, yielding complex **111** as a dark pink solid.

Run 1: yield of **111** = 0.247 g, 0.165 mmol, 33% yield

Run 2: yield of **111** = 0.404 g, 0.27 mmol, 54% yield

Melting point: 162-164 °C

FTIR (neat): 3093, 2935, 1609, 1354, 1273 cm^{-1}.

^{1}H NMR (400 MHz, $CDCl_3$): δ 7.75 (bs, 8H, Ar-H BAr^F), 7.52 (s, 4H, Ar-H BAr^F), 7.49 – 7.42 (m, 6H, Ar-H), 7.34 – 7.31 (m, 4H, Ar-H), 6.96 (s, 2H, Mes Ar-H), 6.94 (d, J = 1.9 Hz, 1H, Im Ar-H), 6.76 (d, J = 1.9 Hz, 1H, Ar-H), 4.60 – 4.49 (m, 2H, PCH_2), 4.38 – 4.35 (m, 2H, COD CH), 3.58 – 3.52 (s, 2H, COD CH), 2.47 (t, J = 10.1 Hz, 2H, CH_2), 2.34 (s, 3H, ArMe), 1.84 (s, 7H, ArMe + COD CH_2), 1.53 (s, 7H, ArMe + COD CH_2) ppm.

^{13}C NMR (101 MHz, $CDCl_3$) δ 170.1 (d, $^{2}J_{C\text{-}P}$ = 10.9 Hz), 161.9 (q, $^{1}J_{C\text{-}B}$ = 50.1 Hz), 140.5, 135.0, 132.8 (d, $J_{C\text{-}P}$ = 10.4Hz), 131.3, 130.7 (d, $J_{C\text{-}P}$ = 49.8 Hz), 129.5, 129.5, 129.4, 128.9, 124.0 (q, $^{1}J_{C\text{-}F}$ = 146 Hz), 117.7, 89.7 (d, $^{2}J_{C\text{-}P}$ = 11.7 Hz), 78.6, 50.0, 30.6 (d, $J_{C\text{-}P}$ = 36.3 Hz), 24.8 (d, $J_{C\text{-}P}$ = 36.3 Hz), 21.2, 18.6 ppm.

^{11}B NMR (128 MHz, $CDCl_3$): δ -6.60 ppm (BAr^F $B(Ar_4)$).

^{31}P NMR (162 MHz, $CDCl_3$): δ 10.2 ppm (PPh_2).

^{19}F NMR (376 MHz, $CDCl_3$): δ -62.4 ppm. (BAr^F $ArCF_3$).

methyl acetylglycinate **147a** [79]

Scheme 1.35

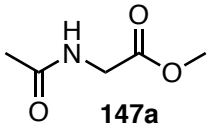

147a

Chemical Formula: $C_5H_9NO_3$
Molecular Weight: 131.1310

Prepared according to *General Procedure C* using a reaction time of 4 h.

Amount of Gly-OMe•HCl: 6.0 g, 48.0 mmol, 1.0 eq.

Amount of triethylamine: 13.4 mL, 144.0 mmol, 3.0 eq.

Amount of acetyl chloride: 3.71 mL, 57.6 mmol, 1.2 eq.

Solvent volume: 100.0 mL DCM.

Product yield: 5.14 g, 38.9 mmol, 81% yield.

Melting point: 48-50 °C (lit. 54-56 °C).[79]

FTIR (neat): 3280, 3080, 2955, 1736, 1637, 1544, 1533 cm^{-1}.

^{1}H NMR (400 MHz, Methanol-d_4): δ 3.94 (s, 2H, C$\underline{H_2}$), 3.74 (s, 3H, OC$\underline{H_3}$), 2.01 (s, 3H, COC$\underline{H_3}$) ppm.

^{13}C NMR (101 MHz, Acetone-d_6): δ 169.8, 169.1, 50.6, 40.1, 21.1 ppm.

Catalyst Screen for methyl acetylglycinate 147a

Scheme 1.35

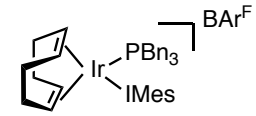

86a

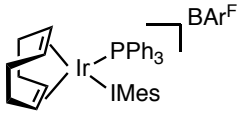

86b

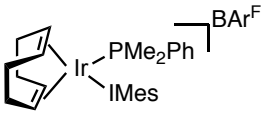

86c

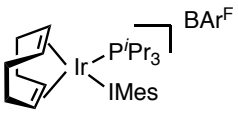

86d

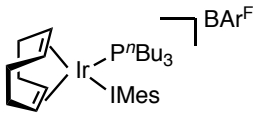

86e

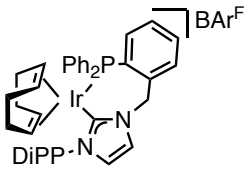

174

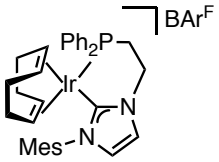

111

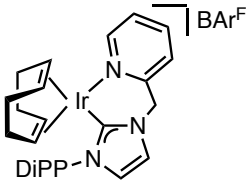

175

The catalyst screen was performed as described in *General Procedure H* utilising the catalysts (5 mol%) shown above and Ac-Gly-OMe **147a** (28.2 mg, 0.215 mmol). Solvent volume (2.5 mL) The product was purified by trituration with diethyl ether. Complexes **174** and **175** were available in-house.[71]

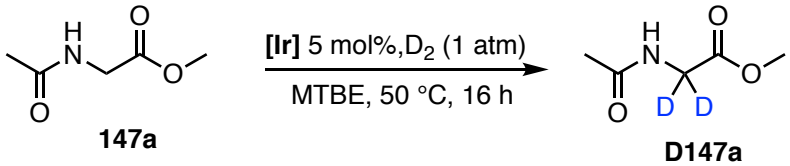

147a **D147a**

^{1}H NMR (400 MHz, Methanol-d_4): δ 3.94 (s, 2H, C$\underline{H_2}$), 3.74 (s, 3H, OC$\underline{H_3}$), 2.01 (s, 3H, COC$\underline{H_3}$) ppm.

Labelling expected against signal at 3.94 ppm, measured against signal at 2.01 ppm.

Table 1.15

Entry	Catalyst	Run 1 (%)	Run 2 (%)	Run 3 (%)	Avg (%)
1	**86a** (0.018 g, 0.01 mmol)	90	91	93	92
2	**86b** (0.017 g, 0.01 mmol)	81	78	86	81
3	**86c** (0.016 g, 0.01 mmol)	87	89	85	87
4	**86d** (0.016 g, 0.01 mmol)	90	88	90	89
5	**86e** (0.017 g, 0.01 mmol)	90	90	90	90
6	**174** (0.017 g, 0.01 mmol)	9	12	9	10
7	**111** (0.018 g, 0.01 mmol)	8	9	12	10
8	**175** (0.015 g, 0.01 mmol)	34	36	31	34

Glycine derivative synthesis

methyl (tert-butoxycarbonyl)glycinate **147d** [86]

Scheme 1.36

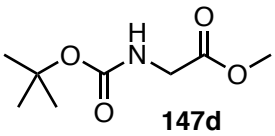

147d

Chemical Formula: $C_8H_{15}NO_4$
Molecular Weight: 189.2110

Prepared according to *General Procedure D* using a reaction time of 16 h.

Amount of Gly-OMe•HCl: 3.0 g, 24.0 mmol, 1.0 eq.

Amount of triethylamine: 9.6 mL, 76.0 mmol, 3.0 eq.

Amount of Boc_2O: 10.2 g, 48.0 mmol, 2.0 eq.

Solvent volume: 100.0 mL DCM.

Product yield: 2.4 g, 12.7 mmol, 53% yield as a yellow oil.

FTIR (neat): 3400, 2978, 2357, 1751, 1697, 1510, 1365 cm $^{-1}$

^{1}H NMR (400 MHz, $CDCl_3$): δ 5.14 – 4.98 (m, 1H, NH), 3.91 (d, *J* = 5.6 Hz, 2H, CH_2), 3.74 (s, 3H OCH_3), 1.44 (s, 9H, $OC(CH_3)_3$) ppm.

^{13}C NMR (101 MHz, Acetone-d_6): δ 171.7, 156.9, 79.5, 52.1, 42.8, 28.7 ppm.

tert-butyl (tert-butoxycarbonyl)glycinate **176** [87]

Scheme 1.36

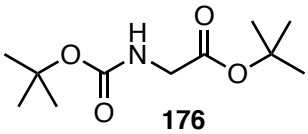

176

Chemical Formula: $C_{11}H_{21}NO_4$
Molecular Weight: 231.2920

tert-Butyl glycinate was synthesised *via* a modified literature procedure. [88] To a 100 mL round-bottom flask was added glycine (4.0 g, 54 mmol, 1.0 eq) and *tert*-butyl acetate (130 mL). The suspension was stirred at 0 °C and 70% perchloric acid in water (7.0 mL, 82 mmol, 1.5 eq). was added dropwise. The resulting solution was stirred overnight at room temperature. After this time, the reaction mixture was diluted with water and carefully quenched at 0 °C with saturated potassium carbonate solution and basified to pH 9. The resulting solution was then extracted with diethyl ether, the combined organic phases dried with sodium sulfate, and concentrated *in vacuo* to yield *tert*-butyl glycinate as a colourless oil. The resulting oil was then dissolved in DCM (200 mL) at 0 °C and trimethylamine (26.0 mL, 162.0 mmol, 3.0 eq) added slowly. After stirring for five minutes, Boc_2O (11.0 g, 54.0 mmol, 1.0 eq) was added dropwise. The reaction mixture was then allowed to slowly rise to room temperature and stirred for 16 h. The reaction mixture was then carefully quenched by addition of saturated sodium bicarbonate solution and extracted with $CHCl_3$. The organic phase was then washed with brine and resulting organic phase was dried with Na_2SO_4, filtered and concentrated *in vacuo*. The resulting residue was then purified by column chromatography (0-20% diethyl ether/petrol) to give **176** as a white solid (2.79 g, 12.42 mmol, 23% yield).

Melting point: 64-66 °C (lit. 64 °C) [87]

FTIR (neat): 3379, 2978, 2939, 1739, 1701, 1689, 1512 cm^{-1}

^{1}H NMR (400 MHz, Acetone-d_6): δ 6.20 – 6.13 (m, 1H, NH), 3.70 (d, J = 6.2 Hz, 2H, CH_2), 1.46 (s, 9H, $OC(CH_3)_3$), 1.43 (s, 9H, $OC(CH_3)_3$) ppm.

^{13}C NMR (101 MHz, Acetone-d_6): δ 170.4, 156.9, 81.4, 79.3, 43.8, 28.7, 28.4 ppm.

Catalyst Screen methyl (*tert*-butoxycarbonyl)glycinate 147d

Scheme 1.36

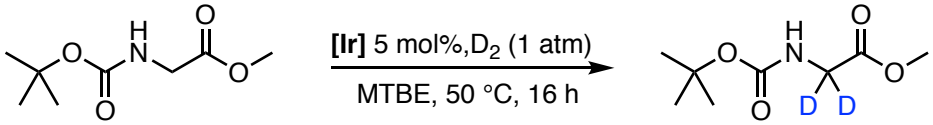

147d **D147d**

The catalyst screen was performed as described in *General Procedure H* with Boc-Gly-OMe **147d** (40.6 mg, 0.215 mmol). Solvent volume was 2.5 mL. The product was purified by trituration with diethyl ether.

^{1}H NMR (400 MHz, $CDCl_3$) δ 3.91 (d, J = 5.6 Hz, 2H, CH_2), 3.74 (s, 3H OCH_3), 1.44 (s, 9H, $OC(CH_3)_3$) ppm.

Labelling expected against signal at 3.91 ppm, measured against signal at 3.74 ppm.

Table 1.16

Entry	Catalyst	Run 1 (%)	Run 2 (%)	Run 3 (%)	Avg (%)
1	**86a** (0.018 g, 0.01 mmol)	49	47	67	54
2	**86d** (0.017 g, 0.01 mmol)	18	20	19	19

Catalyst Screen tert-butyl (tert-butoxycarbonyl)glycinate **176**

Scheme 1.36

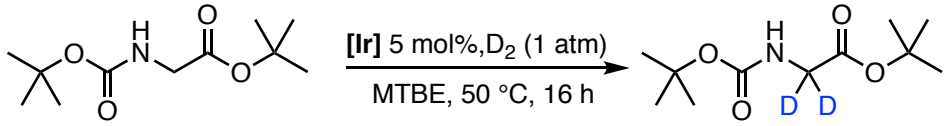

176 **D176**

Performed as described in *General Procedure H* with and Boc-Gly-O^{t}Bu **176** (49.7 mg, 0.215 mmol). Solvent volume was 2.5 mL. The product was purified by flash column chromatography (0-10% MeOH/DCM). Labelling measured using 2,4-di-*tert*-butylphenol **205** in a 1:1 mixture. Post-purification, **205** was added and the mixture analysed by NMR.

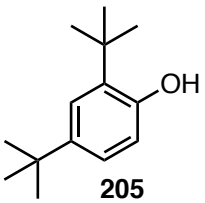

205

205:

^{1}H NMR (400 MHz, $CDCl_3$) δ 7.31 (d, ^4J = 2.5 Hz, 1H, Ar -C<u>H</u>), 7.08 (dd, J = 8.2, 2.5 Hz, 1H, Ar-C<u>H</u>), 6.66 (d, J = 8.3 Hz, 1H, Ar-C<u>H</u>), 1.44 (s, 9H, ArC(C<u>H</u>$_3$)$_3$), 1.32 (s, 9H, ArC(C<u>H</u>$_3$)$_3$) ppm.

176:

^{1}H NMR (400 MHz, $CDCl_3$): δ 5.14 – 4.98 (m, 1H, N<u>H</u>), 3.83 (s, 2H, C<u>H</u>$_2$), 1.48 (d, J = 2.3 Hz, 18H, OC(C<u>H</u>$_3$)$_3$), ppm.

Labelling expected against signal at 3.83 ppm, measured against internal standard signal at 7.31 ppm

Table 1.17

Entry	Catalyst	Run 1 (%)	Run 2 (%)	Run 3 (%)	Avg (%)
1	**86a** (0.018 g, 0.01 mmol)	60	65	63	62
2	**86b** (0.017 g, 0.01 mmol)	44	41	41	42
3	**86d** (0.017 g, 0.01 mmol)	67	79	73	73

Glycine derivative synthesis cntd.

tert-Butyl acetylglycinate **177**

Scheme 1.37

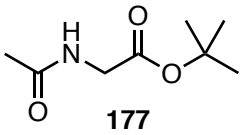

177

Chemical Formula: $C_8H_{15}NO_3$
Molecular Weight: 173.2120

Compound **177** was synthesised *via* a modified literature procedure. [88] To a 100 mL round-bottom flask was added glycine (2.0 g, 27 mmol, 1.0 eq) and *tert*-butyl acetate (65 mL). The suspension was stirred at 0 °C and 70% perchloric acid in water (3.5 mL, 41 mmol, 1.5 eq). was added dropwise. The resulting solution was stirred overnight at room temperature. After this time, the reaction mixture was diluted with water and carefully quenched at 0 °C with saturated potassium carbonate solution then basified to pH 9. The resulting solution was then extracted with diethyl ether, the combined organic phases dried with sodium sulfate, and concentrated *in vacuo* to yield *tert*-butyl glycinate as a colourless oil. The resulting oil was then dissolved in chloroform (100 mL) at 0 °C and trimethylamine (8.85 mL, 54.0 mmol, 2.0 eq) added slowly. After stirring for 5 min, acetyl chloride (2.3 mL, 32.4 mmol, 1.2 eq) was added dropwise. The reaction mixture was then allowed to slowly rise to room temperature and stirred for 16 h. The reaction was then carefully quenched with saturated sodium bicarbonate and extracted with $CHCl_3$. The combined organic phases were dried with Na_2SO_4, filtered and concentrated *in vacuo*. The resulting oil was then purified by column chromatography (50 % EtOAc/Petrol) to afford **177** (1.59 g, 9.18 mmol, 34% yield) as a yellow oil.

FTIR (neat): 3283, 3099, 2978, 1736, 1655, 1541, 1367 cm^{--1}.

^{1}H NMR (400 MHz, Acetone-d_6): δ 7.41 – 7.17 (m, 1H, NH), 3.80 (d, *J* = 5.8 Hz, 2H, CH_2), 1.92 (s, 3H, $COCH_3$), 1.43 (s, 9H, $OC(CH_3)_3$) ppm.

^{13}C NMR (101 MHz, Acetone-d_6): δ 170.4, 169.6, 81.4, 42.4, 28.2, 22.6 ppm.

HRMS (positive ESI): m/z calculated for $C_8H_{16}NO_3$ $[M+H]^+$ 174.1125 found: 174.1123.

Methyl (N-(benzyloxy)carbonyl)glycinate **147d** [89]

Scheme 1.37

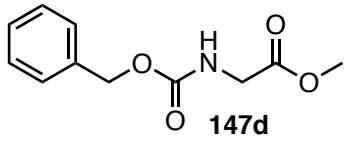

147d

Chemical Formula: $C_{11}H_{13}NO_4$
Molecular Weight: 223.2280

To a stirred suspension of glycine methyl ester hydrochloride (1.5 g, 12 mmol, 1 eq) and benzyl chloroformate (2.3 mL, 15.6 mmol, 1.3 eq) in H_2O (10 mL) was added a solution of $NaHCO_3$ (2 g, 24 mmol, 2 eq) in H_2O (10 mL) slowly at room temperature. The reaction mixture was then stirred for 16 h, after which time EtOAc (20 mL) was added and the phases separated. The aqueous phase was then extracted with EtOAc (3 × 50 mL). The organic phases were then combined, dried with Na_2SO_4 and concentrated *in vacuo*. The resulting residue was then purified by column chromatography (0-50% ethyl acetate/petrol) to afford **147d** as a clear oil (1.27g, 5.76 mmol, 48% yield).

FTIR (neat): 3385, 2953, 2360, 1747, 1701, 1521, 1178 cm^{-1}

^{1}H NMR (400 MHz, $CDCl_3$): δ 7.41 – 7.30 (m, 5H, Ar-H), 5.32 – 5.28 (m, 1H, NH), 5.13 (s, 2H CH_2Ph), 3.99 (d, *J* = 5.6 Hz, 2H, CH_2), 3.76 (s, 3H, OCH_3) ppm.

^{13}C NMR (101 MHz, $CDCl_3$): δ 169.9, 155.7, 135.7, 128.0, 127.7, 127.6, 66.6, 51.9, 42.2 ppm.

tert-butyl glycinate **206** [90]

Scheme 1.37

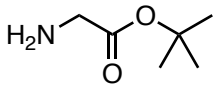

Chemical Formula: $C_6H_{13}NO_2$
Molecular Weight: 131.1750

206

Prepared according to *General Procedure E*.

Amount of Gly-OH: 4.13 g, 53.0 mmol, 1.0 eq.

Amount of ^{t}BuOAc: 212 mL, 159.0 mmol, 3.0 eq.

Amount of 70% $HClO_4$ n water: 6.33 mL, 74.2 mmol, 1.4 eq.

Product yield: 2.49 g, 19.0 mmol, 53% yield.

FTIR (neat): 3286, 2974, 2933, 1699 1701, 1367 cm^{-1}

^{1}H NMR (400 MHz, DMSO-d_6) δ 3.14 (s, 2H, NHC$\underline{H_2}$), 1.42 (s, 9H, OC(C$\underline{H_3}$)$_3$) ppm.

^{13}C NMR (101 MHz, $CDCl_3$): δ 173.0, 80.4, 44.1, 27.5 ppm.

tert-Butyl((benzyloxy)carbonyl)glycinate **178** [91]

Scheme 1.37

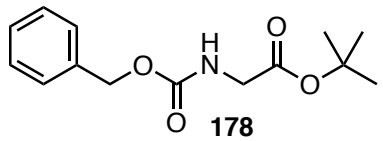

Chemical Formula: $C_{14}H_{19}NO_4$
Molecular Weight: 265.3090

178

To a stirred suspension of glycine *tert*-butyl ester **206** (1.0 g, 7.6 mmol, 1 eq) and benzyl chloroformate (1.47 mL, 9.91 mmol, 1.3 eq) in H_2O (3.2 mL) was added a solution of $NaHCO_3$ (1.27 g, 15.24 mmol, 2 eq) in H_2O (6.4 mL) slowly at room temperature. The reaction mixture was then stirred for 16 h, after which time EtOAc (20 mL) was added and the phases separated. The aqueous phase was then extracted with EtOAc (3 × 50 mL). The organic layers were then combined, dried with Na_2SO_4 and concentrated *in* vacuo. The resulting residue was then purified by column chromatography (0-50% diethyl/petrol) to afford **178** as a clear oil (1.27g, 5.76 mmol, 48% yield).

FTIR (neat): 3354, 2978, 1706, 1517, 1499, 1392 cm^{-1}

^{1}H NMR (400 MHz, $CDCl_3$): δ 7.46 – 7.33 (m, 5H Ar-H), 5.27 – 5.23 (m, 1H, NH), 5.15 (s, 2H, CH_2Ph), 3.90 (d, *J* = 5.4 Hz, 2H, CH_2), 1.49 (s, 9H, $OC(CH_3)_3$) ppm.

^{13}C NMR (101 MHz, $CDCl_3$): δ 168.5, 155.7, 135.8, 128.0, 127.6, 127.6, 81.8, 66.5, 43.0, 27.5 ppm.

HRMS (positive ESI): m/z calculated for $C_{14}H_{20}NO_4$ $[M+H]^+$ 266.1387 found: 266.1389.

Methyl (((9H-fluoren-9-yl)methoxy)carbonyl)glycinate **147c** [92]

Scheme 1.37

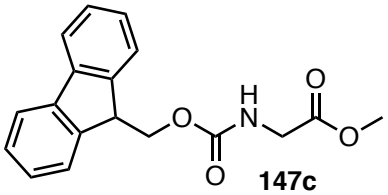

147c

Chemical Formula: $C_{18}H_{17}NO_4$
Molecular Weight: 311.3370

To a stirred suspension of glycine methyl ester hydrochloride (0.5 g, 6.66 mmol, 1 eq) and Fmoc-Cl (1.72 g, 7.33 mmol, 1.1 eq) in DCM (25 mL) was added Et_3N (1.06, 6.66 mmol, 1 eq) at 0 °C. The reaction mixture was then stirred for 16 h. The reaction was then washed successively with 1 N HCl and brine and resulting organic layers were dried with Na_2SO_4, filtered and concentrated *in vacuo*. The resulting residue was then purified by column chromatography (0-50% EtOAc/petrol) to afford **147c (**1.38 g, 4.46 mmol, 67% yield) as a white solid.

Melting point: 112 - 114 °C

FTIR (neat): 3825, 2970, 2360, 1742, 1689, 1556, 1301 cm^{-1}

^{1}H NMR (400 MHz, $CDCl_3$): δ 7.77 (d, *J* = 7.5 Hz, 2H, Ar-H), 7.60 (d, *J* = 7.5 Hz, 2H, Ar-H), 7.40 (t, *J* = 7.4, 2H, Ar-H), 7.31 (t, *J* = 7.2 Hz, 2H, Ar-H), 5.39 – 5.23 (m, 1H, NH), 4.41 (d, *J* = 7.1 Hz, 2H, CH_2Fmoc), 4.24 (t, *J* = 7.1 Hz, 1H, CHFmoc), 4.00 (d, *J* = 5.7 Hz, 2H, $NHCH_2$), 3.76 (s, 3H, OCH_3) ppm.

^{13}C NMR (101 MHz, $CDCl_3$): δ 170.6, 156.4, 143.9, 141.4, 127.9, 127.2, 125.2, 120.1, 67.4, 52.5, 47.3, 42.8 ppm.

tert-Butyl (((9H-fluoren-9-yl)methoxy)carbonyl)glycinate **179** [93]

Scheme 1.37

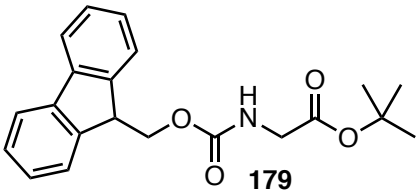

179

Chemical Formula: $C_{21}H_{23}NO_4$
Molecular Weight: 353.4180

Compound **179** was synthesis *via* a modified literature procedure.[94] To a stirred suspension of glycine *tert*-butyl ester **206** (0.5 g, 3.81 mmol, 1 eq) and Fmoc-OSu (1.54 g, 4.58 mmol, 1.2 eq) in dioxane (16 mL) was added Na_2CO_3 (0.49 g, 4.58 mmol, 1.2 eq) in H_2O (2 mL) dropwise at 0 °C. The reaction mixture was then stirred for 16 h. Upon completion of the reaction, the solvent was removed *in vacuo* and the resulting residue dissolved in EtOAc (20 mL) then washed with water (3 × 20 mL), and the resulting organic phase was dried with Na_2SO_4, filtered and concentrated *in vacuo*. The resulting residue was then purified by column chromatography (0-20% EtOAc/petrol) to afford **179** (0.71 g, 2.02 mmol, 53% yield) as a colourless oil.

FTIR (neat): 3379, 2978, 2939, 1739, 1701, 1689, 1512 cm^{-1}

^{1}H NMR (400 MHz, $CDCl_3$): δ 7.79 (d, *J* = 7.4 Hz, 2H, Ar-H), 7.64 – 7.61 (m, 2H, Ar-H), 7.42 (t, *J* = 7.5 Hz, 2H, Ar-H), 7.33 (t, *J* = 7.5 Hz, 2H, Ar-H), 5.48 – 5.33 (m, 1H, NH), 4.42 (d, *J* = 7.2 Hz, 2H, CH_2Fmoc), 4.26 (t, *J* = 7.2 Hz, 1H, CHFmoc), 3.92 (d, *J* = 5.4 Hz, 2H, $NHCH_2$), 1.51 (s, 9H, $OC(CH_3)_3$) ppm.

^{13}C NMR (101 MHz, $CDCl_3$): δ 171.0, 156.4, 144.0, 141.4, 127.9, 127.2, 125.3, 120.1, 82.5, 67.3, 47.3, 43.6, 28.2 ppm.

HRMS (positive ESI): m/z calculated for $C_{21}H_{24}NO_4$ $[M+H]^+$ 354.1700 found: 354.1702.

Labelling of glycine derivatives with catalyst 86a

Scheme 1.37

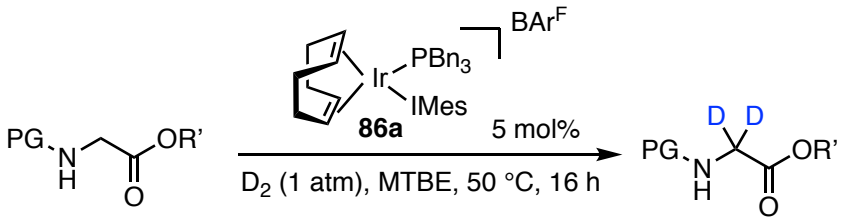

The protecting group screen was performed as described in *General Procedure H.* Solvent volume = 1.25 mL. The products were purified by column chromatography (50:50 diethyl ether/petrol).

Labelling of tert-butyl acetylglycinate, **177**

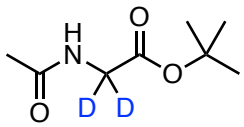

D177

^{1}H NMR (400 MHz, Acetone-d_6): δ 7.41 – 7.17 (m, 1H, NH), 3.80 (d, *J* = 5.8 Hz, 2H, CH_2), 1.92 (s, 3H, $COCH_3$), 1.43 (s, 9H, $OC(CH_3)_3$) ppm.

Labelling expected against signal at 3.80 ppm, measured against signal at 1.92 ppm.

Table 1.18

86a (mg, mmol)	177 (mg, mmol)	Run 1 (%)	Run 2 (%)	Run 3 (%)	Avg (%)
9.53, 0.005	18.6, 0.11	93	83	92	89

Labelling of methyl ((benzyloxy)carbonyl)glycinate **147b**

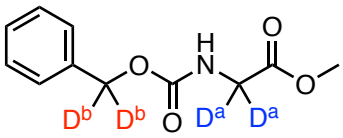

D147b

^{1}H NMR (400 MHz, $CDCl_3$): δ 7.41 – 7.30 (m, 5H, Ar-H), 5.32 – 5.28 (m, 1H, NH), 5.13 (s, 2H CH_2Ph), 3.99 (d, J = 5.6 Hz, 2H, CH_2), 3.76 (s, 3H, OCH_3) ppm.

Labelling expected against signal at 3.99 and 5.13 ppm, measured against signal at 3.76 ppm.

Table 1.19

86a (mg, mmol)	147b (mg, mmol)	Run 1 (%)	Run 2 (%)	Run 3 (%)	Avg (%)
9.53, 0.005	24.0, 0.11	D^a 65 D^b 23	D^a 67 D^b 31	D^a 66 D^b 33	D^a 66 D^b 29

tert-butyl ((benzyloxy)carbonyl)glycinate **178**

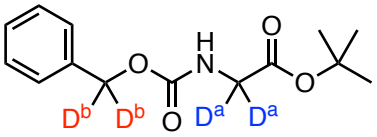

D178

^{1}H NMR (400 MHz, $CDCl_3$): δ 7.46 – 7.33 (m, 5H Ar-H), 5.27 – 5.23 (m, 1H, NH), 5.15 (s, 2H, CH_2Ph), 3.90 (d, J = 5.4 Hz, 2H, CH_2), 1.49 (s, 9H, $OC(CH_3)_3$) ppm.

Labelling expected against signal at 3.90 and 5.15 ppm, measured against signal at 7.46 –

7.33 ppm.

Table 1.20

86a (mg, mmol)	178 (mg, mmol)	Run 1 (%)	Run 2 (%)	Run 3 (%)	Avg (%)
9.53, 0.005	28.4, 0.11	D[a] 68 D[b] 51	D[a] 58 D[b] 40	D[a] 60 D[b] 50	D[a] 62 D[b] 47

Labelling of methyl (((9H-fluoren-9-yl)methoxy)carbonyl)glycinate **147c**

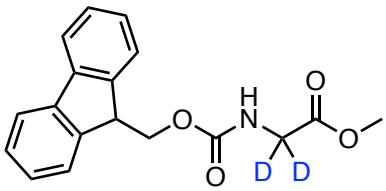

D147c

^{1}H NMR (400 MHz, $CDCl_3$): δ 7.77 (d, *J* = 7.5 Hz, 2H, Ar-H), 7.60 (d, *J* = 7.5 Hz, 2H, Ar-H), 7.40 (t, *J* = 7.4, 2H, Ar-H), 7.31 (t, *J* = 7.2 Hz, 2H, Ar-H), 5.39 – 5.23 (m, 1H, NH), 4.41 (d, *J* = 7.1 Hz, 2H, CH_2Fmoc), 4.24 (t, *J* = 7.1 Hz, 1H, CHFmoc), 4.00 (d, *J* = 5.7 Hz, 2H, NHCH_2), 3.76 (s, 3H, OCH_3) ppm.

Labelling expected against signal at 4.00 ppm, measured against signal at 4.24 ppm.

Table 1.21

86a (mg, mmol)	147c (mg, mmol)	Run 1 (%)	Run 2 (%)	Run 3 (%)	Avg (%)
9.53, 0.005	0.11	53	61	51	55

tert-butyl (((9H-fluoren-9-yl)methoxy)carbonyl)glycinate **179**

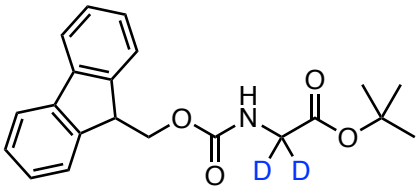

D179

^{1}H NMR (400 MHz, $CDCl_3$): δ 7.79 (d, *J* = 7.4 Hz, 2H, Ar-H), 7.64 – 7.61 (m, 2H, Ar-H), 7.42 (t, *J* = 7.5 Hz, 2H, Ar-H), 7.33 (t, *J* = 7.5 Hz, 2H, Ar-H), 5.48 – 5.33 (m, 1H, NH), 4.42 (d, *J* = 7.2 Hz, 2H, CH_2Fmoc), 4.26 (t, *J* = 7.2 Hz, 1H, CHFmoc), 3.92 (d, *J* = 5.4 Hz, 2H, $NHCH_2$), 1.51 (s, 9H, $OC(CH_3)_3$) ppm.

Labelling expected against signal at 3.92 ppm, measured against signal at 4.26 ppm.

Table 1.22

86a (mg, mmol)	179 (mg, mmol)	Run 1 (%)	Run 2 (%)	Run 3 (%)	Avg (%)
9.53, 0.005	38.0, 0.11	75	80	85	80

1.5.4 Expansion of Deutrium Labelling to Tertiary Amino Acids

methyl acetyl-L- alaninate **148** [95]

Scheme 1.39

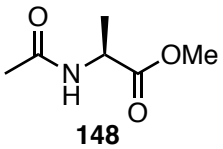

148

Chemical Formula: $C_6H_{11}NO_3$
Molecular Weight: 145.1580

Prepared according to *General Procedure C* using a reaction time of 1 h.

Amount of Ala-OMe•HCl: 7.79 g, 56.0 mmol, 1.0 eq.

Amount of triethylamine: 17.3 mL, 67.0 mmol, 1.2 eq.

Amount of acetyl chloride: 4.75 mL, 112 mmol, 2.0 eq.

Solvent volume: 150 mL $CHCl_3$.

Product yield: 4.38 g, 30.0 mmol, 54% yield.

FTIR (neat): 3308, 2981, 2953, 1739, 1651, 1537 cm^{-1}.

^{1}H NMR (400 MHz, $CDCl_3$): δ 4.64 – 4.52 (m, 1H, C<u>H</u>), 3.79 (s, 3H, OC<u>H</u>$_3$), 2.05 (s, 3H, COC<u>H</u>$_3$), 1.38 (d, J = 7.2, Hz, 3H, C<u>H</u>$_3$) ppm.

^{13}C NMR (101 MHz, Acetone-d_6): δ 172.6, 168.8, 50.9, 47.4, 21.2, 16.4 ppm.

Catalyst screen for methyl acetylalaninate 148

Scheme 1.39

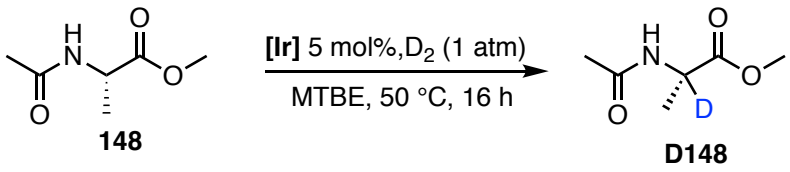

The labelling of alanine derivatives was preformed according to *General Procedure H* with and Ac-Ala-OMe **148** (31.2 mg, 0.215 mmol). Solvent volume was 2.5 mL. The product was purified by column chromatography (0-10% MeOH/DCM).

^{1}H NMR (400 MHz, $CDCl_3$): δ 4.64 – 4.52 (m, 1H, C<u>H</u>), 3.79 (s, 3H, OC<u>H</u>$_3$), 2.05 (s, 3H, COC<u>H</u>$_3$), 1.38 (d, J = 7.2, Hz, 3H, C<u>H</u>$_3$) ppm

Labelling expected against signal at 4.64 – 4.52 ppm, measured against signal at 2.05 ppm.

Table 1.23

Entry	Catalyst	Run 1 (%)	Run 2 (%)	Run 3 (%)	Avg (%)
1	**86a** (0.018 g, 0.01 mmol)	10	20	15	15
2	**86b** (0.017 g, 0.01 mmol)	4	0	6	3
3	**86d** (0.016 g, 0.01 mmol)	17	21	14	17
4	**86e** (0.017 g, 0.01 mmol)	28	22	20	23
5	**174** (0.017 g, 0.01 mmol)	9	12	9	10
6	**111** (0.018 g, 0.01 mmol)	6	7	9	0
7	**175** (0.015 g, 0.01 mmol)	10	2	8	7

Labelling of *tert*-butyl (*tert*-butoxycarbonyl)glycinate 176 with catalyst 111

Scheme 1.42

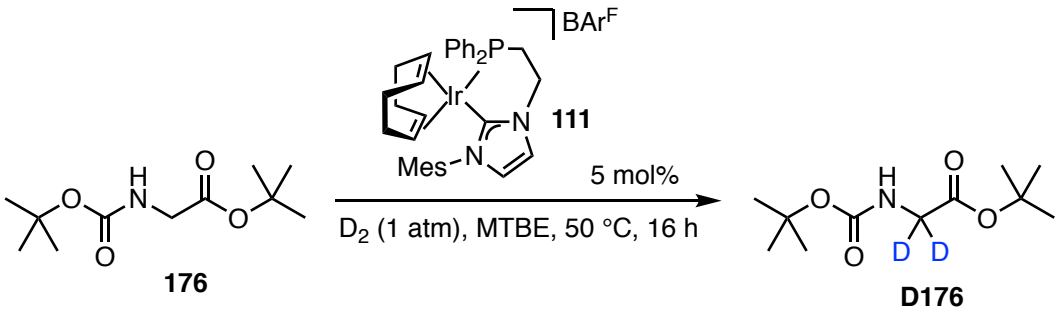

Performed as described in *General Procedure H* with and Boc-Gly-O^{t}Bu **176** (49.7 mg, 0.215 mmol). Solvent volume was 2.5 mL. The product was purified by column chromatography (0-10% MeOH/DCM). Labelling measured using 2,4-di-*tert*-butylphenol **205** in a 1:1 mixture added post purification.

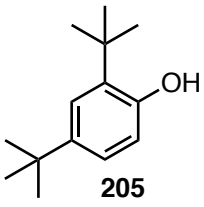

205:

^{1}H NMR (400 MHz, $CDCl_3$) δ 7.31 (d, *J* = 2.5 Hz, 1H, Ar -C<u>H</u>), 7.08 (dd, *J* = 8.2, 2.5 Hz, 1H, Ar-C<u>H</u>), 6.66 (d, *J* = 8.3 Hz, 1H, Ar-C<u>H</u>), 1.44 (s, 9H, ArC(C<u>H</u>$_3$)$_3$), 1.32 (s, 9H, ArC(C<u>H</u>$_3$)$_3$) ppm.

176:

^{1}H NMR (400 MHz, $CDCl_3$): δ 5.15 – 4.98 (m, 1H, N<u>H</u>), 3.83 (s, 2H, C<u>H</u>$_2$), 1.48 (d, *J* = 2.3 Hz, 18H, OC(C<u>H</u>$_3$)$_3$), ppm.

Labelling expected against signal at 3.83 ppm, measured against internal standard signal at 7.31 ppm

Table 1.24

Catalyst	Run 1 (%)	Run 2 (%)	Run 3 (%)	Avg (%)
111 (0.018 g, 0.01 mmol)	45	44	46	45

Synthesis of alanine derivatives

tert-butyl (tert-butoxycarbonyl)alaninate **187** [87]

Scheme 1.44

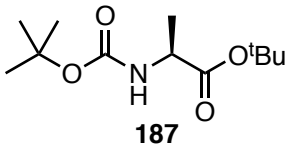

187

Chemical Formula: $C_{12}H_{23}NO_4$
Molecular Weight: 245.3190

To a 250 mL round-bottom flask was added L-alanine (4.0 g, 45 mmol, 1.0 eq) and *tert*-butyl acetate (130 mL). The suspension was stirred at 0 °C and a solution 70% perchloric acid in water (7.0 mL, 67.5 mmol, 1.5 eq). was added dropwise. The resulting solution was stirred overnight at room temperature. After this time, the reaction mixture was diluted with water , then carefully quenched at 0 °C with saturated potassium carbonate solution and basified to pH 9. The resulting solution was then extracted with diethyl ether, and the combined organic

phases dried with sodium sulfate, then concentrated *in vacuo* to yield *tert*-butyl alaninate as a colourless oil. The resulting oil was then dissolved in DCM (200 mL) at 0 °C and trimethylamine (22.2 mL, 135.0 mmol, 3.0 eq) added slowly. After stirring for five min, Boc_2O (9.81 g, 45.0 mmol, 1.0 eq) was added dropwise. The reaction mixture was then allowed to slowly rise to room temperature and stirred for 16 h. The reactionmixture was then carefully quenched by addition of saturated sodium bicarbonate solution and extracted with $CHCl_3$. The resulting organicphase was then washed with brine, dried with Na_2SO_4, filtered and concentrated *in vacuo*. The resulting residue was then purified by column chromatography (0-20% diethyl ether/petrol) to give **187** (6.17 g, 3.15 mmol, 60%) as a colourless oil.

FTIR (neat): 3367, 2978, 1713, 1701, 1503 cm^{-1}

^{1}H NMR (400 MHz, $CDCl_3$): δ 5.26 – 5.02 (m, 1H, NH), 4.25 – 4.11 (m, 1H, CH), 1.44 (s, 9H, $OC(CH_3)_3$), 1.42 (s, 9H, $OC(CH_3)_3$), 1.32 (d, J = 7.1 Hz, 3H, CH_3) ppm.

^{13}C NMR (101 MHz, $CDCl_3$): δ 172.2, 154.5, 81.4, 79.0, 49.5, 28.7, 27.2, 18.5 ppm.

HRMS (positive ESI): m/z calculated for $C_{12}H_{24}NO_4$ $[M+H]^+$ 246.1700 found: 246.1702.

Labelling of *tert*-butyl (*tert*-butoxycarbonyl)alaninate 187 with 86a

Scheme 1.44

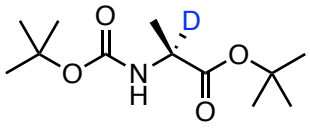

D187

The labelling of alanine derivatives were preformed according to *General Procedure H*. Solvent volume = 1.25 mL. The products were purified by column chromatography (50-100% diethyl ether/petrol).

^{1}H NMR (400 MHz, $CDCl_3$) δ 5.26 – 5.02 (m, 1H, NH), 4.25 – 4.11 (m, 1H, CH), 1.44 (s, 9H, $OC(CH_3)_3$), 1.42 (s, 9H, $OC(CH_3)_3$), 1.32 (d, J = 7.1 Hz, 3H, CH_3) ppm.

Labelling expected against signal at 4.25 – 4.11 ppm, measured against signal at 1.32 ppm

Table 1.25

86a (mg, mmol)	187 (mg, mmol)	Run 1 (%)	Run 2 (%)	Run 3 (%)	Avg (%)
9.53, 0.005	26.4, 0.11	56	62	64	61

Chiral HPLC traces of *rac*-**187** and **D187**:

Column: Chiralpak AD

Flow rate: 1.0 mL/min

Eluent composition: 1.0% *i*PrOH in hexane

Detector: 225 nm

Racemic sample:

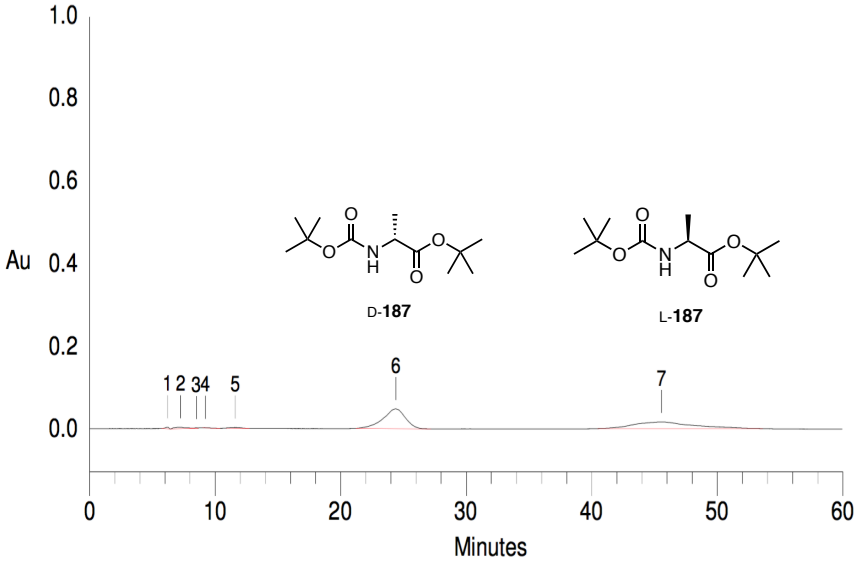

Pk. Num	Ret Time	Component Name	Concentration	Height	Area	Bl. Code	%Delta
1	6.20		0.000	3727	71388	1	
2	7.25		0.000	3190	196812	3	
3	8.50		0.000	221	1759	4	
4	9.20		0.000	512	15156	1	
5	11.60		0.000	1489	83971	1	
6	24.40		0.000	47570	5820578	1	
7	45.57		0.000	16135	5281269	1	
		Totals	0.000	72844	11470932		

Chiral Sample

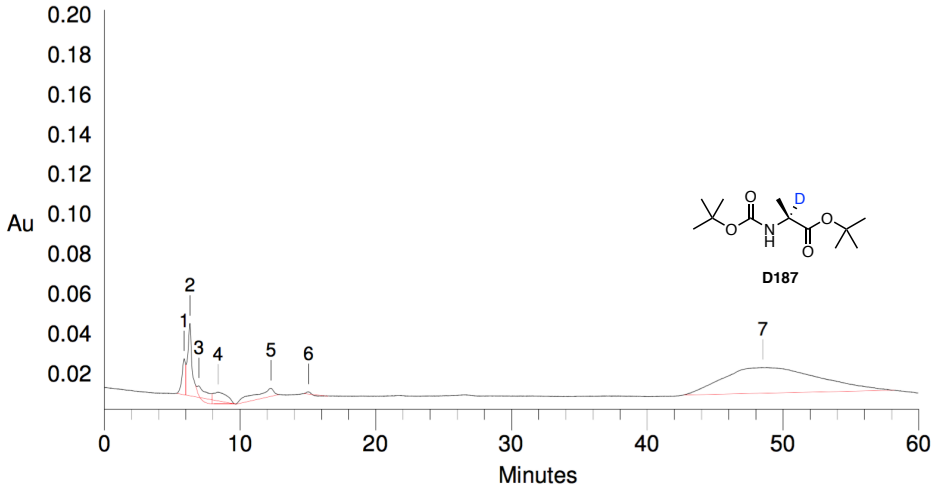

Pk. Num	Ret Time	Component Name	Concentration	Height	Area	Bl. Code	%Delta
1	5.88		0.000	17991	336210	2	
2	6.30		0.000	36212	659957	3	
3	6.97		0.000	4778	326814	4	
4	8.38		0.000	5952	352720	4	
5	12.28		0.000	3989	437390	1	
6	15.05		0.000	1136	7655	1	
7	48.52		0.000	13199	6725609	1	
		Totals	0.000	83257	8846355		

1.5.5 Optimisation of Tertiary Amino Acid Labelling

Screening of NHC

Scheme 1.45

1,3-dimesityl-4,5-dimethyl-1H-imidazol-3-ium chloride **207** [96]

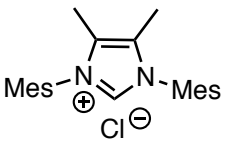

207

Chemical Formula: $C_{23}H_{29}ClN_2$
Molecular Weight: 368.9490

Compound **207** was synthesised *via* a literature procedure.[96] To a 100 mL round-bottom flask was added $MesNH_2$ (33.8 mL, 240 mmol, 2.0 eq), triethyl formate (20 mL, 120 mmol, 1 eq) and glacial acetic acid (0.344 mL, 6 mmol, 0.05 eq). The suspension was stirred at 140 °C for 3 h and the temperature raised to 160 °C for an additional 30 minutes. After this time, the reaction mixture was cooled to room temperature and the resulting off white solid triturated with hexanes to afford *N,N'*-dimesitylformamidine as a white solid (26.3 g, 202 mmol, 84% yield). This material was carried throughto the next synthetic step without further purification. To a flame-dried pressurised vessel was added *N,N'*-dimesitylformamidine (0.84 g, 3 mmol, 1 eq) in acetonitrile. Sequentially, di-*iso*-propylethylamine, (0.59 mL, 3.6 mmol, 1.2 eq) and 3-chloro-2-butanone (0.61 mL, 6.0 mmol, 2 eq) were added and the resulting mixture was stirred at 110 °C for 20 h. Upon full consumption of the formamidine, volatiles were removed under reduced pressure. The residual solid was then suspended in toluene (7.6 mL) and acetic anhydride (0.85 mL, 9.0 mmol, 3 eq) and 37% HCl (0.38 mL, 4.5 mmol, 1.5 eq) were added. The resulting mixture was stirred at 90 °C for 16 h, after which the reaction mixture was suspended in a mixture of DCM/H_2O 1:1 (100 mL). After separation, the aqueous phase was extracted a further three times with DCM (3 × 50 mL). The organic phases were combined and dried with sodium sulfate. Removal of the solvents *in vacuo* afforded the crude reaction product. This was then purified by column chromatography (2.5-10% MeOH/DCM) to afford the product as an off white solid, which was then recrystalised from petroleum ether/diethyl ether to give the pure product **207** as a white solid (0.79 g, 2.13 mmol, 71%).

Melting point: 212 – 215 °C

FTIR (neat): 2970, 2884, 2739, 1678, 1618, 1541, 1479, 1445, 1336 cm^{-1}

^{1}H NMR (400 MHz, $CDCl_3$): δ 10.51 (s, 1H, NC<u>H</u>N), 7.03 (s, 4H, Ar-<u>H</u>), 2.33 (s, 6H, 2 × CH_3), 2.10 (s, 12H, 4 × CH_3), 2.05 (s, 6H, 2 × CH_3) ppm.

^{13}C NMR (101 MHz, $CDCl_3$): δ 141.4, 137.8, 134.7, 130.1, 128.5, 127.6, 21.3, 17.7, 8.7 ppm.

[Ir(COD)ClIMes^{Me}] **106** [58]

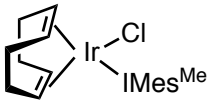

Chemical Formula: $C_{31}H_{40}ClIrN_2$
Molecular Weight: 668.3415

106

Prepared according to *General Procedure A*.

Amount of $[Ir(COD)Cl]_2$: 0.671 g, 1.0 mmol, 0.5 eq

Amount of potassium *tert*-butoxide : 0.224, 2.0 mmol, 1.0 eq.

Amount of $IMes^{Me}$•HCl: 0.733 g, 2.0 mmol, 1.0 eq.

Solvent volume: 18.0 mL THF.

Product yield: 0.735 g, 0.55 mmol, 55% yield.

FTIR (neat): 3003, 2940, 2914, 2873, 2827, 1610, 1484, 1396, 1357, 1315 cm^{-1}

^{1}H NMR (400 MHz, $CDCl_3$): δ 7.04 – 6.95 (m, 4H, Ar-H), 4.11 – 3.96 (m, 2H, COD CH), 3.14 – 2.96 (m, 2H, COD CH), 2.37 (s, 6H, Ar-CH_3), 2.30 (s, 6H, Ar-CH_3), 2.05 (s, 6H, Ar-CH_3), 1.83 (s, 6H, Ar-CH_3), 1.68 – 1.53 (m, 4H, COD CH_2), 1.40 – 1.16 (m, 4H, COD CH_2) ppm.

^{13}C NMR (101 MHz, $CDCl_3$) δ 178.9, 138.5, 137.8, 134.9, 134.4, 129.8, 128.1, 126.0, 81.3, 50.9, 33.6, 29.1, 21.3, 19.8, 18.3, 9.3 ppm.

[Ir(COD)(PBn$_3$)(IMes^{Me})] BAr^F **188**

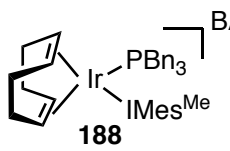

188

Chemical Formula: $C_{84}H_{73}BF_{24}IrN_2P$
Molecular Weight: 1800.4844

Prepared according to *General Procedure B*.

Amount of [Ir(COD)ClIMes^{Me}]: 0.536 g, 0.79 mmol, 1.0 eq.

Amount of NaBAr^F: 0.709 g, 0.79 mmol, 1.0 eq.

Amount of tribenzylphosphine: 0.24 g, 0.79 mmol, 1.0 eq.

Solvent volume: 25.0 mL DCM.

Product yield: 1.10 g, 0.67 mmol, 85% yield.

Melting point: 138 - 142 °C

FTIR (neat): 2970, 2885, 2362, 2341, 1352, 1273, 1120 cm^{-1}.

^{1}H NMR (400 MHz, CDCl$_3$): δ 7.71 (s, 8H, Ar-H BAr^F), 7.52 (s, 4H, Ar-H BAr^F), 7.26 – 7.15 (m, 13H, Ar-H), 6.74 (dt, *J* = 8.3, 1.4 Hz, 6H, Ar-H), 4.62 – 4.57 (m, 2H, COD CH), 3.10 – 3.06 (m, 2H, COD CH), 3.00 (d, $^2J_{P\text{-}H}$ = 8.6 Hz, 6H, P-CH$_2$-Ar), 2.46 (s, 6H, ArCH$_3$), 2.28 (s, 6H, ArCH$_3$), 2.24 (s, 6H, ArCH$_3$), 1.88 (s, 6H, ArCH$_3$), 1.56 – 1.48 (m, 4H, COD CH$_2$), 1.34 – 1.11 (m, 4H, COD CH$_2$) ppm.

^{13}C NMR (101 MHz, CDCl$_3$) δ 174.4 (d, $^2J_{C\text{-}P}$ = 8.7 Hz), 161.2 (q, $^1J_{C\text{-}B}$ = 49.5 Hz), 140.1, 135.9, 134.7, 134.3, 133.6, 132.5, 129.7, 129.4, 129.2, 128.3 (q $^2J_{C\text{-}F}$ = 31.5 Hz), 125.4 (q $^1J_{C\text{-}F}$ = 274 Hz), 116.9, 84.3, 84.1, 74.3, 31.7, 31.5, 30.1, 29.7, 20.5, 19.6, 18.7, 9.0 ppm.

^{11}B NMR (128 MHz, CDCl$_3$): δ -6.64 ppm (BAr^F B(Ar$_4$)).

^{31}P NMR (162 MHz, CDCl$_3$): δ -7.48 ppm (PBn$_3$).

^{19}F NMR (376 MHz, CDCl$_3$): δ -64.3 ppm (BAr^F ArCF$_3$).

HRMS: awaiting

[Ir(COD)ClIPr] **208**[58]

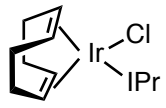

208

Chemical Formula: $C_{35}H_{48}ClIrN_2$
Molecular Weight: 724.4495

Prepared according to *General Procedure A*.

Amount of $[Ir(COD)Cl]_2$: 0.300 g, 0.45 mmol, 0.5 eq

Amount of potassium *tert*-butoxide : 0.10 g, 0.9 mmol, 1.0 eq.

Amount of IPr•HCl: 0.38 g, 0.9 mmol, 1.0 eq.

Solvent volume: 8.0 mL THF.

Product yield: 0.150 g, 0.20 mmol, 45% yield.

FTIR (neat): 2962, 2866, 2058, 1589, 1325 cm^{-1}

^{1}H NMR (400 MHz, $CDCl_3$): δ 7.49 (t, *J* = 7.7 Hz, 2H, Ar-H), 7.44 – 7.30 (s, 4H, Ar-H), 7.04 (s, 2H, Ar-H), 4.30 – 4.15 (m, 2H, COD CH), 3.57 – 3.41 (s, 2H, $CH(CH_3)_2$), 2.98 – 2.86 (m, 2H, COD CH), 2.84 – 2.67 (s, 2H, $CH(CH_3)_2$), 1.85 – 1.17 (m, 18H, COD CH_2 and $CH(CH_3)_2$), 1.12 (d, *J* = 6.9 Hz, 12H, $CH(CH_3)_2$), 0.93 – 0.81 (m, 2H, COD CH_2) ppm.

^{13}C NMR (101 MHz, $CDCl_3$) δ 181.9, 135.7, 129.2, 123.8, 122.4, 82.3, 50.9, 33.0, 28.4, 28.2 25.99, 22.7, 22.0 ppm.

[Ir(COD)(PBn_3)(IPr)] BAr^F **189**

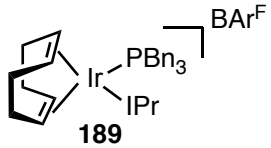

189

Chemical Formula: $C_{88}H_{81}BF_{24}IrN_2P$
Molecular Weight: 1856.5924

Prepared according to *General Procedure B*.

Amount of [Ir(COD)ClIPr]: 0.10 g, 0.138 mmol, 1.0 eq.

Amount of $NaBAr^F$: 0.122 g, 0.138 mmol, 1.0 eq.

Amount of tribenzylphosphine: 0.042 g, 0.138 mmol, 1.0 eq.

Solvent volume: 4.4 mL DCM.

Product yield: 0.065 g, 0.035 mmol, 25% yield.

Melting point: 152 - 153 °C

FTIR (neat): 2980, 2362, 1352, 1274, 1157 cm^{-1}.

^{1}H NMR (400 MHz, $CDCl_3$): δ 7.74 – 7.70 (m, 8H, Ar-H BAr^F), 7.69 – 7.57 (m, 6H, Ar-H), 7.52 (s, 4H, Ar-H, BAr^F), 7.43 – 7.36 (m, 4H, Ar-H), 7.25 – 7.13 (m, 8H, Ar-H), 6.72 6.64 (m, 5H, Ar-H), 4.51 – 4.43 (m, 2H, COD CH), 3.45 – 3.39 (m, 2H, COD CH), 2.91 (d, $^2J_{P\text{-}H}$ = 8.6 Hz, 6H, P-CH_2-Ar), 1.65 – 1.54 (m, 12H, CODCH_2 and Ar$CHCH_3$), 1.44 (d, J = 6.6 Hz, 6H, ArCHCH_3), 1.33 (d, J = 6.7 Hz, 6H, ArCHCH_3), 1.20 (d, J = 6.7 Hz, 6H, ArCHCH_3), 1.13 (d, J = 6.6 Hz, 6H, ArCHCH_3) ppm.

^{13}C NMR (101 MHz, $CDCl_3$) δ 179.4 (d, $^2J_{C\text{-}P}$ = 8.7 Hz), 160.4 (q, $^1J_{C\text{-}B}$ = 49.5 Hz), 145.6, 144.7, 136.5, 134.3, 132.3, 130.9, 129.2, 128.5 (q $^2J_{C\text{-}F}$ = 31.5 Hz), 127.0, 125.4 (q $^1J_{C\text{-}F}$ = 274 Hz), 124.8, 124.4, 122.7, 116.9, 84.4, 84.2, 74.9, 32.7, 32.4, 29.8, 29.6, 29.0, 28.9, 26.5, 25.4, 22.0, 21.6 ppm.

^{11}B NMR (128 MHz, $CDCl_3$): δ -6.64 ppm (BAr^F $B(Ar_4)$).

^{31}P NMR (162 MHz, $CDCl_3$): δ -4.56 ppm (PBn_3).

^{19}F NMR (376 MHz, $CDCl_3$): δ -64.3 ppm (BAr^F $ArCF_3$).

Screening of NHC - Labelling

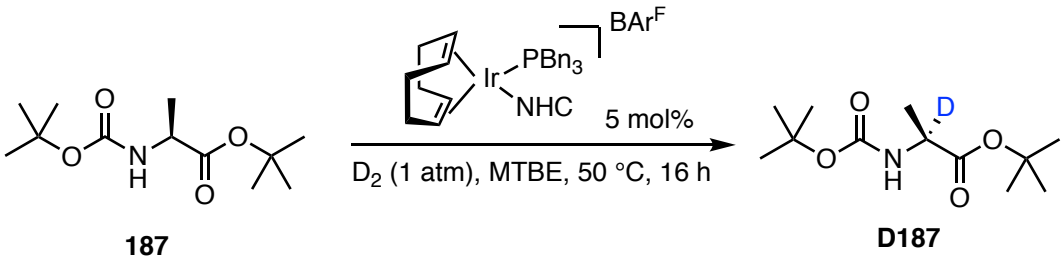

187 **D187**

Reactions were carried out following the *General Procedure H*, using Boc-Ala-O^{t}Bu **187** (26.4 mg, 0.011 mmol, 1 eq). Solvent volume 1.25 mL.

^{1}H NMR (400 MHz, $CDCl_3$) δ 5.26 – 5.02 (m, 1H, NH), 4.25 – 4.11 (m, 1H, CH), 1.44 (s, 9H, OC(CH_3)$_3$), 1.42 (s, 9H, OC(CH_3)$_3$), 1.32 (d, *J* = 7.1 Hz, 3H, CH_3) ppm.

Labelling expected against signal at 4.25 – 4.11 ppm, measured against signal at 1.32 ppm

Table 1.26

NHC	[Ir] (mg, mmol)	Run 1 (%)	Run 2 (%)	Run 3 (%)	Avg (%)
IMes **86a**	9.53, 0.005	56	62	64	61
IMes^{Me} **188**	9.68, 0.005	82	85	86	84
IPr **189**	9.98, 0.005	50	51	50	50

Design of Experiment

Scheme 1.46

Experimental design was used to assess the effect of varying catalyst loading, reaction time and reaction concentration (Conditions: **187**, 26.4 mg, 0.011 mmol, **188** (*catalyst loading*), MTBE (*concentration*), D_2 (1 atm), 50 °C, (*reaction time*)). As such, 'high' and 'low' values for each of these three variables were chosen. To generate a series of experiments to study optimal conditions within the variable ranges chosen, Design Expert™ software v9.0 (Stat_Ease Inc., Minneappolis, Mn) was used. This generated a *2 level, 3 factorial* design containing three centre points, giving 11 experiments in total. The deuterium incorporation of Boc-Ala-O^{t}Bu **187** was used as the response.

Table 1.27

Run[a]	Variable A: Catalyst Loading (mol%)	Amount of 188 (mg)	Variable B: MTBE volume (mL)	Variable C: Reaction Time (h)	Response: Incorporation (%)
1 (000)	7.5	14.6	1.25	10	71
2 (+--)	10.0	19.6	0.63	4	61
3 (000)	7.5	14.6	1.25	10	76
4 (++-)	10.0	19.6	2.50	4	75
5 (-+-)	5.0	9.4	2.50	4	55
6 (000)	7.5	14.6	1.25	10	77
7 (-++)	5.0	9.4	2.50	16	64
8 (--+)	5.0	9.4	0.63	16	43
9 (+-+)	10.0	19.6	0.63	16	48
10 (+++)	10.0	19.6	2.50	16	92
11 (---)	5.0	9.4	0.63	4	48

[a] (+) = high value, (-) low value, and (0) = centre point of a variable. (-+-) = combination of low A, high B, and low C

Entries 1, 3, and 6 represent the centre points of the design. These were employed in order to:

(i) Assess any curvature in the response of conversion changes in the variables.

(ii) Assess the repeatability of the hydrogen isotope exchange reaction.

A response surface was created in the same design program. This generated a half-normal plot, inferring that increasing the catalyst loading and MTBE volume, and the combination of catalyst loading and MTBE volume as well as the combination of solvent volume and reaction time, have a positive impact upon the efficacy of the HIE reaction.

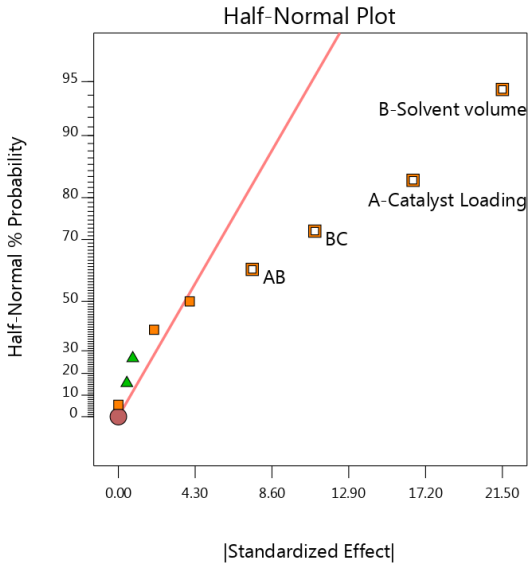

Optimal Conditions from DoE

Scheme 1.46

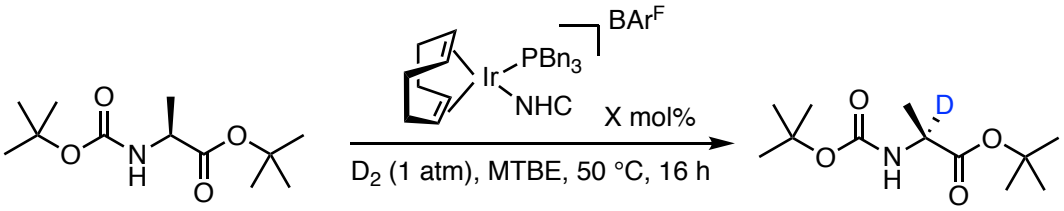

187 **D187**

Reactions were carried out following the *General Procedure H*, using Boc-Ala-O^{t}Bu **187** (26.4 mg, 0.011 mmol, 1 eq), with catalyst (7.5 - 10 mol%) in 1.25 mL of solvent (0.05 M) under D_2 for 16 h at 50 °C, the full details are tabulated below.

^{1}H NMR (400 MHz, $CDCl_3$) δ 5.26 – 5.02 (m, 1H, NH), 4.25 – 4.11 (m,, 1H, CH), 1.44 (s, 9H, OC(CH$_3$)$_3$), 1.42 (s, 9H, OC(CH$_3$)$_3$), 1.32 (d, J = 7.1 Hz, 3H, CH$_3$) ppm.

Labelling expected against signal at 4.25 – 4.11 ppm, measured against signal at 1.32 ppm

Table 1.28

NHC	[Ir] (mol%, mg, mmol)	Run 1 (%)	Run 2 (%)	Run 3 (%)	Avg (%)
$IMes^{Me}$ **188**	7.5, 14.52, (0.008)	90	89	90	90
$IMes^{Me}$ **188**	10, 19.4, (0.011)	92	94	97	93

Solvent Screening for labelling of 189

Graph 1.4

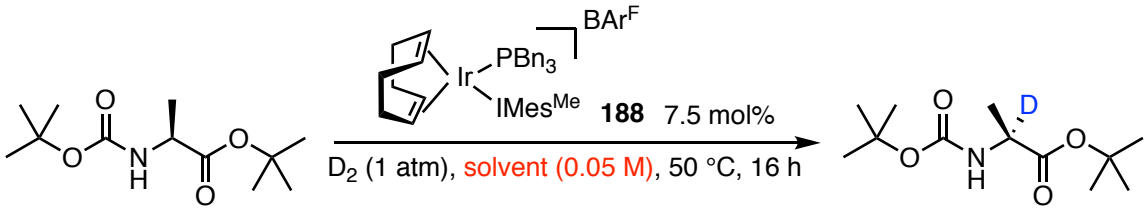

187 **D187**

Reactions were carried out following the *General Procedure H*, using Boc-Ala-O^{t}Bu **187** (26.4 mg, 0.011 mmol, 1 eq), with catalyst **188** in 1.25 mL of solvent (0.05 M) under D_2 for 16 h at 50 °C. The full details are tabulated below.

^{1}H NMR (400 MHz, $CDCl_3$) δ 5.26 – 5.02 (m, 1H, NH), 4.25 – 4.11 (m, 1H, CH), 1.44 (s, 9H, OC(CH_3)$_3$), 1.42 (s, 9H, OC(CH_3)$_3$), 1.32 (d, J = 7.1 Hz, 3H, CH_3) ppm.

Labelling expected against signal at 4.25 – 4.11 ppm, measured against signal at 1.32 ppm

Table 1.29

Entry	Cat. mol%	Solvent	Run 1 (%)	Run 2 (%)	Run 3 (%)	Avg (%)
1	7.5	MTBE	90	89	90	90
2	7.5	CPME	59	55	57	57
3	7.5	^{t}BuOAc	27	27	26	27
4	7.5	EtOAc	18	17	14	16
5	7.5	DCE	9	8	6	8
6	7.5	PhCl	22	24	23	23

1.5.6 Tertiary Amino Acid Labelling Scope

Scheme 1.47

tert-butyl alaninate **209** [97]

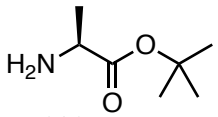

209

Chemical Formula: $C_7H_{15}NO_2$
Molecular Weight: 145.2020

Prepared according to *General Procedure E*.[98]

Amount of Ala-OH: 4.0 g, 44.9 mmol, 1.0 eq.

Amount of ^{t}BuOAc: 180 mL

Amount of $HClO_4$: 5.24 mL, 61.4 mmol, 1.4 eq.

Product yield: 5.21 g, 35.9 mmol, 80% yield.

FTIR (neat): 2974, 1726, 1699, 1367 cm^{-1}

^{1}H NMR (400 MHz, $CDCl_3$) δ 3.39 (q, *J* = 7.0 Hz, 1H, NHC<u>H</u>CH$_3$), 1.44 (s, 9H, OC(C<u>H</u>$_3$)$_3$), 1.26 (d, *J* = 7.0 Hz, 3H, NHCHC<u>H</u>$_3$) ppm.

^{13}C NMR (101 MHz, Acetone-d_6): δ 175.4, 80.2, 50.0, 27.4, 20.2 ppm.

tert-butyl (((9H-fluoren-9-yl)methoxy)carbonyl)alaninate **190** [99]

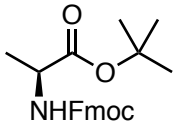

190

Chemical Formula: $C_{22}H_{25}NO_4$
Molecular Weight: 367.4450

Compound **190** was synthesised *via* a modified literature procedure.[94] To a stirred suspension of alanine *tert*-butyl ester **209** (1.83 g, 12.61 mmol, 1 eq) and Fmoc-OSu (5.09 g, 15.13 mmol, 1.2 eq) in dioxane (53 mL) was added Na_2CO_3 1.62 g, 15.13 mmol, 1.2 eq) in H_2O (6 mL) dropwise at 0 °C. The reaction mixture was then stirred for 16 h. Upon completion of the reaction, the solvent was removed *in vacuo* and the resulting residue dissolved in EtOAc (50 mL) then washed with water (3 x 50 mL) and the resulting organic layers were dried with Na_2SO_4, filtered and concentrated *in vacuo*. The resulting residue was then purified by column chromatography (0-20% EtOAc/petrol) to afford **190**, 2.32 g, 6.31 mmol, 50% yield as a white solid.

Melting point: 79 - 81 °C (78-80 °C lit.) [99]

FTIR (neat): 3383, 2980, 2926, 2360, 2331, 1722, 1693, 1529 cm^{-1}

^{1}H NMR (400 MHz, $CDCl_3$): δ 7.79 (d, *J* = 7.5 Hz, 2H, Ar-<u>H</u>), 7.63 (d, *J* = 7.4 Hz, 2H, Ar-<u>H</u>), 7.43 (t, *J* = 7.4 Hz, 2H, Ar-<u>H</u>), 7.34 (td, *J* = 7.4 Hz, ^4J = 1.2 Hz, 2H, Ar-<u>H</u>), 5.41 (d, *J* = 7.7 Hz, 1H, N<u>H</u>), 4.41(d, 2H, C<u>H</u>$_2$Fmoc), 4.31 (t, *J* = 7.3 Hz, 1H, NHC<u>H</u>), 4.25 (t, *J* = 7.1 Hz, 1H, C<u>H</u>Fmoc), 1.51 (s, 9H, OC(C<u>H</u>$_3$)$_3$), 1.43 (d, *J* = 7.1 Hz, NHCHC<u>H</u>$_3$) ppm.

^{13}C NMR (101 MHz, $CDCl_3$): δ 171.8, 155.1, 143.5, 143.4, 140.8, 127.2, 126.6, 124.6, 119.5, 81.5, 66.4, 49.7, 46.7, 27.5, 18.5 ppm.

tert-butyl valinate **210** [100]

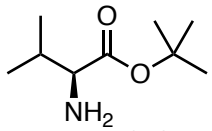

210

Chemical Formula: $C_9H_{19}NO_2$
Molecular Weight: 173.2560

Prepared according to *General Procedure E*. Column conditions: 0-40% EtOAc/petrol.

Amount of L-Val-OH: 2.0 g, 17.0 mmol, 1.0 eq.

Volume of ^{t}BuOAc: 212 mL

Amount of $HClO_4$: 2.21 mL, 26.0 mmol, 1.5 eq.

Product yield: 1.33 g, 7.65 mmol, 45% yield.

FTIR (neat): 3423, 3346, 2980, 1703, 1517, 1365 cm^{-1}

^{1}H NMR (400 MHz, $CDCl_3$) δ 3.16 (d, *J* = 4.9 Hz, 1H, $NH_2C\underline{H}$), 2.01 – 1.93 (m, 1H, $C\underline{H}CH_3$), 1.47 (s, 9H, $OC(C\underline{H_3})_3$), 0.97 (d, *J* = 6.9 Hz, 3H, $CHC\underline{H_3}$), 0.90 (d, *J* = 6.9 Hz, 3H, $CHC\underline{H_3}$) ppm.

tert-butyl (tert-butoxycarbonyl)valinate **191** [101]

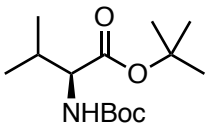

191

Chemical Formula: $C_{14}H_{27}NO_4$
Molecular Weight: 273.3730

Prepared according to *General Procedure D* using a reaction time of 16 *h*.

Amount of Val-O^{t}Bu: 1.0 g, 5.78 mmol, 1.0 eq.

Amount of Boc_2O: 2.90 g, 13.30 mmol, 2.3 eq.

Amount of Et_3N: 1.61 mL, 11.56 mmol, 2.0 eq.

Volume dioxane/water (1:1): 13 mL

Product yield: 1.07 g, 3.93 mmol, 68% yield as a colourless oil.

FTIR (neat): 2972, 2932, 1712, 1497, 1386 cm^{-1}

^{1}H NMR (400 MHz, $CDCl_3$) δ 5.04 (d, *J* = 9.0 Hz, 1H, NH), 4.13 – 4.10 (m, 1H, NH_2CH), 2.19 – 2.07 (m, 1H, $CHCH_3$), 1.49 (s, 9H, $OC(CH_3)_3$), 1.47 (s, 9H, $OC(CH_3)_3$), 0.97 (d, *J* = 6.9, ^4J = 1.1 Hz, 3H, $CHCH_3$), 0.91 (dd, *J* = 6.9, ^4J = 1.1 Hz, 3H, $CHCH_3$) ppm.

^{13}C NMR (101 MHz, $CDCl_3$): δ 171.7, 155.9, 81.7, 79.6, 58.9, 31.6, 28.5, 28.1, 19.1, 17.6 ppm.

HRMS (NSI): m/z calculated $C_{14}H_{28}NO_4$ $[M+H]^+$ 274.2015 found: 274.2013

Synthesis of tert-butyl leucinate **211** [81]

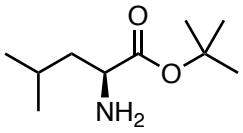

211

Chemical Formula: $C_{10}H_{21}NO_2$
Molecular Weight: 187.2830

Prepared according to *General Procedure E*. Column conditions: 0-20% EtOAc/petrol.

Amount of L-Leu-OH: 1.43 g, 10.9 mmol, 1.0 eq.

Volume of ^{t}BuOAc: 27 mL

Amount of $HClO_4$: 1.5 mL, 17.4 mmol, 1.6 eq.

Product yield: 1.86 g, 8.94 mmol, 82% yield.

FTIR (neat): 3486, 3378, 2988, 2939, 1731cm^{-1}

^{1}H NMR (400 MHz, $CDCl_3$) δ 3.34 – 3.26 (m, 1H, NH_2CH), 1.83 – 1.75 (m, 1H, $CHHCHNH_2$), 1.55 – 1.46 (m, 1H, $CHHCHNH_2$), 1.44 (s, 9H, $OC(CH_3)_3$), 1.39 – 1.31 (m, 1H, $CH(CH_3)_2$), 0.94 – 0.92 (t, *J* = 8.9 Hz, 6H, $CH(CH_3)_2$) ppm.

^{13}C NMR (101 MHz, $CDCl_3$): δ 171.0, 84.7, 81.1, 58.4, 31.0, 27.8, 27.5, 18.4 ppm.

tert-butyl (tert-butoxycarbonyl)- L-leucinate **192** [102]

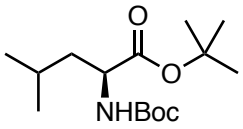

Chemical Formula: $C_{15}H_{29}NO_4$
Molecular Weight: 287.4000

192

Prepared according to *General Procedure D* using a reaction time of 16 h. Column conditions: 5-10% diethyl ether/petrol

Amount of Leu-O^{t}Bu: 1.3 g, 6.94 mmol, 1.0 eq.

Amount of Boc_2O: 3.48 g, 15.96 mmol, 2.3 eq.

Amount of Et_3N: 1.93 mL, 13.89 mmol, 2.0 eq.

Volume dioxane/water (1:1): 15 mL

Product yield: 1.22 g, 4.23 mmol, 61% yield as a colourless oil.

FTIR (neat): 2267, 2976, 2872, 1713, 1501, 1386 cm^{-1}

^{1}H NMR (400 MHz, $CDCl_3$) δ 4.88 (d, *J* = 8.9 Hz, 1H, NH), 4.18 (app. q, *J* = 7.1 Hz, 1H, NH_2CH), 1.76 – 1.66 (m, 1H, $CHCH_3$), 1.61 – 1.52 (m, 2H, $CHCH_2$), 1.47 (s, 9H, $OC(CH_3)_3$), 1.45 (s, 9H, $OC(CH_3)_3$), 0.95 (d, *J* = 6.5 Hz, 6H, 2 × $CHCH_3$) ppm.

^{13}C NMR (101 MHz, $CDCl_3$): δ 172.8, 155.5, 81.6, 79.7, 52.8, 42.3, 28.5, 28.1, 25.0, 23.0, 22.0 ppm.

Synthesis of tert-butyl isolucinate **212** [81]

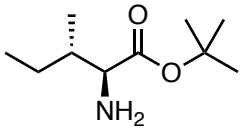

Chemical Formula: $C_{10}H_{21}NO_2$
Molecular Weight: 187.2830

212

Prepared according to *General Procedure E*. Column conditions: 0-60% EtOAc/petrol.

Amount of L-Ile-OH: 1.43 g, 10.9 mmol, 1.0 eq.

Volume of ^{t}BuOAc: 27 mL

Amount of $HClO_4$: 1.5 mL, 17.4 mmol, 1.6 eq.

Product yield: 0.89 g, 4.80 mmol, 44% yield.

FTIR (neat): 2962, 2929, 2875, 1724, 1458 cm^{-1}

^{1}H NMR (400 MHz, $CDCl_3$) δ 3.24 (d, *J* = 4.9 Hz, 1H, $NH_2C\underline{H}$), 1.76 – 1.68 (m, 1H, $CH(C\underline{H}_3)_2$), 1.48 (s, 9H, $OC(C\underline{H}_3)_3$), 1.44 – 1.15 (m, 2H, $CHC\underline{H}_2CH_3$), 0.99 – 0.90 (m, 6H, 2 x $C\underline{H}_3$) ppm.

^{13}C NMR (101 MHz, $CDCl_3$): δ 175.0, 80.9, 59.6, 39.5, 28.3, 25.0, 15.8, 11.9 ppm.

tert-butyl (tert-butoxycarbonyl)- L-isoleucinate **193**

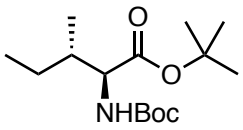

193

Chemical Formula: $C_{15}H_{29}NO_4$
Molecular Weight: 287.4000

Prepared according to *General Procedure D for 16 h*. Column conditions: 5-15% diethyl ether/petrol

Amount of Ile-O^{t}Bu: 0.893 g, 4.76 mmol, 1.0 eq.

Amount of Boc_2O: 2.39 g, 10.95 mmol, 2.3 eq.

Amount of Et_3N: 1.33 mL, 9.53 mmol, 2.0 eq.

Volume dioxane/water (1:1): 10 mL

Product yield: 1.06 g, 3.71 mmol, 78% yield as a colourless oil.

FTIR (neat): 2970, 2931, 1710. 1496, 1365 cm^{-1}

^{1}H NMR (400 MHz, $CDCl_3$) δ 5.06 (d, *J* = 8.9 Hz, 1H, N$\underline{H}$), 4.25 – 3.94 (m, 1H, NHC$\underline{H}$), 1.87 – 1.79 (m, 1H, C$\underline{H}CH_3$), 1.48 (s, 9H, $OC(C\underline{H}_3)_3$), 1.46 (s, 9H, $OC(C\underline{H}_3)_3$), 1.35 – 1.12 (m, 2H, $CHC\underline{H}_2$), 0.94 (dd, *J* = 7.8, 7.1 Hz, 6H, 2 × $CHC\underline{H}_3$) ppm.

^{13}C NMR (101 MHz, $CDCl_3$): δ 171.5, 155.7, 81.8, 79.6, 58.3, 38.5, 28.5, 28.2, 25.3, 15.5, 11.9 ppm.

HRMS (NSI): m/z calculated for $C_{15}H_{30}NO_4$ $[M+H]^+$ 288.2171 found: 288.2169.

Synthesis of tert-butyl O-(tert-butyl)-L-serinate **213** [103]

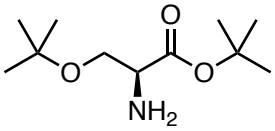

Chemical Formula: $C_{11}H_{23}NO_3$
Molecular Weight: 217.3090

213

Prepared according to *General Procedure E*. Column conditions: 0-30% EtOAc/petrol.

Amount of L-Ser-OH: 1.15 g, 10.9 mmol, 1.0 eq.

Volume of ^{t}BuOAc: 27 mL

Amount of $HClO_4$: 1.5 mL, 17.4 mmol, 1.6 eq.

Product yield: 0.99 g, 4.60 mmol, 42% yield.

Melting point: 40 - 42 °C

FTIR (neat): 3460, 2976, 1721, 1495 cm^{-1}

^{1}H NMR (400 MHz, $CDCl_3$) δ 3.63 – 3.58 (m, 1H, C<u>H</u>NH_2), 3.57 – 3.53 (m, 1H, C<u>H</u>H), 3.46 – 3.43 (m, 1H, CH<u>H</u>), 1.78 (bs, 2H, N<u>H</u>$_2$), 1.47 (s, 9H, OC(C<u>H</u>$_3$)$_3$), 1.18 (s, 9H, OC(C<u>H</u>$_3$)$_3$) ppm.

^{13}C NMR (101 MHz, $CDCl_3$): δ 173.6, 81.1, 73.0, 64.1, 55.8, 28.2, 27.6 ppm.

tert-butyl N-(tert-butoxycarbonyl)-O-(tert-butyl)-L-serinate **194** [104]

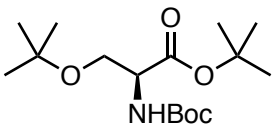

Chemical Formula: $C_{16}H_{31}NO_5$
Molecular Weight: 317.4260

194

Prepared according to *General Procedure D*. Column conditions: 5-50% diethyl ether/petrol.

Amount of Ser(^{t}Bu)-O^{t}Bu: 0.99 g, 4.60 mmol, 1.0 eq.

Amount of Boc_2O: 2.31 g, 10.58 mmol, 2.3 eq.

Amount of Et_3N: 1.28 mL, 9.20 mmol, 2.0 eq.

Volume dioxane/water (1:1): 10 mL

Product yield: 1.35 g, 4.28 mmol, 93% yield as a white solid.

FTIR (neat): 3460, 2976, 2931, 1700, 1720, 1494, 1365 cm^{-1}

^{1}H NMR (400 MHz, $CDCl_3$) δ 5.34 (d, *J* = 9.0 Hz, 1H, 1H, NH), 4.27 (dt, *J* = 9.2 Hz, ^4J = 2.9 Hz, 1H, NHCH), 3.78 (dd, *J* = 8.7 Hz, ^4J = 2.9 Hz, 1H, NHCHCHH), 3.54 (dd, *J* = 8.7 Hz, ^4J = 3.1 Hz, 1H, NHCHCHH), 1.48 (d, *J* = 3.4 Hz, 18H, 2 x OC(CH_3)$_3$), 1.16 (s, 9H, OC(CH_3)$_3$) ppm.

^{13}C NMR (101 MHz, $CDCl_3$): δ 169.5, 155.2, 81.0, 79.0, 72.5, 61.9, 54.1, 27.9, 27.5, 26.8 ppm.

HRMS (NSI): m/z calculated for $C_{16}H_{32}NO_5$ 318.2275 $[M+H]^+$ found: 318.2274

(S)-1-methoxy-1-oxo-3-phenylpropan-2-aminium chloride **214** [105]

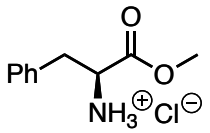

214

Chemical Formula: $C_{20}H_{28}Cl_2N_2O_4$
Molecular Weight: 431.3540

Prepared according to *General Procedure F*.

Amount of L-Phe-OH: 10.0 g, 60.0 mmol, 1.0 eq.

Volume of thionyl chloride: 22.0 mL, 300.0 mmol, 5.0 eq.

Solvent volume : 200.0 mL MeOH.

Product yield: 16.52 g, 60.0 mmol, >99% yield.

Melting point: 124-126 °C (lit. 157 °C)

FTIR (neat): 3040, 2970, 2927, 2821, 1741, 1622, 1454 cm^{-1}.

^{1}H NMR (400 MHz, Methanol-d_4): δ 7.57 – 7.17 (m, 5H, Ar-H), 4.34 (t, *J* = 6.8 Hz, 1H, CH), 3.81 (s, 3H, OCH_3), 3.29 – 3.16 (m, 2H, Ph-CH_2) ppm.

^{13}C NMR (101 MHz, DMSO-d_6) δ 170.5, 136.0, 130.6, 129.8, 128.5, 54.5, 53.7, 37.0 ppm.

methyl acetyl-L-phenylalaninate **150** [106]

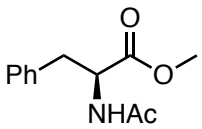

150

Chemical Formula: $C_{12}H_{15}NO_3$
Molecular Weight: 221.2560

Prepared according to *General Procedure G*.

Amount of Phe-OMe•HCl: 2.7 g, 12.0 mmol, 1.0 eq.

Amount of triethylamine: 6.33 mL, 36.0 mmol, 3.0 eq.

Amount of acetic anhydride: 4.30 mL, 36.0 mmol, 1.2 eq.

Solvent volume: 100.0 mL DCM.

Product yield: 2.05 g, 9.24 mmol, 77% yield.

Melting point: 85-88 °C (lit. 86-88 °C)[106]

FTIR (neat): 2978, 2951, 2358, 1732, 1662, 1612 cm^{-1}.

^{1}H NMR (400 MHz, $CDCl_3$): δ 7.37 – 7.25 (m, 3H, Ar-H), 7.15 – 7.09 (m, 2H, Ar-H), 5.92 (s, 1H, NH), 4.91 (dt, *J* = 7.9, 5.7 Hz, 1H, NCH), 3.75 (s, 3H, OCH_3), 3.24 – 3.08 (m, 2H, $PhCH_2$), 2.01 (s, 3H $COCH_3$) ppm.

^{13}C NMR (101 MHz, $CDCl_3$) δ 172.3, 169.8, 136.0, 129.4, 128.8, 127.3, 53.3, 52.5, 38.0, 23.3 ppm.

methyl L-tryptophanate hydrogen chloride **215** [107]

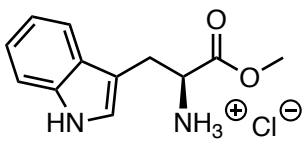

215

Chemical Formula: $C_{12}H_{15}ClN_2O_2$
Molecular Weight: 254.7140

Prepared according to *General Procedure F*.

Amount of L-Trp-OH: 1.0 g, 5.0 mmol, 1.0 eq.

Volume of thionyl chloride: 1.1 mL, 15.0 mmol, 3.0 eq.

Solvent volume : 50.0 mL MeOH.

Product yield: 1.17 g, 4.6 mmol, 92% yield.

Melting point: 210-211 °C (lit. 211-213 °C) [107]

FTIR (neat): 3404, 3351, 2922, 1732, 1661, 1522 cm^{-1}.

^{1}H NMR (400 MHz, DMSO-*d*$_6$) δ 11.19 (s,1H, ArNH), 8.74 (s, 3H, NH_3), 7.53 (d, *J* = 7.9 Hz, 1H, Ar-H), 7.39 (d, *J* = 8.2, 1H, Ar-H), 7.27 (d, *J* = 2.5 Hz, 1H, Ar-H), 7.12 – 7.07 (m, 1H, Ar-H), 7.03 – 6.99 (m, 1H, Ar-H), 4.19 (dd, *J* = 6.9, 5.5 Hz, 1H, $CHNH_2$), 3.63 (s, 3H, OCH_3), 3.42 – 3.28 (m, 2H, $CHCH_2$) ppm.

^{13}C NMR (101 MHz, DMSO-*d*$_6$) δ 169.7, 136.2, 126.9, 124.9, 121.1, 118.6, 117.9, 111.5, 106.3, 52.7, 52.5, 26.0 ppm.

methyl acetyl-L-tryptophanate **196** [108]

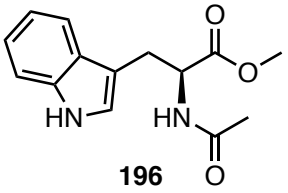

196

Chemical Formula: $C_{14}H_{16}N_2O_3$
Molecular Weight: 260.2930

Prepared according to *General Procedure G* for 1 h.

Amount of Trp-OMe•HCl: 1.17 g, 4.6 mmol, 1.0 eq.

Amount of di*iso*propylethylamine DIPEA: 1.57 mL, 9.2 mmol, 2.0 eq.

Amount of acetic anhydride: 0.43 mL, 4.6 mmol, 1.0 eq.

Solvent volume: 5 mL DCM.

Product yield: 0.404 g, 1.52 mmol, 33% yield.

Melting point: 152 - 154 °C (lit. 154-155 °C) [109]

FTIR (neat): 3404, 3316, 2980 2922, 1732, 1661, 1522 cm^{-1}.

^{1}H NMR (400 MHz, DMSO-d_6) δ 10.86 (s, 1H, ArNH), 8.30 (d, *J* = 7.5 Hz, 1H, NH), 7.49 (d, *J* = 7.8, 1H, Ar-H), 7.34 (d, *J* = 8.1, 1H, Ar-H), 7.15 (d, *J* = 2.4 Hz, 1H, Ar-H), 7.07 (t, *J* = 7.8, 7.0, 1H, Ar-H), 6.99 (t, *J* = 7.3 Hz, 1H, Ar-H), 4.50 (td, *J* = 8.1, 5.8 Hz, 1H, CHNH), 3.58 (s, 3H, OCH_3), 3.23 – 3.11 (m, 1H, CHCHH), 3.05 – 2.97 (m, 1H, CHCHH), 1.82 (s, 3H, $COCH_3$) ppm.

^{13}C NMR (101 MHz, DMSO-d_6) δ 172.5, 169.3, 136.1, 127.1, 124.1 121.0, 118.4, 118.0, 111.4, 109.5, 53.1, 51.7, 27.1, 22.3 ppm

methyl acetyl-1-tosyl-L-tryptophanate **197** [106]

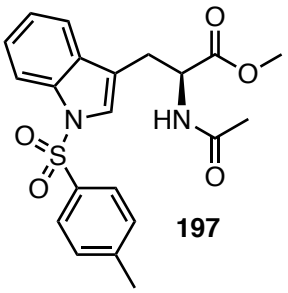

197

Chemical Formula: $C_{21}H_{22}N_2O_5S$
Molecular Weight: 414.4760

To a solution of Ac-Trp-OMe **196** (0.2 g, 0.76 mmol, 1.0 eq) in dry DCM (5 mL) was added NaOH (0.153 g, 3.81 mmol, 5.0 eq) and NBu_4HSO_4 (0.259 g, 0.76 mmol, 1.0 eq). The reaction mixture was stirred at reflux for 10 min. After this time, TsCl (0.436 g, 2.29 mmol, 3.0 eq) was added and the reaction mixture stirred at reflux for a further 1 h. The reaction mixture was then cooled to room temperature and diluted with DCM (15 mL). This resultant solution was then washed with saturated sodium bicarbonate solution (3 × 15 mL), dried with Na_2SO_4 and concentrated *in vacuo*. The resulting residue was purified my flash column chromatography (50-100% EtOAc/petrol) to afford **197** as a yellow oil (0.348 g, 0.72 mmol, 95% yield).

FTIR (neat): 2980, 2955, 1742, 1654, 1366, 1170 cm^{-1}.

^{1}H NMR (400 MHz, $CDCl_3$) δ 8.01 (d, *J* = 8.3 Hz, 1H, Ar-H), 7.83 – 7.71 (m, 2H, Ar-H), 7.50 (d, *J* = 7.7 Hz, 1H, Ar-H), 7.42 – 7.24 (m, 5H, Ar-H), 6.18 (d, *J* = 7.6 Hz, 1H, CHNH), 5.00 – 4.93 (m, 1H, CHNH), 3.71 (s, 3H, OCH_3), 3.44 – 3.11 (m, 2H, $CHCH_2$), 2.38 (s, 3H, $ArCH_3$), 2.00 (s, 3H, $COCH_3$).

^{13}C NMR (101 MHz, $CDCl_3$) δ 171.4, 169.3, 144.5, 134.9, 134.5, 130.3, 129.4, 126.2, 124.4, 123.8, 122.8, 118.8, 116.6, 113.2, 61.1, 52.0, 26.9, 22.6, 21.0 ppm.

methyl acetyl-L-methionate **198** [110]

Scheme 1.47

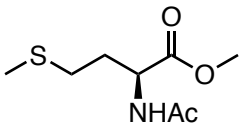

Chemical Formula: $C_8H_{15}NO_3S$
Molecular Weight: 205.2720

198

Prepared according to a literature procedure.[111] To a suspension of amino ester hydrochloride (0.995 g, 5 mmol,1 eq) in 5% Na_2CO_3 (25 mL) was added Ac_2O (15 mL, 159 mmol, 32 eq) in DCM (50 mL). The resulting suspension was stirred for 2 h at room temperature. The reaction mixture was then carefully quenched with saturated sodium bicarbonate and extracted with $CHCl_3$. The resulting organic phase was dried with Na_2SO_4, filtered and concentrated *in vacuo*. The resulting oil was then purified by flash column chromatography (0-5% MeOH/DCM) to afford the title compound as a white solid (0.963 g, 4.7 mmol, 94%).

Melting point: 42-43 °C

FTIR (neat): 2916,2851, 1740, 1653, 1535, 1435 cm^{-1}.

^{1}H NMR (400 MHz, $CDCl_3$) δ 6.26 (bd, 1H, NH), 4.73 (td, J = 7.5, 5.2 Hz, 1H, $CHNH_2$), 3.76 (s, 3H, OCH_3), 2.58 – 2.44 (m, 2H, CH_2SCH_3), 2.17 – 1.91 (m, 2H, $CH_3SCH_2CH_2CHNH$), 2.09 (s, 3H, CH_2SCH_3), 2.04 (s, 3H, $(O)CCH_3$) ppm.

Substrate scope with catalyst 188

Scheme 1.47

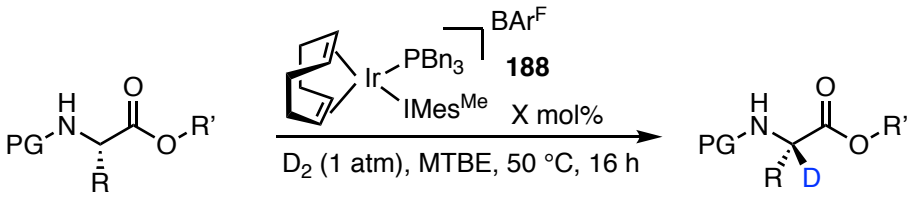

The substrate scope was performed as described in *General Procedure H*. The products were purified by column chromatography (50-100% diethyl ether/petrol) unless otherwise stated. Compound **195** was commercially available. 7.5 mol% [Ir] = 1.8 mL solvent, 10 mol% [Ir] = 2.5 mL solvent.

methyl acetyl-L- alaninate **148**

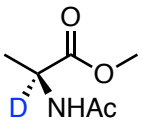

D148

^{1}H NMR (400 MHz, $CDCl_3$): δ 4.64 – 4.52 (m, 1H, C<u>H</u>), 3.79 (s, 3H, OC<u>H</u>$_3$), 2.05 (s, 3H, COC<u>H</u>$_3$), 1.38 (d, *J* = 7.2, Hz, 3H, C<u>H</u>$_3$) ppm

Labelling expected against signal at 4.64 – 4.52 ppm, measured against signal at 2.05 ppm.

Product columned in 0-10% MeOH/DCM.

Table 1.30

188 (mg, mol%, mmol)	148 (mg, mmol)	Run 1 (%)	Run 2 (%)	Run 3 (%)	Avg (%)
14.6, 7.5, 0.008	15.6, 0.11	80	89	-	85

tert-butyl (((9H-fluoren-9-yl)methoxy)carbonyl)alaninate **190**

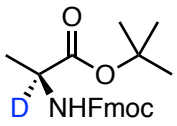

D190

^{1}H NMR (400 MHz, $CDCl_3$): δ 7.79 (d, *J* = 7.5 Hz, 2H, Ar-H), 7.63 (d, *J* = 7.4 Hz, 2H, Ar-H), 7.43 (t, *J* = 7.4 Hz, 2H, Ar-H), 7.34 (td, *J* = 7.4, 1.2 Hz, 2H, Ar-H), 5.41 (d, *J* = 7.7 Hz, 1H, NH), 4.41 (d, 2H, CH_2Fmoc), 4.31 (t, *J* = 7.3 Hz, 1H, NHCH), 4.25 (t, *J* = 7.1 Hz, 1H, CHFmoc), 1.51 (s, 9H, $OC(CH_3)_3$), 1.43 (d, *J* = 7.1 Hz, $NHCHCH_3$) ppm.

Labelling expected against signal at 4.31ppm, measured against signal at 7.79 ppm.

Table 1.31

188 (mg, mol%, mmol)	190 (mg, mmol)	Run 1 (%)	Run 2 (%)	Run 3 (%)	Avg (%)
14.6, 7.5, 0.008	39.5, 0.11	60	65	65	63
19.4, 10 , 0.011	39.5, 0.11	72	75	72	73

tert-butyl (tert-butoxycarbonyl)- L-valinate **191**

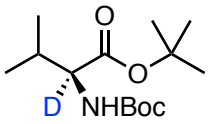

D191

^{1}H NMR (400 MHz, $CDCl_3$) δ 5.04 (d, *J* = 9.0 Hz, 1H, N<u>H</u>), 4.13 – 4.10 (m, 1H, $NH_2C\underline{H}$), 2.19 – 2.07 (m, 1H, $C\underline{H}CH_3$), 1.49 (s, 9H, $OC(C\underline{H_3})_3$), 1.47 (s, 9H, $OC(C\underline{H_3})_3$), 0.97 (d, *J* = 6.9, ^4J = 1.1 Hz, 3H, $CHC\underline{H_3}$), 0.91 (dd, *J* = 6.9, ^4J = 1.1 Hz, 3H, $CHC\underline{H_3}$) ppm.

Labelling expected against signal at 4.13 – 4.10 ppm, measured against signal at 0.97 ppm.

Table 1.32

188 (mg, mol%, mmol)	**191 (mg, mmol)**	**Run 1 (%)**	**Run 2 (%)**	**Run 3 (%)**	**Avg (%)**
14.6, 7.5, 0.008	29.4, 0.11	75	79	79	78
19.4, 10 , 0.011	29.4, 0.11	90	90	91	91

tert-butyl (tert-butoxycarbonyl)- L-leucinate **192**

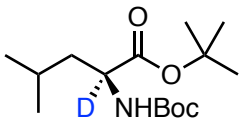

D192

^{1}H NMR (400 MHz, $CDCl_3$) δ 4.88 (d, *J* = 8.9 Hz, 1H, NH), 4.18 (app. q, *J* = 7.1 Hz, 1H, NH_2CH), 1.76 – 1.66 (m, 1H, $CHCH_3$), 1.61 – 1.52 (m, 2H, $CHCH_2$), 1.47 (s, 9H, $OC(CH_3)_3$), 1.45 (s, 9H, $OC(CH_3)_3$), 0.95 (d, *J* = 6.5 Hz, 6H, 2 × $CHCH_3$) ppm.

Labelling expected against signal at 4.18 ppm, measured against signal at 0.95 ppm.

Table 1.33

1988 (mg, mol%, mmol)	192 (mg, mmol)	Run 1 (%)	Run 2 (%)	Run 3 (%)	Avg (%)
14.6, 7.5, 0.008	30.9, 0.11	67	61	60	63
19.4, 10 , 0.011	30.9, 0.11	91	91	-	91

tert-butyl (tert-butoxycarbonyl)- L-isoleucinate **193**

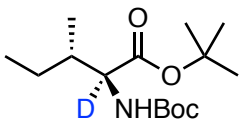

D193

^{1}H NMR (400 MHz, $CDCl_3$) δ 5.06 (d, *J* = 8.9 Hz, 1H, NH), 4.25 – 3.94 (m, 1H, NHCH), 1.87 – 1.79 (m, 1H, CHCH$_3$), 1.48 (s, 9H, OC(CH$_3$)$_3$), 1.46 (s, 9H, OC(CH$_3$)$_3$), 1.35 – 1.12 (m, 2H, CHCH$_2$), 0.94 (dd, *J* = 7.8, 7.1 Hz, 6H, 2 × CHCH$_3$) ppm.

Labelling expected against signal at 4.25 – 3.94 ppm, measured against signal at 0.94 ppm.

Table 1.34

188 (mg, mol%, mmol)	193 (mg, mmol)	Run 1 (%)	Run 2 (%)	Run 3 (%)	Avg (%)
14.6, 7.5, 0.008	30.9, 0.11	91	96	92	93

tert-butyl N-(tert-butoxycarbonyl)-O-(tert-butyl)-L-serinate **194**

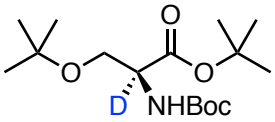

D194

^{1}H NMR (400 MHz, $CDCl_3$) δ 5.34 (d, *J* = 9.0 Hz, 1H, 1H, NH), 4.27 (dt, *J* = 9.2 Hz, ^4J = 2.9 Hz, 1H, NHCH), 3.78 (dd, *J* = 8.7 Hz, ^4J = 2.9 Hz, 1H, NHCHCHH), 3.54 (dd, *J* = 8.7 Hz, ^4J = 3.1 Hz, 1H, NHCHCHH), 1.48 (d, *J* = 3.4 Hz, 18H, 2 × OC(CH$_3$)$_3$), 1.16 (s, 9H, OC(CH$_3$)$_3$) ppm.

Labelling expected against signal at 4.27 ppm, measured against signal at 3.54 ppm.

Table 1.35

188 (mg, mol%, mmol)	194 (mg, mmol)	Run 1 (%)	Run 2 (%)	Run 3 (%)	Avg (%)
14.6, 7.5, 0.008	34.1, 0.11	73	75	78	75
19.4, 10 , 0.011	34.1, 0.11	91	92		91

1-benzyl 2-(tert-butyl) (S)-pyrrolidine-1,2-dicarboxylate **195**

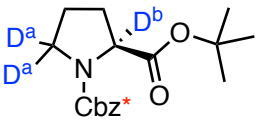

D195

^{1}H NMR (400 MHz, $CDCl_3$) δ 7.50 – 7.28 (m, 5H, ArH), 5.20 – 5.04 (m, 2H, CH_2Ph), 4.30 – 4.20 (m, 1H, NHCH), 3.65 – 3.41 (m, 2H, NCH_2), 2.23 – 1.80 (m, 4H. $NCHCH_2CH_2$), 1.45 (s, 9H, $OC(CH_3)_3$) ppm.

Labelling expected against signals at 5.20 – 5.04, 4.30 – 4.20 and 3.65 – 3.414.27 ppm, measured against signal at 3.54 ppm.

Table 1.36

188 (mg, mol%, mmol)	195 (mg, mmol)	Run 1 (%)	Run 2 (%)	Avg (%)
14.6, 7.5, 0.008	32.8, 0.11	**D^a** 12	17	15
		D^b 41	47	44
		CD_2 (Cbz) 75	86	81

methyl acetyl-L-phenylalaninate **150**

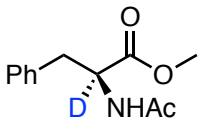

D150

^{1}H NMR (400 MHz, $CDCl_3$) δ 7.37 – 7.25 (m, 3H, Ar-H), 7.15 – 7.09 (m, 2H, Ar-H), 5.92 (s, 1H, NH), 4.91 (dt, *J* = 7.9, 5.7 Hz, 1H, NCH), 3.75 (s, 3H, OCH_3), 3.24 – 3.08 (m, 2H, $PhCH_2$), 2.01 (s, 3H $AcCH_3$) ppm.

Labelling expected against signal at 4.91 ppm, measured against signal at 3.24 – 3.08 ppm.

Product columned in 0-10% MeOH/DCM.

Table 1.37

188 (mg, mol%, mmol)	**150 (mg, mmol)**	**Run 1 (%)**	**Run 2 (%)**	**Run 3 (%)**	**Avg (%)**
		αD 76	72	60	74
19.4, 10 , 0.011	23.8, 0.11	**$C(O)CD_3$** 45	35	29	36

methyl acetyl-L-tryptophanate **196**

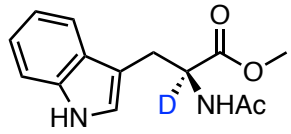

D196

^{1}H NMR (400 MHz, DMSO-d_6) δ 10.86 (s, 1H, ArNH), 8.30 (d, *J* = 7.5 Hz, 1H, NH), 7.49 (d, *J* = 7.8, 1H, Ar-H), 7.34 (d, *J* = 8.1, 1H, Ar-H), 7.15 (d, *J* = 2.4 Hz, 1H, Ar-H), 7.07 (t, *J* = 7.8, 7.0, 1H, Ar-H), 6.99 (t, *J* = 7.3 Hz, 1H, Ar-H), 4.50 (td, *J* = 8.1, 5.8 Hz, 1H, CHNH), 3.58 (s, 3H, OCH_3), 3.23 – 3.11 (m, 1H, CHCHH), 3.05 – 2.97 (m, 1H, CHCHH), 1.82 (s, 3H, $COCH_3$) ppm.

Labelling expected against signal at 4.50 ppm, measured against signal at 7.49 ppm.

Product columned in 0-10% MeOH/DCM.

Table 1.38

188 (mg, mol%, mmol)	196 (mg, mmol)	Run 1 (%)	Run 2 (%)	Run 3 (%)	Avg (%)
		αD 31	40	36	36
19.4, 10 , 0.011	28.0, 0.11	**C(O)CD_3** 15	15	12	14

methyl acetyl-1-tosyl-L-tryptophanate **197**

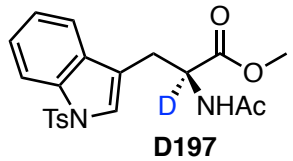

D197

^{1}H NMR (400 MHz, $CDCl_3$) δ 8.01 (d, *J* = 8.3 Hz, 1H, Ar-H), 7.83 – 7.71 (m, 2H, Ar-H), 7.50 (d, *J* = 7.7 Hz, 1H, Ar-H), 7.42 – 7.24 (m, 5H, Ar-H), 6.18 (d, *J* = 7.6 Hz, 1H, CHNH),

5.00 – 4.93 (m, 1H, C<u>H</u>NH), 3.71 (s, 3H, OC<u>H</u>$_3$), 3.44 – 3.11 (m, 2H, CHC<u>H</u>$_2$), 2.38 (s, 3H, ArC<u>H</u>$_3$), 2.00 (s, 3H, COC<u>H</u>$_3$).

Labelling expected against signal at 5.00 – 5.93 ppm, measured against signal at 8.01 ppm.

Table 1.39

188 (mg, mol%, mmol)	197 (mg, mmol)	Run 1 (%)	Run 2 (%)	Run 3 (%)	Avg (%)
19.4, 10 , 0.011	44.5, 0.11	71	-	-	71

methyl acetyl-L-methionate **198**

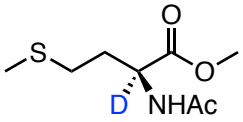

D198

^{1}H NMR (400 MHz, $CDCl_3$) δ 6.26 (bd, 1H, N<u>H</u>), 4.73 (td, J = 7.5, 5.2 Hz, 1H, C<u>H</u>NH$_2$), 3.76 (s, 3H, OC<u>H</u>$_3$), 2.58 – 2.44 (m, 2H, C<u>H</u>$_2$SCH$_3$), 2.17 – 1.91 (m, 2H, CH$_3$SCH$_2$C<u>H</u>$_2$CHNH), 2.09 (s, 3H, CH$_2$SC<u>H</u>$_3$), 2.04 (s, 3H, (O)CC<u>H</u>$_3$) ppm.

Labelling expected against signal at 4.73 ppm, measured against signal at 2.58 – 2.44 ppm.

Product columned in 0-10% MeOH/DCM.

Table 1.40

188 (mg, mol%, mmol)	198 (mg, mmol)	Run 1 (%)	Run 2 (%)	Run 3 (%)	Avg (%)
19.4, 10 , 0.011	22.0, 0.11	62	55	-	59

1.5.7 Limitations of Current Catalyst System

Scheme 1.48

methyl N-(tert-butoxycarbonyl)1-tosyl-L-tryptophanate **201** [112]

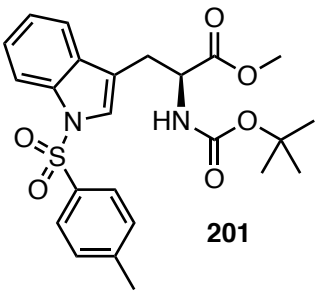

201

Chemical Formula: $C_{24}H_{28}N_2O_6S$
Molecular Weight: 472.5560

To a 25 mL round bottom flask was added *N*-BocTrpOMe (0.28 g, 0.89 mmol, 1 eq), NaOH (0.180 g, 4.45 mmol, 5 eq), NBu_4HSO_4 (0.302 g, 0.89 mmol, 1 eq), and DCM (4.5 mL) and the reaction mixture heated to reflux for 10 min. To this was added TsCl (0.51 g, 2.67 mmol, 3 eq) and the reaction mixture heated to reflux for an additional 1 hour. The reaction mixture was then cooled, concentrated *in vacuo* and diluted with EtOAc (10 mL). The organic phase was washed with saturated $NaHCO_3$, dried over Na_2SO_4, and concentrated *in vacuo*. Purification on silica gel (30 % EtOAc/petrol) afforded the title compounds as a pale yellow solid (0.28 g, 0.59 mmol, 66% yield).

Melting point: 50 - 52 °C (lit. 45 - 48 °C)[112]

FTIR (neat): 3402, 2976, 1741, 1711, 1495, 1447 cm^{-1}.

^{1}H NMR (400 MHz, $CDCl_3$) δ 7.97 (d, *J* = 8.3 Hz, 1H, Ar-H), 7.83 – 7.65 (m, 2H, Ar-H), 7.47 (d, *J* = 7.7 Hz, 1H, Ar-H), 7.38 (s, 1H, Ar-H), 7.37 – 7.19 (m, 4H, Ar-H), 5.10 (d, *J* = 8.0 Hz, 1H, NH), 4.65 (q, *J* = 6.4 Hz, 1H, NHCHCH$_2$), 3.65 (s, 3H, OCH$_3$), 3.29 – 3.13 (m, 2H NHCHCH$_2$), 2.35 (s, 3H, Ar-CH$_3$), 1.46 (s, 9H, OC(CH$_3$)$_3$) ppm.

^{13}C NMR (101 MHz, $CDCl_3$) δ 172.1, 155.1, 150.0, 135.3, 135.2, 130.0, 126.9, 124.9, 124.6, 123.3, 119.6, 117.4, 113.8, 80.2, 53.7, 52.4, 28.4, 28.0, 21.6 ppm.

Labelling of aryl substituted amino acids

Scheme 1.48

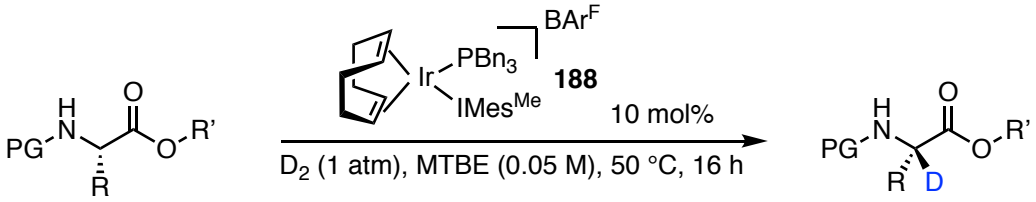

The substrate scope was performed as described in General Procedure H. Compounds **199** and **200** were commercially available. The products were purified by column chromatography (50-100% diethyl ether/petrol) unless otherwise stated. 7.5 mol% [Ir] = 1.8 mL solvent, 10 mol% [Ir] = 2.5 mL solvent.

Labelling of methyl (tert-butoxycarbonyl)-L-tyrosinate **199**

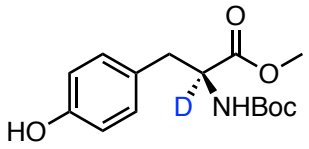

D199

^{1}H NMR (400 MHz, $CDCl_3$) δ 7.03 – 6.89 (m, 2H, Ar-H), 6.73 (d, *J* = 8.0 Hz, 2H, Ar-H), 5.01 (d, *J* = 8.4 Hz, 1H, CHNH), 4.60 – 4.47 (m, 1H, CHNH), 3.71 (s, 3H, OCH_3), 3.06 – 2.91 (m, 2H, $NHCHCH_2$), 1.42 (s, 9H, $OC(CH_3)_3$) ppm.

Labelling expected against signal at 4.60 – 4.47 ppm, measured against signal at 3.06 – 2.91 ppm.

Table 1.41

188 (mg, mol%, mmol)	199 (mg, mmol)	Run 1 (%)	Run 2 (%)	Run 3 (%)	Avg (%)
19.4, 10 , 0.011	31.7, 0.11	0	0	0	0

Labelling of methyl (tert-butoxycarbonyl)-L-phenylalaninate **200**

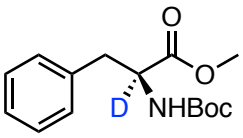

D200

^{1}H NMR (400 MHz, $CDCl_3$) δ 7.39 – 7.21 (m, 3H, Ar-H), 7.18 – 7.05 (m, 2H, Ar-H), 4.98 (d, *J* = 8.1 Hz, 1H, CHNH), 4.60 (q, *J* = 6.7 Hz, 1H, CHNH), 3.72 (s, 3H, OCH_3), 3.17 – 3.02 (m, 2H, $NHCHCH_2$), 1.42 (s, 9H, $OC(CH_3)_3$) ppm.

Labelling expected against signal at 4.60 ppm, measured against signal at 3.17 – 3.02 ppm.

Table 1.42

188 (mg, mol%, mmol)	200 (mg, mmol)	Run 1 (%)	Run 2 (%)	Run 3 (%)	Avg (%)
19.4, 10 , 0.011	30.0, 0.11	0	0	0	0

methyl N-(tert-butoxycarbonyl)1-tosyl-L-tryptophanate **201**

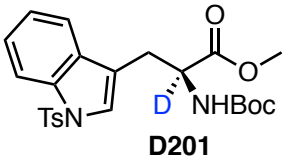

D201

^{1}H NMR (400 MHz, $CDCl_3$) δ 7.97 (d, *J* = 8.3 Hz, 1H, Ar-H), 7.83 – 7.65 (m, 2H, Ar-H), 7.47 (d, *J* = 7.7 Hz, 1H, Ar-H), 7.38 (s, 1H, Ar-H), 7.37 – 7.19 (m, 4H, Ar-H), 5.10 (d, *J* = 8.0 Hz, 1H, NH), 4.65 (q, *J* = 6.4 Hz, 1H, NHCHCH$_2$), 3.65 (s, 3H, OCH$_3$), 3.29 – 3.13 (m, 2H NHCHCH$_2$), 2.35 (s, 3H, Ar-CH$_3$), 1.46 (s, 9H, OC(CH$_3$)$_3$) ppm.

Labelling expected against signal at 4.65 ppm, measured against signal at 3.29 – 3.13 ppm.

Table 1.43

188 (mg, mol%, mmol)	201 (mg, mmol)	Run 1 (%)	Run 2 (%)	Run 3 (%)	Avg (%)
19.4, 10, 0.011	50.8, 0.11	0	0	0	0

Limitations – sulfur containing amino acids

Scheme 1.49

N-Ac-Cystine-OMe **203** [113]

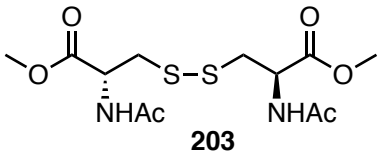

203

Chemical Formula: $C_{12}H_{20}N_2O_6S_2$
Molecular Weight: 352.4200

To a 25 mL round-bottom flask was added *N*-AcCysOMe (0.145 g, 0.81 mmol, 1 eq), Cu(OAc)$_2$ (0.297 g, 1.62 mmol, 2 eq) and 4.0 mL pyridine and the reaction mixture heated to 40 °C for 1 hour. The pyridine was then distilled under vacuum from the reaction mixture and the resulting residue diluted with DCM (5 mL). The organic phase was washed with water, dried over Na_2SO_4, and concentrated *in vacuo*. Purification on silica gel (5% MeOH/DCM) afforded the title compound **203** as a white solid (0.07 g, 0.20 mmol, 49% yield).

Melting point: 123 - 125 °C (lit. 125 - 126 °C) [113]

^{1}H NMR (400 MHz, $CDCl_3$) δ 6.68 (d, *J* = 7.6 Hz, 2H, 2 × NHCH), 4.84 (dt, *J* = 7.6, 5.3 Hz, 2H 2 × NHCH), 3.74 (s, 6H 2 × OCH_3), 3.23 – 3.07 (m, 4H, 2 × SCH_2CHNH), 2.03 (s, 6H, 2 × $COCH_3$) ppm.

^{13}C NMR (101 MHz, $CDCl_3$) δ 171.0, 170.3, 52.9, 51.8, 40.8, 23.1 ppm.

Labelling of sulfur substituted amino acids

Scheme 1.49

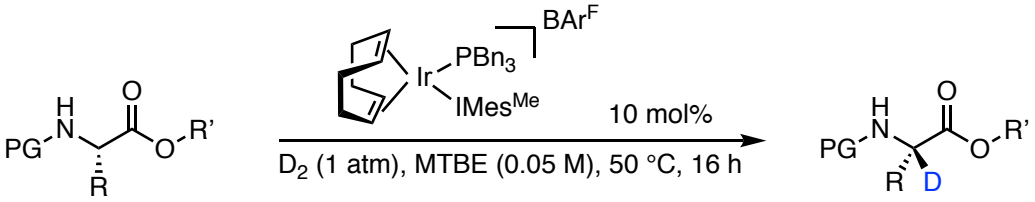

The substrate scope was performed as described in General Procedure H. Compound **202** was commercially available. The products were purified by column chromatography (50-100% diethyl ether/petrol) unless otherwise stated. Solvent volume = 2.5 mL.

Ethyl (tert-butoxycarbonyl)-L-methioninate **202**

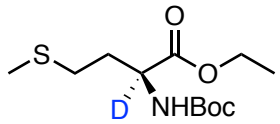

D202

^{1}H NMR (400 MHz, $CDCl_3$) δ 5.11 (bd, 1H, NH), 4.42 – 4.32 (m, 1H, $CHNH_2$), 4.20 (q, *J* = 7.1 Hz, 2H, OCH_2CH_3), 2.53 (dt, *J* = 6.7, 1.6 Hz, 2H, $CH_3SCH_2CH_2$), 2.18 – 2.02 (m, 5H, $CH_3SCH_2CH_2$ and SCH_3), 1.44 (s, 9H, $OC(CH_3)_3$), 1.28 (t, *J* = 7.1 Hz, 3H, OCH_2CH_3) ppm.

Labelling expected against signal at 4.42 – 4.32 ppm, measured against signal at 1.28 ppm.

Table 1.44

188 (mg, mol%, mmol)	202 (mg, mmol)	Run 1 (%)	Run 2 (%)	Run 3 (%)	Avg (%)
19.4, 10 , 0.011	19.8, 0.11	0	0	0	0

N-Ac-Cystine-OMe **203**

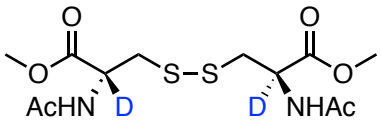

D203

^{1}H NMR (400 MHz, $CDCl_3$) δ 6.68 (d, *J* = 7.6 Hz, 2H, 2 x NHCH), 4.84 (dt, *J* = 7.6, 5.3 Hz, 2H 2 x NHCH), 3.74 (s, 6H 2 x OCH_3), 3.23 – 3.07 (m, 4H, 2 x SCH_2CHNH), 2.03 (s, 2H, 2 x $AcCH_3$) ppm.

Labelling expected against signal at 4.84 ppm, measured against signal at 3.23 – 3.07 ppm.

Table 1.45

188 (mg, mol%, mmol)	203 (mg, mmol)	Run 1 (%)	Run 2 (%)	Run 3 (%)	Avg (%)
19.4, 10 , 0.011	37.8, 0.11	0	0	0	0

1.5.8 Mixed Solvent Systems for Amino Acid Labelling

Labelling of methyl acetylglycinate 147a, solvent screen

Scheme 1.51

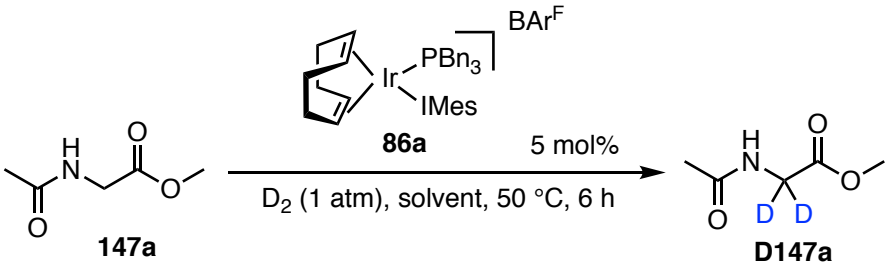

Performed as described in *General Procedure H.* Ac-Gly-OMe **147a** (28.2 mg, 0.215 mmol). Solvent volume (2.5 mL) .The product was purified by trituration with diethyl ether.

^{1}H NMR (400 MHz, Methanol-*d*$_4$): δ 3.94 (s, 2H, C$\underline{H}_2$), 3.74 (s, 3H, OC$\underline{H}_3$), 2.01 (s, 3H, COC$\underline{H}_3$) ppm.

Labelling expected against signal at 3.94 ppm, measured against signal at 2.01 ppm.

Table 1.46

Entry	Solvent	Run 1 (%)	Run 2 (%)	Run 3 (%)	Avg (%)
1	**MTBE**	95	91	88	92
2	**$CHCl_3$**	81	79	67	76
3	**MeOH**	0	0	0	0
4	**EtOH**	0	0	0	0
5	**^{i}PrOH**	0	0	0	0
6	**^{1}AmOH**	0	0	0	0

Labelling of methyl acetylglycinate 147a, MTBE/^{t}AmOH mixtures

Graph 1.5

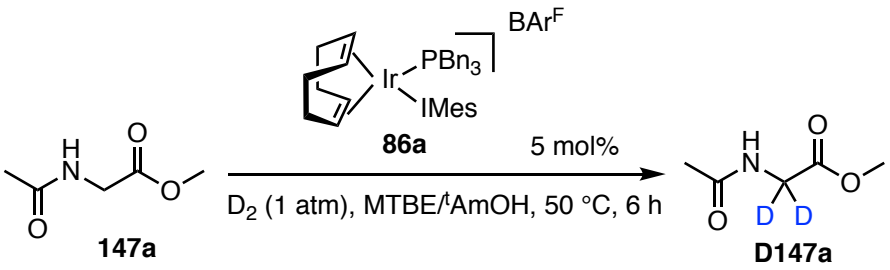

Performed as described in *General Procedure H.* Ac-Gly-OMe **147a** (28.2 mg, 0.215 mmol). Solvent volume (2.5 mL) .The product was purified by trituration with diethyl ether.

^{1}H NMR (400 MHz, Methanol-*d*$_4$): δ 3.94 (s, 2H, C$\underline{H}_2$), 3.74 (s, 3H, OC$\underline{H}_3$), 2.01 (s, 3H, COC$\underline{H}_3$) ppm.

Labelling expected against signal at 3.94 ppm, measured against signal at 2.01 ppm.

Table 1.47

Entry	% ^{t}AmOH in MTBE	Run 1 (%)	Run 2 (%)	Run 3 (%)	Avg (%)
1	**1**	53	47	50	50
2	**10**	69	71	-	70
3	**20**	57	67	69	64
4	**30**	70	80	80	77
5	**40**	69	60	65	65
6	**45**	59	54	54	56
7	**50**	63	48	50	54

Labelling of methyl acetylglycinate 147a, 30% ROH/MTBE mixtures

Graph 1.6

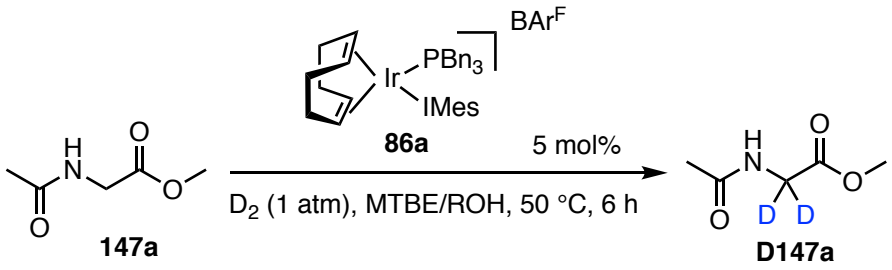

Performed as described in *General Procedure H* with 30% of the reported alcohol in the MTBE solvent. Ac-Gly-OMe **147a** (28.2 mg, 0.215 mmol). Solvent volume (2.5 mL) .The product was purified by trituration with diethyl ether.

^{1}H NMR (400 MHz, Methanol-*d*$_4$): δ 3.94 (s, 2H, C$\underline{H_2}$), 3.74 (s, 3H, OC$\underline{H_3}$), 2.01 (s, 3H, COC$\underline{H_3}$) ppm.

Labelling expected against signal at 3.94 ppm, measured against signal at 2.01 ppm.

Table 1.48

Entry	30% ROH/MTBE	Run 1 (%)	Run 2 (%)	Run 3 (%)	Avg (%)
1	**^{t}AmOH**	70	80	80	77
2	**^{i}PrOH**	31	31	40	34
3	**EtOH**	35	26	32	31
4	**MeOH**	21	26	24	24

Labelling of methyl acetylglycinate 147a, ROH/$CHCl_3$ mixtures

Graph 1.7

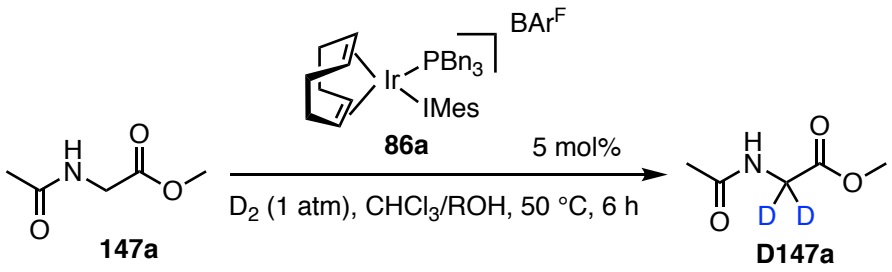

Performed as described in *General Procedure H* with 30% of the reported alcohol in the chloroform solvent. Ac-Gly-OMe **147a** (28.2 mg, 0.215 mmol). Solvent volume (2.5 mL) .The product was purified by trituration with diethyl ether.

^{1}H NMR (400 MHz, Methanol-*d*$_4$): δ 3.94 (s, 2H, C$\underline{H}_2$), 3.74 (s, 3H, OC$\underline{H}_3$), 2.01 (s, 3H, AcC$\underline{H}_3$) ppm.

Labelling expected against signal at 3.94 ppm, measured against signal at 2.01 ppm.

Table 1.49

Entry	Solvent mix	Run 1 (%)	Run 2 (%)	Run 3 (%)	Avg (%)
1	**$CHCl_3$**	81	79	67	76
2	**20:1 $CHCl_3$:^{i}PrOH**	71	76	72	73
3	**10:1 $CHCl_3$: ^{i}PrOH**	49	58	56	54
4	**4:1 $CHCl_3$: ^{i}PrOH**	24	28	27	26
5	**20:1 $CHCl_3$:^{t}AmOH**	64	62	75	67
6	**10:1 $CHCl_3$: ^{t}AmOH**	65	67	64	65

1.5.9 Additional Computational Details

General Comments

Density functional theory (DFT) was employed to calculate the gas-phase electronic structures and energies for all species involved in H/D exchange reactions. All structures thus far have been optimized with the hybrid meta-GGA exchange correlation functional M06. The M06 density functional was used in conjunction with the 6-31(G)(*d*) basis set for main group non-metal atoms and the Stuttgart RSC effective core potential along with the associated basis set for Ir. The participating transition states (TS) are located at the same level of theory. Harmonic vibrational frequencies are calculated (with the incorporation of deuterium wherever state) at the same level of theory to characterize respective minima (reactants, intermediates, and products with no imaginary frequency) and first order saddle points (TSs with one imaginary frequency). The validity of using the 6-31G(d) basis set has previously been checked by comparative single point energy calculations employing the def2-TZVP basis set for all atoms on similar H/D exchange systems. All calculations using the M06 functional have been performed using Gaussian 09 quantum chemistry program package (version A.02). [77]Coordinates and additional computational details are supplied in the appendix

Counterpoise Method for Binding Energy Calculations

Counterpoise method for binding energy calculation requires optimised structures of the free complex (**A**), free substrate (**B**) and the catalyst-substrate complex (**AB**).

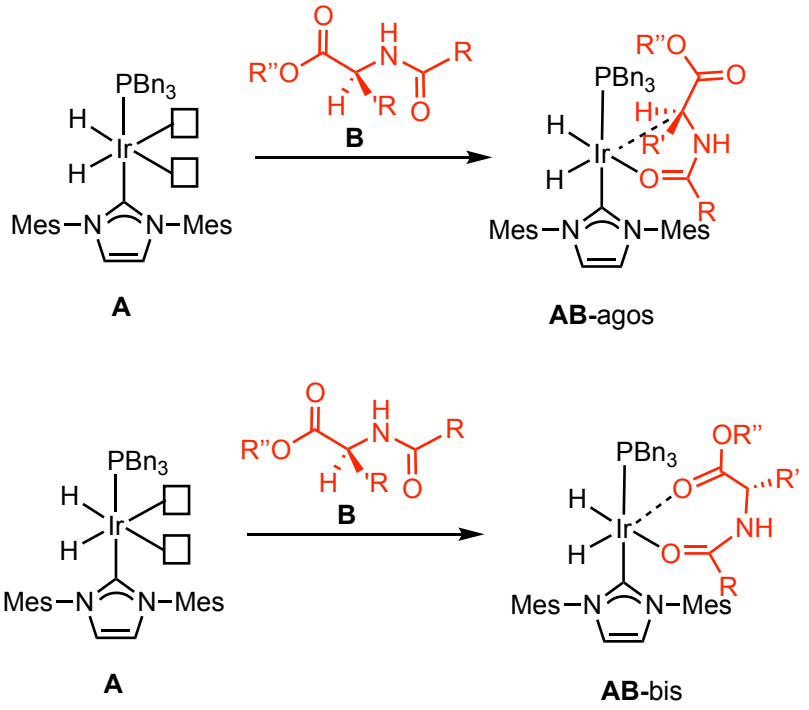

Scheme 0.57

The electronic energy for each of these structures was then used in Equation **1**, in order to deliver the binding energy (ΔE_{Bind}).

$$\Delta E_{Bind} = \left[E_{AB}^{\alpha\beta}(AB) - E_{AB}^{\alpha\beta}(A) - E_{AB}^{\alpha\beta}(B)\right] + \left[\left(E_{AB}^{\alpha}(A) - E_{A}^{\alpha}(A)\right) + \left(E_{AB}^{\beta}(B) - E_{B}^{\beta}(B)\right)\right] \quad \mathbf{1}$$

Key: $E_{geometry}^{basis\ set}(structure)$

Equation **2** can be simplified into terms describing the counterpoise corrected interaction energy (E_{int}) and the sum of distortion energies (E_{dist}), as shown in Equation **2**.

$$\Delta E_{Bind} = E_{int} + E_{dist} \qquad \mathbf{2}$$

A full account of the individual electronic energies and coordinates are reported in the appendix.

Buried Volume Calculations

All percent buried volume ($\%V_{bur}$) data were calculated using the SambVca 2.0 web applications. All structural geometries used as inputs for these calculations were derived from DFT optimised structures. The main input data required for the online software for each ligand are the coordinates of the ligand plus the central metal atom. The metal-ligand bond distance is dictated by the results of the SFT optimisation. Iridium metal atom was selected as the atom coordinated to the centre of the sphere. The ligand atom coordinated to the metal and the metal itself were used to define the z-axis (using default Z-negative option). For NHC ligands, the xz-plane was defined using the two nitrogen atoms flanking the coordinating atom. For phosphines, the xz-plane was defined using the three atoms directly bound to the phosphorus centre. The metal atom was then deleted. Default mesh spacing was kept to 0.1 Å and the sphere radius kept to 3.5 Å. The distance of the coordination point to the centre of the sphere was kept at 0, as the true ligand metal bond distance was already set by the metal atom. Default atomic radii were described by Bondi radii scaled by 1.17. Hydrogen atoms were not included in the calculations. The coordinates of the ligand were first optimized in *Gaussian 09* as part of a full iridium(III) hydride complex cation of the formula $[(NHC)Ir(PR_3)(H)_2(MTBE)_2]^+$, and optimized coordinates converted to .pdb format. The .pdb file was then uploaded to the SambVca web application. Coordinates and SambVca outputs are included in the appendix.

1.6 References

(1) Dowden, H.; Munro, J. *Nat. Rev. Drug Discov.* **2019**, *18*, 495–496.

(2) Lipinski, C. A.; Lombardo, F.; Dominy, B. W.; Feeney, P. J. *Adv. Drug Deliv. Rev.* **1997**, *46*, 3–26.

(3) Wenlock, M. C.; Austin, R. P.; Barton, P.; Davis, A. M.; Leeson, P. D. *J. Med. Chem.* **2003**, *46*, 1250–1256.

(4) Leeson, P. D.; Springthorpe, B. *Nat. Rev. Drug Discov.* **2007**, *6*, 881–890.

(5) Paul, S. M.; Mytelka, D. S.; Dunwiddie, C. T.; Persinger, C. C.; Munos, B. H.; Lindborg, S. R.; Schacht, A. L. *Nat. Rev. Drug Discov.* **2010**, *9*, 203–214.

(6) Mayr, L. M.; Fuerst, P. *J. Biomol. Screen.* **2008**, *13*, 443–448.

(7) Macarron, R.; Banks, M. N.; Bojanic, D.; Burns, D. J.; Cirovic, D.; Garyantes, T.; Green, D. V. S.; Hertzberg, R. P.; Janzen, W. P.; Paslay, J. W.; Schopfer, U.; Sittampalam, G. S. *Nat. Rev. Drug Discov.* **2011**, *10*, 188–195.

(8) Nadin, A.; Hattotuwagama, C.; Churcher, I. *Angew. Chem. Int. Ed.* **2012**, *51*, 1114–1122.

(9) Doveston, R.; Marsden, S.; Nelson, A. *Drug Discov. Today* **2014**, *19*, 813–819.

(10) Doveston, R. G.; Tosatti, P.; Dow, M.; Foley, D. J.; Li, H. Y.; Campbell, A. J.; House, D.; Churcher, I.; Marsden, S. P.; Nelson, A. *Org. Biomol. Chem.* **2015**, *13*, 859–865.

(11) Foley, D. J.; Doveston, R. G.; Churcher, I.; Nelson, A.; Marsden, S. P. *Chem. Commun.* **2015**, *51*, 11174–11177.

(12) Vale, N.; Ferreira, A.; Matos, J.; Fresco, P.; Gouveia, Maria, J. *Molecules* **2018**, *23*, 2318.

(13) Beutner, K. R.; Friedman, D. J.; Forszpaniak, C.; Andersen, P. L.; Wood, M. J. *Antimicrob. Agents Chemother.* **1995**, *39*, 1546–1553.

(14) Chen, J.-R.; Papadimitriou, D. D. A. *US005225204 Patent.* **1993**.

(15) Yoshinaga, F.; Okumura, S.; Tanenholtz, P. E. E.; Application, F.; Data, P. *US3962034* **1976**.

(16) Kaspar, A. A.; Reichert, J. M. *Drug Discov. Today* **2013**, *18*, 807–817.

(17) Fosgerau, K.; Hoffmann, T. *Drug Discov. Today* **2015**, *20*, 122–128.

(18) Lloyd-Jones, G. C.; Muñoz, M. P. *J. Labelled. Compd. Radiopharm.* **2007**, *50*, 1072–1087.

(19) Simmons, E. M.; Hartwig, J. F. *Angew. Chem. Int. Ed.* **2012**, *51*, 3066–3072.

(20) Qiao-Xia, G.; Bao-Jian, S.; Hai-Qing, G.; Tamotsu, T. *Chinese J. Chem.* **2005**, *23*, 341–344.

(21) Heinkele, G.; Mürdter, T. E. *J. Labelled. Compd. Radiopharm.* **2005**, *48*, 457–461.

(22) Furuta, T.; Suzuki, A.; Matsuzawa, M.; Shibasaki, H.; Kasuya, Y. *Steroids* **2003**, *68*, 693–703.

(23) Sajiki, H.; Aoki, F.; Esaki, H.; Maegawa, T.; Hirota, K. *Org. Lett.* **2004**, *6*, 1485–1487.

(24) Davies, H. M. L.; Morton, D. *J. Org. Chem.* **2016**, *81*, 343–350.

(25) Gensch, T.; Hopkinson, M. N.; Glorius, F.; Wencel-Delord, J. *Chem. Soc. Rev.* **2016**, *45*, 2900–2936.

(26) Kar, S.; Goeppert, A.; Sen, R.; Kothandaraman, J.; Surya Prakash, G. K. *Green Chem.* **2018**, *20*, 2706–2710.

(27) Yu, Renyuan, P.; Hesk, D.; Rivera, N.; Pelczer, I.; Chirik, P. J. *Nature* **2016**, *529*, 195–199.

(28) Palmer, W. N.; Chirik, P. J. *ACS Catal.* **2017**, *7*, 5674–5678.

(29) Zarate, C.; Yang, H.; Bezdek, M. J.; Hesk, D.; Chirik, P. J. *J. Am. Chem. Soc.* **2019**, *141*, 5034–5044.

(30) Blake, M. R.; Garnett, J. L.; Gregor, I. K.; Hannan, W.; Hoa, K.; Long, M. A. *J. Chem. Soc. Chem. Commun.* **1975**, 930–932.

(31) Lockley, W. J. S. *J. Labelled. Compd. Radiopharm.* **1984**, *21*, 45–57.

(32) Shapley, J. R.; Schrock, R. R.; Osborn, J. A. *J. Am. Chem. Soc.* **1969**, *91*, 2816–2817.

(33) Heys, J. R. *J. Chem. Soc. Chem. Commun.* **1992**, 680–681.

(34) Heys, J. R.; Shu, A. Y. L.; Senderoff, S. G.; Phillips, N. M. *J. Labelled. Compd. Radiopharm.* **1993**, *33*, 431–438.

(35) Crabtree, R. H.; Felkin, H.; Morris, G. E. *J. Organomet. Chem.* **1977**, *141*, 205–215.

(36) Hesk, D.; Das, P. R.; Evans, B. *J. Labelled. Compd. Radiopharm.* **1995**, *36*, 497–502.

(37) Ellames, G. J.; Gibson, J. S.; Herbert, J. M.; McNeill, A. H. *Tetrahedron* **2001**, *57*, 9487–9497.

(38) Crabtree, R. *Acc. Chem. Res.* **1979**, *12*, 331–337.

(39) Shu, A. Y. L.; Chen, W.; Heys, J. R. *J. Organomet. Chem.* **1996**, *524*, 87–93.

(40) Lee, H. M.; Jiang, T.; Stevens, E. D.; Nolan, S. P. *Organometallics* **2001**, *20*, 1255–1258.

(41) Vázquez-Serrano, L. D.; Owens, B. T.; Buriak, J. M. *Chem. Commun.* **2002**, *3201*, 2518.

(42) Tolman, C. A. *J. Am. Chem. Soc.* **1970**, *92*, 2953–2956.

(43) Tolman, C. A. *Chem. Rev.* **1977**, *77*, 313–348.

(44) Arduengo, A. J.; Harlow, R. L.; Kline, M. *J. Am. Chem. Soc.* **1991**, *113*, 361–363.

(45) Kelly III, R. A.; Clavier, H.; Giudice, S.; Scott, N. M.; Stevens, E. D.; Bordner, J.; Samardjiev, I.; Hoff, C. D.; Cavallo, L.; Nolan, S. P. *Organometallics* **2008**, *27*, 202–210.

(46) Liske, A.; Verlinden, K.; Buhl, H.; Schaper, K.; Ganter, C. *Organometallics* **2013**, *32*, 5269–5272.

(47) Back, O.; Henry-Ellinger, M.; Martin, C. D.; Martin, D.; Bertrand, G. *Angew. Chem. Int. Ed.* **2013**, *52*, 2939–2943.

(48) Clavier, H.; Nolan, S. P. *Chem. Commun.* **2010**, *46*, 841–861.

(49) Brown, J. A.; Irvine, S.; Kennedy, A. R.; Kerr, W. J.; Andersson, S.; Nilsson, G. N. *Chem. Commun.* **2008**, 1115–1117.

(50) Cochrane, A. R. X.; Idziak, C.; Kerr, W. J.; Mondal, B.; Paterson, L. C.; Tuttle, T.; Andersson, S.; Nilsson, G. N. *Org. Biomol. Chem.* **2014**, *12*, 3598–3603.

(51) Kennedy, A. R.; Kerr, W. J.; Moir, R.; Reid, M. *Org. Biomol. Chem.* **2014**, *12*, 7927–7931.

(52) Lightfoot, A.; Schnider, P.; Pfaltz, A. *Angew. Chem. Int. Ed.* **1998**, *37*, 2897–2899.

(53) Drago, D.; Pregosin, P. S.; Pfaltz, A. *Chem. Commun.* **2002**, 286–287.

(54) Brown, J. A.; Cochrane, A. R.; Irvine, S.; Kerr, W. J.; Mondal, B.; Parkinson, J. A.; Paterson, L. C.; Reid, M.; Tuttle, T.; Andersson, S.; Nilsson, G. N. *Adv. Synth. Catal.* **2014**, *356*, 3551–3562.

(55) Mudd, R. J. *PhD Thesis, Univ. Strathclyde* **2016**.

(56) Kerr, W. J.; Lindsay, D. M.; Owens, P. K.; Reid, M.; Tuttle, T.; Campos, S. *ACS Catal.* **2017**, *7*, 7182–7186.

(57) Kerr, W. J.; Mudd, R. J.; Paterson, L. C.; Brown, J. A. *Chem. Eur. J.* **2014**, *20*, 14604–14607.

(58) Kerr, W. J.; Reid, M.; Tuttle, T. *ACS Catal.* **2015**, *5*, 402–410.

(59) Kerr, W. J.; Reid, M.; Tuttle, T. *Angew. Chem. Int. Ed.* **2017**, *56*, 7808–7812.

(60) Kerr, W. J.; Lindsay, D. M.; Reid, M.; Tuttle, T.; Zorzatto, R. *Unpublished Results* **2018**.

(61) Taglang, C.; Martínez-Prieto, L. M.; del Rosal, I.; Maron, L.; Poteau, R.; Philippot, K.; Chaudret, B.; Perato, S.; Sam Lone, A.; Puente, C.; Dugave, C.; Rousseau, B.; Pieters, G. *Angew. Chem. Int. Ed.* **2015**, *54*, 10474–10477.

(62) Pieters, G.; Taglang, C.; Bonnefille, E.; Gutmann, T.; Puente, C.; Berthet, J.-C.; Dugave, C.; Chaudret, B.; Rousseau, B. *Angew. Chem. Int. Ed.* **2014**, *53*, 230–234.

(63) Michelotti, A.; Rodrigues, F.; Roche, M. *Org. Process Res. Dev.* **2017**, *21*, 1741–1744.

(64) Chatterjee, B.; Krishnakumar, V.; Gunanathan, C. *Org. Lett.* **2016**, *18*, 5892–5895.

(65) Loh, Y. Y.; Nagao, K.; Hoover, A. J.; Hesk, D.; Rivera, N. R.; Colletti, S. L.; Davies, I. W.; MacMillan, D. W. C. *Science* **2017**, *358*, 1182–1187.

(66) Kerr, W. J.; Mudd, R. J.; Reid, M.; Atzrodt, J.; Derdau, V. *ACS Catal.* **2018**, *8*, 10895–10900.

(67) Valero, M.; Weck, R.; Güssregen, S.; Atzrodt, J.; Derdau, V. *Angew. Chem. Int. Ed.* **2018**, *57*, 8159–8163.

(68) Cochrane, A. R.; Irvine, S.; Kerr, W. J.; Reid, M.; Andersson, S.; Nilsson, G. N. *J. Labelled. Compd. Radiopharm.* **2013**, *56*, 451–454.

(69) Reid, M. *PhD Thesis, Univ. Strathclyde* **2015**.

(70) Zorzatto, R. *PhD Thesis, Univ. Strathclyde* **2018**.

(71) Knox, G. J. *PhD Thesis, Univ. Strathclyde* **2018**.

(72) Falivene, L.; Cao, Z.; Petta, A.; Serra, L.; Poater, A.; Oliva, R.; Scarano, V.; Cavallo, L. *Nature Chem.* **2019**, *11*, 872–879.

(73) Jover, J.; Cirera, J. *Dalt. Trans.* **2019**, *48*, 15036–15048.

(74) Hesk, D. Merck.

(75) Boys, S. F.; Bernardi, F. *Mol. Phys.* **1970**, *19*, 553–566.

(76) Armarego, W. L. .; Chai, C. L. . *Purification of Laboratory Chemicals*, Seventh Ed.; Elsevier Ltd, 2013.

(77) Gaussian 09, M. J. Frisch, G. W. Trucks, H. B. Schlegel, G. E. Scuseria, M. A. Robb, J. R. Cheeseman, G. Scalmani, V. Barone, G. A. Petersson, H. Nakatsuji, X. Li, M. Caricato, A. Marenich, J. Bloino, B. G. Janesko, R. Gomperts, B. Mennucci, H. P. Hratchi, and D. J. F. *Gaussian Inc., Wallingford CT* **2016**, *53*, 1689–1699.

(78) Kerr, W. J.; Mudd, R. J.; Owens, P. K.; Reid, M.; Brown, J. A.; Campos, S. *J. Labelled. Compd. Radiopharm.* **2016**, 10–12.

(79) Croft, a K.; Foley, M. K. *Org. Biomol. Chem.* **2008**, *6*, 1594.

(80) Gillie, A. D.; Jannapu Reddy, R.; Davies, P. W. *Adv. Synth. Catal.* **2016**, *358*, 226–239.

(81) Plastina, P.; Fazio, A.; Attya, M.; Sindona, G.; Gabriele, B. *Nat. Prod. Res.* **2012**, *26*, 1799–1805.

(82) Giovani, S.; Penzo, M.; Butini, S.; Brindisi, M.; Gemma, S.; Novellino, E.; Campiani, G.; Blackman, M. J.; Brogi, S. *RSC Adv.* **2015**, *5*, 22431–22448.

(83) Kerr, W. J.; Mudd, R. J.; Brown, J. A. *Chem. Eur. J.* **2016**, *22*, 4738–4742.

(84) Occhipinti, G.; Jensen, V. R.; Törnroos, K. W.; Frøystein, N. Å.; Bjørsvik, H.-R. *Tetrahedron* **2009**, *65*, 7186–7194.

(85) Wolf, J.; Labande, A.; Daran, J.-C.; Poli, R. *J. Organomet. Chem.* **2006**, *691*, 433–443.

(86) Vong, K. K. H.; Maeda, S.; Tanaka, K. *Chem. Eur. J.* **2016**, *22*, 18865–18872.

(87) Horikawa, R.; Fujimoto, C.; Yazaki, R.; Ohshima, T. *Chem. Eur. J.* **2016**, *22*, 12278–12281.

(88) Chen, H.; Feng, Y.; Xu, Z.; Ye, T. *Tetrahedron* **2005**, *61*, 11132–11140.

(89) Seashore-Ludlow, B.; Villo, P.; Somfai, P. *Chem. Eur. J.* **2012**, *18*, 7219–7223.

(90) Mock, J. N.; Taliaferro, J. P.; Lu, X.; Patel, S. K.; Cummings, B. S.; Long, T. E. *Bioorg. Med. Chem. Lett.* **2012**, *22*, 4854–4858.

(91) Konnert, L.; Lamaty, F.; Martinez, J.; Colacino, E. *J. Org. Chem.* **2014**, *79*, 4008–4017.

(92) Di Gioia, M. L.; Gagliardi, A.; Leggio, A.; Leotta, V.; Romio, E.; Liguori, A. *RSC Adv.* **2015**, *5*, 63407–63420.

(93) Di Gioia, M. L.; Costanzo, P.; De Nino, A.; Maiuolo, L.; Nardi, M.; Olivito, F.; Procopio, A. *RSC Adv.* **2017**, *7*, 36482–36491.

(94) Liu, H.; Pattabiraman, V. R.; Vederas, J. C. *Org. Lett.* **2007**, *9*, 4211–4214.

(95) Fleming, J. T.; Wills, C.; Waddell, P. G.; Harrington, R. W.; Higham, L. J. *Dalton Trans.* **2016**, *45*, 15660–15670.

(96) Hirano, K.; Urban, S.; Wang, C.; Glorius, F. *Org. Lett.* **2009**, *11*, 1019–1022.

(97) Yeh, T.-L.; Liao, C.-C.; Uang, B.-J. *Tetrahedron* **1997**, *53*, 11141–11152.

(98) Tallon, S.; Manoni, F.; Connon, S. J. *Angew. Chem. Int. Ed.* **2015**, *54*, 813–817.

(99) Deboves, H. J. C.; Montalbetti, C. A. G. N.; Jackson, R. F. W. *J. Chem. Soc. Perkin Trans. 1* **2001**, 1876–1884.

(100) Chen, H.; Feng, Y.; Xu, Z.; Ye, T. *Tetrahedron* **2005**, *61*, 11132–11140.

(101) Barrett, A. G. M.; Pilipauskas, D. *J. Org. Chem.* **1990**, *55*, 5170–5173.

(102) Evans, V.; Mahon, M. F.; Webster, R. L. *Tetrahedron* **2014**, *70*, 7593–7597.

(103) Souto, A.; Montaos, M. A.; Balado, M.; Osorio, C. R.; Rodríguez, J.; Lemos, M. L.; Jiménez, C. *Bioorg. Med. Chem.* **2013**, *21*, 295–302.

(104) Gibson, F. S.; Bergmeier, S. C.; Rapoport, H. *J. Org. Chem.* **1994**, *59*, 3216–3218.

(105) Da Costa, C. F.; Pinheiro, A. C.; De Almeida, M. V.; Lourenço, M. C. S.; De Souza, M. V. N. *Chem. Biol. Drug Des.* **2012**, *79*, 216–222.

(106) Pan, X.; Liu, Z. *Tetrahedron* **2014**, *70*, 4602–4610.

(107) Williams, T. J.; Reay, A. J.; Whitwood, A. C.; Fairlamb, I. J. S. *Chem. Commun.* **2014**,

50, 3052–3054.

(108) Ruiz-Rodríguez, J.; Albericio, F.; Lavilla, R. *Chem. Eur. J.* **2010**, *16*, 1124–1127.

(109) Reay, A. J.; Williams, T. J.; Fairlamb, I. J. S. *Org. Biomol. Chem.* **2015**, *13*, 8298–8309.

(110) Foster, M. S.; Oldham, C. D.; May, S. W. *Tetrahedron Asymm.* **2011**, *22*, 283–293.

(111) Di Gioia, M.; Leggio, A.; Le Pera, A.; Liguori, A.; Perri, F.; Siciliano, C. *European J. Org. Chem.* **2004**, *2004*, 4437–4441.

(112) Su, S.; Kakeya, H.; Osada, H.; Porco, J. A. *Tetrahedron* **2003**, *59*, 8931–8946.

(113) KrouzÌelka, J.; Linhart, I. *European J. Org. Chem.* **2009**, *2009*, 6336–6340.

Chapter Two

2.1 Proposed Work

2.1.1 Solution Phase Labelling of Peptides

Following the extensive and highly successful studies on the deuteration of α- amino acids described in Chapter One, we sought to extend our deuterium labelling protocol to the HIE of small peptide molecules. The emergence of peptidic drug molecules in clinical trials and, in turn, the drug market, makes the investigation of their metabolic behaviour extremely important.[1] As a result, the incorporation of isotopic labels into peptides under mild conditions is of high priority. Currently within the literature, as discussed previously, there are few mild and efficient methods to overcome this challenge. Peptide molecules present a considerable challenge as substrates for HIE compared to single amino acid residues. The number of Lewis basic sites and the ubiquity of C-H bonds available for activation present two significant problems: akin to amino acids, additional Lewis basic sites could allow the peptide substrate to chelate to the iridium catalyst, therefore hindering the C-H activation process; and secondly, selectivity at a specific residue may be extremely challenging as a result of the various directing groups and activated positions within a peptide. An example of this is shown in Figure 2.1, where potential directing groups and their corresponding activated positions are highlighted, taking into account activation by only a 5-mmi. Concomitant binding of two of the carbonyl groups within this molecule would result in an off-cycle intermediate detrimental to the productive labelling pathway.

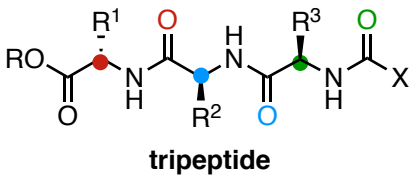

Figure 2.1

To initiate our studies on HIE for peptide molecules, we first aimed to investigate simple dipeptide molecules. To probe the activity and selectivity of our developed iridium(I) catalysts, we first sought to investigate peptides containing a secondary and tertiary amino acid (Scheme 2.1). Secondary amino acid glycine would be incorporated into dipeptides at both the *N* and *C* termini, and combined with several tertiary amino acid residues. This would allow us to observe whether we could achieve complete selectivity at the glycine residue, independent of the nature of the tertiary amino acid, or whether the tertiary position will compete. Additionally, alteration of the protecting group may impart a selectivity switch, whereby the internal amide within the peptide backbone may become a more competent directing group compared to a large carbamate directing group (such as Fmoc-) at the *N* terminus.

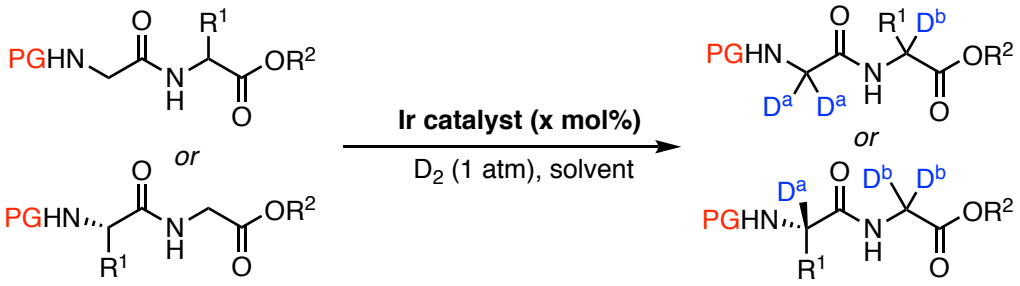

Scheme 2.1

Continuing our work on dipeptides, we will endeavour to extend our developed methodology to peptides containing solely tertiary amino acid residues. This will again give us the opportunity to gain insight into selectivity within these small peptidic systems between substituted amino acids.

In a further advance to our solution phase peptide labelling, we hope to extend our methodology in incremental steps to tripeptides (Scheme 2.2). Once again, various peptide sequences and protecting group combinations will be investigated to allow additional insight and expand our substrate peptide substrate scope.

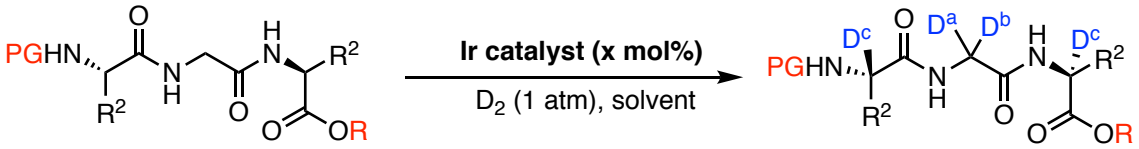

Scheme 2.2

2.1.2 HIE of Peptides on Solid Phase

Alongside our investigation into the HIE of peptide molecules in solution, we proposed that development of a HIE protocol for peptides on solid phase resin would be extremely beneficial, particularly for industrial chemists. The synthesis of peptide sequences are routinely carried out through solid-phase peptide synthesis (SPPS),[2] with excess reagents and side products easily removed by washing the resin bound peptide pre-cleavage. As this method is very convenient for the chemist, if an isotopically labelled peptide is required, it would be beneficial to access the isotopically enriched peptide before final cleavage and purification. In addition, the limited solubility of peptides compared to small singular amino acid residues is a prominent consideration at the outset of our studies. The use of covalently bound peptides on an insoluble solid support negates the requirement of a soluble peptide within the reaction medium. This could aid the HIE development process considerably. Of course, there are some potential complications to this method: solvents applicable to both efficient swelling of the resin (required for solid phase peptide chemistry) and HIE will be required; and, there are several practical considerations to this set-up which may provide additional issues. These matters will be discussed *vide infra*.

To commence our studies in this area, we first wanted to investigate HIE on solid phase for an established and robust system. To this end, we aimed to centre our labelling studies on a singular amino acid residue covalently bound to resin (Scheme 2.3).

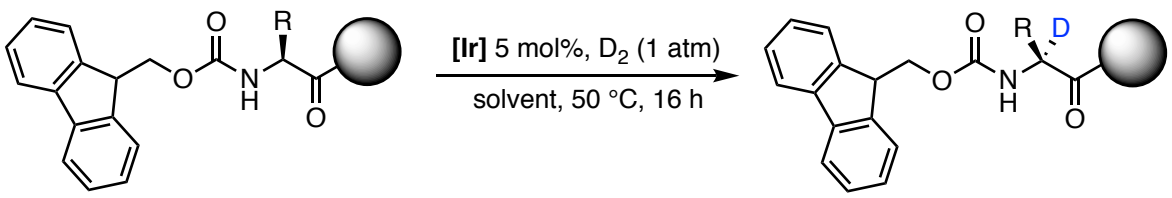

Scheme 2.3

With a HIE protocol in hand for the deuteration of a single amino acid residue, small tripeptide sequences bound to a solid support will be investigated. A range of resin supports will be investigated to determine the most suitable solid support for the proposed HIE methodology.

2.2 Results and Discussion

2.2.1 Labelling of Dipeptides Containing Glycine

To extend our HIE protocol from amino acids to more complex dipeptide systems, Ac-Gly-Phe-OMe was utilised as a model substrate. Although concerned around the lower solubility of dipeptides compared to amino acids, the conditions employed were akin to the labelling of Ac-Gly-OMe (Scheme 2.4), discussed in Chapter One, Section 1.3.1.

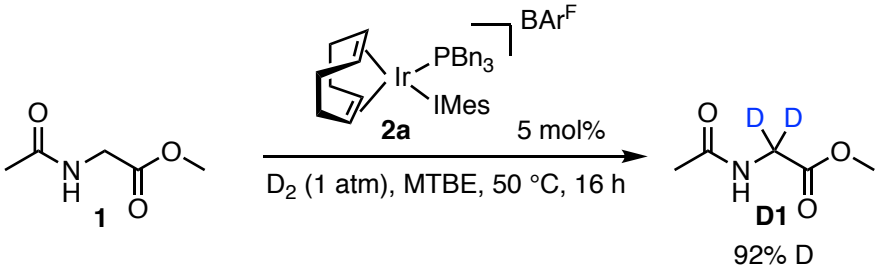

Scheme 2.4

At the outset of the investigation, it was deemed necessary to conduct a catalyst screen for the dipeptide model substrate. The nature and size of the ligand set around iridium could be crucial to the efficient labelling of these larger, more complex substrates. Whilst the bidentate catalysts had previously shown poor activity with the α-amino acids due to the formation of an unproductive intermediate through chelation of both carbonyls of the protected amino acid, the enhanced size of the peptide substrates could require a smaller ligand set around iridium, provided by such a bidentate system. Of course, the increased number of Lewis basic sites within the peptide molecules opens further opportunity for unproductive chelation of the substrates to the catalyst, and so it was also possible that the activity of the bidentate systems could remain similar to the HIE of α-amino acids.

It was extremely pleasing to observe that the deuteration of Ac-Gly-Phe-OMe **3** with monodentate complex **2a** displayed almost complete chemo-selectivity for the glycine residue, with a very respectable 61% incorporation observed at 5 mol% catalyst loading (Scheme 2.5). Although labelling at the phenylalanine was minimal, measurable amounts

were observed. Monodentate complex **2b** also allowed incorporation into the glycine residue, although only to moderate levels of 35%. Lamentably, although perhaps not surprisingly, the activity of the chelated complexes **4-6** showed poor activity compared to monodentate **2a**. This being said, complex **4** displayed similar activity to monodentate complex **2b**. Further, it was interesting to note that **2a** remained the most efficient for HIE process, similar to the labelling of Ac-Gly-OMe **1**.

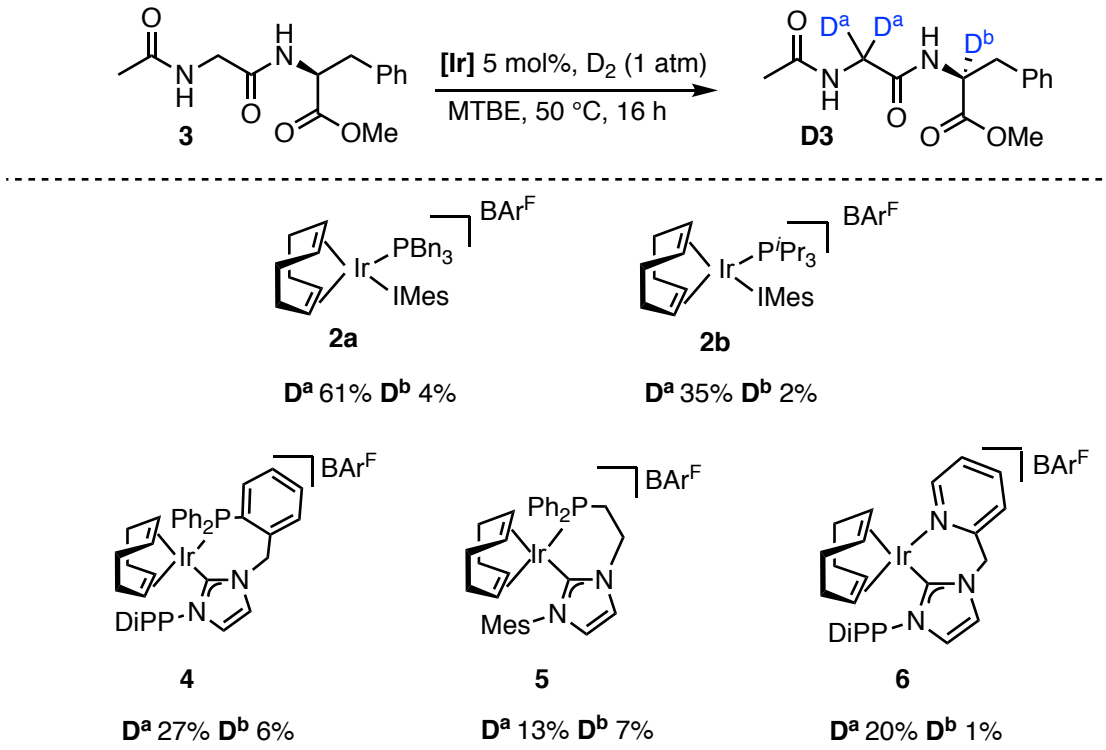

Scheme 2.5

With an efficient catalyst identified, we followed up our previous work on the application of mixed solvent systems for the HIE of amino acids, to identify whether such a system would allow for better solubility of Ac-Gly-Phe-OMe **3**, and subsequently more efficient levels of labelling. Pure chloroform was investigated alongside 10:1 mixtures of chloroform/alcohol (Graph 2.1). No incorporation was observed at the phenylalanine residue in these instances. Disappointingly, whilst all solvent systems afforded incorporation at the glycine residue, and although the substrate appeared to have better solubility in these systems, the incorporation remained lower than when MTBE was utilised in the HIE process. This suggests that the nature of the solvent is very important for catalyst turnover, with the bulky, less coordinating alcohol ^{t}AmOH affording better incorporation than ^{i}PrOH when mixed with chloroform.

Nonetheless, although the results appear somewhat disappointing, it is pleasing to observe incorporation in these mixed solvent systems. Whilst dipeptide **3** is sparingly soluble in MTBE at 50 °C, it is unlikely that larger, more complex peptide molecules will be completely insoluble, and mixed solvent systems may be the only viable route in these cases.

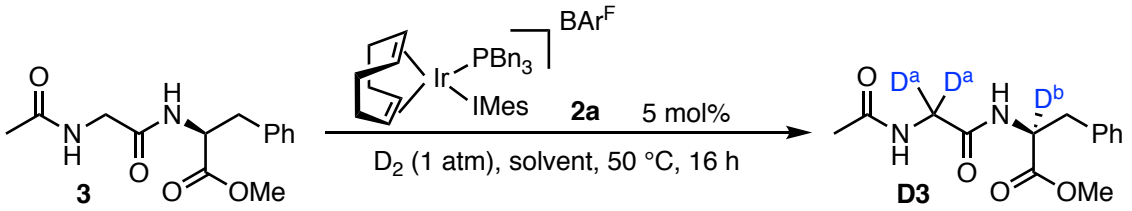

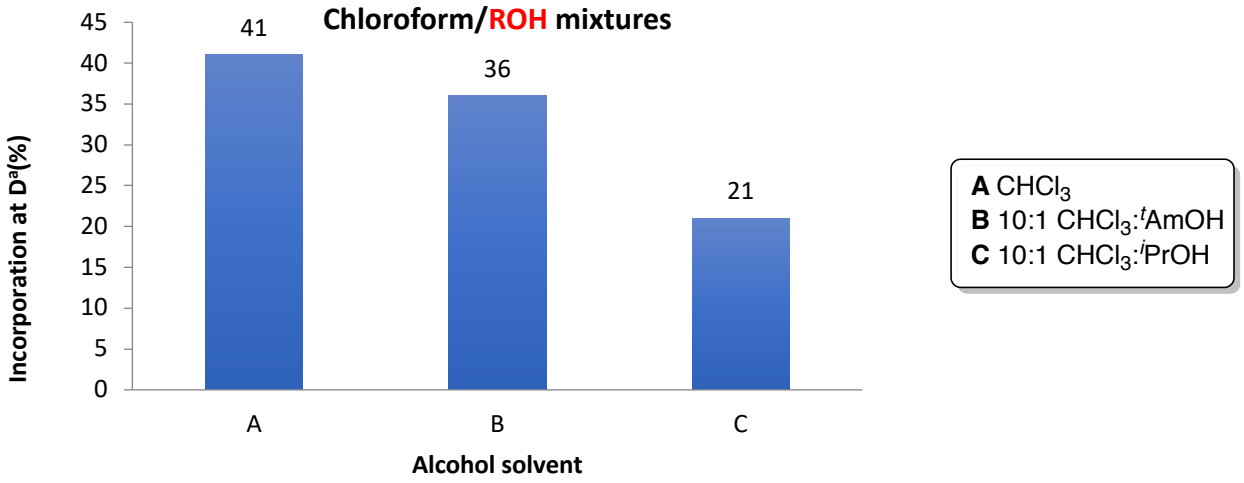

Graph 2.1

Based on our work on the HIE of amino acids, catalyst **7** had been identified as an extremely competent catalyst for the isotopic labelling of tertiary amino acid residues. Employment of the more electron rich $IMes^{Me}$ discourages formation of inactive intermediates where binding through both carbonyls of the substrate to iridium hindered the formation of the productive agostically bound substrate, and subsequently decreased the likelihood of C-H activation occurring. With the additional Lewis basic sites present within even simple dipeptide molecules, it was proposed that employment of this catalyst could allow higher levels of labelling than those observed with catalyst **2a (**Scheme 2.6**)**. To our delight, catalyst **7** indeed allowed an increase in isotopic incorporation at the glycine residue to an impressive 77%.

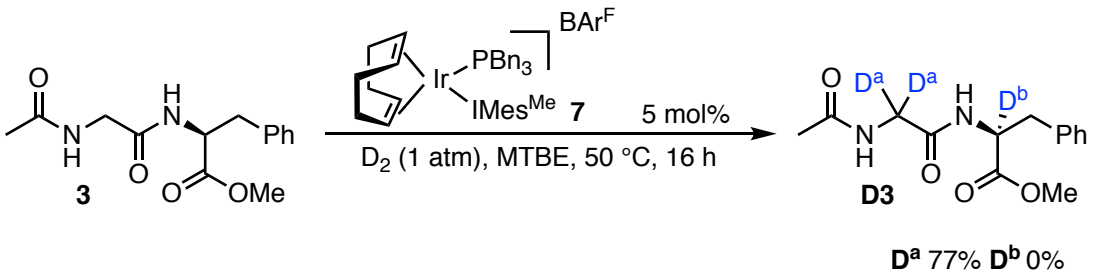

Scheme 2.6

Following our success with Ac-Gly-Phe-OMe **3** under the developed conditions, we sought to extend the scope of dipeptides containing glycine residues. Phenylalanine had previously been a challenging residue in HIE (see Chapter One), with only select protecting groups compatible with a successful C-H activation process. Therefore, it was perhaps unsurprising that chemo-selectivity could be achieved at glycine in Ac-Gly-Phe-OMe **3**. When designing our substrate scope, we endeavoured to include residues which may compete with glycine, and also become isotopically enriched under the reaction conditions. In an attempt to increase the level of isotopic enrichment observed, we chose to modestly increase the catalyst loading to 10 mol%, akin to the labelling of tertiary amino acids. The results are highlighted in Scheme 2.7. High levels of labelling remained at the glycine residues within dipeptides Boc-Gly-Val-O^{t}Bu **D8** and Cbz-Val-Gly-O^{t}Bu **D9**, and it is interesting to note that regardless of whether the glycine residue is at the *N* or *C* terminus, good levels of labelling are observed at the methylene position. Also noteworthy, and in line with our amino acid labelling protocol, was the tolerance of a carbamate directing group such as Boc- or Cbz-. For substrate **D8**, where the valine residue resides at the *C* terminus of the dipeptide, a deuterium enrichment of 18% was observed at the methine position, directed through a 5-mmi of the internal amide within the peptide backbone. This is an interesting result, and depending on the desired outcome, conditions could potentially be manipulated to either encourage higher incorporation at both residues concomitantly or alternatively, gain selectivity at the glycine residue perhaps by lowering the catalyst loading or altering the concentration of the reaction medium. Arguably more intriguing, was the isotopic labelling of Cbz-Val-Gly-O^{t}Bu **D9**. The glycine residue was labelled to excellent levels of 82%, with direction from the internal amide. However, in this instance, with the valine residue at the *N* terminus, high deuteration was observed at the α position of this residue, with 62% isotopic enrichment. To our surprise,

isotopic enrichment was also observed on the side chain of valine, with the methine position of the *iso*-propyl group labelled to 26%. This position lacks the presence of a heteroatom α to it, which is considered beneficial for productive C-H activation. Secondly, within our labelling studies on valine alone, no incorporation was observed on the side chain. This could be the result of the mode of binding of the substrate within the peptide, with some element of secondary structure placing the C-H bond in close proximity to the iridium centre and thereby allowing formation of an agostic interaction and subsequent C-H activation. The formation of a 5-mmi at this position is available through coordination of the internal amide. Finally, it was interesting to note that unlike our HIE of singular amino acids, the Cbz- protecting group within **D9** displayed no deuterium incorporation at the benzyl position. Unfortunately, dipeptide **D10** containing cyclic amino acid proline, displayed poor levels of isotopic enrichment at both the glycine and proline residues. Screening of alternative catalyst motifs, or modification of the current conditions could allow further advancement in the labelling of this sequence.

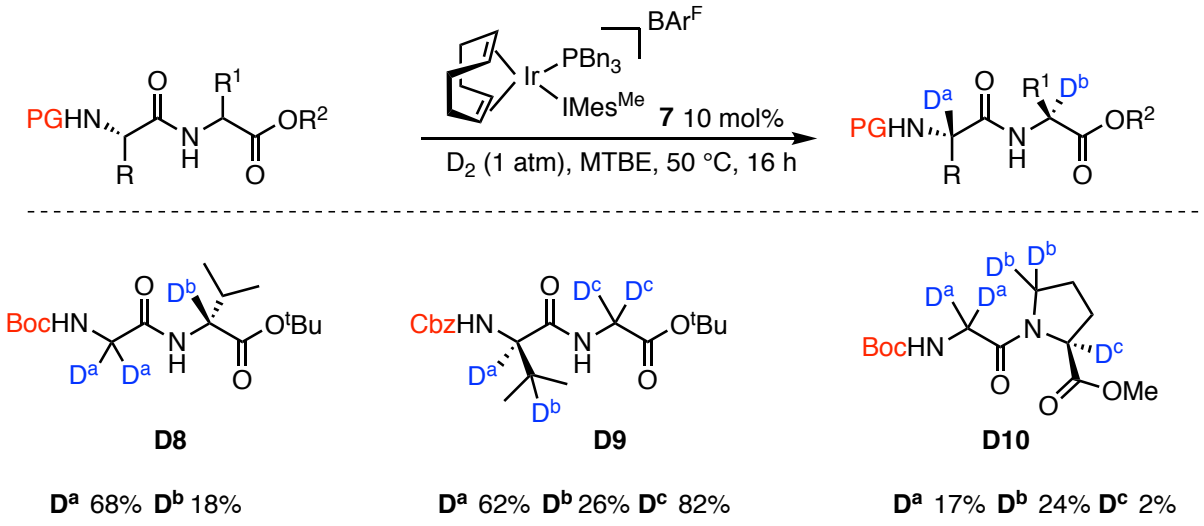

Scheme 2.7

The substrates investigated *above* show interesting selectivities depending upon several key factors. Whilst a rationale for the levels of labelling observed in the sequences cannot be fully elucidated, the level of enrichment appears to be dependent on the position of the residue, the combination of residues within a sequence, and the protecting group of choice. This opens up

the option of exploring further combinations and peptide sequences to further elucidate the selectivity. Encouragingly, the ability to label other residues in a concomitant fashion in the presence of a glycine residue was a promising advancement in the field. Incorporation of several deuterium atoms within a sequence may be beneficial, particularly when considering the utility of a deuterated peptide within mass spectrometry studies.

2.2.2 Labelling of Dipeptides Containing Tertiary Amino Acids

Next, we sought to expand the scope of the HIE of dipeptides to sequences which contained only tertiary amino acid residues, where C-H activation is more challenging. Again, the insight into potential chemoselectivity within a sequence would allow us to gather information on the residues most likely to be accessible for deuteration in larger peptidic systems. Under identical conditions to the labelling of glycine containing dipeptides, a variety of peptide sequences were efficiently labelled (Scheme 2.8). For dipeptides containing phenylalanine at the *C* terminus (**D11**, **D12**, **D13**), no incorporation was observed at the methine position of this residue. Interestingly, Boc-Ile-Phe-O^{t}Bu **D11** afforded deuterium incorporation selectively at the Ile residue with an appreciable 56% incorporation. No incorporation was observed on the side chain in contrast to Cbz-Val-Gly-O^{t}Bu **D9**. An absence of diastereomeric signals within the ^{1}H NMR spectra confirmed that the HIE of peptides molecules, like amino acids, was stereoretentive. For Boc-Ala-Phe-OMe **D12**, a similar trend was observed, with 46% isotopic incorporation observed at the alanine methine position. When switching the protecting group to Cbz- in **D13,** the level of isotopic incorporation dropped to 34%, while the benzylic position of the carbamate remained unlabelled. This observation is in accordance with the glycine containing peptides. In contrast, however, if the residues were switched, to give Cbz-Phe-Ala-O^{t}Bu **D14**, a change in chemoselectivity was observed. Although deuterium incorporation remained highest at the methine position within alanine (29%), the HIE process was not chemo-selective, with isotopic enrichment observed at both the methine position of phenylalanine and the benzylic position of the carbamate protecting group (26% and 20% respectively). This highlights the complexity of even small peptides compared to single amino acid residues.

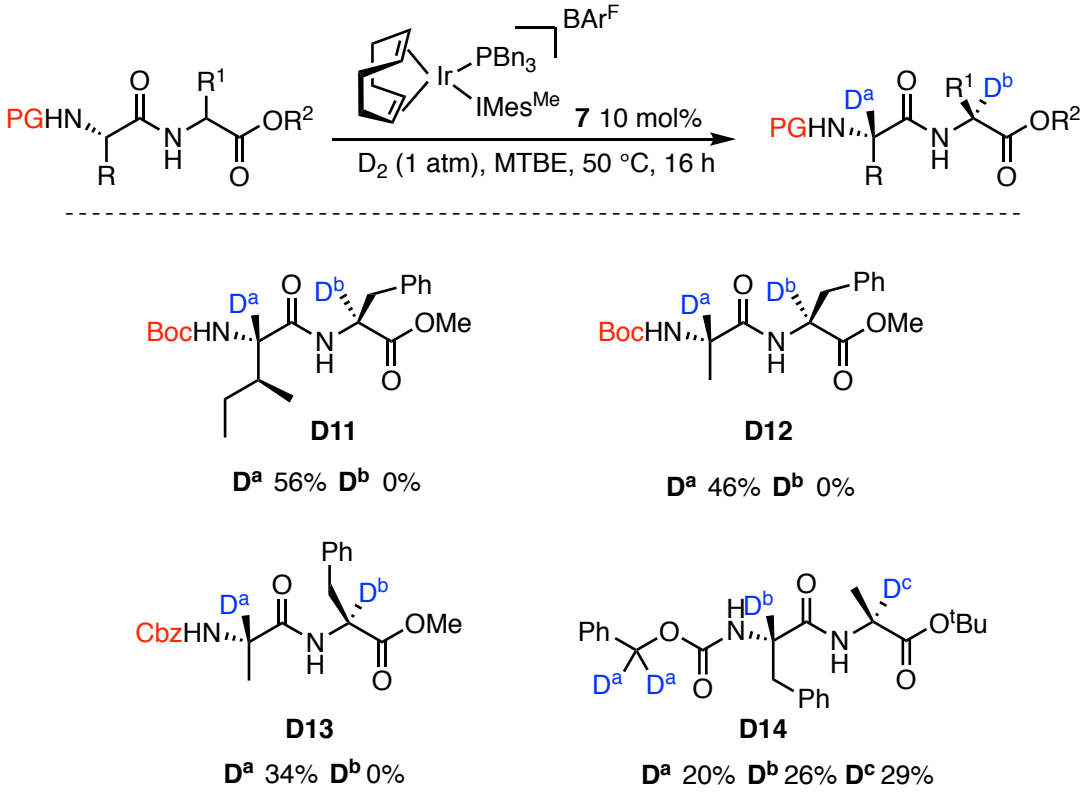

Scheme 2.8

It was extremely encouraging to observe high activity of our Ir(I) catalysts for HIE of tertiary amino acid residues within dipeptide molecules, something which, to the best of our knowledge, is unprecedented in the literature with Ir(I) catalysts.

2.2.3 Isotopic Labelling of Tripeptides

In a further extension of our work, we next investigated the labelling of glycine-containing tripeptide Ac-Phe-Gly-Phe-O^{t}Bu **15**. All tripeptides utilised throughout were commercial unless otherwise stated. Since complex **2a** is a competent catalyst for the labelling of glycine residues, this catalyst was utilised to optimise the HIE of **15** (Table 2.1). Similarly to our dipeptide substrates, Ac-Phe-Gly-Phe-O^{t}Bu **15** contains several possible directing groups, and labelling sites. To achieve regioselective glycine labelling, direction through the internal carbonyl *via* a 5-mmi would be required. The common *tert*-butyl ester moiety was chosen for *C* terminus protection to aid with solubility of the peptide sequence, and a range of

organic solvents were investigated. At low catalyst loading of 5 mol% (entries 1 and 2) it was disappointing to observe very low levels of deuteration, regardless of the nature of the solvent. This being said, it was extremely pleasing to observe high levels (65%, 59%) of isotopic enrichment at the diastereotopic C-H bonds of the methylene position at a moderate catalyst loading of 10 mol% in MTBE (entry 3). Further organic solvents such as DCE, EtOAc and ^{t}BuOAc (entries 4-6) were investigated, however MTBE remained the most efficient solvent, regardless of the apparent lack of solubility of the peptide substrate in the reaction medium. Pleasingly, the HIE reaction was completely selective for labelling at the glycine residue. This could have excellent utility, enabling the chemist to determine which residue may be labelled within a larger peptide. Interestingly, increasing the catalyst loading to 20 mol% allowed further enhancement in the level of deuterium incorporated with MTBE or EtOAc as solvent. At this catalyst loading, EtOAc outperformed MTBE with high levels of 83% and 82% observed at the diastereotopic C-H bonds of the glycine residue. HIE reactions at higher levels of catalyst loading resulted in a detrimental effect on the chemo-selectivity of the reaction, with deuterium incorporation observed at the methine position of the phenylalanine residues.

Table 2.1

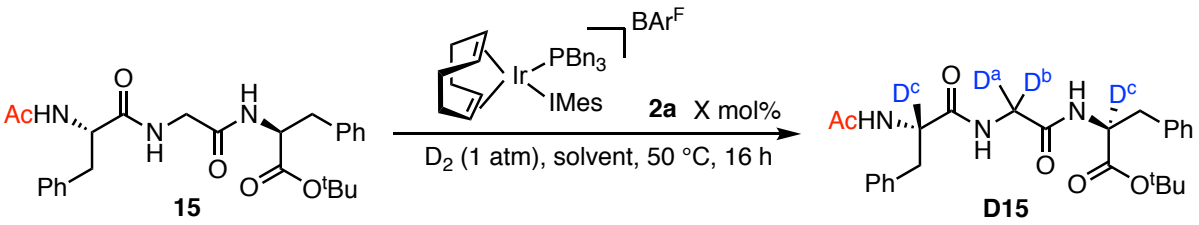

Entry	Solvent	Molarity (M)	x mol%	D^a (%)	D^b (%)	D^c (%)
1	MTBE	0.10	5	17	14	0
2	$CHCl_3$	0.10	5	4	3	0
3	MTBE	0.05	10	65	58	0
4	DCE	0.05	10	28	29	0
5	EtOAc	0.05	10	44	48	0
6	^{t}BuOAc	0.05	10	28	29	0
7	MTBE	0.05	20	77	69	9
8	DCE	0.05	20	25	22	2
9	EtOAc	0.05	20	83	82	12

Following our success with Ac-Phe-Gly-Phe-O^{t}Bu **15**, we turned our attention to examining the tolerability of our conditions to alternative protecting groups at the *N* and *C* termini (Scheme 2.9). Previous studies for the HIE of amino acid and small dipeptides had identified both **2a** and **7** as highly active catalysts and so both were examined concomitantly. A move

to the smaller methyl ester at the *C* terminus in Ac-Phe-Gly-Phe-OMe **D18** saw deuteration completely suppressed in MTBE. A move to a more polar solvent EtOAc did afford isotopic incorporation, although the level was extremely low. Cbz- protected **D16** performed extremely well under the HIE conditions. This is attributed to the increased solubility of this substrate in the reaction solvent, with a remarkable 94% and 95% labelling at the methylene of the glycine residue with catalyst **2a**. Once again, moving to the smaller ester in **D19** required a move to EtOAc to obtain an impressive 72% and 74% isotopic enrichment at the glycine residue with catalyst **7**. No incorporation was observed at the benzylic position of the Cbz- protecting group. In general, for substrates bearing the larger *tert*-butyl ester, **2a** was the most active catalyst. In contrast, for the majority of substrates catalyst **7** afforded higher incorporations for methyl ester substrates. For tripeptides protected with Ac- or Cbz-, solvent choice was highly dependent on the ester group. For the more lipophilic *tert*-butyl ester, MTBE was the optimal solvent, whilst for methyl esters, EtOAc allowed higher incorporations. Fmoc- protected substrates did not follow the same trend, with a switch in the optimal solvent observed. Fmoc-Phe-Gly-Phe-O^{t}Bu **D17** performed poorly under our HIE conditions, with only moderate levels of deuterium incorporated. In contrast to our previous substrates, a move to a methyl ester in **D20** allowed greatly enhanced levels of isotopic enrichment. These results highlight the dependency of the HIE reaction on the nature of the protecting groups on a peptide substrate. Even a small change in the nature of the capping groups can cause significant changes in the level of deuterium incorporation observed on the same peptide sequence. Unsurprisingly, solubility appears to be crucial to allow excellent levels of incorporation, as is demonstrated by substrates **D16** and **D18**. Whilst the level of labelling is dependent on the nature of the protecting groups, it was extremely pleasing to see that under our mild conditions, all substrates were labelled. This is an encouraging advancement, and has allowed identification of suitable protecting groups for the HIE of small peptide molecules.

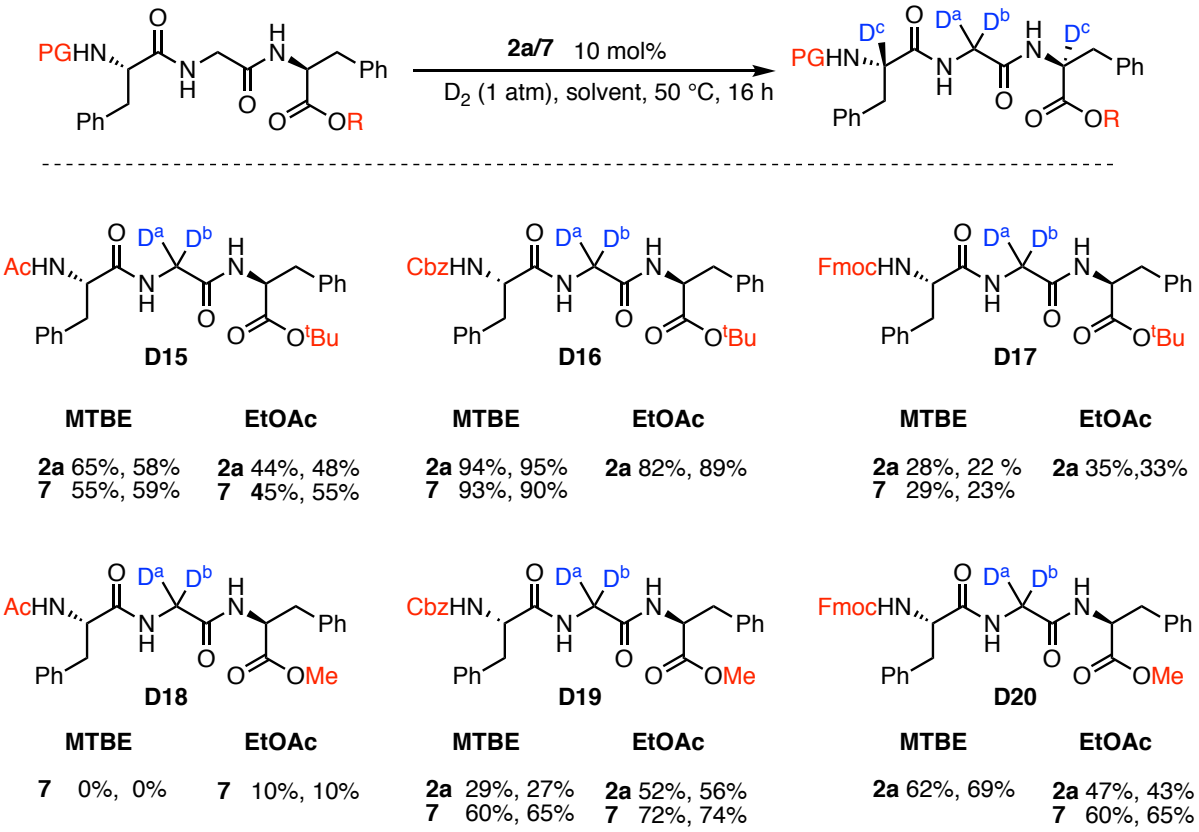

Results represented as: incorporations of (D^a, D^b)
No incorporation at D^c observed

Scheme 2.9

Based on our previous results for the HIE of phenylalanine residues, and recognizing that this was one of the more challenging motifs we have come across, we next turned our attention to tripeptides containing glycine and a tertiary amino acid which is highly competent under our HIE conditions. Investigation of the chemoselectivity and dependency of the HIE outcome on the protecting group in PG-Ala-Gly-Ala-OR' derivatives was carried out with catalyst **7**, and the results are shown in Scheme 2.10. The level of isotopic incorporation achieved and chemoselectivity were indeed highly dependent on the nature of the protecting group. For Ac- protected peptides, complete chemoselectivity for the glycine residue was not observed (**D21** and **D24**). **D21** performed poorly compared to peptide **D15**, where alanine residues are substituted for phenylalanine. In contrast to **D15**, isotopic labelling was not only observed at the glycine residue, but additional incorporation was observed at the methine positions within the alanine residues. Intriguingly, for Ac-Ala-Gly-Ala-OMe **D24**, incorporation was observed not only at the α positions of the amino acid residues, but also at the CH_3 of the methyl ester. This is the only peptide substrate thus far to display isotopic enrichment on the ester

functionality. Akin to the Phe-Gly-Phe peptides, Cbz- protected **D22** and **D25** displayed complete chemo-selectivity for the glycine residue. Remarkable levels of isotopic enrichment were observed for **D22** in EtOAc, with 98% and 97% observed at the diastereotopic C-H bonds in the glycine residue. The discrepancy in chemo-selectivity between Cbz- and Ac-protected tripeptides in this study may be due to the nature of the directing group. In both cases, incorporation at the methylene of the glycine residue arises through the formation of a 5-mmi through coordination of the internal amide. Incorporation at alanine will be delivered from a 5-mmi by coordination of the nitrogen protecting group. In the case of **D21**, the Ac-protecting group affords an amide directing group, whereas with Cbz- a carbamate directing group is present. The carbamate will bind significantly less strongly to the metal centre compared to an internal amide, and so it is perhaps unsurprising we observe incorporation only at the glycine residue. On the other hand, in **D21** two amide directing groups compete and this could be the reasoning for the lack of selectivity and incorporation at both sites. Perhaps the most intriguing results from this study come from substrates **D23** and **D26**, bearing an Fmoc- protecting group. In addition to labelling at both the alanine and glycine α positions, deuterium incorporation was observed on the methyl side chain of the alanine residues. Whilst minimal in **D26**, compound **D23** displayed high levels of 56% incorporation at this position. Similar to the labelling of the valine side chain in dipeptide **D9**, it was surprising to see deuterium enrichment at this position, where there is a lack of adjacent activating heteroatom. Incorporation at this position could again be a result of secondary structure, where the methyl groups are brought into close proximity to the metal centre and are thereby activated towards C-H insertion.

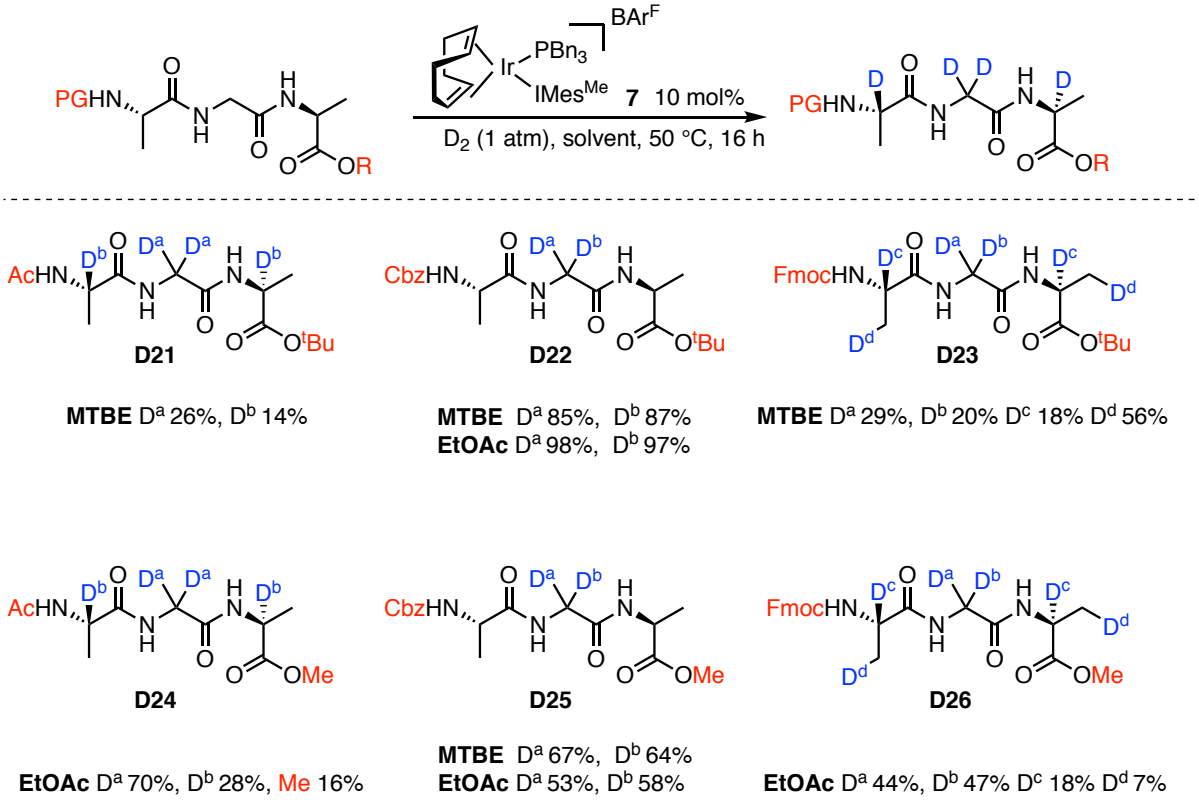

Scheme 2.10

The labelling results from the two tripeptide sequences highlight the sheer complexity brought about with even small peptide molecules. We were delighted that each of the protected peptides could be deuterated under the mild HIE conditions, regardless of the nature of the directing group. This being said, HIE of these molecules appears to be highly dependent on both protecting group choice and solubility. The change in selectivity observed with alteration of the protecting group allows the chemist the opportunity to manipulate the system to achieve incorporation at one or more desired sites within these peptide molecules. As expected, the somewhat limited solubility of some of the tripeptide substrates greatly hinders the level of labelling achieved. Therefore, an alternative approach, where solubility would be less important was investigated.

2.2.4 Labelling of a Glycine Residue on Solid Support

With the aim of increasing the number of residues within our peptide sequences for HIE, we wanted to address the issue of solubility observed even with the small tripeptide systems. To do this, we envisaged carrying out our labelling reactions on peptides which were covalently bound to a solid phase resin. All solid phase bound peptides were obtained commercially, unless otherwise stated in the Experimental section. Peptide synthesis is routinely carried out on solid phase, through SPPS, with the general process highlighted (Scheme 2.11).[2] Manipulation of our peptide substrates directly after their synthesis, and before cleavage from the resin, allows several advantages. The HIE reaction would take place within the polymer network (polymer beads swell in organic solvents to produce a network). This exerts a strong solvating effect on the peptide chains, thereby alleviating any solubility concerns. Use of a polymer supported peptide for HIE would also allow facile catalyst removal on completion of the reaction. However, there are also some key concerns: finding a solvent which is applicable to both swelling the chosen resin and the HIE process could be challenging (often solvents such as DMF or DCM are used to swell SPPS resin and are not compatible within our HIE protocol on amino acids); and secondly, manipulation of solid phase bound peptides usually avoids mechanical stirring to ensure the integrity of the resin beads. This will not be an option for our HIE reaction conditions, where stirring is required to ensure complete dissolution of deuterium gas throughout the system. Additionally, shaking apparatus typically utilised do not allow for rigorous extrusion of air, required for the HIE labelling reactions.

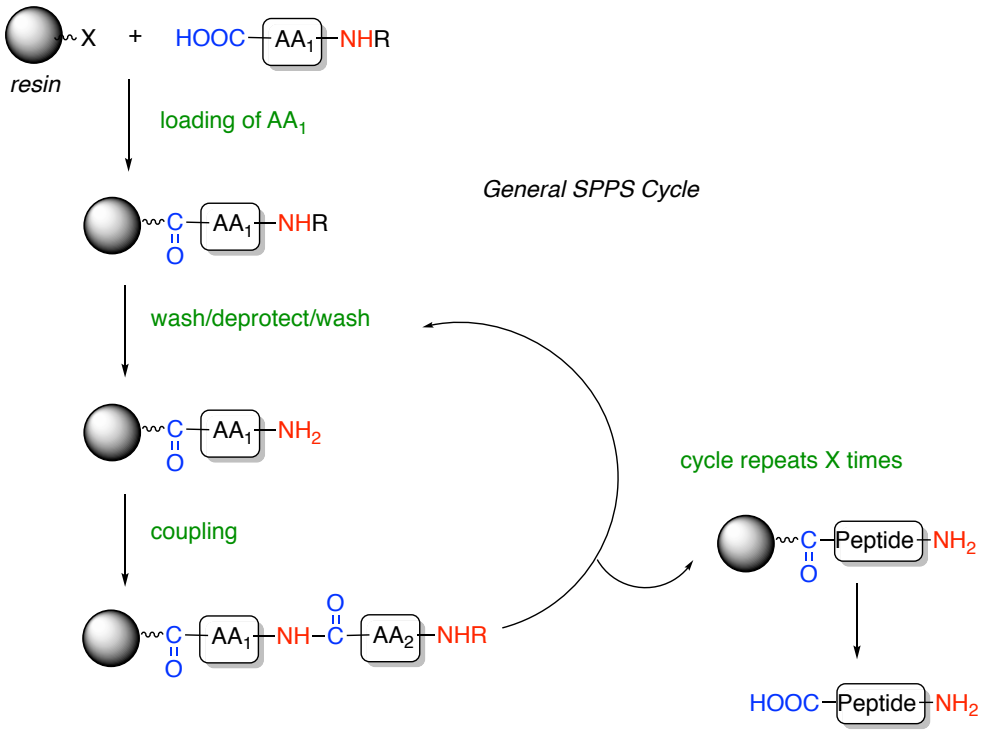

Scheme 2.11

To initiate our studies, we chose to investigate perhaps the simplest system available, an Fmoc- protected glycine residue covalently bound to resin. The commonly employed Wang resin was identified as a suitable solid support for our studies (Figure 2.2).

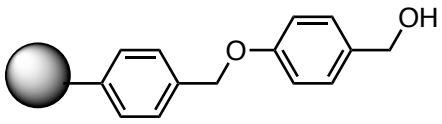

Wang resin

Figure 2.2

Identification of a solvent suitable for both HIE and swelling of the chosen Wang resin was imperative, and so the labelling of model system Fmoc-Gly-O^{t}Bu **27** was conducted in solution phase (Graph 2.2). Several solvents known to swell Wang resin were tested to identify their level of activity in the HIE of this glycine residue. The optimal solvent could then be applied to the labelling on resin. Unfortunately, MTBE is not a suitable solvent for

labelling on resin as this solvent is commonly used to shrink resin post synthesis. Incorporation in this solvent was included to benchmark the other solvents. Ethereal solvent CPME afforded good levels of deuterium incorporation at 59%. EtOAc was also a competent labelling solvent with 43% incorporation observed. Disappointingly, 2-MeTHF performed poorly under the HIE conditions (13%D).

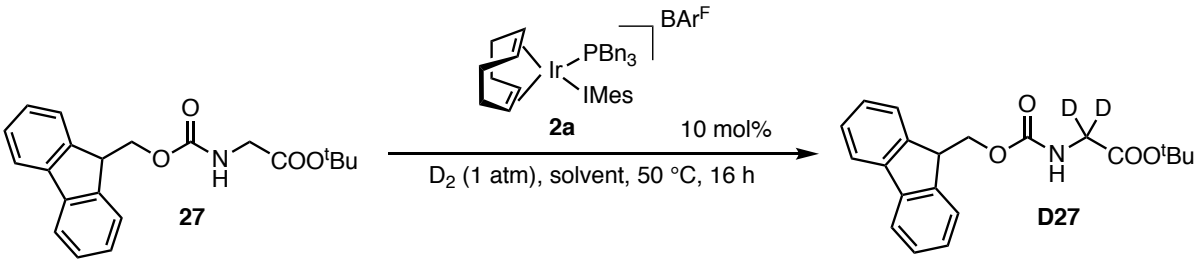

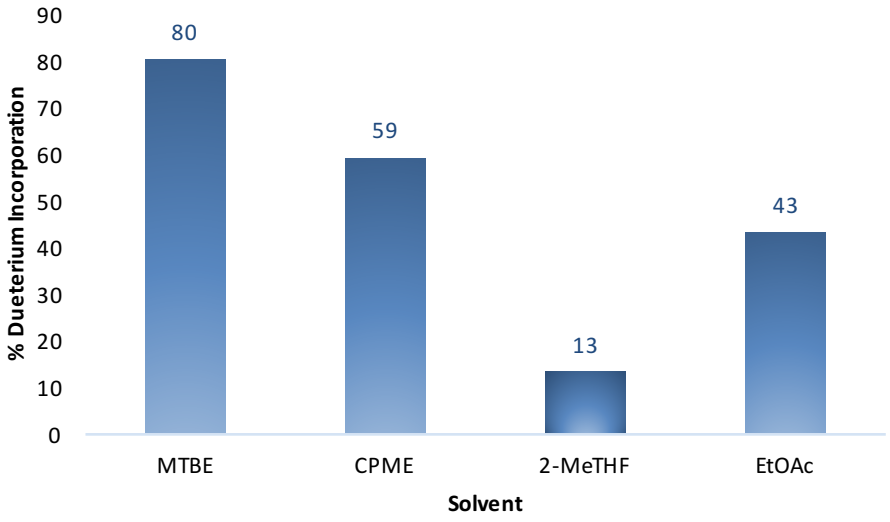

Graph 2.2

Based on our solvent screen, we initiated studies on the HIE of glycine covalently bonded to Wang resin **28** (Scheme 2.12). Our two most active catalysts **2a** and **7** were investigated. To our delight, small amounts of deuterium were incorporated on the glycine residue employing **2a** as the catalyst in both CPME and EtOAc. With EtOAc showing the highest levels of labelling, HIE with catalyst **7** was carried out in this solvent. Pleasingly, excellent levels of incorporation were observed, with 77% deuterium at the methylene position. This was a landmark result and confirmed that labelling of amino acid residues on solid phase resin was achievable under our mild reaction conditions. Practically, we were able to stir the resin to allow gas dissolution with minimal detriment to the resin. The superiority of EtOAc for HIE

was contradictory to the results observed in the solvent screening for **D27**. This highlights the importance of a solvent's ability to not only be an efficient HIE solvent, but additionally be competent at swelling the chosen resin.

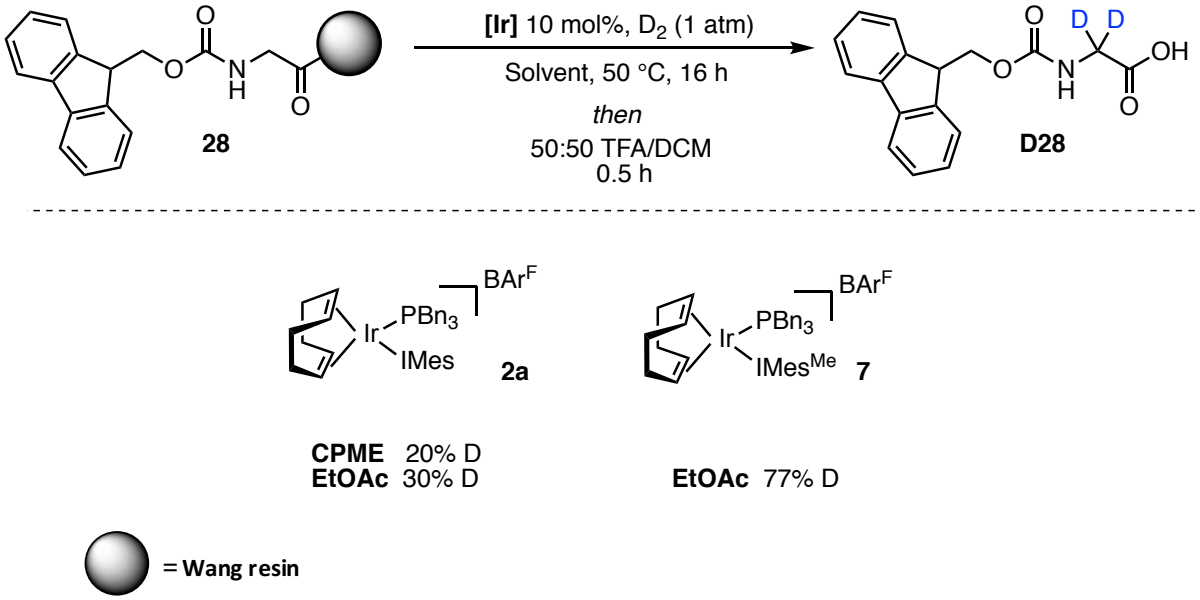

Scheme 2.12

2.2.5 Isotopic Labelling of a Tripeptide on Solid Phase

Following our success in labelling **28**, we ambitiously turned our attention to the labelling of a tripeptide sequence on solid phase. We chose to investigate the sequences we had previously studied in our solution phase labelling of tripeptides (Scheme 2.13). To our disappointment, no incorporation was observed for tripeptide **29** under the developed conditions.

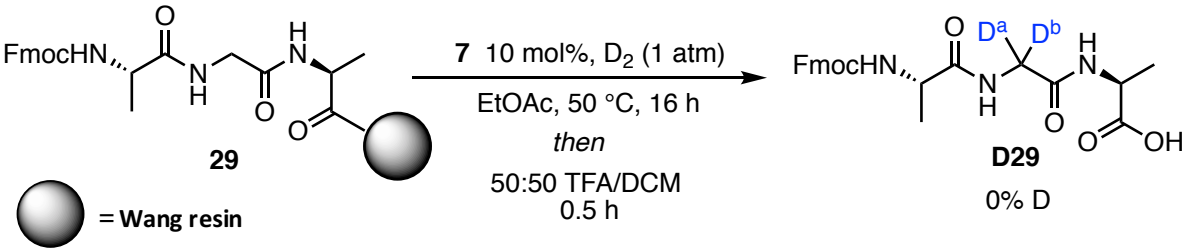

Scheme 2.13

Although initially disappointed by the results, we hypothesised that the lack of activity observed may be a result of the SPPS synthesis of **29**. Large volumes of dimethylformamide (DMF) would be used in the synthetic procedure and if small amounts remained, or indeed other non-covalently bound impurities, these could irreversibly bind to the iridium(I) catalyst and inhibit the catalytic process. To test this, the resin was first washed with several portions of DCM to eliminate potential impurities. The DCM was then removed under vacuum and the resin swollen in the HIE reaction solvent (EtOAc). The treated resin was then subjected to the HIE conditions (Scheme 2.13). To our delight, washing with room temperature DCM allowed incorporations of 41% and 23% at the diastereotopic C-H bonds in **29**. It was interesting to note that there was a diastereotopic preference in the C-H activation step. Incorporation could be pushed to excellent levels of 83% and 80% respectively if the resin was first washed in refluxing DCM. Incorporations were interpreted from the crude reaction mixture after cleavage. Moving forward, it was decided to wash the resin with only room temperature DCM. Whilst this may seem counterintuitive, we wanted to ensure chemical integrity of the sample, and therefore avoided washing at raised temperatures.

Table 2.2

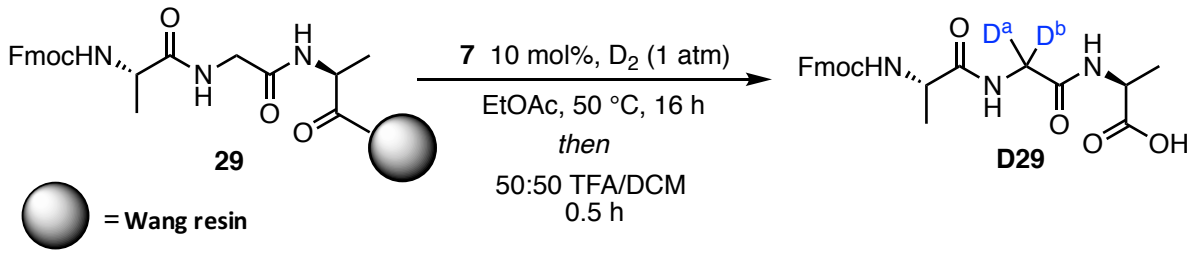

Entry	Washing	% Deuteration D^a	% Deuteration D^b
1	-	0	0
2	DCM	41	23
3	Δ DCM	83	80

At this stage of the project, we were delighted to have access to a Trisorber manifold at Research Triangle Institute (RTI) laboratories where reactions under reduced pressure of deuterium gas could be conducted. Due to the hazardous nature of tritium gas, tritiation reactions are exclusively carried out on these manifolds and so investigation of our deuterium protocol on such a system would allow greater transferability to the corresponding tritium system. Due to the practical set up of these reactions, and the scales typically utilised for tritiation chemistries, the reactions were run at small scale and analysed by liquid chromatography mass spectrometry (LCMS). Analysis of the crude reaction mixture allows the percentage of mono- and di- deuterated tripeptide post cleavage to be estimated (Table 2.3). The reaction were run at a reduced pressure of deuterium (300 mm). Concentration was very important for our deuterium protocol, as shown with entries 1 and 2. Increasing the catalyst loading from 10 mol% to 25 mol% (entry 2 *vs* entry 4) appeared to have no beneficial effect on the level of incorporation observed. Interestingly, when the temperature of the reaction was raised to 65 °C in entry 5, an impressive increase to 44% and 14% of mono- and di- deuterated **D29** was achieved. This is an encouraging result, and shows that

similar levels of incorporation can be accessed on a small scale, under reduced pressure, with only a modest increase in temperature. As a reaction temperature of 65 °Ç is reaching the boiling point of EtOAc (77 °C), and given that the reaction is under reduced pressure, we wanted to investigate some higher boiling solvents. CPME and DCE were investigated for the HIE reaction (entries 6 and 7), with CPME showing appreciable incorporation of deuterium. A mixed solvent system of CPME/EtOAc (4:1) was also tested (entry 8), allowing 40% mono- and 6% di- deuterated peptide. Owing to the practical set up of this reaction, and although performed on a smaller scale than our traditional HIE experiments, the quantity of peptide was significantly more than would be subjected to a manifold if a small molecule was to be labelled. This means the deuterium is no longer in a large excess and this could result in the lower levels of labelling observed.

Table 2.3

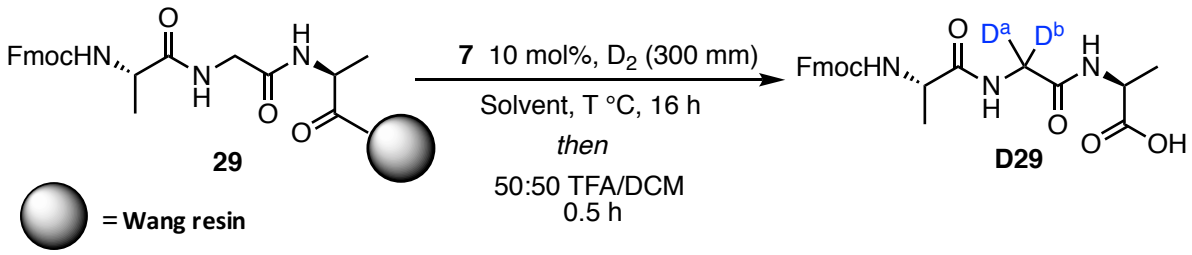

Entry	Solvent	Temp (°C)	X (mol%)	Conc. (M)	% 1-D	% 2-D
1	EtOAc	50	10	0.00054	5	0
2	EtOAc	50	10	0.0043	16	2
3	EtOAc	50	25	0.0105	6	2
4	EtOAc	50	25	0.0043	15	1
5	EtOAc	65	10	0.0043	44	14
6	CPME	65	10	0.0043	31	11
7	DCE	65	10	0.0043	5	0
8	CPME/ EtOAc (4:1)	65	10	0.0043	40	6

To investigate the transferability of our process, we next carried out the corresponding tritiation on a tritium manifold (Scheme 2.14), again undertaken at RTI laboratories. Under the reaction conditions, a specific activity of 2.53 Ci/mmol was achieved. Although this is low, it is exciting to achieve tritiated product on such a complex system, and is an excellent proof of concept reaction. Additionally, akin to the deuterium experiments, tritium is the limiting reagent in these reactions and so therefore isotopic enrichment becomes limited. Further optimisation on the deuteration reaction to increase the levels of incorporation, could allow a process, which, when applied to the tritiation conditions, could generate useable

levels of tritiated product for ADMET studies. Secondly, further practical considerations may allow the scale of substrate used to be decreased and the tritium to then be in excess.

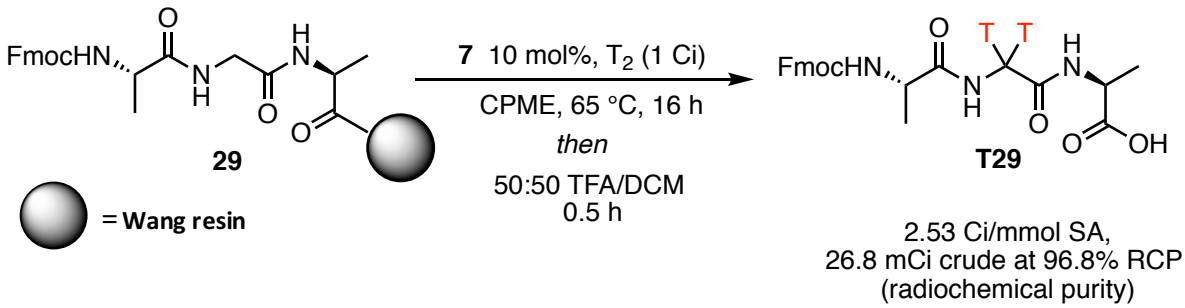

Scheme 2.14

As an extension to our investigations, we next wanted to consider alternative solid supports for the HIE of peptides. Two alternative resins were investigated: chlorotrityl resin, and the poly(ethylene)glycol (PEG) based resin ChemMatrix. In the case of ChemMatrix a Rink amide linker is utilised to covalently bond the amino acid residue (Figure 2.3). These resins are commonly used within SPPS. ChemMatrix displays excellent swelling properties compared to other resins and as a result, this was of great interest for our HIE methodology.

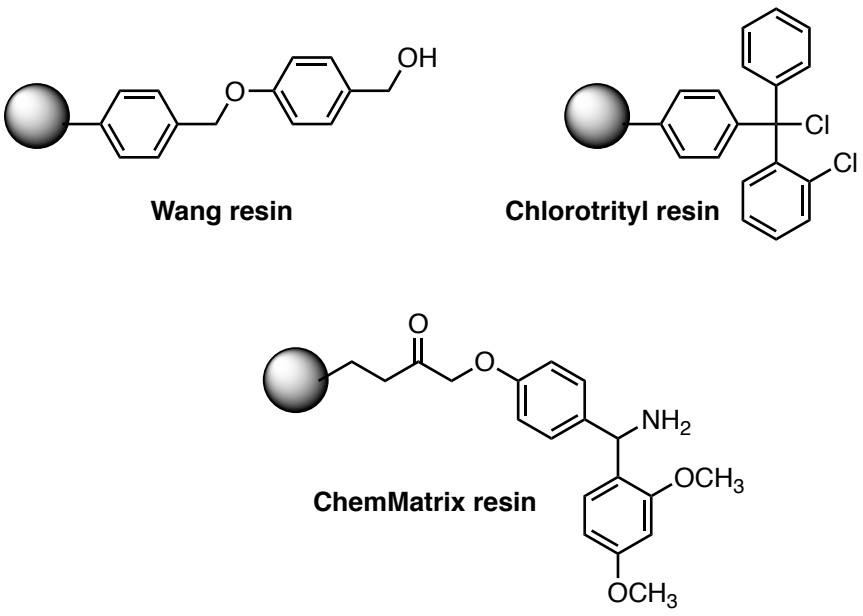

Figure 2.3

To investigate the effect of alternative resins, we first had to synthesise the solid supported peptides (Table 2.4). The desired resin was loaded with the first amino acid residue through formation of the anhydride, and subsequent coupling with the resin linker. Deprotection of the Fmoc- group under basic conditions, and coupling with the next residue was repeated on a cycle until the desired sequence was achieved. All peptides were synthesised effectively, and the loading of each resin reported.

Table 2.4

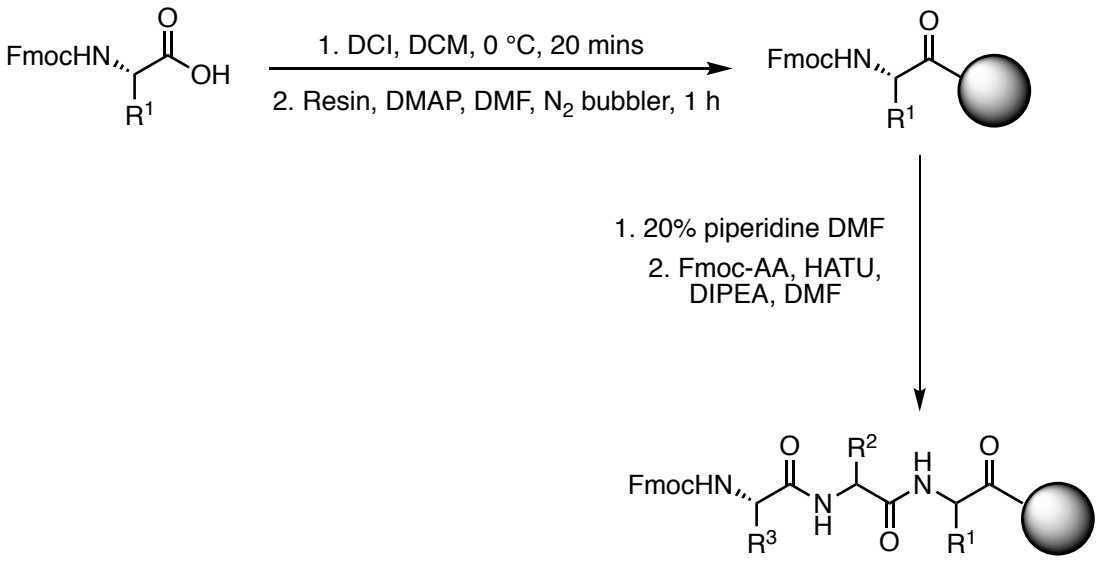

Resin Loading	Sequence	Loading of Peptide
Wang (1.11 mmol/g)	Fmoc-AGA-Wang **29**	0.78 mmol/g
ChemMatrix-Rink (0.45 mmol/g)	Fmoc-AGA-CM **30**	0.20 mmol/g
Wang (1.11 mmol/g)	Fmoc-FAF-Wang **31**	0.69 mmol/g

With the desired solid phase peptides in hand, we could investigate the effect of altering the solid support on our HIE reaction. Pleasingly, ChemMatrix resin displayed significantly better swelling properties in EtOAc compared to Wang, and as a result, higher levels of incorporation. This appears to be the most promising resin for future investigations in the area. On the other hand, chlorotrityl resin did not appear to swell in the reaction solvent, and

therefore no deuterium incorporation was observed for this solid support. Whilst this resin was not suitable, it is encouraging to observe deuteriation of solid phase peptides on two different resins. This makes the methodology more applicable to the industrial isotope chemist, who may not have a direct input on which resin the peptide sequence is synthesised on.

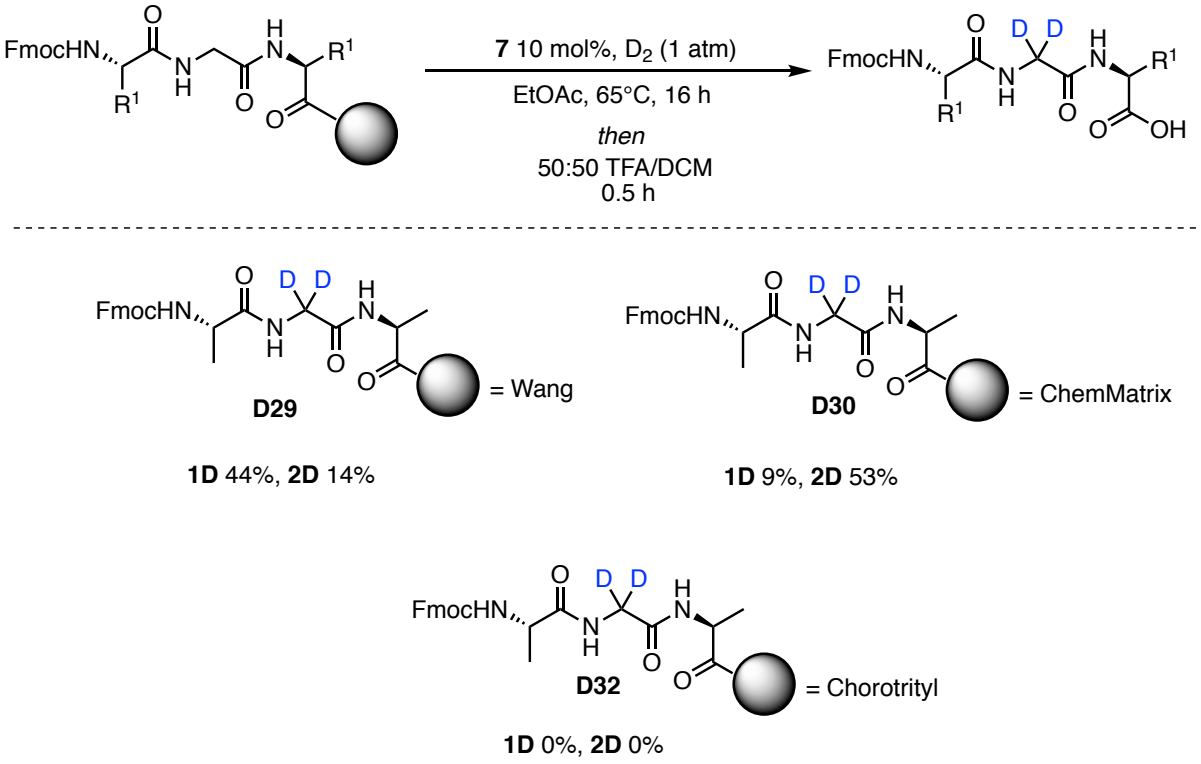

Scheme 2.15

Finally, we wanted to investigate a tripeptide which did not contain a glycine residue, to observe if isotopic enrichment could be achieved at tertiary amino acid residues on solid phase. Therefore, **31** was subjected to the HIE conditions. Despite lower activity than **29**, tripeptide **31** was deuterated to low levels. Although the levels would currently not be high enough for the utility of **D31** within pharmacokinetic studies, as a proof of concept result this is extremely encouraging. Further optimisation of the conditions could allow enhanced levels of labelling within this peptide sequence.

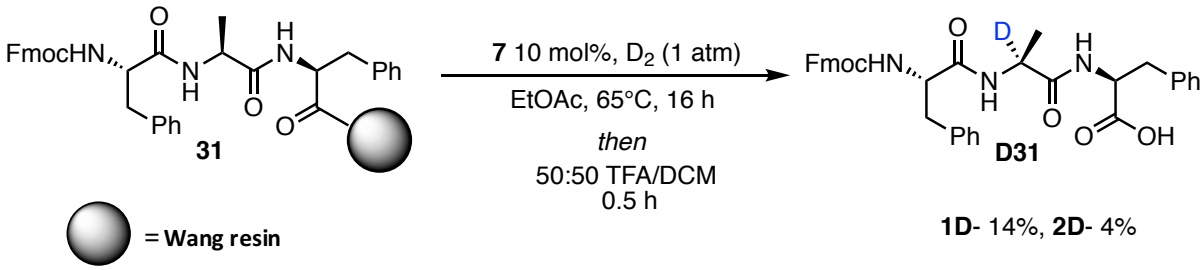

Scheme 2.16

Although the HIE of peptide molecules bound to a solid support has provided both chemical and practical challenges, the levels of incorporation achieved under relatively mild conditions has been very encouraging. There is scope to further optimise the process to enable higher levels of incorporation. This methodology could be extremely useful for larger, insoluble peptides which cannot feasibly be labelled under our current solution phase HIE protocol.

2.3 Conclusions

The work described within this chapter presents an important advancement in the field of Ir(I) catalysed HIE. Firstly, our developed methodology for the HIE of amino acids was extended to glycine containing dipeptide molecules (Scheme 2.17). Various tertiary residues were investigated, alongside a range of common protecting groups, with excellent levels of deuterium incorporation observed at glycine residues. Some interesting chemoselectivity was observed, with some dipeptides labelling only at the glycine residue. Other dipeptides displayed labelling at both residues, and in one case unprecedented labelling at the side chain within valine.

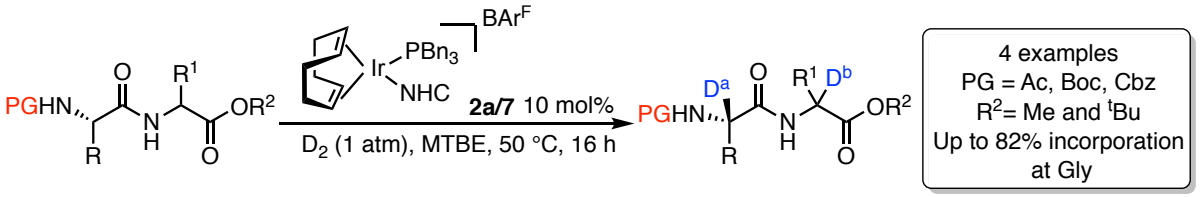

Scheme 2.17

In a further extension, dipeptides consisting of only tertiary amino acids were investigated. Moderate levels of incorporation were observed for the four dipeptides investigated. Interesting selectivity was observed dependent on the positioning of particular residues, and the directing group employed. Labelling at a variety of amino acid residues within small peptides was achieved under mild conditions, demonstrating the progress made to date in developing this area.

To exemplify the high activity of our Ir(I) catalysts, we next targeted a range of tripeptide molecules. Investigations focused on the exploration of a range of protecting groups to obtain information on compatibility within our HIE reaction, and if selectivity could be obtained. Excellent levels of incorporation were observed for tripeptides protected by Cbz- at the *N*

terminus, and this was largely attributed to the better solubility of these substrates in the reaction media. For tripeptides containing the Phe-Gly-Phe sequence, complete selectivity was observed for isotopic incorporation at the methylene position of glycine. In contrast, for the Ala-Gly-Ala sequence, for some of the derivatives, labelling was also observed at the alanine residues. Intriguingly, deuterium incorporation was additionally observed at the side chain of Fmoc- protected Ala-Gly-Ala peptides, an unactivated position which could have underwent C-H activation due to secondary structure.

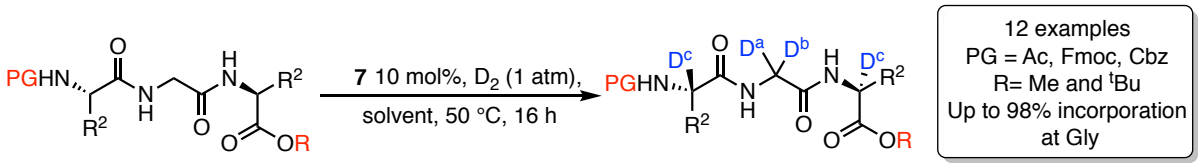

Scheme 2.18

Lastly, in an attempt to negate solubility issues, our HIE methodology was investigated using solid supported peptide molecules. This is an extremely efficient way to label peptides immediately after their synthesis *via* SPPS and allows for easy catalyst removal post reaction. Whilst there were some practical points to consider, this method proved to be extremely promising, with good levels of deuterium incorporated at tripeptide sequence **D30** (Scheme 2.19). Whilst there is room for further optimisation and expansion, this body of work is an exciting advancement in the area, with the possibility of widespread utility.

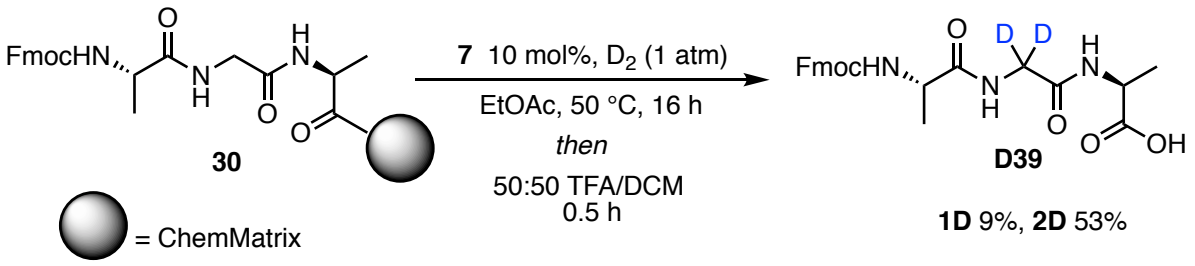

Scheme 2.19

2.4 Future Work

The methodology presented within this chapter has laid the foundations for the application of our catalysts to the HIE of peptide molecules. In venturing further into this area, a more thorough study of selectivity of the methodology to label at certain amino acids over the other is critical. This will allow prediction of the potential to access specific residues within larger peptidic systems. To obtain more information in this area, the labelling of tripeptides should be expanded to sequences containing solely tertiary amino acid residues (Figure 2.4). An interesting sequence to investigate would be sequence **33** consisting solely of a single amino acid residue. This would allow us to gain information on the preference of activation at a specific site in the sequence and the dependency on the nature of the directing group. HIE on peptide **34** would probe the activation of the challenging phenylalanine residues when utilised in combination with another tertiary amino acid. Sequences containing three different residues such, as **35** and **36**, would also provide further insight into the selectivity of our HIE process. A move to tripeptides containing challenging residues, such as sulfur containing amino acids, would be an exciting extension to the work.

Potential tripeptide substrates:

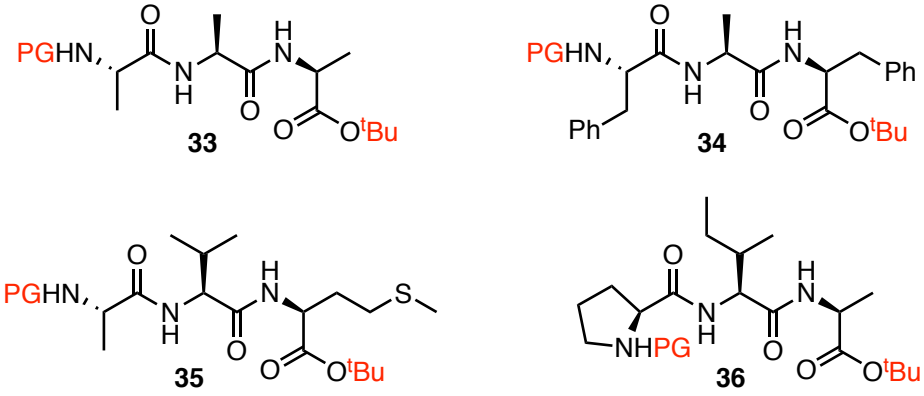

Figure 2.4

Further application of our methodology could centre around the HIE of natural or peptidic drugs (Figure 2.5). Endogenous opioid neurotransmitter Leu-enkephalin is found naturally in the human brain. This peptide, containing five natural amino acid residues, would be an excellent substrate, with high levels of incorporation expected at the methylene glycine positions. Another peptide of interest is peptide drug Carfilzomib, used in the treatment of multiple myeloma. HIE of these peptides would highlight the utility of our methodology in the labelling of biologically relevant peptide motifs, that are within reach of our current methodology.

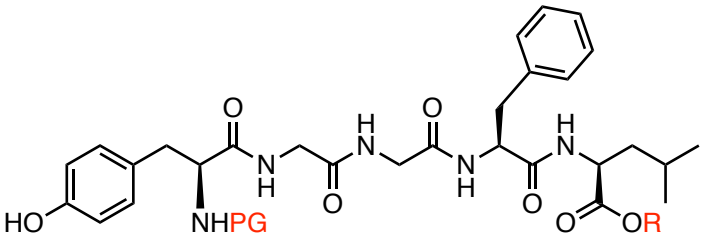

Leu-enkephalin

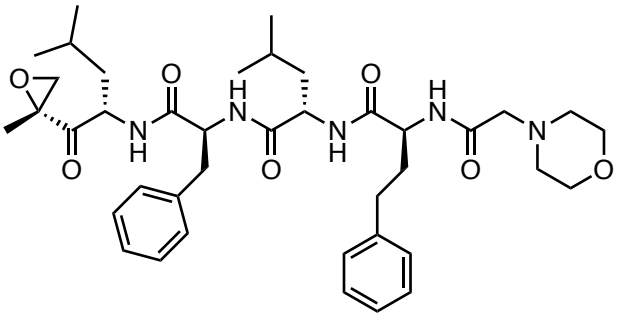

Carfilzomib

Figure 2.5

In an effort to extend the developed methodology, the labelling of peptides bearing a thioester at the *C* terminus, for application in Native Chemical Ligation (NCL) could be investigated. NCL reacts the thioester with an *N*-terminal cysteine residue of a separate peptide, resulting in formation of a thioester. Subsequently, the amine on the cysteine residue undergoes nucleophilic attack with the ester carbonyl allowing a S/N shift, resulting in a native amide bond (Scheme 2.20). This would allow access to isotopically labelled peptides which would otherwise currently be very challenging, as the presence of the thiol on the cysteine residue currently inhibits our HIE process. Additionally, the thioester may be a more competent

directing group compared to an amide and therefore the solvent scope could greatly increase, beneficial for the labelling of often insoluble peptide molecules.

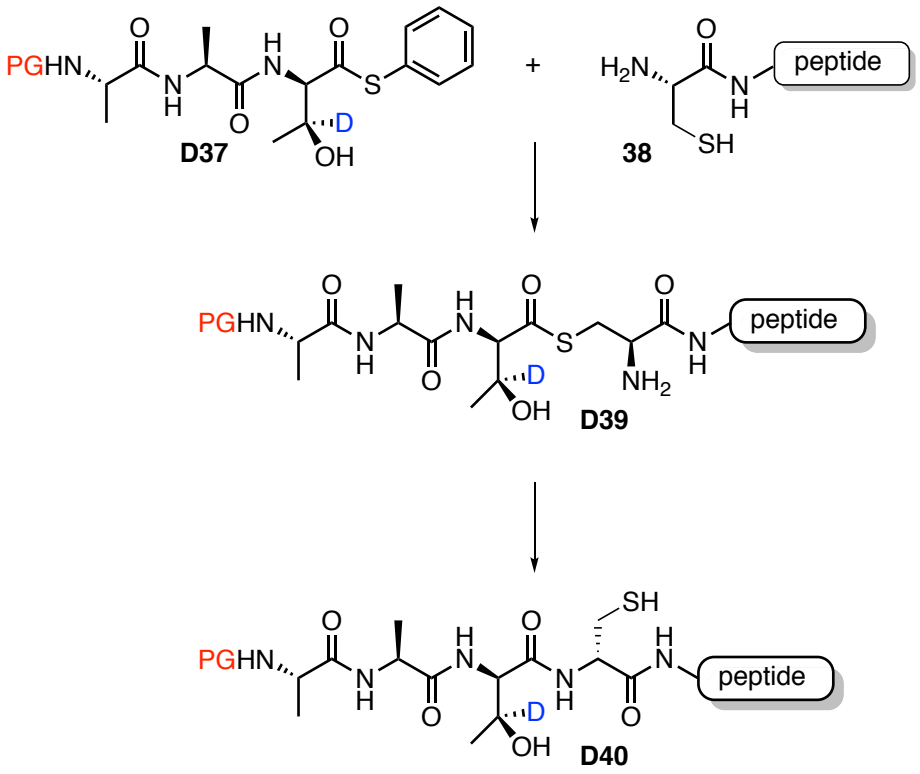

Scheme 2.20

A prominent issue within the HIE of amino acid and peptide molecules thus far has been the unproductive binding of substrates to iridium through two carbonyl moieties, resulting in an off-cycle, unproductive intermediate. This results in lower levels of deuterium incorporation, and a more challenging process overall. In an attempt to combat this, it may be worthwhile to investigate installation of a Lewis acidic (LA) site on one of the ligands, which could perhaps co-ordinate the second carbonyl, and allow for formation of the desired agostic interaction between the metal centre and the C-H bond to be activated (Figure 2.6). Potential ligands and the positioning of the LA on the aromatic ring could first be investigated *in silico,* and promising ligands synthesised and investigated experimentally under the HIE conditions. This approach has the potential to eliminate the unproductive substrate binding mode, allowing higher concentration of agostically bound substrate in solution and therefore better access to the productive C-H activation process. Of course, this will not be an easy task, and

may require several substrates and Lewis acids to be tested. However, this could be an important advancement for peptide molecules where there are many Lewis basic sites which could cause interreference with the productive labelling pathway.

Coordination of second carbonyl moiety:

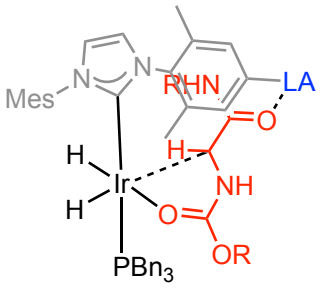

Chelation of carbonyl by LA on NHC

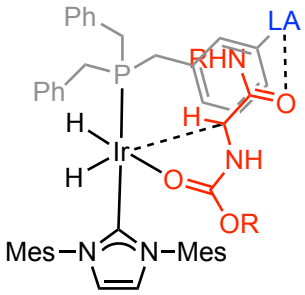

Chelation of carbonyl by LA on phosphine

Potential Lewis acids:

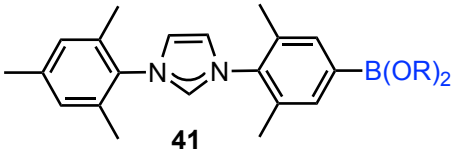

41

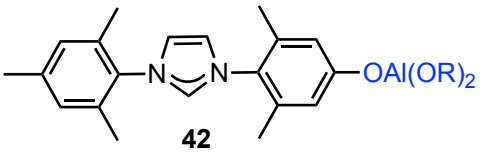

42

Figure 2.6

The work in this chapter has provided proof of concept reactivity for the labelling of peptide residues bound to solid phase. This is an exciting area, which could have widespread application. The labelling of resin bound substrates appears to rely heavily on the capability of the solvent (for both swelling and activity in HIE). The investigation into alternative resin supports concluded that ChemMatrix may be more suitable to the labelling process than the previously utilised Wang resin owing to its more optimal swelling properties. Therefore, it is important to investigate a wider range of solvents for the HIE process of peptides bound to this resin (Scheme 2.21). Solvents such as CPME, 2-MeTHF, ^{t}BuOAc and other solvents shown to swell this resin could be investigated. This may allow us to achieve even higher levels of isotopic enrichment. Mixed solvent systems may also be a viable avenue for

investigation. Mixing a solvent which displays favourable swelling properties with one which is more suited to the HIE process could allow a further enhancement (e.g CPME/EtOAc, DCM/EtOAc). Additionally, owing to the more sterically crowded environment of these substrates, a catalyst screen may be beneficial. Employment of catalysts with a smaller ligand set (such as PMe_2Ph in place of PBn_3) may afford higher levels of incorporation, or indeed, differing selectivity.

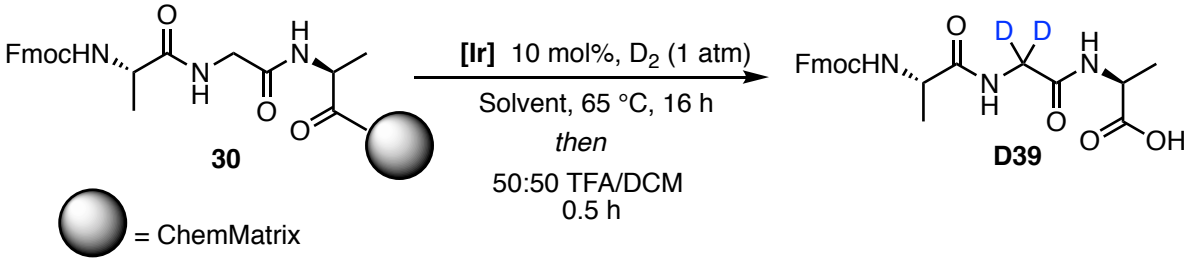

Scheme 2.21

Previous work within the Kerr group has described the labelling of Boc- protected indole and pyrazoles motifs.[3] Employment of $[(COD)Ir(PMe_2Ph)IMes]PF_6$ in DCM at room temperature allowed incorporation at the C-2 position of an indole directed through a Boc- group. Employment of this methodology to resin bound peptides could allow isotopic enrichment on the side chains of a peptidic sequence (Scheme 2.22). This would extend our methodology from observing isotopic enrichment at the α position of amino acid residues. Interestingly, throughout the work described, for sp^3 systems employing an amide or carbamate directing group, DCM has not been a compatible solvent for HIE. However, this approach could afford activation at sp^2 side chains and offer excellent selectivity for the site of enrichment. Additionally, utilisation of DCM would be extremely beneficial as this is an excellent solvent in SPPS and is routinely used to swell a variety of solid support resins. If successful, this approach could be extended to the labelling through other side chains bearing directing groups, such as serine, threonine and histidine.

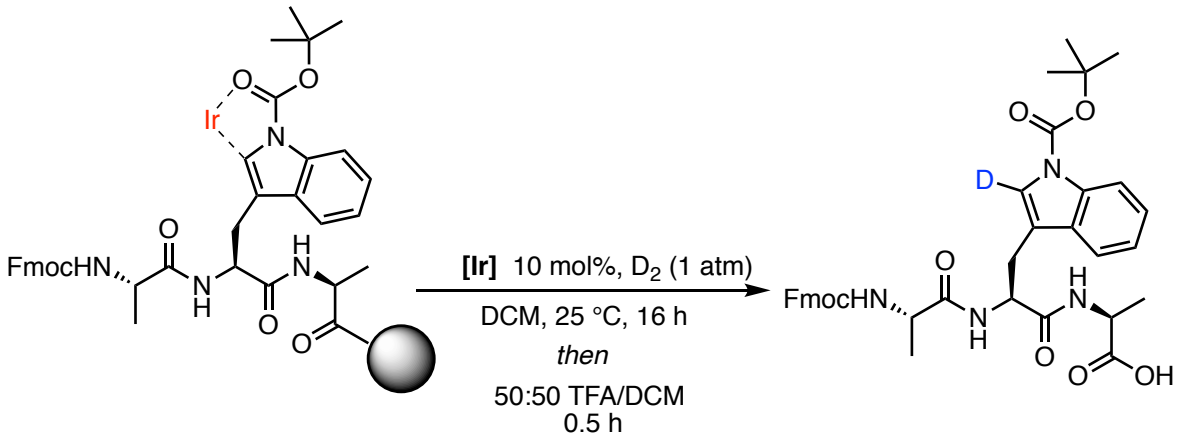
Ir
FmocHN
[Ir] 10 mol%, D2 (1 atm)
DCM, 25 °C, 16 h
then
50:50 TFA/DCM
0.5 h
D
OH

Scheme 2.22

2.5 Experimental

2.5.1 General Information

All reagents were obtained from commercial suppliers (Alfa Aesar, Sigma Aldrich, Apollo Scientific, Fluorochem or Strem) and were used without further purification unless otherwise stated. If purification was required this was carried out using standard laboratory methods.[4] All glassware was flame dried and cooled under a stream of nitrogen, unless otherwise stated.

Unless stated, peptide samples were purchased from Biopeptek and used without further purification, other than purifications described herein.

All solvents were distilled over calcium hydride under an argon atmosphere and stored over molecular sieves. Petroleum ether refers to ether with a boiling point range of 40-60 °C.

Thin layer chromatography was carried out using Camlab silica plates coated with fluorescent indicator UV254. Plates were analysed using a Mineralight UVGL-25 lamp, or developed using vanillin or $KMnO_4$ solution.

IR spectra were obtained on a Perking Elmer Spectrometer 1. All samples were analysed neat unless otherwise stated and are reported in cm^{-1}.

^{1}H, ^{13}C, ^{11}B, ^{19}F, and ^{31}P NMR spectra were recorded on a Bruker DPX 400 spectrometer at 400 MHz, 101 MHz, 128 MHz, 376 MHz, and 162 MHz, respectively. Chemical shifts are reported in ppm. Coupling constants are reported in Hz and refer to $^{3}J_{HH}$ interactions unless stated otherwise.

LCMS analysis was carried out with a Waters ZQ LCMS system with an Acquity UPLC CSH C18 column (50 mm x 2.1 mm) with a flow rate of 1 mL/min. An A:B gradient of 97:3 to 3:97 was used, where mobile phase A = 10 mmol ammonium bicarbonate in waters adjusted to pH 10, and mobile phase B = Acetonitrile.

For tritiation procedures: HPLC analysis was Gemini NX C18 4.6 ×50 mm, 3 u, 0.1% Aq TFA for 6 mins followed by a step gradient to 100% 0.1% TFA in MeCN, 1cc/min, 212 nm. Other equipment used was Waters 2695 Alliance HPLC with a 2996 PDA detector and Perkin Elmer C150 Radioflow detetctor.

DFT was used to calculate gas-phase electronic structures and associated energies. All structures were optimized using the M06L functional. This was utillised in conjunction with 6-31G9D) basis set for the main group atoms. Stuttgart RSC effective core potential with associated basis set was utilised for iridium. All calculations were performed using Gaussian 09 quantum package. Please see appendix for coordinates and further information.

For synthesis of Ir(I) complexes, please see the experimental section for Chapter One.

2.5.2 General Procedure for SPPS of Peptides

All peptides were assembled on Wang or ChemMatrix-Rink amide resin, and so the first amino acid residues were converted to the active, symmetrical amino acid anyhydride by dissolving the amino acid (10 eq.) in dry DCM (3 mL/mmol amino acid, with a few drop of DMF, if necessary, to ensure full dissolution). DIC (5.0 eq.) dissolved in minimal dry DCM was added to the flask and the mixture was then stirred at 0 °C for 10 min. If required, additional DMF was added to redissolve any precipitate. The reaction mixture was then allowed to warm to room temperature and stirred for a further 10 min and the solvent reduced *in vacuo*. The anhydride formed was then manually loaded onto the resin (1.0 eq) using a Merrifield bubbler, attached to a vacuum line, a nitrogen line and a large RBF for waste, following the steps highlighted in Table 2.5.

Table 2.5

Step	Solvent/Reagents	Volume (mL)	Time (min)	Mixing	Iterations
Swell	DCM	5	30	-	-
Wash	DMF	5	0.5	N_2 bubbling	5
Esterification	Amino acid anhydride (5 equiv.), DMAP (1 equiv.), DMF	5	0.5	N_2 bubbling	-
Wash	DMF	5	0.5	N_2 bubbling	5
Wash	DCM	5	0.5	N_2 bubbling	5
Wash	Diethyl ether	5	0.5	N_2 bubbling	5
Vacuum Dry	-	-	30	-	-
Loading Test	20 % piperidine in DMF	10	10	Sonication	2
Swell	DCM	5	30	-	-
Wash	DMF	5	0.5	N_2 bubbling	5

The success of the manual loading of each amino acid residue was assessed by means of a Fmoc loading test. ~ 10 mg of resin was added to two 10 mL volumetric flasks and dissolved in 20 % piperidine in DMF solution (10 mL) then sonicated for 15 minutes. The sample absorption was then monitored by UV at 302 nm against a blank solution. The loading was then calculated using an equation derived from the Beer-Lambert Law, and an average was taken of the two values calculated.

$$L = \frac{A\ x\ 20}{m\ x\ 7.8}$$

The loading value determined was used to calculate the masses of subsequent amino acid residues required for the assembly of the desired peptides, which is done so by an automated process as highlighted in the tables below.

Table 2.6 automated coupling of second amino acid

Table 2.7 automated coupling of final amino acid residue

All amino acids were supplied by Protein Technologies in pre-weighed cartridges of 5 and 20 mmol. Each synthesis was conducted at 0.4 M. Each amino acid residue required was dissolved in DMF until the desired concentration was reached. Additionally, each solvent bottle required for the synthesis was to be made up so that the only volumes of solvent required were available, to reduce wastage, e.g. DMF; DCM; 20 % piperidine in DMF; 15 % acetic anhydride in DMF; 0.8 M DIPEA in DMF and 0.4 M HATU in DMF.

Table 2.6

Step	Solvent/Reagents	Volume (mL)	Time (min)	Mixing	Iterations
Swell	DCM	6	10	Shaking	2
Wash	DMF	6	1	Shaking	1
Top Wash	DMF	6	1	Shaking	3
Deprotection	20 % piperidine in DMF	6	10	Shaking	2
Wash	DMF	6	1	Shaking	1
Top Wash	DMF	6	1	Shaking	3
Coupling	Amino acid (2 mL), HATU (2 mL), DIPEA (2 mL), DMF	6	20	Shaking	-
Wash	DMF	6	1	Shaking	1
Top Wash	DMF	6	1	Shaking	3
Capping	15 % Acetic Anhydride in DMF	6	10	Shaking	1
Wash	DMF	6	1	Shaking	1
Top Wash	DMF	6	1	Shaking	3

Table 2.7

Step	Solvent/Reagents	Volume (mL)	Time (min)	Mixing	Iterations
Deprotection	20 % piperidine in DMF	6	10	Shaking	2
Wash	DMF	6	1	Shaking	1
Top Wash	DMF	6	1	Shaking	3
Coupling	Amino acid (2 mL), HATU (2 mL), DIPEA (2 mL), DMF	6	20	Shaking	1
Wash	DMF	6	1	Shaking	1
Top Wash	DMF	6	1	Shaking	3
Capping	15 % Acetic Anhydride	6	10	Shaking	1
Wash	DMF	6	1	Shaking	1
Top Wash	DMF	6	1	Shaking	3
Top Wash	DCM	6	1	Shaking	4
Drain Dry	-	-	15	-	1

2.5.3 General Procedures

General Procedure A - Boc Protection of Amino Acids [5]

To a round-bottom flask was added the amino acid (1.0 eq) and dioxane-water (1:1, 0.4 M) at 0 °C. To this was added triethylamine (1.0 eq) and Boc_2O (1.0 eq) and the reaction mixture stirred for 5 h. After this time, the volatiles were removed by evaporation, and after re-dissolving in water, the solution was washed with diethyl ether. The pH was set to 2 using 1 N HCl and the resulting solution extracted with ethyl acetate. The combined organic phases were dried over sodium sulfate and concentrated *in vacuo* to afford the title compounds.

General Procedure B - Formation of tert-butyl Esters [6]

To a round-bottom flask was added the amino acid (1.0 eq) and *tert*-butyl acetate. The suspension was stirred at 0 °C and 70% perchloric acid in water (X eq) was added *via* a syringe pump (5 mL/h). The resulting solution was stirred overnight at room temperature. After this time, the reaction mixture was diluted with water and carefully quenched at 0 °C with saturated potassium carbonate solution then basified to pH 9. The resulting solution was then extracted with chloroform, the combined organic phases dried with sodium sulfate, and concentrated *in vacuo.* The resulting residue was then purified by column chromatography (EtOAc/Petrol) to afford the title compounds.

General Procedure C – Coupling of Amino Acids [7]

To a flame-dried round-bottom flask under an atmosphere of argon was added PG-AA-OH (1.0 eq), AA-OR•HCl (1 eq), HATU (1 eq), DMAP (1.0 eq), and dry DCM (0.1 M). To this mixture was added DIPEA (3.5 eq) dropwise and the resulting mixture allowed to stir overnight at room temperature. After this time, the reaction mixture was washed with 1 N NaOH, 1 N HCl, and brine sequentially. The organic phases were dried over sodium sulfate,

and concentrated *in vacuo*. Flash chromatography afforded the title compounds.

General Procedure D – HIE Protocol

Reactions were all performed using a Radley's 12-chamber carousel. Each of the carousel tubes were dried overnight in an oven at 180 °C. and allowed to cool under vacuum. Each tube was charged with the *N*-protected amino ester (0.011mmol) and the relevant catalyst (5 mol%). To each tube was added MTBE or other solvent depending upon the study (2.5 mL), and the solutions cooled to -78 °C. The atmosphere was exchanged with three vacuum/D_2 cycles and the tubes were sealed and immediately placed in a heating block pre-heated to the desired temperature (25 °C or 50 °C). The reactions were stirred for 16 h after which time the solvent was removed *in vacuo*. The resulting residue was triturated or purified by column chromatography to remove catalyst. The level of incorporation was determined by ^{1}H NMR spectroscopic analysis, with the integrals of the labelling positions measured against a peak corresponding to a position where labelling was not expected. The level of deuteration was then calculated using the formula:

$$Deuteration\ (\%) = \ 100 - [100 \times \left(\frac{Residual\ Integral}{Expected\ Integral}\right)]$$

General Procedure E – HIE Protocol for Resin Bound Peptides in a Round-Bottom Flask

The desired substrate was place in a hydrophobic frit attached to a fish-tank and repeatedly washed with dry DCM. The distilled reaction solvent was then added to the resin bound substrate and left to swell for 1 hour. After this time, the reaction solvent was removed *via* filtration and the solid substrate added to a flame dried 100 mL round-bottom flask (bearing a double stopcock) under an argon atmosphere. Solvent and catalyst were then added to the reaction flask, which was then cooled to -78 C. The flask was evacuated and refilled with deuterium from a balloon, and the process repeated three times. The flask was then placed on a heating block at 50 °C and the stopper clamped. After 16 h, the solvent was then removed

via filtration under vacuum on a fish-tank. The result resin bound peptide was transferred to a falcon tube and TFA/DCM (1:1, 5 mL) added. The tube was placed under shaking for 30 min, before the solution was again filtered. The filtrate was then concentrated *in vacuo* and azeotroped with chloroform several times.

Where appropriate, the level of incorporation was determined by ^{1}H NMR spectroscopic analysis, with the integrals of the labelling positions measured against a peak corresponding to a position where labelling was not expected. The level of deuteration was then calculated using the formula:

$$Deuteration\ (\%) = \ 100 - [100 \times \left(\frac{Residual\ Integral}{Expected\ Integral}\right)]$$

Where analysis by ^{1}H NMR was not appropriate, the level of incorporation of deuterium was verified by LCMS, by observing the shift in the isotope distribution in the starting material (M) to show M+1 (D_1), M+2 (D_2), M+3 (D_3) etc. for the labelled compound.

General Procedure E – HIE Protocol for Resin Bound Peptides on a Manifold

The desired substrate was place in a hydrophobic frit attached to a fish-tank and repeatedly washed with dry DCM. The resin bound peptide was then placed in a deuterium/tritium vessel and the distilled reaction solvent added to the resin bound substrate and left to swell for 1 hour. After this time, the catalyst was added to the reaction mixture, and the vessel was attached to the deuterium manifold, frozen with liquid nitrogen, evacuated, and subjected to 3 freeze pump thaw cycles before being finally frozen in liquid nitrogen. Deuterium gas (400 mm) was then added, and the reaction mixture thawed and then stirred overnight at 50 °C. On completion of the reaction, the solvent was then removed *via* filtration under vacuum on a fish-tank. The resulting resin-bound peptide was transferred to a falcon tube and TFA/DCM (1:1, 5 mL) added. The tube was placed under shaking for 30 mins, before the solution was

again filtered. The filtrate was then concentrated *in vacuo* and azeotroped with chloroform several times.

The level of incorporation of deuterium was verified by LCMS, by observing the shift in the isotope distribution in the starting material (M) to show M+1 (D_1), M+2 (D_2), M+3 (D_3) etc. for the labelled compound.

2.5.4 Labelling of Dipeptides Containing Glycine

tert-butyl (tert-butoxycarbonyl)glycinate **43**[5]

Scheme 2.5

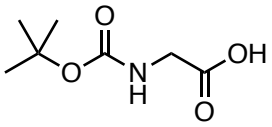

43

Chemical Formula: $C_7H_{13}NO_4$
Molecular Weight: 175.1840

Prepared according to *General Procedure B*.

Amount of Glycine: 3.0 g, 40.0 mmol, 1.0 eq.

Amount of triethylamine: 5.54 mL, 40.0 mmol, 1.0 eq.

Amount of Boc_2O: 8.72 g, 40.0 mmol, 1.0 eq.

Solvent volume: 100 mL dioxane-water (1:1)

Product yield: 4.20 g, 24.0 mmol, 60% yield as a white solid.

Melting point: 80-83 °C (78.5 °C lit.)[5]

FTIR (neat): 3381, 2974, 1720, 1686, 1527 cm^{-1}

^{1}H NMR (400 MHz, Acetone-d_6) δ 6.23 – 6.13 (m, 1H, NH), 3.82 (d, J = 6.1 Hz, 2H, CH_2), 1.42 (s, 9H, $OC(CH_3)_3$) ppm.

^{13}C NMR (101 MHz, Acetone-d_6): δ 171.8, 156.7, 79.2, 42.3, 28.5 ppm.

methyl (tert-butoxycarbonyl)glycyl-L-phenylalaninate **44** [8]

Scheme 2.5

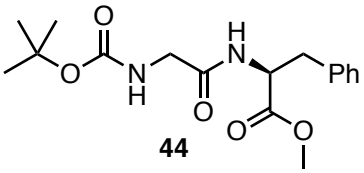

44

Chemical Formula: $C_{17}H_{24}N_2O_5$
Molecular Weight: 336.3880

Prepared according to *General Procedure C.*

Amount of Boc-Gly-OH **43**: 2.5 g, 14.3 mmol, 1.0 eq.

Amount of Phe-OMe•HCl: 3.08 g, 14.3 mmol, 1.0 eq

Amount of HATU: 5.44 g, 14.3 mmol, 1.0 eq.

Amount of DMAP: 1.74 g, 14.3 mmol, 1.0 eq.

Amount of DIPEA: 8.79 mL, 50.1 mmol, 3.5 eq.

Solvent volume: 140 mL dry DCM.

Product yield: 5.35 g, 14.3, >99% yield as a yellow oil.

FTIR (neat): 3271, 2935, 2872, 1739, 1714, 1680, 1624, 1506 cm^{-1}.

^{1}H NMR (400 MHz, $CDCl_3$) δ 7.38 (s, 1H, NH), 7.35 (s, 1H, NH), 7.35 – 7.9 (m, 5H, Ar-CH), 4.80 – 4.69 (m, 1H, NHCH), 3.77 – 3.71 (m, 2H, NHCH_2), 3.68 (s, 3H, OCH_3), 3.10-3.07 (m, 1H), 3.00-2.96 (m, 1H), 1.52 (s, 9H, OC(CH_3)$_3$) ppm.

^{13}C NMR (101 MHz, $CDCl_3$): δ 171.8, 169.3, 156.7, 136.1, 129.0, 127.8, 126.3, 80.2, 53.5, 51.1, 48.2, 37.5, 28.5 ppm.

methyl acetylglycyl-L-phenylalaninate **3** [9]

Scheme 2.5

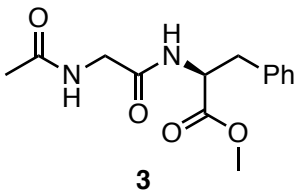

3

Chemical Formula: $C_{14}H_{18}N_2O_4$
Molecular Weight: 278.3080

Methyl (*tert*-butoxycarbonyl)glycyl-*L*-phenylalaninate **44** (4.80 g, 14.3 mmol, 1.0 eq) was added to a round bottom flask along with 40 % TFA in DCM (100 mL). The reaction mixture was then stirred for 16 h. After this time, the reaction was concentrated *in vacuo*. The resulting oil was dissolved in $CHCl_3$ (150 mL) at 0 °C. To this was added dropwise triethylamine (7.03 mL, 42.9 mmol, 3.0 eq) and acetyl chloride (1.1 mL, 15.73 mmol, 1.1 eq) and the reaction mixture stirred overnight. The reaction mixture was quenched with saturated sodium bicarbonate solution, and extracted with chloroform. The combined organic phases were then dried with sodium sulfate, filtered and concentrated in vacuo. The crude compound was purified by silica gel column chromatography (1% MeOH/DCM) to yield **3** (2.90 g, 10.43 mmol, 73%) as a white solid.

Melting point: 104-107 °C

FTIR (neat): 3275, 3066, 2754, 1751, 1660, 1649 1566 cm^{-1}

^{1}H NMR (400 MHz, Acetone-d_6): δ 7.48 – 7.42 (m, 1H, NH), 7.41 – 7.35 (m, 1H, NH), 7.31 – 7.18 (m, 5H, Ar-CH), 4.69 (td, J = 7.8, 5.7 Hz, 1H, CHCH$_2$Ph), 3.82 (dd, J = 5.7, ^4J = 1.2 Hz, 2H, CH$_2$NH), 3.65 (s, 3H, OCH$_3$), 3.10 – 3.09 (m, 1H, CHHPh), 3.00 – 2.96 (m, 1H, CHHPh), 1.92 (s, 3H, COCH$_3$) ppm.

^{13}C NMR (101 MHz, Acetone-d_6): δ 171.2, 169.4, 168.5, 136.4, 128.8, 127.7, 126.3, 53.2, 51.2, 41.9, 36.7, 21.3 ppm.

Catalyst Screen for the Labelling of methyl acetylglycyl-L-phenylalaninate, **3**

Scheme 2.5

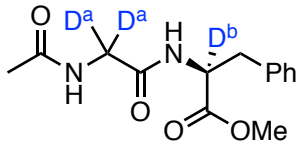

D3

Performed as described in *General Procedure D* using **3** (59.8 mg, 0.215 mmol) and 2.5 mL MTBE Data presented in Table 2.8.

^{1}H NMR (400 MHz, Acetone-d_6): δ 7.48 – 7.42 (m, 1H, NH), 7.41 – 7.35 (m, 1H, NH), 7.31 – 7.18 (m, 5H, Ar-CH), 4.69 (td, J = 7.8, 5.7 Hz, 1H, CHCH$_2$Ph), 3.82 (dd, J = 5.7, ^4J = 1.2 Hz, 2H, CH$_2$NH), 3.65 (s, 3H, OCH$_3$), 3.10 – 3.09 (m, 1H, CHHPh), 3.00 – 2.96 (m, 1H, CHHPh), 1.92 (s, 3H, COCH$_3$) ppm.

Labelling expected against signal at 4.69 ppm and 3.82 ppm, measured against signal at 1.92 ppm

Table 2.8

Entry	Catalyst	D	Run 1 (%D)	Run 2 (%D)	Run 3 (%D)	Avg (%D)
1	**2a** (0.018 g, 0.01 mmol)	**D[a]**	64	61	56	61
		D[b]	4	5	3	4
2	**2b** (0.017 g, 0.01 mmol)	**D[a]**	31	39	36	35
		D[b]	6	0	0	2
3	**4** (0.017 g, 0.01 mmol)	**D[a]**	27	25	30	27
		D[b]	10	0	7	6
4	**5** (0.018 g, 0.01 mmol)	**D[a]**	11	15	12	13
		D[b]	8	7	6	7
5	**6** (0.015 g, 0.01 mmol)	**D[a]**	18	24	18	20
		D[b]	0	3	0	1

Mixed Solvent Screen for the Labelling of methyl acetylglycyl-L-phenylalaninate, **3** with **2a**

Graph 2.1

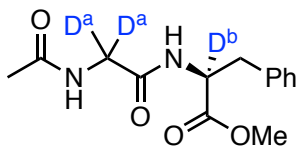

D3

Performed as described in *General Procedure D*. No incorporation was observed at D^b. **3** (59.8 mg, 0.215 mmol), **2a** (0.018 g, 0.01 mmol) and 2.5 mL MTBE**.**

^{1}H NMR (400 MHz, Acetone-d_6): δ 7.48 – 7.42 (m, 1H, NH), 7.41 – 7.35 (m, 1H, NH), 7.31 – 7.18 (m, 5H, Ar-CH), 4.69 (td, J = 7.8, 5.7 Hz, 1H, CHCH$_2$Ph), 3.82 (dd, J = 5.7, ^4J = 1.2 Hz, 2H, CH$_2$NH), 3.65 (s, 3H, OCH$_3$), 3.10 – 3.09 (m, 1H, CHHPh), 3.00 – 2.96 (m, 1H, CHHPh), 1.92 (s, 3H, COCH$_3$) ppm.

Labelling expected against signal at 4.69 ppm and 3.82 ppm, measured against signal at 1.92 ppm

Entry	Solvent	Run 1 (%)	Run 2 (%)	Run 3 (%)	Avg (%)
1	**$CHCl_3$**	43	42	38	41
2	**10:1 $CHCl_3$:^{t}AmOH**	36	35	37	36
3	**10:1 $CHCl_3$:^{i}PrOH**	22	20	21	21

Labelling of methyl acetylglycyl-L-phenylalaninate, **3** with **7**

Scheme 2.6Scheme 2.5

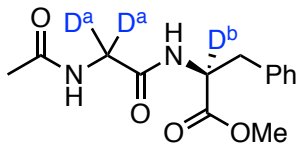

D3

Performed as described in *General Procedure D.* No incorporation was observed at D^b. Solvent volume = 2.5 mL.

^{1}H NMR (400 MHz, Acetone-d_6): δ 7.48 – 7.42 (m, 1H, NH), 7.41 – 7.35 (m, 1H, NH), 7.31 – 7.18 (m, 5H, Ar-CH), 4.69 (td, J = 7.8, 5.7 Hz, 1H, CHCH$_2$Ph), 3.82 (dd, J = 5.7, ^4J = 1.2

Hz, 2H, C<u>H</u>$_2$NH), 3.65 (s, 3H, OC<u>H</u>$_3$), 3.10 – 3.09 (m, 1H, C<u>H</u>HPh), 3.00 – 2.96 (m, 1H, CH<u>H</u>Ph), 1.92 (s, 3H, COC<u>H</u>$_3$) ppm.

Labelling expected against signal at 4.69 ppm and 3.82 ppm, measured against signal at 1.92 ppm

7 Mass (mg, mol%, mmol)	3 (mg, mmol)	Run 1 (%)	Run 2 (%)	Run 3 (%)	Avg (%)
19.3, 5, 0.01	59.8, 0.215	78	75	79	77

Boc-Gly-Val-O^{t}Bu **8** [10]

Scheme 2.7

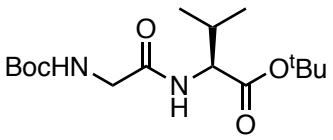

Chemical Formula: $C_{16}H_{30}N_2O_5$
Molecular Weight: 330.4250

8

Prepared according to *General Procedure C.* Columned on silica gel 1% MeOH/DCM.

Amount of Boc-Gly-OH **43**: 0.17 g, 0.97 mmol, 1.0 eq.

Amount of ValO^{t}Bu•HCl: 0.20 g, 0.97 mmol, 1.0 eq

Amount of HATU: 0.37 g, 0.97 mmol, 1.0 eq.

Amount of DMAP: 0.12 g, 0.97 mmol, 1.0 eq.

Amount of DIPEA: 0.59 mL, 3.40 mmol, 3.5 eq.

Solvent volume: 9.5 mL dry DCM.

Product yield: 0.15 g, 0.46 mmol, 47% yield as a colourless oil.

FTIR (neat): 3333, 2972, 1720, 1665, 1508 cm^{-1}.

^{1}H NMR (400 MHz, $CDCl_3$) δ 6.66 (d, J = 8.8 Hz, 1H, NH-Val), 5.32 (d, J = 6.2 Hz, 1H, NH-Gly), 4.41 (dd, J = 8.8, 4.5 Hz, 1H, Hα-Val), 3.87 – 3.74 (m, 2H, Hα-Gly), 2.12 (hept d, J = 6.8, 4.6 Hz, 1H, Hβ-Val), 1.43 (s, 9H, $OC(CH_3)_3$), 1.42 (s, 9H, $OC(CH_3)_3$), 0.90 (d, *J* = 6.9 Hz, 3H, $CHCHCH_3$), 0.86 (d, *J* = 6.9 Hz, 3H, $CHCHCH_3$) ppm.

^{13}C NMR (101 MHz, $CDCl_3$): δ 171.0, 169.5, 156.1, 82.1, 80.2, 57.4, 44.5, 31.5, 28.4, 28.1, 18.9, 17.6 ppm.

Cbz-Val-Gly-O^{t}Bu **9** [11]

Scheme 2.7

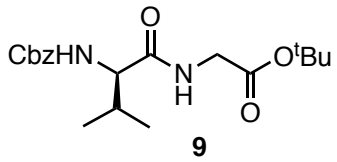

9

Prepared according to *General Procedure C.* Columned on silica gel 1% MeOH/DCM.

Amount of Cbz-Val-OH: 0.23 g, 0.90 mmol, 1.0 eq.

Amount of ValO^{t}Bu•HCl: 0.15 g, 0.90 mmol, 1.0 eq.

Amount of HATU: 0.37 g, 0.90 mmol, 1.0 eq.

Amount of DMAP: 0.12 g, 0.90 mmol, 1.0 eq.

Amount of DIPEA: 0.59 mL, 3.15 mmol, 3.5 eq.

Solvent volume: 8.8 mL dry DCM.

Product yield: 0.26 g, 0.68 mmol, 78% yield as a white solid.

Melting point: 135 - 138 °C (lit. 139 – 141 °C). [11]

FTIR (neat): 3286, 2978, 2868, 1740, 1693, 1649, 1533, 1290 cm^{-1}.

^{1}H NMR (400 MHz, $CDCl_3$) δ 7.46 – 7.23 (m, 5H, ArH), 6.75 – 6.67 (m, 1H, NH-Val), 5.61 (d, J = 8.9 Hz, 1H, NH-Gly), 5.18 – 5.07 (m, 2H, CH_2Ar), 4.17 – 4.12 (m, 1H, Hα-Val), 4.06 – 3.78 (m, 2H, Hα-Gly), 2.16 (h, *J* = 6.6 Hz, 1H, Hβ-Val), 1.47 (s, 9H, OC(CH_3)$_3$), 0.99 (d, *J* = 6.8 Hz, 3H, CHCHCH_3), 0.95 (d, *J* = 6.8 Hz, 3H, CHCHCH_3) ppm.

^{13}C NMR (101 MHz, $CDCl_3$): δ 171.5, 168.8, 156.6, 136.4, 128.6, 128.2, 128.1, 82.4, 67.1, 60.4, 42.1, 31.2, 28.1, 19.3, 17.9 ppm.

Boc-Gly-Pro-OMe **10** [8]

Scheme 2.7

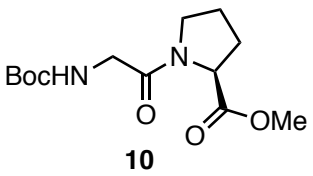

10

Chemical Formula: $C_{13}H_{22}N_2O_5$
Molecular Weight: 286.3280

Prepared according to *General Procedure C.* Columned on silica gel 1% MeOH/DCM.

Amount of Boc-Gly-OH: 0.39 g, 2.20 mmol, 1.0 eq.

Amount of ProOMe•HCl: 0.49 g, 2.20 mmol, 1.0 eq.

Amount of HATU: 0.84 g, 2.20 mmol, 1.0 eq.

Amount of DMAP: 0.27 g, 2.20 mmol, 1.0 eq.

Amount of DIPEA: 1.34 mL, 7.70 mmol, 3.5 eq.

Solvent volume: 21.5 mL dry DCM.

Product yield: 0.26 g, 0.68 mmol, 78% yield as a colourless oil.

FTIR ($CHCl_3$): 3354, 2974, 2878, 1742, 1713, 1653, 1506, 1390 cm^{-1}.

^{1}H NMR (400 MHz, $CDCl_3$) δ 5.43 – 5.32 (m, 1H, NH), 4.45 (major rotamer), 4.34 (minor rotamer) (dd, *J* = 8.6, 3.6 Hz, 1H, NCHC(O)OCH_3), 4.20 – 4.10 (minor rotamer), 3.97 – 3.80 (major rotamer) (m, 2H, CH_2NH), 3.69 (minor rotamer), 3.66 (major rotamer) (s, 3H, OCH_3),

3.60 – 3.41 (m, 2H, C$\underline{H}_2$CHC(O)OCH$_3$), 2.20 – 1.88 (m, 4H, NC$\underline{H}_2$C$\underline{H}_2$CH$_2$), 1.37 (s, 9H, OC(C$\underline{H}_3$)$_3$) ppm.

^{13}C NMR (101 MHz, CDCl$_3$): δ 172.3 (major rotamer), 171.9 (minor rotamer), 167.7 (minor rotamer), (167.4 major rotamer), 155.8, 79.5, 58.8 (major rotamer), 58.4 (minor rotamer), 52.8 (minor rotamer), 52.3 (major rotamer), 46.6 (minor rotamer), 45.8 (major rotamer), 43.0, 31.4, 29.0 (minor rotamer), 28.3 (major rotamer), 24.6 (major rotamer), 22.2 (minor rotamer) ppm.

Labelling substrate scope of dipeptides containing glycine

Scheme 2.7

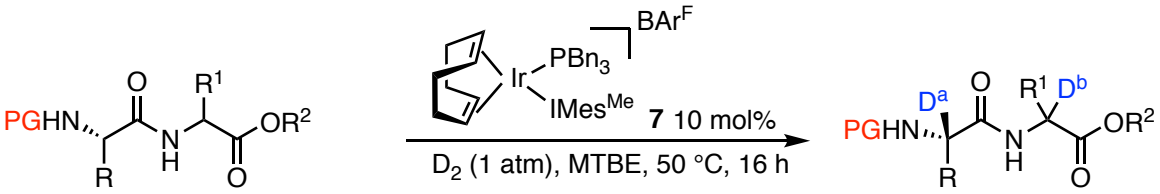

The substrate scope was performed as described in *General Procedure D*. The products were purified by column chromatography (0-5% MeOH/petrol) unless otherwise stated.

Boc-Gly-Val-O^{t}Bu **8**

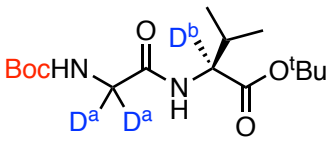

D8

^{1}H NMR (400 MHz, $CDCl_3$) δ 6.66 (d, J = 8.8 Hz, 1H, NH-Val), 5.32 (d, J = 6.2 Hz, 1H, NH-Gly), 4.41 (dd, J = 8.8, 4.5 Hz, 1H, Hα-Val), 3.87 – 3.74 (m, 2H, Hα-Gly), 2.12 (heptd, J = 6.8, 4.6 Hz, 1H, Hβ-Val), 1.43 (s, 9H, $OC(CH_3)_3$), 1.42 (s, 9H, $OC(CH_3)_3$), 0.90 (d, J = 6.9 Hz, 3H, $CHCHCH_3$), 0.86 (d, J = 6.9 Hz, 3H, $CHCHCH_3$) ppm.

Labelling expected against signal at 4.41 ppm and 3.87 – 3.74 ppm, measured against signal at 0.86 ppm.

Table 2.9

7 (mg, mol%, mmol)	8 (mg, mmol)	Run 1 (%)	Run 2 (%)	Avg (%)
19.6, 10 mol%, 0.011	35.5, 0.11	**D**^{a} 72	63	68
		D^b 17	18	18

Cbz-Val-Gly-O^{t}Bu **9**

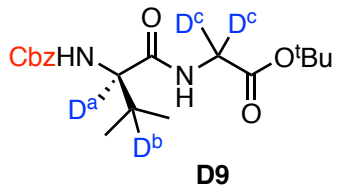

D9

^{1}H NMR (400 MHz, $CDCl_3$) δ 7.46 – 7.23 (m, 5H, ArH), 6.75 – 6.67 (m, 1H, NH-Val), 5.61 (d, J = 8.9 Hz, 1H, NH-Gly), 5.18 – 5.07 (m, 2H, CH_2Ar), 4.17 – 4.12 (m, 1H, Hα-Val), 4.06 – 3.78 (m, 2H, Hα-Gly), 2.16 (h, J = 6.6 Hz, 1H, Hβ-Val), 1.47 (s, 9H, $OC(CH_3)_3$), 0.99 (d, *J* = 6.8 Hz, 3H, $CHCHCH_3$), 0.95 (d, J = 6.8 Hz, 3H, $CHCHCH_3$) ppm.

Labelling expected against signal at 4.17 – 4.12 ppm, 4.06 – 3.78 and 2.16 ppm, measured against signal at 0.95 ppm. Product triturated with Et_2O.

Table 2.10

7 (mg, mol%, mmol)	9 (mg, mmol)	Run 1 (%)	Run 2 (%)	Run 3 (%)	Avg (%)
19.6, 10 mol%, 0.011	42.2, 0.11	**D**[a] 65	61	59	62
		D[b] 30	29	18	26
		D[c] 87	86	73	82

Boc-Gly-Pro-OMe **10**

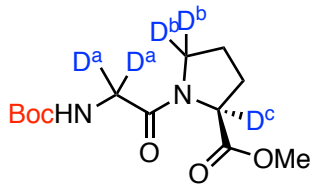

^{1}H NMR (400 MHz, $CDCl_3$) δ 5.43 – 5.32 (m, 1H, NH), 4.45 (major rotamer), 4.34 (minor rotamer) (dd, *J* = 8.6, 3.6 Hz, 1H, NCHC(O)OCH_3), 4.20 – 4.10 (minor rotamer), 3.97 – 3.80 (major rotamer) (m, 2H, CH_2NH), 3.69 (minor rotamer), 3.66 (major rotamer) (s, 3H, OCH_3), 3.60 – 3.41 (m, 2H, CH_2CHC(O)OCH_3), 2.20 – 1.88 (m, 4H, NCH_2C$H_2$$CH_2$), 1.37 (s, 9H, OC($CH_3$)$_3$) ppm.

Labelling expected against signal at 4.45 (major rotamer), 4.34 (minor rotamer) ppm, 4.20 – 4.10 (minor rotamer), 3.97 – 3.80 (major rotamer) ppm and 3.60 – 3.41 ppm, measured against signal at 3.66 ppm.

Table 2.11

7 (mg, mol%, mmol)	10 (mg, mmol)	Run 1 (%)	Run 2 (%)	Run 3 (%)	Avg (%)
19.6, 10 mol%, 0.011	30.8, 0.11	**D**[a] 20	19	11	17
		D[b] 23	24	25	24
		D[c] 6	1	0	2

2.5.5 Labelling of Dipeptides Containing Tertiary Amino Acids

(tert-butoxycarbonyl)alaninate **45** [12]

Scheme 2.8

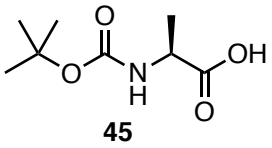

45

Chemical Formula: $C_8H_{15}NO_4$
Molecular Weight: 189.2110

To a 200 mL round-bottom flask was added alanine (2.0 g, 22.45 mmol, 1.0 eq) and MeOH (100 mL). To this was added triethylamine (3.43 mL, 24.69 mmol, 1.1 eq) and Boc_2O (9.82 g, 44.9 mmol, 2 eq) and the reaction mixture heated to reflux for 1 h. After this time, the volatiles were removed by evaporation, and after being taken up in 1 N HCl at 0 °C, the solution was washed with EtOAc (3 × 50 mL). The combined organic phases were dried over sodium sulfate and concentrated *in vacuo*. Diethyl ether was then added to the resulting residue, and the solid filtered yielding **45** (2.5 g, 13.47 mmol, 60%) as a white solid.

Melting point: 82 - 84 °C (lit. 81 - 82 °C)[12]

FTIR (neat): 3400, 2983, 2910, 1734, 1685, 1458, 1155 cm^{-1}

^{1}H NMR (400 MHz, $CDCl_3$) δ 5.08 (s, 1H, NH), 4.42 – 4.16 (m, 1H, CH), 1.47 (s, 9H, $OC(CH_3)_3$), 1.45 (app d, 3H, $CHCH_3$) ppm.

^{13}C NMR (101 MHz, $CDCl_3$): δ176.8, 155.0, 79.8, 48.6, 27.8, 17.8 ppm.

Boc-Ala-Phe-OMe **12** [13]

Scheme 2.8

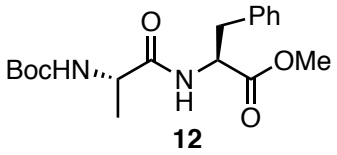

12

Chemical Formula: $C_{18}H_{26}N_2O_5$
Molecular Weight: 350.4150

Prepared according to a modified literature procedure. [14] To a flame-dried round-bottom flask under an atmosphere of argon was added Phe-OMe•HCl (1.25 g, 5.82, mmol,1.1 eq), and Et_3N (0.81 mL, 5.82 mmol,.1.1 eq) in $CHCl_3$ (15 mL) at 0 °C. Boc-Ala-OH **45** (1.0 g, 5.29 mmol, 1.0 eq) and DCC (1.09 g, 5.29 mmol, 1.0 eq) were added sequentially and the mixture allowed to stir in an ice bath for 1h, before slowly raising to room temperature and stirring overnight. After 16 h, a few drops of AcOH was added and allowed to stir for 15 mins. The reaction mixture was then filtered through celite and washed with water, 10% citric acid solution and 5% $NaHCO_3$ solution sequentially. The organic phases were dried over sodium sulfate, and concentrated *in vacuo*. The resulting residue was recrystalised from petrol affording **12** (1.37 g, 3.54 mmol, 67% yield) as a yellow oil.

FTIR (neat): 3655, 3301, 2970, 2929, 1736, 1689, 1653, 1624, 1472 cm^{-1}.

^{1}H NMR (400 MHz, $CDCl_3$) δ 7.33 – 7.18 (m, 3H, Ar-H) 7.13 – 7.03 (m, 2H, Ar-H), 6.54 (d, J = 7.9 Hz, 1H, NH), 4.96 (s, 1H, NH), 4.92 – 4.85 (m, 1H, $NHCHCH_2Ph$), 4.26 – 4.09 (m, 1H, $NHCHCH_3$) 3.71 (s, 3H, OCH_3), 3.22 – 3.02 (m, 2H, CH_2Ph), 1.44 (s, 9H, $OC(CH_3)_3$), 1.31 (d, J = 7.0 Hz, 3H, $CHCH_3$) ppm.

^{13}C NMR (101 MHz, $CDCl_3$): δ 172.3, 171.8, 155.5, 135.9, 129.4, 128.7, 127.3, 80.2, 53.3, 52.5, 50.3, 38.2, 28.4, 18.4 ppm.

Cbz-Ala-Phe-OMe **13** [15]

Scheme 2.8

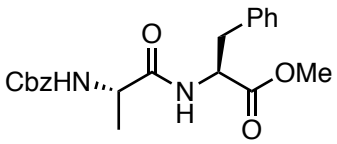

13

Chemical Formula: $C_{21}H_{24}N_2O_5$
Molecular Weight: 384.4320

Procedure adapted from *General Procedure C.* To a flame-dried round-bottom flask under an atmosphere of argon was added Phe-OMe•HCl (1.06 g, 4.93 mmol,1.1 eq), Cbz-Ala-OH (1.0 g, 4.48 mmol, 1 eq) and DCM (45 mL). DIPEA (2.34 mL, 13.44 mmol, 3.0 eq) and T3P (1.73 mL, 5.82 mmol, 1.3 eq) were added sequentially and the mixture allowed to stir for 16 h. The reaction mixture was then washed with brine, the organicphases were dried over sodium sulfate, and concentrated *in vacuo.* The resulting residue was purified by flash column chromatography (25 – 50% EtOAc/Petrol) to afford **13** as a white solid (0.91 g, 2.37 mmol, 53% yield).

Melting point: 95 - 97 °C (98 °C lit.)[15]

^{1}H NMR (400 MHz, $CDCl_3$) δ 7.45 – 7.34 (m, 5H, ArH), 7.32 – 7.25 (m, 3H, ArH), 7.13 – 7.07 (m, 2H, ArH), 6.50 – 6.41 (m, 1H, NH), 5.30 – 5.21 (m, 1H, NH), 5.21 – 5.06 (m, 2H, CH_2Ph), 4.90 – 4.84 (m, 1H, Hα-Phe), 4.29 – 4.19 (m, 1H, Hα-Ala), 3.75 (s, 3H, OCH_3), 3.24 – 3.01 (m, 2H, $CHCH_2$Ph), 1.36 (d, J = 7.0 Hz, 3H, $CHCH_3$) ppm.

^{13}C NMR (101 MHz, $CDCl_3$): δ 171.8, 171.2, 156.0, 136.3, 135.8, 129.4, 128.8 128.7, 128.4, 128.2, 127.3, 67.2, 53.3, 52.5, 50.6, 38.0, 18.5 ppm.

Cbz-Phe-Ala-O^{t}Bu **14** [16]

Scheme 2.8

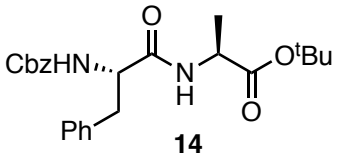

14

Chemical Formula: $C_{24}H_{30}N_2O_5$
Molecular Weight: 426.5130

Prepared according to *General Procedure C.* Columned on silica gel 30% EtOAc/Petrol.

Amount of Cbz-Phe-OH: 2.0 g, 6.69 mmol, 1.0 eq.

Amount of AlaO^{t}Bu•HCl: 0.97 g, 6.69 mmol, 1.0 eq.

Amount of HATU: 2.54 g, 6.69 mmol, 1.0 eq.

Amount of DMAP: 0.82 g, 6.69 mmol, 1.0 eq.

Amount of DIPEA: 4.07 mL, 23.41 mmol, 3.5 eq.

Solvent volume: 65 mL dry DCM.

Product yield: 0.77 g, 2.0 mmol, 30% yield as a white solid.

^{1}H NMR (400 MHz, $CDCl_3$) δ 7.41 – 7.14 (m, 10H, ArH), 6.32 (d, *J* = 7.1 Hz, 1H, NH), 5.28 (d, *J* = 10.4 Hz, 1H, NH), 5.09 (s, 2H, CH_2Ph), 4.46 – 4.40 (d, *J* = 7.4 Hz, 1H, 1H Hα-Phe), 4.39 – 4.31 (m, 1H, Hα-Ala), 3.12 (dd, ^{2}J = 13.8, *J* = 6.4 Hz, 1H, CHCH_2Ph), 3.04 (dd, ^{2}J = 13.7, *J* = 6.8 Hz, 1H, CHCH_2Ph), 1.44 (s, 9H, OC(CH_3)$_3$), 1.30 (d, *J* = 7.1 Hz, 3H, CHCH_3) ppm.

^{13}C NMR (101 MHz, $CDCl_3$): δ 171.7, 170.2, 155.8, 136.3, 129.8, 128.8, 128.7 128.6, 128.3, 128.2, 127.2, 82.3, 67.2, 56.2, 48.9, 38.7, 28.1, 18.7 ppm.

Dipeptide Labelling with catalyst 7

Scheme 2.8

The substrate scope was performed as described in *General Procedure D*. The products were purified by column chromatography (0-100% diethyl ether/petrol) unless otherwise stated. Solvent volume = 1.25 mL MTBE. Substrate **11** was commercially available.

Boc-Ile-Phe-OMe **11**

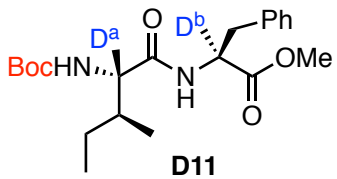

D11

^{1}H NMR (400 MHz, $CDCl_3$) δ 7.36 – 7.24 (m, 3H, Ar-H), 7.18 – 7.10 (m, 2H, Ar-H), 6.29 (d, *J* = 7.5 Hz, 1H, NHCH), 4.99 (s, 1H, NHCH), 4.95 – 4.84 (m, 1H, NHCHCH$_2$Ph), 3.94 (q, *J* = 5.7, 4.0 Hz, 1H, NHCH), 3.74 (s, 3H, OCH$_3$), 3.21 – 3.05 (m, 2H, CH$_2$Ph), 1.91 – 1.81 (m, 1H, CH(CH$_3$)CH$_2$), 1.62 – 1.58 (m, 1H, CH(CH$_3$)CHH), 1.47 (s, 9H, 1.15 – 1.04 (s, 1H, CH(CH$_3$)CHH), 0.93 – 0.87 (m, 6H, 2 x CH$_3$) ppm.

Labelling expected against signal at 4.95 – 4.84 ppm and 3.94 ppm, measured against signal at 0.93 – 0.87 ppm.

Table 2.12

7 (mg, mol%, mmol)	11 (mg, mmol)	Run 1 (%)	Run 2 (%)	Run 3 (%)	Avg (%)
19.6, 10 mol%, 0.011	42.2, 0.11	**D^a** 50	58	60	56
		D^b 0	0	0	0

Boc-Ala-Phe-OMe, **12**

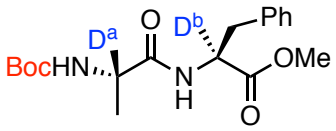

D12

^{1}H NMR (400 MHz, $CDCl_3$) δ 7.33 – 7.18 (m, 3H, Ar-H) 7.13 – 7.03 (m, 2H, Ar-H), 6.54 (d, *J* = 7.9 Hz, 1H, NH), 4.96 (s, 1H, NH), 4.92 – 4.85 (m, 1H, NHCHCH$_2$Ph), 4.26 – 4.09 (m, 1H, NHCHCH$_3$) 3.71 (s, 3H, OCH$_3$), 3.22 – 3.02 (m, 2H, CH$_2$Ph), 1.44 (s, 9H, OC(CH$_3$)$_3$), 1.31 (d, *J* = 7.0 Hz, 3H, CHCH$_3$) ppm.

Labelling expected against signal at 4.92 – 4.85 ppm and 4.26 – 4.09 ppm, measured against signal at 1.31 ppm.

Table 2.13

7 (mg, mol%, mmol)	12 (mg, mmol)	Run 1 (%)
19.6, 10 mol%, 0.011	37.6, 0.11	**D**[a] 46
		D[b] 0

Cbz-Ala-Phe-OMe **13**

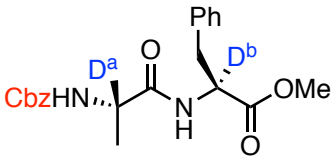

D13

^{1}H NMR (400 MHz, $CDCl_3$) δ 7.45 – 7.34 (m, 5H, ArH), 7.32 – 7.25 (m, 3H, ArH), 7.13 – 7.07 (m, 2H, ArH), 6.50 – 6.41 (m, 1H, NH), 5.30 – 5.21 (m, 1H, NH), 5.21 – 5.06 (m, 2H, CH_2Ph), 4.90 – 4.84 (m, 1H, Hα-Phe), 4.29 – 4.19 (m, 1H, Hα-Ala), 3.75 (s, 3H, OCH_3), 3.24 – 3.01 (m, 2H, $CHCH_2$Ph), 1.36 (d, J = 7.0 Hz, 3H, $CHCH_3$) ppm.

Labelling expected against signal at 4.90 – 4.85 ppm and 4.29 – 4.19 ppm, measured against signal at 1.36 ppm.

Table 2.14

7 (mg, mol%, mmol)	13 (mg, mmol)	Run 1 (%)	Run 2 (%)	Run 3 (%)	Avg (%)
19.6, 10 mol%, 0.011	41.3, 0.11	**D**[a] 33	32	37	34
		D[b] 0	0	0	0

Cbz-Phe-Ala-O^{t}Bu **14**

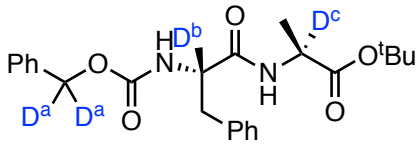

D14

^{1}H NMR (400 MHz, $CDCl_3$) δ 7.41 – 7.14 (m, 10H, ArH), 6.32 (d, *J* = 7.1 Hz, 1H, NH), 5.28 (d, *J* = 10.4 Hz, 1H, NH), 5.09 (s, 2H, CH_2Ph), 4.46 – 4.40 (d, *J* = 7.4 Hz, 1H, 1H Hα-Phe), 4.39 – 4.31 (m, 1H, Hα-Ala), 3.12 (dd, ^2J = 13.8, *J* = 6.4 Hz, 1H, CHCH_2Ph), 3.04 (dd, ^2J = 13.7, *J* = 6.8 Hz, 1H, CHCH_2Ph), 1.44 (s, 9H, OC(CH_3)$_3$), 1.30 (d, *J* = 7.1 Hz, 3H, CHCH_3) ppm.

Labelling expected against signal at 4.46 – 4.40 ppm and 4.39 – 4.31 ppm, measured against signal at 1.30 ppm.

Table 2.15

7 (mg, mol%, mmol)	14 (mg, mmol)	Run 1 (%D)	Run 2 (%)	Run 3 (%)	Avg (%)
19.6, 10 mol%, 0.011	45.8, 0.11	**D**[a] 21	22	18	20
		D[b] 25	25	29	26
		D[c] 18	29	41	29

2.5.6 Isotopic Labelling of Tripeptides

Solvent and Catalyst Loading Screen for Ac-Phe-Gly-Phe-O^{t}Bu 15

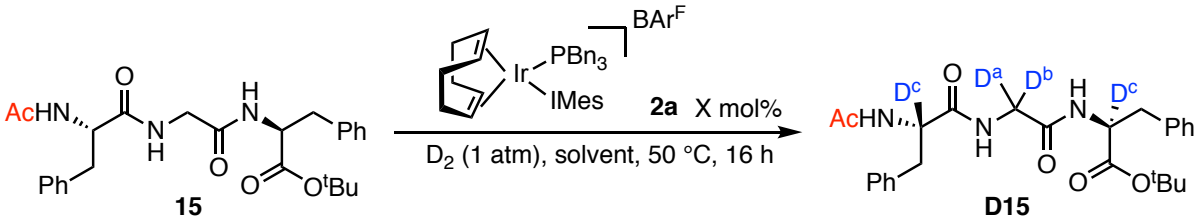

Table 2.1

The solvent and catalyst loading screen was performed as described in *General Procedure D* on half scale. Peptides utilised in this section were all commercially available. Mass of **15** = 25.1 mg, 0.054 mmol. Solvent volume = 1.25 mL. The products were purified by trituration with diethyl ether.

^{1}H NMR (400 MHz, MeOD-*d*$_4$) δ 7.46 – 7.09 (m, 10H, Ar-H), 4.59 – 4.53 (m, 2H, 2 ×CHNH), 3.91 (d, ^2J = 16.8 Hz, 1H, NHCHH), 3.69 (d, ^2J = 16.8 Hz, 1H, NHCHH), 3.25 – 2.99 (m, 4H, 2 ×PhCH$_2$), 1.91 (s, 3H, C(O)CH$_3$), 1.40 (s, 9H, OC(CH$_3$)$_3$) ppm.

Labelling expected against signal at 4.59 – 4.53, 3.91 and 3.69 ppm, measured against signal at 1.91 ppm.

Table 2.16

Solvent	**Molarity (M)**	**2a mol%**	**Incorporation D^a (%)**	**Incorporation D^b (%)**	**Incorporation D^c (%)**
MTBE	0.10	5	17	14	0
$CHCl_3$	0.10	5	4	3	0
MTBE	0.05	10	65	58	0
DCE	0.05	10	28	29	0
EtOAc	0.05	10	44	48	0
^{t}BuOAc	0.05	10	28	29	0
MTBE	0.05	20	77	69	9
DCE	0.05	20	25	22	2
EtOAc	0.05	20	83	82	12

Labelling Scope for Phe-Gly-Phe Sequences

Scheme 2.9

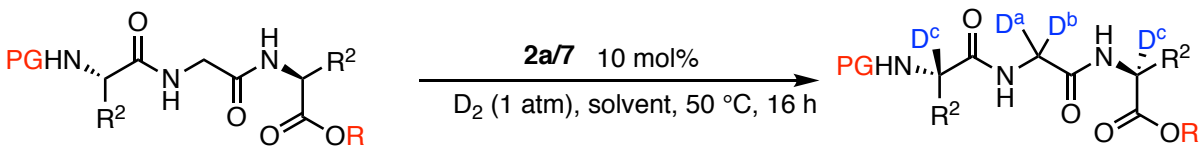

The tripeptide labelling was performed as described in *General Procedure D* on half scale (0.054 mmol substrate). Peptides utilised in this section were all commercially available. Solvent volume = 1.25 mL. The products were purified by trituration with diethyl ether.

Ac-Phe-Gly-Phe-O^{t}Bu ***16***

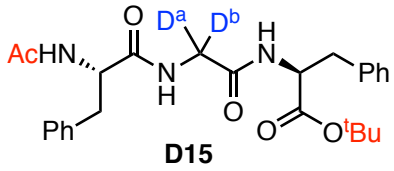

D15

^{1}H NMR (400 MHz, MeOD-*d*$_4$) δ 7.46 – 7.09 (m, 10H, Ar-H), 4.59 – 4.53 (m, 2H, 2 ×CHNH), 3.91 (d, ^2J = 16.8 Hz, 1H, NHCHH), 3.69 (d, ^2J = 16.8 Hz, 1H, NHCHH), 3.25 – 2.99 (m, 4H, 2 ×PhCH$_2$), 1.91 (s, 3H, C(O)CH$_3$), 1.40 (s, 9H, OC(CH$_3$)$_3$) ppm.

Labelling expected against signal at 4.59 – 4.53, 3.91 and 3.69 ppm, measured against signal at 1.91 ppm.

Table 2.17

[Ir] (mg, mol%, mmol)	15 (mg, mmol)	Solvent	D^a (%)	D^b (%)
2a, 9.53, 10, 0.0054	25.1, 0.054	**MTBE**	65	58
		EtOAc	44	48
7, 9.80, 10, 0.0054	25.1, 0.054	**MTBE**	55	59
		EtOAc	45	55

Cbz-Phe-Gly-Phe-O^{t}Bu ***16***

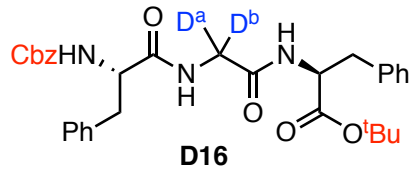

D16

^{1}H NMR (400 MHz, MeOD-*d*$_4$) δ 7.37 – 7.18 (m, 15H, Ar-H), 5.12 – 4.98 (m, 2H, NHC(O)OCH_2Ph), 4.60 – 4.51 (m, 1H, NHCH), 4.37 – 4.31 (m, 1H, NHCH), 3.95 (d, ^2J = 16.9 Hz, 1H, NHCHH), 3.68 (d, ^2J = 16.9 Hz, 1H, NHCHH), 3.23 – 2.87 (m, 4H, 2 ×CH_2Ph), 1.39 (s, 9H, OC(CH_3)$_3$) ppm.

Labelling expected against signal at 3.95 and 3.68 ppm, measured against signal at 3.23 – 2.87 ppm.

Table 2.18

[Ir] (mg, mol%, mmol)	16 (mg, mmol)	Solvent	D^a (%)	D^b (%)
2a, 9.53, 10, 0.0054	30.1, 0.054	**MTBE**	94	95
		EtOAc	82	89
7, 9.80, 10, 0.0054	30.1, 0.054	**MTBE**	93	90

Fmoc-Phe-Gly-Phe-O^{t}Bu ***17***

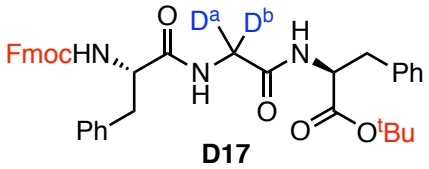

D17

^{1}H NMR (400 MHz, $CDCl_3$) δ 7.76 (d, *J* = 8.1 Hz, 2H, Ar-H), 7.51 (t, *J* = 7.5 Hz, 2H, Ar-H), 7.40 (t, *J* = 7.5 Hz, 2H, Ar-H), 7.32 – 7.11 (m, 12H, Ar-H), 6.48 – 6.39 (m, 1H, NH), 5.33 – 5.22 (m, 1H, NH) 4.76 – 4.68 (m, 1H, NHCH), 4.48 – 4.40 (m, 3H, OCH_2CH), 4.17 (t, *J* = 6.5 Hz, 1H, NHCH), 3.99 (d, ^2J = 13.2 Hz, 1H, NHCHH), 3.74 (d, ^2J = 13.2 Hz, 1H, NHCHH), 3.19 – 2.95 (m, 4H, 2 CH_2Ph) 1.39 (s, 9H, $OC(CH_3)_3$) ppm.

Labelling expected against signal at 3.99 and 3.74 ppm, measured against signal at 3.19 – 2.95 ppm.

Table 2.19

[Ir] (mg, mol%, mmol)	17 (mg, mmol)	D^a (%)	D^b (%)
2a, 9.53, 10, 0.0054	34.7, 0.054	**MTBE** 28	22
		EtOAc 35	33
7, 9.80, 10, 0.0054	34.7, 0.054	**MTBE** 29	23

Ac-Phe-Gly-Phe-OMe ***18***

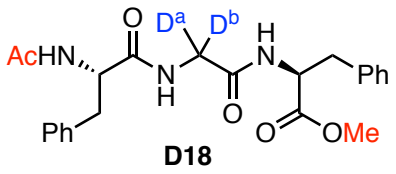

D18

^{1}H NMR (400 MHz, MeOD-*d*$_4$) δ 7.34 – 7.14 (m, 10H, Ar-H), 4.68 (dd, *J* = 8.5, 5.7 Hz, 1H, CHNH), 4.53 (dd, *J* = 9.0, 5.9 Hz, 1H, CHNH), 3.91 (d, ^2J = 16.9 Hz, 1H, NHCHH), 3.70 (br s, 4H, OCH_3 and NHCHH), 3.23 – 3.14 (m, 2H, $PhCH_2$), 3.04 (dd, ^2J = 13.9, *J* = 8.5 Hz, 1H, PhCHH), 2.91 (dd, ^2J = 13.8, *J* = 9.0 Hz, 1H, PhCHH), 1.91 (s, 3H, $C(O)CH_3$) ppm.

Labelling expected against signal at 3.91 and 3.70 ppm, measured against signal at 3.04 ppm.

Table 2.20

[Ir] (mg, mol%, mmol)	18 (mg, mmol)	Solvent	D^a (%)	D^b (%)
7, 9.80, 10, 0.0054	22.8, 0.054	**MTBE**	0	0
		EtOAc	10	10

*Cbz-Phe-Gly-Phe-OMe **19***

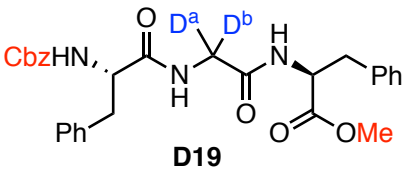

D19

^{1}H NMR (400 MHz, MeOD-*d*$_4$) δ 7.34 – 7.17 (m, 15H, Ar-H), 5.07 – 4.98 (m, 2H, C(O)OCH_2Ph), 4.68 (dd, *J* = 8.4, 5.8 Hz, 1H, NHCH), 4.32 (dd, *J* = 9.1, 5.9 Hz, 1H, NHCH), 3.94 (d, *J* = 16.9 Hz, 1H, NHCHH), 3.69 (s, 3H, OCH_3), 3.65 - 3.61 (d, *J* = 6.8 Hz, 1H, NHCHH), 3.20 – 2.86 (m, 4H, 2 ×CH_2Ph) ppm.

Labelling expected against signal at 3.94 and 3.65 – 3.61 ppm, measured against signal at 3.20 – 2.86 ppm.

Table 2.21

[Ir] (mg, mol%, mmol)	19 (mg, mmol)	Solvent	D^a (%)	D^b (%)
2a, 9.53, 10, 0.0054	27.8, 0.054	**MTBE**	29	27
		EtOAc	52	56
7, 9.80, 10, 0.0054	27.8, 0.054	**MTBE**	60	65
		EtOAc	72	74

Fmoc-Phe-Gly-Phe-OMe ***20***

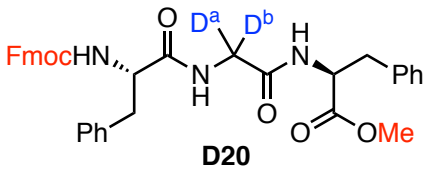

D20

^{1}H NMR (400 MHz, MeOD-*d*$_4$) δ 7.79 (d, *J* = 7.5 Hz, 2H, Ar-H), 7.57 (t, *J* = 6.1 Hz, 2H, Ar-H), 7.39 (t, *J* = 7.5 Hz, 2H, Ar-H), 7.35 – 7.10 (m, 12H, Ar-H), 4.73 – 4.60 (m, 1H, NHCH), 4.38 – 4.21 (m, 3H, OCH_2CH), 4.16 (t, *J* = 6.9 Hz, 1H, NHCH), 3.97 (d, $_2J$ = 17.0 Hz, 1H, NHCHH), 3.66 (bs, 4H, CH_3 and NHCHH), 3.21 – 2.86 (m, 4H, 2 × CH_2Ph) ppm.

Labelling expected against signal at 3.97 and 3.66 ppm, measured against signal at 7.79 ppm.

Table 2.22

[Ir] (mg, mol%, mmol)	20 (mg, mmol)	Solvent	D^a (%)	D^b (%)
2a, 9.53, 10, 0.0054	32.5, 0.054	**MTBE**	62	69
		EtOAc	47	43
7, 9.80, 10, 0.0054	32.5, 0.054	**EtOAc**	60	65

Labelling Scope for Ala-Gly-Ala Sequences

Scheme 2.10

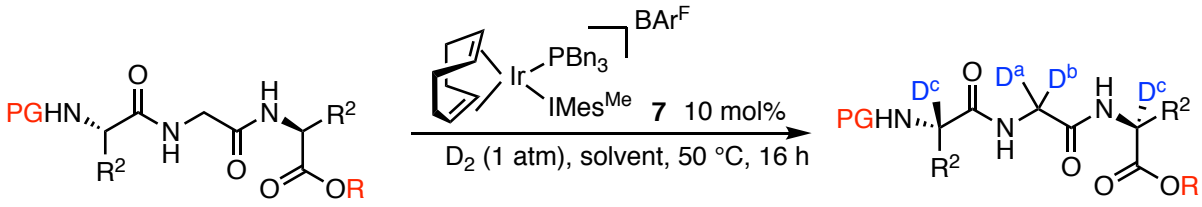

The tripeptide labelling was performed as described in *General Procedure D* on half scale (0.054 mmol substrate). The products were purified by trituration with diethyl ether. Peptides utilised in this section were all commercially available. Solvent volume = 1.25 mL.

Ac-Ala-Gly-Ala-O^{t}Bu **21**

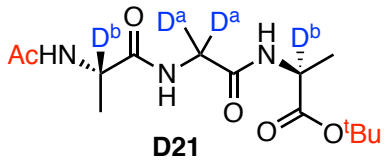

D21

^{1}H NMR (400 MHz, MeOD-*d*$_4$) δ 4.34 – 4.27 (m, 2H, 2 × NHC<u>H</u>CH$_3$), 3.96 – 3.81 (m, 2H, NHC<u>H</u>$_2$), 2.00 (s, 3H, C(O)C<u>H</u>$_3$), 1.48 (s, 9H, OC(C<u>H</u>$_3$)$_3$), 1.39 (d, *J* = 7.1 Hz, 3H, NHCHC<u>H</u>$_3$), 1.37 (d, *J* = 7.4 Hz, 3H, NHCHC<u>H</u>$_3$) ppm.

Labelling expected against signal at 4.34 – 4.27 ppm and 3.96 – 3.81 ppm and measured against signal at 1.91 ppm.

Table 2.23

[Ir] (mg, mol%, mmol)	21 (mg, mmol)	Solvent	D^a (%)	D^b (%)
7, 9.80, 10, 0.0054	16.9, 0.054	**MTBE**	26	14

Cbz-Ala-Gly-Ala-O^{t}Bu **22**

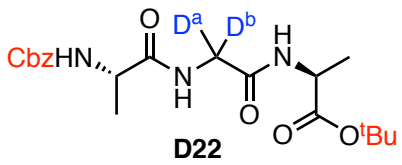

D22

^{1}H NMR (400 MHz, $CDCl_3$) δ 7.47 – 7.32 (m, 5H, Ar-H), 6.88 (s, 1H, NHCH), 6.79 (s, 1H, NHCH), 5.40 (d, J = 6.9 Hz, 1H, NHCH$_2$), 5.20 – 5.06 (m, 2H, CH$_2$Ph), 4.47 – 4.39 (m, 1H, NHCH), 4.27 – 4.20 (m, 1H, NHCH), 4.10 (dd, ^2J = 16.8, J = 5.9 Hz, 1H, NHCHH), 3.90 (dd, ^2J = 16.8, J = 5.1 Hz, 1H, NHCHH), 1.48 (s, 9H, OC(CH$_3$)$_3$), 1.43 (d, J = 7.1 Hz, 3H, CH$_3$), 1.40 (d, J = 7.2 Hz, 3H, CH$_3$) ppm.

Labelling expected against signal at 4.10 and 3.90 ppm, measured against signal at 1.40 ppm.

Table 2.24

[Ir] (mg, mol%, mmol)	22 (mg, mmol)	Solvent	D^a (%)	D^b (%)
7, 9.80, 10, 0.0054	21.9, 0.054	**MTBE**	85	87
		EtOAc	98	97

Fmoc-Ala-Gly-Ala-O^{t}Bu **23**

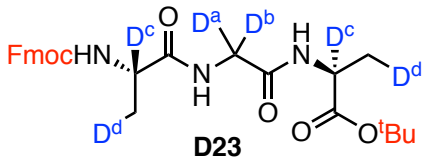

D23

^{1}H NMR (400 MHz, $CDCl_3$) δ 7.79 (d, *J* = 7.6 Hz, 2H, Ar-H), 7.60 (d, *J* = 7.4 Hz, 2H, Ar-H), 7.42 (t, *J* = 7.5 Hz, 2H, Ar-H), 7.33 (t, *J* = 7.5 Hz, 2H, Ar-H), 6.68 – 6.69 (m, 2H, 2 × NH), 5.46 – 5.37 (m, 1H, NH), 4.51 – 4.41 (m, 3H, OCH_2CH), 4.30 – 4.20 (m, 2H, $NHCHCH_3$), 4.08 (dd, ^2J = 16.8, *J* = 5.1 Hz, 1H, NHCHH), 3.74 (dd, ^2J = 16.2, *J* = 5.1 Hz, 1H, NHCHH), 1.49 (s, 9H, $OC(CH_3)_3$), 1.38 (d, *J* = 7.2 Hz, 3H, $NHCHCH_3$), 1.20 (d, *J* = 6.5 Hz, 3H, $NHCHCH_3$) ppm.

Labelling expected against signal at 4.30 – 4.20, 4.08, 3.74, 1.38 and 1.20 measured against signal at 7.79 ppm.

Table 2.25

[Ir] (mg, mol%, mmol)	23 (mg, mmol)	Solvent	D^a (%)	D^b (%)	D^c (%)	D^d (%)
7, 9.80, 10, 0.0054	24.4, 0.054	**MTBE**	29	20	18	56

Ac-Ala-Gly-Ala-OMe **24**

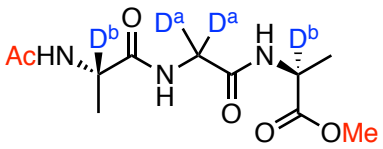

D24

^{1}H NMR (400 MHz, MeOD-*d*$_4$) δ 4.45 (q, *J* = 7.3 Hz, 1H, NHC<u>H</u>CH$_3$), 4.28 (q, *J* = 7.2 Hz, 1H, NHC<u>H</u>CH$_3$), 3.99 – 3.81 (m, 2H, NHC<u>H</u>$_2$), 3.73 (s, 3H, OC<u>H</u>$_3$), 2.00 (s, 3H, C(O)C<u>H</u>$_3$), 1.41 (d, *J* = 7.3 Hz, 3H, NHCHC<u>H</u>$_3$), 1.38 (d, *J* = 7.2 Hz, 3H, NHCHC<u>H</u>$_3$) ppm.

Labelling expected against signal at 4.45, 4.28 and 3.99 – 3.81 ppm and measured against signal at 2.00 ppm.

Table 2.26

[Ir] (mg, mol%, mmol)	24 (mg, mmol)	Solvent	D^a (%)	D^b (%)	OMe (%)
7, 9.80, 10, 0.0054	14.7, 0.054	**EtOAc**	70	28	16

Cbz-Ala-Gly-Ala-OMe ***25***

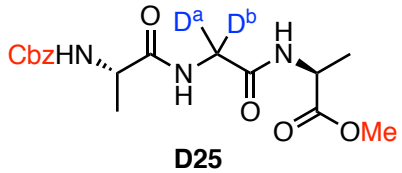

D25

^{1}H NMR (400 MHz, CDCl$_3$) δ 7.42 – 7.32 (m, 5H, Ar-<u>H</u>), 6.92 (s, 2H, 2 × N<u>H</u>CH), 5.41 (d, *J* = 6.8 Hz, 1H, N<u>H</u>CH$_2$), 5.19 – 5.06 (m, 2H, C<u>H</u>$_2$Ph), 4.58 (p, *J* = 7.2 Hz, 1H, NHC<u>H</u>), 4.24

(p, J = 7.0 Hz, 1H, NHC<u>H</u>), 4.12 (dd, ^2J = 17.0, J = 6.1 Hz, 1H NHCH<u>H</u>), 3.89 (dd, ^2J = 16.8, J = 5.1 Hz, 1H, NHC<u>H</u>H), 3.75 (s, 3H, OC<u>H</u>$_3$), 1.43 (d, J = 7.1 Hz, 6H, 2 ×C<u>H</u>$_3$) ppm.

Labelling expected against signal at 4.12 and 3.89 ppm, measured against signal at 3.75 ppm.

Table 2.27

[Ir] (mg, mol%, mmol)	25 (mg, mmol)	Solvent	D^a (%)	D^b (%)
7, 9.80, 10, 0.0054	19.6, 0.054	**MTBE**	67	64
		EtOAc	53	58

Fmoc-Ala-Gly-Ala-O^{t}Bu **26**

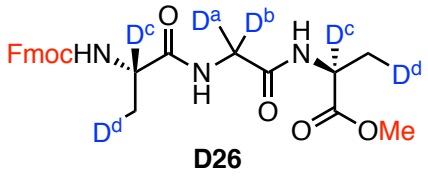

D26

^{1}H NMR (400 MHz, $CDCl_3$) δ 7.77 (d, J = 7.6 Hz, 2H, Ar-<u>H</u>), 7.64 – 7.54 (m, 2H, Ar-<u>H</u>), 7.43 – 7.38 (m, 2H, Ar-<u>H</u>), 7.31 (t, J = 7.4 Hz, 2H, Ar-<u>H</u>), 6.82 (s, 1H, N<u>H</u>), 6.71 (s, 1H, N<u>H</u>), 5.30 (d, J = 6.5 Hz, 1H, N<u>H</u>), 4.55 (p, J = 7.2 Hz, 1H, OCH$_2$C<u>H</u>), 4.43 (d, J = 7.0 Hz, 2H, OC<u>H</u>$_2$CH), 4.21 (t, J = 6.8 Hz, 2H, NHC<u>H</u>CH$_3$), 4.10 (dd, ^2J = 16.7, J = 5.1 Hz, 1H, NHC<u>H</u>H), 3.88 (dd, ^2J = 16.9, J = 5.2 Hz, 1H, NHCH<u>H</u>), 3.73 (s, 3H, OC<u>H</u>$_3$), 1.42 (d, J = 7.2 Hz, 3H, NHCHC<u>H</u>$_3$), 1.39 (d, J = 6.5 Hz, 3H, NHCHC<u>H</u>$_3$) ppm.

Labelling expected against signal at 4.43, 4.21, 4.10, 3.88, 1.42 and 1.39, measured against signal at 7.79 ppm.

Table 2.28

[Ir] (mg, mol%, mmol)	26 (mg, mmol)	Solvent	D^a (%)	D^b (%)	D^c (%)	D^d (%)
7, 9.80, 10, 0.0054	26.6, 0.054	**EtOAc**	44	47	18	7

2.5.7 Labelling of a Glycine Residue on Solid Support

Solvent screen for the isotopic labelling of 27

Graph 2.2

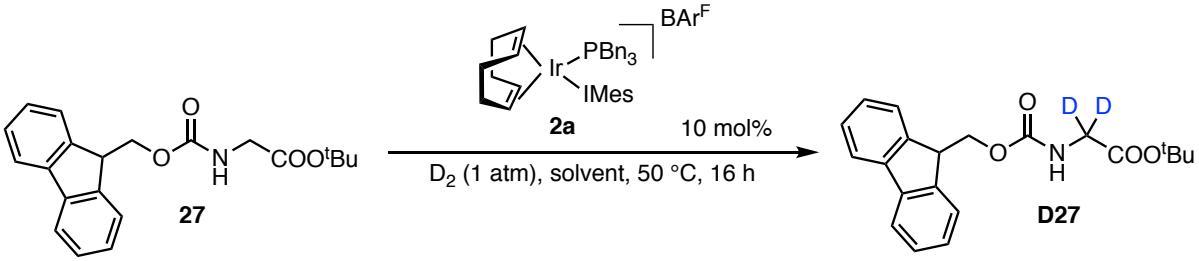

The labelling reactions were performed as described in *General Procedure D*. Mass **27** = 38.0 mg (0.11 mmol) and mass **2a** = 19.1 mg, 10 mol%, 0.011 mmol. Solvent volume = 2.5 mL. The products were purified by column chromatography (0 – 10% MeOH/DCM).

^{1}H NMR (400 MHz, $CDCl_3$): δ 7.79 (dt, *J* = 7.4, 0.9 Hz, 2H, Ar-H), 7.64 – 7.61 (m, 2H, Ar-H), 7.42 (tt, *J* = 7.5, 1.0 Hz, 2H, Ar-H), 7.33 (td, *J* = 7.5, 1.2 Hz, 2H, Ar-H), 5.48 – 5.33 (m, 1H, NH), 4.42 (d, *J* = 7.2 Hz, 2H, CH_2Fmoc), 4.26 (t, *J* = 7.2 Hz, 1H, CHFmoc), 3.92 (d, *J* = 5.4 Hz, 2H, $NHCH_2$), 1.51 (s, 9H, $OC(CH_3)_3$) ppm.

Labelling expected against signal at 3.92 ppm, measured against signal at 4.26 ppm.

Table 2.29

Entry	Solvent	Run 1 (%)	Run 2 (%)	Run 3 (%)	Avg (%)
1	MTBE	75	80	85	80
2	CPME	64	57	57	59
3	2-MeTHF	14	10	14	13
4	EtOAc	44	42	43	43

Labelling of 28

Scheme 2.12

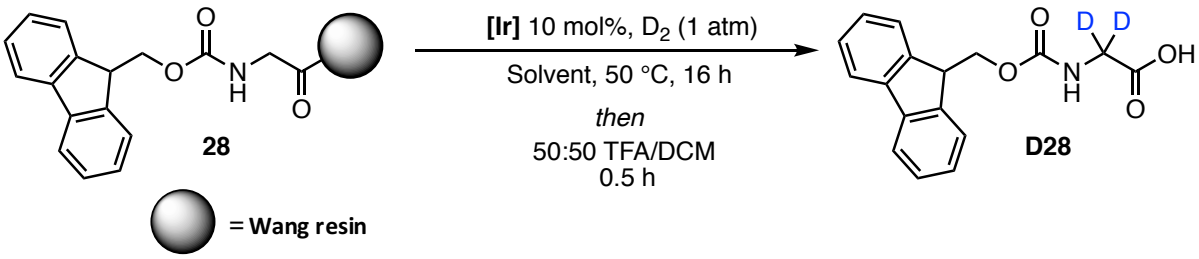

28 was commercially available. The labelling reactions were performed as described in *General Procedure E*. The loading of the Wang residue was assessed by means of a Fmoc-loading test. ~ 10 mg of resin is added to two 10 mL volumetric flasks and dissolved in 20 % piperidine in DMF solution (10 mL) and sonicated for 15 minutes. The sample absorption was then monitored by UV at 302 nm against a blank solution. The loading was then calculated using an equation derived from the Beer-Lambert law and an average was taken of the two values calculated.

$$L = \frac{A\ x\ 20}{m\ x\ 7.8}$$

Loading of peptide = 0.378 mmol/g

Amount of resin bound peptide = 283 mg, 0.11 mmol

Solvent volume = 2.5 mL

NMR of cleaved 28:

^{1}H NMR (400 MHz, MeOD-*d*$_4$) δ 7.76 (d, *J* = 7.8, Hz, 2H, Ar-H), 7.63 (d, *J* = 7.2 Hz, 2H, Ar-H), 7.35 (t, *J* = 7.4 Hz, 2H, Ar-H), 7.27 (t, *J* = 7.4 Hz, 2H, Ar-H), 4.31 (d, *J* = 6.7 Hz, 2H, CH$_2$Fmoc), 4.19 (t, *J* = 6.8 Hz, 1H, CHFmoc), 3.78 (d, *J* = 5.7 Hz, 1H, NHCHH), 3.67 (d, *J* = 6.1 Hz, 1H, NHCHH) ppm.

Labelling expected against signal at 3.78 and 3.67 ppm, measured against signal at 4.19 ppm.

Table 2.30

[Ir] (mg, mol%, mmol)	Solvent	D (%)
2a, 19.1, 10, 0.011	**CPME**	20
	EtOAc	30
7, 19.6, 10, 0.011	**EtOAc**	77

2.5.8 Isotopic Labelling of a Tripeptide on Solid Phase

Initial labelling of 29

Scheme 2.13

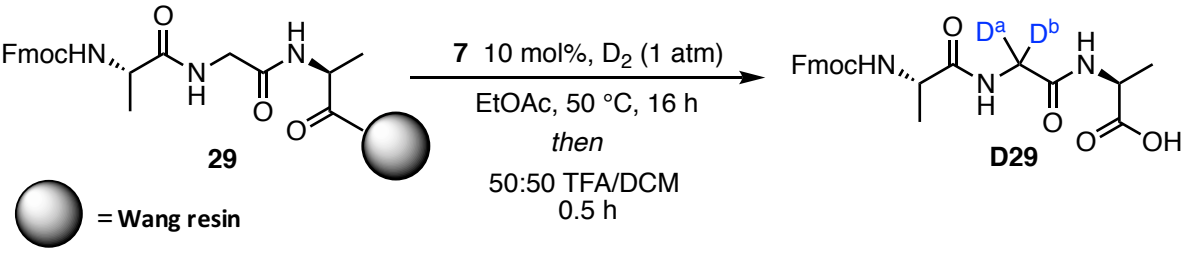

The labelling reactions were performed as described in *General Procedure E*. No prior washing of resin was conducted. The loading of the Wang residue was assessed by means of a Fmoc- loading test. ~ 10 mg of resin is added to two 10 mL volumetric flasks and dissolved in 20 % piperidine in DMF solution (10 mL) and sonicated for 15 minutes. The sample absorption was then monitored by UV at 302 nm against a blank solution. The loading was then calculated using an equation derived from the Beer-Lambert law and an average was taken of the two values calculated.

$$L = \frac{A\ x\ 20}{m\ x\ 7.8}$$

Loading of peptide = 0.99 mmol/g

Amount of resin bound peptide = 108 mg, 0.11 mmol

Solvent volume = 2.5 mL

NMR of cleaved 29:

^{1}H NMR (400 MHz, MeOD-*d*$_4$): δ 7.82 (d, *J* = 7.7 Hz, 2H, Ar-H), 7.68 (d, *J* = 7.5 Hz, 2H, Ar-H), 7.41 (q, *J* = 7.5 Hz, 2H, Ar-H), 7.33 (t, *J* = 7.4 Hz, 2H, Ar-H), 4.52 – 4.30 (m, 3H, CH$_2$Fmoc and CHFmoc), 4.27 – 4.22 (m, 1H, CHCH$_3$), 4.12 – 4.06 (m, 1H, CHCH$_3$), 3.93 (d, *J* = 16.9 Hz, 1H, NHCHH), 3.84 (d, *J* = 16.7 Hz, 1H, NHCHH), 1.37 (t, *J* = 7.0 Hz, 6H, 2 × CH$_3$) ppm.

Labelling expected against signal at 3.93 and 3.84 ppm, measured against signal at 7.82 ppm.

Table 2.31

[Ir] (mg, mol%, mmol)	Solvent	D^a (%)	D^b (%)
7, 19.6, 10, 0.011	**EtOAc**	0	0

Labelling of 29 after washing resin with DCM

Table 2.2

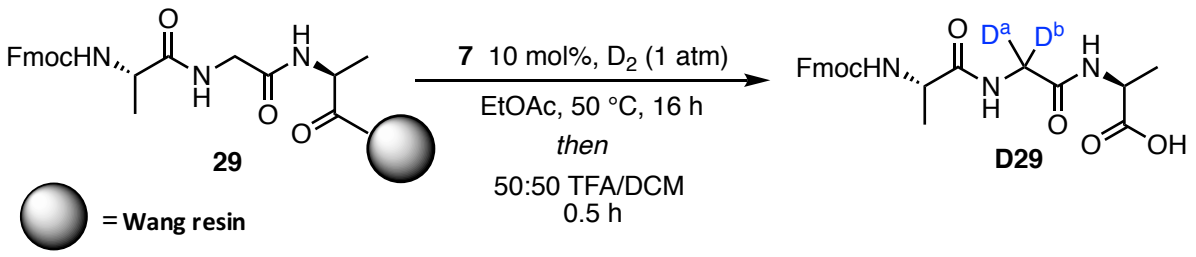

The labelling reactions were performed as described in *General Procedure E*. Procedure as above. For washing resin: resin was placed in a fritted tube attached to vacuum and 10 × DCM washings (5 mL). For refluxing DCM, resin was washed using a soxhlet.

Loading of peptide = 0.27 mmol/g

Amount of resin bound peptide = 399 mg, 0.11 mmol

EtOAc volume = 2.5 mL

NMR of cleaved 29:

^{1}H NMR (400 MHz, MeOD-*d*$_4$): δ 7.82 (d, *J* = 7.7Hz, 2H, Ar-H), 7.68 (d, *J* = 7.5 Hz, 2H), Ar-H, 7.41 (q, *J* = 7.5, 2H, Ar-H), 7.33 (t, *J* = 7.4 Hz, 2H, Ar-H), 4.52 – 4.30 (m, 3H, CH$_2$Fmoc and CHFmoc), 4.27 – 4.22 (m, 1H, CHCH$_3$), 4.12 – 4.06 (m, 1H, CHCH$_3$), 3.93 (d, *J* = 16.9 Hz, 1H, NHCHH), 3.84 (d, *J* = 16.7 Hz, 1H, NHCHH), 1.37 (t, *J* = 7.0 Hz, 6H, 2 x CH$_3$) ppm.

Labelling expected against signal at 3.93 and 3.84 ppm, measured against signal at 7.82 ppm.

Table 2.32

[Ir] (mg, mol%, mmol)	Washing	D^a (%)	D^b (%)
7, 19.6, 10, 0.011	**DCM**	41	23
	Δ DCM	83	80

Optimisation of Labelling of 29 under reduced pressure

Table 2.3

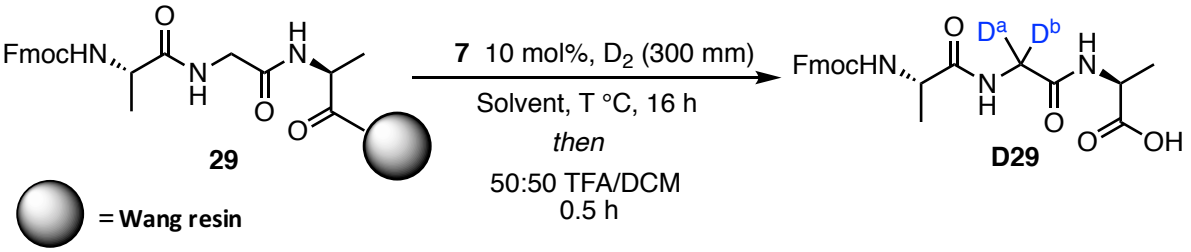

The labelling reactions were performed as described in *General Procedure F*. Loading test performed as described above.

Loading of peptide = 0.37 mmol/g

Amount of resin bound peptide = 58 mg, 0.02 mmol

Incorporation was analysed by LCMS and the labelling position assumed based upon our previous findings. Retention time: 5.94 min, 440.2 $(M+H)^+$

Table 2.33

Entry	Solvent	Temp (°C)	7 (mol%)	Conc. (M)	% 1-D	% 2-D
1	EtOAc	50	10 (3.8 mg)	0.00054	5	0
2	EtOAc	50	10 (3.8 mg)	0.0043	16	2
3	EtOAc	50	25 (9.5 mg)	0.0105	6	2
4	EtOAc	50	25 (9.5 mg)	0.0043	15	1
5	EtOAc	65	10 (3.8 mg)	0.0043	44	14
6	CPME	65	10 (3.8 mg)	0.0043	31	11
7	DCE	65	10 (3.8 mg)	0.0043	5	0
8	CPME/ EtOAc (4:1)	65	10 (3.8 mg)	0.0043	40	6

Tritiation of 29

Scheme 2.14

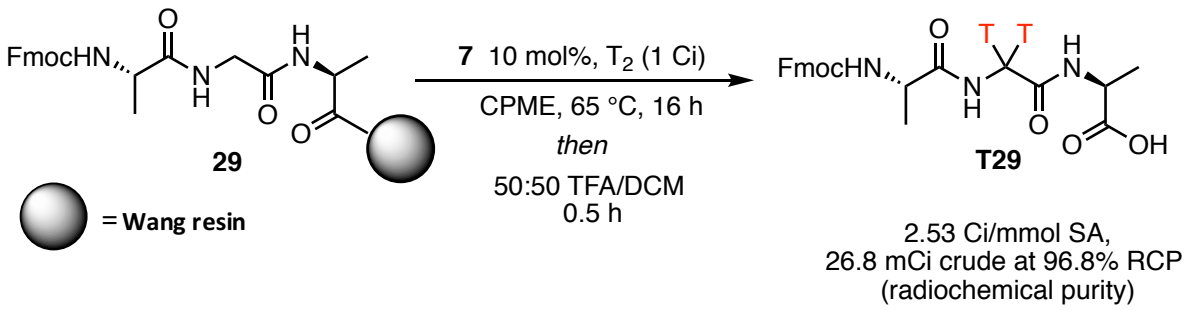

Fmoc-Ala-Gly-Ala-Wang **29** (pre-washed with DCM) was weighed into a tritiation vessel (58 mg, 0.02 mmol) and to this was added EtOAc (0.4 mL). The resin was allowed to swell for 15 mins before a solution of **7** (3.80 mg, 10 mol%) in EtOAc (0.1 mL) was added. This was then attached to a tri-sorber and evacuated. Tritium was then added to the reaction vessel under cooling with liquid nitrogen and the reaction stirred for 16 h at 65 °C. Spent tritium was then reabsorbed from the reaction vessel. At this point the solvent was then removed, and several drops of ethanol added, and again concentrated two further times. At this point the resin was taken up in DCM/TFA (50:50, 1 mL) and allowed to stir for 30 mins. The reaction mixture was then filtered and several drops of ethanol added, and again concentrated. The reaction mixture was then analysed by HPLC and LC-MS analysis. A total of 26.8 mCi of **T29** at a radiochemical purity of 96.8% was isolated. The position was confirmed by ^{3}H NMR spectroscopic analysis.

Incorporation was analysed by LCMS and the labelling position assumed based upon our previous findings. Retention time: 5.94 min, 441.2 $[M(T)+H]^{+}$

^{1}H NMR (400 MHz, MeOD-*d*$_4$): δ 7.82 (d, *J* = 7.7Hz, 2H, Ar-H), 7.68 (d, *J* = 7.5 Hz, 2H), Ar-H, 7.41 (q, *J* = 7.5 Hz, 2H, Ar-H), 7.33 (t, *J* = 7.4 Hz, 2H, Ar-H), 4.52 – 4.30 (m, 3H, CH$_2$Fmoc and CHFmoc), 4.27 – 4.22 (m, 1H, CHCH$_3$), 4.12 – 4.06 (m, 1H, CHCH$_3$), 3.93 (d, *J* = 16.9 Hz, 1H, NHCHH), 3.84 (d, *J* = 16.7 Hz, 1H, NHCHH), 1.37 (t, *J* = 7.0 Hz, 6H, 2 × CH$_3$) ppm.

Labelling expected against signal at 3.93 and 3.84 ppm.

^{3}H NMR (533 MHz, DMSO-*d*$_6$): δ 3.72 – 3.66 (m, 2H, NHCH$_2$) ppm.

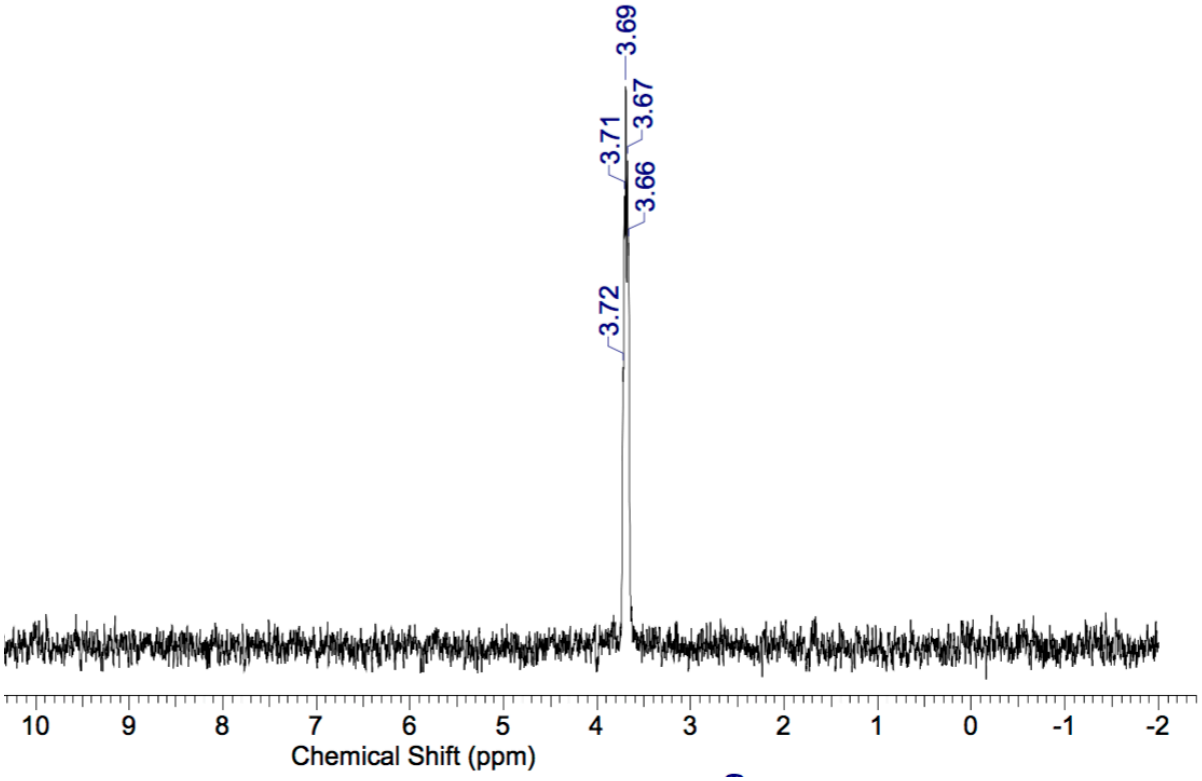

Synthesis of solid phase peptides by SPPS

Table 2.4

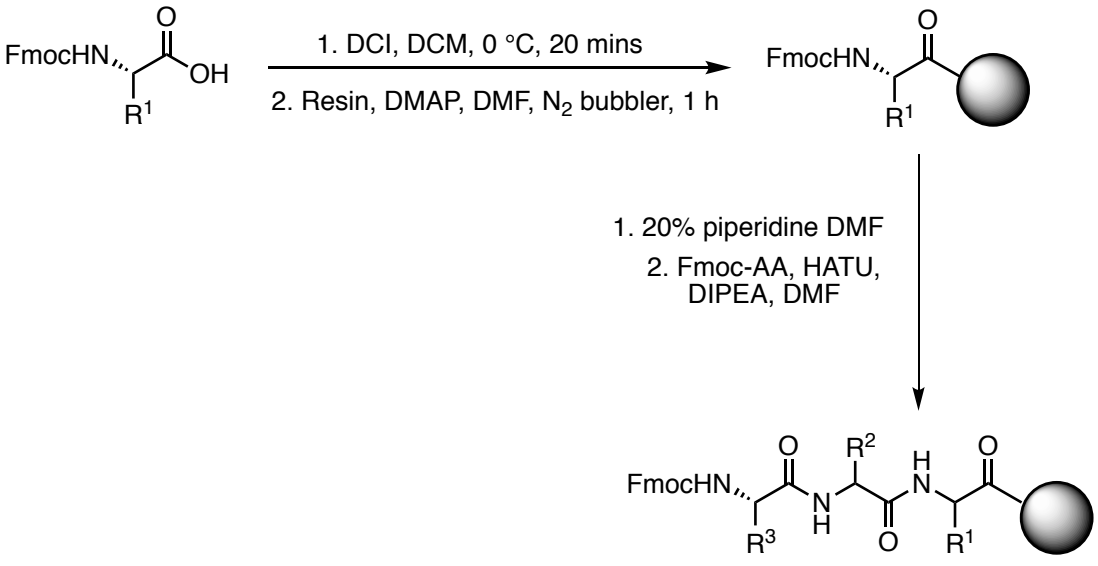

Resin bound peptides were synthesised according to General Procedure for SPPS of Peptides. 500 mg of each resin was used for the initial loading of the first residue. The quantities for each sequence are shown below and the final loadings described in Table 2.34.

Fmoc-Ala-Gly-Ala-Wang **29**

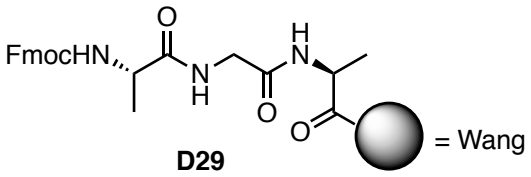

D29

Amount of Fmoc-Ala-OH: 1.29 g, 5.55 mmol, 10 eq.

Amount of Wang resin: 0.50 g, 0.55 mmol, 1.0 eq.

Amount of DIC: 0.35 g, 2.77 mmol, 5.0 eq.

Amount of DMAP: 0.067 g, 0.55 mmol, 1.0 eq.

Volume DCM: 16.65 mL

Fmoc-Ala-Gly-Ala-ChemMatrix-Rink **30**

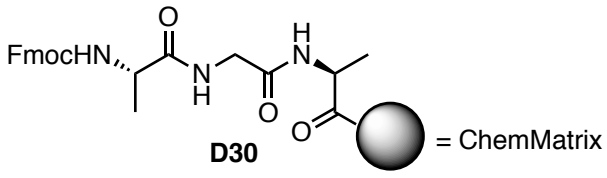

D30

Amount of Fmoc-Ala-OH: 0.388 g, 2.5 mmol, 10 eq.

Amount of resin: 0.50 g, 0.25 mmol, 1.0 eq.

Amount of DIC: 0.158 g, 1.25 mmol, 5.0 eq.

Amount of DMAP: 0.030 g, 0.25 mmol, 1.0 eq.

Volume DCM: 7.5 mL

Fmoc-Phe-Gly-Phe-Wang **31**

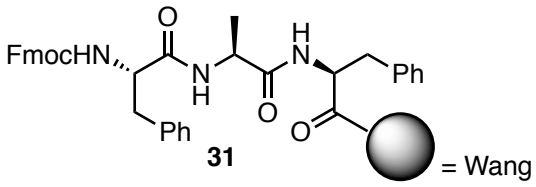

31

Amount of Fmoc-Phe-OH: 2.15 g, 5.55 mmol, 10 eq.

Amount of Wang resin: 0.50 g, 0.55 mmol, 1.0 eq.

Amount of DIC: 0.35 g, 2.77 mmol, 5.0 eq.

Amount of DMAP: 0.067 g, 0.55 mmol, 1.0 eq.

Volume DCM: 16.65 mL

Table 2.34

Resin Loading	L of FmocAA-Resin	Sequence	L of Peptide
Wang (1.11 mmol/g)	0.74 mmol/g	Fmoc-AGA-Wang **29**	0.78 mmol/g
ChemMatrix-Rink (0.45 mmol/g)	0.45 mmol/g	Fmoc-AGA-CM **30**	0.20 mmol/g
Wang (1.11 mmol/g)	1.09 mmol/g	Fmoc-FAF-Wang **31**	0.69 mmol/g

L= loading

Investigation of alternative resin supports

Scheme 2.15

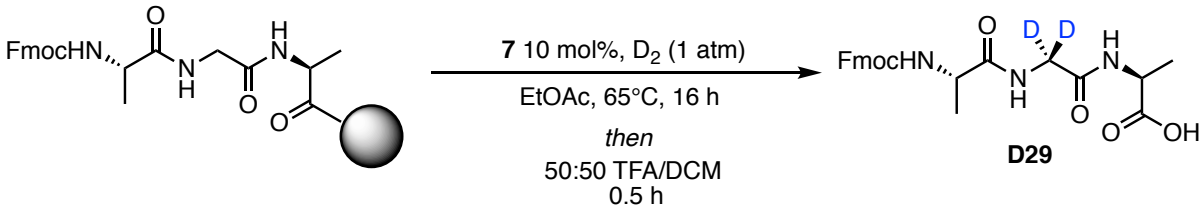

The labelling reactions were performed as described in *General Procedure E*. Loading test procedure as above. Solvent volume = 1.25 mL.

Incorporation was analysed by LCMS and the labelling position assumed based upon our previous findings. Retention time: 5.94 min, 440.2 $(M+H)^+$

Table 2.35

Entry	Resin	Peptide (mg, mmol)	7 (mg, mmol)	% 1-D	% 2-D
1	Wang **29** (0.78 mmol/g)	68.5, 0.05	9.6, 0.005	44	14
2	ChemMatrix **30** (0.20 mmol/g)	268, 0.05	9.6, 0.005	9	53
3	Chlorotrityl **32** (0.99 mmol/g)	108, 0.11	19.6, 0.011	0	0

Labelling of 31

Scheme 2.16

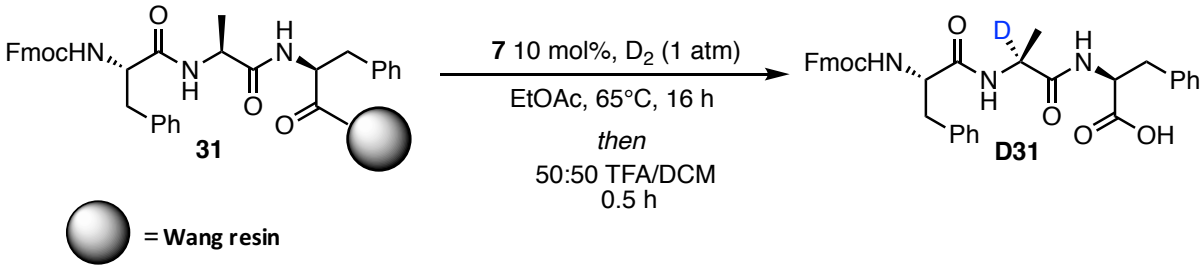

The labelling reactions were performed as described in *General Procedure E*. Loading test procedure as above. Solvent volume 1.25 mL.

Incorporation was analysed by LCMS and the labelling position assumed based upon our previous findings. Retention time: 7.24 min, 604.2 $(M-H)^-$

[Ir] (mg, mol%, mmol)	31 (mg, mmol)	% 1-D	% 2-D
7, 19.6, 10, 0.011	77.5, 0.11	14	4

2.6 References

(1) Fosgerau, K.; Hoffmann, T. *Drug Discov. Today* **2015**, *20*, 122–128.

(2) Palomo, J. M. *RSC Adv.* **2014**, *4*, 32658–32672.

(3) Kerr, W. J.; Lindsay, D. M.; Owens, P. K.; Reid, M.; Tuttle, T.; Campos, S. *ACS Catal.* **2017**, *7*, 7182–7186.

(4) Armarego, W. L.; Chai, C. L. . *Purification of Laboratory Chemicals*, Seventh Ed.; Elsevier, **2013**.

(5) Voskuhl, J.; Waller, M.; Bandaru, S.; Tkachenko, B. A.; Fregonese, C.; Wibbeling, B.; Schreiner, P. R.; Ravoo, B. J. *Org. Biomol. Chem.* **2012**, *10*, 4524.

(6) Plastina, P.; Fazio, A.; Attya, M.; Sindona, G.; Gabriele, B. *Nat. Prod. Res.* **2012**, *26*, 1799–1805.

(7) Bolla, M. L.; Azevedo, E. V.; Smith, J. M.; Taylor, R. E.; Ranjit, D. K.; Segall, A. M.; McAlpine, S. R. *Org. Lett.* **2003**, *5*, 109–112.

(8) Morisset, E.; Chardon, A.; Rouden, J.; Blanchet, J. *Eur. J. Org. Chem.* **2020**, *2020*, 388–392.

(9) Gamon, L. F.; Nathanael, J. G.; Taggert, B. I.; Henry, F. A.; Bogena, J.; Wille, U. *Chem. Eur. J.* **2015**, *21*, 14924–14930.

(10) Pérez-Picaso, L.; Escalante, J.; Olivo, H. F.; Rios, M. Y. *Molecules* **2009**, *14*, 2836–2849.

(11) Barbayianni, E.; Stephens, D.; Grkovich, A.; Magrioti, V.; Hsu, Y-H.; Dolatzas, P.; Kalogiannidis, D.; Dennis, E. A.; Kokotos, G. *Bioorg. Med. Chem.* **2009**, *17*, 4833–4843.

(12) Maheswara Rao, B. L.; Nowshuddin, S.; Jha, A.; Divi, M. K.; Rao, M. N. A. *Synth. Commun.* **2017**, *47*, 2127–2132.

(13) Suárez-Picado, E.; Quiñoá, E.; Riguera, R.; Freire, F. *Angew. Chem. Int. Ed.* **2020**, *59*, 4537–4543.

(14) Ariyoshi, Y. *Bull. Chem. Soc. Jpn.* **1984**, *57*, 3197–3202.

(15) Kaur, B.; Kaur, M.; Kaur, N.; Garg, S.; Bhatti, R.; Singh, P. *J. Med. Chem.* **2019**, *62*, 6363–6376.

(16) Filp, U.; Pekošak, A.; Poot, A. J.; Windhorst, A. D. *Eur. J. Org. Chem.* **2017**, *2017*, 5592–5596.

Chapter Three

3.1 Introduction

3.1.1 Mesoionic Carbenes

The introduction of NHCs as ligands for transition metal chemistry has proven a landmark advancement in the area. As discussed in Chapter One, the synthetic flexibility and strong M-L bonds of NHCs has driven a large focus in developing ligand motifs in this arena. Traditionally, the main synthetic modifications have centered around modifications of 2-imidazolylidene type carbenes (Arduengo carbenes **A**, Figure 3.1). Modifications typically were through substitution of the R groups residing on the two nitrogen atoms, or modulation of the backbone (introduction of substituents or saturation). Modification of the ring size and bonding patterns of imidazolylidene carbenes (such as **B**) came much later.[1] In addition to this is the introduction of alternative heterocyclic scaffolds (**C**-**I**), which display less heteroatom stabilization. Owing to the decreased stabilization observed, the pre-carbenic site is less acidic compared to Arduengo type carbenes, and upon complexation provides a highly basic ligand with stronger donor properties.[2] These key differences in basicity and the exploration of enhanced synthetic opportunities have influenced researchers to study these motifs more closely as potential ligands in transition metal chemistry.

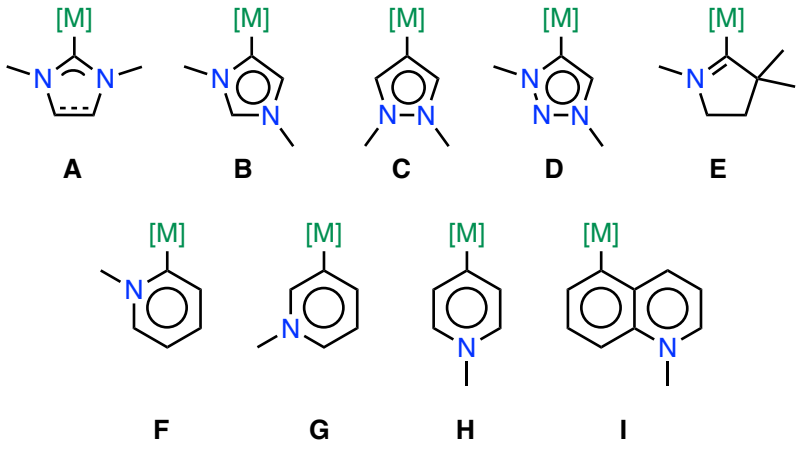

Figure 3.1

The term "abnormal carbene" was first introduced to describe **B** type carbenes, where binding of the imidazolyidene was not through the 'normal' 2- position.[3] The term has been outsourced to any NHC which cannot be represented by a neutral covalent structure. These are typically 5- or 6- membered rings that have a positive and negative charge which are partially delocalized but cannot be described by a singular resonance form. A move in terminology has seen the emergence of the term "mesoionic carbenes" (MICs), allowing a better description of this delocalized charge.[4] To further divide NHC classes, the terms "remote" or "non-remote" have been introduced to describe the positioning of the heteroatoms. Examples of the different carbene classes are highlighted in Figure 3.2. Non-remote carbenes (**A** and **B**) have one or more heteroatoms α- to the carbonic site. In contrast, the heteroatoms are absent in this position for remote carbenes (**C** and **H**). Introduction of these sub-classes for NHCs has significantly broadened the scope and utility of NHC ligands within organometallic chemistry.

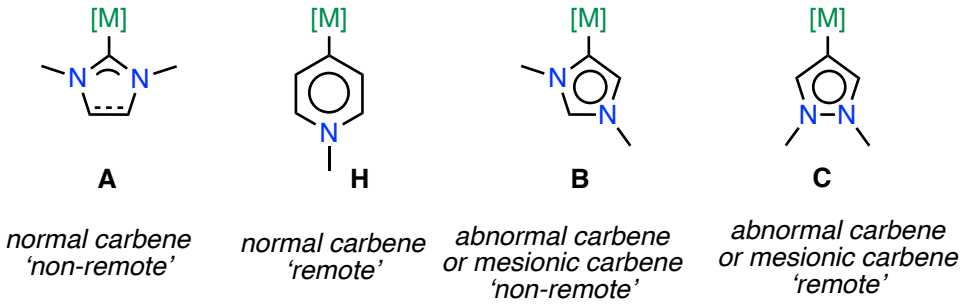

Figure 3.2

3.1.2 Mesoionic Imidazolylidene Ligands

Predominantly, the area of mesoionic carbenes has been saturated with investigation into the application of imidazole-4-ylidines **B**. The initial discovery of C4/5-imidazolylidene bonding

to a metal was the serendipitous formation of iridium complex **2** in 2001 by Crabtree *et al* (Scheme 3.1).[5]

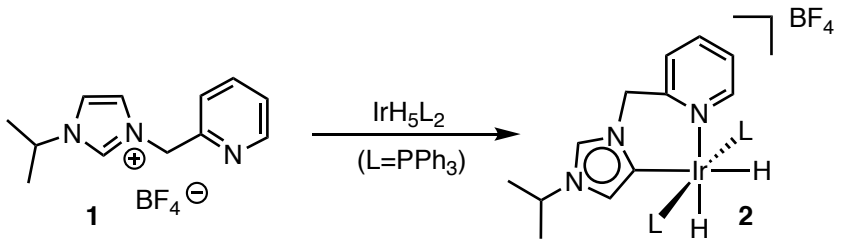

Scheme 3.1

Subsequently, a number of organometallic complexes with this mode of bonding have been reported, opening up new reactivity modes. Catalytically active complexes with various metals have been synthesised, including palladium complexes for cross-coupling reactions,[6–8] rhodium complexes for Si-H bond activations,[9] ruthenium hydrogenation catalysts[10,11] and gold complexes which promote cyclisation reactions.[12] Focusing on iridium, several complexes with catalytic applications have been discovered. An example is complex **6** (Scheme 3.2), a chelated iridium(I) complex with application in transfer hydrogenation.[13,14] Initial phosphine coordination to $[Ir(COD)Cl]_2$ affords **5a**, followed by activation at the C-4 position in a reversible fashion. Base-mediated reductive elimination then allows access to complex **6**. Modification of the *N*-group, or application of a hard chloride counterion, also affords bonding through the C-4 position, with no bonding at C-2 observed. This selectivity may be a result of the propensity of Ir(I) for C=C bonds, or an enhanced steric influence at the metal centre through bonding of the bulky, constrained phosphine. Alternative synthetic approaches to access bonding through C-4 or -5 has been achieved through oxidative addition, transmetallation and deprotonation of the imidazolium to the free base. Interestingly, both **5b** and **6** have been shown to catalyse the transfer hydrogenation of aryl ketones with high rates of success comparative to the corresponding C-2 bound imidazole catalyst motif.

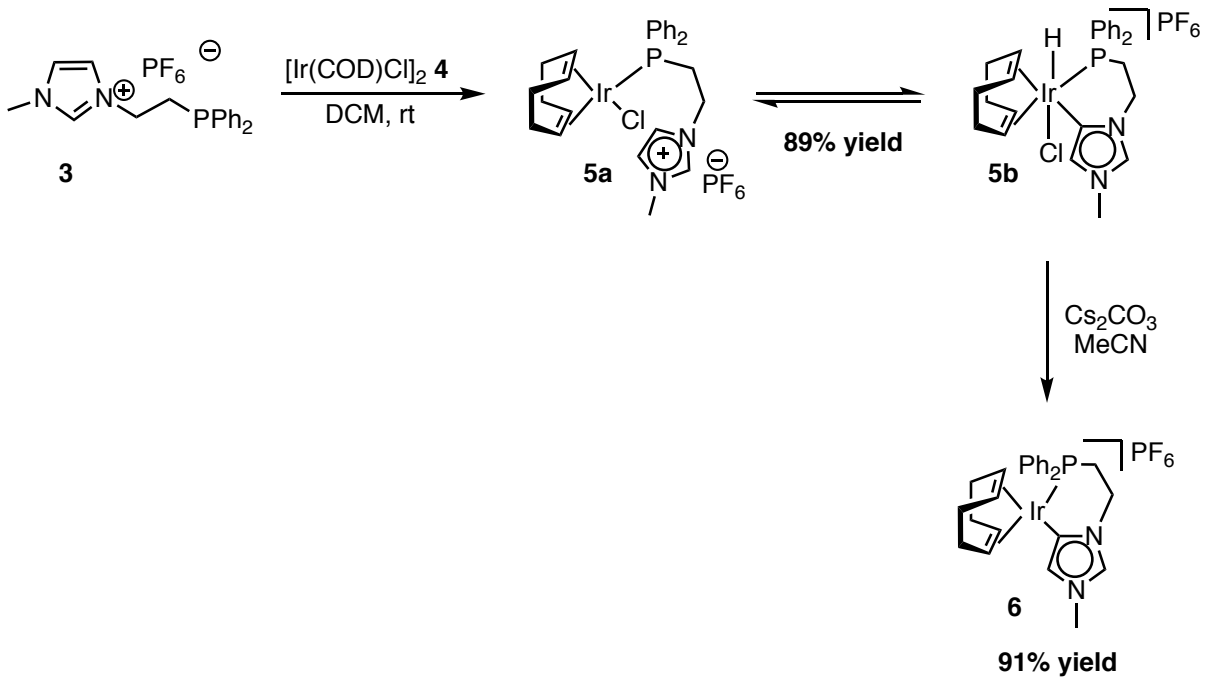

Scheme 3.2

Another factor which governs the success and mode of bonding for imidazolylidene NHCs to transition metals is the starting metal complex. In 2005, Danopoulos and co-workers reported the formation of several NHC-M complexes (M= Rh or Ir), where different modes of bonding were observed depending upon the starting metal complex (Scheme 3.3).[15] Attempted complexation of the pre-formed carbene of **7** *in situ* to $[Ir(COD]Cl]_2$ **4** did not give reliable conversion to **8**. Reaction directly with the imidazolium salt **7**, in the absence of base, unsurprisingly generated phosphine-only bound complex **9**. On the other hand, a move to the more reactive $[Ir(COD)(\mu\text{-}H)(\ \mu\text{-}Cl)_2]_2$ **11** yielded a five coordinate Ir(I) complex **12**. In this instance, the complex generated displayed square pyramidal geometry, with the bromide residing at the apical position. Perhaps owing to the increased steric congestion, abnormal binding was observed for the NHC. Interesting to investigate, would be the complexation of imidazolium salts bearing a more diffuse, non-binding counterion, which would likely result in the formation of a C-2 bound NHC. In line with this, the authors also investigated the binding of a NHC-pyridyl chelated phosphine. Reaction of the corresponding free carbene with $[Ir(COD)Cl_2]$ **4** and $NaBAr^F$ did indeed form a C-2 bound NHC. This report highlights

the complex behaviour of NHC ligands and their bonding modes with various transition metal complexes.

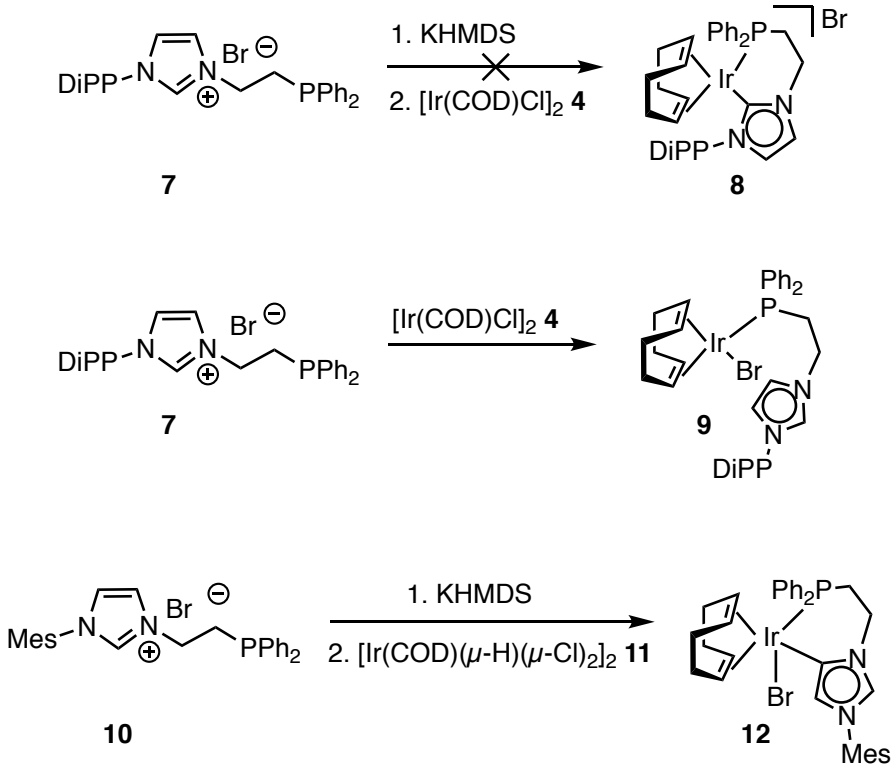

Scheme 3.3

Of particular influence to the mode of bonding displayed by NHC ligands is its steric influence around the metal centre. Braunstein and co-workers targeted the complexation of bis(imidazolium) salt **13** (Scheme 3.4) to generate iridium(III) pincer complexes.[16] Where the use of *iso*-propyl or *n*-butyl substituents on the imidazole NHC generated pincer complexes where metalation was observed exclusively at the 2- position, use of large adamantyl groups led to complex **14**, where a mixed normal/abnormal NHC bonding mode is observed. Generation of these complexes has been described to occur through formation of a mono-NHC Ir(I) complex, which subsequently undergoes oxidative addition with the second imidazolium to form the pincer complex. Coordination of the second imidazolium in ligand **13** is *via* the C-4 coordination mode, to relieve steric congestion at the metal centre. Isomerisation was not observed upon exchange of the spectator ligands in **14** to generate dihydride **15**. As well as altering the steric environment around the metal centre, the complex

is more electron rich in this coordination mode, and this will be discussed in more detail below.

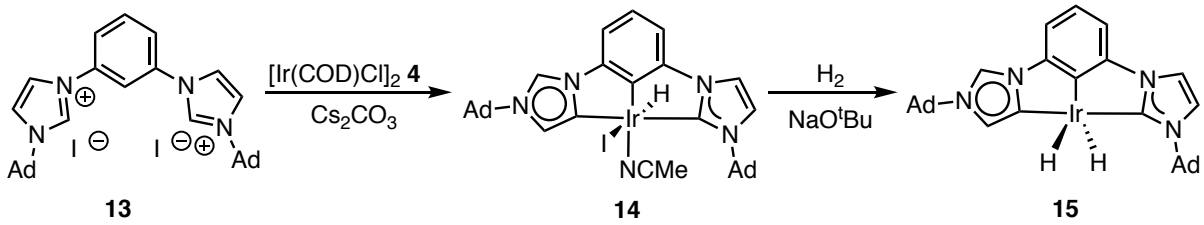

Scheme 3.4

In an extension to his earlier work, Crabtree envisaged preparing abnormal carbene ligands which were monodentate, to determine whether chelation in his previous examples had provided enhanced stability of this binding mode.[17] Refluxing imidazolium salt **16** with $IrH_5(PPh_3)_2$ and pyridine in THF afforded abnormal carbene bound complex **17** (Scheme 3.5). The least sterically hindered carbon in the imidazole ring was selectively bound to iridium to form the iridium(III) species. Although this complex was synthesised in a facile manner akin to its chelated counterpart, the stability of the abnormal monodentate carbene complex **15** was significantly lower than observed for related chelate complex **2**. Complex **2** was shown to be air-stable at room temperature in a chloroform solution for a number of days, whilst **17** displayed decomposition under similar conditions.

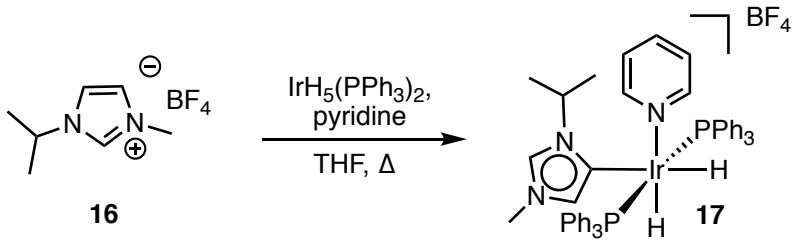

Scheme 3.5

Crabtree *et al*. additionally investigated the generation of Ir(I) complexes bearing mesoionic imidazolylidene ligands.[17] In this instance, the starting complex was lacking the presence of sterically encumbered ligands, such as PPh_3 in the generation of **17**. In the absence of steric effects to control the complexation mode, several challenges arose. Due to the inherently higher acidity of the C-2 position, standard synthetic procedures to form NHC complexes

would afford a normal bound carbene. To avoid this, and further study the properties and stability of the abnormal NHC-Ir(I) complexes, the C-2 position in imidazolium **18** was blocked (Scheme 3.6). The NHC was then complexed through a transmetallation procedure, whereby initial formation of a silver carbene and reaction with **4** generates complex **19** in 45% yield, with an abnormal bonding mode observed. Disappointingly, the absence of a substituent at the C-5 position afforded a silver carbene complex which degraded *via* protonolysis. Complex **19** was a yellow solid which displayed stability in air in both the solid and solution states.

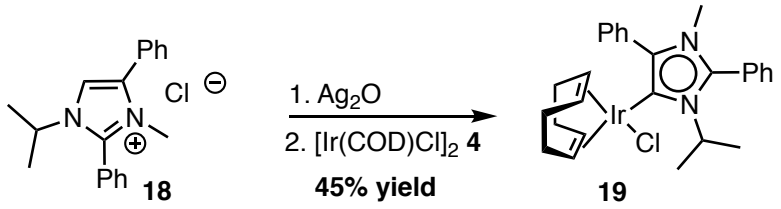

Scheme 3.6

Whilst limited in the substitution pattern required around the monodentate imidazolium salt, it is pleasing to note the success and stability in the synthesis of iridium(I) complexes bearing mesoionic carbene ligands. Also noteworthy is the generation of chelated mesoionic iridium(I) carbene complexes such as **6**. Such complexes have shown alteration in catalytic activity comparative to their counterparts (where a normal bonding mode of the NHC is observed). This is apparent with a variety of metal complexes. The differentiation in chelation mode between abnormal and normal imidazolyidene ligands affords complexes which differ in their electronic properties, alongside alteration of the steric environment around the metal centre. Discussion of the electronic differences and the methods commonly utilised to investigate such attributes will be discussed *vide infra*.

3.1.3 Mesoionic Triazolylidene Ligands

A more recent addition to the abnormal carbene arena has been the introduction of triazolylidene ligands. Such NHC ligands are becoming increasingly popular and this is owed

to the attractive synthesis of their ligand precursor, a triazolium salt. These motifs are typically synthesised *via* a [2+3] cycloaddition between an alkyne and an azide, termed a 'click' reaction (CuAAC),[18] described in Scheme 3.7. The click reaction is highly regioselective, and tolerates a variety of functional groups, providing access to a wide breadth of substitution patterns on the triazole scaffold. One-pot syntheses of triazoles have been reported from aniline starting materials, negating the issue of potentially unstable azide starting materials which through this strategy are generated *in situ*.[19] Perhaps a key drawback, is the substitution of the N-3 position, which requires an electrophile, such as an alkyl halide or triflate. N-3 alkyl-substituted free triazolylidenes can, in some cases, undergo decomposition by attack of the carbene to the alkyl group of a second unit, allowing de-alkylation. Therefore, aryl substitution at this position is also sought.

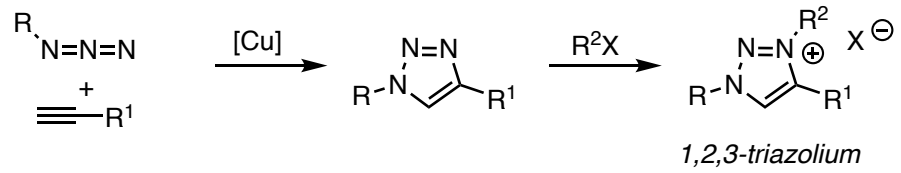

Scheme 3.7

To circumvent this drawback, synthesis of N-3 arylated triazolium salts can be achieved through cycloaddition of 1,3-diaryl-2-azoniaallene salts with alkynes (Scheme 3.8) in the presences of hypochlorite and KPF_6.[19,20] The discussed methods allow generation of diverse triazolium precursors for triazolylidene MICs, and whilst the application of these NHCs in transition metal catalysis is in its early stages, the number and robustness of the methods to synthesise their precursors is noteworthy and well established.

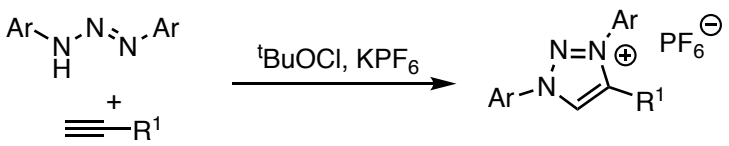

Scheme 3.8

Initial application of triazolylidene MICs as ligands in organometallic chemistry was demonstrated by Albrecht *et al* in 2008.[21] A variety of metal complexes were synthesised (Scheme 3.9) from triazolium **20**, which was in turn prepared *via* CuAAC chemistry. Direct metalation of triazolium **20** with $Pd(OAc)_2$ afforded di-nuclear complex **21**. Complexes of ruthenium, **23**; iridium, **24a**; and rhodium, **24b**, were accessed through transmetallation from silver carbene **22**. Ligand precursor **20** displayed high affinity in binding to several metal centres and this was an encouraging advancement in the area with the authors noting that diversification of the substituents on the triazolylidene would be facile through the CuAAC methodology. This study confirmed that triazole based MICs could be an interesting avenue of investigation for researchers, and as a result, several reports of the use of these MICs followed, with comprehensive studies into their synthesis, properties and catalytic applications investigated

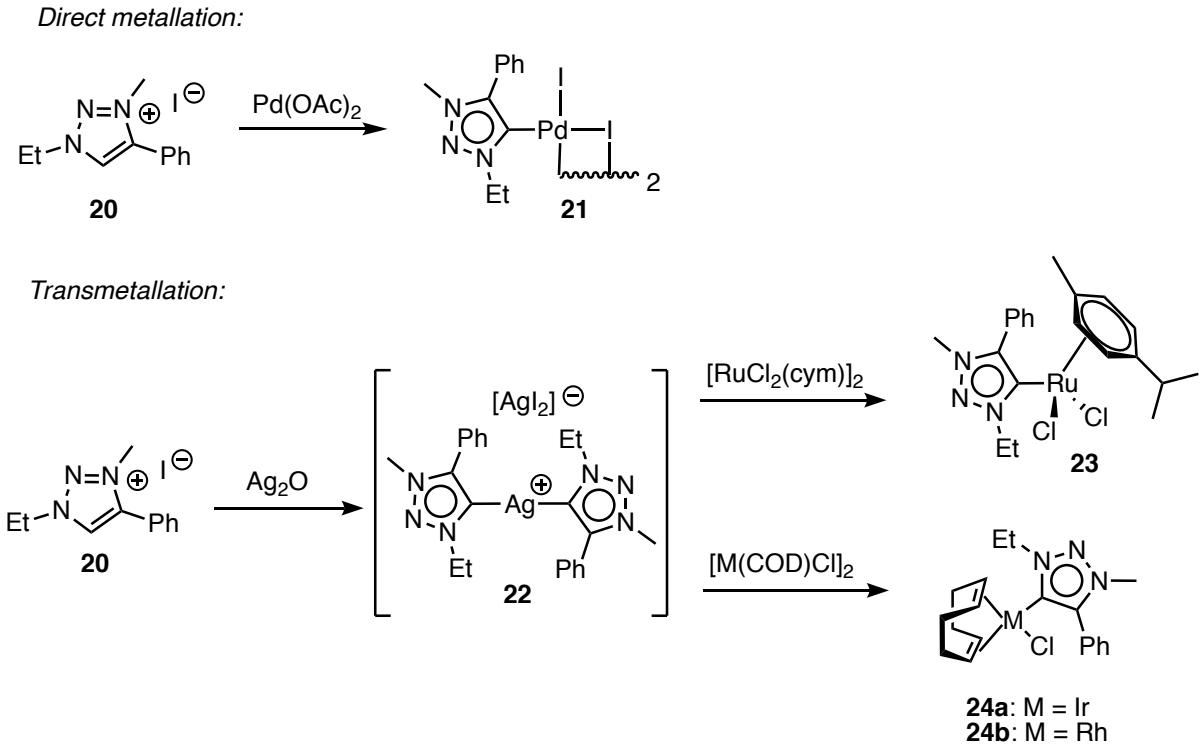

Scheme 3.9

3.1.4 Synthesis of Triazolylidene Metal Complexes

Significant research into the most suitable method for complexation of triazolium salts to metal complexes has been undertaken. Complexation can be accomplished *via* a variety of

methods and the optimal synthetic procedure depends highly on the metal centre. Alongside direct metalation and transmetallation from the corresponding silver complex, deprotonation with an external base or ligand bound to the precursor metal salt, and ligand post-modification have been utilised. Perhaps the most common approach is transmetallation from a triazolylidene silver complex. Similar to Arduengo-type NHC silver complexes, triazolylidene silver complexes are diverse in structure and can exist as either a neutral [Ag(trz)X] complex or a cationic $[Ag(trz)_2][AgX_2]$ complex and the success of transmetallation appears to be independent of the structure adopted. For transmetallation to another metal, the silver carbene species are generally formed *in situ* and identified my ^{1}H NMR spectroscopy; however, in a manner akin to traditional NHC ligands, silver carbene MICs have been isolated, although these instances are small in comparison to Arduengo NHCs. Initial isolated silver complexes were limited to bulky triazolylidene ligands, and it wasn't until more recently that simpler triazolylidene silver complexes were reported (Scheme 3.10).[22] Silver carbenes **26** and **27** were generated from the corresponding triazolium salt **25a/b**. Activation of MeCN during the reaction of **25b** with Ag_2O afforded the resultant neutral cyano carbene **26**. These crystalline materials were characterized by NMR spectroscopy and X-ray diffraction, allowing characterization of some of the first simple triazolylidene silver carbene complexes.

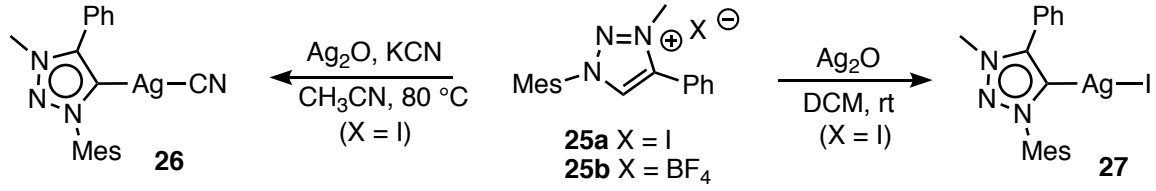

Scheme 3.10

To further explore the properties and activity of these isolated silver complexes, the authors investigated both **26** and **27** as a catalyst for the formation of oxazolines from aldehydes and isocyanoacetates (Scheme 3.11). These complexes were extremely efficient, generating excellent yields of oxazoline product. The anionic ligand does not seem to impart significant influence on the catalytic activity of these complexes, suggesting a lability of the anion. It could therefore be postulated that for use in transmetallation, the nature of the anionic ligand may not have a profound on effect on reactivity. This being said, for several complexes, the presence of nitrile anions may be detrimental to the process. This body of work highlights

very effectively the importance in choice of conditions in the formation of a silver carbene complex.

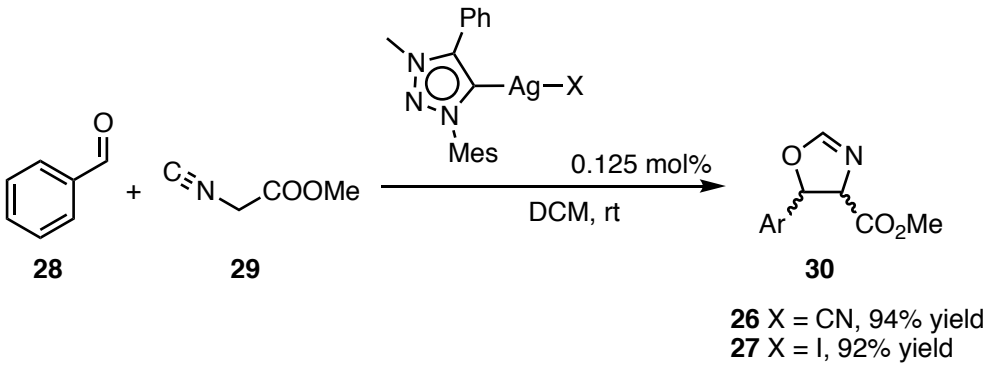

Scheme 3.11

Silver carbene transmetallation can be widely utilised for the introduction of triazolylidene MICs to various transition metal complexes. This strategy is not limited to monodentate triazolylidene motifs, but can also be used for bidentate systems, as well as hemilabile triazolylidene ligands. In 2017, Albrecht reported the use of transmetallation to form Ir(I) and Ir(III) complexes bearing a hemi-labile ligand derived from **31** (Scheme 3.12).[23] Silver complexes were not isolated in this instance, but it is postulated that the generated silver species could reside with the hemi-labile methoxy motif also bound to the silver atom. Competent transmetallation to Ir(I), affording **32**, and Ir(III), producing **34**, occurred, highlighting the tolerability of transmetallation *via* a silver carbene to triazolylidene motifs bearing additional functionality and Lewis basic groups.

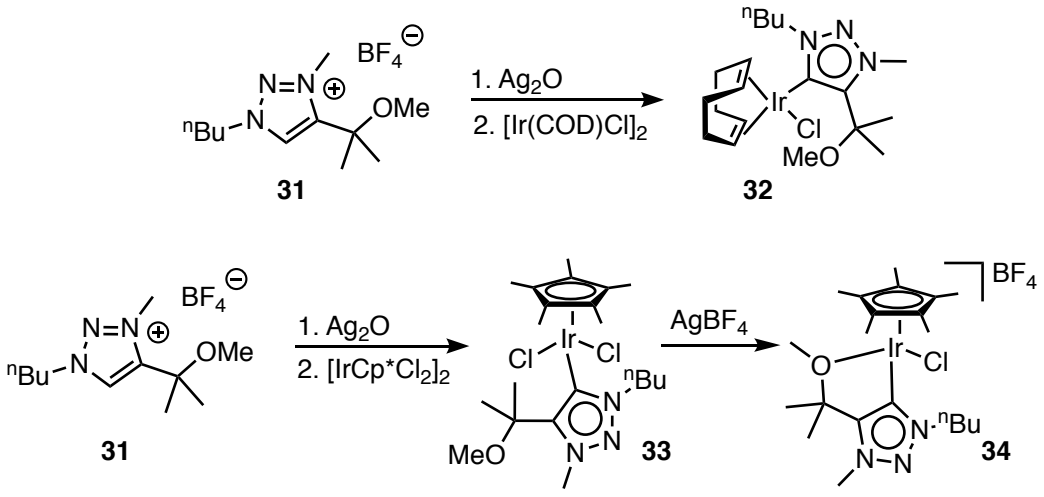

Scheme 3.12

Transmetallation is not limited to the use of silver complexes, and indeed copper intermediates have also been utilised for transmetallation (Scheme 3.13). Bis(copper) complex **35**, bearing both an imidazolylidene and a triazolylidene ligand, has been employed for the successful transmetallation to both Pd and Rh, to afford complexes **36a** and **36b**.[24] The use of copper as a transmetallation intermediate is attractive for ligands which are sensitive to oxidation, as Cu(I) intermediates are much less oxidizing than Ag(I) species. This greatly widens the scope of ligands which can be introduced through the transmetallation protocol.

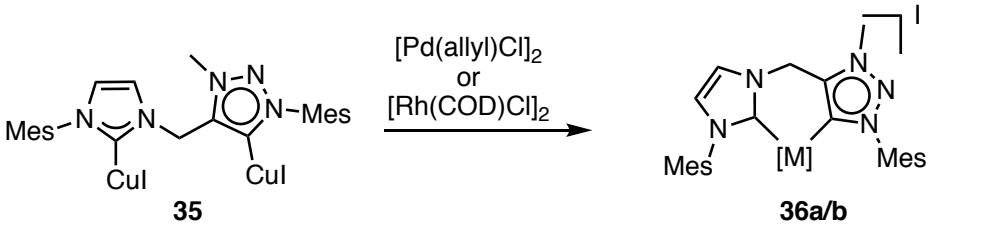

35 **36a/b**

36a [M] = Pd(allyl), 82% yield
36b [M] = Rh(COD), 73% yield

Scheme 3.13

Alongside transmetallation protocols, generation of the free carbene with a strong base, such as KHMDS or KO^{t}Bu, is a popular approach. The bridged NHC/MIC species discussed above for copper mediated transmetallation can additionally be complexed to transition metals *via* a free carbene approach (Scheme 3.14).[24] When salt **37** is deprotonated in the presence of an excess of base, deprotonation of both heterocycles occurs, and reaction with $[Rh(COD)Cl]_2$ affords the monometallic bis(carbene) complex **36b** in 82% yield. Through this method, new avenues can be accessed. If **37** is deprotonated using substoichiometric quantities of base, deprotonation selectively occurs at the imidazolium NHC, and thereby yields the imidazolylidene-bound complex **38**, bearing a pendant triazolium motif. Addition of a second equivalent of base, alongside a secondary metal precursor, induces deprotonation of the triazolium, and subsequent coordination to the second metal, accessing di-metallic species **39** in excellent yield. The free carbene route strategically makes use of the relative pKa values of the starting heterocycles, enabling the chemist to control selectively the metal complex that is formed. This method clearly highlights a sufficiently large difference in acidity of the triazolium and imidazolium salts for selectivity to be observed.

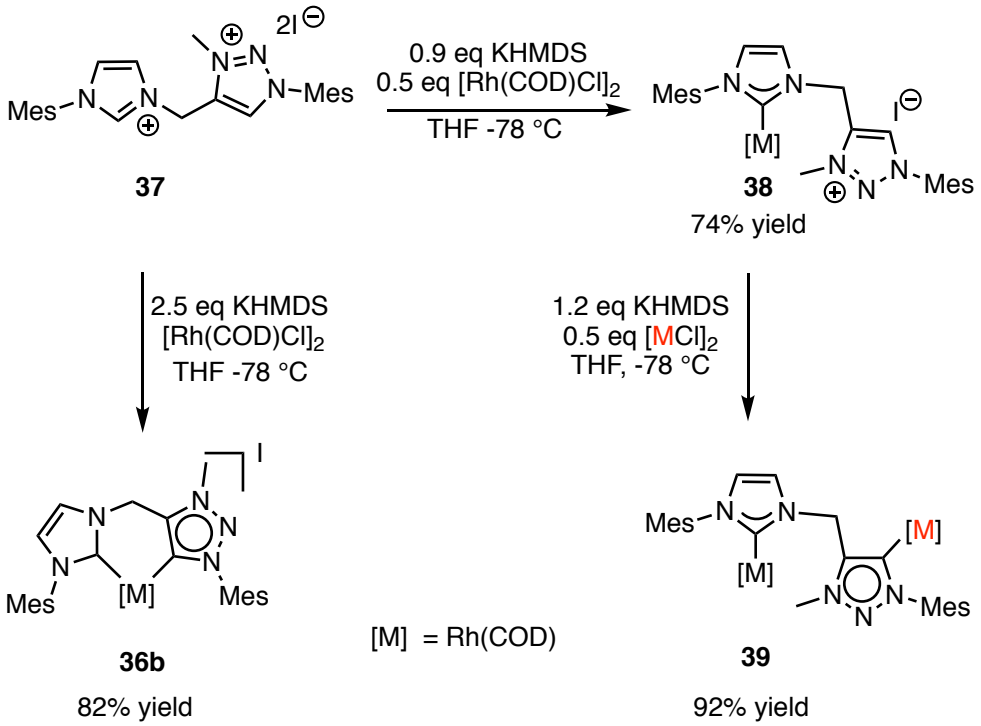

Scheme 3.14

Direct metalation of triazolium salts with a suitable metal precursor is also a popular synthetic choice for the complexation of these types of MICs. This approach has been particularly common in the generation of palladium complexes, however there have also been several reports for iridium, rhodium and nickel. Activation can be induced by several different methods: activation by a metal precursor which bears basic ligands; activation through addition of an external proton scavenger; or through the use of chelating groups to promote cyclometallation. Use of a metal precursor bearing an internal base is a relatively mild process and is generally thermally induced. This is a common approach for complexes of Ir and Rh, where $[M(COD)(OMe)]_2$ is generally employed as the metal precursor. Cowie and co-workers employed this strategy to afford triazolylidene complexes **41a/b**, bearing a pendant triazolium which could be further manipulated to afford di-metallic species (Scheme 3.15).[25] This mode of reactivity is very efficient, with high yields observed for both iridium and rhodium complexes. In addition, to allow direct metalation, $[M(COD)(OMe)]_2$ can be prepared *in situ* by reaction of $[M(COD)Cl]_2$ with NaH in the presence of MeOH.

40

41a M = Ir 81% yield
41b M = Rh 82% yield

Scheme 3.15

Chelate directed bond activation can be extremely useful for systems which contain more than one activatable C-H bond within the triazolium, such as in ligand precursor **42** (Scheme 3.16).[26] Coordination of the pyridyl nitrogen to iridium directs the metal to the triazolium C-5 position selectively, and typically for a cyclometallation reaction. Use of a transmetallation protocol was not suitable, in this case, as formation of a silver complex and subsequent reaction with $[IrCp^*Cl_2]_2$ gave a mixture of products, with bonding through both available positions observed. This highlights the importance of method selection for the successful coordination of MIC ligands, and the necessity to consider what governs the selectivity in each particular case.

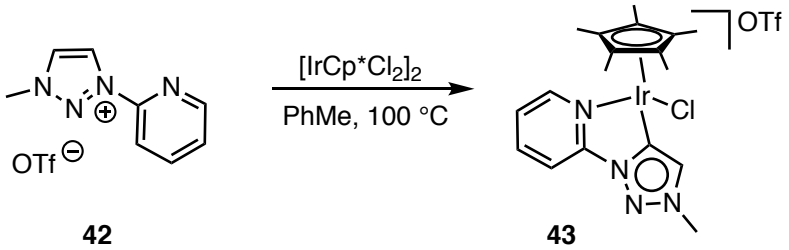

42 **43**

Scheme 3.16

Ligand post modification is the final way in which triazolylidene complexes are synthesised. This route involves initial complexation of a triazole to the metal centre, followed by synthetic manipulation at the triazole to form the triazolylidene. This synthetic approach was utilised by Gandelman *et al*. in 2011 to form palladium pincer complex **46** (Scheme 3.17).[27] Metallation of **44** allows access to triazolide **45**, which, upon alkylation at N-3, is transformed into the desired triazolylidene complex.

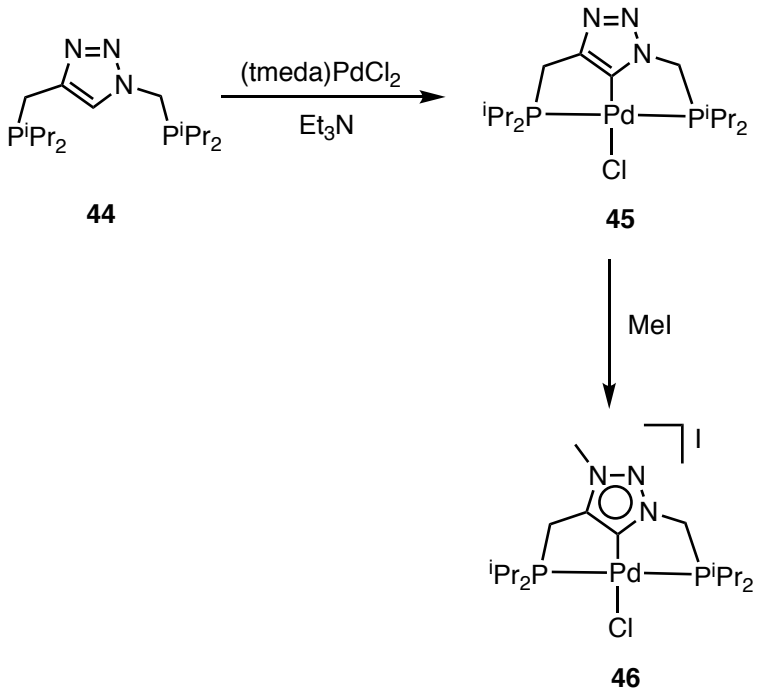

44 **45** **46**

Scheme 3.17

3.1.5 Properties of MICs

To better understand the chemistry of MIC complexes, and how they compare to traditional Arduengo-type NHCs, several attempts have been made to characterise the properties of these ligand motifs. An important aspect to consider of an organometallic complex designed to facilitate catalysis is the electronics of the system. In order to do this, we must first understand the donor properties of the ligands complexed to the metal centre. As previously discussed in Chapter One, the most common parameter utilised to describe the electronic properties of NICs is the Tolman electronic Parameter (TEP). Whilst commonly accessed through the analysis of the CO stretching frequency from IR spectroscopy in nickel complexes of the form $[NiL(CO)_3]$, use of the less toxic iridium and rhodium complexes $[MCl(L)(CO)_2]$ have also been used for correlation. Accordingly, analysis of the CO stretching frequencies from Ir/Rh complexes can be converted to the TEP through equation (1).[17]

$$TEP = 0.847[\nu_{av}(CO)] + 336\ cm^{-1} \qquad \text{Equation (1)}$$

Several TEPs of a variety of both NHC and imidazole and triazole MICs have been reported in the literature, and are summarised and compared in Table 3.1. According to the data, the donor ability of abnormal bound imidazolylidenes **48** is significantly better than those for Arduengo-type carbenes **47**. The lower values clearly show that the imidazole MICs are significantly better electron donors than their C2 counterparts. Even **48c**, bearing an electron withdrawing aryl ring is significantly more donating than complex **47**. Triazolylidene complexes **49** reside between imidazole-2-ylidenes and imidazole-4-ylidenes in terms of electron donating ability. The presence of an additional nitrogen in the triazolylidenes may explain their lower donor ability relative to imidizaole-4-ylidenes.

Table 3.1

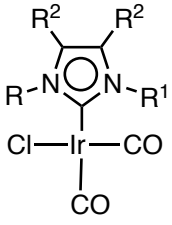

47

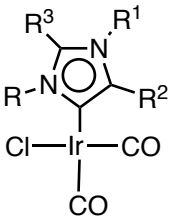

48

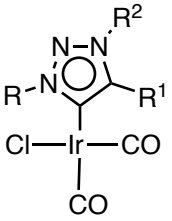

49

Complex	R	R^1	R^2	R^3	TEP/cm^{-1}
47a	DiPP	DiPP	H	-	2051 [28]
47b	Mes	Mes	H	-	2051 [28]
47c	Cy	Cy	H	-	2050 [29]
47d	Ad	Ad	H	-	2050 [29]
48a	^{i}Pr	Me	Ph	Ph	2039 [3]
48b	DiPP	DiPP	Ph	Ph	2038 [30]
48c	DiPP	DiPP	4-CF_3Ph	Ph	2041 [30]
49a	DiPP	DiPP	Me	-	2046 [28]
49b	Mes	Mes	Me	-	2046 [28]
49c	Et	Ph	Me	-	2047 [21]
49d	DiPP	OEt	DiPP	-	2047 [19]

Although descriptive of the donor properties of a ligand to a metal centre, stereoelectronic effects can impact the CO ligands and their stretching frequencies without modification of the true donor properties of the carbene ligand.[31] Therefore, parallel techniques are often employed to confirm the donor abilities. Such techniques can be the formation of metal

hydrides and analysis of the ^{1}H NMR spectra, x-ray photoelectron spectroscopy of palladium NHC complexes, and the investigation of palladium complexes by ^{13}C NMR spectroscopy. Yuan and Huynh investigated the donor ability of triazolylidenes by complexation to a palladium complex bearing an $^{i}Pr_2$-bimy ligand ($^{i}Pr_2$-bimy = 1,3-diisopropylbenzimidaolin2-ylidene), (Figure 3.3).[32] ^{13}C NMR spectroscopy was used to elucidate the donor ability of the ligand *trans* to the bimy ligand. The Pd bound C_{bimy} displays a sensitivity depending upon the nature of the ligand *trans* to it. This technique confirms the notion that triazolylidenes fall between normal and abnormal imidazolylidenes. In addition, subtle shifts were observed due to the inductive effects of the substituents on the triazolylidene ligand.

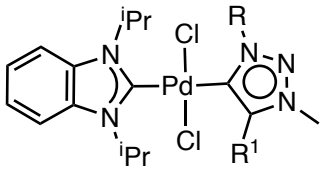

50

Figure 3.3

For triazolylidene complexes, the vast repertoire of products (and therefore ligand precursors) from CuAAC reactions is substantial. This has led to the investigation of various ligands which have the ability to be polydentate, with triazolium salts bearing phosphine,[27] carboxylate,[33] alcohol,[23] amine,[34] thioethers[35] and chiral substituents[36] all reported (Figure 3.4). Often, protecting groups are utilised in the synthesis of these triazolium salts to avoid over alkylation at potentially nucleophilic sites. The linker between the two chelating motifs can also be readily altered.

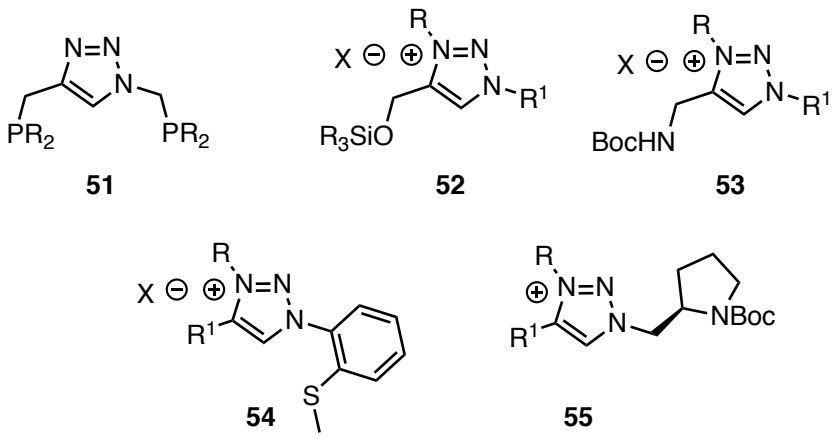

51 **52** **53**

54 **55**

Figure 3.4

Similarly to imidazolylidene NHCs, the soft base character of these formally neutral carbon donor ligands results in the most stable complexes for triazolylidenes being softly Lewis acidic metals, such as rhodium, iridium and platinum. Harder first row transition metals are more susceptible to degradation, with triazolylidene Fe(II) complexes reported to be stable in the solid state but degrading in solution.[37] The synthetic versatility which can be achieved for triazoliums, and their stability in a number of transition metal complexes, makes these perhaps the most attractive precursors for MICs, and opens a variety of potential applications.

3.1.6 Application of MICs in Ir(I) Catalysis

MICs are beginning to emerge as competent ligand motifs with a range of different metal complexes. As well as those described above, MICs have been reported for a number of applications: Pd catalysed cross couplings;[38] Ru catalysed olefin metathesis;[19] Pd/Ru hydrogenation,[39] and Ir/Ru catalysed oxidative coupling,[40,41] Ir/Rh catalysed hydrosilylation,[26,42] amongst other applications. This range of applications shows that MICs are an attractive ligand class. The combination of soft ligand character, with a high tolerance towards oxidative conditions and strong donor properties, makes for efficient catalysis by organometallic complexes bearing such motifs. Alongside the application of Ir catalysts described, both imidazolylidene and triazolylidene MICs have been reported to catalyse transfer hydrogenation of ketones and enones. In 2011, Li and co-workers reported the application of abnormal complex **6** for transfer hydrogenation (Scheme 3.18).[14] This abnormal analogue displayed higher activity than its normal-bound NHC counterpart. The reaction was tolerant of a variety of substrates, including electron-withdrawing substituents on the aryl ring to give product **56**, a cyclic ketone affording **57**, acyclic ketone to give **58** and an aldehyde substrate allowing formation of primary alcohol **59**. Additionally, enones were a compatible substrate for this process, where reduction of the C=C and C=O bonds is observed concomitantly, affording product **60**.

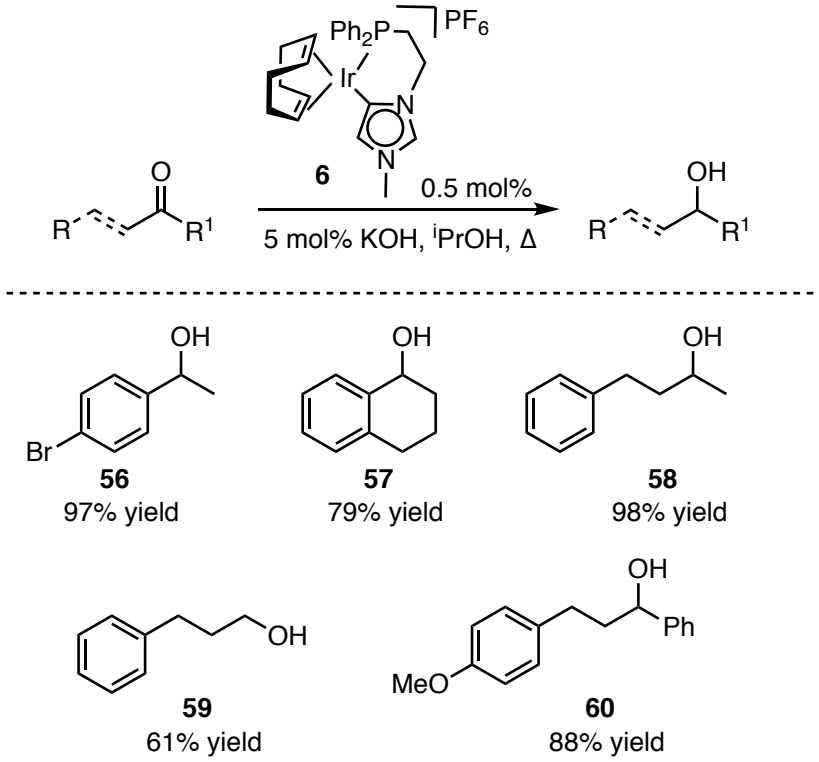

Scheme 3.18

Ir(I) triazolylidene complexes have also been applied as catalysts for transfer hydrogenation. However it was not until 2017, much later than the application of imidazolylidene MICs, that the first report was published, by Albrecht *et al* (Scheme 3.19).[23] This complex was extremely efficient in catalysing the transfer hydrogenation of ketones, aldehydes and imines. Of particular note, was the tolerance of the heteroaromatic ring in product **64**. The coordinating nitrogen in the pyridyl ring could feasibly cause issues through chelation to the iridium centre, however the reaction process was excellent yielding. Electron-withdrawing substituents such as that in **61** performed better under the reaction conditions than those with electron-donating substituents on the aryl ring.

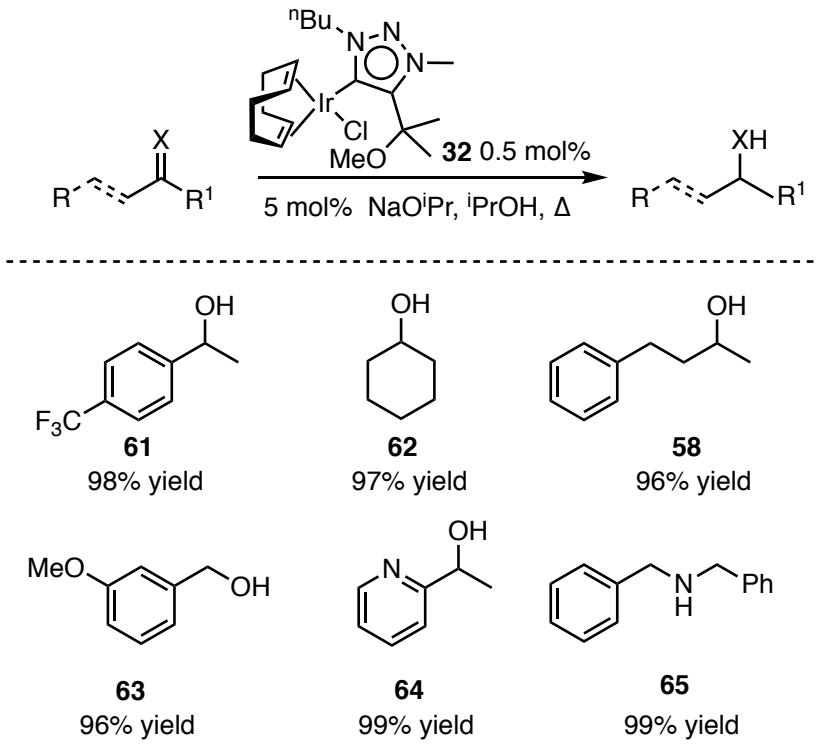

Scheme 3.19

Perhaps the most pertinent example to that of the work done by the Kerr group, is the application of an Ir(I) triazolylidene catalyst in the HIE of aromatic anilines (Scheme 3.20). [43] A base-mediated HIE process with catalyst **66** allowed excellent deuteration *ortho* to the amine in several primary aniline substrates. Secondary and tertiary anilines were not tolerated in this approach. This methodology was tolerant of a rage of aromatic substituents and functionality within the molecule. For *ortho*-methyl substituted **D71**, incorporation was observed at the methyl groups. The presence of an inorganic base was imperative for the reaction to proceed, and the authors suggested a non-covalent interaction between the K^+ counterion with both the NH_2 group and the aryl ring present on the MIC. The author additionally compared the activity of **66** with Kerr catalyst [Ir(COD)IMesCl] and observed starkly different outcomes. When the Kerr catalyst bearing an Arduengo-type NHC, was utilised in the HIE of **69**, deuteration was observed solely at the position *ortho* to the sulfonamide directing group. This shows an interesting switch in reactivity between the NHC and MIC. Whilst the omission of base makes the two processes not directly comparable, it is interesting that the MIC does not appear to direct through traditional directing groups for Ir(I)

HIE such as the amide in **D68**, or the sulfonamide in **D69**. Although this may be attributed to the more strongly coordinating amine and the presence of base within the system, it would be extremely interesting to investigate the application of **66** in a non-base mediated HIE process for anilines. The increased σ-donating ability of the MIC may be less efficient at binding a poorly Lewis basic group such as a sulfonamide, and may not allow incorporation. This being said, the differing electronic and steric environment of these types of NHCs makes them very attractive for application in HIE particularly for cases where more electron density is required at the iridium centre than traditionally afforded by an Arduengo-type NHC.

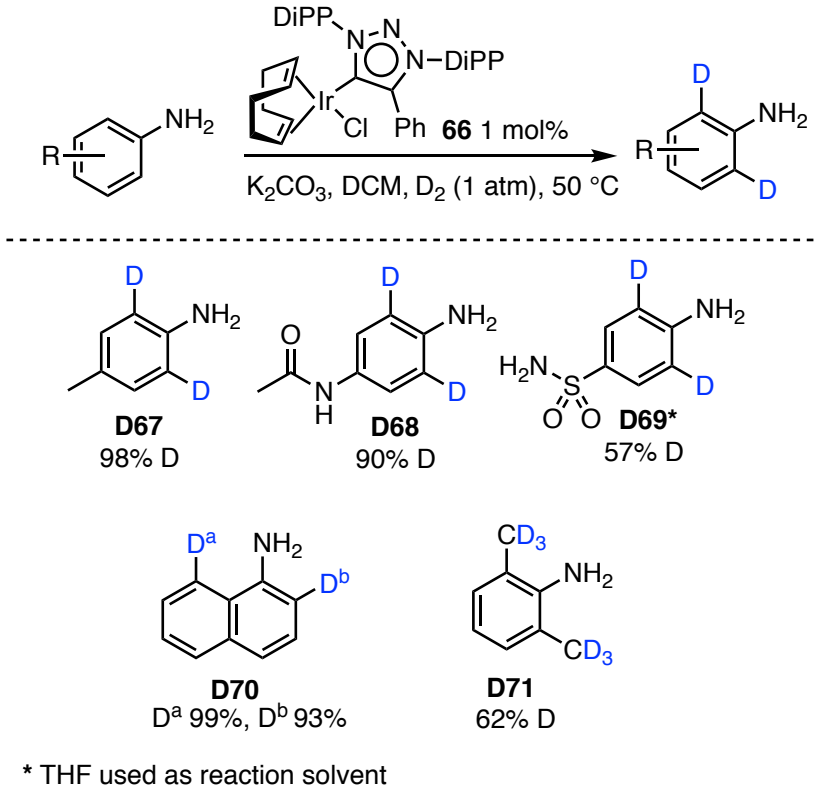

Scheme 3.20

3.2 Proposed Work

The activity of organometallic complexes in catalytic processes is highly dependent on the steric and electronic environment experienced at the metal centre. This makes ligand choice crucial, and small changes in the ligand set results in vastly altered catalytic capabilities. Through our work on the HIE of α-amino acids (described in Chapter One), we discovered that by simply altering the NHC from IMes to $IMes^{Me}$, for example, we could enhance the activity of our Ir(I) catalysts significantly, hypothesised to be a result of the increase in electron density at the metal centre, which disfavoured the formation off-cycle intermediates (Scheme 3.21).

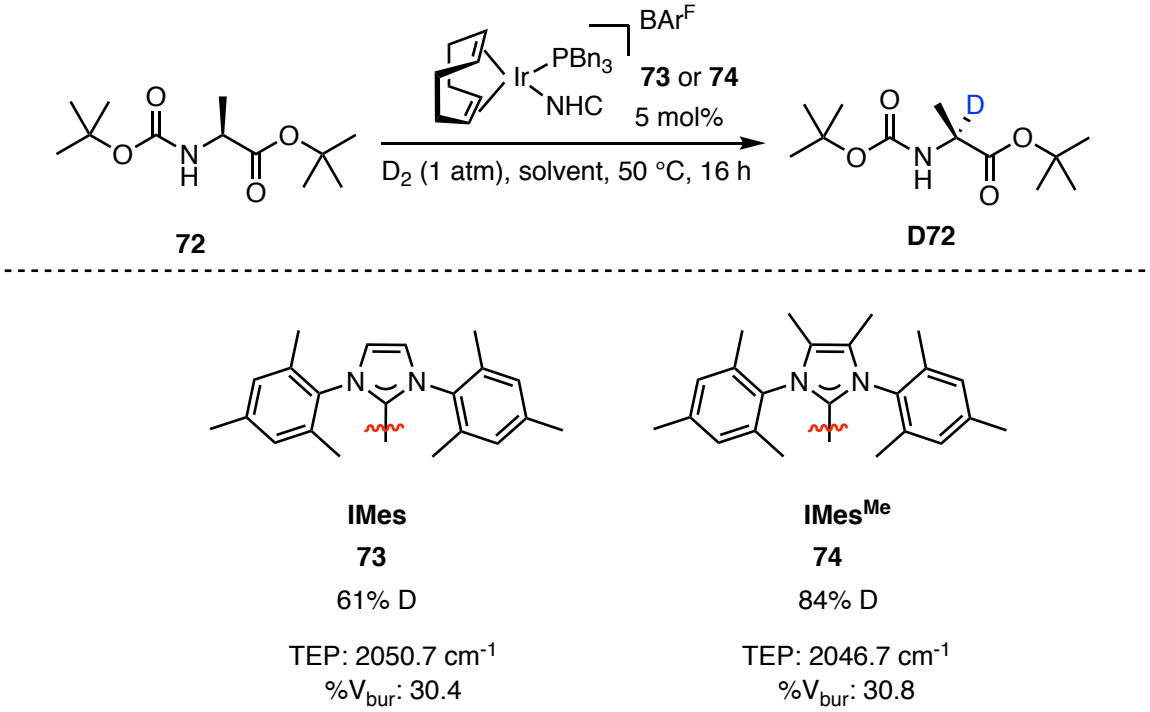

Scheme 3.21

Whilst complex **74** was an extremely efficient catalyst for the labelling of a variety of tertiary α-amino acids, as well as for the HIE of small peptides (described in Chapter Two), some limitations were observed. For residues with sp^2 substitution (such as phenylalanine), or those containing sulfur functionality, only very specific substrates were labelled efficiently.

Use of common protecting groups such as Boc- were not tolerated under the reaction conditions for these substrates. At the onset of the work described in the chapter herein, it was deemed necessary to better understand the complete drop in activity observed with these substrates. It was proposed that DFT could be utilised to probe the origin of the incompatibility of catalyst and substrate in these instances (Scheme 3.22). Throughout our investigation into the deuteration of amino acids, DFT has revealed that the formation of an intermediate where the substrate is bound through both carbonyls (**B**) results in an unproductive, off-cycle species. This limits the amount of intermediate **A** where the substrate is bound through both the directing group and a productive agostic interaction between the metal centre and C-H bond to be activated. We proposed that for larger substrates with sp^2 substitution, the agostically bound intermediate **A** may be approaching the steric limits of the current catalyst system. In contrast, for unproductive intermediate **B**, the R group is positioned away from the metal centre, and so the steric impact is less pronounced. This could lead to intermediate **B** being inherently more stable, and therefore hamper the desired C-H activation process.

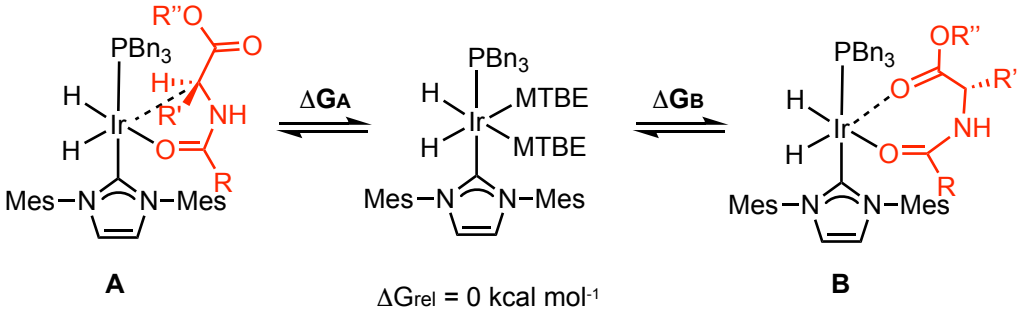

Scheme 3.22

To address this, and with the aim to develop a catalyst system tolerant of large peptide molecules, it was proposed that *in silico* screening of alternative ligand motifs could provide novel Ir(I) complexes which would successfully label these challenging substrates. If our hypothesis is correct, it would appear that a catalyst with a smaller ligand set would be required to accommodate the additional steric bulk of these substrates. Employment of a bidentate tethered system would generate a complex with significantly more space around the metal centre for substrate binding. However, use of chelated catalysts currently available

within the group in the labelling of amino acids was unfruitful. This was attributed to the high preference for the substrate to bind through both carbonyls, generating the unproductive intermediate. In a manner akin to the strategy employed for the monodentate complexes, it was hypothesised that perhaps a more electron-rich tethered ligand would allow the space required for substrate binding, whilst disfavouring the unproductive binding through both carbonyls as a result of the iridium centre being less Lewis acidic.

Substitution of either the NHC or the phosphine in the chelated systems could allow for such a more suitable catalyst system. In terms of the NHC, the emergence of MICs in the organometallic arena attracted our interest in them as a potential ligand class to utilise. The synthetic versatility of triazolium precursors, and their enhanced donor ability compared to normal NHCs, led us to hypothesise whether the use of a triazolylidene NHC in place of an imidazolylidene would result in a more effective catalyst system (Figure 3.5). Several points on the ligand could be diversified, including the aryl ring, tether length, nature of tether and alteration of the second Lewis basic site.

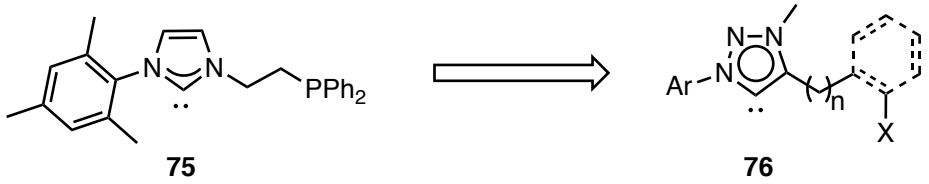

75 **76**

Figure 3.5

Upon identification of a suitable ligand by DFT screening, ligand synthesis and complexation will ensue. If successful, the novel complex will be investigated in the labelling of the previously challenging amino acid substrates.

In addition to the synthesis of novel chelated MIC systems, substitution of the imidazolylidene ligand in catalyst **73** for a triazolylidene will allow the opportunity to investigate the differences in activity and characteristics of MIC containing catalysts. This will allow insight into the potential application of these systems for HIE reactions.

3.3 Results and Discussion

3.3.1 Limitations of Imidazolylidene Ir(I) Complexes in the HIE of Amino Acids

Our investigation into the labelling of α- amino acids led to the development of novel Ir(I) catalyst **74** (Scheme 3.23). Whilst an impressive substrate scope of amino acids could be deuterated under mild conditions (a total of 18 amino acid derivatives, with various common protecting groups) there remained some limitations. As previously discussed, sp^2 containing amino acids could only be labelled successfully with small protecting groups. Whilst labelling was achieved through an acyl- protecting group, we aimed to develop a system which could tolerate larger, more common and synthetically tractable directing groups such as Boc- within these substrates. In addition to the lack of activity observed with sp^2 protected amino acids, sulfur containing residues such as methionine derivative **D80** and disulfide cystine **D81** also did not appear to be suitable substrates for HIE catalysed by **74**. It was hypothesised that the catalyst may be at its steric limit with these substrates, and unable to form the required agostic interaction, and instead be resting in an off-cycle species where the substrate is bound through both carbonyls and steric congestion at the metal centre is reduced. With a view to apply our HIE protocol to larger peptidic systems in the future, it was important to find a catalyst system which could better accommodate the steric constraints provided by these substrates.

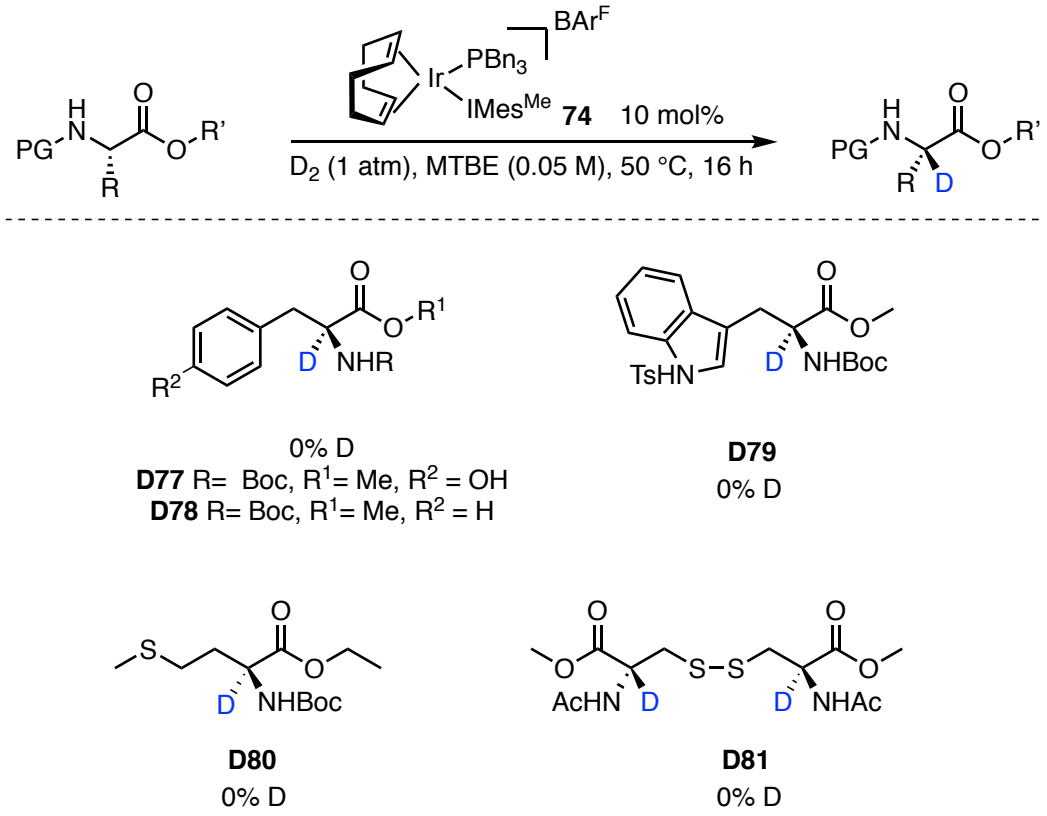

Scheme 3.23

To confirm our hypothesis suggesting larger substrates present a steric problem, we investigated these systems *in silico*. The relative Gibbs free energy and the binding energies for various substrates bound to the metal centre agostically (**A**) and in bis-carbonyl **B** were compared for phenylalanine and methionine derived substrates. For binding mode **B**, it would appear that the R group would impact the steric environment at the metal centre much less and so this mode would therefore be more stable, and indeed display a higher binding energy for the bulky substrates to the catalyst. For those substrates which contain smaller directing groups, and label effectively, this difference should be less pronounced. The energy associated with binding for each geometry was calculated using the basis set superposition error (BSSE) counterpoise method.[44] In addition, the Gibbs free energy (ΔG_{rel}) was also calculated for each structure (Table 3.2). When analyzing the ΔG_{rel} values for each binding mode **A**, and **B**, for each of the four substrates, it can be seen that for those substrates where, experimentally no deuterium incorporation is observed, the unproductive bis-carbonyl bound substrate is inherently more stable (by up to 5.8 – 9.3 kcal mol^{-1}), highlighted by substrates **78**, **80** and **81**. On the other hand, for those substrates where deuterium incorporation is observed (**82** and **83**), the ΔG_{rel} values for **A** and **B** are much closer in energy (0.5 – 0.7 kcal mol^{-1} difference between two modes). The energetic cost of binding also appears to have a

significant effect on whether labelling is observed. For sterically less encumbered substrates Ac-Phe-OMe **82** and Ac-Met-OMe **83**, the energy for binding in mode **A**, where the desired agostic interaction is formed, is more stable than the unproductive bis-carbonyl binding mode **B**. The more efficient binding, combined with the similar stabilities of **A** and **B** in this instance, results in sufficient quantities of the agostic complex **A** in solution, in turn facilitating C-H activation and successful deuterium incorporation. Akin to the ΔG_{rel} values, the differences in binding energies for **A** and **B** for the larger, more encumbered substrates Boc-Phe-OMe **78**, Boc-Met-OEt **80** and Ac-Cys-OMe)$_2$ **81** are more pronounced. For each of these substrates, ΔE_{bindB} is significantly stronger than ΔE_{bindA}. These values, combined with the enhanced stability observed for binding mode **B**, results in a potential unproductive resting state off-cycle. This greatly decreases the presence of productive binding mode **A** in solution and therefore hampers C-H activation and subsequent deuterium incorporation. Experimental and theoretical observations are in agreement, with no isotopic labelling observed for these substrates.

Table 3.2

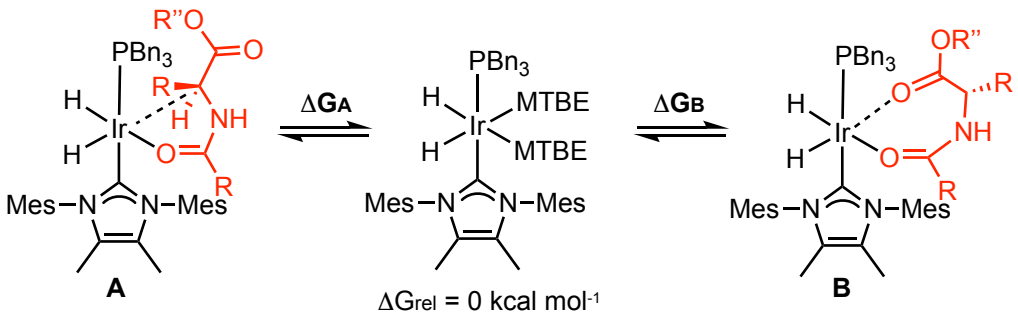

AA	ΔG_A (kcal mol^{-1})	ΔG_B (kcal mol^{-1})	ΔE_{bindA} (kcal mol^{-1})	ΔE_{bindB} (kcal mol^{-1})	%D*
Ac-Phe-OMe **82**	-14.6	-13.9	-19.7	-16.7	60
Boc-Phe-OMe **78**	-9.1	-16.8	-6.5	-14.4	0
Ac-Met-OMe **83**	-16.9	-17.4	-16.5	-12.9	59
Boc-Met-OEt **80**	-14.8	-20.6	-12.5	-15.4	0
$(Ac\text{-}Cys\text{-}OMe)_2$ **81**	-25.6	-34.9	-20.1	-26.6	0

*See Chapter One, Section 1.3.4 and 1.3.5

Further investigation of the computationally optimised structures (used to elucidate Gibbs Free energy values in Table 3.2) for both agostically-bound and bis-carbonyl bound **78** highlighted the steric influence of this substrate (Figure 3.6). When Boc-Phe-OMe **78** is bound agostically, the phenyl ring is position so as to impart a steric clash with the ligand set, and this could be the reason for both poor relative stability, and a weak binding interaction. In contrast, when **78** is bound *via* both carbonyl groups, the phenyl group is now positioned pointing out in to solvent space. No steric clash is observed with the ligand set, and therefore this conformer will be much more stable.

Agostically bound substrate 78:

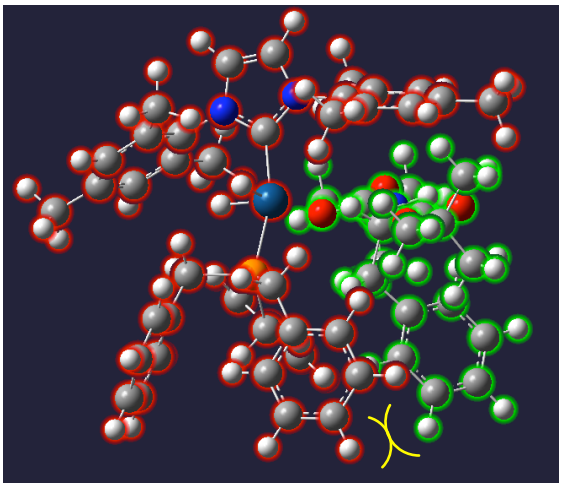

Bis-carbonyl bound substrate 78:

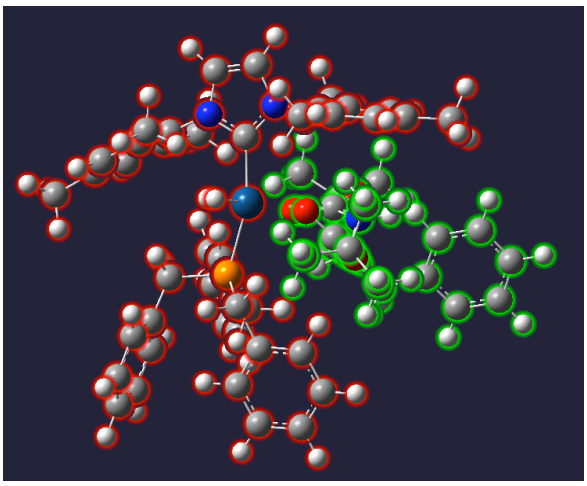

Figure 3.6

Although through judicious choice of protecting groups, isotopic labelling can be achieved for amino acids such as phenylalanine and methionine, we sought to find a catalyst system which was tolerant of larger, more common carbamate protecting groups. In addition, it appears that the monodentate catalysts are at their steric limit with these substrates, and so discovery of a smaller catalyst to allow larger peptidic substrates was targeted. Although chelated NHC/P catalysts showed poor activity in the HIE of amino acids previously (owing to the propensity to bind through both carbonyls), we hypothesised that use of an NHC/P with enhanced electron density could disfavour binding through this unproductive bis carbonyl, while concomitantly opening up the metal centre, and enabling accommodation of larger substrates.

3.3.2 In Silico Screening of Novel Chelating Ligands

Next, we investigated a range of novel chelating NHC ligands *in silico*. We calculated the binding energy of the substrate through both modes (agostically bound and bis carbonyl bound) with sterically encumbered substrate Boc-Phe-O^{t}Bu. The energy associated with binding for each geometry was calculated using the basis set superposition error (BSSE) counterpoise method.[44] In addition the Gibbs free energy (ΔG_{rel}) was also calculated for each

structure (Figure 3.7). For Ir(I) imidazolylidene catalyst **84**, it can be seen that the unproductive binding mode through both carbonyls is the stronger interaction, by 3.4 kcal mol^{-1}. Replacing the phosphine with a phenol motif in **85**, also provided a catalyst system where binding through both carbonyls on the amino acid was preferred. However, we were delighted to observe that replacement of the imidazolylidene ring in **84**, for a triazolylidene, giving **86**, provided a system, which, although the binding through both carbonyls appeared to remain the most efficient, this was only by a small margin compared to the productive binding mode (0.7 kcal mol^{-1}). At elevated temperatures, this energy difference will be negligible and according to the DFT calculations, HIE should proceed for this catalyst system. The biding energies for **86** are stronger than those observed previously, however this may aid the HIE process. Diversification of ligand **86** was then investigated, with tether length **87**, nature of tether **88** and aryl ring substituents, **89-92**, modified. Unfortunately, lengthening the tether had a detrimental effect on the preference for mode of binding, with the chelated substrate the stronger interaction. Introduction of two *iso*-propyl substituents on the aromatic ring in **89** appeared very promising initially, with the binding energies suggesting the preferred mode of binding was the productive agostic interaction. However, closer analysis of the Gibbs free energy highlighted that the substrate bound through both carbonyls was inherently more stable (by 10 kcal mol^{-1}). Ligand **91** also appeared very attractive, and indeed, was the only other ligand motif where binding through the agostic interaction was preferred. Binding to **92** appeared unfavourable.

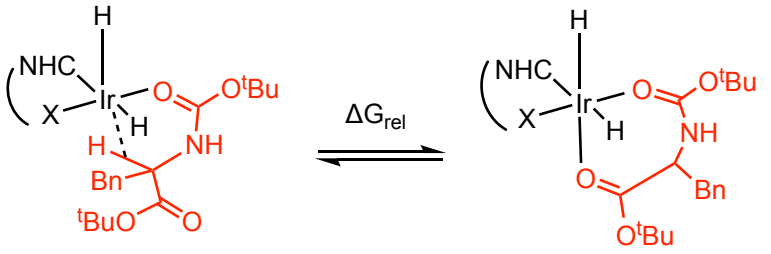

$\Delta E_{bind(agos)}$ = kcal mol^{-1} $\Delta E_{bind(chel)}$ = kcal mol^{-1}

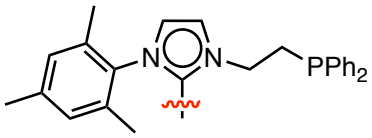

84

$\Delta G_{rel=}$ -3.96 kcal mol^{-1}

$\Delta E_{bind(agos)}$= -28.9 kcal mol^{-1}

$\Delta E_{bind(chel)}$= -32.3 kcal mol^{-1}

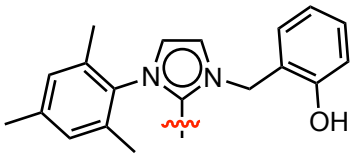

85

$\Delta G_{rel=}$ -0.98 kcal mol^{-1}

$\Delta E_{bind(agos)}$= -13.8 kcal mol^{-1}

$\Delta E_{bind(chel)}$= -19.0 kcal mol^{-1}

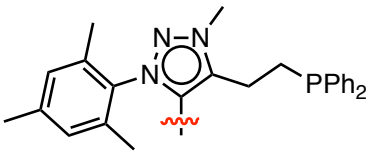

86

$\Delta G_{rel=}$ +0.97 kcal mol^{-1}

$\Delta E_{bind(agos)}$= -32.8 kcal mol^{-1}

$\Delta E_{bind(chel)}$= -33.5 kcal mol^{-1}

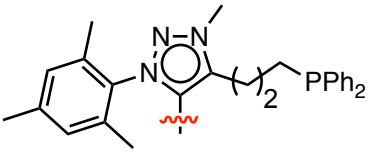

87

$\Delta G_{rel=}$ -1.85 kcal mol^{-1}

$\Delta E_{bind(agos)}$= -14.8 kcal mol^{-1}

$\Delta E_{bind(chel)}$= -21.2 kcal mol^{-1}

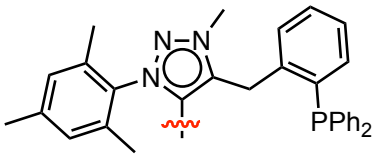

88

$\Delta G_{rel=}$ +0.40 kcal mol^{-1}

$\Delta E_{bind(agos)}$= -19.7 kcal mol^{-1}

$\Delta E_{bind(chel)}$= -21.2 kcal mol^{-1}

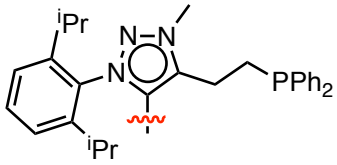

89

$\Delta G_{rel=}$ -10.12 kcal mol^{-1}

$\Delta E_{bind(agos)}$= -17.1 kcal mol^{-1}

$\Delta E_{bind(chel)}$= -11.4 kcal mol^{-1}

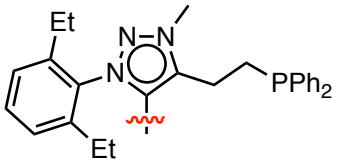

90

$\Delta G_{rel=}$ +4.92 kcal mol^{-1}

$\Delta E_{bind(agos)}$= -23.8 kcal mol^{-1}

$\Delta E_{bind(chel)}$= -24.9 kcal mol^{-1}

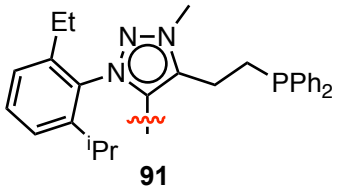

91

$\Delta G_{rel=}$ +1.41 kcal mol^{-1}

$\Delta E_{bind(agos)}$= -19.2 kcal mol^{-1}

$\Delta E_{bind(chel)l}$= -16.4 kcal mol^{-1}

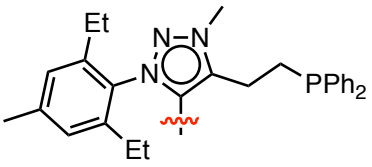

92

$\Delta G_{rel=}$ +2.56 kcal mol^{-1}

$\Delta E_{bind(agos)}$= +16.8 kcal mol^{-1}

$\Delta E_{bind(chel)}$= +2.1 kcal mol^{-1}

Figure 3.7

Although **91** appeared extremely promising, due to availability of starting materials, and with an aim to achieve a binding energy of between 25- 35 kcal mol^{-1} for the substrate to catalyst, complex **86**, bearing a mesityl ring, was first targeted (Figure 3.8). When a synthetic route was established, complex **91** would then be investigated.

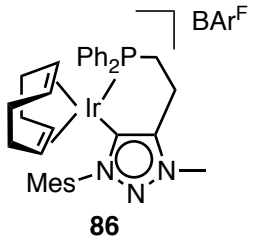

86

Figure 3.8

With our experience of chelated Ir(I) complexes limited in comparison to monodentate Ir(I) complexes, and with a complete change in the nature of the NHC to be utilised, we additionally aimed to investigate a monodentate triazolylidene complex. Monodentate imidazolylidene complexes have shown excellent utility in the labelling of amino acids, and so this strategy would provide a good benchmark and allow insight into the effect of changing the nature of the carbene ligands.

3.3.3 Investigation of a Monodentate Triazolylidene Catalyst

Owing to the lengthy synthesis associated with chelated NHC/P ligands, we sought to first investigate replacing the traditional Arduengo-type NHC in complexes **73** and **74** with the triazolylidene MIC counterpart. This would allow us to not only investigate suitable methods to complex triazolium precursors to our Ir(I) catalysts, but, additionally, would result in the opportunity to gain an understanding of their catalytic activity and properties as a comparison (Figure 3.9). This would allow us invaluable insight into the nature of the triazolylidene complexes, and enable us to apply our learnings to the synthesis of our more complex chelating MIC/P system.

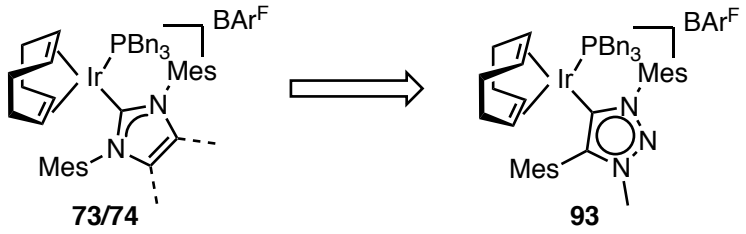

Figure 3.9

To draw comparison to the chelated ligand system identified, and indeed the traditional monodentate Ir(I) catalysts, we performed *in silico* calculations to probe the potential activity of novel triazolylidene catalyst **93** in the labelling of simple amino acid substrates (Figure 3.10). Unfortunately, when considering the labelling of Ac-Gly-OMe, the triazolylidene monodentate catalyst (TMes) appears to be less efficient compared to the traditional IMes catalyst. The unproductive bis carbonyl species **B'** displays a stronger binding energy than the productive agostically bound substrate **A'**. Drawing from our computational investigations with other iridium catalysts, this would suggest labelling levels would be lower compared to the IMes catalyst, where the productive, agostically-bound substrate **A** is a more efficient binding mode than the off-cycle intermediate **B**. In addition, for the IMes catalyst, **A** is significantly more energetically stable than **B**. In contrast, the relative Gibbs free energies for the two binding modes with the TMes catalyst display a similar level of thermodynamic stability. Further, the binding energy for the agostic complex with the TMes catalyst **A'** is extremely low (-13.9 kcal mol^{-1} compared to the IMes catalyst **A** (-20.5 kcal mol^{-1})). This would again result in lowered activity, with solvent displacement through substrate coordination a significant challenge in this instance.

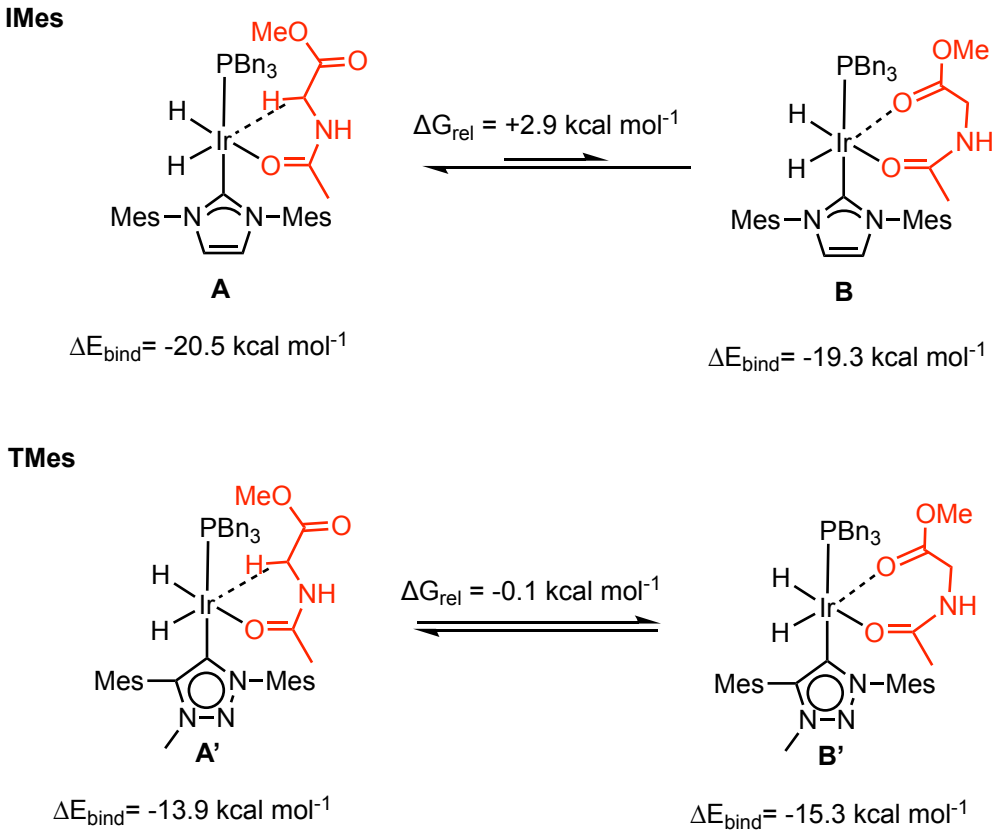

Figure 3.10

The competency of the monodentate triazolylidene catalyst with additional amino acid substrates was further probed (Table 3.3). Pleasingly, for substrate Ac-Gly-O^{t}Bu **95**, the DFT results imply that this could be a competent substrate and catalyst combination for successful HIE. Whilst the binding energies are not as strong as would be preferable, the agostically bound substrate displays a stronger binding energy $\Delta E_{bindA'}$ compared to the off-cycle species $\Delta E_{bindB'}$. Experimental investigation of the HIE of this process with catalyst **93** under the previously optimised conditions would be very beneficial and allow information on whether these catalyst activate and perform similarly to their imidazolylidene counterparts. It was unfortunate to note that phenylalanine substrates **96** and **97** did not appear to bind efficiently to the metal centre through *in silico* screening. In addition, in agreement with the imidazolylidene analogues, bis-carbonyl species **B'** appeared to be the most efficient binding mode in these substrates, regardless of the nature of the protecting groups (in a departure to the trend observed with imidazolylidene analogues).

Table 3.3

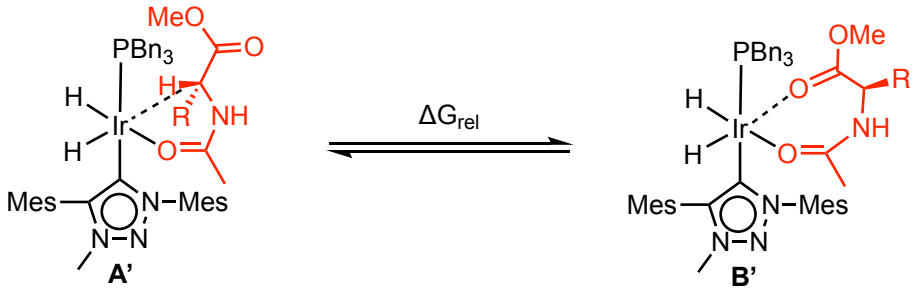

Entry	AA	ΔG_{rel} (kcal mol^{-1})	$\Delta E_{bindA'}$ (kcal mol^{-1})	$\Delta E_{bindB'}$ (kcal mol^{-1})
1	Ac-Gly-OMe **94**	-0.1	-13.9	-15.3
2	Ac-Gly-O^{t}Bu **95**	+1.9	-15.3	-14.0
3	Ac-Phe-OMe **96**	-4.9	-10.0	-16.9
4	Boc-Phe-O^{t}Bu **97**	-4.3	-6.9	-11.4

Although from the small substrate scope screened *in silico*, results for catalyst **93** did not suggest there would be much activity with several substrates, the synthesis of this complex was nonetheless deemed important. As alluded to earlier, investigation of the synthesis, activation and characteristics of this complex would enable a more thorough understanding of this class of novel complexes.

To facilitate the synthesis of complex **93**, synthesis of the required Mes-acetylene for the key CuAAC reaction was undertaken. Initial formation of the TMS- protected alkyne **99** was investigated (Table 3.4). Use of literature conditions[45] led to a poor reaction yield of 14% (entry 1), with 70% starting material isolated post reaction. Alternative conditions from the published literature[46] were also investigated however no desired product was isolated in this case (entry 2). Performing the Sonagashira coupling in neat triethylamine at a raised temperature of 70 °C pleasingly allowed access to **99** in a good yield of 69% (entry 3). Upon increasing the scale of the reaction to 8.70 mmol, excellent yields of product could be observed (entries 4 and 5).

Table 3.4

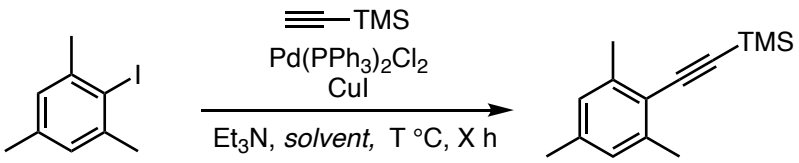

98 **99**

Entry	Conditions	Scale (mmol)	Yield(%)	Yield SM (%)
1	DMF, 50 °C, 16 h	2.18	14	70
2	rt, 3 h	2.18	-	89
3	70 °C, 16 h	2.18	69	-
4	70 °C, 16 h	8.70	90	-
5	70 °C, 16 h	8.70	94	-

With **99** in hand, we began the remaining synthetic sequence towards the desired triazolium salt (Scheme 3.24). Deprotection of **99** to afford the terminal alkyne **100** proceeded in moderate yields on both small and larger scales. The key CuAAC reaction with Mes-N_3 **101** afforded triazole **102** in good yield on large scale. Subsequent methylation of the most nucleophilic site yielded triazolium salt **103**. The resultant salt then underwent salt metathesis to generate the desired triazolium precursor **104** in excellent yield on small scale. This synthesis is modular and the aryl groups or nitrogen substitution could be altered with ease to provide a quick and efficient synthesis of a variety of triazolium salt precursors, as has been discussed and reported within the literature.

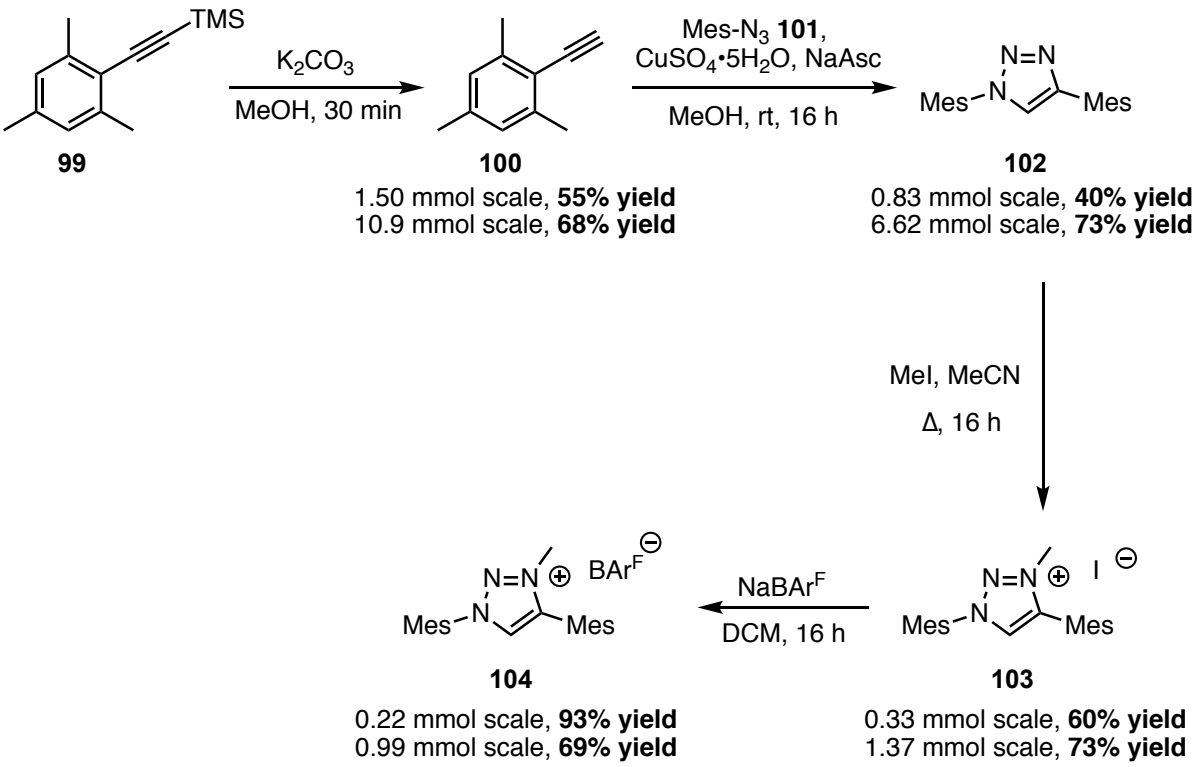

Scheme 3.24

Next, we turned our attention to the complexation of **104** and the resultant formation of desired monodentate catalyst **93**. Previously within the Kerr group, synthesis of NHC/phosphine monodentate catalysts has been carried out in one of two ways. The first is initial formation of the chlorocarbene complex, followed by phosphine displacement. The second utilizes a one-pot procedure where both the NHC and phosphine ligand are complexed concomitantly. The decision was made to attempt complexation *via* the second route as this would be more comparable to the proposed complexation of a chelated triazole/phosphine motif where both the NHC and phosphine functionality are present within the same ligand. To our delight, catalyst **93** was accessed in moderate yield on small scale. Increasing the scale moderately to 0.40 mmol, led to an excellent increase in yield to 72%. Also pleasing, was the stability of complex **93** to silica gel purification, in accordance with the imidazolylidene analogues. In addition, the complex was similarly air stable.

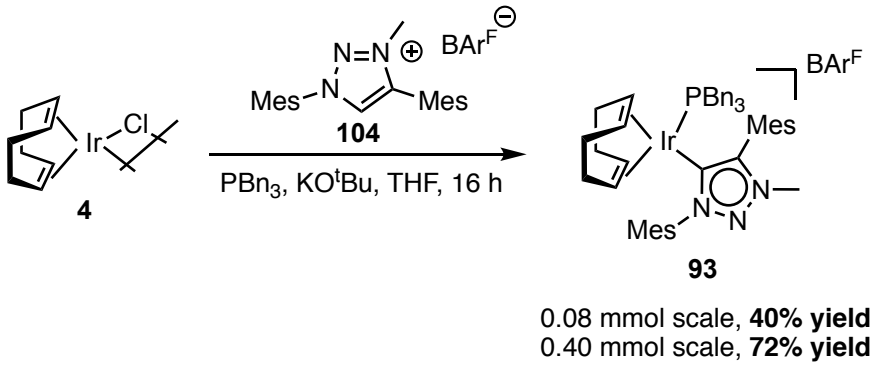

Scheme 3.25

*3.3.4 Isotopic Labelling with Novel Catalyst **93***

To confirm the hypothesis drawn from our computational studies, and to investigate the activation of our novel complex **93**, we next applied the complex in the HIE reaction of Ac-Gly-O^{t}Bu **105** (Scheme 3.26). It was extremely encouraging to note that the levels of labelling achieved with catalysts **73** and **93** were near identical, highlighting the competency of the triazolylidene monodentate complex under our HIE conditions. It was important to confirm that complex **93** could be activated and catalyse the reaction in a manner akin to **73**. This being said, no further labelling was investigated with this complex for amino acid labelling, as computational probing did not suggest this motif would outperform the imidazolylidene catalysts in any of the systems examined. This lower proposed activity does not detract from the discovery of this novel ligand set, and this catalyst may find application for a variety of other substrates suitable for HIE. In addition, the successful complexation and stability of complex **93** encouraged us in the targeting of chelated MIC/P ligands, where the likelihood of them being competent catalysts for the HIE of amino acids and peptides is enhanced, as suggested by DFT calculations. Before targeting these motifs, we wanted to further investigate the steric and electronic properties of Ir(I) catalysts bearing a triazolylidene MIC to confirm that we were indeed accessing complexes with higher levels of electron density at the metal centre through increased donation from the MIC, compared to an Arduengo-type NHC.

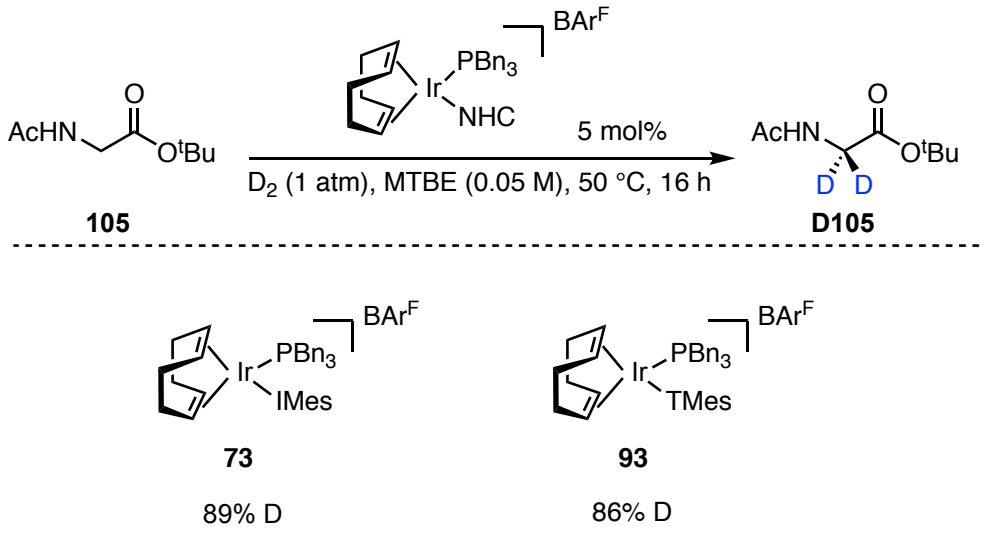

Scheme 3.26

3.3.5 Characterisation of Triazolylidene Complexes

To better analyse the effects of substituting a normal NHC for an abnormal carbene ligand, studies into the steric and electronic properties of various Ir(I) complexes was desired. Considering a series of complexes, we wanted to confirm whether the electronics were significantly altered through modification off the NHC (Figure 3.11). Additionally, we aimed to investigate the steric influence of each NHC.

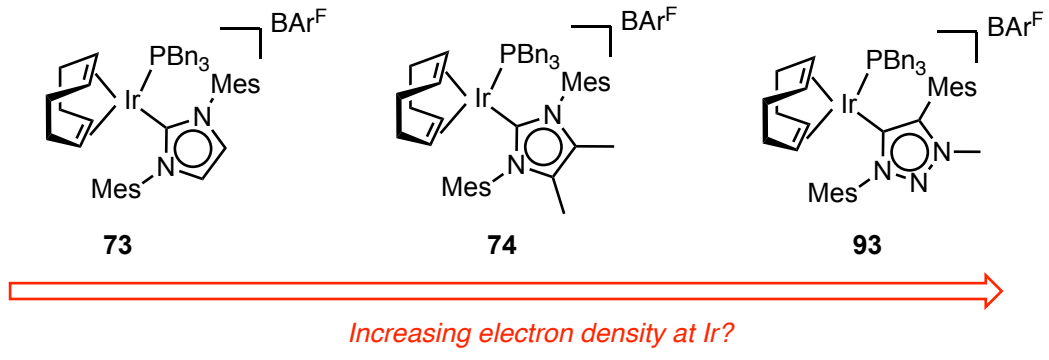

Figure 3.11

Initially, the overall σ-donating ability was investigated through the formation of Ir(III) dihydride species. Previously, analysis of NMR measurements of these catalytically relevant species have been utilised, with hydride ligands being solely σ-bonding in nature, allowing analysis of the σ-donating ability of the NHC.[47,48] These complexes are stable in solution for prolonged periods of time and are generated in monomeric form by application of acetonitrile solvent to stabilise the intermediate. To investigate the differences in the NHC's donating ability, both NHC/P systems and NHC/Cl systems were investigated. To facilitate this, synthesis of the required triazolylidene/chloride complex was required (Scheme 3.27). Triazolium salt **103** was deprotonated, and the free carbene reacted with $[Ir(COD)Cl]_2$ **4** to generate the desired neutral complex **106** in a moderate 62% yield.

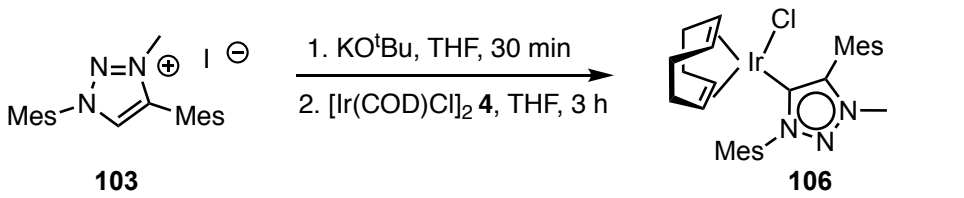

103 **106**

0.22 mmol scale, **62% yield**

Scheme 3.27

Returning to the formation of the Ir(III) dihydrides, this process was practically very accessible. A small quantity (around 10 mg) of each pre-catalyst was dissolved in deuterated acetonitrile in an oven dried NMR tube. H_2 gas was bubbled through the solution through a rubber septum allowing generation of the activated dihydride complex (Scheme 3.28). Examining the hydride shifts in the ^{1}H NMR spectra for a series of NHC/P activated catalysts **107-110**, where we would expect the complexes to become more electron-rich through the series, revealed that indeed changing the phosphine from PPh_3 in **107** to PBn_3 in **108** did indeed afford a more electron rich complex. Additionally, introduction of methyl substituents on the NHC backbone in **109** resulted in a more σ-donating complex. Triazolylidene complex **110** was an anomaly in this series of complexes, with the hydride shifts appearing to suggest this complex is less σ-donating than the imidazolylidene counterparts **108** and **109**. This is contrary to what we would expect for the triazolylidene, where less heteroatom stabilisation

should result in a more donating NHC. NHC/Cl complexes **111-113** were also investigated, with a similar trend observed.

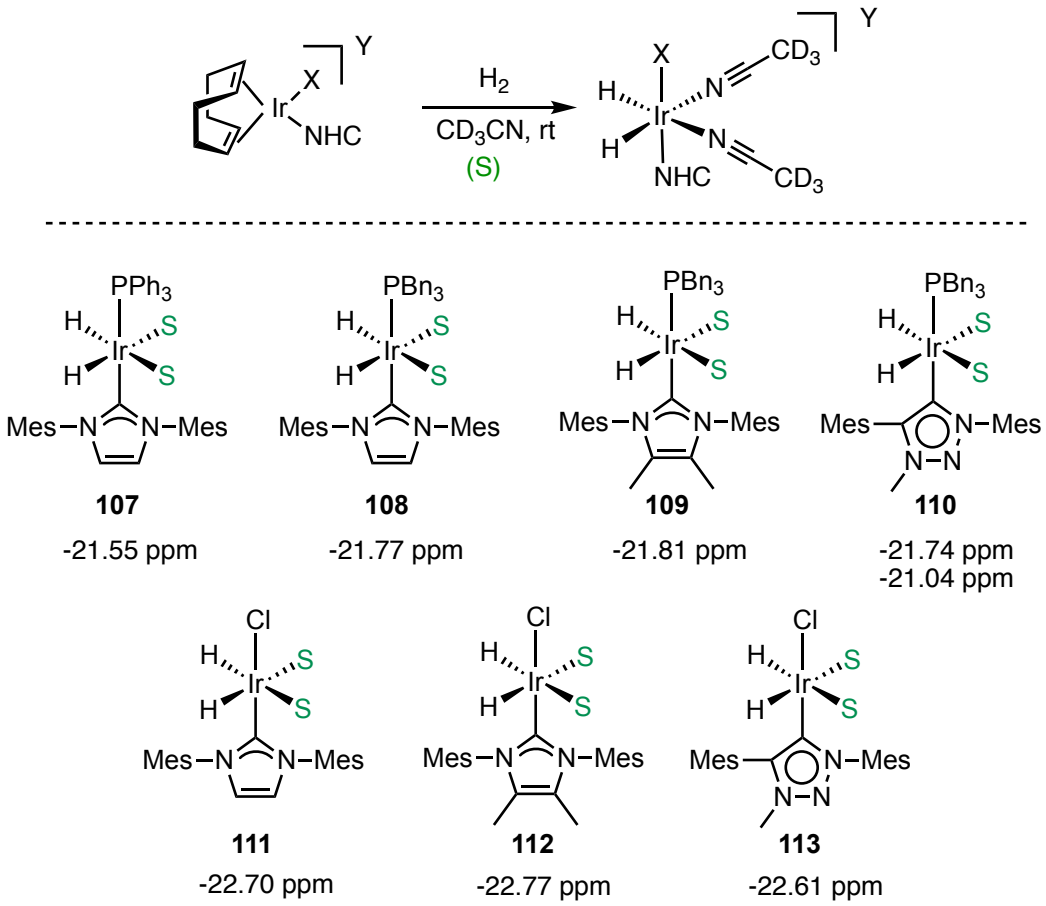

*Complexes **107-110** are cationic, anions ommited for clarity*
*Complexes **111-113** are neutral with no Y counterion*

Scheme 3.28

Whilst the hydride shift of the Ir(III) dihydrides provides information on the σ-donating ability of a ligand, it does not take into account π-backbonding. There is expected to be significant differences in the π-acidity between these NHC classes, and so it was deemed important to investigate them further. As previously discussed, the CO stretches of Ir complexes can be utilised as a direct probe for the electronic properties of ligands. Various reports of such studies have previously been made, including triazolylidene-ligated Ir complexes. We further hoped to examine our catalyst series to obtain more information on the electronic differences observed. Initially, NHC/Cl complexes were investigated (Table

3.5). Synthesis of the required carbonyl complexes and subsequent analysis by infrared (IR) spectroscopy allowed the CO vibration frequencies to be collected. The CO stretching frequencies were lower for the triazolylidene complex **116** compared to the imidazolylidene counterparts **114** and **115**. TEP values could then be calculated for each complex. The vibrational study was in agreement with previous studies into the electronic properties of these NHCs,[28] where the application of a triazolylidene MIC results in a more electron rich complex as a result of the ligands superior donor properties.

Table 3.5

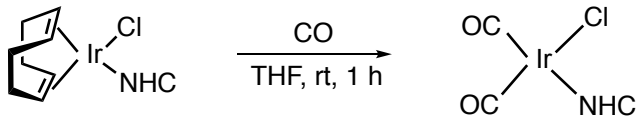

Complex	NHC	Yield %	ν(CO)/cm^{-1}	TEP/cm^{-1}
114	IMes	86%	2056, 1969	2041
115	IMes^{Me}	66%	2052, 1967	2038
116	TMes	36%	2052, 1965	2037

In an extension to this work, we synthesised the CO complexes in the NHC/P states phosphine, to further probe these partnerships.[48] The chloro-carbonyl complexes previously generated were dissolved in DCM and reacted with the required phosphine to generate the desired complexes. Once again, the CO vibrational shifts were compared *via* IR analysis (Table 3.6). Pleasingly, these results were in accordance with the data generated from the di-carbonyl complexes generated from the NHC/Cl precursors, where the triazolyidene containing (TMes) **120** complex was the most electron rich of the series. Differences between imidazolylidene complexes **117**, **118** and **119** were also observed in accordance with the previously generated data.

Table 3.6

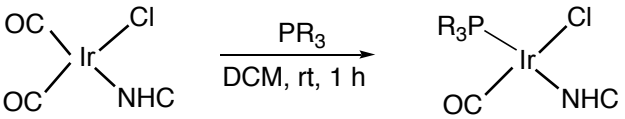

Complex	NHC	PR_3	Yield %	ν(CO)/cm^{-1}
117	IMes	PPh_3	89	1937
118	IMes	PBn_3	71	1931
119	$IMes^{Me}$	PBn_3	58	1929
120	TMes	PBn_3	56	1928

The results generated through the three distinct investigations into the electronic properties of this range of Ir(I) catalysts developed highlighted the need for a multivariant approach to investigation. This allows a better overall appreciation for the understanding of the properties of these catalysts. Whilst the investigation of hydride shifts in Ir(III) dihydrides displayed discrepancies in the expected trends, the analysis of CO complexes allowed a more robust general analysis of the electronic properties.

Alongside altering the electronic properties of the ligand, the use of a triazolylidene NHC in place of an imidazolylidene NHC may also significantly alter the steric environment. Percentage buried volume ($\%V_{bur}$) calculations were utilised to gain more information regarding any steric differences between the triazolylidene/imidazolylidene complexes. Akin to previous $\%V_{bur}$ study, DFT calculations were utilised to generate an optimised geometry of a bis-solvated intermediate which is part of the proposed catalytic cycle (Figure 3.12).

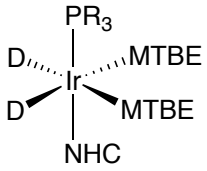

Figure 3.12

SambVca online software was then utilised to calculate the $\%V_{bur}$ values from the optimised coordinates. In addition to investigating the steric environment of the monodentate complexes, the proposed chelating MIC/P system was also investigated (Table 3.7). Whilst the $\%V_{bur}$ for complexes **73** and **74**, bearing imidazolylidene ligands were similar, despite the addition of methyl substituents on the backbone of **74**, triazolylidene **93** displayed a decreased $\%V_{bur}$, suggesting this ligand is smaller than its imidazolyl counterparts. This catalyst may therefore find application for substrates where the directing group is sterically encumbered, or activation through a larger metallocycle (for example a 6-mmi) is required. Interestingly, chelated complex **86** has a significantly smaller ligand sphere compared to the monodentate complexes, as hypothesised, and it is hoped this would allow accommodation of larger amino acid and peptide substrates.

Table 3.7

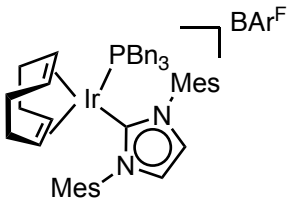

73

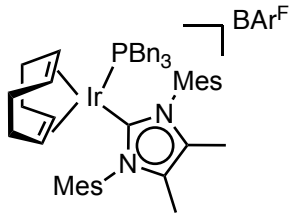

74

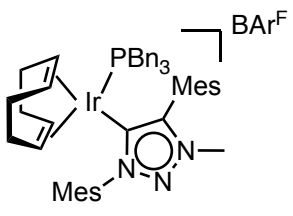

93

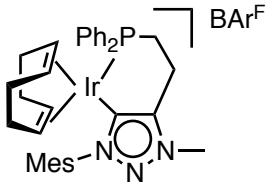

86

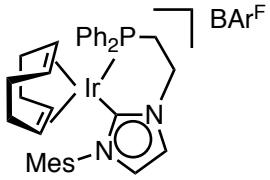

84

Complex	NHC	%V_{bur}P	%V_{bur}NHC	%V_{bur}P+NHC
73	**IMes**	24.6	30.4	55.0
74	**IMes^{Me}**	24.5	30.7	55.2
93	**TMes**	24.8	29.0	53.8
86	**TMes/P**	-	-	48.6
84	**IMes/P**	-	-	49.1

3.3.6 Attempted Synthesis of MIC/P Complex

With an increased understanding of the behaviour and properties of an Ir(I) TMes complex, we embarked on the synthesis of a chelated triazolylidene ligand. To enable synthesis of MIC/P complex **86**, triazolium salt **121** was targeted. The initial retrosynthetic approach to this ligand is highlighted in Scheme 3.26. Salt **121** would be accessed from phosphination of a suitable leaving group, X, in **122** with subsequent salt metathesis to the BAr^F analogue.

Iodide salt **122** could be synthesised from manipulation of alcohol **123**. Triazolium **123**, bearing a pendant alcohol has previously been prepared within the literature and is accessed through a CuAAC reaction of azide **101** and alkynyl-alcohol **124**, followed by methylation of the nitrogen atom with methyl iodide.[49] This route employs late stage phosphination of the ligand motif, preventing this group being taken through the Click reaction, which could cause significant issues. In addition, for previous Ir(I) chelating catalysts such as **84**, phosphination is the penultimate step, allowing limited exposure to silica for this oxidation-sensitive functionality.

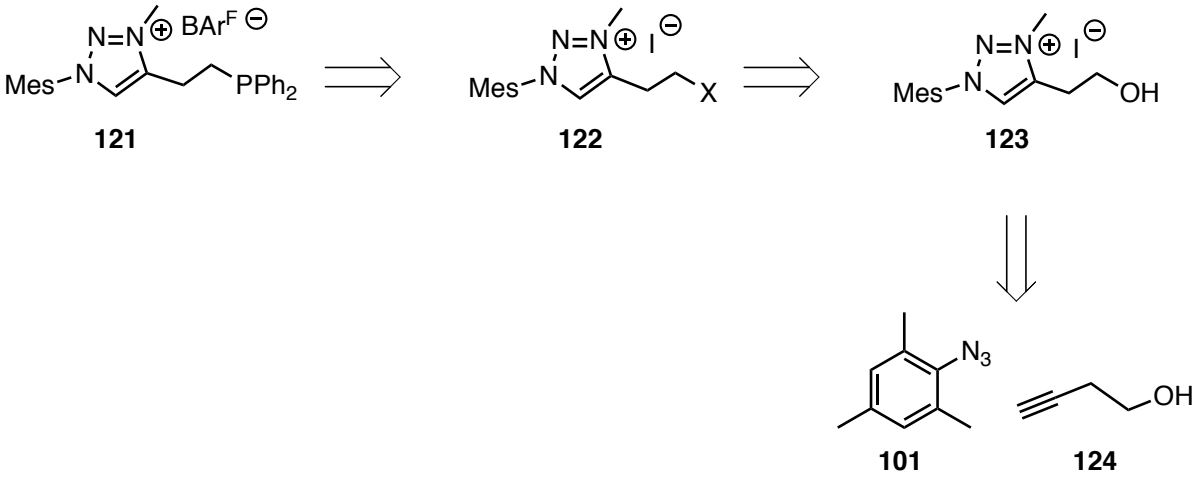

Scheme 3.29

Following the literature precedent, our synthesis began with copper-catalysed CuAAC reaction of alkyne **124** with Mes-N_3 **101** (Scheme 3.30).[49] This proceeded in moderate yields on both small and larger scale. Triazole **125** was then methylated according to the literature procedure with methyl iodide in refluxing acetonitrile, yielding iodide salt **123** in good to moderate levels. Subsequent bromination to **126** showed poor reproducibility, with rapidly decreasing yields observed at a small increase in scale. Bromide salt **126** was extremely hygroscopic and difficult to handle. As a result, this precursor was synthesised and rapidly utilised in the next step. To our disappointment, phosphination conditions previously ustilised by our group for the synthesis of chelated imidazolium/phosphine ligands proved unfruitful in the synthesis of **121**. Although employed in our previous synthetic endeavours, this step

has always been somewhat capricious. Introduction of the phosphine at an earlier stage of the reaction, on substrates which were not hygroscopic in nature, was thus targeted.

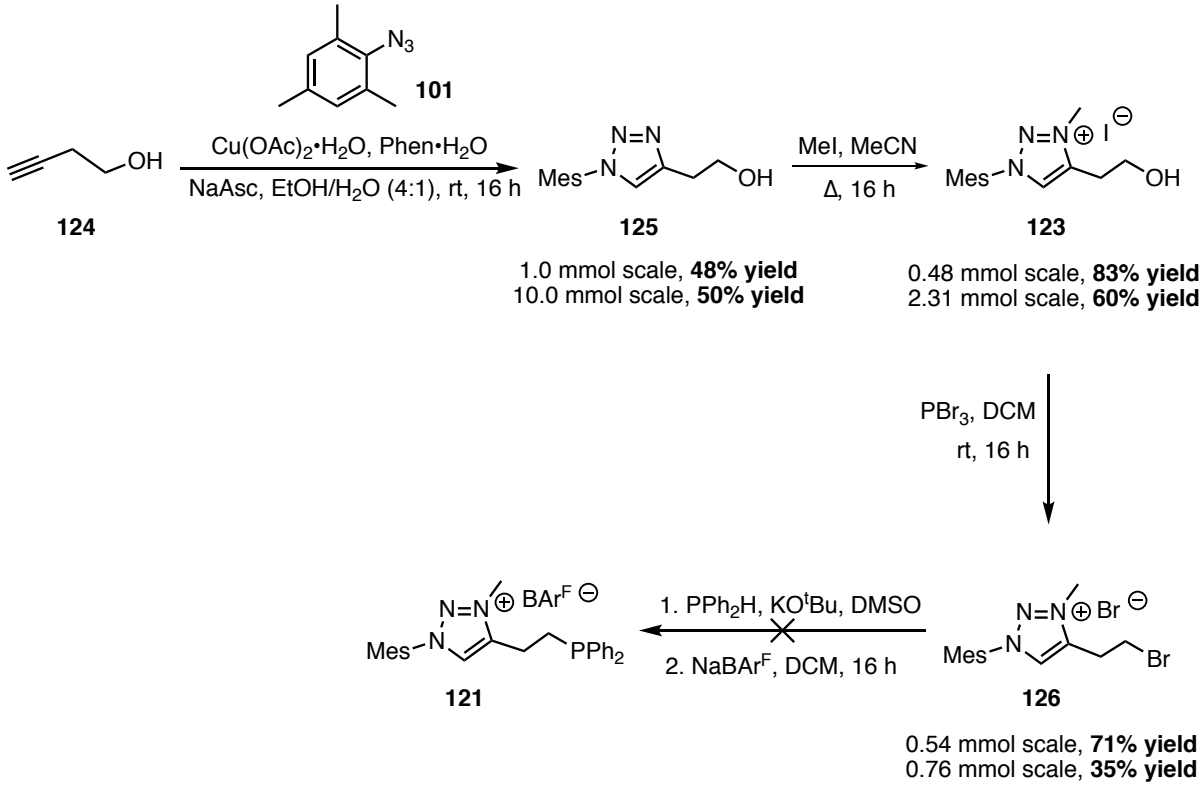

Scheme 3.30

To enable installation of the phosphine at an earlier stage of the synthetic sequence, a protected phosphine was required to enable alkyne **129** to be suitable for CuAAC chemistry (Scheme 3.31). Similarly to the previously investigated route, the ligand precursor **121** would be accessed from an iodide salt **127** *via* salt metathesis. **127** could be generated through methylation and reduction of the borane protected functionality in **128**. Triazole **128** could be synthesised through CuAAC reaction of **101** and **129**. Borane is a commonly employed protecting group for phosphines, allowing modification of the reactivity at phosphorous as well as providing air and moisture stability.[50] Deprotection of borane protecting groups is usually achieved through application of a Lewis basic amine to generate the free phosphine and resultant amino-borane.

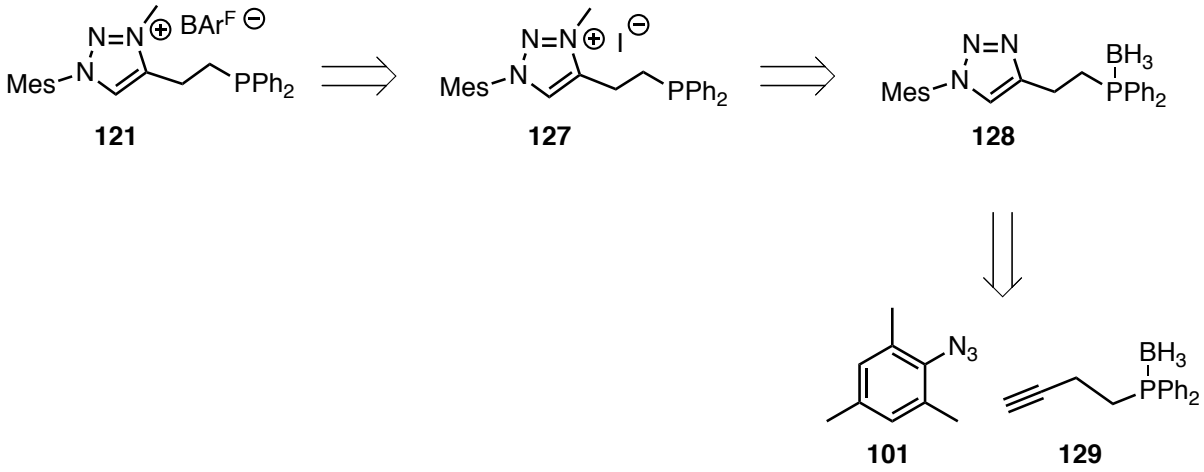

Scheme 3.31

Novel alkyne **129** was synthesised in four steps from alkynyl alcohol **124** (Scheme 3.32). Tosylation of this motif proceeded well on large scale, with up to 70% yield achieved. TMS protection of the terminal alkyne in **130** proceeded in excellent yields of up to 90% on smaller scale to generate **131**. Phosphination of tosylate **131** initially proceeded in an extremely poor yield of 15%. Increasing the scale of the reaction enhanced the yield of **132** to a maximum of 40%. Finally, deprotection of the silyl protecting group in good yield allowed synthesis of required alkyne **129**.

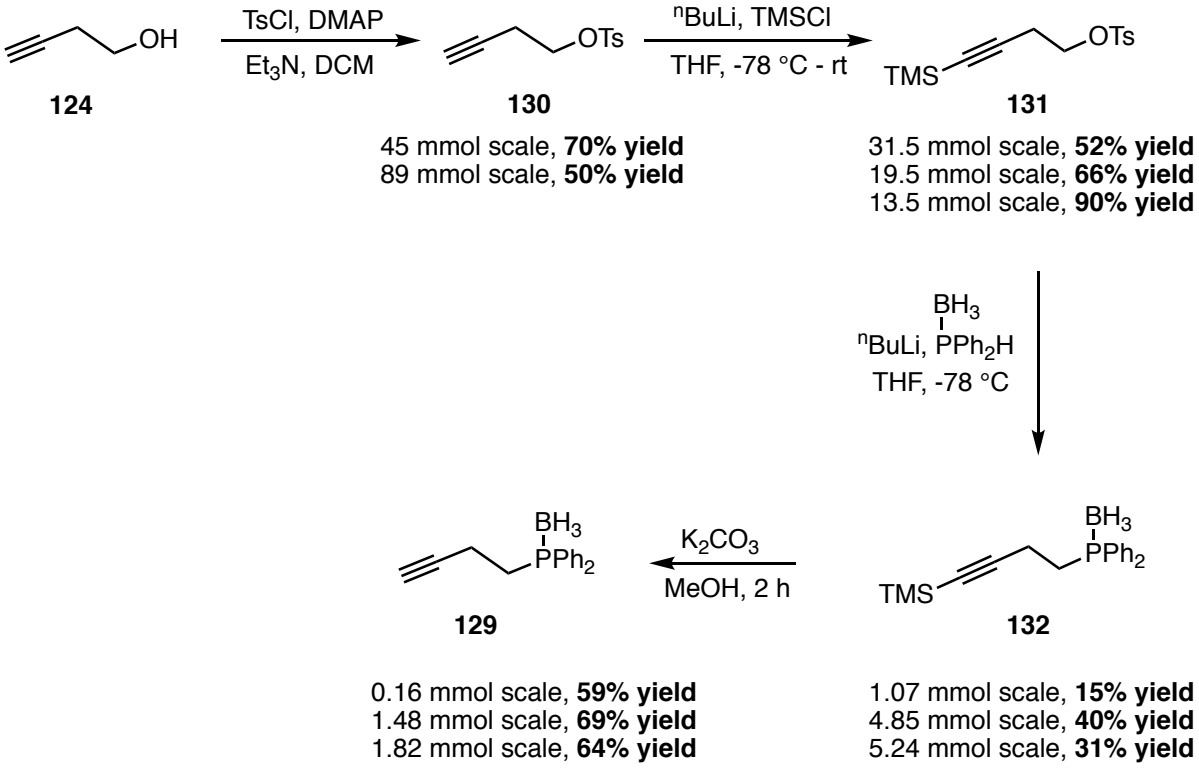

Scheme 3.32

With alkyne **129** in hand, synthesis of triazole **128** bearing a protected phosphine, was synthesised *via* CuAAC reaction in moderate yields of 40 and 34% (Scheme 3.33). Although low yielding, investigation of the remainder of the synthetic route was the priority, with optimisation of the CuAAC conditions planned if the synthesis of **121** through this route was viable. Disappointingly, salt metathesis of **133** to BAr^F analogue **134** proceeded in extremely low yield. Subsequent deprotection with DABCO was unfruitful, with a complex mixture of products isolated from the reaction mixture. At this point, encouraged by the synthetic route so far, we next envisaged investigation of the phosphine protected as its corresponding oxide, as this would allow significantly more reduction methods to generate the free phosphine later in the synthesis.

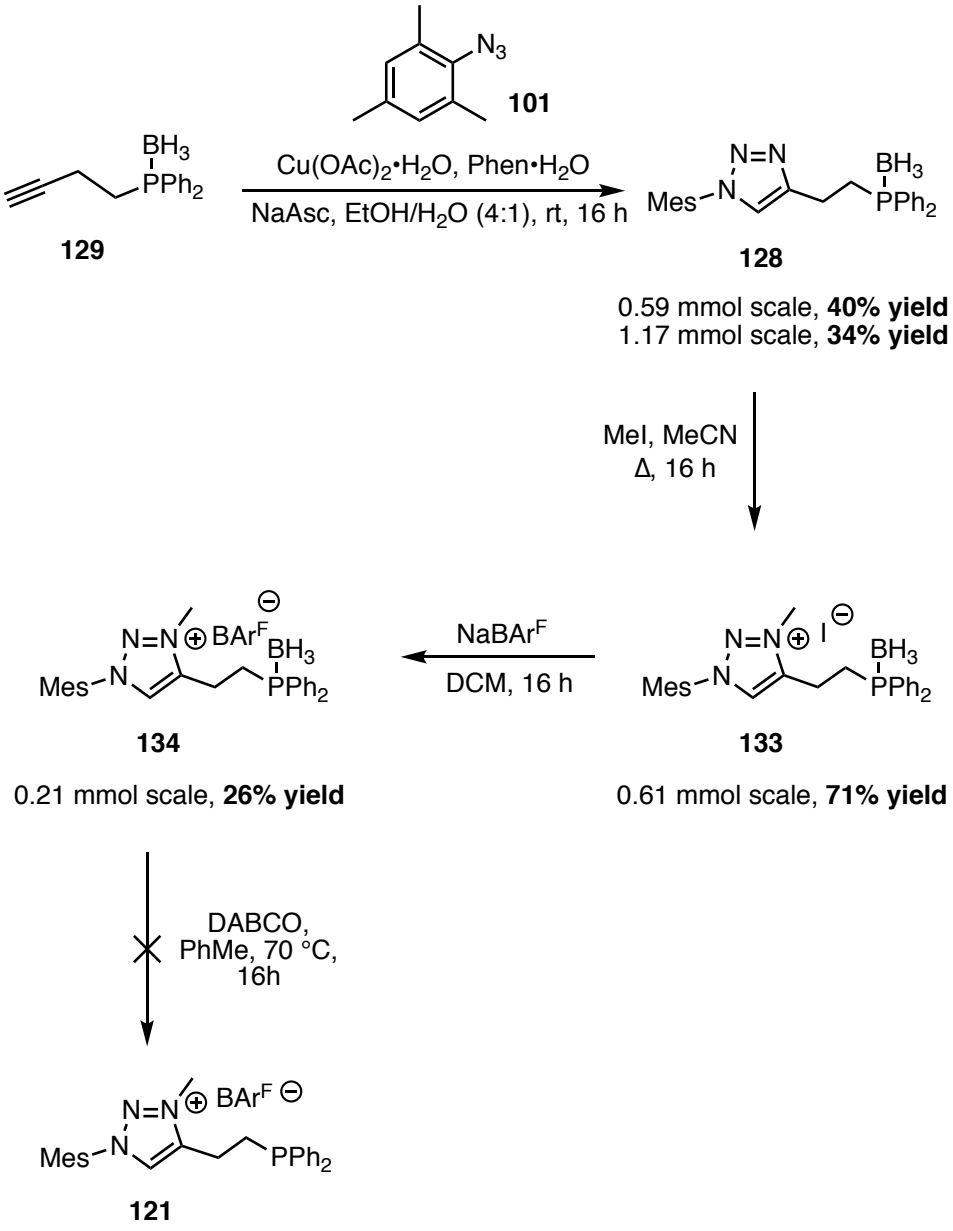

Scheme 3.33

Modification of the protecting group on the phosphine to the phosphine oxide would allow a very similar synthetic pathway to that investigated for the borane-protected counterpart (Scheme 3.34). Reduction of the phosphine oxide could be investigated on either the iodide or BAr^F salt, and various literature precedent phosphine oxide reduction are available for investigation. Synthesis of **134** was required to enable this synthetic sequence.

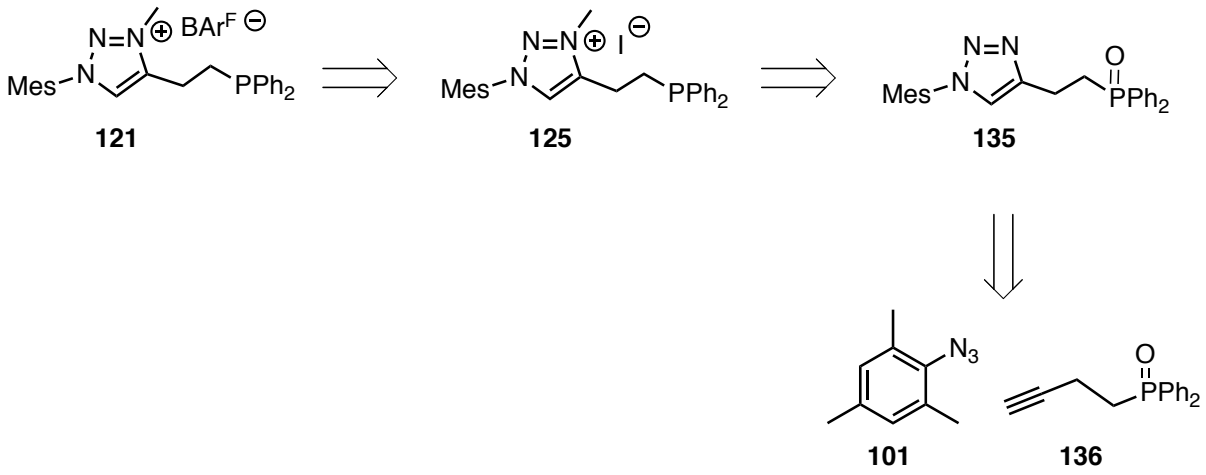

Scheme 3.34

Generation of the required alkynyl-phosphine oxide click precursor **136** proved to be challenging. Employing slightly adapted literature conditions for the synthesis of this compound (where previously a bromide electrophile was utilised) resulted in no product formation (Scheme 3.35).[51] This was disappointing as, if successful, this would have been an extremely concise synthesis of our desired alkyne.

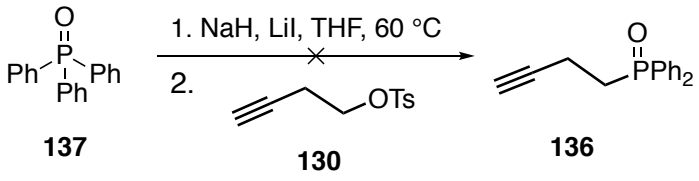

Scheme 3.35

Other methods commonly employed within the literature for similar compounds were also investigated to no avail (Scheme 3.36).[52] Deprotonation of **138** under basic conditions and reaction with **138** unfortunately did not lead to the successful synthesis of alkyne **136**. At this stage, we decided to employ a similar strategy to that utilised in the formation of the borane-protected phosphine.

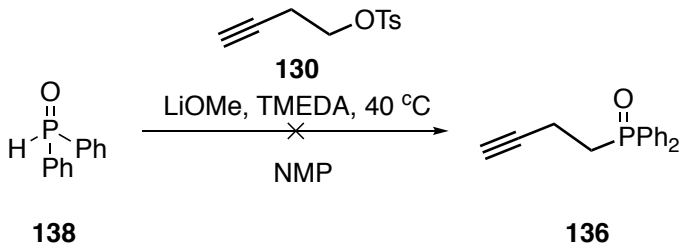

Scheme 3.36

Although this synthetic procedure was lengthy in comparison to the previously attempted literature conditions, to our delight, synthesis of **136** could be achieved *via* our previously utilised phosphination conditions (Scheme 3.37). Order of addition was critical to afford pure isolated product, with addition of the electrophile to the deprotonated nucleophile most successful. Slow addition was also necessary to yield **137** in moderate quantities. Deprotection of the TMS group using K_2CO_3 afforded the desired alkyne **136** in excellent yield.

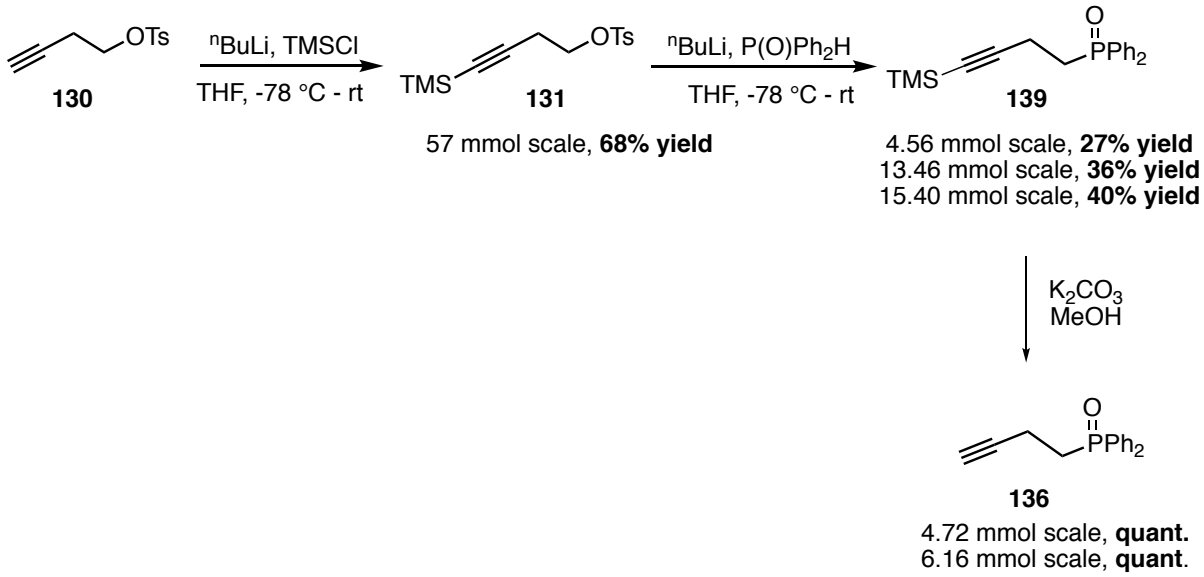

Scheme 3.37

To our delight, when the phosphine oxide was employed in place of the borane protected phosphine in the click reaction, significantly better yields were achieved, with up to 87% of triazole **135** generated (Scheme 3.38). Methylation to iodide salt **140** also proceeded in excellent yield on small scale. Subsequent salt metathesis also yielded **141** in very high yield.

At this stage of the synthesis, we decided to investigate both the iodide salt **140** and the more soluble BAr^F salt **141**, in the reduction of the phosphine oxide motif.

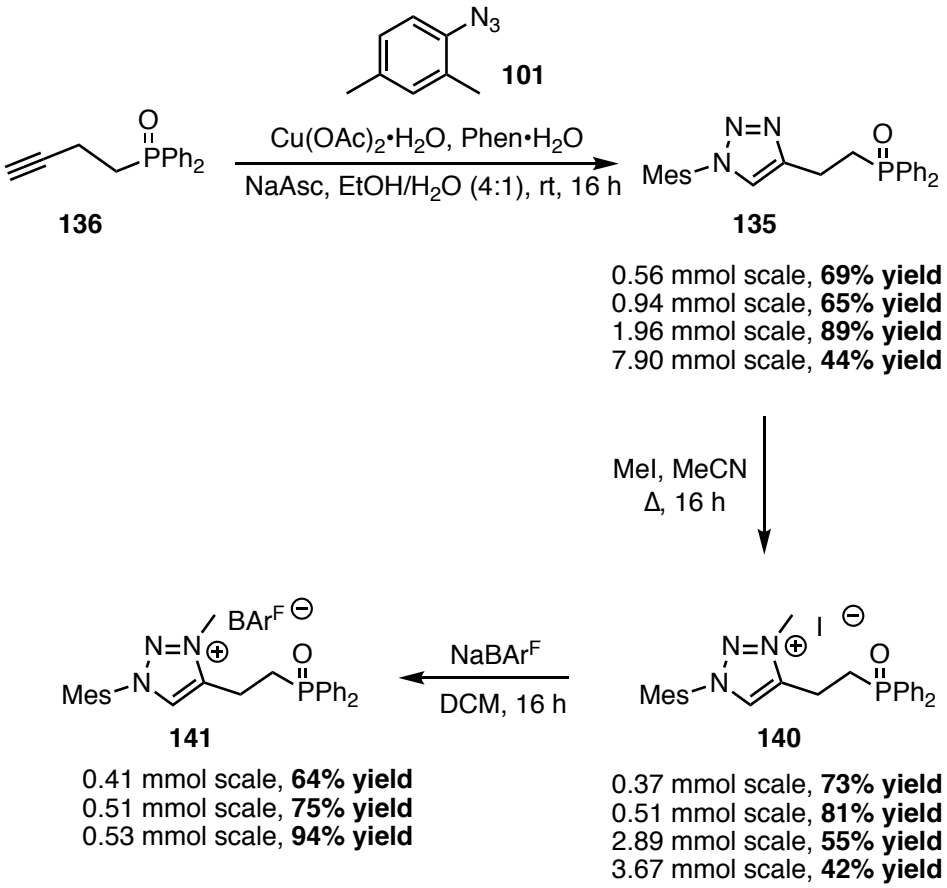

Scheme 3.38

Reduction of iodide salt **140** was first investigated. Use of DIBAL-H (1M in toluene) as the reducing agent was initially unproductive (Table 3.8) as iodide **140** was completely insoluble in toluene (entry 1). Addition of a more solubilizing solvent, such as THF or DCM (entries 1 and 2) unfortunately also did not allow reduction. It was hypothesised that perhaps the strongly coordinating iodide anion is rendering the phosphine oxide sterically inaccessible.

Table 3.8

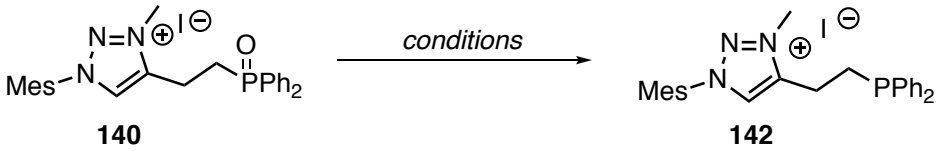

140 **142**

Entry	Conditions	Yield
1	DIBAL-H (1 M PhMe), 0 °C – rt, 3 h	trace
2	DIBAL-H (1 M PhMe), THF, 0 °C – rt, 3 h	trace
3	DIBAL-H (1 M PhMe), DCM, 0 °C – rt, 3 h	0%

In a final attempt to reduce the iodide salt **140**, an iodine-catalysed reduction where a sacrificial phosphine is utilised, was investigated.[53] In this case, the oxide is transferred to the relatively electron-rich tributylphosphine from the relatively electron-deficient phosphine oxide (Table 3.11). Pleasingly, the reaction did proceed in this case, with initial conditions providing a 2:1 ratio of starting material:product in the crude mixture. Increasing the reaction time to 16 h (entry 2), improved the ratio of product; however, a reaction time of 72 h caused significant degradation of both starting material and product (entry 3). The reaction temperature was then increased modestly to 40 °C (entries 4 and 5), delivering a good ratio of 1:5 starting material:product. Although the reaction proceeded well at 40 °C over 5 hours, the main issue with this methodology was separation of starting material, product and excess sacrificial phosphine. The material generated from entry **5** was subjected to salt metathesis; however, although product was observed in the NMR spectrum of the crude material, no pure product could be isolated in this case. At this point it was decided to concentrate on the reduction of the more soluble BAr^F salt **141**.

Table 3.9

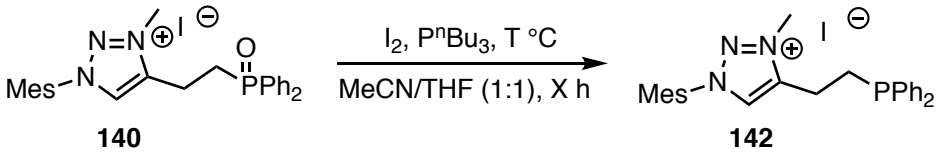

140 **142**

Entry	X h	T °C	140:142 in ^{31}P NMR
1	2	rt	2:1
2	16	rt	1.5:1
3	72	rt	degradation
4	2	40	1:1
5	5	40	1:5

To initiate studies with the BAr^F salt **141**, a range of literature conditions were investigated (Table 3.10). Unfortunately, trichlorosilane reduction (entry 1),[54] copper-mediated reduction (entry 2)[55] and cerium modified $LiAlH_4$ reaction (entry 3)[56] were unsuccessful, with complete recovery of starting material observed in all cases. Pleasingly, DIBAL-H (25% in hexane) did allow access to **121** in modest yields over 4 hours (entry 4).[57] It is worth noting at this stage that product **121** is extremely sensitive to oxidation on silica gel. To limit this process, oven-dried silica and degassed solvent were used, and the prepared column was flushed with argon before purification of the product. In addition, a relatively short band of silica was required to limit exposure time.

Table 3.10

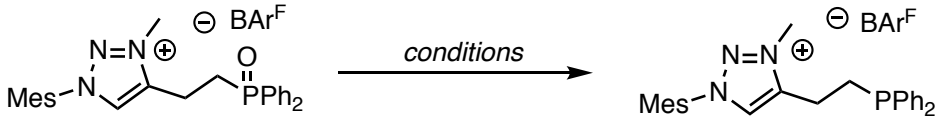

141 **121**

Entry	Conditions	Yield 121 (%)	Yield 141(%)
1	$SiCl_3H$, $CHCl_3$, rt, 4 h	0	Quant.
2	$Cu(OTf)_2$, TMDS, PhMe, 100 °C, 2 h	0	Quant.
3	$LiAlH_4$, $CeCl_3$, THF, 40 °C, 2 h	0	Quant.
4	DIBAL-H (25% in hexane), rt, 4 h	35	-

With promising results utilizing DIBAL-H (25% in hexane) for the reduction of **141**, this reaction was further investigated. Due to the insolubility of the starting material in hexane, toluene was added to enhance the solubility of the material in the reaction mixture (Table 3.11). To our delight, the reaction was reproducible on a variety of scales, with up to 46% of product **121** isolated (entry 3). Increasing the temperature of the reaction mixture to 40 °C, however, led to a complex reaction profile, and isolation of impure material.

Table 3.11

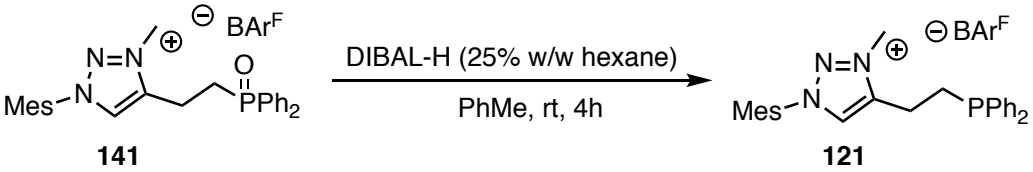

141 **121**

Entry	Scale (mmol)	T (°C)	Yield 121(%)
1	0.08	rt	32
2	0.23	rt	32
3	0.23	rt	46
4	0.52	rt	41
5	0.08	40	30 (impure)

With complex **121** in hand, complexation to iridium could then be investigated. As complexation of monodentate triazolium ligands had behaved in a similar manner to Ir(I) catalysts bearing an imidazolylidene, we first employed previous conditions for the synthesis of NHC/P chelating Ir(I) catalysts (Table 3.12, entry 1). Whilst crude NMR analysis suggested formation of product, attempts at isolation on silica gel caused complete degradation of the material. Although product was observed in the ^{1}H and ^{31}P NMR spectra, the predominant species within the spectra appeared to still bear the triazolium proton. It was hypothesised that this could be a result of coordination of two phosphine groups from two distinct ligand molecules, bearing pendant triazolium salts. Changing the order of addition, whereby the ligand **121** was first deprotonated and then metal precursor **4** added, a similar outcome was observed upon purification. Although the crude NMR spectra appeared less complex in this instance, degradation of the material on silica occurred. In a final attempt, trituration with hexane was utilised as the purification procedure. However, rather disappointingly, this also appeared to degrade the material. In this case, it appears that the triazolylidene catalyst motif is significantly less stable compared to its imidazolylidene counterpart. This being said, reaction on this scale makes purification challenging, and

reaction with more material may lead to more successful attempts at the complexation reaction.

Table 3.12

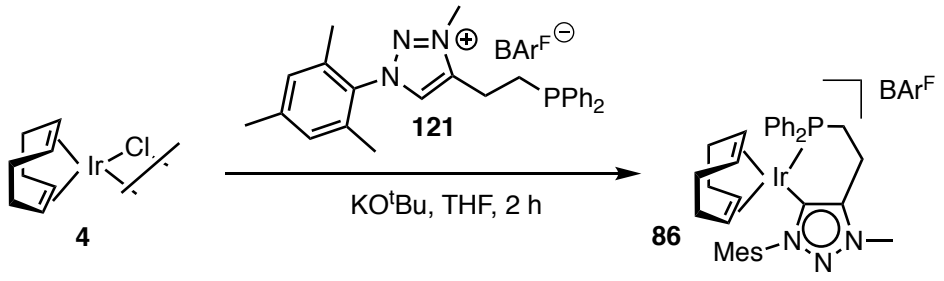

Entry	Scale (mmol)	Addition	Isolation	Yield 86 (%)
1	0.10	[Ir] +L, then KO^{t}Bu	Silica column	0
2	0.134	KO^{t}Bu + L, then [Ir]	Silica column	0
3	0.134	KO^{t}Bu + L, then [Ir]	Triturate (hexane)	0

Although a disappointing outcome, and the apparent instability of complex **86**, a robust synthesis of MIC/P bidentate ligand was developed. Substituents on the the N-1 position could be easily modified through the strategy, with a range of azides available for CuACC chemistry. In this regard, a larger aryl ring may provide enhanced stability. In addition, the methyl substituent at N-3 could easily be altered. Larger scale complexation attempts, with resulting cleaner reaction profiles may allow for the successful isolation of **86**. Transmetallation procedures from silver or copper complexes could also be investigated. These MIC/P ligand chelating motifs appear very interesting through DFT studies, and with optimisation of complexation/stabilizing groups, successful synthesis and application may yet be achievable.

3.4 Conclusion

To conclude this chapter, we have investigated the use of alternative abnormal NHCs as potential ligands for Ir(I) Kerr catalysts for HIE. Firstly, we have successfully synthesised an Ir(I) monodentate HIE catalyst bearing a triazolylidene MIC (Figure 3.13). This ligand motif was synthesised and complexed in good yields of up to 72%. Pleasingly, the synthesis was facile akin to the imidazolylidene counterpart. Also encouraging, was the stability of this catalyst, which proved to be stable to silica and displayed stability in solid and solution state for prolonged periods of time. DFT calculations were utilised to predict the activity of catalyst **93** in the HIE of amino acid motifs. Whilst for several substrates this appeared to be less active than the imidazolylidene complex, experimentally, excellent levels of labelling were observed for the labelling of Ac-Gly-O^{t}Bu. It was exciting to observe similar levels of activity with NHCs of a different nature, and this expands the scope of NHCs which can be utilised in the development of Ir(I) catalysts for both HIE and hydrogenation reactions, alike.

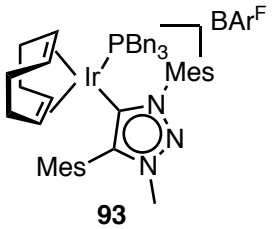

93

Figure 3.13

In addition to applying the novel triazolylidene catalyst to HIE reactions, we sought to characterise this complex, to provide comparison between the NHC classes. Electronic and steric parameters were investigated through a combination of experimental and theoretical techniques. Tolman electronic parameter (TEP) data suggests that, as expected, use of a triazolylidene ligand in place of the traditional imidazolylidene ligand used in Kerr catalysts, provides a more electron-rich Ir(I) metal precatalyst. Sterically, the MIC catalyst **93** appear to

be smaller than the imidazolylidene counterpart with $\%V_{bur}$ of 53.8% and 55.0%, respectively. The subtle differences in steric and electronic properties of these two catalyst classes, widely broadens the scope of potential HIE reactions. The smaller catalysts may better accommodate substrates for HIE which contain large directing groups, or where activation through a more challenging metallocycle, such as a 6- mmi, is required. Increased electron density observed at **93** may also find application where strongly coordinating Lewis basic groups are an issue. Synthesis and application of triazolylidene **93** has been encouraging, and application of this class of catalyst in HIE reactions could widen the scope of potential substrates. In addition, the use of a triazolium ligand precursor allows facile derivatization of the "wing tip" groups and nitrogen substitution on the ring, as a result of their modular and facile synthesis through CuAAC chemistry.

In an attempt to overcome the limitations of our developed monodentate Ir(I) catalysed HIE of amino acid motifs, where large substrates were troublesome, *in silico* screening of potential chelating motifs was carried out. Identification of a MIC/P chelated complex **86** (Figure 3.14) provided a synthetic target. This ligand motif, unlike its imidazolylidene counterpart, was predicted to not favour unproductive, off-cycle binding modes of the amino acid substrates to a significant degree. This was encouraging, as a smaller chelated ligand was perhaps now suitable through increasing the electron density at the metal, and discouraging unwanted Lewis base coordination. The smaller size of this ligand compared to monodentate systems was proposed to better accommodate the more challenging, sterically encumbered amino acid substrates.

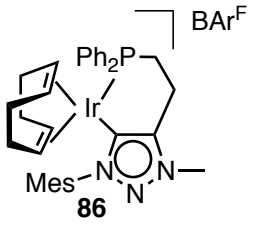

86

Figure 3.14

To access complex **86**, the synthesis of triazolium precursor **121** was targeted (Figure 3.15). Within the literature, there are few examples of MIC/P chelating ligand systems. Where there are some examples where the triazole remains neutral, synthesis of the triazolium/phosphine is rare. Whilst this has been achieved, in this work, the synthesis of ligand precursor **121** proved challenging. Where late stage introduction of the phosphine functionality was unachievable, utilization of a protected phosphine allowed generation of **121**. Removal of the phosphine protecting group was not facile. However, this being said, ligand **121** could be synthesised in 7 steps. Once again, the use of CuAAC chemistry to build this motif allows the opportunity to widely diversify the substitution of the triazolium ring, as a result of the abundance of azide and alkyne precursors.

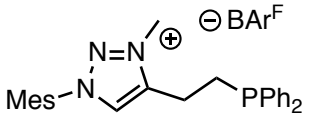

121

Figure 3.15

Unfortunately, the few attempts made at complexation of ligand **121** to Ir were unsuccessful, and this catalyst appeared to be unstable on the small scales employed. Although this is disappointing, the catalyst could perhaps be rendered more stable through introduction of, for example, aryl substitution on the triazole ring.

3.5 Future Work

Due to the apparent instability of catalyst **86**, and with a robust route to the ligand precursor **121** now developed, complexation attempts on larger scale will verify any stability issues. Additionally, alternative complexation methods could be utilised. The first, and perhaps most promising, route would be *via* transmetallation from copper or silver (Scheme 3.39). The silver carbene complex could be characterized pre-complexation and its stability evaluated. Transmetallation could potentially allow a cleaner reaction profile, where purification is more facile compared to generating the free carbene *in situ*.

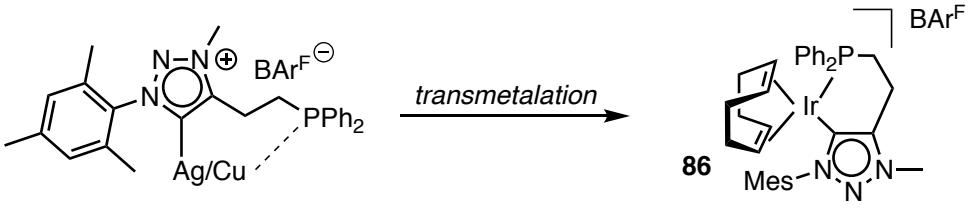

Scheme 3.39

A second method which could be utilised, is to first complex the triazole, and then alkylate to form the substituted ring, post metalation. This method would allow insight into the relative stability with the triazole motif *vs* the triazolium. Information could also be gained as to whether modification of the N-3 substituent to something larger than a methyl would induce greater stability.

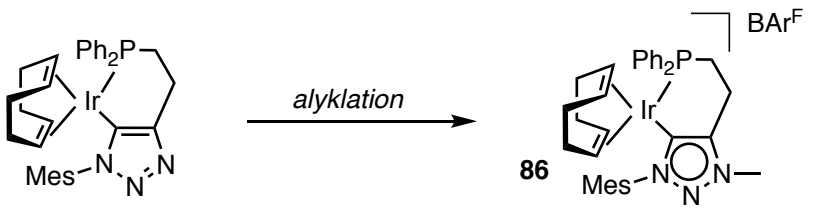

Scheme 3.40

Finally, attempts could be made to make the MIC/P ligated catalyst more stable. This could be achieved through introduction of more sterically encumbered groups on the ligand motif, such as those shown in Figure 3.16. These motifs would initially be investigated through DFT to predict their competency in HIE reactions, before being synthesised experimentally.

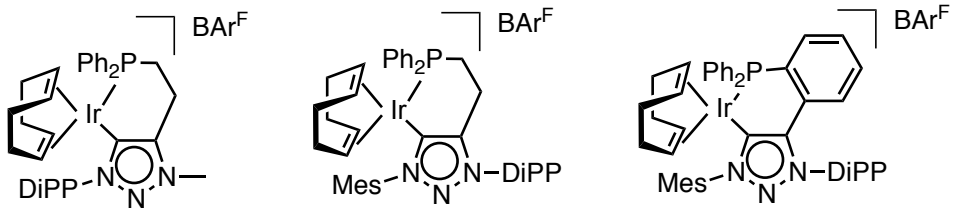

Figure 3.16

3.6 Experimental

3.6.1 General Information

All reagents were obtained from commercial suppliers (Alfa Aesar, Sigma Aldrich, Apollo Scientific, Fluorochem or Strem) and were used without further purification unless otherwise stated. If purification was required this was carried out using standard laboratory methods.[58] All glassware was flame-dried and cooled under a stream of nitrogen, unless otherwise stated.

Tetrahydrofuran was purified by heating to reflux over sodium wire, employing benzophenone ketyl as an indicator, before being distilled under a nitrogen atmosphere. All other solvents were distilled over calcium hydride under an argon atmosphere and stored over molecular sieves. Petroleum ether refers to ether with a boiling point range of 40-60°C.

Thin layer chromatography was carried out using Camlab silica plates coated with fluorescent indicator UV254. Plates were analysed using a Mineralight UVGL-25 lamp, or developed using vanillin or $KMnO_4$ solution.

Flash column chromatography was carried out using Prolab silica gel (230-400 μm mesh).

IR spectra were obtained on a Perking Elmer Spectrometer 1. All samples were analysed neat unless otherwise stated, and wavenumber values are reported in cm^{-1}.

^{1}H, ^{13}C, ^{11}B, ^{19}F and ^{31}P NMR spectra were recorded on a Bruker DPX 400 spectrometer at 400 MHz, 101 MHz, 128 MHz, 376 MHz, and 162 MHz, respectively. Chemical shifts are reported in ppm. Coupling constants are reported in Hz and refer to $^{3}J_{HH}$ interactions unless stated otherwise.

High resolution mass spectra were recorded on a Finnigan MAT 90XLT instrument at either the EPSRC Mass Spectrometry facility at the University of Wales, Swansea or the Mass Spectrometry facility at the University of Edinburgh.

DFT theory was used to calculate gas-phase electronic structures and associated energies. All structures were optimized using the M06L functional. This was utilised in conjunction with 6-31G9D) basis set for the main group atoms. Stuttgart RSC effective core potential with associated basis set was utilised for iridium. All calculations were performed using Gaussian 09 quantum package. Please see appendix for coordinates and further information.

3.6.2 General Procedures

General Procedure A – Deprotection of Silyl Protected Alkynes with K_2CO_3.[59]

The chosen TMS-alkyne (1 eq) was dissolved in MeOH and K_2CO_3 (X eq) was added. The resulting mixture was allowed to stir at room temperature for the desired time (0.5 – 4 h). The reaction mixture was then filtered through celite and concentrated *in vacuo*. The resulting alkynes were then purified by column chromatography to afford the title compound.

General Procedure B – Methylation of Triazoles with Me-I.[49]

Methyl iodide (5 eq) was added to a solution of the required triazole (1 eq) in acetonitrile (4.3 mL/mmol) and the resulting solution heated at reflux for 16 h. After cooling to room temperature, the solvent was concentrated *in vacuo* to ½ the original volume and diethyl ether was added until a precipitate was formed. The resultant solid was collected *via* filtration and washed with cold deiethyl ether to afford the title compound after drying.

General Procedure C – Salt Metathesis with $NaBAr^F$.

To a flame-dried round-bottom flask, was added the respective iodide triazolium salt (1 eq) , $NaBAr^F$ (1.10 eq) and dry DCM. The reaction mixture was then stirred at room temperature for 16 h. After this time, the reaction mixture was concentrated *in vacuo*, and the product purified by column chromatography to yield the title compound.

General Procedure D – Preparation of Complexes of Type [(CO)$_2$Ir(NHC)Cl][19]

To a flame-dried Schlenk tube containing [(COD)Ir(NHC)Cl] was added dry THF. To the resulting solution, $CO_{(g)}$ was bubbled for 30 min, followed by stirring for a further 1 h under a CO atmosphere. The Schlenk tube was then replaced with an atmosphere of argon, before being concentrated *in vacuo*. The crude reaction mixture was then purified by column chromatography (50% DCM/hexane) to afford the title compound as a pale yellow solid.

General Procedure E – Preparation of Complexes of Type [(CO)Ir(NHC)(PR$_3$)Cl] from [Ir(COD)(NHC)Cl]

Ir complexes of the type [Ir(COD)(NHC)Cl] were added to a flame-dried Schlenk tube under an argon atmosphere and dissolved in dry THF. To the resulting solution, $CO_{(g)}$ was bubble for 30 minutes, followed by stirring for a further 1 h under a CO atmosphere. The Schlenk tube was then replaced with an atmosphere of argon, and this solution concentrated *in vacuo*. DCM was then added, followed by the desired phosphine (1.0 eq) in one portion, with effervescence observed. After stirring for 1 h, the reaction mixture was concentrated *in vacuo* and diethyl ether added to allow trituration of the desired yellow solid product.

General Procedure F – Preparation of Complexes of Type [(CO)Ir(NHC)(PR$_3$)Cl] from [(CO)$_2$Ir(NHC)Cl].

Ir complexes of the type [$(CO)_2$Ir(NHC)Cl] were added to a flame-dried Schlenk tube under an argon atmosphere and dissolved in dry DCM. The phosphine (1 eq) was added to the mixture in one portion, with effervescence observed. After stirring for 1 h, the reaction mixture was concentrated *in vacuo* and diethyl ether added to allow trituration of the desired yellow solid product.

General Procedure G – Phosphination of alkyne-tosylates

$HP(X)Ph_2$ (1 eq) was added to a flame-dried round-bottom flask under an argon atmosphere and dry THF added. The reaction flask was cooled to -78 °C and ^{n}BuLi (1 eq) added dropwise. The tosylate electrophile was added dropwise at -78 °C as a THF solution and stirred for 15 min. The reaction mixture was then slowly brought to room temperature and allowed to stir overnight. After this time, the mixture was quenched with water and extracted with EtOAc. The resulting product was then purified by column chromatography.

General Procedure H – CuAAC reaction with $Cu(OAc)_2$ [49]

To a round-bottom flask was added $Cu(OAc)_2 \cdot H_2O$ (5 mol%), 1,10-phenenthroline monohydrate (5 mol%) and sodium L-ascorbate (1 eq). After dilution with a mixture of $EtOH/H_2O$ (4:1), the resulting suspension was stirred at room temperature for 5 mins. After this time the desired alkyne (1 eq) and azide (1.2 eq) were added to the reaction mixture and allowed to stir at room temperature for 16 h. The organic phase was then extracted with DCM, washed with brine, dried with sodium sulfate and concentrated *in vacuo*. The crude product was purified by column chromatography to yield the title product.

General Procedure I – Reduction with DIBAL-H [57]

To a flame dried flask under an atmosphere of argon was added the respective phosphine oxide (1.0 eq) and solvent. The reaction mixture was then cooled to 0 °C before slow addition of DIBAL-H (X eq). The reaction mixture was then allowed to slowly warm to room temperature and stirred for the allotted time. At this point, the reaction mixture was quenched by addition of NaOH (2M), diluted with degassed DCM and washed with a saturated solution of Rochelle's salt. The organic phase was dried with sodium sulfate and concentrated *in vacuo*. The crude mixture was then purified by trituration or column chromatography (note: oven dried silica, degassed solvents and argon were used for purification).

*3.6.3 Synthesis of Monodentate MIC Complex **93***

(mesitylethynyl)trimethylsilane **99** [60]

Table 3.4

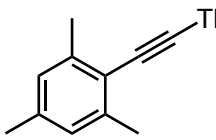

Chemical Formula: $C_{14}H_{20}Si$
Molecular Weight: 216.3990

99

Synthesis of compound **99** was attempted *via* the three following synthetic procedures:

Entry 1 [45]

A mixture of Mes-I **98** (0.536 g, 2.18 mmol, 1 eq), TMS-acetlyene (0.33 mL, 2.40 mmol, 1.1 eq), $Pd(PPh_3)_2Cl_2$ (12.46 mg, 0.07 mmol, 3 mol%), CuI (24.9 mg, 0.13 mmol, 6 mol%) and Et_3N (1.09 mL, 7.85 mmol, 3.6 eq) and DMF (3.6 mL) was stirred at 50 °C for 6 h. After this time, the reaction mixture was cooled to room temperature and H_2O was added. The solution was extracted with diethyl ether and the organic phases washed with brine, dried over sodium

sulfate and concentrated *in vacuo*. The residue was then purified by column chromatography (hexane) to yield **99** (66 mg, 0.31 mmol, 14% yield).

Entry 2 [46]

To a microwave vial were added Mes-I **98** (0.536 g, 2.18 mmol, 1 eq) and Et_3N (5.0 mL, 36.0 mmol, 16.5 eq). After three cycles of freeze-pump-thaw, $Pd(PPh_3)_2Cl_2$ (15.3 mg, 0.22 mmol, 10 mol%) and CuI (8.81 mg, 0.44 mmol, 20 mol%) were added under argon. Addition of TMS-acetlyene (0.61 mL, 4.36 mmol, 2 eq) afforded a green suspension which was stirred at room temperature for 2 h. The reaction mixture was then reduced *in vacuo*, dissolved in DCM and washed with water. The organic phase was then dried with sodium sulfate and concentrated. The residue was then purified by column chromatography (hexane) to yield only starting material **98** (89% recovery).

Entries 3-5

To a mixture of Mes-I **98** (1 eq), $Pd(PPh_3)_2Cl_2$ (10 mol%), CuI (10 mol%) and Et_3N was added TMS-acetlyene (1 eq) and the resulting suspension allowed to stir at 70 °C for 16 h under an argon atmosphere. After cooling, the reaction mixture was then diluted with diethyl ether and washed with 2 M HCl. The organic phase was then combined, dried with sodium sulfate and concentrated *in vacuo*. The resulting residue was then purified by column chromatography (hexane) to yield **99** as a yellow oil.

Table 3.13

Entry	Amount of 98		Amount of $Pd(PPh_3)_2Cl_2$		Amount of CuI		Amount of TMS-acetlyene		Amount of Et_3N	Product Yield		
	mg	mmol	mg	mmol	mg	mmol	mL	mmol	mL	mg	mmol	%
3	536	2.18	15.3	0.22	4.41	0.22	0.31	2.18	0.49	324	1.50	69
4	2139	8.70	61.1	0.87	17.6	0.87	1.24	8.70	1.96	1691	7.83	90
5	2139	8.70	61.1	0.87	17.6	0.87	1.24	8.70	1.96	1754	8.12	94

FTIR (neat): 2955, 2855, 2147, 1611, 1437, 1248 cm^{-1}.

^{1}H NMR (400 MHz, $CDCl_3$): δ 6.94 (s, 2H, Ar-H), 2.52 (s, 6H, $ArCH_3$), 2.37 (s, 3H, $ArCH_3$), 0.40 (s, *J* = $Si(CH_3)_3$ ppm.

^{13}C NMR (101 MHz, $CDCl_3$) δ 140.6, 137.9, 127.6, 120.2, 103.2, 101.8, 21.5, 21.0, 0.3 ppm.

2-ethynyl-1,3,5-trimethylbenzene **100** [60]

Scheme 3.24

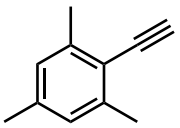

Chemical Formula: $C_{11}H_{12}$
Molecular Weight: 144.2170

100

Prepared according to *General Procedure A*. Product purified by column chromatography (hexane). Data presented as: (a) amount of **99**, (b) volume of MeOH, (c) amount of K_2CO_3, and (d) yield.

Run 1

(a) 0.324 g, 1.50 mmol, 1.0 eq, (b) 20.0 mL, (c) 0.214 g, 1.50 mmol, 1.0 eq, and (d) 0.119 g, 0.83 mmol, 55% yield.

Run 2

(a) 2.35 g, 10.9 mmol, 1.0 eq, (b) 145 mL, (c) 1.56 g, 10.9 mmol, 1.0 eq, and (d) 1.06 g, 7.41 mmol, 68% yield.

^{1}H NMR (400 MHz, $CDCl_3$): δ 6.88 (s, 2H, Ar-H)3.48 (s, 1H, C-C≡H), 2.43 (s, 6H, $ArCH_3$), 2.29 (s, 3H, $ArCH_3$) ppm.

^{13}C NMR (101 MHz, $CDCl_3$) δ 141.0, 138.2, 127.7, 119.1, 84.6, 81.5, 21.4, 21.0 ppm.

2-azido-1,3,5-trimethylbenzene **101**[60]

Scheme 3.24

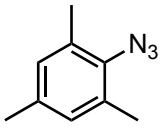

Chemical Formula: $C_9H_{11}N_3$
Molecular Weight: 161.2080

101

To a 250 mL, three-necked round bottom flask was charged trimethylaniline (13.51 g, 0.10 mol) and water (110 mL). Concentrated HCl (17.4 mL, 0.21 mol) was added to the mixture under vigorous stirring at 0 °C. After stirring at this temperature for 20-30 min, a freshly

prepared ice cold solution of $NaNO_2$ (7.16, 0.10 mol) in water (30 mL) was added dropwise *via* a dropping funnel. The internal temperature was kept below 5 °C. After complete addition, the reaction mixture was stirred for an additional 10 min. After this time, a freshly prepared solution of NaN_3 (6.75 g, 0.10 mol) in water (40 mL) was added to the reaction mixture *via* a dropping funnel, whilst keeping the internal temperature below 5 °C. Once the addition was complete, the mixture was stirred for an additional 30 min at 0 °C, followed by stirring at room temperature for 3 h. The reaction mixture was then extracted with EtOAc. The combined organic phases were dried over sodium sulfate and concentrated *in vacuo*. The crude residue was then purified by column chromatography (hexane) to afford **101** as a yellow oil (13.03 g, 0.08 mol, 81% yield).

^{1}H NMR (400 MHz, $CDCl_3$): δ 6.87 (s, 2H, Ar-H), 2.36 (s, 6H, $ArCH_3$), 2.29 (s, 3H, $ArCH_3$) ppm.

^{13}C NMR (101 MHz, $CDCl_3$) δ 135.4, 134.5, 131.9, 129.6, 20.8, 18.1 ppm.

1,4-dimesityl-1H-1,2,3-triazole **102** [61]

Scheme 3.24

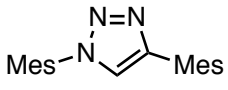

Chemical Formula: $C_{20}H_{23}N_3$
Molecular Weight: 305.4250

102

To a round bottom flask were charged mesitylazide **101** (1.0 eq) in MeOH, then sodium L-ascorbate (20 mol%), $CuSO_4 \cdot H_2O$ (15 mol%) and mesitylacetylene **100** (1.0 eq) were. The reaction mixture was stirred at room temperature for 16 h. At this point, H_2O was added and the mixture washed with EtOAc. The combined organic phases were dried over sodium sulfate and concentrated *in vacuo*. The residue was then purified by column chromatography (20% EtOAc/petrol) to afford **102** as a colourless solid.

Table 3.14

Run	Amount of 101		Amount of 100		Amount of $CuSO_4 \cdot H_2O$		Amount of NaAsc		Amount MeOH	Product Yield		
	mg	mmol	mg	mmol	mg	mmol	mg	mmol	mL	mg	mmol	%
1	134	0.83	120	0.83	19.9	0.12	33.2	0.17	0.42	110	0.33	40
2	1069	6.62	957	6.62	164	0.99	258	1.32	3.35	1610	4.83	73

Melting point: 150-152 °C (lit. 152-154 °C).[61]

FTIR (neat): 3034, 2961, 1610, 1354, 1274, cm^{-1}.

^{1}H NMR (400 MHz, $CDCl_3$): δ 7.42 (s, 1H, NC<u>H</u>CN), 7.02 (s, 2H, Ar-<u>H</u>), 6.96 (s, 2H, Ar-<u>H</u>), 2.36 (s, 3H, ArC<u>H</u>$_3$), 2.32 (s, 3H, ArC<u>H</u>$_3$), 2.18 (s, 6H, ArC<u>H</u>$_3$), 2.04 (s, 6H, ArC<u>H</u>$_3$) ppm.

^{13}C NMR (101 MHz, $CDCl_3$) δ 145.5, 140.1, 138.3, 137.9, 135.2, 133.7, 129.2, 128.5, 127.2, 124.6, 21.3, 20.8, 17.4 ppm.

1,4-dimesityl-3-methyl-1H-1,2,3-triazol-3-ium iodide **103** [61]

Scheme 3.24

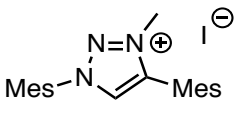

Chemical Formula: $C_{21}H_{26}IN_3$
Molecular Weight: 447.3645

103

Prepared according to *General Procedure B*. Data presented as: (a) amount of **102**, (b) volume of MeCN, (c) amount of MeI, and (d) yield.

Run 1

(a) 0.110 g, 0.32 mmol, 1.0 eq, (b) 1.86 mL, (c) 0.217 mL, 1.66 mmol, 5.0 eq, and (d) 0.10 g, 0.20 mmol, 60% yield.

Run 2

(a) 0.471 g, 1.37 mmol, 1.0 eq, (b) 7.96 mL, (c) 0.929 mL, 7.11 mmol, 5.0 eq, and (d) 0.50 g, 1.0 mmol, 73% yield.

Melting point: 204-206 °C (lit. 200-202 °C).[61]

FTIR (neat): 3057, 2956, 1611, 1576, 1458 cm^{-1}.

^{1}H NMR (400 MHz, $CDCl_3$): δ 9.36 (s, 1H, NC<u>H</u>CN), 7.08 (s, 2H, Ar-<u>H</u>), 7.07 (s, 2H, Ar-<u>H</u>), 4.26 (s, 3H, NC<u>H</u>$_3$), 2.39 (s, 3H, ArC<u>H</u>$_3$), 2.37 (s, 3H, ArC<u>H</u>$_3$), 2.20 (s, 6H, ArC<u>H</u>$_3$), 2.20 (s, 6H, ArC<u>H</u>$_3$) ppm.

^{13}C NMR (101 MHz, $CDCl_3$) δ 142.8, 142.8, 142.7, 138.1, 134.3, 132.6, 131.2, 130.1, 129.6, 117.1, 39.4, 21.4, 20.9, 18.0 ppm.

1,4-dimesityl-3-methyl-1H-1,2,3-triazol-3-ium BAr^F **104**

Scheme 3.24

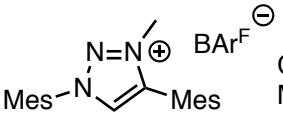

Chemical Formula: $C_{53}H_{38}BF_{24}N_3$
Molecular Weight: 1183.6797

104

Prepared according to *General Procedure C*. Data presented as: (a) amount of **103**, (b) volume of DCM, (c) amount of NaBAr^F, and (d) yield.

Run 1

(a) 0.10 g, 0.22 mmol, 1.0 eq, (b) 2.0 mL, (c) 0.215 g, 0.24 mmol, 1.1 eq, and (d) 0.242 g, 0.20 mmol, 93% yield.

Run 2

(a) 0.45 g, 0.99 mmol, 1.0 eq, (b) 9.0 mL, (c) 0.976 g, 1.09 mmol, 1.1 eq, and (d) 0.823 g, 0.68 mmol, 69% yield.

Melting point: 110-112 °C

FTIR (neat): 2986, 2968, 2901, 1613, 1354, 1273 cm^{-1}.

^{1}H NMR (400 MHz, $CDCl_3$): δ 8.01 (s, 1H, NC<u>H</u>CN), 7.68 (bs, 8H, Ar-<u>H</u> BAr^F), 7.49 (bs, 4H, Ar-<u>H</u> BAr^F), 7.09 (s, 2H, Ar-<u>H</u>), 7.08 (s, 2H, Ar-<u>H</u>), 4.01 (s, 3H, NC<u>H</u>$_3$), 2.39 (s, 3H, ArC<u>H</u>$_3$), 2.36 (s, 3H, ArC<u>H</u>$_3$), 2.01 (s, 12H, ArC<u>H</u>$_3$) ppm.

^{13}C NMR (101 MHz, $CDCl_3$) δ 161.8 (q, $^{1}J_{C\text{-}B}$ = 49.0 Hz), 144.3, 144.1, 143.8, 137.4, 135.0, 133.6, 130.7, 130.6, 130.5, 130.1, 129.1 (q, $^{2}J_{C\text{-}F}$ = 32.6 Hz), 124.6 (q, $^{1}J_{C\text{-}F}$ = 273.1 Hz), 117.6, 115.8, 37.8, 21.3, 21.2, 19.7, 16.9 ppm.

^{11}B NMR (128 MHz, $CDCl_3$): δ -6.68 ppm (BAr^F $B(Ar_4)$).

^{19}F NMR (376 MHz, Methanol-*d_4*): δ -62.5 ppm (BAr^F $ArCF_3$).

HRMS (positive ESI): m/z calculated for $C_{21}H_{26}N_3$ $[M]^+$: 320.212,. found: 320.2123.

HRMS (negative ESI): m/z calculated for [$C_{32}H_{12}BF_{24,}$ BArF]$^-$: 863.0654, found: 863.0656.

[Ir(COD)(PBn$_3$)(TMes)] BAr^F **93**

Scheme 3.25

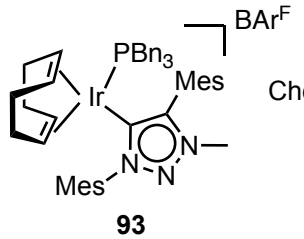

93

Chemical Formula: $C_{82}H_{70}BF_{24}IrN_3P$
Molecular Weight: 1787.4449

Bis(1,5-cyclooctadiene)diiridium(I) dichloride (1 eq) was added to a flame-dried, argon-cooled Schlenk tube and stirred under vacuum for 5 min. THF was added and the mixture stirred until solids had dissolved. After this time, tribenzylphosphine (1 eq) was added in one portion, resulting in an orange to yellow colour change. After allowing the reaction mixture to stir for 15 min at room temperature, triazolium **104** (2 eq) was then added and the reaction mixture stirred for 5 min. At this point, potassium *tert*-butoxide (1.5 eq) was added, causing a yellow to bright red colour change, and the mixture allowed to stir for 16 h. The solvent was then removed *in vacuo*, and purification by column chromatography (50% DCM in petrol) afforded the title compound as a red solid.

Table 3.15

Run	Amount of Ir dimer 4		Amount of PBn_3		Amount of 104		Amount of KO^tBu		Amount THF	Product Yield		
	mg	mmol	mg	mmol	mg	mmol	mg	mmol	mL	mg	mmol	%
1	27	0.04	24	0.08	95	0.08	13.4	0.12	0.50	57	0.03	40
2	136	0.20	120	0.40	475	0.40	67	0.60	2.5	551	0.29	72

Melting point: decomp >178 °C

FTIR (neat): 3032, 2922, 2332, 1609, 1495, 1454, 1352 cm^{-1}.

^{1}H NMR (400 MHz, $CDCl_3$): δ 7.70 (bs, 8H, Ar-H BAr^F), 7.50 (bs, 4H, Ar-H BAr^F), 7.25 – 7.14 (m, 13H, Ar-H), 6.87 (d, J = 7.2 Hz, 6H, Ar-H), 4.67 – 4.55 (m, 0.5H, COD CH), 4.41 – 4.30 (m, 1.5H, COD CH), 3.81 (s, 3H, NCH_3), 3.14 – 3.08 (m, 2H, COD CH), 2.75 (d, $^2J_{P\text{-}H}$ = 8.7 Hz, 6H, P-CH_2-Ar), 2.47 (s, 3H, $ArCH_3$), 2.44 (s, 3H, $ArCH_3$), 2.42 (s, 3H, $ArCH_3$), 2.36 (s, 3H, $ArCH_3$), 2.22 (s, 3H, $ArCH_3$), 2.20 (s, 3H, $ArCH_3$), 1.81 – 1.23 (m, 8H, COD CH_2) ppm.

^{13}C NMR (101 MHz, $CDCl_3$) δ 165.9 (d, $^{2}J_{C\text{-}P}$ = 7.7 Hz), 161.84 (q, $^{1}J_{C\text{-}B}$ = 50.0 Hz), 145.3, 142.3, 142.1, 139.4, 137.9, 136.4, 135.9, 135.0, 134.8, 132.8, 132.7, 130.6, 130.2, 130.1, 130.0, 129.9, 129.7, 128.4d ($^{2}J_{C\text{-}F}$ = 32.4 Hz), 127.6, 124.1 (q $^{1}J_{C\text{-}F}$ = 271.1 Hz), 120.6, 117.6, 88.5, 88.4, 86.2, 86.1, 75.0, 74.9, 37.1, 31.7, 31.4, 29.9, 29.5, 21.8, 21.4, 21.3, 20.1, 19.9 ppm.

^{11}B NMR (128 MHz, $CDCl_3$): δ -6.64 ppm (BAr^F $B(Ar_4)$).

^{31}P NMR (162 MHz, $CDCl_3$): δ -8.1 ppm PBn_3.

^{19}F NMR (376 MHz, Methanol-*d_4*): δ -64.3 ppm (BAr^F $ArCF_3$).

HRMS (positive ESI): m/z calculated for $C_{29}H_{37}N_3Ir$ $[M]^+$: 620.2611, found: 620.2578.

HRMS (negative ESI): m/z calculated for [$C_{32}H_{12}BF_{24}$, BArF]$^-$ 863.0654, found: 863.0679.

*3.6.4 Isotopic Labelling with Catalyst **93***

Scheme 3.26

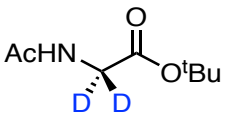

D105

Reactions were performed using a Radley's 12-chamber carousel. Each of the carousel tubes were dried overnight in an oven at 180 °C and allowed to cool under vacuum. Each tube was charged with **105** (18.6 mg, 0.11mmol, 1.0 eq) and the relevant catalyst (5 mol%). To each tube was added MTBE (1.25 mL), and the solutions cooled to -78 °C. The atmosphere was exchanged with three vacuum/D_2 cycles and the tubes were sealed and immediately placed in a heating block pre-heated to 50 °C. The reactions were stirred for 16 h after which time the solvent was removed *in vacuo*. The resulting residue was purified by column chromatography (0 – 10% MeOH/DCM) The level of incorporation was determined by ^{1}H NMR spectroscopic analysis, with the integrals of the labelling positions measured against a peak corresponding to a position where labelling was not expected. The level of deuteration was then calculated using the formula:

$$Deuteration\,(\%) = \; 100 - [100 \times \left(\frac{Residual\ Integral}{Expected\ Integral}\right)$$

^{1}H NMR (400 MHz, Acetone-d_6): δ 7.41 – 7.17 (m, 1H, NH), 3.80 (d, *J* = 5.8 Hz, 2H, CH_2), 1.92 (s, 3H, $COCH_3$), 1.43 (s, 9H, $OC(CH_3)_3$) ppm.

Labelling expected against signal at 3.80 ppm, measured against signal at 1.92 ppm.

Table 3.16

[Ir]	[Ir] (mg, mmol)	Run 1 (%)	Run 2 (%)	Run 3 (%)	Avg (%)
73	9.53, 0.005	93	83	92	89
93	9.60, 0.005	83	90	84	86

*3.6.5 Characterisation of Triaozlylidene Complex **93***

[Ir(COD)(TMes)Cl] BAr^F **106**

Scheme 3.27

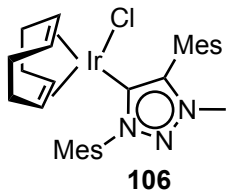

106

Chemical Formula: $C_{29}H_{37}ClIrN_3$
Molecular Weight: 655.3019

Triazolium salt **103** (100 mg, 0.22 mmol, 1.0 eq) and potassium *tert*-butoxide (24.64 mg, 0.22 mmol, 1.0 eq) were added to a flame-dried, argon cooled Schlenk tube and stirred under vacuum for 5 min. THF (3.5 mL) was added and the mixture stirred under argon for 30 min. After this time the solution was allowed to settle until the precipitate settled at the bottom of the vessel. In a separate flame-dried Schlenk tube was added bis(1,5-cyclooctadiene)diiridium(I) dichloride **4** (73 mg, 0.11 mmol, 0.5 eq) in THF (3.5 mL). The deprotonated triazolium salt was then transferred to the Schlenk tube containing **4** *via* syringe transfer. The resulting solution was then stirred for 3 h. The solvent was then removed *in vacuo*, and column chromatography (50% ethyl acetate in petrol) afforded the title compound **106** as a yellow solid (90 mg, 0.14 mmol, 62% yield).

Melting point: >230 °C (decomposition) .

FTIR (neat): 3005, 2914, 2361, 1734, 1609, 1443, 1325 cm^{-1}

^{1}H NMR (400 MHz, $CDCl_3$): δ 7.10 – 6.83 (m, 4H, Ar-H), 4.20 – 4.13 (m, 2H, COD CH), 3.75 (s, 3H, NCH_3), 2.92 – 2.86 (m, 2H, COD CH_2), 2.37 (s, 3H, $ArCH_3$), 2.35 (s, 3H, $ArCH_3$), 2.23 (s, 12H, $ArCH_3$), 1.88 – 1.20 (m, 8H, COD CH_2) ppm.

^{13}C NMR (102 MHz, $CDCl_3$): δ 170.9, 144.3, 139.9, 139.7, 139.0, 136.6, 135.5, 128.9, 128.7, 124.4, 81.0, 51.6, 36.1, 33.7, 29.4, 21.5, 21.4, 21.3, 18.9 ppm.

HRMS (ESI): m/z calculated for $C_{29}H_{37}N_3ClIr$ $[M]^+$ 655.22999 found: 655.22700.

Formation of MeCN/dihydride Complexes **107 – 113**

Scheme 3.28

The complex of interest (~ 10 mg) was dissolved in 0.7 mL MeCN-d_3 amd transferred to an oven-dried NMR tube sealed with a rubber septum. Hydrogen gas was bubbled through the solution carefully for 30 min with an exit needle in place. For chloro-carbene complexes **111 – 113**, a longer activation time of 1 h was utilised. After this time, the sample was analysed directly by ^{1}H NMR at 300 K.

Due to the 'quick screen' method utilised, full analysis of ^{1}H and ^{13}C NMR is not provided for each derivative. However, for each complex, complete disappearance of the COD olefinic proton signals was observed, as expected.

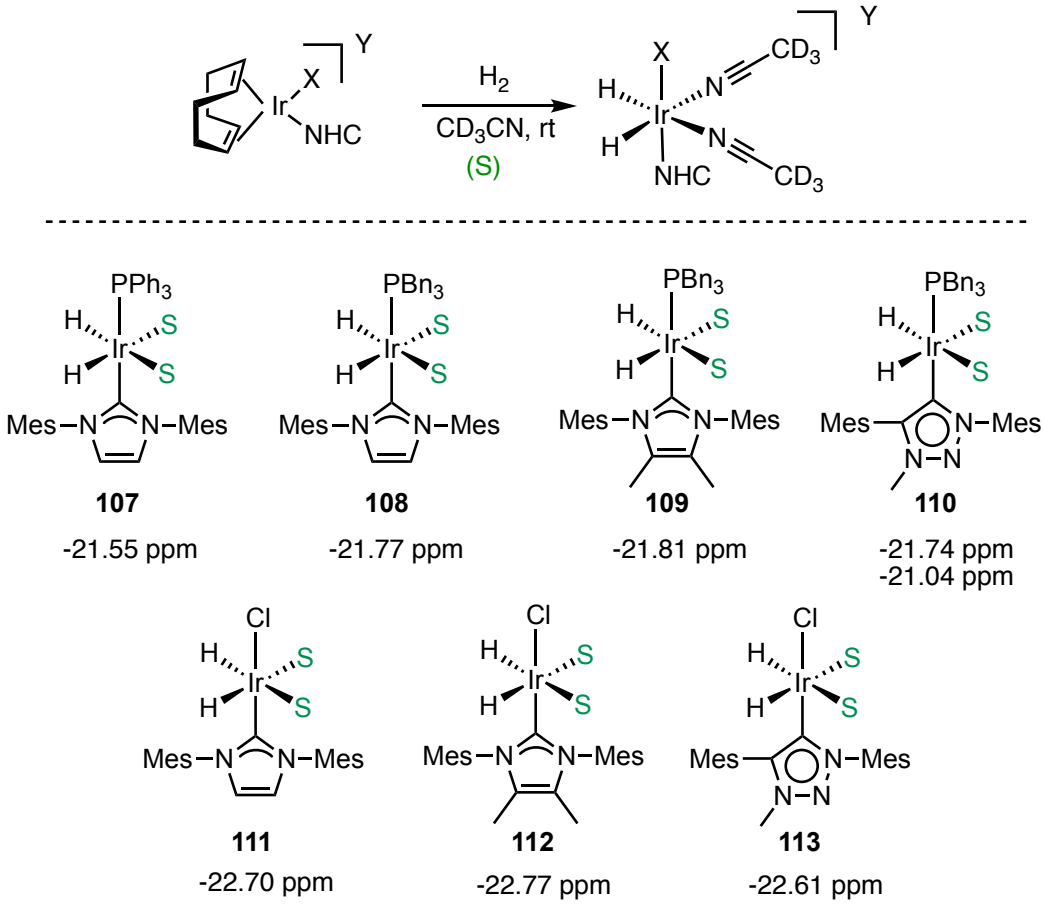

*Complexes **107-110** are cationic, anions ommited for clarity*
*Complexes **111-113** are neutral with no Y counterion*

[(CO)$_2$Ir(IMes)Cl] **114**

Table 3.5

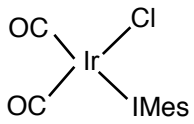

114

Chemical Formula: $C_{23}H_{24}ClIrN_2O_2$
Molecular Weight: 588.1235

Prepared according to *General Procedure D*. Data presented in Table 3.17 for mass of [Ir(COD)(IMes)Cl] **143**.

Table 3.17

143 Mass (mg)	143 (mmol)	THF (mL)	Yield 114
48 mg	0.075	1.2	38 mg, 0.065 mmol, 86% yield

Melting point: >215 °C (decomposition) .

FTIR (neat): 3140, 2961, 2859, 2056, 1969, 1483, 1229 cm^{-1}.

^{1}H NMR (400 MHz, $CDCl_3$): δ 7.11 (s, 2H, Ar-H), 7.01 (bs, 4H, Ar-H), 2.37 (s, 6H, $ArCH_3$), 2.22 (s, 12H, $ArCH_3$) ppm.

^{13}C NMR (102 MHz, $CDCl_3$): δ 180.2, 176.2, 168.5, 139.6, 135.3, 135.0, 129.4, 123.8, 21.3, 18.6 ppm

HRMS (ESI): *pending*

$[(CO)_2Ir(IMes^{Me})Cl]$ **115**

Table 3.5

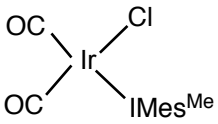

Chemical Formula: $C_{25}H_{28}ClIrN_2O_2$
Molecular Weight: 616.1775

115

Prepared according to *General Procedure D*. Data presented in Table 3.17 for mass of [Ir(COD)($IMes^{Me}$)Cl] **144**.

Table 3.18

144 Mass (mg)	144 (mmol)	THF (mL)	Yield 115
100 mg	0.15	1.2	61 mg, 0.099 mmol, 66% yield

Melting point: >228 °C (decomposition) .

FTIR (neat): 2972, 2922, 2052, 1967, 1485, 1383 cm^{-1}.

^{1}H NMR (400 MHz, $CDCl_3$): δ 7.00 (bs, 4H, Ar-H), 2.36 (bs, 6H, $ArCH_3$), 2.15 (s, 12H, $ArCH_3$), 1.88 (s, 6H, $ArCH_3$) ppm.

^{13}C NMR (102 MHz, $CDCl_3$): δ 180.5, 173.0, 169.0, 139.3, 135.6, 133.3, 129.4, 126.9, 21.4, 18.5, 9.2. ppm

HRMS (ESI): *pending*

$[(CO)_2Ir(TMes)Cl]$ **116**

Table 3.5

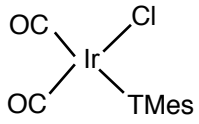

Chemical Formula: $C_{23}H_{25}ClIrN_3O_2$
Molecular Weight: 603.1379

116

Prepared according to *General Procedure D*. Data presented in Table 3.17 for mass of [Ir(COD)(TMes)Cl] **106**.

Table 3.19

106 Mass (mg)	106 (mmol)	THF (mL)	Yield 116
94 mg	0.16	1.2	34.7 mg, 0.058 mmol, 36% yield

Melting point: 208 – 210 °C.

FTIR (neat): 2916, 2052, 1965, 1611, 1354, 1277 cm^{-1}.

^{1}H NMR (400 MHz, $CDCl_3$): δ 7.02 (s, 4H, Ar-H), 3.86 (s, 3H, NCH_3), 2.38 (s, 3H, $ArCH_3$), 2.37 (s, 3H, $ArCH_3$), 2.20 (s, 6H, $ArCH_3$), 2.17 (s, 6H, $ArCH_3$) ppm.

^{13}C NMR (102 MHz, $CDCl_3$): δ 181.2, 169.1, 166.8, 146.8, 140.8, 140.6, 138.4, 135.7, 134.9, 134.8, 129.4, 129.1, 128.8, 122.7, 36.4, 31.7, 28.2, 21.5, 20.8, 18.3, 14.3 ppm.

HRMS (ESI): *pending*

[(CO)Ir(IMes)Cl(PPh_3)] **117**

Table 3.6

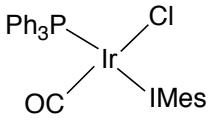

117

Chemical Formula: $C_{40}H_{39}ClIrN_2OP$
Molecular Weight: 822.4052

Prepared according to *General Procedure E*. Data presented in Table 3.17 for mass of [Ir(COD)(IMes)Cl] **143**.

Table 3.20

143 (mg)	143 (mmol)	THF (mL)	PPh_3 (mg)	PPh_3 (mmol)	DCM (mL)	Yield
100	0.15	1.2	39	0.15	4.6	110 mg, 0.13 mmol, 89%

Melting point: >200 °C (decomposition).

FTIR (neat): 3049, 2945, 2914, 1937, 1481, 1433 cm^{-1}.

^{1}H NMR (400 MHz, $CDCl_3$): δ 7.48 – 7.32 (m, 10H, Ar-H), 7.30 – 7.17 (m, 5H, Ar-H), 7.08 (s, 2H, Ar-H), 7.02 (s, 4H, Ar-H), 2.42 (s, 6H, $ArCH_3$), 2.29 (s, 12H, $ArCH_3$) ppm.

^{13}C NMR (102 MHz, $CDCl_3$): δ 179.5 (d, $^2J_{C-P}$ = 120.0 Hz), 171.7 (d, $^2J_{C-P}$ = 10.3 Hz), 138.4, 136.3, 136.0, 135.0, 134.9, 134.1, 133.9, 133.7, 133.6, 129.5, 129.0, 127.6, 127.5, 122.8, 122.7, 21.4, 19.1 ppm.

^{31}P NMR (162 MHz, $CDCl_3$): δ 23.6 ppm PPh_3.

HRMS (ESI): *pending*

[(CO)Ir(IMes)Cl(PBn_3)] **118**

Table 3.6

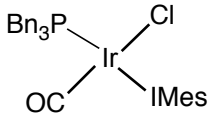

118

Chemical Formula: $C_{43}H_{45}ClIrN_2OP$
Molecular Weight: 864.4862

Prepared according to *General Procedure F*. Data presented in Table 3.17 for mass of *[$(CO)_2$Ir(IMes)Cl]* **114**

.

Table 3.21

114 (mg)	114 (mmol)	PBn_3 (mg)	$PBn3_3$ (mmol)	DCM (mL)	Yield
57	0.097	29.5	0.097	3.0	61 mg, 0.069 mmol, 71%

Melting point: 152 -154 °C.

FTIR (neat): 2961, 1931, 1493, 1260 cm^{-1}.

^{1}H NMR (400 MHz, $CDCl_3$): δ 7.28 – 6.98 (m, 21H, Ar-H), 3.12 (d, $^2J_{P-H}$ = 9.4 Hz, 6H, P-CH_2-Ar), 2.44 (s, 6H, ArCH_3), 2.33 (s, 12H, ArCH_3) ppm.

^{13}C NMR (102 MHz, $CDCl_3$): δ 180.4 (d, $^2J_{C-P}$ = 118.7 Hz), 171.9 (d, $^2J_{C-P}$ = 12.2 Hz), 138.6, 136.5, 135.9, 135.1, 135.0, 130.7, 130.6, 129.2, 127.9, 126.0, 123.0, 122.9, 30.7 (d, $^1J_{C-P}$ = 26.9 Hz) 21.4, 18.8 ppm.

^{31}P NMR (162 MHz, $CDCl_3$): δ 6.6 ppm PBn_3.

HRMS (ESI): *pending*

[(CO)Ir($IMes^{Me}$)Cl(PBn_3)] **119**

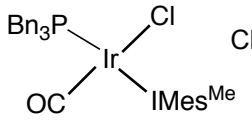

Chemical Formula: $C_{45}H_{49}ClIrN_2OP$
Molecular Weight: 892.5402

119

Prepared according to *General Procedure F*. Data presented in Table 3.17 for mass of *[$(CO)_2$Ir(IMes)Cl]* **115**

.

Table 3.22

115 (mg)	115 (mmol)	PBn_3 (mg)	$PBn3_3$ (mmol)	DCM (mL)	Yield
61	0.099	30.0	0.099	3.0	51 mg, 0.057 mmol, 58%

Melting point: >210 °C (decomposition).

FTIR (neat): 3057, 2870, 1929, 1493, 1375 cm^{-1}.

^{1}H NMR (400 MHz, $CDCl_3$): δ 7.38 – 7.25 (m, 3H, Ar-H), 7.21 – 7.07 (m, 16H, Ar-H), 3.11 (d, $^{2}J_{P-H}$ = 9.4 Hz, 6H, P-CH_2-Ar), 2.45 (s, 6H, ArCH_3), 2.27 (s, 12H, ArCH_3), 1.94 (s, 6H, ArCH_3) ppm.

^{13}C NMR (102 MHz, $CDCl_3$): δ 177.1 (d, J = 120.1 Hz), 172.2 (d, J = 10.9 Hz), 138.2, 136.3, 135.2, 135.1, 134.9, 130.8, 130.6, 129.2, 127.9, 125.9, 125.8, 125.7, 30.7 (d, ^{1}J = 27.1 Hz), 21.4, 18.7, 9.5 ppm.

^{31}P NMR (162 MHz, $CDCl_3$): δ 6.3 ppm PBn_3.

HRMS (ESI): *pending*

[(CO)Ir(TMes)Cl(PBn_3)] **120**

Table 3.6

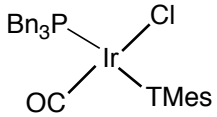

Chemical Formula: $C_{43}H_{46}ClIrN_3OP$
Molecular Weight: 879.5007

120

Prepared according to *General Procedure E*. Data presented in Table 3.17 for mass of [Ir(COD)(TMes)Cl] **106**.

Table 3.23

106 (mg)	106 (mmol)	THF (mL)	PBn_3 (mg)	PBn_3 (mmol)	DCM (mL)	Yield
94	0.16	1.2	48.6	0.16	4.6	79 mg, 0.09 mmol, 56%

Melting point: >110 – 112 °C

FTIR (neat): 3057, 2961, 2856, 1928, 1492, 1450 cm^{-1}.

^{1}H NMR (400 MHz, $CDCl_3$): δ 7.24 – 7.10 (m, 19H, Ar-H), 3.91 (s, 3H, NCH_3), 3.17 (d, $^2J_{P\text{-}H}$ = 9.4 Hz, 6H, P-CH_2-Ar), 2.49 (s, 3H, $ArCH_3$), 2.47 (s, 3H, $ArCH_3$), 2.35 (s, 6H, $ArCH_3$), 2.31 (s, 6H, $ArCH_3$) ppm.

^{13}C NMR (102 MHz, $CDCl_3$): δ 171.7, 169.5 (d, ^2J = 110.7 Hz), 165.8, 139.2, 139.0, 138.3, 137.2, 137.2, 134.8, 134.8, 134.7, 130.3, 130.2, 130.1, 128.8, 128.7, 128.5, 128.3, 128.2, 127.92, 127.8, 127.3, 125.4, 35.7, 33.7 (d, ^1J = 19.6 Hz), 30.3 (d, ^1J = 26.2 Hz), 27.6, 20.9, 20.90, 20.2, 17.8 ppm.

^{31}P NMR (162 MHz, $CDCl_3$): δ 9.8 ppm PBn_3.

HRMS (ESI): *pending*

3.6.6 Synthesis of MIC/P Ligand

2-(1-mesityl-1H-1,2,3-triazol-4-yl)ethan-1-ol **125** [49]

Scheme 3.30

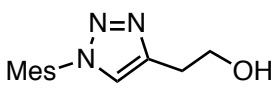

Chemical Formula: $C_{13}H_{17}N_3O$
Molecular Weight: 231.2990

125

Prepared according to *General Procedure H*. Product purified by column chromatography (0-15% MeOH/DCM). Data presented as: (a) amount of $Cu(OAc)_2 \cdot H_2O$, (b) amount of 1,10-phenanthroline monohydrate, (c) amount of NaAsc, (d) amount 3-butyn-1-ol **124**, (e) amount Mes-N_3 **101**, (f) amount EtOH/H_2O (4:1), and (g) yield.

Run 1

(a) 9.98 mg, 5 mol%, 0.05 mmol, (b) 9.91mg, 5 mol%, 0.05 mmol, (c) 0.198 g, 1 mmol, 1.0 eq (d) 0.076 mL, 1 mmol, 1.0 eq, (e) 0.193 g, 1.2 mmol, 1.2 eq, (f) 5 mL, and (g) 0.112 g, 0.48 mmol, 48% yield as a yellow oil.

Run 2

(a) 99.8 mg, 5 mol%, 0.5 mmol (b) 99.1 mg, 5 mol%, 0.5 mmol (c) 1.981 g, 10 mmol, 1.0 eq (d) 0.76 mL, 10 mmol, 1.0 eq, (e) 1.93 g, 12 mmol, 1.2 eq, (f) 50 mL, and (g) 0.932 g, 4 mmol, 50% yield as a yellow oil.

FTIR (neat): 3310 (broad), 3138, 3028, 2951, 2874, 1493, 1379 cm^{-1}.

^{1}H NMR (400 MHz, $CDCl_3$): δ 7.44 (s, 1H, NC<u>H</u>CN), 6.98 (s, 2H, Ar-<u>H</u>), 4.03 (t, *J* = 5.9 Hz, 2H, $CH_2C\underline{H}_2OH$), 3.06 (t, *J* = 5.9 Hz, 2H, $C\underline{H}_2CH_2OH$), 2.35 (s, 3H, $ArC\underline{H}_3$), 1.95 (s, 6H, $ArC\underline{H}_3$) ppm.

^{13}C NMR (101 MHz, $CDCl_3$) δ 145.3, 139.7, 134.9, 133.4, 128.9, 123.6, 61.3, 28.8, 21.0, 17.1 ppm.

HRMS (NSI): m/z calculated for $C_{13}H_{18}N_3O$ $[M+H]^+$: 232.1451, found: 232.1250.

4-(2-hydroxyethyl)-1-mesityl-3-methyl-1H-1,2,3-triazol-3-ium iodide **123** [49]

Scheme 3.30

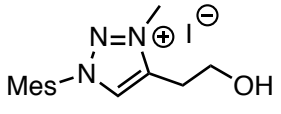

123

Chemical Formula: $C_{14}H_{20}IN_3O$
Molecular Weight: 373.2385

Prepared according to *General Procedure B*. Data presented as: (a) amount of triazole **125**, (b) volume of MeCN, (c) amount of MeI, and (d) yield.

Run 1

(a) 0.111 g, 0.48 mmol, 1.0 eq, (b) 2.10 mL, (c) 0.15 mL, 2.4 mmol, 5.0 eq, and (d) 0.147 g, 0.40 mmol, 83% yield.

Run 2

(a) 0.532 g, 2.31 mmol, 1.0 eq, (b) 10.0 mL, (c) 0.71 mL, 11.5 mmol, 5.0 eq, and (d) 0.513 g, 1.39 mmol, 60% yield.

Melting point: 158-161 °C (lit. 159-161 °C).[49]

FTIR (neat): 3304, 3055, 2878, 1578, 1487, 1335 cm^{-1}.

^{1}H NMR (400 MHz, DMSO-*d*$_6$) δ 9.02 (s, 1H, NC<u>H</u>CN), 7.20 (s, 2H, Ar-<u>H</u>), 5.10 (s, 1H, O<u>H</u>), 4.36 (s, 3H, NC<u>H</u>$_3$), 3.81 (t, *J* = 6.6 Hz, 2H, $CH_2C\underline{H}_2OH$), 3.12 (t, *J* = 6.0 Hz, 2H, $C\underline{H}_2CH_2OH$), 2.36 (s, 3H, ArC<u>H</u>$_3$), 2.02 (s, 6H, ArC<u>H</u>$_3$) ppm.

^{13}C NMR (101 MHz, DMSO-*d*$_6$) δ 143.2, 141.6, 134.2, 131.3, 130.9, 129.3, 58.0, 38.1, 26.6, 20.6, 16.6 ppm.

HRMS (NSI): *pending*

4-(2-bromoethyl)-1-mesityl-3-methyl-1H-1,2,3-triazol-3-ium bromide **126**

Scheme 3.30

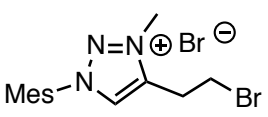

126

Chemical Formula: $C_{14}H_{19}Br_2N_3$
Molecular Weight: 389.1350

To a 25 mL round-bottom flask was added triazolium **123** (1.0 eq) and DCM. The solution was cooled to 0 °C and PBr_3 (0.87 eq) added dropwise. The reaction was stirred at room temperature for 16 h, and then cooled to 0 °C and quenched with saturated aqueous sodium bicarbonate. The mixture was then extracted with DCM and organic phases collected, dried with sodium sulfate and concentrated *in vacuo* to yield **174** as an extremely hygroscopic off-white solid.

Prepared according to above procedure. Data presented as: (a) amount of **123**, (b) volume of DCM mL, (c) amount of PBr_3, and (d) yield.

Run 1

(a) 0.20 g, 0.54 mmol, 1.0 eq, (b) 3.0 mL, (c) 0.047 mL, 0.47 mmol, 0.87 eq, and (d) 0.147 g, 0.47 mmol, 71% yield.

Run 2

(a) 0.28 g, 0.76 mmol, 1.0 eq, (b) 4.2 mL, (c) 0.066 mL, 0.66 mmol, 0.87 eq, and (d) 0.084 g, 0.27 mmol, 35% yield.

FTIR (neat): 3431, 2916, 1576, 1443 cm^{-1}.

^{1}H NMR (400 MHz, DMSO-d_6, apparent mixture of rotamers) δ 9.17 (bs, 1H, NC<u>H</u>N), 7.38 – 6.92 (m, 2H, Ar-<u>H</u>), 4.39 (s, 2H, NC<u>H</u>$_3$), 4.38 (s, 1H, NC<u>H</u>$_3$), 3.93 (t, J = 6.6 Hz, 1.5H, C<u>H</u>$_2$CH$_2$Br), 3.66 – 3.54 (m, 2.5H, CH$_2$C<u>H</u>$_2$Br), 2.37 (s, 3H, ArC<u>H</u>$_3$), 2.04 (s, 2H, ArC<u>H</u>$_3$), 2.03 (s, 4H, ArC<u>H</u>$_3$) ppm.

^{13}C NMR (101 MHz, DMSO-d_6, apparent mixture of rotamers) δ 142.7, 141.8, 134.2, 131.3, 131.2, 131.1, 129.4, 38.2, 29.9, 29.3, 26.9, 26.3, 20.6, 16.6, 16.5 ppm.

HRMS (NSI): Could not be successfully obtained, due to instability of product.

4-(2-(diphenylphosphaneyl)ethyl)-1-mesityl-3-methyl-1H-1,2,3-triazol-3-ium BAr^F **121**

Scheme 3.30

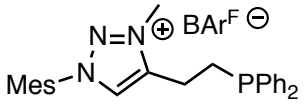

Chemical Formula: $C_{58}H_{40}BF_{24}N_3P$
Molecular Weight: 1276.7239

121

A flame-dried 10 mL round-bottom flask was placed under inert atmosphere *via* three vacuum/argon cycles. The flask was charged with potassium *tert*-butoxide (52.6 mg, 0.47 mmol, 1.0 eq) and DMSO (0.71 mL). To this was added diphenylphosphine (0.079 mL, 0.49 mmol, 1.05 eq) and the reaction mixture stirred for 1 h. A separate flame-dried 10 mL round-bottom flask was placed under an inert atmosphere with three vacuum/argon cycles, and subsequently charged with triazolium bromide **174** (0.180 g, 0.47 mmol, 1.0 eq) and DMSO (0.71 mL). The DMSO solution of potassium diphenylphosphide was then added dropwise, *via* syringe, and stirred for 2 h. Water (7.0 mL) was then added to the reaction mixture and the product extracted with DCM. The organic layer was separated, and placed under an inert atmosphere. $NaBAr^F$ (0.458 g, 0.52 mmol, 1.10 eq) was added and the reaction stirred for 16 h at room temperature. After this time, the reaction mixture was concentrated *in vacuo*, and the residue purified by column chromatography (50% DCM/petrol), however no product was obtainedfrom the reaction and mass degradation was observed.

but-3-yn-1-yl 4-methylbenzenesulfonate **130** [62]

Scheme 3.32

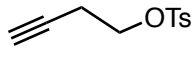

Chemical Formula: $C_{11}H_{12}O_3S$
Molecular Weight: 224.2740

130

Prepared following a literature procedure.[63] To a flame-dried flask was added 4-dimethylaminopyridine (DMAP, 0.01 eq), then the flask was flushed on a vacuum/argon cycle three times. DCM was then added to the reaction flask. After addition of the alcohol (1 eq) and Et_3N (1.1 eq), the flask was cooled to 0 °C, and 4-toluenesulfonyl chloride added in portions. The flask was then allowed to warm to room temperature and stirred overnight. The

mixture was then diluted with water and extracted with DCM. The organic phases were collected, dried with sodium sulfate and concentrated *in vacuo*. The resulting residue was purified by column chromatography (0 – 50% EtOAc/Petrol) to yield **130** as a white solid.

Prepared according to above procedure. Data presented as: (a) amount of 3-butyn-1-ol **124**, (b) volume of DCM mL, (c) amount DMAP (d) amount Et_3N, (e) amount TsCl, and (f) yield.

Run 1

(a) 3.4 mL, 44.6 mmol, 1.0 eq, (b) 152 mL, (c) 54 mg, 0.45 mmol, 0.01 eq, (d) 6.8 mL, 49.0 mmol, 1.1 eq, (e) 9.35 g, 49.0 mmol, 1.1 eq, and (f) 6.90 g, 31.2 mmol, 70% yield.

Run 2

(a) 8.8 mL, 89 mmol, 1.0 eq, (b) 300 mL, (c) 108 mg, 0.89 mmol, 0.01 eq, (d) 13.6 mL, 98 mmol, 1.1 eq, (e) 18.7 g, 98 mmol, 1.1 eq, and (f) 10.0 g, 44.5 mmol, 50% yield.

Melting point: 42-44 °C.

FTIR (neat): 3288, 2963, 1597, 1356, 1173 cm^{-1}.

^{1}H NMR (400 MHz, $CDCl_3$) δ 7.81 (d, *J* = 8.0 Hz, 2H, Ar-H), 7.40 – 7.31 (d, *J* = 8.0 Hz, 2H, Ar-H), 4.11 (t, *J* = 7.1Hz, 2H, CH_2CH_2O), 2.56 (td, *J* = 7.0, ^4J = 2.6 Hz, 2H, CH_2CH_2O), 2.46 (s, 3H, $ArCH_3$), 1.97 (t, ^4J = 2.7 Hz, 1H, C≡CH) ppm.

^{13}C NMR (101 MHz, $CDCl_3$) δ 145.1, 132.9, 130.0, 128.1, 78.5, 70.9, 67.6, 21.7, 19.5 ppm.

4-(trimethylsilyl)but-3-yn-1-yl 4-methylbenzenesulfonate **131** [64]

Scheme 3.32

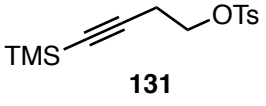

131

Chemical Formula: $C_{14}H_{20}O_3SSi$
Molecular Weight: 296.4560

To a stirred solution of but-3-yn-1-yl 4-methylbenzenesulfonate **130** in dry THF was added ^{n}BuLi (2.16 M in hexane) at -78 °C, and the mixture allowed to stir for 1 h. At this point, trimethylsilyl chloride (TMS-Cl) was added and stirring continued for another hour. The reaction mixture was slowly brought to room temperature with stirring for 4 h. The reaction was quenched by addition of 2% Na_2CO_3 solution and extracted with diethyl ether. The combined organic phases were then dried with Na_2SO_4 and concentrated *in vacuo*. The resulting reside was purified by column chromatography (10% EtOAc/petrol) to obtain **131** as a white solid.

Prepared according to above procedure. Data presented as: (a) amount of **130**, (b) volume of THF mL, (c) volume ^{n}BuLi (d) volume TMS-Cl and (e) yield.

Run 1

(a) 7.09 g, 31.5 mmol, 1.0 eq, (b) 60 mL, (c) 15.3 mL, 33.1 mmol, 1.05 eq, (d) 6.04 mL, 47.3 mmol, 1.5 eq, and (e) 4.88 g, 16.4 mmol, 52% yield.

Run 2

(a) 4.39 g, 19.5 mmol, 1.0 eq, (b) 37 mL, (c) 9.49 mL, 20.5 mmol, 1.05 eq, (d) 3.74 mL, 29.3 mmol, 1.5 eq, and (e) 3.84 g, 12.9 mmol, 66% yield.

Run 3

(a) 3.04 g, 13.5 mmol, 1.0 eq, (b) 26 mL, (c) 6.57 mL, 14.2 mmol, 1.05 eq, (d) 2.59 mL, 20.3 mmol, 1.5 eq, and (e) 3.63 g, 12.2 mmol, 90% yield.

Melting point: 44-46 °C.

FTIR (neat): 2958, 2899, 2180, 1736, 1597, 1362, 1175 cm^{-1}.

^{1}H NMR (400 MHz, $CDCl_3$) δ 7.69 (d, *J* = 8.0 Hz, 2H, Ar-H), 7.23 (d, *J* = 8.0 Hz, 2H, Ar-H), 3.97 (t, *J* = 7.3 Hz, 2H, CH_2CH_2O), 2.47 (t, *J* = 7.3 Hz, 2H, CH_2CH_2O), 2.34 (s, 3H, $ArCH_3$), 0.00 (s, 9H, $Si(CH_3)_3$) ppm.

^{13}C NMR (101 MHz, $CDCl_3$) δ 145.1, 133.1, 130.0, 128.1, 100.5, 87.6, 67.7, 21.8, 20.9, 0.0 ppm.

diphenyl(4-(trimethylsilyl)but-3-yn-1-yl)phosphane borane **132**

Scheme 3.32

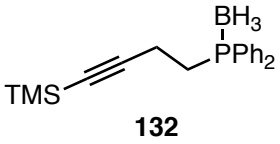

132

Chemical Formula: $C_{19}H_{26}BPSi$
Molecular Weight: 324.2858

Prepared according to *General Procedure G*. Purification by column chromatography (hexane:EtOAc:MeOH 55:45:2). Data presented as: (a) amount of $HP(BH_3)Ph_2$, (b) volume of THF mL, (c) volume ^{n}BuLi (d) amount tosylate **131** and (e) yield.

Run 1

(a) 0.214 g, 1.07 mmol, 1.0 eq, (b) 4.0 mL, (c) 0.43 mL (2.5 M in hexane),, 1.07 mmol, 1.0 eq, (d) 0.349 g, 1.18 mmol, 1.1 eq, and (e) 0.052 g, 0.16 mmol, 15% yield.

Run 2

(a) 0.97 g, 4.85 mmol, 1.0 eq, (b) 13.0 mL, (c) 1.95 mL (2.16 M in hexane), 4.85 mmol, 1.0 eq, (d) 1.59 g, 5.34 mmol, 1.1 eq, and (e) 0.610 g, 1.94 mmol, 40% yield.

Run 3

(a) 1.05 g, 5.24 mmol, 1.0 eq, (b) 14.0 mL, (c) 2.10 mL (2.16 M in hexane), 5.24 mmol, 1.0 eq, (d) 1.71 g, 5.76 mmol, 1.1 eq, and (e) 0.520 g, 1.62 mmol, 31% yield.

Melting point: 44-46 °C.

FTIR (neat): 3077, 2957, 2378, 2240, 2176, 1437 cm^{-1}

^{1}H NMR (400 MHz, $CDCl_3$) δ 7.73 – 7.63 (m, 5H, Ar-H), 7.57 – 7.40 (m, 5H, Ar-H), 2.61 – 2.38 (m, 4H, CH_2CH_2P), 1.46 – 0.91 (m, 3H, BH_3), 0.12 (s, 9H, $Si(CH_3)_3$) ppm.

^{13}C NMR (101 MHz, $CDCl_3$) δ 132.2 (d, $^{3}J_{C\text{-}P}$ = 9.0 Hz), 131.6, 129.0 (d, $^{2}J_{C\text{-}P}$ = 10.0 Hz), 128.7 (d, $^{1}J_{C\text{-}P}$ = 33.4 Hz), 105.4 (d, $^{3}J_{C\text{-}P}$ = 18.1 Hz), 85.8, 25.5 (d, $^{1}J_{C\text{-}P}$ = 35.7 Hz), 14.6, 0.1 ppm.

^{11}B NMR (128 MHz, $CDCl_3$): δ -40.7 (q, $^{1}J_{B\text{-}H}$ = 101.0 Hz) ppm

^{31}P NMR (162 MHz, $CDCl_3$): δ 15.7 ppm

HRMS *pending*

but-3-yn-1-yldiphenylphosphino borane **129**

Scheme 3.32

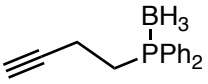

Chemical Formula: $C_{16}H_{18}BP$
Molecular Weight: 252.1038

129

Prepared according to *General Procedure A*. Purification by column chromatography (hexane:EtOAc:MeOH 55:45:2). Data presented as: (a) amount of **132**, (b) volume of MeOH, (c) amount of K_2CO_3, and (d) yield as a colourless oil.

Run 1

(a) 52 mg, 0.16 mmol, 1.0 eq, (b) 1.0 mL, (c) 59.2 mg, 0.43 mmol, 2.7 eq, and (d) 23.8 mg, 0.09 mmol, 59% yield.

Run 2

(a) 480 mg, 1.48 mmol, 1.0 eq, (b) 9.2 mL, (c) 546.5 mg, 4.0 mmol, 2.7 eq, and (d) 270.1 mg, 1.02 mmol, 69% yield.

Run 3

(a) 592 mg, 1.82 mmol, 1.0 eq, (b) 11.0 mL, (c) 674 mg, 4.91 mmol, 2.7 eq, and (d) 307.2 mg, 1.16 mmol, 59% yield.

FTIR (neat): 3283, 3057, 2959, 2916, 2378, 2344, 1676, 1585, 1433, 1107 cm^{-1}.

^{1}H NMR (400 MHz, $CDCl_3$) δ 7.77 – 7.62 (m, 4H, Ar-H), 7.56 – 7.40 (m, 6H, Ar-H), 2.56 – 2.37 (m, 4H, CH_2CH_2P), 1.96 (t, ^{4}J = 2.5 Hz, 1H, C≡CH), 1.40 – 0.53 (m, 3H, BH_3) ppm.

^{13}C NMR (101 MHz, $CDCl_3$) δ 131.7 (d, $^{3}J_{C\text{-}P}$ = 9.4 Hz), 131.0, 128.5 (d, $^{2}J_{C\text{-}P}$ = 10.8 Hz), 128.1 (d, $^{1}J_{C\text{-}P}$ = 56.2 Hz), 82.3 (d, $^{3}J_{C\text{-}P}$ = 19.2 Hz), 68.9, 25.0 (d, $^{1}J_{C\text{-}P}$ = 35.8 Hz), 12.6 ppm.

^{11}B NMR (128 MHz, $CDCl_3$): δ -40.8 (q, $^{1}J_{B\text{-}H}$ = 101.9 Hz) ppm

^{31}P NMR (162 MHz, $CDCl_3$): δ 16.0 ppm

HRMS *pending*

4-(2-(diphenylphosphenylborane)ethyl)-1-mesityl-1H-1,2,3-triazole **128**

Scheme 3.33

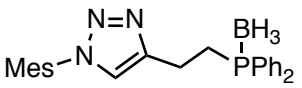

Chemical Formula: $C_{25}H_{29}BN_3P$
Molecular Weight: 413.3118

128

Prepared according to *General Procedure H*. Product purified by column chromatography (0 – 10% MeOH/DCM). Data presented as: (a) amount of $Cu(OAc)_2 \cdot H_2O$, (b) amount of 1,10-phenanthroline monohydrate, (c) amount of NaAsc, (d) amount of alkyne **129**, (e) amount Mes-N_3 **101**, (f) amount EtOH/H_2O (4:1), and (g) yield.

Run 1

(a) 5.9 mg, 5 mol%, 0.03 mmol, (b) 5.9 mg, 5 mol%, 0.03 mmol, (c) 0.117 g, 0.59 mmol, 1.0 eq, (d) 0.152 g, 0.59 mmol, 1.0 eq, (e) 0.115 g, 0.71mmol, 1.2 eq, (f) 3.0 mL, and (g) 0.097 g, 0.24 mmol, 40% yield as a colourless oil.

Run 2

(a) 11.58 mg, 5 mol%, 0.06 mmol, (b) 11.60 mg, 5 mol%, 0.06 mmol,(c) 0.232 g, 1.17 mmol, 1.0 eq (d) 0.330 g, 1.17 mmol, 1.0 eq, (e) 0.223 g, 1.40 mmol, 1.2 eq, (f) 6.0 mL, and (g) 0.157 g, 0.4 mmol, 34% yield as a colourless oil.

FTIR ($CHCl_3$): 3134, 2924, 2857, 1491, 1437 cm^{-1}.

^{1}H NMR (400 MHz, $CDCl_3$) δ 7.83 – 7.73 (m, 4H, Ar-H), 7.53 – 7.43 (m, 6H, Ar-H), 7.36 (s, 1H, NCHN), 6.96 (s, 2H, Ar-H), 3.10 – 2.96 (m, 2H, CH_2CH_2P), 2.90 – 2.72 (m, 2H, CH_2CH_2P), 2.34 (s, 3H, $ArCH_3$), 1.90 (s, 6H, $ArCH_3$), 1.74 – 0.35 (m, 3H, BH_3) ppm.

^{13}C NMR (101 MHz, $CDCl_3$) δ 140.1, 135.2, 133.6, 132.4 (d, $^2J_{C\text{-}P}$ = 9.0 Hz), 131.5, 129.3, 129.2, 129.1 (d, $^1J_{C\text{-}P}$ = 56.2 Hz), 129.0, 123.1, 25.4 (d, $^1J_{C\text{-}P}$ = 37.0 Hz), 21.2, 19.8, 17.4 ppm.

^{11}B NMR (128 MHz, $CDCl_3$): δ -39.9 ppm

^{31}P NMR (162 MHz, $CDCl_3$): δ 15.9 ppm

HRMS *pending*

4-(2-(diphenylphosphenylborane)ethyl)-1-mesityl-1H-1,2,3-triazolium iodide **133**

Scheme 3.33

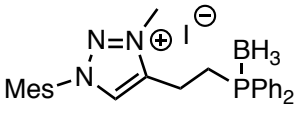

Chemical Formula: $C_{26}H_{32}BIN_3P$
Molecular Weight: 555.2512

133

Prepared according to *General Procedure B*. Data presented as: (a) amount of triazole **128**, (b) volume of MeCN, (c) amount of MeI, and (d) yield.

Run 1

(a) 0.254 g, 0.61 mmol, 1.0 eq, (b) 2.65 mL, (c) 0.189 mL, 3.1 mmol, 5.0 eq, and (d) 0.147 g, 0.43 mmol, 71% yield as a beige solid.

Melting point: 90-92 °C.

FTIR (neat): 3435, 3219, 2965, 2359, 2328, 1587, 1485, 1435 cm^{-1}.

^{1}H NMR (400 MHz, $CDCl_3$, rotameric mixture) δ 9.15 (s, 0.7H, NC<u>H</u>CN), 8.86 (s, 0.3H, NC<u>H</u>CN), 8.22 – 8.07 (m, 2.8 H, Ar-<u>H</u>), 7.95 – 7.82 (m, 1.2 H, Ar-<u>H</u>), 7.76 – 7.65 (m, 4H, Ar-<u>H</u>), 7.54 – 7.44 (m, 2H, Ar-<u>H</u>), 7.02 (s, 0.6H, Ar-<u>H</u>), 7.00 (s, 1.4H, Ar-<u>H</u>), 4.58 – 4.44 (m, 2H, NC<u>H</u>$_3$), 4.33 (s, 1H, NC<u>H</u>$_3$), 3.51 – 3.39 (m, 2H, CH_2C<u>H</u>$_2$P), 3.01 – 2.92 (m, 2H, C<u>H</u>$_2CH_2$P), 2.16 (s, 3H, ArC<u>H</u>$_3$), 2.11 (s, 3.5H, ArC<u>H</u>$_3$), 2.00 (s, 2.5H, ArC<u>H</u>$_3$), 1.74 – 1.64 (m, 3H, B<u>H</u>$_3$) ppm.

^{13}C NMR (101 MHz, $CDCl_3$, rotameric mixture) δ 143.0, 142.5, 140.2, 135.4, 135.2, 135.0, 134.9, 133.1 (d, $^{2}J_{C\text{-}P}$ = 10.8 Hz), 132.7, 130.8, 130.7, 130.6, 129.5 (d, $^{1}J_{C\text{-}P}$ = 66.4 Hz), 40.5, 21.3 (d, J = 9.4 Hz), 19.5, 18.5, 17.6, 17.4 ppm.

^{11}B NMR (128 MHz, $CDCl_3$): δ -41.4 ppm

^{31}P NMR (162 MHz, $CDCl_3$): δ 24.1 ppm

HRMS (positive ESI): m/z calculated for $C_{26}H_{32}N_3BP$ $[M+H]^+$: 428.2411, found: 428.2421.

4-(2-(diphenylphosphenylborane)ethyl)-1-mesityl-1H-1,2,3-triazolium BAr^F **134**

Scheme 3.33

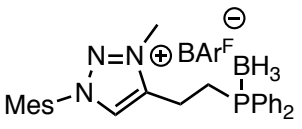

134

Chemical Formula: $C_{58}H_{43}B_2F_{24}N_3P$
Molecular Weight: 1290.5579

Prepared according to *General Procedure C.* Product purified by column chromatography (0-15% MeOH/DCM). Data presented as: (a) amount of **133**, (b) volume of DCM, (c) amount of $NaBAr^F$, and (d) yield.

Run 1

(a) 114 mg, 0.21 mmol, 1.0 eq, (b) 2.3 mL, (c) 204 mg, 0.22 mmol, 1.1 eq, and (d) 70 mg, 0.06 mmol, 26% yield as a yellow oil.

FTIR (neat): 2986, 2970, 2901, 1608, 1352 cm^{-1}.

^{1}H NMR (400 MHz, $CDCl_3$): δ 8.23 (s, 1H, NC<u>H</u>CN), 7.70 – 7.58 (m, 13H, Ar-<u>H</u>), 7.55-7.51 (m, 3H, Ar-<u>H</u>), 7.50 – 7.48 (m, 6H, Ar-<u>H</u>), 7.09 – 7.02 (m, 2H, Ar-<u>H</u>), 4.11 (s, 3H, NC<u>H</u>$_3$), 3.10 – 3.00 (m, 2H, $CH_2C\underline{H}_2P$), 2.72 – 2.58 (m, 2H, $C\underline{H}_2CH_2P$), 2.39 (s, 3H, ArC<u>H</u>$_3$), 1.95 (s, 6H, ArC<u>H</u>$_3$), 1.31 – 0.88 (s, 3H, B<u>H</u>$_3$) ppm.

^{13}C NMR (101 MHz, $CDCl_3$) δ 161.8 (q, $^{1}J_{C\text{-}B}$ = 49.7 Hz), 140.8, 136.0, 134.9, 134.7, 132.4, 131.8 (d, $^{3}J_{C\text{-}P}$ = 10.7 Hz), 131.0 (d, $^{2}J_{C\text{-}P}$ = 12.7 Hz), 129.4, 129.1 (d, $^{1}J_{C\text{-}P}$ = 56.4 Hz), 129.0 (q, $^{2}J_{C\text{-}F}$ = 29.6 Hz), 128.7, 124.7 (q, $^{1}J_{C\text{-}F}$ = 274.1 Hz), 123.7, 117.6, 29.6, 22.9 (d, J = 52.6 Hz), 21.2, 18.5, 17.2 ppm

^{11}B NMR (128 MHz, $CDCl_3$): δ -6.8, -41.9 ppm

^{31}P NMR (162 MHz, $CDCl_3$): δ 22.8 ppm

^{19}F NMR (376 MHz, $CDCl_3$): δ -62.4 ppm

HRMS: *pending*

4-(2-(diphenylphosphaneyl)ethyl)-1-mesityl-3-methyl-1H-1,2,3-triazol-3-ium BAr^F **121**

Scheme 3.33

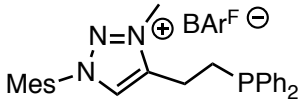

Chemical Formula: $C_{58}H_{40}BF_{24}N_3P$
Molecular Weight: 1276.7239

121

Prepared according to a modified literature procedure. [65] A flame-dried 10 mL round-bottom flask was placed under inert atmosphere with three vacuum/argon cycles. The flask was charged with **134** (70 mg, 0.054 mmol, 1.0 eq) and DABCO (4.22 mg, 0.07 mmol, 1.2 eq), and toluene (1 mL) added. The reaction mixture was stirred at 70 °C for 16 h. The solution

was then cooled to room temperature and concentrated *in* vacuo. The residue purified by column chromatography (50% DCM/petrol), to yield a complex mixture of inseparable products.

Attempted synthesis of but-3-yn-1-yldiphenylphosphine oxide **136** - 1

Scheme 3.35

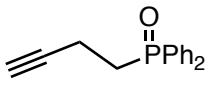

Chemical Formula: $C_{16}H_{15}OP$
Molecular Weight: 254.2688

136

Attempted according to a modified literature procedure.[51] To a mixture of triphenylphosphine oxide (139.7 mg, 0.5 mmol, 1.0 eq), NaH (40 mg, 1.0 mmol, 2.0 eq) and LiI (66.9 mg, 0.5 mmol, 1.0 eq) in a 25 mL reaction vessel was added THF (2.5 mL). The reaction mixture was stirred at 60 °C for 16 h. The reaction mixture was then cooled to 0 °C and tosylate **130** added (119.4 mg, 0.53 mmol, 1.1 eq). The reaction mixture was then stirred at this temperature for 1 h. The reaction mixture was then quenched by addition of saturated ammonium chloride solution at 0 °C, and extracted with ethyl acetate. The combined organic phases were washed with brine, dried with sodium sulfate and concentrated *in vacuo*. Purification by column chromatography (hexane:EtOAc:MeOH, 55:45:2) failed to yield product **136**.

Attempted synthesis of but-3-yn-1-yldiphenylphosphine oxide **136** - 2

Scheme 3.36

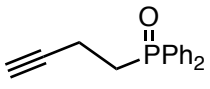

Chemical Formula: $C_{16}H_{15}OP$
Molecular Weight: 254.2688

136

Attempted according to a modified literature procedure.[52] To a flame-dried Schlenk flask under argon, was added diphenylphosphine oxide (101 mg, 0.5 mmol, 1.0 eq) and LiOMe (19 mg, 0.5 mmol, 1.0 eq). TMEDA (07.49 μL, 0.05 mmol, 0.1 eq), NMP (0.5 mL) and tosylate **130** (56.0 mg, 0.25 mmol, 0.5 eq) were added in turn and the resulting solution stirred at 40 °C for 24 h. At this point, the reaction mixture was quenched by addition of H_2O, and extracted with DCM. The combined organic phases were then dried with sodium sulfate and concentrated *in vacuo*. Purification by column chromatography (hexane:EtOAc:MeOH, 55:45:2) failed to yield product **136**.

diphenyl(4-(trimethylsilyl)but-3-yn-1-yl)phosphine oxide **139**

Scheme 3.37

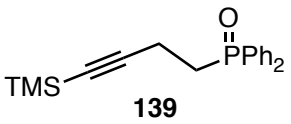

139

Chemical Formula: $C_{19}H_{23}OPSi$
Molecular Weight: 326.4508

Prepared according to *General Procedure G*. Purification by column chromatography (hexane:EtOAc:MeOH 55:45:2). Data presented as: (a) amount of $HP(O)Ph_2$, (b) volume of THF mL, (c) volume ^{n}BuLi (d) amount tosylate **131** and (e) yield as a white solid.

Run 1

(a) 0.92 g, 4.56 mmol, 1.0 eq, (b) 18.0 mL, (c) 2.19 mL (2.08 M in hexane), 4.56 mmol, 1.0 eq, (d) 1.36 g, 4.56 mmol, 1.0 eq and (e) 0.40 g, 1.23 mmol, 27% yield.

Run 2

(a) 2.72 g, 13.46 mmol, 1.0 eq, (b) 52.0 mL, (c) 6.47 mL (2.08 M in hexane), 13.46 mmol, 1.0 eq, (d) 4.0 g, 13.46 mmol, 1.0 eq and (e) 1.582 g, 4.85 mmol, 36% yield.

Run 3

(a) 3.11 g, 15.40 mmol, 1.0 eq, (b) 60.0 mL, (c) 7.41 mL (2.08 M in hexane), 15.40 mmol, 1.0 eq, (d) 4.58 g, 15.40 mmol, 1.0 eq and (e) 2.0 g, 6.16 mmol, 40% yield.

Melting point: 84-87 °C.

FTIR (neat):, 2986, 2900, 2181, 1597, 154 cm^{-1}.

^{1}H NMR (400 MHz, $CDCl_3$) δ 7.83 – 7.69 (m, 5H, Ar-H), 7.55 – 7.44 (m, 5H, Ar-H), 2.58 – 2.49 (m, 4H, CH_2CH_2P), 0.10 (s, 9H, $Si(CH_3)_3$) ppm.

^{13}C NMR (101 MHz, $CDCl_3$) δ 132.4 (d, $^{1}J_{C-P}$ = 99.6 Hz), 132.1, 131.0 (d, $^{3}J_{C-P}$ = 9.3 Hz), 128.8 (d, $^{2}J_{C-P}$ = 12.2 Hz), 105.4 (d, $^{3}J_{C-P}$ = 18.5 Hz), 85.7, 29.9 (d, $^{1}J_{C-P}$ = 50.2 Hz), 12.9, 0.1 ppm.

^{31}P NMR (162 MHz, $CDCl_3$): δ 30.8 ppm

HRMS (NSI): m/z calculated for $C_{19}H_{24}OPSi$ $[M+H]^+$: 327.1329, found: 327.1318.

but-3-yn-1-yldiphenylphosphine oxide **136** [51]

Scheme 3.37

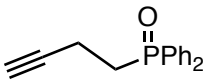

Chemical Formula: $C_{16}H_{15}OP$
Molecular Weight: 254.2688

136

Prepared according to *General Procedure A*. Purification by column chromatography (hexane:EtOAc:MeOH 55:45:2). Data presented as: (a) amount of **139**, (b) volume of MeOH, (c) amount of K_2CO_3, and (d) yield as a colourless oil.

Run 1

(a) 1.542 g, 4.72 mmol, 1.0 eq, (b) 30.0 mL, (c) 1.741 g, 12.74 mmol, 2.7 eq, and (d) 1.19 g, 4.72 mmol, >99% yield.

Run 2

(a) 2.01 g, 6.16 mmol, 1.0 eq, (b) 40.0 mL, (c) 2.273 g, 16.63 mmol, 2.7 eq, and (d) 1.55 g, 6.16 mmol, >99% yield.

FTIR (neat): 3310, 2914, 2847, 1629, 1545 cm^{-1}.

^{1}H NMR (400 MHz, $CDCl_3$) δ 7.83 – 7.67 (m, 4H, Ar-H), 7.61 – 7.36 (m, 6H, Ar-H), 2.58 – 2.44 (m, 4H, CH_2CH_2P), 1.92 (t, J = 2.4 Hz, 1H, C≡CH) ppm.

^{13}C NMR (101 MHz, $CDCl_3$) δ 132.4 (d, $^{1}J_{C\text{-}P}$ = 97.1 Hz), 132.1, 130.9 (d, J = 9.3 Hz), 128.9 (d, $^{2}J_{C\text{-}P}$ = 12.2 Hz), 82.8 (d, $^{3}J_{C\text{-}P}$ = 19.8 Hz), 69.5, 29.4 (d, $^{1}J_{C\text{-}P}$ = 50.2 Hz), 11.6 ppm.

^{31}P NMR (162 MHz, $CDCl_3$): δ 31.1 ppm

(2-(1-mesityl-1H-1,2,3-triazol-4-yl)ethyl)diphenylphosphine oxide **135**

Scheme 3.38

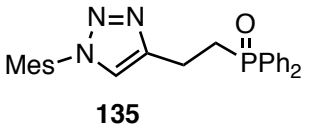

135

Chemical Formula: $C_{25}H_{26}N_3OP$
Molecular Weight: 415.4768

Prepared according to *General Procedure H*. Product purified by column chromatography (0-10% MeOH/DCM). Data presented as: (a) amount of $Cu(OAc)_2 \cdot H_2O$, (b) amount of 1,10-phenanthroline monohydrate, (c) amount of NaAsc, (d) amount of alkyne **129**, (e) amount Mes-N_3 **101**, (f) amount EtOH/H_2O (4:1), and (g) yield.

Run 1

(a) 5.6 mg, 5 mol%, 0.03 mmol, (b) 5.6 mg, 5 mol%, 0.03 mmol, (c) 0.112 g, 0.56 mmol, 1.0 eq, (d) 0.42 g, 0.56 mmol, 1.0 eq, (e) 0.110 g, 0.67 mmol, 1.2 eq, (f) 3.0 mL, and (g) 0.162 g, 0.39 mmol, 69% yield as a colourless oil.

Run 2

(a) 9.4 mg, 5 mol%, 0.05 mmol, (b) 9.4 mg, 5 mol%, 0.05 mmol, (c) 0.188 g, 0.94 mmol, 1.0 eq, (d) 0.240 g, 0.94 mmol, 1.0 eq, (e) 0.184 g, 1.13 mmol, 1.2 eq, (f) 5.0 mL, and (g) 0.253 g, 0.61 mmol, 65% yield as a colourless oil.

Run 3

(a) 19.7 mg, 5 mol%, 0.098 mmol, (b) 19.7 mg, 5 mol%, 0.098 mmol, (c) 0.391 g, 1.96 mmol, 1.0 eq, (d) 0.50 g, 1.96 mmol, 1.0 eq, (e) 0.383 g, 2.35 mmol, 1.2 eq, (f) 17.0 mL, and (g) 0.723 g, 1.74 mmol, 89% yield as a colourless oil.

Run 4

(a) 79.4 mg, 5 mol%, 0.4 mmol, (b) 79.4 mg, 5 mol%, 0.4 mmol, (c) 1.58 g, 7.90 mmol, 1.0 eq, (d) 2.02 g, 7.90 mmol, 1.0 eq, (e) 1.54 g, 9.48 mmol, 1.2 eq, (f) 69.0 mL, and (g) 1.412 g, 3.48 mmol, 44% yield as a colourless oil.

FTIR ($CHCl_3$): 3674, 2970, 2901, 2359, 1437 cm^{-1}.

^{1}H NMR (400 MHz, $CDCl_3$) δ 7.89 – 7.74 (m, 4H, Ar-H), 7.52 – 7.41 (m, 6H, Ar-H), 7.36 (s, 1H, NCHN), 6.92 (s, 2H, Ar-H), 3.19 – 3.05 (m, 2H, CH_2CH_2P), 2.91 – 2.75 (m, 2H, CH_2CH_2P), 2.29 (s, 3H, $ArCH_3$), 1.86 (s, 6H, $ArCH_3$) ppm.

^{13}C NMR (101 MHz, $CDCl_3$) δ 146.3, 139.9, 135.0, 133.5, 132.6 (d, $^1J_{C\text{-}P}$ = 99.5 Hz), 131.9, 130.8 (d, $^3J_{C\text{-}P}$ = 9.3 Hz), 129.0, 128.8 (d, $^2J_{C\text{-}P}$ = 12.3 Hz), 123.0, 29.4 (d, $^1J_{C\text{-}P}$ = 71.0 Hz), 21.1, 18.0, 17.3 ppm.

^{31}P NMR (162 MHz, $CDCl_3$): δ 31.9 ppm

HRMS: *pending*

4-(2-(diphenylphosphenyloxide)ethyl)-1-mesityl-1H-1,2,3-triazolium iodide **140**

Scheme 3.38

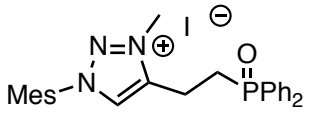

140

Chemical Formula: $C_{26}H_{29}IN_3OP$
Molecular Weight: 557.4162

Prepared according to *General Procedure B*. Data presented as: (a) amount of triazole **135**, (b) volume of MeCN, (c) amount of MeI, and (d) yield.

Run 1

(a) 0.152 g, 0.37 mmol, 1.0 eq, (b) 1.85 mL, (c) 0.230 mL, 1.85 mmol, 5.0 eq, and (d) 0.177 g, 0.23 mmol, 73% yield as a beige solid.

Run 2

(a) 0.210 g, 0.51 mmol, 1.0 eq, (b) 2.55 mL, (c) 0.317 mL, 2.55 mmol, 5.0 eq, and (d) 0.230 g, 0.35 mmol, 81% yield as a beige solid.

Run 3

(a) 1.19 g, 2.89 mmol, 1.0 eq, (b) 14.5 mL, (c) 1.80 mL, 14.5 mmol, 5.0 eq, and (d) 1.04 g, 1.59 mmol, 55% yield as a beige solid.

Run 4

(a) 1.51g, 3.67 mmol, 1.0 eq, (b) 18.4 mL, (c) 2.29 mL, 18.4 mmol, 5.0 eq, and (d) 1.01 g, 1.54 mmol, 42% yield as a beige solid.

Melting point: >200 °C (decomposition).

FTIR (neat): 3661, 2986, 2901, 2358. 1433 cm^{-1}.

^{1}H NMR (400 MHz, $CDCl_3$) δ 9.02 (s, 1H, NC<u>H</u>CN), 7.98 – 7.79 (m, 4H, Ar-<u>H</u>), 7.71 – 7.39 (m, 6H, Ar-<u>H</u>), 7.00 (s, 2H, Ar-<u>H</u>), 4.39 (s, 3H, NC<u>H</u>$_3$), 3.57 – 3.41 (m, 2H, $CH_2C\underline{H}_2P$), 3.31 – 3.20 (m, 2H, C<u>H</u>$_2$$CH_2P$), 2.35 (s, 3H, ArC<u>H</u>$_3$), 2.06 (s, 6H, ArC<u>H</u>$_3$) ppm.

^{13}C NMR (101 MHz, $CDCl_3$) δ 144.9, 144.8, 142.6, 136.0, 134.5, 132.5, 131.3 (d, $^{1}J_{C\text{-}P}$ = 84.3 Hz), 131.0 (d, $^{3}J_{C\text{-}P}$ = 9.3 Hz), 129.9, 129.2 (d, $^{2}J_{C\text{-}P}$ = 11.5 Hz), 39.4, 28.0 (d, $^{1}J_{C\text{-}P}$ = 69.6 Hz), 18.2, 18.1 ppm.

^{31}P NMR (162 MHz, $CDCl_3$): δ 32.2 ppm

HRMS (NSI): m/z calculated for $C_{26}H_{29}IN_3OPNa$ $[M+Na]^+$: 580.0996, found: 580.0979.

4-(2-(diphenylphosphenyloxide)ethyl)-1-mesityl-1H-1,2,3-triazolium BAr^F **141**

Scheme 3.38

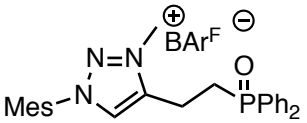

141

Chemical Formula: $C_{58}H_{40}BF_{24}N_3OP$
Molecular Weight: 1292.7229

Prepared according to *General Procedure C.* Product purified by column chromatography (5-10% MeOH/DCM). Data presented as: (a) amount of **140**, (b) volume of DCM, (c) amount of $NaBAr^F$, and (d) yield as a beige solid.

Run 1

(a) 230 mg, 0.41 mmol, 1.0 eq, (b) 4.0 mL, (c) 398 mg, 0.45 mmol, 1.1 eq, and (d) 340 mg, 0.26 mmol, 64% yield as a yellow oil.

Run 2

(a) 286 mg, 0.51 mmol, 1.0 eq, (b) 5.0 mL, (c) 398 mg, 0.56 mmol, 1.1 eq, and (d) 500 mg, 0.38 mmol, 75% yield as a yellow oil.

Run 3

(a) 297 mg, 0.53 mmol, 1.0 eq, (b) 5.2 mL, (c) 414 mg, 0.58 mmol, 1.1 eq, and (d) 656 mg, 0.50 mmol, 94% yield as a yellow oil.

Melting point: >140-142 °C.

FTIR (neat): 3764, 2986, 2970, 2359, 1354, 1275 cm^{-1}.

^{1}H NMR (400 MHz, $CDCl_3$): δ 8.26 (s, 1H, NC<u>H</u>CN), 7.70 – 7.64 (m, 11H, Ar-<u>H</u>), 7.61 – 7.55 (m, 2H, Ar-<u>H</u>), 7.54 – 7.47 (m, 9H, Ar-<u>H</u>), 7.05 (s, 2H, Ar-<u>H</u>), 4.15 (s, 3H, NC<u>H</u>$_3$), 3.18 – 3.04 (m, 2H, $CH_2C\underline{H}_2P$), 2.76 – 2.63 (m, 2H, $C\underline{H}_2CH_2P$), 2.37 (s, 3H, ArC<u>H</u>$_3$), 1.95 (s, 6H, ArC<u>H</u>$_3$) ppm.

^{13}C NMR (101 MHz, $CDCl_3$) δ 161.8 (q, $^{1}J_{C\text{-}B}$ = 49.8 Hz), 143.7, 143.6, 134.9, 133.9, 133.2, 131.3, 130.8, 130.5, 130.3 (d, J = 12.4 Hz), 130.2, 129.0 (q, $^{2}J_{C\text{-}F}$ = 30.5 Hz), 129.5 (d, J = 12.3 Hz), 124.6 (q, $^{1}J_{C\text{-}F}$ = 271.9 Hz), 117.6, 38.1, 27.1 (d, J = 69.4 Hz), 21.3, 17.0 ppm.

^{11}B NMR (128 MHz, $CDCl_3$): δ -6.6 ppm

^{31}P NMR (162 MHz, $CDCl_3$): δ 30.9 ppm

^{19}F NMR (376 MHz, $CDCl_3$): δ -62.4 ppm

HRMS (positive ESI): m/z calculated for $C_{26}H_{30}N_3OP$ $[M+H]^+$: 430.2043, found: 430.2041.

HRMS (negative ESI): m/z calculated for $[C_{32}H_{12}BF_{24}, BArF]^-$: 863.0654, found: 863.0650.

Attempted synthesis of 4-(2-(diphenylphosphine)ethyl)-1-mesityl-1H-1,2,3-triazolium iodide **142**

Table 3.8

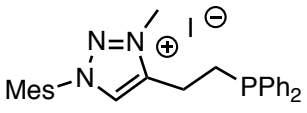

142

Chemical Formula: $C_{26}H_{29}IN_3P$
Molecular Weight: 541.4172

Prepared according to *General Procedure I* for 3 h. Data presented as: (a) amount of triazolium iodide **140**, (b) volume of solvent, (c) amount of DIBAL-H (1 M PhMe), and (d) yield.

Run 1

(a) 50 mg , 0.09 mmol, 1.0 eq, (b) 0 mL, (c) 0.18 mL, 0.18 mmol, 2.0 eq, and (d) trace product observed.

Run 2

(a) 50 mg , 0.09 mmol, 1.0 eq, (b) 0.18 mL THF, (c) 0.18 mL, 0.18 mmol, 2.0 eq, and (d) trace product observed.

Run 3

(a) 50 mg , 0.09 mmol, 1.0 eq, (b) 0.18 mL DCM, (c) 0.18 mL, 0.18 mmol, 2.0 eq, and (d) no product observed.

Attempted synthesis of 4-(2-(diphenylphosphine)ethyl)-1-mesityl-1H-1,2,3-triazolium iodide **142**

Table 3.9

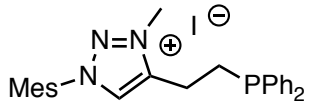

142

Chemical Formula: $C_{26}H_{29}IN_3P$
Molecular Weight: 541.4172

Attempted according to a patent procedure. [53] Triazolium iodide **140** (100 mg, 0.18 mmol, 1.0 eq) was placed in a flame-dried microwave vial under argon and charged with I_2 (5 mg, 20 μ mol) and P^nBu_3 (0.185 mL, 0.74 mmol, 4.1 eq) in degassed MeCN/THF 1:1 (1 mL). The

mixture was stirred for the allotted time and at the allotted temperature. The solvent was then removed *in vacuo* and the crude mixture analysed by ^{31}P NMR spectroscopy.

Table 3.24

Entry	X h	T °C	140:142 in ^{31}P NMR
1	2	rt	2:1
2	16	rt	1.5:1
3	72	rt	degradation
4	2	40	1:1
5	5	40	1:5

Towards the synthesis of 4-(2-(diphenylphosphaneyl)ethyl)-1-mesityl-3-methyl-1H-1,2,3-triazol-3-ium BAr^F **121**

Table 3.10

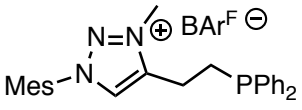

121

Chemical Formula: $C_{58}H_{40}BF_{24}N_3P$
Molecular Weight: 1276.7239

Synthesis of compound **121** was attempted *via* the four following synthetic procedures:

Entry 1

Attempted according to a modified literature procedure. [54] Phosphine oxide **141** (189 mg, 0.15 mmol, 1.0 eq) was dissolved in anhydrous chloroform (0.36 mL). Trichlorosilane (0.22

mL, 2.25 mmol, 15 eq) was added and the resulting solution stirred under an argon atmosphere for 4 h. The reaction mixture was then quenched by slow addition of saturated sodium bicarbonate solution and extracted with chloroform, then all combined extracts concentrated *in vacuo*. The residue was purified by column chromatography (50% DCM/petrol), to yield only starting material **141**.

Entry

Attempted according to a modified literature procedure.[55] To a flame-dried Schlenk tube was added $Cu(OTf)_2$ (2.0 mg, 0.006 mmol, 15 mol%) and phosphine oxide **141** (50 mg, 0.04 mmol, 1.0 eq). Under argon, dry toluene (0.3 mL) and TMDS (13.68 μL, 0.08 mmol, 2.0 eq) were added and the reaction mixture stirred at 100 °C for 2 h. The solvent was removed under vacuum. Analysis of the crude material by ^{31}P NMR spectroscopy revealed no reaction had taken place, and starting material remained.

Entry 3

Attempted according to a modified literature procedure. [56] $CeCl_3$ (21.2 mg, 0.06 mmol, 1.5 eq) was dried in a Schlenk tube under vacuum for 1 h at 135 °C. Once cooled to room temperature, phosphine oxide **141** (50 mg, 0.04 mmol, 1.0 eq) and THF (0.13 mL) were added, followed by $LiAlH_4$ (3.0 mg, 0.08 mmol, 2 eq). The reaction mixture was then heated to 40 °C and stirred for 2 h. The reaction mixture was then quenched by slow addition of water and extracted with chloroform, then all combined extracts concentrated *in vacuo*. Analysis of the crude material by ^{31}P NMR spectroscopy revealed no reaction had taken place, and starting material remained.

Entry 4

Prepared according to *General Procedure I* for 4 h. Data presented as: (a) amount of triazolium iodide **140**, (b) volume of solvent, (c) amount of DIBAL-H (25% hexane), and (d) yield.

(a) 100 mg , 0.08 mmol, 1.0 eq, (b) 0 mL, (c) 1.2 mL, 0.32 mmol, 4.0 eq, and (d) 36 mg, 0.03 mmol, 35% yield.

Note: Data for compound **121** presented after further successful reactions.

4-(2-(diphenylphosphaneyl)ethyl)-1-mesityl-3-methyl-1H-1,2,3-triazol-3-ium BAr^F **121**

Table 3.11

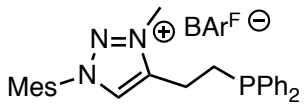

121

Chemical Formula: $C_{58}H_{40}BF_{24}N_3P$
Molecular Weight: 1276.7239

Prepared according to *General Procedure I* for 4 h. Data presented as: (a) amount of triazolium iodide **140**, (b) volume of solvent, (c) amount of DIBAL-H (25% hexane), and (d) yield.

Entry 1

(a) 100 mg , 0.08 mmol, 1.0 eq, (b) 0.5 mL PhMe, (c) 1.2 mL, 0.32 mmol, 4.0 eq, and (d) 31 mg, 0.026 mmol, 32% yield.

Entry 2

(a) 300 mg , 0.23 mmol, 1.0 eq, (b) 1.5 mL PhMe, (c) 3.6 mL, 0.93 mmol, 4.0 eq, and (d) 69 mg, 0.074 mmol, 32% yield.

Entry 3

(a) 300 mg , 0.23 mmol, 1.0 eq, (b) 1.5 mL PhMe, (c) 3.6 mL, 0.93 mmol, 4.0 eq, and (d) 98.6 mg, 0.106 mmol, 46% yield.

Entry 4

(a) 681 mg , 0.52 mmol, 1.0 eq, (b) 3.4 mL PhMe, (c) 12.1 mL, 3.15 mmol, 6.0 eq, and (d) 198 mg, 0.213 mmol, 41% yield.

Entry 5 – 40 °C

(a) 100 mg , 0.08 mmol, 1.0 eq, (b) 0.5 mL PhMe, (c) 1.2 mL, 0.32 mmol, 4.0 eq, and (d) 28.6 mg, 0.024 mmol, 30% yield of impure product.

Melting point: >140-142 °C.

FTIR (neat): 3388, 2961, 2862, 2342, 1717, 1354 cm^{-1}.

^{1}H NMR (400 MHz, $CDCl_3$): δ 7.94 (s, 1H, NC<u>H</u>CN), 7.68 (bs, 8H, Ar-<u>H</u>), 7.50 (bs, 4H, Ar-<u>H</u>), 7.41 – 7.35 (m, 10H, Ar-<u>H</u>), 7.05 (s, 2H, Ar-<u>H</u>), 4.04 (s, 3H, NC<u>H</u>$_{3z}$), 3.02 – 2.95 (m, 2H, $CH_2C\underline{H}_2P$), 2.48 (t, J = 7.4 Hz, 2H, $C\underline{H}_2CH_2P$), 2.36 (s 3H, ArC<u>H</u>$_3$), 1.91 (s, 6H, ArC<u>H</u>$_3$) ppm.

^{13}C NMR (101 MHz, $CDCl_3$) δ 161.8 (q, $^{1}J_{C\text{-}B}$ = 49.4 Hz), 145.0, 144.0, 134.9, 133.7, 132.6 (d, $^{2}J_{C\text{-}P}$= 18.4 Hz), 130.6, 130.3 (d, $^{2}J_{C\text{-}P}$= 18.4 Hz), 129.4, 129.3, 129.0 (q, $^{2}J_{C\text{-}F}$ = 32.7 Hz), 128.0, 124.6 (q, $^{1}J_{C\text{-}F}$ = 272.4 Hz), 117.6, 38.10, 25.6, 21.3, 17.0 ppm.

^{11}B NMR (128 MHz, $CDCl_3$): δ -6.6 ppm

^{31}P NMR (162 MHz, $CDCl_3$): δ -20.5 ppm

^{19}F NMR (376 MHz, $CDCl_3$): δ -62.4 ppm

HRMS: *pending*

3.6.7 Attempted Complexation of MIC/P Ligand

Cycloocta-1,5-diene(3-(2-(diphenylphosphanyl)ethyl)-1-mesityl triazol ylidene)iridium terakis[3,5-bis(trifluoromethyl)phenyl]borate, **96**

Table 3.12

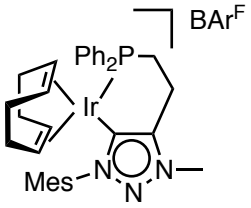

86

Synthesis of compound **86** was attempted *via* the three following synthetic procedures:

Entry 1

To a flame dried Schlenk tube was added $[Ir(COD)Cl]_2$ **4** (33 mg, 0.049 mmol, 0.5 eq) and **121** (124.5 mg, 0.097 mmol, 1.0 eq). The mixture was then dissolved in THF (1.0 mL) and ^{t}BuOK (10.9 mg, 0.097 mmol,1.0 eq) was added. The reaction was stirred at room temperature for 2 h, after which the solvent was removed *in vacuo*. The resulting residue was purified by column chromatography (50% DCM/petrol). No product was isolated.

Entry 2

To a flame dried Schlenk tube was added ^{t}BuOK (15.1 mg, 0.134 mmol,1.0 eq) and **121** (170 mg, 0.134 mmol, 1.0 eq). The mixture was then dissolved in THF (1.0 mL) and $[Ir(COD)Cl]_2$ **4** (45.2 mg, 0.067 mmol, 0.5 eq) was added. The reaction was stirred at room temperature for

2 h, after which the solvent was removed *in vacuo*. The resulting residue was purified by column chromatography (50% DCM/petrol). No product was isolated.

Entry 3

To a flame dried Schlenk tube was added ^{t}BuOK (15.1 mg, 0.134 mmol,1.0 eq) and **121** (170 mg, 0.134 mmol, 1.0 eq). The mixture was then dissolved in THF (1.0 mL) and $[Ir(COD)Cl]_2$ **4** (45.2 mg, 0.067 mmol, 0.5 eq) was added. The reaction was stirred at room temperature for 2 h, after which the solvent was removed *in vacuo*. The resulting residue was purified by trituration with hexane. No product was isolated.

3.6.8 Additional Computational details

General Comments

Density functional theory (DFT) was employed to calculate the gas-phase electronic structures and energies for all species involved in H/D exchange reactions. All structures thus far have been optimized with the hybrid meta-GGA exchange correlation functional M06. The M06 density functional was used in conjunction with the 6-31(G)(*d*) basis set for main group non-metal atoms and the Stuttgart RSC effective core potential along with the associated basis set for Ir. The participating transition states (TS) are located at the same level of theory. Harmonic vibrational frequencies are calculated (with the incorporation of deuterium wherever state) at the same level of theory to characterize respective minima (reactants, intermediates, and products with no imaginary frequency) and first order saddle points (TSs with one imaginary frequency). The validity of using the 6-31G(d) basis set has previously been checked by comparative single point energy calculations employing the def2-TZVP basis set for all atoms on similar H/D exchange systems. All calculations using the M06 functional have been performed using Gaussian 09 quantum chemistry program package (version A.02). Coordinates and additional computational details are supplied in the appendix.

Counterpoise Method for Binding Energy Calculations

Counterpoise method for binding energy calculation requires optimised structures of the free complex (**A**), free substrate (**B**) and the catalyst-substrate complex (**AB**).

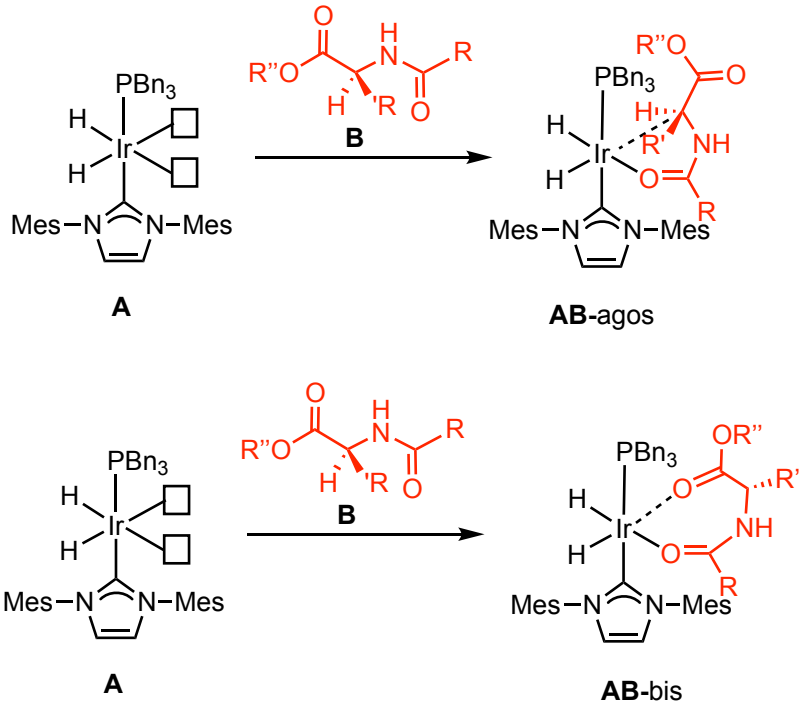

Scheme 3.41

The electronic energy for each of these structures was then used in Equation **1**, in order to deliver the binding energy (ΔE_{Bind}).

$$\Delta E_{Bind} = \left[E_{AB}^{\alpha\beta}(AB) - E_{AB}^{\alpha\beta}(A) - E_{AB}^{\alpha\beta}(B)\right] + \left[\left(E_{AB}^{\alpha}(A) - E_{A}^{\alpha}(A)\right) + \left(E_{AB}^{\beta}(B) - E_{B}^{\beta}(B)\right)\right] \quad \mathbf{1}$$

Key: $E_{geometry}^{basis\ set}(structure)$

Equation **2** can be simplified into terms describing the counterpoise corrected interaction energy (E_{int}) and the sum of distortion energies (E_{dist}), as shown in Equation **2**.

$$\boxed{\Delta E_{Bind} = E_{int} + E_{dist}} \qquad \mathbf{2}$$

A full account of the individual electronic energies and coordinates are reported in the appendix.

Buried Volume Calculations

All percent buried volume ($\%V_{bur}$) data were calculated using SambVca 2.0 web applications. All structural geometries used as inputs for these calculations were derived from DFT optimised structures. The main input data required for the online software for each ligand are the coordinates of the ligand plus the central metal atom. The metal-ligand bond distance is dictated by the results of the SFT optimisation. Iridium metal atom was selected as the atom coordinated to the centre of the sphere. The ligand atom coordinated to the metal and the metal itself were used to define the z-axis (using default Z-negative option). For NHC ligands, the xz-plane was defined using the two nitrogen atoms flanking the coordinating atom. For phosphines, the xz-plane was defined using the three atoms directly bound to the phosphorus centre. The metal atom was then deleted. Default mesh spacing was kept to 0.1 Å and the sphere radius kept to 3.5 Å. The distance of the coordination point to the centre of the sphere was kept at 0, as the true ligand metal bond distance was already set by the metal atom. Default atomic radii were described by Bondi radii scaled by 1.17. Hydrogen atoms were not included in the calculations. The coordinates of the ligand were first optimized in *Gaussian 09* as part of a full iridium(III) hydride complex cation of the formula $[(NHC)Ir(PR_3)(H)_2(MTBE)_2]^+$, and optimized coordinates converted to .pdb format. The .pdb file was then uploaded to the SambVca web application. Coordinates and SambVca outputs are included in the appendix.

3.7 References

(1) Arduengo, A. J.; Harlow, R. L.; Kline, M. *J. Am. Chem. Soc.* **1991**, *113*, 361–363.

(2) Magill, A. M.; Cavell, K. J.; Yates, B. F. *J. Am. Chem. Soc.* **2004**, *126*, 8717–8724.

(3) Chianese, A. R.; Kovacevic, A.; Zeglis, B. M.; Faller, J. W.; Crabtree, R. H. *Organometallics* **2004**, *23*, 2461–2468.

(4) Crabtree, R. H. *Coord. Chem. Rev.* **2013**, *257*, 755–766.

(5) Gründemann, S.; Kovacevic, A.; Albrecht, M.; Faller Robert, J. W.; Crabtree, R. H. *Chem. Commun.* **2001**, 2274–2275.

(6) Rottschäfer, D.; Schürmann, C. J.; Lamm, J.-H.; Paesch, A. N.; Neumann, B.; Ghadwal, R. S. *Organometallics* **2016**, *35*, 3421–3429.

(7) John, A.; Shaikh, M. M.; Ghosh, P. *Dalt. Trans.* **2009**, 10581–10591.

(8) Karthik, V.; Gupta, V.; Anantharaman, G. *Organometallics* **2014**, *33*, 6218–6222.

(9) Krüger, A.; Albrecht, M. *Chem. Eur. J.* **2012**, *18*, 652–658.

(10) Witt, J.; Pöthig, A.; Kühn, F. E.; Baratta, W. *Organometallics* **2013**, *32*, 4042–4045.

(11) Filonenko, G. A.; Cosimi, E.; Lefort, L.; Conley, M. P.; Copéret, C.; Lutz, M.; Hensen, E. J. M.; Pidko, E. A. *ACS Catal.* **2014**, *4*, 2667–2671.

(12) Manzano, R.; Rominger, F.; Hashmi, A. S. K. *Organometallics* **2013**, *32*, 2199–2203.

(13) Song, G.; Wang, X.; Li, Y.; Li, X. *Organometallics* **2008**, *27*, 1187–1192.

(14) Gong, X.; Zhang, H.; Li, X. *Tetrahedron Lett.* **2011**, *52*, 5596–5600.

(15) Stylianides, N.; Danopoulos, A. A.; Tsoureas, N. *J. Organomet. Chem.* **2005**, *690*, 5948–5958.

(16) Zuo, W.; Braunstein, P. *Organometallics* **2012**, *31*, 2606–2615.

(17) Chianese, A. R.; Kovacevic, A.; Zeglis, B. M.; Faller, J. W.; Crabtree, R. H. *Organometallics* **2004**, *23*, 2461–2468.

(18) Liang, L.; Astruc, D. *Coord. Chem. Rev.* **2011**, *255*, 2933–2945.

(19) Bouffard, J.; Keitz, B. K.; Tonner, R.; Guisado-Barrios, G.; Frenking, G.; Grubbs, R.

H.; Bertrand, G. *Organometallics* **2011**, *30*, 2617–2627.

(20) Wirschun, W.; Jochims, J. C. *Synthesis (Stuttg).* **1997**, *1997*, 233–241.

(21) Mathew, P.; Neels, A.; Albrecht, M. *J. Am. Chem. Soc.* **2008**, *130*, 13534–13535.

(22) Heath, R.; Müller-Bunz, H.; Albrecht, M. *Chem. Commun.* **2015**, *51*, 8699–8701.

(23) Mazloomi, Z.; Pretorius, R.; Pàmies, O.; Albrecht, M.; Diéguez, M. *Inorg. Chem.* **2017**, *56*, 11282–11298.

(24) Mendoza-Espinosa, D.; Alvarez-Hernández, A.; Angeles-Beltrán, D.; Negrón-Silva, G. E.; Suárez-Castillo, O. R.; Vásquez-Pérez, J. M. *Inorg. Chem.* **2017**, *56*, 2092–2099.

(25) Zamora, M. T.; Ferguson, M. J.; Cowie, M. *Organometallics* **2012**, *31*, 5384–5395.

(26) Petronilho, A.; Woods, J. A.; Mueller-Bunz, H.; Bernhard, S.; Albrecht, M. *Chem. Eur. J.* **2014**, *20*, 15775–15784.

(27) Schuster, E. M.; Botoshansky, M.; Gandelman, M. *Dalt. Trans.* **2011**, *40*, 8764–8787.

(28) Terashima, T.; Inomata, S.; Ogata, K.; Fukuzawa, S. *Eur. J. Inorg. Chem.* **2012**, *2012*, 1387–1393.

(29) Kelly III, R. A.; Clavier, H.; Giudice, S.; Scott, N. M.; Stevens, E. D.; Bordner, J.; Samardjiev, I.; Hoff, C. D.; Cavallo, L.; Nolan, S. P. *Organometallics* **2008**, *27*, 202–210.

(30) Ung, G.; Bertrand, G. *Chem. Eur. J.* **2011**, *17*, 8269–8272.

(31) Song, G.; Zhang, Y.; Li, X. *Organometallics* **2008**, *27*, 1936–1943.

(32) Yuan, D.; Huynh, H. V. *Organometallics* **2012**, *31*, 405–412.

(33) Delgado-Rebollo, M.; Canseco-Gonzalez, D.; Hollering, M.; Mueller-Bunz, H.; Albrecht, M. *Dalton Trans.* **2014**, *43*, 4462–4473.

(34) Strydom, I.; Guisado-Barrios, G.; Fernández, I.; Liles, D. C.; Peris, E.; Bezuidenhout, D. I. *Chem. Eur. J.* **2017**, *23*, 1393–1401.

(35) Hohloch, S.; Su, C.-Y.; Sarkar, B. *Eur. J. Inorg. Chem.* **2011**, *2011*, 3067–3075.

(36) Karthikeyan, T.; Sankararaman, S. *Tetrahedron Lett.* **2009**, *50*, 5834–5837.

(37) Johnson, C.; Albrecht, M. *Organometallics* **2017**, *36*, 2902–2913.

(38) Mitsui, T.; Sugihara, M.; Tokoro, Y.; Fukuzawa, S. *Tetrahedron* **2015**, *71*, 1509–1514.

(39) Wang, D.; Astruc, D. *Chem. Rev.* **2015**, *115*, 6621–6686.

(40) Prades, A.; Peris, E.; Albrecht, M. *Organometallics* **2011**, *30*, 1162–1167.

(41) Valencia, M.; Pereira, A.; Müller-Bunz, H.; Belderraín, T. R.; Pérez, P. J.; Albrecht, M. *Chem. Eur. J.* **2017**, *23*, 8901–8911.

(42) Nishiki, K.; Ota, H.; Ogo, S.; Sano, T.; Sadakane, M. *Eur. J. Inorg. Chem.* **2015**, *2015*, 2714–2723.

(43) Liu, W.; Cao, L.; Zhang, Z.; Zhang, G.; Huang, S.; Huang, L.; Zhao, P.; Yan, X. *Org. Lett.* **2020**, *22*, 2210–2214.

(44) Boys, S. F.; Bernardi, F. *Mol. Phys.* **1970**, *19*, 553–566.

(45) Sugimoto, K.; Hayashi, R.; Nemoto, H.; Toyooka, N.; Matsuya, Y. *Org. Lett.* **2012**, *14*, 3510–3513.

(46) Brand, J. P.; Chevalley, C.; Scopelliti, R.; Waser, J. *Chem. Eur. J.* **2012**, *18*, 5655–5666.

(47) Torres, O.; Martín, M.; Sola, E. *Organometallics* **2009**, *28*, 863–870.

(48) Cochrane, A. R.; Kennedy, A. R.; Kerr, W. J.; Lindsay, D. M.; Reid, M.; Tuttle, T. *Catalysts* **2020**, *10*, 161.

(49) Mendoza-Espinosa, D.; Rendón-Nava, D.; Alvarez-Hernández, A.; Angeles-Beltrán, D.; Negrón-Silva, G. E.; Suárez-Castillo, O. R. *Chem. - An Asian J.* **2017**, *12*, 203–207.

(50) Lloyd-Jones, G. C.; Taylor, N. P. *Chem. Eur. J.* **2015**, *21*, 5423–5428.

(51) Tejo, C.; Pang, J. H.; Ong, D. Y.; Oi, M.; Uchiyama, M.; Takita, R.; Chiba, S. *Chem. Commun.* **2018**, *54*, 1782–1785.

(52) Yang, C.-T.; Han, J.; Liu, J.; Li, Y.; Zhang, F.; Gu, M.; Hu, S.; Wang, X. *RSC Adv.* **2017**, *7*, 24652–24656.

(53) Laven, G.; Kullberg, M. *WO2011/123037 A1* **2011**, 32.

(54) Soellner, M. B.; Tam, A.; Raines, R. T. *J. Org. Chem.* **2006**, *71*, 9824–9830.

(55) Li, Y.; Das, S.; Zhou, S.; Junge, K.; Beller, M. *J. Am. Chem. Soc.* **2012**, *134*, 9727–9732.

(56) Imamoto, T.; Takeyama, T.; Kusumoto, T. *Chem. Lett.* **1985**, *14*, 1491–1492.

(57) Busacca, C. A.; Raju, R.; Grinberg, N.; Haddad, N.; James-Jones, P.; Lee, H.; Lorenz, J. C.; Saha, A.; Senanayake, C. H. *J. Org. Chem.* **2008**, *73*, 1524–1531.

(58) Armarego, W. L. .; Chai, C. L. . *Purification of Laboratory Chemicals*, Seventh Ed.; Elsevier Ltd, 2013.

(59) Kojima, T.; Hiraoka, S. *Org. Lett.* **2014**, *16*, 1024–1027.

(60) Kloss, F.; Köhn, U.; Jahn, B. O.; Hager, M. D.; Görls, H.; Schubert, U. S. *Chem. - An Asian J.* **2011**, *6*, 2816–2824.

(61) Nakamura, T.; Ogata, K.; Fukuzawa, S. *Chem. Lett.* **2010**, *39*, 920–922.

(62) Erixon, K. M.; Dabalos, C. L.; Leeper, F. J. *Org. Biomol. Chem.* **2008**, *6*, 3561–3577.

(63) Boon, B. A.; Green, A. G.; Liu, P.; Houk, K. N.; Merlic, C. A. *J. Org. Chem.* **2017**, *82*, 4613–4624.

(64) Jana, G. K.; Sinha, S. *Tetrahedron Lett.* **2012**, *53*, 1671–1674.

(65) Detz, R. J.; Heras, S. A.; de Gelder, R.; van Leeuwen, P. W. N. M.; Hiemstra, H.; Reek, J. N. H.; van Maarseveen, J. H. *Org. Lett.* **2006**, *8*, 3227–3230.